frontiers | Research Topics

Insights in neuro-otology: 2021 and 2022

Edited by
Michael Strupp, Hans Straka and Sun-Young Oh

Published in
Frontiers in Neurology

FRONTIERS EBOOK COPYRIGHT STATEMENT

The copyright in the text of individual articles in this ebook is the property of their respective authors or their respective institutions or funders. The copyright in graphics and images within each article may be subject to copyright of other parties. In both cases this is subject to a license granted to Frontiers.

The compilation of articles constituting this ebook is the property of Frontiers.

Each article within this ebook, and the ebook itself, are published under the most recent version of the Creative Commons CC-BY licence. The version current at the date of publication of this ebook is CC-BY 4.0. If the CC-BY licence is updated, the licence granted by Frontiers is automatically updated to the new version.

When exercising any right under the CC-BY licence, Frontiers must be attributed as the original publisher of the article or ebook, as applicable.

Authors have the responsibility of ensuring that any graphics or other materials which are the property of others may be included in the CC-BY licence, but this should be checked before relying on the CC-BY licence to reproduce those materials. Any copyright notices relating to those materials must be complied with.

Copyright and source acknowledgement notices may not be removed and must be displayed in any copy, derivative work or partial copy which includes the elements in question.

All copyright, and all rights therein, are protected by national and international copyright laws. The above represents a summary only. For further information please read Frontiers' Conditions for Website Use and Copyright Statement, and the applicable CC-BY licence.

ISSN 1664-8714
ISBN 978-2-83252-028-4
DOI 10.3389/978-2-83252-028-4

About Frontiers

Frontiers is more than just an open access publisher of scholarly articles: it is a pioneering approach to the world of academia, radically improving the way scholarly research is managed. The grand vision of Frontiers is a world where all people have an equal opportunity to seek, share and generate knowledge. Frontiers provides immediate and permanent online open access to all its publications, but this alone is not enough to realize our grand goals.

Frontiers journal series

The Frontiers journal series is a multi-tier and interdisciplinary set of open-access, online journals, promising a paradigm shift from the current review, selection and dissemination processes in academic publishing. All Frontiers journals are driven by researchers for researchers; therefore, they constitute a service to the scholarly community. At the same time, the *Frontiers journal series* operates on a revolutionary invention, the tiered publishing system, initially addressing specific communities of scholars, and gradually climbing up to broader public understanding, thus serving the interests of the lay society, too.

Dedication to quality

Each Frontiers article is a landmark of the highest quality, thanks to genuinely collaborative interactions between authors and review editors, who include some of the world's best academicians. Research must be certified by peers before entering a stream of knowledge that may eventually reach the public - and shape society; therefore, Frontiers only applies the most rigorous and unbiased reviews. Frontiers revolutionizes research publishing by freely delivering the most outstanding research, evaluated with no bias from both the academic and social point of view. By applying the most advanced information technologies, Frontiers is catapulting scholarly publishing into a new generation.

What are Frontiers Research Topics?

Frontiers Research Topics are very popular trademarks of the *Frontiers journals series*: they are collections of at least ten articles, all centered on a particular subject. With their unique mix of varied contributions from Original Research to Review Articles, Frontiers Research Topics unify the most influential researchers, the latest key findings and historical advances in a hot research area.

Find out more on how to host your own Frontiers Research Topic or contribute to one as an author by contacting the Frontiers editorial office: frontiersin.org/about/contact

Insights in neuro-otology: 2021 and 2022

Topic editors
Michael Strupp — Ludwig Maximilian University of Munich, Germany
Hans Straka — Ludwig Maximilian University of Munich, Germany
Sun-Young Oh — Jeonbuk National University, Republic of Korea

Citation
Strupp, M., Straka, H., Oh, S.-Y., eds. (2023). *Insights in neuro-otology: 2021 and 2022*. Lausanne: Frontiers Media SA. doi: 10.3389/978-2-83252-028-4

Table of contents

06 Editorial: Insights in neuro-otology: 2021 and 2022
Michael Strupp, Hans Straka and Sun-Young Oh

11 Preoperative Significance of Ipsilateral Manual Neck Compression in Patients With Pulsatile Tinnitus Secondary to Sigmoid Sinus Dehiscences and Diverticula
Seung Jae Lee, Sang-Yeon Lee, Byung Yoon Choi, Ja-Won Koo, Sung Hwa Hong and Jae-Jin Song

21 Development and Content Validity of the Bilateral Vestibulopathy Questionnaire
Lisa van Stiphout, Israt Hossein, Merel Kimman, Susan L. Whitney, Andrianna Ayiotis, Michael Strupp, Nils Guinand, Angélica Pérez Fornos, Josine Widdershoven, Ángel Ramos-Macías, Vincent Van Rompaey and Raymond van de Berg

29 The Effect of Galvanic Vestibular Stimulation on Visuospatial Cognition in an Incomplete Bilateral Vestibular Deafferentation Mouse Model
Thanh Tin Nguyen, Gi-Sung Nam, Gyu Cheol Han, Chuyen Le and Sun-Young Oh

39 Vestibular Cochlear Manifestations in COVID-19 Cases
Kathiravan Kaliyappan, Yu-Chen Chen and Vijaya Prakash Krishnan Muthaiah

47 Patterns of Vestibular Impairment in Bilateral Vestibulopathy and Its Relation to Etiology
Lisa van Stiphout, Maksim Pleshkov, Florence Lucieer, Bieke Dobbels, Vergil Mavrodiev, Nils Guinand, Angelica Pérez Fornos, Josine Widdershoven, Michael Strupp, Vincent Van Rompaey and Raymond van de Berg

61 A Randomized, Double-Blind, Sham-Controlled Trial of Transcranial Direct Current Stimulation for the Treatment of Persistent Postural-Perceptual Dizziness (PPPD)
Jooyeon Jamie Im, Seunghee Na, Sanghoon Kang, Hyeonseok Jeong, Eek-Sung Lee, Tae-Kyeong Lee, Woo-Young Ahn, Yong-An Chung and In-Uk Song

71 Purification of Fibroblasts From the Spiral Ganglion
Annett Anacker, Karl-Heinz Esser, Thomas Lenarz and Gerrit Paasche

85 Heading Direction Is Significantly Biased by Preceding Whole-Body Roll-Orientation While Lying
Alexander Andrea Tarnutzer, Vasco Duarte da Costa, Denise Baumann and Simone Hemm

100 B81 Bone Vibrator-Induced Vestibular-Evoked Myogenic Potentials: Normal Values and the Effect of Age
Yuzhong Zhang, Zichen Chen, Huandi Zhao, Jiali Shen, Bo Zhong, Qiong Wu, Jun Yang, Yulian Jin, Qing Zhang and Pengyu Ren

112 The Role of Neck Input in Producing Corrective Saccades in the Head Impulse Test
Shinichi Iwasaki, Teru Kamogashira, Chisato Fujimoto, Kayoko Kabaya, Makoto Kinoshita and Tatsuya Yamasoba

119 Is There an "Acquired Idiopathic Head-Shaking Nystagmus"?—A Discussion of Mechanisms and Clinical Implications Based on a Case Report
Filipp M. Filippopulos, Andreas Zwergal and Doreen Huppert

124 Commentary: Is There an "Acquired Idiopathic Head-Shaking Nystagmus?": A Discussion of Mechanisms and Clinical Implications Based on a Case Report
Sun-Uk Lee and Ji-Soo Kim

126 Comparison of Clinical Balance and Visual Dependence Tests in Patients With Chronic Dizziness With and Without Persistent Postural-Perceptual Dizziness: A Cross-Sectional Study
Charlotte De Vestel, Willem De Hertogh, Vincent Van Rompaey and Luc Vereeck

138 Case Report: Diagnosis of Petrous Apex IgG4-Related Disease by Middle Cranial Fossa Craniotomy and Temporal Bone Biopsy
Louis Hofmeyr, Gerrida Herbst, Elias Pretorius, Brian Sarembock, Kathryn Taylor and David Roytowski

143 Description of a New Labyrinthine Dehiscence: Horizontal Semicircular Canal Dehiscence at the Tympanic Segment of the Facial Nerve
Gerard Gianoli, James Soileau and Bradley Shore

152 Olfactory, Auditory, and Vestibular Performance: Multisensory Impairment Is Significantly Associated With Incident Cognitive Impairment
Jacob C. Lucas, Zack Arambula, Alexandra M. Arambula, Katherine Yu, Nathan Farrokhian, Linda D'Silva, Hinrich Staecker and Jennifer A. Villwock

166 Simultaneous Dual Recordings From Vestibular Hair Cells and Their Calyx Afferents Demonstrate Multiple Modes of Transmission at These Specialized Endings
Donatella Contini, Gay R. Holstein and Jonathan J. Art

176 Low Gain Values of the Vestibulo-Ocular Reflex Can Optimize Retinal Image Slip
Stefan Glasauer and Hans Straka

188 Self-Reported Measures Have a Stronger Association With Dizziness-Related Handicap Compared With Physical Tests in Persons With Persistent Dizziness
Lene Kristiansen, Liv H. Magnussen, Kjersti T. Wilhelmsen, Silje Maeland, Stein Helge G. Nordahl, Anders Hovland, Richard Clendaniel, Eleanor Boyle and Birgit Juul-Kristensen

199 Transcriptional Down-Regulation of Major Histocompatibility Complex as a Possible Pathogenesis for Meniere's Disease
Kwang-Dong Choi, Eun Hye Oh, Hyun Sung Kim, Hyang-Sook Kim, Ji-Yun Park, Seo Young Choi and Jae-Hwan Choi

207 Correlation of clinical parameters with endolymphatic hydrops on MRI in Meniere's disease
Seung Cheol Han, Young Seok Kim, Yehree Kim, Sang-Yeon Lee, Jae-Jin Song, Byung Yoon Choi, Ji-Soo Kim, Yun Jung Bae and Ja-Won Koo

217 A preliminary trial of botulinum toxin type A in patients with vestibular migraine: A longitudinal fMRI study
Sun-Young Oh, Jin-Ju Kang, Sohui Kim, Jong-Min Lee, Ji-Soo Kim and Marianne Dieterich

228 Thresholds for vestibular and cutaneous perception and oculomotor response induced by galvanic vestibular stimulation
Thanh Tin Nguyen, Jin-Ju Kang and Sun-Young Oh

240 Recent developments in the understanding of the interactions between the vestibular system, memory, the hippocampus, and the striatum
Paul F. Smith

253 Comparison of EOG and VOG obtained eye movements during horizontal head impulse testing
Maksim Pleshkov, Vasilii Zaitsev, Dmitrii Starkov, Vladimir Demkin, Herman Kingma and Raymond van de Berg

263 The frequency and relationship with vestibular function test results of positional preference in acute vestibular neuritis
Ji-Yun Park, Hyung Lee and Hyun Ah Kim

frontiers | Frontiers in Neurology

TYPE Editorial
PUBLISHED 07 December 2022
DOI 10.3389/fneur.2022.1104573

Check for updates

OPEN ACCESS

EDITED AND REVIEWED BY
Toshihisa Murofushi,
Teikyo University Mizonokuchi Hospital, Japan

*CORRESPONDENCE
Michael Strupp
michael.strupp@
med.uni-muenchen.de

SPECIALTY SECTION
This article was submitted to Neuro-Otology, a section of the journal Frontiers in Neurology

RECEIVED 21 November 2022
ACCEPTED 28 November 2022
PUBLISHED 07 December 2022

CITATION
Strupp M, Straka H and Oh S-Y (2022) Editorial: Insights in neuro-otology: 2021 and 2022.
Front. Neurol. 13:1104573.
doi: 10.3389/fneur.2022.1104573

COPYRIGHT
© 2022 Strupp, Straka and Oh. This is an open-access article distributed under the terms of the Creative Commons Attribution License (CC BY). The use, distribution or reproduction in other forums is permitted, provided the original author(s) and the copyright owner(s) are credited and that the original publication in this journal is cited, in accordance with accepted academic practice. No use, distribution or reproduction is permitted which does not comply with these terms.

Editorial: Insights in neuro-otology: 2021 and 2022

Michael Strupp[1]*, Hans Straka[2] and Sun-Young Oh[3]

[1]Department of Neurology and German Center for Vertigo and Balance Disorders, Ludwig-Maximilians-University, Munich, Germany, [2]Faculty of Biology, Ludwig-Maximilians-University, Planegg, Germany, [3]Department of Neurology, School of Medicine, Jeonbuk National University, Jeonju, South Korea

KEYWORDS

vertigo, dizziness, vestibulo-ocular research, bilateral vestibulopathy, acute unilateral vestibulopathy, nystagmus, Menière's disease, functional dizziness

Editorial on the Research Topic
Insights in neuro-otology: 2021 and 2022

Introduction

The Research Topic "*Insights in neuro-otology: 2021 and 2022*" covers, as the title indicates, a broad range of topics from basic research on the vestibular system to clinical studies and trials. It brings together many influential researchers in their specific areas of expertise and presents relevant key findings from the last 2 years. Thereby, it also connects the various levels of research and will stimulate translational and back-translational research. Twenty-seven articles with a total of 126 authors were published in this Research Topic, and so far, it has received more than 22,000 views and has been downloaded more than 3,700 times. This Editorial briefly summarizes the background and the key findings and conclusions of the various contributions, providing an overview that will hopefully prompt the reader to read these articles in full.

Basic and applied vestibular research

The connection between mammalian type I hair cells and calyx afferents forms a highly specialized synapse that is excellently suited for the transmission of high-frequency, high-acceleration head motion profiles. Contini et al. coherently describe, in a mini review, the multiple communication modes of the calyx synapse. The conventional glutamatergic quantal transmission on the millisecond timescale by these synapses is assisted by low-pass filtered transduction currents mediated by potassium ions that accumulate in the synaptic cleft. This mechanism depolarizes hair cells and afferents and thereby enhances the conventional transmission, both pre- and post-synaptically. A third form of transmission in the microsecond range exploits the large voltage- and ion-sensitive cleft-facing conductances of the hair cells and the calyx, adding collectively to the large range of response dynamics of irregular firing vestibular afferent fibers.

Cultures of isolated spiral ganglion cells usually contain cell bodies of auditory afferent fibers but also cochlear fibroblasts, which, in the case of cochlear implants, can produce undesired fibrous tissue around the electrode. Anacker et al. succeeded in purifying fibroblasts following removal of neurons, and by increasing the ratio of fibroblast to glial cells, verified by differential staining for vimentin, S100B-protein, and 200-kD neurofilament. Using Thy1-glycoprotein and p75NGFR immunolabeling allowed fluorescence-based cell sorting, providing an almost pure cochlear fibroblast cell culture. These cells exhibit a fibroblast-specific morphology, are stable for multiple proliferation rounds, and robustly survive cryopreservation. This offers the possibility of conducting *in vitro* studies to find possible conceptual solutions for minimizing fibrous scar formation.

In their study with 25 healthy participants, Tarnutzer et al. demonstrate that heading direction is significantly biased by preceding short-term whole-body roll orientation while lying horizontally. This finding underlines the broad impact of a shifting internal estimate of the direction of gravity. The authors conclude that, in a broader context, the observed bias in perceived straight ahead emphasizes that getting up in the morning is a vulnerable period with an increased risk of falls and fall-related injuries due to an inability of optimally tuned internal estimates of the direction of gravity and the direction of straight ahead. This article therefore has a direct impact and helps to explain the high risk of falls after a good night's sleep.

Many animal and clinical studies have extensively reported prominent and long-lasting spatial cognitive deficits in bilateral vestibulopathy (BVP), along with some evidence of hippocampal atrophy. Nguyen, Nam et al. report that these impairments were ameliorated by application of five consecutive daily sessions of noisy galvanic vestibular stimulation (nGVS), as evidenced by the substantial improvement of poor behavioral performance during the Y-maze and MWM tasks in mice with a surgically incomplete BVP. This weak galvanic current, which acts at the sensory endorgans and the spike trigger zone of primary vestibular afferents (inhibitory anode and excitatory cathode that can be amplified by the "stochastic resonance" phenomenon) and assists in rebalancing bilateral vestibular inputs, has recently shown positive effects in improving spatial cognition as well as postural and locomotion deficits in patients with BVP with residual function.

Vestibulo-ocular reflexes (VOR) stabilize retinal images by counter-rotating the eyes during head movements, ideally with a unity gain. However, in many species, and in elderly humans or patients with a vestibular impairment, the VOR gain is far from compensatory. Glasauer and Straka suggest in their study that such a suboptimal VOR gain reflects an adaptation to the sensory and motor signal variability. Since sensorimotor noise can disturb stabilizing eye movements, minimization of the overall retinal image slip should incorporate the effects of both noise components and the dynamic constraints of the signal processing. This premise was confirmed in *Xenopus laevis*, where computational calculations correspond to the observed variability of eye movements and the overall low VOR gain. This thus indicates that lower VOR gains in elderly humans or recovered vestibular patients may be an optimal adaptation given higher noise levels rather than a direct consequence of the principal damage.

Vestibular function is clinically evaluated by the video head impulse test combined with video-oculography (VOG), even though the latter method is occasionally challenging due to pupil detection issues. This prompted Pleshkov et al. to compare VOG with electro-oculography (EOG) as a technically more robust method for eye motion quantification. Horizontal eye movements in healthy human subjects were recorded with VOG and EOG during bidirectional head impulses and recorded magnitudes were cross-correlated and statistically evaluated. Eye movements obtained with either method correlated well with each other. However, EOG recordings were symmetric for bidirectional head impulses, while VOG recordings yielded a clear left-right asymmetry. This outcome suggests that EOGs are well-suited for eye movement recordings and might in fact represent a more objective technology.

A so far unknown positional preference was evaluated by Park et al. during the acute phase of an acute unilateral vestibulopathy by assessing the severity of vertigo with a visual analog scale (VAS). Patients were characterized with VOG, including standard tests such as spontaneous nystagmus during sitting, head rolling to both sides or ocular and cervical vestibular-evoked myogenic potentials. About a third of the patients complained of more severe vertigo during lying on the affected side compared to the healthy side with (36%) or without (30%) visual fixation. Both groups had significantly higher VAS and maximal slow phase velocities of the spontaneous nystagmus in all positions except lying on the impaired side, compared to those without positional preference. In the absence of other differences between the groups, the positional preference might reflect damage to the activation of the tonic but not the phasic otolithic system.

Head-shaking nystagmus can derive from asymmetric peripheral vestibular signals or from lesions, mostly in the cerebellum, that affect the velocity storage. In a case study, Filippopulos et al. report on a patient with recurrent episodes of vertigo, induced by fast head movements and accompanied by a severe head-shaking nystagmus with a long time constant. In the absence of other criteria for vestibular/auditory or neurological disorders, the authors suggest the presence of a clinical entity termed "acquired idiopathic head shaking nystagmus" as a rare cause of episodic vertigo with a distinct pathology of the cerebellar velocity storage mechanism that becomes apparent during fast head movements.

Based on the similarity of the recurrent spontaneous vertigo and absence of other pathological signs, Lee and Kim in a commentary suggest that this patient suffers from a

similar pathology as a previously described group of patients. Based on the characterization of these latter patients, the authors suggest that an unstable, asymmetric velocity-storage mechanism is the common pathological mechanism for the benign recurrent vertigo with head-shaking nystagmus and for acquired idiopathic head-shaking nystagmus.

Vestibular dysfunction can be detected by observing corrective saccades/re-fixation saccades that return the eyes to the target during a head impulse test. Corrective saccades are defined as covert or overt depending on whether the onset occurs before or after the end of the head impulse, respectively. In the absence of a clear mechanistic origin, Iwasaki et al. examined the role of neck proprioceptive signals as a trigger for these saccades. In patients with vestibular dysfunction, head and eye movements were recorded during the head or body impulse test, where during the latter maneuver, the head is fixed to the body. While the number of corrective covert saccades was similar in both conditions, there were significantly fewer overt saccades during the body impulse test. This result suggests that neck somatosensory inputs contribute to the generation of overt saccades, thereby reinforcing the VOR during high-frequency head movements.

Clinical vestibular research

There have already been many publications on vestibulo-cochlear manifestations in COVID-19 cases with contradicting findings, but one must always consider that there were vestibular disorders even before this pandemic. Kaliyappan et al. critically review basic mechanisms that may lead to an impairment of vestibular and audiological function by SARS-CoV-2, namely the role of the angiotensin-converting enzyme 2 receptor in various parts of the brain. However, critically viewing the many case reports and new case series published so far, there is currently no evidence for a major impact of SARS-CoV-2 on either the peripheral vestibular or the auditory system, which is also true for the vaccines against SARS-CoV-2. There is still a great need for clinically relevant and validated scales to quantify the impact of vestibular disorders on functionality and quality of life.

In their article, Kristiansen et al. describe the variations in signs and symptoms in 107 patients with persistent dizziness using physical tests and self-reported outcomes across three severity levels of the Dizziness Handicap Inventory (DHI). Participants performed physical tests, psychological measures and various scales for the quality of life. There was a trend toward worse scores on physical tests and self-reported measurements with increasing DHI severity level. However, several signs and symptoms may not be detected by the DHI and therefore the authors recommend a combination of outcomes in patients with persistent dizziness.

Another article in this Research Topic focuses on a similar topic: development and content validity of the bilateral vestibulopathy (BVP) questionnaire by van Stiphout, Hossein et al. The aim was to measure the burden and severity of the full spectrum of bilateral vestibulopathy symptoms and to assess its impact on daily life. A two-step approach was used: (1) initial item generation and (2) phase and content validity testing. This questionnaire consists of two sections: (1) 50 items scored on a six-point Likert scale, e.g., on imbalance and cognitive symptoms; and (2) four items on a visual analog scale from 0 to 100 on limitations in daily life, perceived health and expectations regarding recovery. The authors conclude that this questionnaire can be used to characterize current self-reported symptoms and disability and the burden of disease and as an outcome measure in clinical practice and clinical studies.

Another article by van Stiphout, Pleshkov et al. also focuses on BVP, namely the patterns of vestibular impairment and its relationship to etiology. A total of 173 subjects from three tertiary referral centers in Europe with the diagnosis of BVP according to the Barany Society diagnostic criteria were included. They underwent a full diagnostic workup. The major findings were as follows: vHIT and caloric testing seem to be more sensitive for measuring vestibular impairment, whereas the Torsion Swing Test is more suited to measuring residual vestibular function. No striking patterns of vestibular impairment in relation to etiology were found. Finally, the authors advised that one should carefully examine every patient for its overall pattern of vestibular impairment in order to make well-informed and personalized therapeutic decisions, i.e., if vestibular implants are considered in the future.

There are currently three types of stimulation for vestibular evoked myogenic potentials: air-conducted sound, bone-conducted vibration and galvanic vestibular stimulation. For bone-conducted vibration, various bone vibrators have been used, e.g., the mini-shaker and the RadioEar. In a methodologically important study, Zhang et al. evaluated normal values and the effect of aging on bone vibrator-induced cervical and ocular vestibular evoked myogenic potentials (cVEMPs and oVEMPs). With aging, the cVEMP response amplitude decreased, while the threshold and the latency increased. The same was true for oVEMPs. This shows the importance of each laboratory with a sufficient number of patients ideally generating its own reference values in healthy individuals for different age groups.

Menière's disease is evidently the result of various underlying etiologies leading to such a phenotype. In addition to genetic factors, inflammation is one of the underlying etiological factors. Using transcriptome analysis, Choi et al. compared 39 patients with Menière's disease with 39 controls using peripheral blood monocular cells to evaluate differentially expressed genes. Four hundred and fifteen genes were upregulated and

581 were downregulated in the Menière's disease group. The downregulated genes were mainly associated with the immune system pathways, including the major histocompatibility complex, which may contribute to the development of Meniere's disease and may have implications for a targeted treatment in the future based on the genetic profile of each patient: precision medicine.

Using the "HYDROPS" (HYbriD of the reversed image of positive endolymph signal and native image of positive perilymph signal) imaging magnetic resonance (MR) protocol, Han et al. describe a significant positive correlation between some clinical and laboratory parameters in Menière's disease (MD), including the diagnostic scale of MD (possible, probable, and definite), pure tone average, low tone average, and canal paresis, but no such correlation with disease duration. These findings suggest that MR-based radiological evaluation of endolymphatic hydrops (EH) is useful for determining the extent and severity of MD, as well as the pathophysiological relationship between Menière's disease and EH.

In a case series, Gianoli et al. describe a new form of labyrinthine dehiscence: horizontal semicircular canal dehiscence at the tympanic segment of the facial nerve in 16 patients. The tympanic segment of the facial nerve crosses over the ampullated end of the horizontal semicircular canal. This type could also be the source of persistent symptoms after regular superior semicircular canal dehiscence surgery.

In a case report, Hofmeyr et al. describe the precise diagnosis of petrous apex IgG4-related disease by middle cranial fossa craniotomy and temporal bone biopsy in a patient with diplopia and unilateral headache, which had major therapeutic consequences because, after a precise histological diagnosis, the patient was treated with steroids, which led to a complete recovery.

Given the recent evidence that high-intensity galvanic stimulation (GVS) current can cause spatial cognitive performance errors, GVS threshold determination is required to optimize intervention. Nguyen, Kang et al. show that in a simultaneous analysis of the three impacts of vestibular and cutaneous perception and oculomotor response, induced by direct current galvanic vestibular stimulation (DC-GVS) with surface electrodes placed at the bilateral mastoid in healthy subjects, the mean vestibular threshold was lower than the mean oculomotor threshold but similar to the mean cutaneous threshold. This vestibular threshold was influenced by gender characteristics (significantly higher in males than in females) but not by the GVS paradigm (cathode right anode left vs. cathode left anode right).

In a review of studies published over the last 2 years exploring the contribution of the vestibular system to motor and cognitive processes, Smith provides insight into the interactions of vestibular information and hippocampal and striatal functions. Recent findings of vestibular impairments in Parkinson's disease and Alzheimer's disease have important implications for a comprehensive understanding and optimal treatment of these disorders.

In a model to evaluate the influence of individual sensory impairments, Lucas et al. discovered that olfactory dysfunction, gait impairment, and sensorineural hearing loss were significantly associated with increased risk of cognitive impairment, with olfactory dysfunction being the strongest predictor of cognitive impairment. Subjects with dysfunction in all three domains had a higher risk of cognitive impairment than those with impairment in fewer than two domains, indicating that multisensory dysfunction may contribute synergistically to cognitive impairment. These findings support the hypothesis that cognitive impairment and dementia are associated with sensory impairments in a variety of domains, common in elderly subjects, and early therapeutic intervention potentially prevents cognitive decline.

Oh et al. show that injection of botulinum toxin type A (BTX-A) in patients with vestibular migraine (VM) resistant to conventional prophylactic therapies significantly reduces the frequency of migraine and vertigo episodes and improves the Headache Impact Test-6 (HIT-6) score, Migraine Disability Assessment (MIDAS), Dizziness Handicap Inventory (DHI), Vertigo Symptom Scale (VSS), and anxiety and depression scores 2 months after treatment. Analysis of resting-state functional MRI data also revealed an increased functional connectivity of the right superior temporal gyrus, left post-central gyrus, right supramarginal gyrus, and right middle temporal gyrus, all of which were negatively correlated with the MIDAS score. This suggests that BTX-A may enhance intrinsic vestibular, nociceptive, and cross-modal interactions within the multisensory cortical network and is effective at improving vertigo and migraine attacks in VM.

De Vestel et al. conducted a cross-sectional study to compare clinical balance and visual dependence tests among persistent postural-perceptual dizziness (PPPD) patients, dizzy non-PPPD patients, and healthy subjects (HS) to determine whether these clinical tests can help to identify PPPD. PPPD patients were more visually dependent with significantly higher Visual Vertigo Analog Scale (VVAS) scores but did not have a worse postural balance compared to dizzy non-PPPD patients. This suggests that the VVAS had the highest discriminative value for identifying PPPD in chronic dizziness.

For the treatment of PPPD, Im et al. report that active transcranial direct current stimulation (tDCS) was not significantly more effective than sham tDCS for alleviating dizziness symptoms in a randomized, double-blind, sham-controlled trial of tDCS. The applied tDCS (20 min per session, 15 sessions over 3 weeks), targeting the dorsolateral prefrontal cortex, did not achieve significant symptom reduction, indicating the need for further research in PPPD using different stimulation protocols of tDCS with respect to stimulation site or number of sessions.

Author contributions

All authors listed have made a substantial, direct, and intellectual contribution to the work and approved it for publication.

Conflict of interest

The authors declare that the research was conducted in the absence of any commercial or financial relationships that could be construed as a potential conflict of interest.

Publisher's note

All claims expressed in this article are solely those of the authors and do not necessarily represent those of their affiliated organizations, or those of the publisher, the editors and the reviewers. Any product that may be evaluated in this article, or claim that may be made by its manufacturer, is not guaranteed or endorsed by the publisher.

frontiers in Neurology

ORIGINAL RESEARCH
published: 17 March 2022
doi: 10.3389/fneur.2022.869244

Preoperative Significance of Ipsilateral Manual Neck Compression in Patients With Pulsatile Tinnitus Secondary to Sigmoid Sinus Dehiscences and Diverticula

Seung Jae Lee[1†], *Sang-Yeon Lee*[2,3,4†], *Byung Yoon Choi*[1,3], *Ja-Won Koo*[1,3], *Sung Hwa Hong*[5] *and Jae-Jin Song*[1,3,4*]

[1] Department of Otorhinolaryngology-Head and Neck Surgery, Seoul National University Bundang Hospital, Seongnam, South Korea, [2] Department of Otorhinolaryngology-Head and Neck Surgery, Seoul National University Hospital, Seoul, South Korea, [3] Department of Otorhinolaryngology-Head and Neck Surgery, Seoul National University College of Medicine, Seoul, South Korea, [4] Sensory Organ Research Institute, Seoul National University Medical Research Center, Seoul, South Korea, [5] Department of Otorhinolaryngology-Head and Neck Surgery, Samsung Changwon Hospital, Sungkyunkwan University School of Medicine, Changwon, South Korea

OPEN ACCESS

Edited by:
In Seok Moon,
Yonsei University Health System,
South Korea

Reviewed by:
Gi Jung Im,
Korea University, South Korea
Wuqing Wang,
Fudan University, China

***Correspondence:**
Jae-Jin Song
jjsong96@gmail.com;
jjsong96@snubh.org

[†] These authors have contributed equally to this work and share first authorship

Specialty section:
This article was submitted to Neuro-Otology, a section of the journal Frontiers in Neurology

Received: 04 February 2022
Accepted: 21 February 2022
Published: 17 March 2022

Citation:
Lee SJ, Lee S-Y, Choi BY, Koo J-W, Hong SH and Song J-J (2022) Preoperative Significance of Ipsilateral Manual Neck Compression in Patients With Pulsatile Tinnitus Secondary to Sigmoid Sinus Dehiscences and Diverticula. Front. Neurol. 13:869244. doi: 10.3389/fneur.2022.869244

Venous pulsatile tinnitus (PT) is characterized by an auditory perception of pulse-synchronous sound, suppressed by compression of the ipsilateral internal jugular vein. We sought to determine the preoperative prognostic significance of the effect of ipsilateral neck manual compression on the PT loudness and audiometric changes in patients with sigmoid sinus dehiscences (SS-Deh) and diverticula (SS-Div) by comparing postoperative improvements in ipsilateral low-frequency hearing loss (LFHL) in pure-tone audiogram (PTA) and PT symptoms. Twenty-two subjects with PT originating from SS-Deh/Div were recruited. Air-conduction hearing thresholds were measured using PTA at three time points: twice preoperatively (with neutral neck position and with ipsilateral manual compression of internal jugular vein) and once at 3-months postoperatively with neutral neck position. We defined a positive neck compression effect as a threshold improvement of $\geq$ 10 dB HL at 250 or 500 Hz after manual neck compression. All but two subjects presented with ipsilateral LFHL in the neutral position. The average hearing threshold in the neutral position markedly improved after manual neck compression, indicating that LFHL originated from the masking effect of venous PT. All subjects had subjective improvements in PT and LFHL after sigmoid sinus surgeries, confirming that LFHL resulted from the masking effect of PT. Additionally, improvement of LFHL after neck compression could be regarded as a positive prognostic indicator after surgery. Collectively, elimination of PT loudness and improvement of LFHL with manual compression over the ipsilateral neck may suggest the venous origin of the PT and predict a favorable outcome following repair of SS-Deh/SS-Div.

Keywords: tinnitus, pulsatile tinnitus, pure-tone audiometry, hearing loss, jugular veins, compression

INTRODUCTION

Tinnitus can be pulsatile or non-pulsatile depending on the characteristics of the perceived sound (1). Non-pulsatile tinnitus, often referred to as subjective tinnitus, is presumably caused by functional changes in the auditory and non-auditory cortices (2, 3). Meanwhile, pulsatile tinnitus (PT) is caused by altered vascular hemodynamics, such as turbulent blood flow or vibration of a dehiscent vascular wall, or abnormal perception of the sound of normal flow, such as third-window lesions due to bony defects of the inner ear. Venous PT is characterized by auditory perception of a pulse-synchronous sound, which is usually suppressed by compressing internal jugular vein on the symptomatic side (4, 5).

Detailed otoendoscopy, physical examination, and radiologic evaluation are necessary for evaluating PT and selecting appropriate surgical candidates (6–8). In particular, high-resolution imaging modalities, such as contrast-enhanced temporal bone computed tomography and angiography (TB-CTA), depict details of the vascular abnormalities that may precipitate PT with reference to the surrounding structures. Nonetheless, some abnormalities (e.g., high-riding jugular bulb with or without dehiscence) are incidentally found among patients without PT and radiologic images may be normal in patients with PT. Therefore, better objective tests are required to identify lesions causing PT and predict symptomatic improvement after treatment. Previous studies reported that sigmoid sinus dehiscence (SS-Deh) and sigmoid sinus diverticulum (SS-Div), which were the most frequent vascular abnormalities in patients with venous PT, were also found in individuals without PT (4, 9–11).

Increasing evidence suggests that objective tests, including transcanal sound recording and spectro-temporal analysis (TSR-STA) (1, 12), can objectively demonstrate pulse-synchronous patterns of vascular PT and predict the origin thereof. Furthermore, preoperative ipsilateral low-frequency hearing loss (LFHL) has been reported as an objective audiological marker of PT, which improves following treatment in most cases (13). LFHL may predict postoperative audiological improvement on pure-tone audiometry (PTA) at low frequencies including 250 or 500 Hz, suggesting normalization of the underlying abnormal vascular pathology and alleviation of PT. Therefore, we hypothesized that audiological evaluation while applying manual neck compression would circumvent the masking effect of PT, thereby detecting the causative lesion of PT and helping to select the appropriate surgical candidates.

In this study, we explored the preoperative diagnostic and prognostic values of the effect of manual compression over the ipsilateral neck on the PT loudness and audiometric changes in patients with SS-Div or SS-Deh by comparing the ipsilateral LFHL and PT pre- and post-operatively. By confirming our a priori hypothesis, we may be able to understand the pathophysiological mechanisms of SS-Div/SS-Deh-associated PT and contribute to the development of diagnostic techniques for PT.

MATERIALS AND METHODS

Subjects

We screened PT patients who presented to Seoul National University Bundang Hospital, South Korea, between January 2019 and May 2021. This study included patients with radiologically documented SS-Div/SS-Deh and preoperative ipsilateral LFHL (pure-tone threshold $\geq$ 10 dB HL at 250 or 500 Hz compared to the symptom-free side) who underwent SS resurfacing or reshaping by a single surgeon (J-J.S.). Other arterial, venous or non-vascular etiologies of PT including intracranial arteriovenous fistulae and aneurysms, aberrant carotid artery, jugular bulb abnormalities or vascular neoplasms were excluded in our study (14). Twenty-two patients were included in this study and all of them underwent standard physical examinations at the outpatient clinic including thorough inspection and auscultation of head and neck area, and otoendoscopic examinations. The study was approved and patient consent was waived by the Institutional Review Board of the Clinical Research Institute (no. B-2107-699-105) and was conducted in accordance with the Declaration of Helsinki.

Audiological Evaluations

The patients underwent PTA pre- and post-operatively. Air conduction thresholds for seven octave frequencies (250, 500, 1,000, 2,000, 4,000, and 8,000 Hz) were evaluated using PTA in a soundproof booth. Serial audiograms were performed to determine the PTA threshold at all frequencies, at 3 time points: preoperatively with neutral neck position, preoperatively with ipsilateral manual compression of the internal jugular vein, and 3 months postoperatively with neutral neck position. A recent study investigated audiometric threshold shifts from PT due to SS wall anomalies, demonstrating PT can cause an average of 6 dB, and uncommonly up to 30 dB, of low-frequency hearing threshold shift in the affected ear (15). Since there is no gold standard for the definition of ipsilesional LFHL (i.e., pseudo-LFHL, PLFHL), we have defined it as a threshold difference of $\geq$ 10 dB HL at 250 or 500 Hz between ipsi- and contra-lesional neutral positions which fell within the middle range based on previous literature. Positive manual neck compression effect was defined as a threshold improvement of $\geq$ 10 dB HL at 250 or 500 Hz after manual compression.

Subjective Tinnitus Evaluations

At the initial visit, a structured interview about the PT characteristics was conducted. The patients completed a comprehensive questionnaire, which included the Numerical Rating Scale (NRS) and Tinnitus Handicap Inventory (THI) (16), to assess subjective tinnitus loudness and severity pre- and post-operatively. Pre- and post-operative NRS and THI scores were obtained at 1 day before and after surgery. The NRS consisted of 2 elements designed to assess the degree of annoyance (NRS-A; range, 0–10) and subjective loudness of tinnitus (NRS-L; range, 0–10).

Radiologic Evaluations

The patients underwent contrast-enhanced TB-CTA using Philips 128 CT scanners (Philips Medical Systems, Eindhoven,

TABLE 1 | Demographic and clinical characteristics of our cohort.

Pt. No.	Sex	Age	Side	Sx.Duration (mo)	Diagnosis	Operation name
1	F	24	R	48	(R) SS diverticulum	(R) SS resurfacing
2	F	42	R	9	(R) SS dehiscence	(R) SS reshaping
3	F	32	L	60	(L) SS dehiscence	(L) SS reshaping
4	F	30	R	4	(R) SS dehiscence	(R) SS reshaping
5	F	42	R	3	(R) SS diverticulum	(R) SS resurfacing
6	F	27	R	13	(R) SS dehiscence	(R) SS reshaping scheduled
7	F	45	R	24	(R) SS dehiscence	(R) SS reshaping
8	M	29	R	12	(R) SS dehiscence	(R) SS reshaping
9	F	25	R	10	(R) SS dehiscence	(R) SS reshaping
10	F	40	R	36	(R) SS dehiscence	None
11	F	28	R	24	(R) SS diverticulum	(R) SS resurfacing
12	F	36	L	9	(L) SS dehiscence	(L) SS reshaping
13	F	26	R	36	(R) SS dehiscence	(R) SS reshaping
14	F	33	R	2	(R) SS dehiscence	(R) SS reshaping
15	F	37	R	4	(R) SS diverticulum	(R) SS resurfacing
16	F	41	L	48	(L) SS diverticulum	(L) SS resurfacing scheduled
17	M	45	R	120	(R) SS diverticulum	(R) SS resurfacing scheduled
18	F	19	R	12	(R) SS dehiscence	None
19	F	36	L	84	(L) SS diverticulum	(L) SS resurfacing
20	F	23	L	8	(L) SS dehiscence	None
21	F	26	R	48	(R) SS dehiscence	(R) SS reshaping scheduled
22	F	20	L	48	(L) SS diverticulum	(L) SS resurfacing

Pt. No., patient number; M, male; F, female; R, right; L, left; Sx., symptom; mo, month; SS, sigmoid sinus.
Of 22 subjects, 20 (90.9%) were women. The mean age of subjects was 33.1 ± 6.6 years (range, 19–45 years). Sixteen subjects (72.7 %) presented with right-sided pulsatile tinnitus (PT) and six (27.3 %) with left-sided PT. The mean duration of PT symptoms was 30.1 ± 17.3 months (range, 2–120 months). According to temporal bone computed tomography and angiography (TB-CTA), 14 (63.6%) and 8 (36.4%) showed SS-Deh and SS-Div, respectively. Of the 15 subjects who underwent surgery, 6 (40.0%) and 9 (60.0%) underwent SS resurfacing due to SS-Div and SS reshaping due to SS-Deh, respectively.

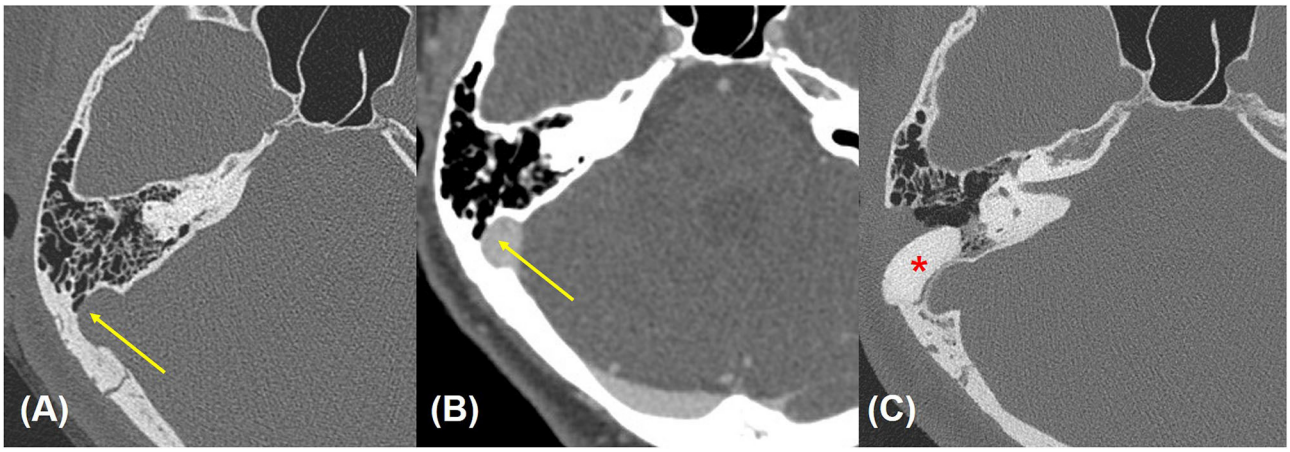

FIGURE 1 | Preoperative **(A,B)** and postoperative **(C)** temporal bone computed tomographic angiography (TB-CTA) images of Subject 4. Focal bony dehiscence at the lateral wall of the right transverse-sigmoid junction is observed [yellow arrow points to precontrast **(A)** and contrast-enhanced **(B)** images]. **(C)** Postoperative TB-CTA image showing calcium hydroxyapatite well *in situ* at the previously noted defect site (red asterisk).

The Netherlands). TB-CTA was performed using tube energy of 120 kVp, a quality reference value of 250 mA, and a detector configuration of 2 × 0.625 mm. The CT scan slices were of 0.7 mm and the scan length was 16 cm. Additionally, contrast-enhanced brain magnetic resonance imaging (MRI) with magnetic resonance angiography (MRA) were performed to identify pathognomonic findings related to dural arteriovenous fistula, pseudotumor cerebri, and idiopathic intracranial

hypertension. Specifically, we examined for transverse sinus stenosis and empty sella, which are radiological biomarkers of diseases associated with PT (4). A neuroradiologist and an otolaryngologist (S.J.L), who were blinded to clinical findings, independently reviewed the images of brain neurovascular structures and cervical neck to detect abnormal findings associated with PT.

Surgical Intervention

A typical cortical mastoidectomy was performed using the retro-auricular approach. As for the SS-Div cases, the diverticulum was completely skeletonized and manually reduced to the level of the adjacent SS wall, and the bony dehiscence surrounding the diverticulum was reconstructed by extraluminal placement of temporalis fascia and Mimix™ hydroxyapatite bone cement (Walter Lorenz Surgical Inc., Jacksonville, FL, USA). Meanwhile, for the SS-Deh cases, the SS and its dehiscent or thinned portions were also skeletonized for reshaping of the SS. The dominant SS was gently decompressed using autologous materials, and the SS-Deh was carefully reconstructed using temporalis fascia and bone cement as described in previous literature of ours (11, 17, 18).

Statistical Analysis

Data are presented as mean ± standard deviation (SD). Statistical analyses were performed using SPSS software (version 20; IBM Corp., Armonk, NY, USA). The statistical results were depicted using the GraphPad Prism software (version 9.0.0; GraphPad Software Inc., San Diego, CA, USA). The hearing thresholds were pair-wise compared at each frequency between the ipsilateral and contralateral sides, between ipsilateral neutral and manual compression positions, and between pre- and post-operative neutral positions using Wilcoxon signed-rank test. Pre- and post-operative subjective symptoms in terms of NRS and THI scores were compared using the aforementioned methods. P-value < 0.05 was considered statistically significant.

TABLE 2 | Effect of ipsilesional neck compression on low-frequency hearing thresholds.

Pt. No.	250 Hz			500 Hz			PLFHL	Ipsilesional neck compression effect
	Ipsi-lesional neutral (dB HL)	Contra-lateral neutral (dB HL)	Ipsi-lesional neck com. (dB HL)	Ipsi-lesional neutral (dB HL)	Contra-lateral neutral (dB HL)	Ipsi-lesional neck com. (dB HL)		
1	20	5	5	15	5	5	O	O
2	35	5	10	20	10	15	O	O
3	30	10	15	30	10	20	O	O
4	30	5	15	15	10	15	O	O
5	20	10	20	10	5	10	O	X
6	20	10	15	20	10	15	O	X
7	20	10	15	5	5	10	O	X
8	35	5	10	20	0	5	O	O
9	35	20	15	20	15	10	O	O
10	20	5	20	15	5	20	O	X
11	15	5	10	15	10	10	O	X
12	20	5	5	15	5	5	O	O
13	25	20	20	20	20	10	X	O
14	20	10	10	20	10	10	O	O
15	25	10	15	25	10	10	O	O
16	40	10	10	30	10	5	O	O
17	35	5	10	20	5	15	O	O
18	30	10	15	30	10	10	O	O
19	45	5	25	40	10	25	O	O
20	20	15	20	20	15	15	X	X
21	25	5	5	10	5	5	O	O
22	40	10	30	30	15	20	O	O

Pt. No., patient number; PTA, pure tone audiogram; PLFHL, pseudo-low-frequency hearing loss; com., compression.

In the neutral position, all but two subjects (Subjects 13 and 20) had ipsilateral low-frequency hearing loss (LFHL) (i.e., pseudo-low-frequency hearing loss, PLFHL) compared to the contralateral side. Sixteen subjects (72.7 %) had a positive ipsilateral effect of manual neck compression (i.e., improvement of ≥ 10 dB HL at 250 or 500 Hz), as proposed by our study. In the neutral position, the average hearing thresholds at 250 and 500 Hz were significantly higher in the ipsilateral side than the contralateral side (27.5 ± 8.2 dB HL vs. 8.9 ± 4.5 dB HL at 250 Hz, 20.2 ± 7.9 dB HL vs. 9.1 ± 4.4 dB HL at 500 Hz, respectively; both $p < 0.001$). After manual neck compression, the average hearing threshold markedly improved from 27.5 ± 8.2 dB HL to 14.3 ± 6.3 dB HL at 250 Hz and from 20.2 ± 8.0 dB HL to 12.1 ± 5.6 dB HL at 500 Hz (both $p < 0.001$).

RESULTS

Demographic Characteristics

Table 1 presents the demographic and clinical characteristics of the 22 subjects (20 women and two men). The mean age of subjects was 33.1 ± 6.6 years (range, 19–45 years). Sixteen subjects (72.7 %) presented with right-sided PT and six (27.3 %) presented with left-sided PT. The mean duration of PT symptoms was 30.1 ± 17.3 months (range, 2–120 months). SS-Deh and SS-Div were observed on TB-CTA in 14 (63.6 %) and 8 (36.4 %) subjects, respectively. Fifteen subjects (80.0 %) underwent SS operations; six of them were diagnosed with SS-Div and underwent SS resurfacing, while nine underwent SS reshaping due to SS-Deh. Postoperatively, SS and its dehiscence or diverticulum were found to be completely corrected in all subjects after reviewing TB-CTA taken 3 months after surgical interventions. A representative case of SS-Deh is demonstrated in **Figure 1**.

Effect of Manual Neck Compression on Audiological Manifestation

The pre- and post-operative audiological profiles of both 250 and 500 Hz are summarized in **Table 2**. In the neutral position, all but two subjects (Subjects 13 and 20, 90.9%) had ipsilateral LFHL compared to the contralateral side. The average hearing thresholds of neutral position at both 250 and 500 Hz were significantly different between the ipsilateral and contralateral sides (27.5 ± 8.2 dB HL and 8.9 ± 4.5 dB HL at 250 Hz, 20.2 ± 7.9 dB HL and 9.1 ± 4.4 dB HL at 500 Hz, respectively; both $p < 0.001$, the Wilcoxon signed-rank test). Sixteen subjects (72.7 %) had a positive ipsilateral effect of manual compression (i.e., improvement of ≥ 10 dB HL at 250 or 500 Hz). The average hearing threshold markedly improved from 27.5 ± 8.2 dB HL to 14.3 ± 6.3 dB HL at 250 Hz and from 20.2 ± 8.0 dB HL to 12.1 ± 5.6 dB HL at 500 Hz (both $p < 0.001$, the Wilcoxon signed-rank test) after manual neck compression, indicating that the LFHL was a result of the masking effect of venous PT. However, manual compression did not elicit a significant difference in hearing thresholds at other frequencies (1,000, 2,000, 4,000, or 8,000 Hz) compared to the neutral position.

Pre- and Postoperative Audiological Manifestations

Baseline and 3-month postoperative data for the audiological evaluations were available for 11 subjects. The postoperative average thresholds at 250 and 500 Hz (9.1 ± 3.6 dB HL and 10.0 ± 4.3 dB HL, respectively) significantly improved compared to the preoperative ipsilateral average pure-tone thresholds at the same frequencies ($p = 0.005$ and 0.033, the Wilcoxon signed rank test, respectively). The hearing thresholds at other frequencies (1,000, 2,000, 4,000, and

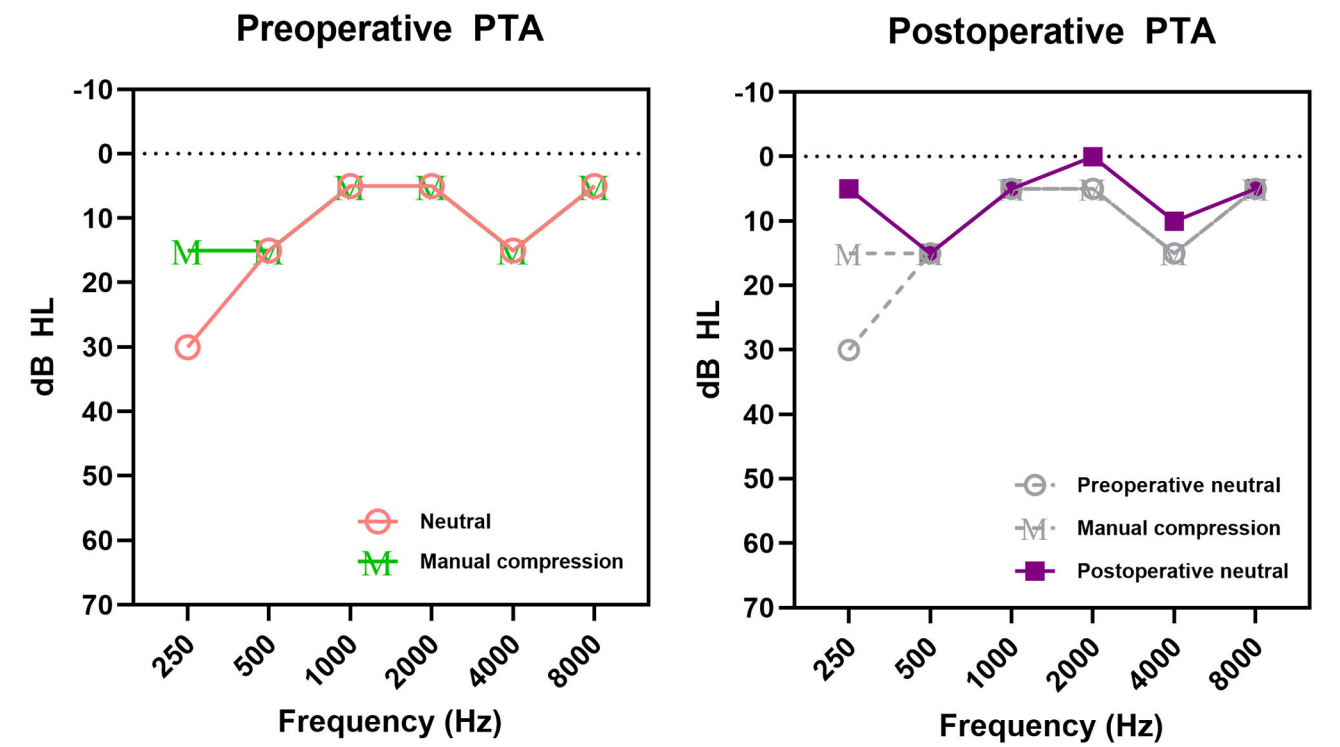

FIGURE 2 | Pure-tone audiogram (PTA) of Subject 4 with pulsatile tinnitus and ipsilateral low-frequency hearing loss (LFHL). Ipsilateral LFHL was defined as a hearing threshold >10 dB HL at 250 or 500 Hz compared to the opposite symptom-free side; positive neck compression effect was defined as a threshold decrease of ≥ 10 dB HL at 250 or 500 Hz after manual compression. Changes in ipsilateral pure-tone thresholds after neck compression and surgical treatment are demonstrated. M in preoperative PTA represents hearing thresholds after manual compression.

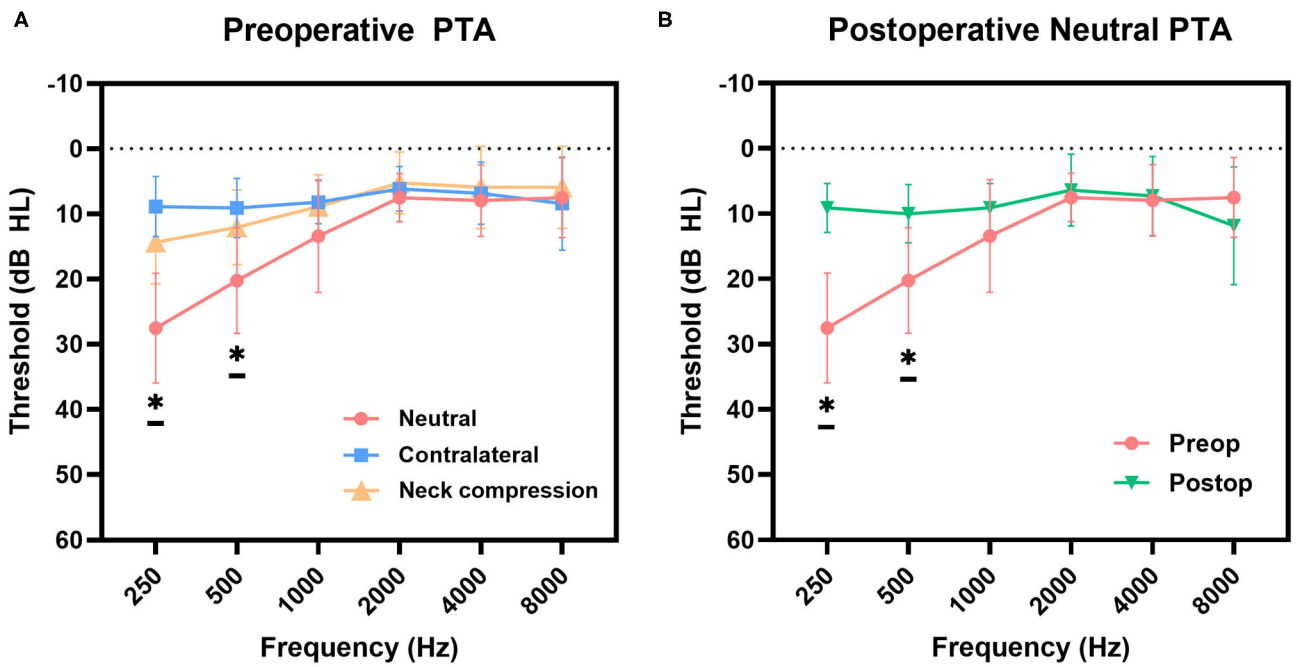

FIGURE 3 | (A) Mean preoperative hearing thresholds of pure-tone audiogram (PTA) were compared pair-wise between the neutral and contralateral side, and between neutral and post-manual compression by Wilcoxon singed-rank test. Statistical significance results ($p < 0.05$) were obtained at 250 ($p < 0.001$) and 500 Hz ($p < 0.001$), respectively. **(B)** Average postoperative thresholds at 250 and 500 Hz significantly improved from those for the preoperative neutral position ($p = 0.005$ and $p = 0.033$, respectively, Wilcoxon signed-rank test), indicating successful treatment. The asterick "*" means that there is a statistical significance between Neutral and both Contralateral and Neck compression thresholds, between preop and postop thresholds.

8,000 Hz) did not change postoperatively compared to the preoperative values. **Figure 2** depicts the pre- and post-manual compression and postoperative PTA for a representative case. Importantly, the PTA thresholds at 250 and 500 Hz did not show any significant differences between preoperative audiometry parameters with ipsilesional neck compression compared to the postoperative ones ($p = 0.053$ and $p = 0.603$, respectively; **Figure 3**). Therefore, the average PTA improvements at 250 Hz and 500 Hz following manual neck compression indicated the degree of postoperative PTA improvements.

Subjective Outcomes

The median NRS-A significantly decreased from 7 (range, 4–10) to 1 (range, 0–3) ($p = 0.001$ by Wilcoxon signed-rank test), and the median NRS-L also significantly decreased from 7 (range, 5–10) to 1 (range, 0–6) ($p = 0.001$ by Wilcoxon signed-rank test) postoperatively (**Figure 4**). Furthermore, subjective PT improvements, as evidenced by change in median THI score, significantly improved from 60 (range, 22–82) preoperatively to 10 (range, 0–52) postoperatively ($p = 0.002$, Wilcoxon signed-rank test; **Figure 4**). Detailed scores of pre- and postoperative subjective outcomes are indicated in **Table 3**. In addition to written questionnaire results, all subjects answered that their symptoms had completely disappeared or much abated immediately and 3 months after the surgical interventions.

Negative Effect of Manual Neck Compression

Five out of 22 subjects (22.7%; Subject 5, 6, 7, 10, and 11) had negative manual compression effect (i.e., lack of improvement of $\geq$ 10 dB HL at 250 or 500 Hz) preoperatively, despite the presence of ipsilateral LFHL and radiologically-evident SS abnormalities. Only one subject (Subject 20) showed neither LFHL nor positive manual neck compression effect. Nonetheless, Subject 5, 7, and 11 underwent surgical interventions for each SS abnormality, which showed markedly improved postoperative PT symptoms with THI score (from 80 to 20, severe to mild; from 30 to 0, mild to none; from 60 to 36, severe to mild, respectively) and hearing thresholds at both 250 and 500 Hz. Subject 10 and 20 were not operated on due to mild PT symptoms. Their symptoms remained stable during the follow-up period. Although the PT symptom was severe in Subject 18 with both LFHL and positive neck compression effects, she did not want to undergo surgical treatment.

DISCUSSION

Since the first study by Sismanis proposed that digital pressure could be applied over the internal jugular vein to diagnose PT (19), many physicians have performed this examination to preoperatively characterize PT. The current study investigated the preoperative diagnostic and prognostic values of the effect of ipsilateral neck manual compression on the PT loudness and

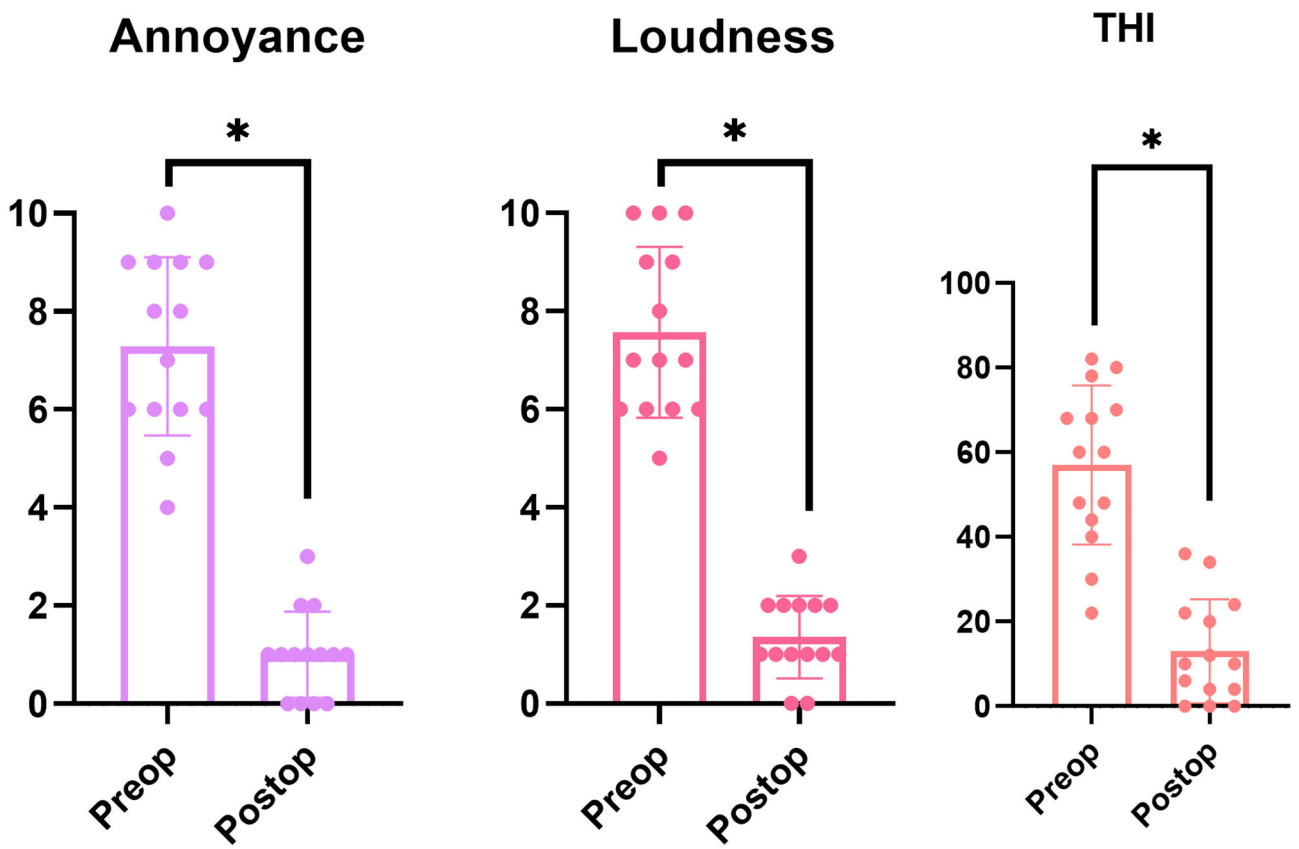

FIGURE 4 | Pre- and post-operative Numerical Rating Scale (NRS) Annoyance and Loudness scales and Tinnitus Handicap Inventory (THI) scores. NRS Annoyance and Loudness scales significantly decreased after surgery in all 12 subjects ($p = 0.001$, Wilcoxon signed-rank test). With regard to THI scores, all 12 subjects reported significant improvement in postoperative tinnitus-related symptoms, with a statistically significant decrease from 54.1 ± 18.0 preoperatively to 14.3 ± 12.1 postoperatively ($p = 0.002$, Wilcoxon signed-rank test). NRS, numerical rating scale; THI, tinnitus handicap inventory. All 3 categories also showed statistical significance between preop and postop scores, which are also indicated with the asterick.

associated audiometric changes in subjects with SS-Deh and SS-Div. The new examination method, PTA with ipsilesional manual neck compression, may aid in having an initial diagnostic impression in SS-Div/SS-Deh-associated PT and identifying appropriate candidates for surgery.

Friedmann et al. suggested that cardiac venous pulsations from the dominant vein continuously collide with the inner venous walls and expand the dehiscent vascular portions, thereby increasing the diameter of the right-sided dominant vein (20). Furthermore, based on Poiseuille's law, the volumetric flow rate is mechanistically proportional to the radius to the fourth power. Variations in the SS geometry may accelerate the disruption of local laminar flow and cause continuous outward pressure, leading to SS-Deh and formation/enlargement of SS-Div (21). Therefore, turbulent blood flow due to hemodynamic changes, as well as vibration of a dehiscent vascular wall, even in the absence of turbulent flow, can transmit sounds into the cochlea, resulting in PT. Kao et al. discovered that distinct flow patterns (i.e., vortex pattern) within the internal jugular vein, which rely on the shape and position of the jugular bulbs, are closely associated with PT (22). The intensity of the vascular bruit is reflected by the venous flow velocity, which causes turbulence as it enters the SS. When the flow in the internal jugular vein is temporarily arrested due to external pressure (e.g., manual neck compression), venous flow velocity is minimized to an almost static condition, thereby eliminating the pulsatile perception (23). In the current study, the majority of subjects (16 subjects, 72.7%) showed positive neck compression effect and this phenomenon was consequently verified as the existence of venous origin of PT. Furthermore, our group again confirmed that SS resurfacing/reshaping, including external decompression or reduction of the SS, has produced satisfying long-term treatment outcomes.

Importantly, the combination of PTA and ipsileisional manual neck compression may help to confirm the venous origin of PT and may predict favorable surgical outcomes. In our previous study, subjects with PT and radiologically-evident vascular pathology near the cochlea frequently presented with ipsilateral LFHL (11, 12, 18). Previous studies have reported that intravascular flow produces PT, which is synchronous to the heartbeat. Additionally, the frequency spectrum of the first heart sound is primarily distributed in the low frequency range of 50–200 Hz (24). Specifically, in the cases of SS-Div/SS-Deh, it has been proven that pulse-synchronous acoustic characteristics are relatively low sound pressure levels within low-frequency range

TABLE 3 | Pre- and postoperative tinnitus questionnaire results.

	Preoperative symptom scores				Postoperative symptom scores			
Pt. No.	**NRS Annoyance**	**NRS Loudness**	**THI**		**NRS Annoyance**	**NRS Loudness**	**THI**	
1		N/A				N/A		
2	6	6	22	Mild	0	0	0	No
3	4	6	48	Moderate	3	1	24	Mild
4	6	6	40	Moderate	1	2	12	No
5	9	10	80	Severe	0	0	20	Mild
6		N/A				N/A		
7	6	6	30	Mild	1	1	0	No
8	5	7	44	Moderate	1	2	6	No
9	8	8	48	Moderate	1	1	10	No
10		N/A				N/A		
11	9	5	60	Severe	2	2	36	Mild
12	9	10	60	Severe	1	2	4	No
13	7	7	68	Severe	2	3	34	Mild
14	6	7	68	Severe	0	1	22	Mild
15	10	10	82	Severe	0	2	4	No
16		N/A				N/A		
17		N/A				N/A		
18		N/A				N/A		
19	9	9	78	Severe	1	1	0	No
20		N/A				N/A		
21		N/A				N/A		
22	8	9	70	Severe	1	1	10	No

Pt., patient; No., number; NRS, numerical rating scale; THI, tinnitus handicap inventory; N/A, not available.
The median Numerical Rating Scale Annoyance and Loudness markedly decreased from 7 (range, 4–10) preoperatively to 1 (range, 0–3) postoperatively ($p = 0.001$) and from 7 (range, 5–10) preoperatively to 1 (range, 0–6) postoperatively ($p = 0.001$), respectively. Also, the median Tinnitus Handicap Inventory score significantly improved from 60 (range, 22–82) preoperatively to 10 (range, 0–52) postoperatively ($p = 0.002$).

using TSR-STA (1). Therefore, PT may mask low-frequency sounds and result in LFHL. Our results are consistent with those of previous studies, which reported that the average PTA thresholds in the neutral position were significantly higher than those on the contralateral symptom-free side. In the present study, all but two subjects (Subjects 13 and 20) with ipsilateral LFHL had SS-Div/SS-Deh and the majority of the enrolled subjects had a positive manual compression effect in the affected ear. Furthermore, subjective PT improvements correlated with marked improvements in hearing thresholds at low frequencies after SS resurfacing/reshaping, similar to the threshold levels for the normal contralateral ear. These results suggest that the effect of ipsilesional manual neck compression on LFHL would be comparable to that of SS resurfacing/reshaping. Oh et al. reported that five patients with PT due to a dehiscent high jugular bulb demonstrated resolution of symptoms by ipsilateral internal jugular vein compression (25). In addition, Sismanis and Sismanis et al. reported resolution or improvement of PT by ipsilateral internal jugular vein compression, coupled with an improvement of LFHL, in patients with benign intracranial hypertension (19, 26). Expanding upon the improvement of LFHL in these previous studies, our study is meaningful in that the improvement in audiometric profiles can be visualized with the help of our new examination method and thus PTA with manual neck compression may aid in confirming a venous origin of PT and predicting a favorable surgical outcome.

This study had several limitations that should be addressed in future studies. First, the sample size was relatively small and only subjects with SS abnormalities were evaluated. A larger number of participants with various etiologies should be included in future studies. Second, this study only used TB-CTA or MRI/MRA to evaluate vascular abnormalities, which may have reduced the strength of evidence of alleviation of subjective symptoms. As previously mentioned, TSR-STA can also be used to evaluate the surgical outcomes (18, 27). Pre- and post-manual compression TSR-STA may provide an objective evaluation of PT changes, which will help clinicians identify patients who may benefit from surgery. Third, improvements in low-frequency hearing thresholds under manual compression showed wide variation. For instance, Subject 16 showed an improvement of 30 dB HL in the PTA thresholds at 250 Hz, while Subject 13 showed only an improvement of 5 dB HL at 250 Hz, despite applying manual compression. According to our hypothesis, if ipsilesional manual compression of the internal jugular vein is successful, the PTA threshold at low frequencies should improve up to the level of the normal contralateral ear because digital compression of the internal jugular vein limits the generation of PT. This variation among subjects may result from possible differences

in the compression intensity among subjects. Therefore, future follow-up studies should minimize these errors by controlling the intensity of compression (i.e., to the level of disappearance or stark alleviation of PT). Fourth, evaluation of the frequency of PT using 250 and 500 Hz can be somewhat less comprehensive since spectro-temporal analyses may present pulse-synchronous fluctuation of tinnitus frequency above 500 Hz occasionally. Thus, evaluating additional low frequencies (e.g., 750 Hz) will be helpful to better understand the effect of manual neck compression on pulse-synchronous acoustic characteristics of PT in the future studies. Nevertheless, we believe that our findings of convenient and cost-effective use of PTA with manual neck compression are clinically meaningful, especially when the PTA shows ipsilateral LFHL in PT patients.

CONCLUSION

This was the first study to explore the preoperative significance of ipsilateral manual neck compression in patients with pulsatile tinnitus secondary to SS-Deh/Div. A positive manual compression effect in the affected ear strongly suggested postoperative improvements in ipsilateral LFHL and PT symptoms. Temporary improvement in PT and LFHL with manual compression over the ipsilateral neck may help to confirm the venous origin of the PT and predict a favorable surgical outcome following repair of SS-Deh or SS-Div.

DATA AVAILABILITY STATEMENT

The original contributions presented in the study are included in the article/supplementary material, further inquiries can be directed to the corresponding author.

ETHICS STATEMENT

The studies involving human participants were reviewed and approved by Institutional Review Board of the Clinical Research Institute (no. B-2107-699-105). The patients/participants provided their written informed consent to participate in this study. Written informed consent was obtained from the individual(s) for the publication of any potentially identifiable images or data included in this article.

AUTHOR CONTRIBUTIONS

J-JS designed the study. SL led the analysis, interpretation of the results, and drafted the first manuscript. S-YL, BC, J-WK, and SH reviewed and revised the manuscript for intellectual contents. SL, S-YL, BC, J-WK, SH, and J-JS contributed to all aspects of the investigation, including data collection, analysis, interpretation of the results, and revision of the manuscript for important intellectual contents. All authors approved the final version of the manuscript and agree to be accountable for all aspects of the work.

FUNDING

This work was supported by grants from the National Research Foundation of Korea funded by the Korean government (MSIP) (no. NRF-2022R1A2B5B02002139; recipient: J-JS).

ACKNOWLEDGMENTS

The manuscript was edited and revised by highly qualified native English-speaking editors at Textcheck (submission code: 21091514).

REFERENCES

1. Song JJ, An GS, Choi I, De Ridder D, Kim SY, Choi HS, et al. Objectification and differential diagnosis of vascular pulsatile tinnitus by transcanal sound recording and spectrotemporal analysis: a preliminary study. *Otol Neurotol.* (2016) 37:613–20. doi: 10.1097/MAO.0000000000001005
2. Song JJ, De Ridder D, Schlee W, Van De Heyning P, Vanneste S. "Distressed aging": the differences in brain activity between early- and late-onset tinnitus. *Neurobiol Aging.* (2013) 34:1853–63. doi: 10.1016/j.neurobiolaging.2013.01.014
3. Lee SY, Choi BY, Koo JW, De Ridder D, Song JJ. Cortical oscillatory signatures reveal the prerequisites for tinnitus perception: a comparison of subjects with sudden sensorineural hearing loss with and without tinnitus. *Front Neurosci.* (2020) 14:596647. doi: 10.3389/fnins.2020.596647
4. Sismanis A. Pulsatile tinnitus: contemporary assessment and management. *Curr Opin Otolaryngol Head Neck Surg.* (2011) 19:348–57. doi: 10.1097/MOO.0b013e3283493fd8
5. Baguley D, Mcferran D, Hall D. Tinnitus. *Lancet.* (2013) 382:1600–7. doi: 10.1016/S0140-6736(13)60142-7
6. Liyanage SH, Singh A, Savundra P, Kalan A. Pulsatile tinnitus. *J Laryngol Otol.* (2006) 120:93–7. doi: 10.1017/S0022215105001714
7. Ahsan SF, Seidman M, Yaremchuk K. What is the best imaging modality in evaluating patients with unilateral pulsatile tinnitus? *Laryngoscope.* (2015) 125:284–5. doi: 10.1002/lary.24822
8. Carlson ML, Sweeney AD, Pelosi S, Wanna GB, Glasscock ME 3rd, Haynes DS. Glomus tympanicum: a review of 115 cases over 4 decades. *Otolaryngol Head Neck Surg.* (2015) 152:136–142. doi: 10.1177/0194599814555849
9. Grewal AK, Kim HY, Comstock RH 3rd, Berkowitz F, Kim HJ, Jay AK. Clinical presentation and imaging findings in patients with pulsatile tinnitus and sigmoid sinus diverticulum/dehiscence. *Otol Neurotol.* (2014) 35:16–21. doi: 10.1097/MAO.0b013e31829ab6d7
10. Eisenman DJ, Raghavan P, Hertzano R, Morales R. Evaluation and treatment of pulsatile tinnitus associated with sigmoid sinus wall anomalies. *Laryngoscope.* (2018) 128(Suppl. 2):S1–13. doi: 10.1002/lary.27218
11. Lee SY, Kim MK, Bae YJ, An GS, Lee K, Choi BY, et al. Longitudinal analysis of surgical outcome in subjects with pulsatile tinnitus originating from the sigmoid sinus. *Sci Rep.* (2020) 10:18194. doi: 10.1038/s41598-020-75348-3
12. Lee SJ, Lee SY, An GS, Lee K, Choi BY, Koo JW, et al. Treatment outcomes of patients with glomus tympanicum tumors presenting with pulsatile tinnitus. *J Clin Med.* (2021) 10:2348. doi: 10.3390/jcm10112348
13. Jeon HW, Kim SY, Choi BS, Bae YJ, Koo JW, Song JJ. Pseudo-low frequency hearing loss and its improvement after treatment may be objective signs of significant vascular pathology in patients with pulsatile tinnitus. *Otol Neurotol.* (2016) 37:1344–9. doi: 10.1097/MAO.0000000000001179
14. Sismanis A, Smoker WR. Pulsatile tinnitus: recent advances in diagnosis. *Laryngoscope.* (1994) 104:681–8. doi: 10.1288/00005537-199406000-00007
15. Bhatnagar K, Lataille AT, Eisenman DJ. Patterns of audiometric threshold shifts from pulsatile tinnitus due to sigmoid sinus wall anomalies. *Am J Otolaryngol.* (2020) 41:102647. doi: 10.1016/j.amjoto.2020.102647

16. Newman CW, Jacobson GP, Spitzer JB. Development of the tinnitus handicap inventory. *Arch Otolaryngol Head Neck Surg.* (1996) 122:143–8. doi: 10.1001/archotol.1996.01890140029007
17. Song JJ, Kim YJ, Kim SY, An YS, Kim K, Lee SY, et al. Sinus wall resurfacing for patients with temporal bone venous sinus diverticulum and ipsilateral pulsatile tinnitus. *Neurosurgery.* (2015) 77:709–17. discussion 717. doi: 10.1227/NEU.0000000000000902
18. Kim SH, An GS, Choi I, Koo JW, Lee K, Song JJ. Pre-treatment objective diagnosis and post-treatment outcome evaluation in patients with vascular pulsatile tinnitus using transcanal recording and spectro-temporal analysis. *PLoS ONE.* (2016) 11:e0157722. doi: 10.1371/journal.pone.0157722
19. Sismanis A. Otologic manifestations of benign intracranial hypertension syndrome: diagnosis and management. *Laryngoscope.* (1987) 97:1–17. doi: 10.1288/00005537-198708001-00001
20. Friedmann DR, Eubig J, Mcgill M, Babb JS, Pramanik BK, Lalwani AK. Development of the jugular bulb: a radiologic study. *Otol Neurotol.* (2011) 32:1389–95. doi: 10.1097/MAO.0b013e31822e5b8d
21. Sutera SP, Skalak R. The history of Poiseuille's law. *Annu Rev Fluid Mech.* (1993) 25:1–20. doi: 10.1146/annurev.fl.25.010193.000245
22. Kao E, Kefayati S, Amans MR, Faraji F, Ballweber M, Halbach V, et al. Flow patterns in the jugular veins of pulsatile tinnitus patients. *J Biomech.* (2017) 52:61–7. doi: 10.1016/j.jbiomech.2016.12.008
23. Berguer R, Nowak P. Treatment of venous pulsatile tinnitus in younger women. *Ann Vasc Surg.* (2015) 29:650–3. doi: 10.1016/j.avsg.2014.12.039
24. Stein PD, Sabbah HN, Lakier JB, Magilligan DJ Jr, Goldstein D. Frequency of the first heart sound in the assessment of stiffening of mitral bioprosthetic valves. *Circulation.* (1981) 63:200–3. doi: 10.1161/01.CIR.63.1.200
25. Oh SJ, Kim D, Lee JI, Ko JK, Choi SW, Kong SK, et al. Transvenous stent-assisted coil embolization for management of dehiscent high jugular bulb with tinnitus and contralateral hypoplastic venous sinuses. *Otol Neurotol.* (2019) 40:1253–9. doi: 10.1097/MAO.0000000000002349
26. Sismanis A, Butts FM, Hughes GB. Objective tinnitus in benign intracranial hypertension: an update. *Laryngoscope.* (1990) 100:33–6. doi: 10.1288/00005537-199001000-00008
27. Lee SY, Song SK, Park SJ, Park HG, Choi BY, Koo JW, et al. Jugular bulb resurfacing with bone cement for patients with high dehiscent jugular bulb and ipsilateral pulsatile tinnitus. *Otol Neurotol.* (2019) 40:192–9. doi: 10.1097/MAO.0000000000002093

Conflict of Interest: The authors declare that the research was conducted in the absence of any commercial or financial relationships that could be construed as a potential conflict of interest.

Publisher's Note: All claims expressed in this article are solely those of the authors and do not necessarily represent those of their affiliated organizations, or those of the publisher, the editors and the reviewers. Any product that may be evaluated in this article, or claim that may be made by its manufacturer, is not guaranteed or endorsed by the publisher.

Copyright © 2022 Lee, Lee, Choi, Koo, Hong and Song. This is an open-access article distributed under the terms of the Creative Commons Attribution License (CC BY). The use, distribution or reproduction in other forums is permitted, provided the original author(s) and the copyright owner(s) are credited and that the original publication in this journal is cited, in accordance with accepted academic practice. No use, distribution or reproduction is permitted which does not comply with these terms.

frontiers in Neurology

ORIGINAL RESEARCH
published: 17 March 2022
doi: 10.3389/fneur.2022.852048

Development and Content Validity of the Bilateral Vestibulopathy Questionnaire

Lisa van Stiphout[1], Israt Hossein[1], Merel Kimman[2], Susan L. Whitney[3], Andrianna Ayiotis[4,5], Michael Strupp[6], Nils Guinand[7], Angélica Pérez Fornos[7], Josine Widdershoven[1,8], Ángel Ramos-Macías[9], Vincent Van Rompaey[8] and Raymond van de Berg[1]*

[1] Division of Balance Disorders, Department of Otorhinolaryngology and Head and Neck Surgery, Maastricht University Medical Center, School for Mental Health and Neuroscience, Maastricht, Netherlands, [2] Department of Clinical Epidemiology and Medical Technology Assessment (KEMTA), Maastricht University Medical Center, Maastricht, Netherlands, [3] Department of Physical Therapy, School of Health and Rehabilitation Sciences, University of Pittsburgh, Pittsburgh, PA, United States, [4] Department of Otolaryngology–Head and Neck Surgery, Johns Hopkins University School of Medicine, Baltimore, MD, United States, [5] Department of Biomedical Engineering, Johns Hopkins University School of Medicine, Baltimore, MD, United States, [6] Department of Neurology, German Center for Vertigo, Ludwig-Maximilians University, Munich, Germany, [7] Service of Otorhinolaryngology Head and Neck Surgery, Department of Clinical Neurosciences, Geneva University Hospitals, Geneva, Switzerland, [8] Department of Otorhinolaryngology and Head and Neck Surgery, Faculty of Medicine and Health Sciences, Antwerp University Hospital, University of Antwerp, Antwerp, Belgium, [9] Department of Otolaryngology, Head and Neck Surgery, Complejo Hospitalario Universitario Insular Materno Infantil de Gran Canaria, Las Palmas, Spain

OPEN ACCESS

Edited by:
Leonardo Manzari, MSA ENT Academy Center, Italy

Reviewed by:
Nicolas Perez-Fernandez, University Clinic of Navarra, Spain
Giovanni Galeoto, Sapienza University of Rome, Italy

***Correspondence:**
Lisa van Stiphout
lisa.van.stiphout@mumc.nl

Specialty section:
This article was submitted to Neuro-Otology, a section of the journal Frontiers in Neurology

Received: *10 January 2022*
Accepted: *15 February 2022*
Published: *17 March 2022*

Citation:
van Stiphout L, Hossein I, Kimman M, Whitney SL, Ayiotis A, Strupp M, Guinand N, Pérez Fornos A, Widdershoven J, Ramos-Macías Á, Van Rompaey V and van de Berg R (2022) Development and Content Validity of the Bilateral Vestibulopathy Questionnaire. Front. Neurol. 13:852048. doi: 10.3389/fneur.2022.852048

Background: To date, the burden and severity of the full spectrum of bilateral vestibulopathy (BVP) symptoms has not yet been measured in a standardized manner. Since therapeutic interventions aiming to improve BVP symptoms are emerging, the need for a new standardized assessment tool that encompasses the specific aspects of BVP arises. Therefore, the aim of this study was to develop a multi-item Patient Reported Outcome Measure (PROM) that captures the clinically important symptoms of BVP and assesses its impact on daily life.

Methods: The development of the Bilateral Vestibulopathy Questionnaire (BVQ) consisted of two phases: (I) initial item generation and (II) face and content validity testing. Items were derived from a literature review and individual semi-structured interviews focusing on the full spectrum of reported BVP symptoms (I). Subsequently (IIa), individual patient interviews were conducted using "thinking aloud" and concurrent verbal probing techniques to assess the comprehensibility of the instructions, questions and response options, and the relevance, missing domains, or missing items. Interviews continued until saturation of input was reached. Finally, international experts with experience in the field of the physical, emotional, and cognitive symptoms of BVP participated in an online focus group to assess the relevance and comprehensiveness of the BVQ (IIb).

Results: The BVQ consisted of two sections. The first section included 50 items scored on a six-point Likert scale arranged into seven constructs (i.e., imbalance, oscillopsia, other physical symptoms, cognitive symptoms, emotional symptoms, limitations and behavioral changes and social life). The second section consisted of four items, scored on a visual analog scale from 0 to 100, to inquire about limitations in daily life, perceived health and expectations regarding future recovery. Interviews with BVP patients [$n = 8$,

50% female, mean age 56 years (range 24–88 years)] and the expert meeting confirmed face and content validity of the developed BVQ.

Conclusion: The BVQ, which was developed to assess the spectrum of BVP symptoms and its impact on daily life, proved to have good face and content validity. It can be used to characterize current self-reported symptoms and disability and to evaluate symptom burden before and after therapeutic interventions in future research and clinical practice.

Keywords: bilateral vestibulopathy, Patient Reported Outcome Measure (PROM), questionnaire, vestibular impairment, symptoms bilateral vestibulopathy

INTRODUCTION

Bilateral vestibulopathy (BVP) is a chronic disorder which is defined by bilateral loss or reduction of vestibular function due to deficits of the vestibular organs, vestibular nerves, the brain, or a combination of the above (1, 2). The leading symptoms of BVP include oscillopsia during walking or quick head/body movements (movement-induced blurred vision), unsteadiness when walking or standing and worsening of unsteadiness on uneven ground or in darkness (2). Previous literature demonstrated that BVP also results in cognitive or emotional complaints (3–6). In particular, an association between BVP and symptoms such as sadness, fear, anger, difficulties with dual tasking and spatial anxiety was described (3–11). This ultimately results in behavioral changes such as avoiding activities or performing activities more slowly and with greater attention (6). Together these symptoms negatively impact daily functioning and quality of life and increase socio-economic burden (12–15).

BVP can pose a diagnostic challenge since it is a heterogeneous disorder with multiple identified etiologies and with various clinical characteristics due to different involvement within the vestibular system (16–24). Currently, BVP is diagnosed using the criteria from the Classification Committee of the Bárány Society, which include symptoms of oscillopsia and imbalance, together with a reduced vestibular function measured with caloric testing and/or video head impulse test and/or torsion swing test (2). Since the current BVP criteria were developed as a diagnostic tool, they primarily focus on physical complaints combined with measuring vestibular reflexes and not on the full spectrum of BVP symptoms (i.e., it is not designed to portray the burden of disease in patients with BVP). Additionally, earlier research has demonstrated that the extent of the perceived dizziness related handicap is often not correlated with results from vestibular reflex tests (25, 26). Therefore, evaluating the burden of disease cannot be accomplished by focusing on the diagnostic criteria alone.

Generic questionnaires such as the Short-Form Health Survey (SF-36), the Health-Utilities-Index (HUI) and EuroQol-5D-5L (EQ-5D-5L) but also more specific questionnaires such as the Dizziness Handicap Inventory (DHI) and Hospital Anxiety and Depression Scale (HADS) have been used to characterize symptoms, quality of life and emotional health in BVP populations (6, 12). However, due to the generic nature of these questionnaires, they are evidently not able to accurately capture the full spectrum and the specific aspects of BVP symptoms relevant to patients (6, 27).

To date, the burden and severity of the full spectrum of BVP symptoms are not measured in a standardized way. Since therapeutic interventions focusing on improving BVP symptoms are emerging (e.g., the vestibular implant, balance belt and noisy galvanic stimulation), the need for a standardized assessment tool that embraces the specific aspects of BVP arises (28–39). Thorough evaluation of BVP symptoms and disease burden via patient-relevant and disease-specific parameters before and after therapeutic interventions is also crucial for measuring the effectiveness of these interventions (40, 41). A targeted questionnaire has the potential to improve clinical decision making as it enables clinicians and patients to establish realistic and shared treatment goals, taking patient preferences into account (42–45).

Consequently, the development of a multi-item Patient Reported Outcome Measure (PROM), that captures the clinically important and patient-relevant symptoms of the BVP population would be of value. The aim of this study was to develop a PROM to assess the spectrum of BVP symptoms and its impact on daily life. The development and face and content validity testing of the Bilateral Vestibulopathy Questionnaire (BVQ) are described in this article.

CONCEPTUAL MODEL AND CONTEXT

Results from a qualitative study assessing symptoms of patients with BVP were used as foundation for the conceptual framework of the BVQ (6, 46). This conceptual framework is centered around the full spectrum of BVP symptoms and categorizes them in three different domains: the physical, cognitive, and emotional domain. The burden of these symptoms increases when performing certain activities such as cycling or driving a car, leading to limitations in carrying out these activities (47). Consequently, patients show altered behavior such as slowing down or paying more attention while performing activities or even avoiding specific activities (6). Since BVP symptoms and BVP patients' behavior are interrelated, the conceptual model embodies all three domains of BVP symptoms and BVP behavioral concepts [adapted from the model of altered behavior due to BVP when performing activities by Lucieer et al. (6), **Figure 1**].

The BVQ was developed for use in patients with BVP. It was developed for evaluative applications to characterize the current self-reported symptoms and disability and to depict symptom burden before and after therapeutic interventions (41). Furthermore, the questionnaire is aimed to be used as an addition

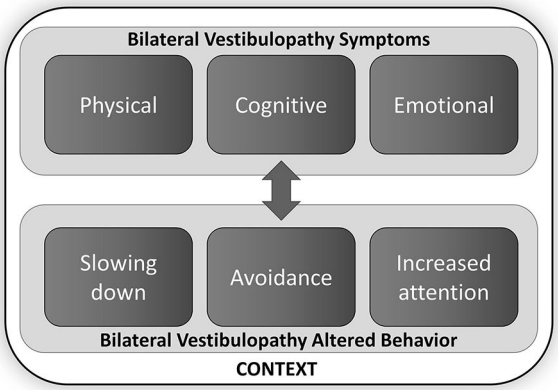

FIGURE 1 | Conceptual framework of the Bilateral Vestibulopathy Questionnaire (BVQ) [adapted from Lucieer et al. (6)]. The spectrum of BVP symptoms is categorized in three different domains (the physical, cognitive, and emotional domain), which can lead to context-specific behavioral changes. Double arrow indicates the interrelation between concepts.

to the diagnostic BVP criteria to portray symptom severity, for patient counseling, and shared clinical decision making in a research and clinical setting (2, 42–45).

METHODS

The development of the BVQ consisted of two phases: (I) initial item generation and (II) face and content validity testing. Phase II included cognitive interviews to gain insight in patients' perspectives (IIa) and an international expert meeting for obtaining input from several BVP experts (IIb). All phases of development are in agreement with the COSMIN guideline for PROM development (48).

Initial Item Generation

The initial items for the BVQ were formulated by a panel of experts consisting of two otorhinolaryngologists with an expertise in Vestibular Medicine, a vestibular researcher with a focus on BVP and an expert in health outcome research and PROM development. The themes and items were derived from a previous literature review and individual semi-structured patient interviews focusing on the full spectrum of reported symptoms of BVP (5, 6). A detailed procedure regarding the systematic review and qualitative data analysis was described by Lucieer et al. (5, 6). Discussions with the panel of experts were used to define the first longlist of relevant items for inclusion in the questionnaire, the questionnaire instructions, the recall period, the response options and lay-out. This first version was formulated in Dutch. The questionnaire was translated to English, in consultation with a native English speaker, and sent to another group of experts located in Europe and the United States (two otorhinolaryngologists with an expertise in Vestibular Medicine, one neurologist with an expertise in Vestibular Medicine, one neural prosthesis research specialist with an expertise in vestibular implantation, one physical therapist focusing on balance disorders and one vestibular researcher with a focus on BVP and vestibular implantation). Open feedback was asked on the initial items, different types of response options, the questionnaire instructions and recall period. Feedback of all experts was incorporated to remodel the first longlist version for face and content validity testing. The version for face and content validity testing was translated from English back to Dutch. The first version of the BVQ is presented in the result section of this report (phase I).

Face and Content Validity Test

Cognitive Patient Interviews

Individual patient interviews ($n = 8$) were conducted to assess the comprehensibility of the instructions, questions and response options, and the relevance, missing domains or missing items. Patients with BVP diagnosed at the Maastricht University Medical Center+ according to the diagnostic criteria of the Bárány Society were asked to participate in this study (2). Inclusion criteria for BVP included imbalance and/or oscillopsia during walking or head movements, a reduced bithermal caloric response (sum of bithermal maximal peak slow phase velocity bilaterally $<6°/s$), and/or a reduced vestibular-ocular-reflex (VOR) gain as measured by horizontal vHIT (bilateral VOR gain < 0.6) and/or torsion swing test (VOR gain < 0.1). It was required that patients were able to speak the Dutch language and to understand written Dutch. Interviews were conducted individually, either face-to-face or virtually, depending on the patient's preference, and continued until saturation of input was reached. Saturation was reached when interviews no longer provided new information in addition to previous interviews.

Interviews were conducted in Dutch following a semi-structured interview guide and consisted of two phases (**Supplementary Data Sheet 1**). At first, an open discussion took place in which patients were instructed to define what items should be included in a BVP questionnaire. During the second phase, the BVQ was provided to patients and they were asked to read the instruction, questions, and their answers aloud [i.e., a think-aloud technique was used (49)]. Patients were asked to verbalize their thoughts while answering the questions. If patients were unclear or were hesitating in formulating their thoughts or answers, the interviewer probed further into the response to gain additional information about the interpretation and understanding of the items, construct, or overall questionnaire. The interviewer used both spontaneous and pre-scripted probes during the interview. The interviews were moderated and facilitated by experienced researchers with medical backgrounds and trained in interviewing patients and qualitative data analysis (LvS and IH). Neither the interviewer nor the observer had established patient relationships prior to conducting this study. All interviews were recorded and transcribed verbatim and the transcripts were anonymized. The transcripts were subjected to manual qualitative analysis by two data coders (LvS and IH). Coding was carried out by highlighting quotations or phrases in the text and assigning each quotation or phrase a code representing predefined

categories. Consensus meetings were organized between the two researchers to identify (in)consistencies in their findings and to confirm whether the interpretations were correct. All codes were summarized in a spreadsheet database, which was used for evaluating whether to delete, alter, add, or preserve items from the questionnaire. The methods, findings, analysis and interpretations of the interviews were reported in accordance with the consolidated criteria for reporting qualitative research (COREQ; **Supplementary Data Sheet 2**) (50).

Based on the results from the first set of cognitive interviews ($n = 4$), revisions were made to the questionnaire items and instructions during two consecutive panel expert meetings (LvS, IH, MK, RvdB). To confirm face and content validity of the revised items, further cognitive interviews were conducted. Based on the results from the final set of interviews ($n = 4$), some minor revisions were made to the questionnaire during a panel expert meeting to facilitate patient understanding of the items. Results from all interviews were combined and presented as the results from phase II of this report.

Expert Meeting

International experts with extensive experience in the field of the physical, emotional, and cognitive symptoms of BVP and mechanism of altered behavior due to BVP were invited to participate in an online focus group to assess the relevance and comprehensiveness of the BVQ. The meeting was led by two trained moderators (RvdB and LvS). Five experts (one otorhinolaryngologist with an expertise in Vestibular Medicine, one neurologist with an expertise in Vestibular Medicine, one physical therapist focusing on balance disorders and two vestibular researchers with a focus on BVP and vestibular implantation) discussed items that were selected during initial item generation (phase I) and the cognitive interviews (phase IIa) via a semi-structured interview format (**Supplementary Data Sheet 3**). The English version of the BVQ was used, due to the participation of international experts. Each item was discussed with respect to its relevance in clinical practice and the overall questionnaire was commented on whether it included all the relevant constructs and items of BVP (comprehensiveness). During this meeting, the final set of questions was selected in consensus. The meeting was recorded and transcribed verbatim and the transcripts were anonymized. The transcript was subjected to manual qualitative analysis by two data coders (LvS and IH) and data analysis was performed as described for the cognitive patient interviews (phase IIa). This phase led to the final version of the BVQ, which was sent to the patient group from phase IIa to confirm comprehensibility of any changes suggested by the experts.

Ethical Considerations

This study was conducted in accordance with the legislation and ethical standards on human experimentation in the Netherlands and in accordance with the Declaration of Helsinki (amended version 2013). The medical ethical committee of Maastricht UMC+ approved this study (METC 2020-2215) and written informed consent was obtained from all patients participating in this study.

RESULTS

Initial Item Generation

Items elicited from the systematic literature review, the individual patient interviews, the panel of experts' discussions and the online survey to six international experts resulted in a longlist consisting of two sections. The first section included seven constructs with a total of 44 items scored on a six-point (Likert-type) scale: three constructs regarding physical symptoms (imbalance, oscillopsia and other physical symptoms), one construct encompassing cognitive symptoms, one construct encompassing emotional symptoms, one construct comprising limitations and behavioral changes, and one construct regarding social life. A six-point Likert scale was chosen, since literature showed that patients were less likely to choose a neutral option out of convenience and could therefore provide answers with a higher discrimination compared to a five-point Likert scale (51). The 6-point Likert-scale included the following points: "never," "rarely," "sometimes," "regularly," "frequently," and "always." Six items in the behavioral construct included a "not applicable" answer option since these items could not be answered by some patients in specific cases (e.g., not being able to drive a car yourself when not having a driver's license). The second part consisted of three scale items, scored on a visual analog scale from 0 to 100, to inquire about limitations in daily life (two items) and perceived health at the moment of completing the questionnaire. Both sections contained short instructions. It was emphasized that the items were focused on the symptoms patients have experienced due to BVP. Patients were encouraged to choose the answer that best suited their situation. The chosen recall period was one week since BVP symptoms can vary per day, depending on the patient's daily activities. Furthermore, a recall period of one week was considered to be most suitable for evaluative assessments after therapy. A shorter recall period may cause over- or underestimation of symptoms and a longer recall period could increase the risk of recall bias (52, 53).

An overview of the content and items constructed during this phase is shown in **Supplementary Data Sheet 4 Table 1**.

Face and Content Validity Test

Cognitive Patient Interviews

Eight BVP patients [(50% female, mean age 56 years (range 24–88 years)] were approached to participate in this study and completed the initial round of individual interviews. Included BVP etiologies were idiopathic ($n = 2$), DFNA9 ($n = 2$), Cogan's syndrome ($n = 1$), head trauma ($n = 1$), ototoxicity due to gentamicin treatment ($n = 1$), and meningitis ($n = 1$). All included patients fulfilled the Bárány Society Criteria and had no comorbidities. The mean bithermal caloric response was 1.3°/s and 1.5°/s for the right and left ear respectively. The mean VOR gain was 0.1 measured with torsion swing test and 0.22 bilaterally measured with horizontal vHIT.

Two rounds of individual cognitive interviews were organized with four participants included in each round. All interviews lasted between 75 and 120 min with an average duration of 93 min. The first round of interviews consisted of four online video-recorded meetings [mean age 36 years (range 24–53

years)]. The relatively young age included in the first round was due to the online nature of the first round of interviews during the COVID-19 pandemic, since younger participants were more willing and able to participate online. Elderly participants were more comfortable with face-to-face interviews.

From the first round of interviews some issues were identified regarding the formulation of items or missing items that required alteration of the BVQ. Based on feedback from the first set of interviews, revisions were made to the questionnaire items and instructions during a panel expert meeting (LvS, IH, MK, RvdB). To confirm face and content validity of the (revised) BVQ, a second round of interviews was conducted. This round consisted of four face-to-face interviews [mean age 77 years (range 68–88 years)] and resulted in some minor adjustments.

Results from the interviews indicated that all constructs were considered relevant and overall that the questions were clear and concise. Some minor textual changes were required to increase comprehensibility. For example, some patients mentioned that the items about "falling" and "tripping" were similar in phrasing. Therefore, the formulation of the item about "tripping" was changed to "trip without falling" (construct imbalance). The word "dizziness" was changed to "lightheadedness" since some patients experienced difficulty with the word "dizziness" in combination with standing up fast (construct other physical symptoms). Next to this, patients reported wanting to make a comparison with their situation before their diagnosis of BVP regarding the items "forgetfulness" and "concentration" (construct cognition). Lastly, to increase the comprehensibility and ease of reading, the words "limit" and "avoid" were underlined (construct limitations and behavioral changes) and the order of the scale questions was altered to create a more logical sequence.

The interviews pointed out that items were missing regarding imbalance when changing positions (construct imbalance), problems with multitasking (construct cognition), and emotions such as sadness, embarrassment, and loneliness (construct emotion). An item regarding the potential positive influence of BVP on social interactions was difficult or unpleasant to answer according to the patients and was therefore removed from the questionnaire.

All patients were able to answer the questions on a six-point Likert scale and appreciated the differences between steps on the scale from "never" to "always." The "not applicable" response option for some items was found relevant. However, two patients mentioned that the "not applicable" answer option was not clearly visible when completing the questionnaire. Therefore, after the first round of cognitive interviews an instruction was added above this construct to point out this extra answer option.

All instructions were clear to patients and sufficiently concise. However, some patients did not relate all their symptoms to having BVP and answered some questions with "never" although they clearly expressed experiencing these symptoms. Therefore, minor textual changes were made to the introduction after the first round of interviews to increase clarity. No changes in recall period were made since the majority of the patients pointed out that one week was an appropriate recall period for the questionnaire.

The second round of interviews indicated that no more substantial changes were needed, and face and content validity were considered good. Overall, the interviews pointed out that patients felt that the questionnaire covered all relevant aspects of BVP and that it made them feel heard. The length of the questionnaire was not experienced as bothersome. Instead, patients clearly expressed that the length of the questionnaire made them feel that they were taken seriously. Finally, after inquiring, all patients indicated that the COVID-19 pandemic did not affect the completion of the questionnaire.

An overview of the content and items altered during this phase is shown in **Supplementary Data Sheet 4 Table 2**.

Expert Meeting

The validity of the BVQ was discussed with regard to the relevance and comprehensiveness with international experts with extensive experience in the field of BVP during a 90 min online expert meeting. In general, experts advised to make minor textual changes which resulted in shorter and more concise items (e.g., "I feel tired" instead of "I feel tired due to my symptoms"). These alterations made the questionnaire more concise. Three items were added to make the questionnaire complete: one item regarding oscillopsia while walking (construct oscillopsia), one item regarding difficulties with multitasking while walking (construct cognition), and one scale question regarding expectations concerning future recovery. No changes were made to the instructions, recall period or response options and no items were removed from the questionnaire.

To verify that the comprehensibility of the questionnaire remained unchanged after incorporating the alterations from the expert meeting and to test all items in their final form, the questionnaire was discussed with five patients [40% female, mean age 65 years (range 39–88 years)] from phase IIa. All five patients confirmed comprehensibility and relevance of all items and the comprehensiveness of the overall questionnaire. The final instrument included 54 items (i.e., 50 items scored on a six-point Likert scale and four VAS items) which is shown in **Supplementary Data Sheet 4 Table 3**.

DISCUSSION

This paper describes the development and face and content validity testing of the Bilateral Vestibulopathy Questionnaire (BVQ), a PROM to assess the spectrum of BVP symptoms and their impact on functioning and daily life. Face and content validity tests with eight BVP patients and five international experts confirmed the relevance, comprehensibility, and comprehensiveness of the developed BVQ, which included 50 items arranged into seven constructs (imbalance, oscillopsia, other physical symptoms, cognitive symptoms, emotional symptoms, limitations and behavioral changes and social life) and four scale items.

Specific PROMs, such as the BVQ, can be used in clinical practice to [1] improve communication between patients and health care professionals, [2] facilitate personalized care

and shared clinical decision making and [3] improve patient satisfaction (54–59). Moreover, in research and clinical settings, regular assessment of patients' symptoms and functioning with PROMs can be useful for obtaining information about patients' experiences regarding their disorder and symptom evolution, and for monitoring and evaluating treatment effectiveness (54–56). The latter is especially important when introducing novel treatment strategies such as the vestibular implant. By administering the BVQ before and after a new intervention, it can be used complementary to vestibular reflex testing as a valuable outcome measure for evaluating treatment efficacy over time in future research and clinical practice.

To evaluate quality of life, symptom burden and emotional health in BVP populations both generic and specific questionnaires were used previously (6, 12). One of the main advantages of generic questionnaires is the large applicability. In other words, generic questionnaires can be administered in various patient populations and as a result, they can be valuable for comparison of symptoms or quality of life between different patient populations (60, 61). They are however less sensitive to small changes and may include domains which are not applicable for every patient population. This is also seen in the BVP population for generic questionnaires such as the EQ-5D-5L and the HUI3, as previous literature illustrated that these questionnaires did not fully capture BVP symptom burden (5). Firstly, this can be explained by the items included in generic questionnaires. For example, domains such as dexterity (HUI3) and pain (HUI3 and EQ-5D-5L) are less relevant symptoms in the BVP population. Next to this, the HUI3 does not distinguish between static or dynamic visual acuity (domain vision). The latter, which is an important symptom in the BVP population (oscillopsia) and has a major impact on quality of life, is not measured accurately in this way. Secondly, previous literature showed that chronically changed situations can alter patients views of what is considered normal, a phenomenon called adaptation (62). It is hypothesized that this also applies for the BVP population. Consequently, the HUI3 and EQ-5D-5L overall index scores would not give an accurate representation of BVP symptom burden and quality of life. To overcome this issue, the BVQ includes specific aspects of BVP symptoms and contexts relevant to patients.

It is stated that more specific questionnaires such as the DHI and HADS have greater sensitivity for small changes in health state or symptom burden, but at the same time have the disadvantage that they mainly focus on only one aspect of health or quality of life (63). However, the symptoms experienced by BVP patients are much broader than the items included in the DHI and HADS (6). As a result, the use of these questionnaires alone can overlook many aspects important to patients living with BVP. The BVQ includes the full extent of BVP symptoms and is therefore expected to provide a better representation of the perceived symptom burden and to be more sensitive to disease-specific changes. Subsequently, the BVQ should be more suitable for evaluation of treatment effectiveness.

A limitation of this study was the relatively small number of participants for the individual patient interviews ($n = 8$) and expert meeting ($n = 5$). However, since interviews continued until data saturation was reached, the number of BVP patients included for face and content validity testing was adequate (48, 50). Moreover, no overlap between patients included in phase I (initial item generation) and phase IIa (face and content validity testing) was ensured. Furthermore, the expert meeting was held internationally, to ensure good quality feedback from well-known experts in the field of BVP. Additionally, a minor risk of sampling bias could not be prevented since patients willing to participate in this study were highly motivated and willing to contribute to the development of a PROM for BVP. Therefore, possibly patients with stronger opinions and/or severe symptoms and disease burden were overrepresented in this study. To minimize the risk of sampling bias, a variety of patients were selected with differences in age, symptom duration, sex, educational backgrounds, and etiologies.

Future work on the BVQ includes testing of the construct validity and reliability using quantitative methods in a large study population. After assessment of all psychometric properties, the BVQ will be translated into different languages followed by cross-cultural validation to facilitate its use internationally.

CONCLUSION

The BVQ, which was developed to assess the spectrum of BVP symptoms and its impact on daily life, proved to have good face and content validity. It can be used to characterize current self-reported symptoms and disability and to depict symptom burden before and after therapeutic interventions.

DATA AVAILABILITY STATEMENT

The raw data supporting the conclusions of this article will be made available by the authors, without undue reservation.

ETHICS STATEMENT

This study was conducted in accordance with the legislation and ethical standards on human experimentation in the Netherlands and in accordance with the Declaration of Helsinki (amended version 2013). The Medical Ethical Committee of Maastricht UMC+ approved this study (METC 2020-2215) and written informed consent was obtained from all patients participating in this study.

AUTHOR CONTRIBUTIONS

LS, MK, and RB designed the study. LS wrote the manuscript. LS, RB, MK, SW, AA, Á-RM, MS, and VV contributed to developing the first longlist. LS and IH performed cognitive

patient interviews and conducted the analysis. LS and RB conducted the expert meeting. MK and RB supervised the writing and edited the manuscript. SW, MS, NG, AP, JW, Á-RM, and VV reviewed the manuscript. All authors contributed to the article and approved the submitted version.

SUPPLEMENTARY MATERIAL

The Supplementary Material for this article can be found online at: https://www.frontiersin.org/articles/10.3389/fneur.2022.852048/full#supplementary-material

REFERENCES

1. Hain TC, Cherchi M, Yacovino DA. Bilateral vestibular loss. *Semin Neurol.* (2013) 33:195–203. doi: 10.1055/s-0033-1354597
2. Strupp M, Kim JS, Murofushi T, Straumann D, Jen JC, Rosengren SM, et al. Bilateral vestibulopathy: diagnostic criteria consensus document of the classification Committee of the Bárány Society. *J Vestib Res.* (2017) 27:177–89. doi: 10.3233/VES-170619
3. Brandt T, Schautzer F, Hamilton DA, Brüning R, Markowitsch HJ, Kalla R, et al. Vestibular loss causes hippocampal atrophy and impaired spatial memory in humans. *Brain.* (2005) 128(Pt 11):2732–41. doi: 10.1093/brain/awh617
4. Kremmyda O, Hüfner K, Flanagin VL, Hamilton DA, Linn J, Strupp M, et al. Beyond dizziness: virtual navigation, spatial anxiety and hippocampal volume in bilateral vestibulopathy. *Front Hum Neurosci.* (2016) 10:139. doi: 10.3389/fnhum.2016.00139
5. Lucieer F, Duijn S, Van Rompaey V, Pérez Fornos A, Guinand N, Guyot JP, et al. Full spectrum of reported symptoms of bilateral vestibulopathy needs further investigation-a systematic review. *Front Neurol.* (2018) 9:352–352. doi: 10.3389/fneur.2018.00352
6. Lucieer FMP, Van Hecke R, van Stiphout L, Duijn S, Perez-Fornos A, Guinand N, et al. Bilateral vestibulopathy: beyond imbalance and oscillopsia. *J Neurol.* (2020) 267:241–55. doi: 10.1007/s00415-020-10243-5
7. Popp P, Wulff M, Finke K, Rühl M, Brandt T, Dieterich M. Cognitive deficits in patients with a chronic vestibular failure. *J Neurol.* (2017) 264:554–63. doi: 10.1007/s00415-016-8386-7
8. Dobbels B, Mertens G, Gilles A, Claes A, Moyaert J, van de Berg R, et al. Cognitive function in acquired bilateral vestibulopathy: a cross-sectional study on cognition, hearing, and vestibular loss. *Front Neurosci.* (2019) 13:340. doi: 10.3389/fnins.2019.00340
9. Dobbels B, Peetermans O, Boon B, Mertens G, Van de Heyning P, Van Rompaey V. Impact of bilateral vestibulopathy on spatial and nonspatial cognition: a systematic review. *Ear Hear.* (2019) 40:757–65. doi: 10.1097/AUD.0000000000000679
10. Dobbels B, Lucieer F, Mertens G, Gilles A, Moyaert J, van de Heyning P, et al. Prospective cohort study on the predictors of fall risk in 119 patients with bilateral vestibulopathy. *PLoS ONE.* (2020) 15:e0228768. doi: 10.1371/journal.pone.0228768
11. Schöberl F, Pradhan C, Grosch M, Brendel M, Jostes F, Obermaier K, et al. Bilateral vestibulopathy causes selective deficits in recombining novel routes in real space. *Sci Rep.* (2021) 11:2695. doi: 10.1038/s41598-021-82427-6
12. Guinand N, Boselie F, Guyot JP, Kingma H. Quality of life of patients with bilateral vestibulopathy. *Ann Otol Rhinol Laryngol.* (2012) 121:471–7. doi: 10.1177/000348941212100708
13. Grill E, Strupp M, Müller M, Jahn K. Health services utilization of patients with vertigo in primary care: a retrospective cohort study. *J Neurol.* (2014) 261:1492–8. doi: 10.1007/s00415-014-7367-y
14. Kovacs E, Wang X, Grill E. Economic burden of vertigo: a systematic review. *Health Econ Rev.* (2019) 9:1–14. doi: 10.1186/s13561-019-0258-2
15. Wang X, Strobl R, Holle R, Seidl H, Peters A, Grill E. Vertigo and dizziness cause considerable more health care resource use and costs: results from the KORA FF4 study. *J Neurol.* (2019) 266:2120–8. doi: 10.1007/s00415-019-09386-x
16. Ishiyama G, Ishiyama A, Kerber K, Baloh RW. Gentamicin ototoxicity: clinical features and the effect on the human vestibulo-ocular reflex. *Acta Otolaryngol.* (2006) 126:1057–61. doi: 10.1080/00016480600606673
17. Zingler VC, Weintz E, Jahn K, Botzel K, Wagner J, Huppert D, et al. Saccular function less affected than canal function in bilateral vestibulopathy. *J Neurol.* (2008) 255:1332–6. doi: 10.1007/s00415-008-0887-6
18. Zingler VC, Weintz E, Jahn K, Huppert D, Cnyrim C, Brandt T, et al. Causative factors, epidemiology, and follow-up of bilateral vestibulopathy. *Ann N Y Acad Sci.* (2009) 1164:505–8. doi: 10.1111/j.1749-6632.2009.03765.x
19. Greco A, Gallo A, Fusconi M, Magliulo G, Turchetta R, Marinelli C, et al. Cogan's syndrome: an autoimmune inner ear disease. *Autoimmun Rev.* (2013) 12:396–400. doi: 10.1016/j.autrev.2012.07.012
20. de Varebeke SP, Termote B, Van Camp G, Govaerts PJ, Schepers S, Cox T, et al. Focal sclerosis of semicircular canals with severe DFNA9 hearing impairment caused by a P51S COCH-mutation: is there a link? *Otol Neurotol.* (2014) 35:1077–86. doi: 10.1097/MAO.0000000000000283
21. Szmulewicz DJ, McLean CA, MacDougall HG, Roberts L, Storey E, Halmagyi GM. CANVAS an update: clinical presentation, investigation and management. *J Vestib Res.* (2014) 24:465–74. doi: 10.3233/VES-140536
22. van de Berg R, van Tilburg M, Kingma H. Bilateral Vestibular Hypofunction: Challenges in Establishing the Diagnosis in Adults. *ORL J Otorhinolaryngol Relat Spec.* (2015) 77:197–218. doi: 10.1159/000433549
23. Lucieer F, Vonk P, Guinand N, Stokroos R, Kingma H, van de Berg R. Bilateral vestibular hypofunction: insights in etiologies, clinical subtypes, and diagnostics. *Front Neurol.* (2016) 7:26. doi: 10.3389/fneur.2016.00026
24. Tarnutzer AA, Bockisch CJ, Buffone E, Weiler S, Bachmann LM, Weber KP. Disease-specific sparing of the anterior semicircular canals in bilateral vestibulopathy. *Clin Neurophysiol.* (2016) 127:2791–801. doi: 10.1016/j.clinph.2016.05.005
25. Gofrit SG, Mayler Y, Eliashar R, Bdolah-Abram T, Ilan O, Gross M. The association between vestibular physical examination, vertigo questionnaires, and the electronystagmography in patients with vestibular symptoms: a prospective study. *Ann Otol Rhinol Laryngol.* (2017) 126:315–21. doi: 10.1177/0003489417691298
26. Yip CW, Strupp M. The Dizziness handicap inventory does not correlate with vestibular function tests: a prospective study. *J Neurol.* (2018) 265:1210–8. doi: 10.1007/s00415-018-8834-7
27. Jacobson GP, Calder JH. Self-perceived balance disability/handicap in the presence of bilateral peripheral vestibular system impairment. *J Am Acad Audiol.* (2000) 11:76–83.
28. Della Santina CC, Migliaccio AA, Patel AH. A multichannel semicircular canal neural prosthesis using electrical stimulation to restore 3-d vestibular sensation. *IEEE Trans Biomed Eng.* (2007) 54(6 Pt 1):1016–30. doi: 10.1109/TBME.2007.894629
29. Golub JS, Ling L, Nie K, Nowack A, Shepherd SJ, Bierer SM, et al. Prosthetic implantation of the human vestibular system. *Otol Neurotol.* (2014) 35:136–47. doi: 10.1097/MAO.0000000000000003
30. Iwasaki S, Yamamoto Y, Togo F, Kinoshita M, Yoshifuji Y, Fujimoto C, et al. Noisy vestibular stimulation improves body balance in bilateral vestibulopathy. *Neurology.* (2014) 82:969–75. doi: 10.1212/WNL.0000000000000215
31. Perez Fornos A, Guinand N, van de Berg R, Stokroos R, Micera S, Kingma H, et al. Artificial balance: restoration of the vestibulo-ocular reflex in humans with a prototype vestibular neuroprosthesis. *Front Neurol.* (2014) 5:66. doi: 10.3389/fneur.2014.00066
32. Perez Fornos A, Cavuscens S, Ranieri M, van de Berg R, Stokroos R, Kingma H, et al. The vestibular implant: a probe in orbit around the human balance system. *J Vestib Res.* (2017) 27:51–61. doi: 10.3233/VES-170604
33. Ramos de Miguel A, Falcon Gonzalez JC, Ramos Macias A. Vestibular response to electrical stimulation of the otolith organs. Implications in the development of a vestibular implant for the improvement of the sensation of gravitoinertial accelerations. *J Int Adv Otol.* (2017) 13:154–61. doi: 10.5152/iao.2017.4216

34. Fujimoto C, Egami N, Kawahara T, Uemura Y, Yamamoto Y, Yamasoba T, et al. Noisy galvanic vestibular stimulation sustainably improves posture in bilateral vestibulopathy. *Front Neurol.* (2018) 9:900. doi: 10.3389/fneur.2018.00900
35. Iwasaki S, Fujimoto C, Egami N, Kinoshita M, Togo F, Yamamoto Y, et al. Noisy vestibular stimulation increases gait speed in normals and in bilateral vestibulopathy. *Brain Stimul.* (2018) 11:709–15. doi: 10.1016/j.brs.2018.03.005
36. Guyot J-P, Perez Fornos A. Milestones in the development of a vestibular implant. *Curr Opin Neurol.* (2019) 32:145–53. doi: 10.1097/WCO.0000000000000639
37. Kingma H, Felipe L, Gerards M-C, Gerits P, Guinand N, Perez-Fornos A, et al. Vibrotactile feedback improves balance and mobility in patients with severe bilateral vestibular loss. *J Neurol.* (2019) 266:19–26. doi: 10.1007/s00415-018-9133-z
38. Starkov, D., Guinand, N., Lucieer, F., Ranieri, M., Cavuscens, S., Pleshkov, M., et al. (2019). Restoring the high-frequency dynamic visual acuity with a vestibular implant prototype in humans. *Audiol Neurotol* 25:91–5. doi: 10.1159/000503677
39. Chow MR, Ayiotis AI, Schoo DP, Gimmon Y, Lane KE, Morris BJ, et al. Posture, gait, quality of life, and hearing with a vestibular implant. *N Engl J Med.* (2021) 384:521–32. doi: 10.1056/NEJMoa2020457
40. Stegenga J. Measuring effectiveness. *Stud Hist Philos Sci C.* (2015) 54:62–71. doi: 10.1016/j.shpsc.2015.06.003
41. Field J, Holmes MM, Newell D. PROMs data: can it be used to make decisions for individual patients? A narrative review. *Patient Relat Outcome Meas.* (2019) 10:233–41. doi: 10.2147/PROM.S156291
42. Wright JG. Evaluating the outcome of treatment. Shouldn't We be asking patients if they are better? *J Clin Epidemiol.* (2000) 53:549–53. doi: 10.1016/S0895-4356(99)00225-5
43. Greenhalgh J, Long AF, Flynn R. The use of patient reported outcome measures in routine clinical practice: lack of impact or lack of theory? *Soc Sci Med.* (2005) 60:833–43. doi: 10.1016/j.socscimed.2004.06.022
44. Marshall S, Haywood K, Fitzpatrick R. Impact of patient-reported outcome measures on routine practice: a structured review. *J Eval Clin Pract.* (2006) 12:559–68. doi: 10.1111/j.1365-2753.2006.00650.x
45. Bitton A, Onega T, Tosteson AN, Haas JS. Toward a better understanding of patient-reported outcomes in clinical practice. *Am J Manag Care.* (2014) 20:281–3. doi: 10.3390/healthcare10020253
46. van Stiphout L, Lucieer F, Guinand N, Pérez Fornos A, van de Berg M, Van Rompaey V, et al. Bilateral vestibulopathy patients' perspectives on vestibular implant treatment: a qualitative study. *J Neurol.* (2021). doi: 10.1007/s00415-021-10920-z. [Epub ahead of print].
47. Uwents MH, Jorissen C, Van Ombergen A, Dobbels B, van de Berg R, Janssens de Varebeke S, et al. Driving ability in patients with dizziness: a systematic review. *Eur Arch Otorhinolaryngol.* (2021). doi: 10.1007/s00405-021-06881-8. [Epub ahead of print].
48. Terwee CB, Prinsen C, Chiarotto A, De Vet H, Bouter LM, Alonso J, et al. *COSMIN Methodology for Assessing the Content Validity of PROMs–User Manual*. Amsterdam: VU University Medical Center (2018).
49. Güss CD. What is going through your mind? Thinking aloud as a method in cross-cultural psychology. *Front Psychol.* (2018) 9:1292. doi: 10.3389/fpsyg.2018.01292
50. Tong A, Sainsbury P, Craig J. Consolidated criteria for reporting qualitative research (COREQ): a 32-item checklist for interviews and focus groups. *Int J Qual Health Care.* (2007) 19:349–57. doi: 10.1093/intqhc/mzm042
51. Chomeya R. Quality of psychology test between likert scale 5 and 6 points. *J Soc Sci.* (2010) 6:399–403. doi: 10.3844/jssp.2010.399.403
52. Stull DE, Leidy NK, Parasuraman B, Chassany O. Optimal recall periods for patient-reported outcomes: challenges and potential solutions. *Curr Med Res Opin.* (2009) 25:929–42. doi: 10.1185/03007990902774765
53. Norquist JM, Girman C, Fehnel S, DeMuro-Mercon C, Santanello N. Choice of recall period for patient-reported outcome (PRO) measures: criteria for consideration. *Qual Life Res.* (2012) 21:1013–20. doi: 10.1007/s11136-011-0003-8
54. Higginson IJ, Carr AJ. Measuring quality of life: Using quality of life measures in the clinical setting. *BMJ.* (2001) 322:1297–300. doi: 10.1136/bmj.322.7297.1297
55. Chen J, Ou L, Hollis SJ. A systematic review of the impact of routine collection of patient reported outcome measures on patients, providers and health organisations in an oncologic setting. *BMC Health Serv Res.* (2013) 13:211. doi: 10.1186/1472-6963-13-211
56. Greenhalgh J, Abhyankar P, McCluskey S, Takeuchi E, Velikova G. How do doctors refer to patient-reported outcome measures (PROMS) in oncology consultations? *Qual Life Res.* (2013) 22:939–50. doi: 10.1007/s11136-012-0218-3
57. Kotronoulas G, Kearney N, Maguire R, Harrow A, Di Domenico D, Croy S, et al. What is the value of the routine use of patient-reported outcome measures toward improvement of patient outcomes, processes of care, and health service outcomes in cancer care? A systematic review of controlled trials. *J Clin Oncol.* (2014) 32:1480–501. doi: 10.1200/JCO.2013.53.5948
58. Santana M-J, Feeny D. Framework to assess the effects of using patient-reported outcome measures in chronic care management. *Qual Life Res.* (2014) 23:1505–13. doi: 10.1007/s11136-013-0596-1
59. Greenhalgh J, Gooding K, Gibbons E, Dalkin S, Wright J, Valderas J, et al. How do patient reported outcome measures (PROMs) support clinician-patient communication and patient care? A realist synthesis. *J Patient Rep Outcomes.* (2018) 2:42. doi: 10.1186/s41687-018-0061-6
60. Nelson EC, Eftimovska E, Lind C, Hager A, Wasson JH, Lindblad S. Patient reported outcome measures in practice. *BMJ.* (2015) 350:g7818. doi: 10.1136/bmj.g7818
61. Murphy M, Hollinghurst S, Salisbury C. Identification, description and appraisal of generic PROMs for primary care: a systematic review. *BMC Fam Pract.* (2018) 19:41. doi: 10.1186/s12875-018-0722-9
62. Leibold ML, Holm MB, Raina KD, Reynolds CF 3rd, Rogers JC. Activities and adaptation in late-life depression: a qualitative study. *Am J Occup Ther.* (2014) 68:570–7. doi: 10.5014/ajot.2014.011130
63. Patrick DL, Deyo RA. Generic and disease-specific measures in assessing health status and quality of life. *Med Care.* (1989) 27:S217–232. doi: 10.1097/00005650-198903001-00018

Conflict of Interest: LS was supported through funding of MED-EL (Innsbruck, Austria). RB, AP, and NG received funding for travel from MED-EL. MS is Joint Chief Editor of the Journal of Neurology, Editor in Chief of Frontiers of Neuro-otology and Section Editor of F1000 and has received speaker's honoraria from Abbott, Auris Medical, Biogen, Eisai, Grünenthal, GSK, Henning Pharma, Interacoustics, J&J, MSD, NeuroUpdate, Otometrics, Pierre-Fabre, TEVA, UCB, and Viatris. MS also receives support for clinical studies from Decibel, U.S.A., Cure within Reach, U.S.A. and Heel, Germany and acts as a consultant for Abbott, AurisMedical, Heel, IntraBio and Sensorion. SW is a paid consultant for Intelligent Automation (a BlueHalo Company). The funders had no role in study design, data collection, data analysis, interpretation of data, decision to publish, or preparation of the manuscript.

The remaining authors declare that the research was conducted in the absence of any commercial or financial relationships that could be construed as a potential conflict of interest.

Publisher's Note: All claims expressed in this article are solely those of the authors and do not necessarily represent those of their affiliated organizations, or those of the publisher, the editors and the reviewers. Any product that may be evaluated in this article, or claim that may be made by its manufacturer, is not guaranteed or endorsed by the publisher.

Copyright © 2022 van Stiphout, Hossein, Kimman, Whitney, Ayiotis, Strupp, Guinand, Pérez Fornos, Widdershoven, Ramos-Macías, Van Rompaey and van de Berg. This is an open-access article distributed under the terms of the Creative Commons Attribution License (CC BY). The use, distribution or reproduction in other forums is permitted, provided the original author(s) and the copyright owner(s) are credited and that the original publication in this journal is cited, in accordance with accepted academic practice. No use, distribution or reproduction is permitted which does not comply with these terms.

frontiers in Neurology

ORIGINAL RESEARCH
published: 18 March 2022
doi: 10.3389/fneur.2022.857736

The Effect of Galvanic Vestibular Stimulation on Visuospatial Cognition in an Incomplete Bilateral Vestibular Deafferentation Mouse Model

Thanh Tin Nguyen[1,2,3], *Gi-Sung Nam*[2,4], *Gyu Cheol Han*[5], *Chuyen Le*[3,6]* and *Sun-Young Oh*[1,2,7]*

[1] Jeonbuk National University College of Medicine, Jeonju, South Korea, [2] Department of Neurology, Jeonbuk National University Hospital and School of Medicine, Jeonju, South Korea, [3] Department of Pharmacology, Hue University of Medicine and Pharmacy, Hue University, Hue, Vietnam, [4] Department of Otorhinolaryngology-Head and Neck Surgery, Chosun University College of Medicine, Gwangju, South Korea, [5] Department of Otolaryngology-Head and Neck Surgery, Gachon University of Medicine and Science, Graduate School of Medicine, Incheon, South Korea, [6] Department of General-Endocrinology and Internal Medicine, Hue University Hospital, Hue, Vietnam, [7] Research Institute of Clinical Medicine of Jeonbuk National University-Biomedical Research Institute of Jeonbuk National University Hospital, Jeonju, South Korea

OPEN ACCESS

Edited by:
Andreas Zwergal, Ludwig Maximilian University of Munich, Germany

Reviewed by:
Paul Smith, University of Otago, New Zealand
Max Wuehr, Ludwig Maximilian University of Munich, Germany

***Correspondence:**
Chuyen Le
lechuyen@huemed-univ.edu.vn; lchuyen@hueuni.edu.vn
Sun-Young Oh
ohsun@jbnu.ac.kr

Specialty section:
This article was submitted to Neuro-Otology, a section of the journal Frontiers in Neurology

Received: *19 January 2022*
Accepted: *15 February 2022*
Published: *18 March 2022*

Citation:
Nguyen TT, Nam G-S, Han GC, Le C and Oh S-Y (2022) The Effect of Galvanic Vestibular Stimulation on Visuospatial Cognition in an Incomplete Bilateral Vestibular Deafferentation Mouse Model. Front. Neurol. 13:857736. doi: 10.3389/fneur.2022.857736

Objectives: To evaluate the efficacy of galvanic vestibular stimulation (GVS) for recovering from the locomotor and spatial memory deficits of a murine bilateral vestibular deafferentation (BVD) model.

Methods: Male C57BL/6 mice ($n = 36$) were assigned to three groups: bilateral labyrinthectomy with (BVD_GVS group) and without (BVD_non-GVS group) the GVS intervention, and a control group with the sham operation. We used the open field and Y maze, and Morris water maze (MWM) tests to assess locomotor and visuospatial cognitive performance before (baseline) and 3, 7, and 14 days after surgical bilateral labyrinthectomy. For the GVS group, a sinusoidal current at the frequency at 1 Hz and amplitude 0.1 mA was delivered for 30 min daily from the postoperative day (POD) 0 to 4 *via* electrodes inserted subcutaneously close to both the bony labyrinths.

Results: Short-term spatial memory was significantly impaired in bilaterally labyrinthectomized mice (BVD_non-GVS group), as reflected by decreased spontaneous alternation performance in the place recognition test and time spent in the novel arm and increased same arm return in the Y-maze test, compared with the control. Long-term spatial memory was also impaired, as indicated by a longer escape latency in the hidden platform trial and a lower percentage of time spent in the target quadrant in the probe trial of the MWM. GVS application significantly accelerated the recovery of locomotion and short-term and long-term spatial memory deficits in the BVD mice.

Conclusions: Our data demonstrate that locomotion, short-term, and long-term (at least 2 weeks) spatial memory were impaired in BVD mice. The early administration of sinusoidal GVS accelerated the recovery of those locomotion and spatial memory deficiencies. GVS could be applied to patients with BVD to improve their locomotion and vestibular cognitive functioning.

Keywords: vestibular, labyrinthectomy, galvanic vestibular stimulation, functional recovery, spatial navigation, higher vestibular cognition

INTRODUCTION

Given that anatomical end organs are extremely sensitive to physical acceleration, the vestibular system is needed to coordinate motion and balance (1, 2). To adequately accomplish that complex task, the vestibular system possesses an incredibly delicate sensory synergy and is linked to motor organs through reflexes such as the vestibulo-ocular reflex (VOR), vestibulospinal reflex (VSR), and vestibulocollic reflex (3). In addition, the vestibular system plays a highly significant role in cognitive functions, particularly visuospatial memory (2, 4, 5). Recently, imaging and histologic evidence have proposed pathways, including thalamocortical, theta-generating, cerebellocortical, head direction pathways (2, 6, 7), from the peripheral vestibular organs to the hippocampus, which is involved in the multiple learning and memory processes (8–10). Once it arrives in the brain, the vestibular information derived from peripheral organs swiftly becomes convergent, multisensory-integrated (1, 2, 11, 12). Accordingly, the loss of vestibular inputs causes not only vertigo, dizziness, visual instability, and disturbed balance (because of impairment of the vestibulo-thalamo-cortical pathways, VOR, and VSR), but also deficits in spatial navigation and memory tasks, body representation, and bodily self-consciousness (through dysfunctions in the vestibular cortex and hippocampus) (13). Although unilateral vestibular deafferentation (UVD) might cause some degree of visuospatial memory deficits (14–16), bilateral vestibular deafferentation (BVD) can create prominent spatial cognitive deficiencies (17–19) that can last for up to 10 years (20). Furthermore, bilateral hippocampal atrophy was documented following BVD in the clinical investigations (20, 21).

Vestibular deafferentation induces several functional and structural changes in the brain (21), including vestibular compensation, which encompasses restoration, habituation, and adaptation (21). Vestibular compensation takes place in various brain regions, including the vestibular nuclei, spinal cord, cerebellum, and cortices with different biochemical substrates (22), in an attempt to partially ameliorate the vestibular dysfunctions. Clinical prognosis in BVD is usually poor compared with the unilateral vestibular loss (21) because in BVD, peripheral recovery is incomplete, and the central mechanisms are confined to sensory substitution, including lowering the thresholds of other sensory (auditory, visual, proprioceptive, and tactile) processing and boosting reciprocal intersensory interactions. Therefore, a substantial proportion of patients with bilateral vestibulopathy do not recover significantly and live with prolonged spatial memory problems (23). Complete BVD animal models that use vestibular neurectomy, chemical labyrinthectomy, or complete removal of both the otolith organ and the semicircular canals (SCCs) (17–19, 24, 25) have produced permanent impairments in the spatial cognition (17, 18, 25). In this study, we used an incomplete BVD model by causing confined bilateral damage to only the posterior SCCs. Given that a restricted injury level is accompanied by a better possibility of recovery, our incomplete BVD model appears to be a promising candidate for evaluating new rehabilitation strategies for bilateral vestibular-related deficits.

Over the past 100 years, galvanic vestibular stimulation (GVS) has been extensively applied in the pathological situations to examine the role of vestibular signals in visual stability, postural balance, locomotor control, and spatial cognition (26–28). By modulating the firing rate of vestibular afferents of both vestibular nerves and hair cells, GVS has been demonstrated to ameliorate several vestibular-related functional deficits, not only visual stability, motor coordination, and posture but also cognitive and memory impairments, particularly in UVD (14, 15, 29, 30). Accordingly, 5 sessions of direct current, bilateral, bipolar GVS improved UVD-induced short- and long-term spatial memory deficits when the cathode (excitatory) was placed on the lesion side (14, 15). We designed this study to evaluate the efficacy of GVS for recovery from the spatial memory and navigation deficits caused by the vestibular deafferentation in a murine BVD model.

METHODS

Animals

A total of thirty-six 9-week-old male C57BL/6 mice (Animal Technology, Koatech, Kyonggi-Do, Korea), weighing 20–25 g, were randomly allocated into 3 groups: bilateral labyrinthectomy (BL) with GVS intervention (BVD_GVS group, $n = 12$), BL without GVS intervention (BVD_non-GVS group, $n = 12$), and the control group ($n = 12$). The mice were housed separately and kept in the laboratory conditions with *ad libitum* feeding. All the efforts were made to reduce the number of mice used and to minimize potential suffering.

Surgical labyrinthectomy was chosen because of its relative simplicity, reliability, instantly symptom-induced, and faster-recovered ability in comparison to vestibular neurectomy or chemical labyrinthectomy. The surgical BL procedure was done in the BVD_GVS and BVD_non-GVS groups, which were described in our published studies (14, 15, 30). Through a small hole made in the posterior SCC with a diamond otologic drill, the perilymph fluid was aspirated for 3 min, and then the hole was filled with collagen to prevent further leakage (14, 15, 30). Using this surgical approach, we created a minor lesion (incomplete) in the vestibular apparatus while retaining the intact auditory organ. Meanwhile, sham surgery without labyrinthectomy was applied for mice in the control group. All the surgical and GVS application-prepared procedures were conducted under inhaled anesthesia by isoflurane gas (Ifran, O_2 5 L/min, 2.0, Hana Pharm Co. Ltd., Kyonggi-Do, Korea).

The animal procedures used in this study were consistent with the Assessment and Accreditation of Laboratory Animal Care International and were reviewed and approved by the Animal Care Committee of the Gachon University of Medicine and Science (IRB MRI2019-0008).

Study Design

To acquire baseline levels for motor and swimming capacity, we evaluated swimming ability and the open field (OF) and Y maze tests before conducting BL. Only mice that showed freely move and swimming were assigned to the three experimental groups. Following the surgery, the OF and Y maze behavioral

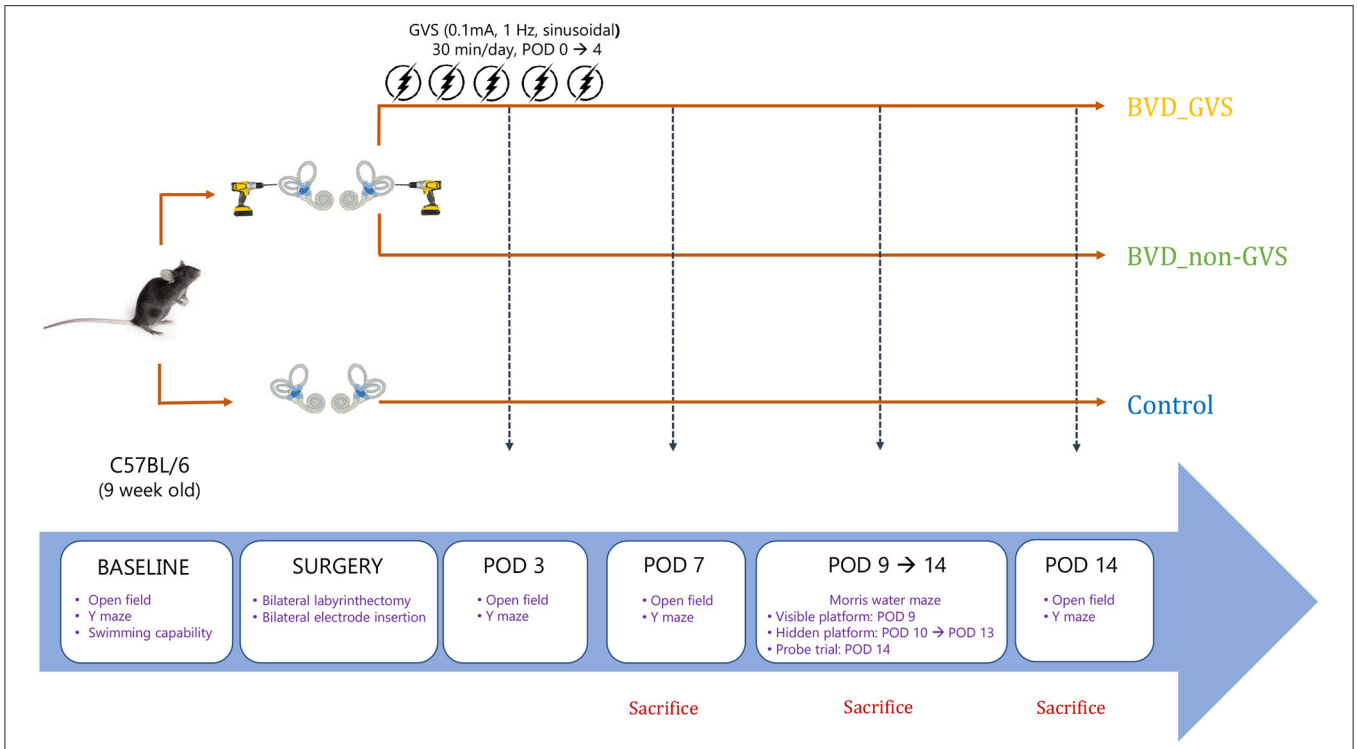

FIGURE 1 | A schematic representation of the experimental design and schedules for GVS application. BVD, bilateral vestibular deafferentation; GVS, galvanic vestibular stimulation; POD, postoperative day.

tests were checked on postoperative days (PODs) 3, 7, and 14 to determine locomotor activities and spatial cognition. Meanwhile, the Morris water maze (MWM) training sessions were conducted for 5 consecutive days from POD 9 to 13, and the probe trial was performed on POD 14 to measure the long-term spatial memory (**Figure 1**). All the behavioral assessments were performed at the time between 11:00–15:00 to reduce the time-of-day impacts on the locomotor and exploratory activities.

The GVS application was implemented with the same paradigm of the electrode implantation and technical system described in our earlier works (14, 15, 30). As we have highlighted the beneficial effects of subthreshold GVS in our earlier studies with UVD model, we applied a subthreshold current in this study (14, 15, 30). Based on the analog-model pilot experiment, the GVS threshold was determined using oculomotor threshold or GVS-induced nystagmus monitoring which is a feasible and widespread applied approach in animals. As a result, a subthreshold, bipolar, sinusoidal GVS current of 0.1 mA and 1 Hz was generated by a computer-controlled stimulator (A-M Systems Model 2100 Isolated Stimulator, A-M Systems Inc., United States, and CED micro1401-4 Cambridge Electronic Design Ltd, United Kingdom) and delivered during a 30-min period daily, consecutively for 5 days. The restraint procedure during GVS application with no current was likewise applied for mice in the control and BVD_non-GVS groups.

Behavioral Observations

Assessments of the air-righting reflex and contact righting were used to behaviorally evaluate vestibular function following BL. In the air-righting reflex test, we held the mice in a supine position and dropped (roughly 40 cm) onto a soft surface. Meanwhile, in the contact-righting test, we laid the mice supine on a horizontal surface and another horizontal surface was placed in contact with their feet. Vestibular-intact mice will immediately right themselves in both the tests (18, 24).

Open Field Test

The OF apparatus and the protocols for assessing the locomotor activities of the mice have been documented in our previous papers (14, 15, 30). In which, we employed a circular arena (37 cm diameter × 53 cm height) and an overhead tracking camera (HD 1080p C920, Logitech, Switzerland) mounted at the center. With the 2-min task for mice, we sought to collect 2 major metrics comprising the total path length across the whole ground (mm) (**Figure 2A**), and the percentage of time spent in the outer (peripheral) zone as an indicator of anxiety (31) (**Figure 2B**).

Y Maze

The Y maze apparatus and the protocols for measuring the short-term memory have been described in our previous papers (14, 15). In which, a plastic Y-shaped maze with three arms (51 × 18 × 32 cm; labeled A, B, C) orientated at 120 angles from each other and an overhead tracking camera (HD 1080p C920, Logitech, Switzerland) mounted at the center were employed.

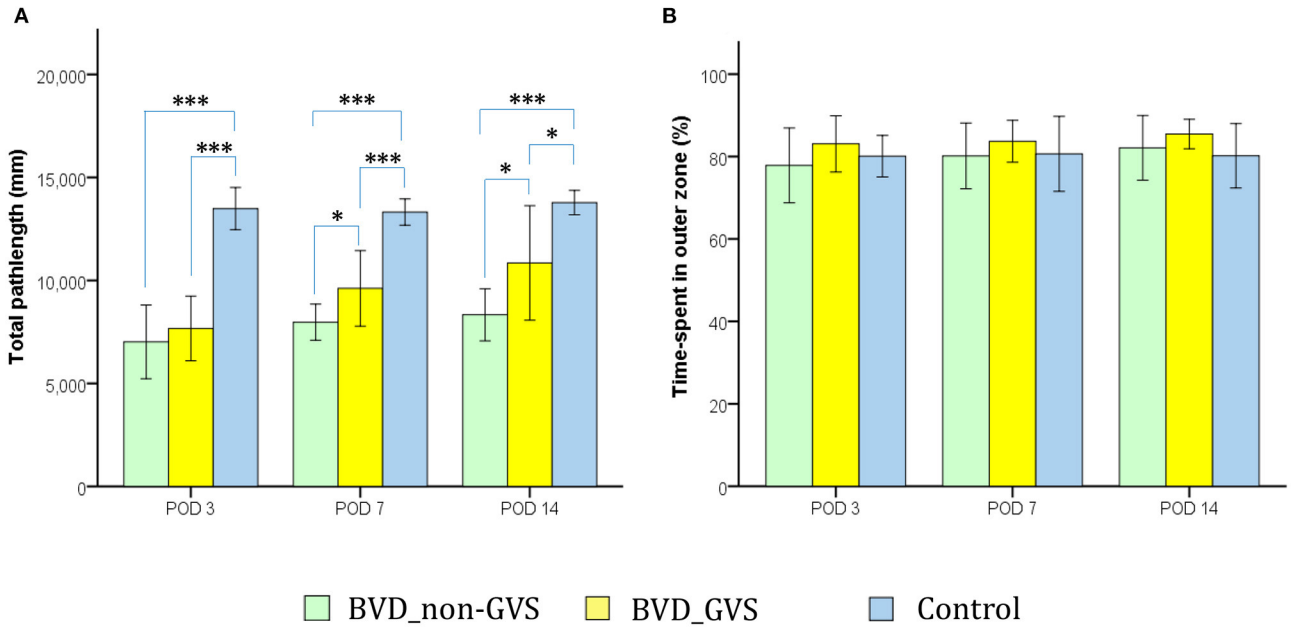

FIGURE 2 | Evaluation of the locomotor activity of mice in an open-field (OF) task. Locomotion impairment was indicated by a significant decrease in the total path length. The values of the BVD_non-GVS group were lower than those of the control group on PODs 3 ($p < 0.001$, Bonferroni test), 7 ($p < 0.001$, Bonferroni test), and 14 ($p < 0.001$, Bonferroni test). GVS improved the total path length during OF activity on PODs 7 ($p = 0.031$, LSD test) and 14 ($p = 0.027$, LSD test) **(A)**. The percentage of time spent in the outer zone, which is an indicator of anxiety, did not differ among the three groups **(B)**. Values are indicated as the mean ± SD. Statistical significances were calculated using one-way ANOVA with post-hoc tests. *Significant differences between two groups: * $p < 0.05$; *** $p < 0.001$.

With the 6-min task for mice, we sought to gather three principal parameters that reflect short-term memories comprising; (i) the spontaneous alternation performance (SAP: defined as entries into all the three arms consecutively, e.g. ABC, BCA...) represents the spatial working memory (32, 33) (**Figure 3A**), (ii) the same arm return (SAR: defined as visiting the same arm repeatedly, e.g., AA, BB, CC) represents the spatial working memory error (33, 34) (**Figure 3B**), and (iii) the place recognition test [PRT: defined as the percentage of time spent in the B arm (after unblocking)—designated as the novel arm] represents the spatial working and reference memory (14, 15, 33) (**Figure 3C**). We measured these SAP, SAR, and PRT scores at baseline and PODs 3, 7, and 14 (**Figure 1**).

Morris Water Maze Task

The MWM was used to evaluate spatial memory and navigation, and the apparatus and experimental protocols as described in our earlier works (14, 15). The paradigm was comprised of a plastic circular water tank (175 diameter and 62 cm high) with opaque made water, an acrylic circular escape platform (15 cm in diameter), four distal visual cues corresponding to four directions (east, south, west, and north), and a camera (HD 1080p C920; Logitech International SA, Lausanne, Switzerland) mounted in the center above the tank. Given the 24-h intervals between the last training session and the probe trial session, MWM was appropriate for assessing the long-term memory and learning process (20, 35–37). We sought to collect two major parameters, (i) the amount of time that elapsed before the animal climbed onto the platform to escape the water (escape latency) during the hidden platform training session (**Figure 4A**) (ii) the percentage of time spent in the target quadrant (SE quadrant) during the probe trial (**Figure 4B**). We also examined an auxiliary metric, the mean swim velocity using a visible platform test done 30 min following the probe trial to assess sensorimotor ability and motivation (38).

Statistical Analysis

We analyzed the data with SPSS Statistics version 23.0 (IBM Corp., Armonk, NY, USA). The normality of the distribution was assessed using the Shapiro-Wilk test for each parameter. The repeated measures ANOVA or the Friedman Tests were used to analyze the interaction between surgical conditions—time as a first-level analysis. The parametric variables are shown as the mean ± SD, and statistical significances were calculated using *post-hoc* one-way ANOVA accompanied by a test of the homogeneity of variances (Levene test): (i) if $p > 0.05$, ANOVA (between-group comparison) and the LSD test or Bonferroni test (multiple comparisons) were used; (ii) if $p < 0.05$, the Robust test (between group comparison) and Tamhane test (multiple comparisons) were used. Non-parametric variables are given as the median [interquartile range], and significant differences were determined using the Kruskal-Wallis test (between-group comparison) accompanied by the Mann-Whitney *U* test or the Wilcoxon signed-rank test (pairwise comparisons). All the tests were performed at a 0.05 level of significance.

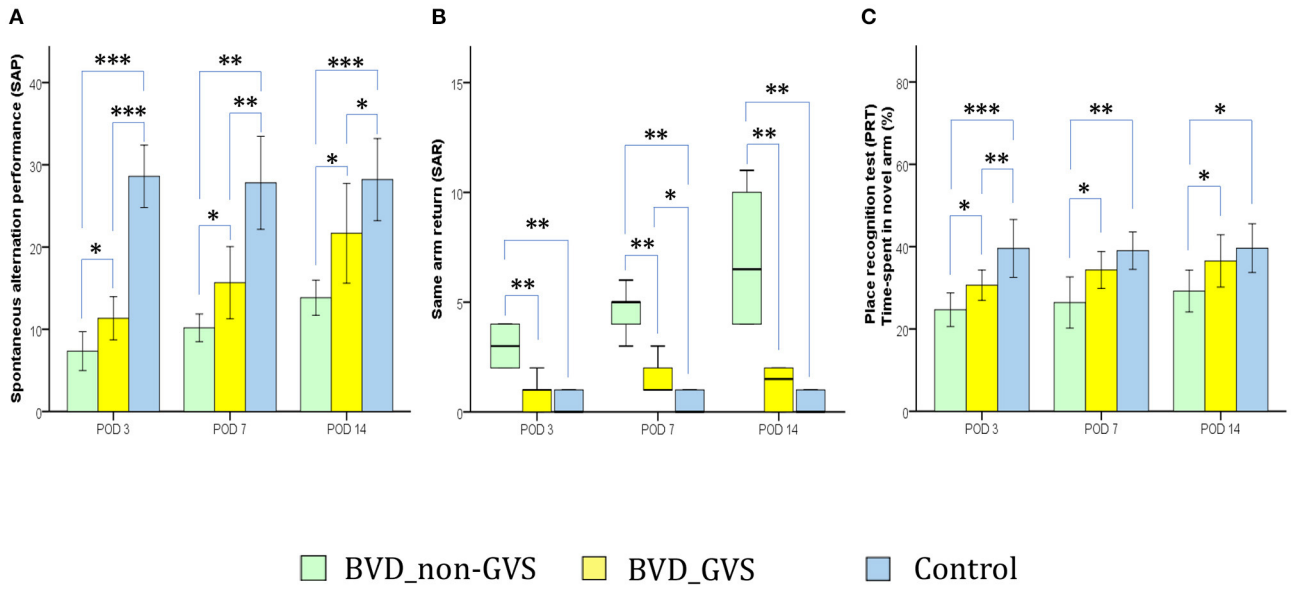

FIGURE 3 | Evaluation of locomotor activity and spatial navigation in the Y maze test. The spontaneous alternation performance (SAP), an indicator of spatial working memory and locomotor activity, was decreased in the BVD_non-GVS group compared with the control group on PODs 3 ($p < 0.001$, Bonferroni test), 7 ($p < 0.001$, Tamhane test), and 14 ($p < 0.001$, Bonferroni test). The values of the BVD_GVS group were better than those of the BVD_non-GVS group on PODs 3 ($p = 0.018$, LSD test), 7 ($p = 0.049$, Tamhane test), and 14 ($p = 0.02$, Bonferroni test) **(A)**. The same arm return (SAR), which indicates the degree of attentional difficulty during active working-memory performance, was significantly higher in the BVD_non-GVS group than in the control group on PODs 3 ($p = 0.005$, Mann-Whitney U test), 7 ($p = 0.005$, Mann-Whitney U test), and 14 ($p = 0.005$, Mann-Whitney U test). The BVD_GVS group showed better values than the BVD_non-GVS group on PODs 3 ($p = 0.006$, Mann-Whitney U test), 7 ($p = 0.004$, Mann-Whitney U test), and 14 ($p = 0.003$, Mann-Whitney U test) **(B)**. In the PRT, an indicator of spatial reference memory, the BVD_non-GVS group scored significantly worse than the control mice on PODs 3 ($p < 0.001$, Bonferroni test), 7 ($p = 0.002$, Bonferroni test), and 14 ($p = 0.017$, Bonferroni test). The PRT performance improved significantly in the BVD_GVS group, compared with the BVD_non-GVS group, on PODs 3 ($p = 0.033$, LSD test), 7 ($p = 0.038$, Bonferroni test), and 14 ($p = 0.031$, LSD test) **(C)**. The SAP and PRT values are given as the mean ± SD, and the p values were calculated using one-way ANOVA with *post-hoc* tests. The SAR values are given as the median (95% confidence interval), and those p values were calculated using the Kruskal-Wallis test and Mann-Whitney U-test. *Significant differences between two groups: * $p < 0.05$; ** $p < 0.01$; *** $p < 0.001$.

RESULTS

The results of the air-righting and contact-righting tests confirmed the vestibular dysfunction in all the BL mice; the control mice-righted themselves instantly. In the air-righting reflex test examining the ability to right themselves in the air, the control mice all landed on their feet, whereas the BL mice tended to land on their backs or sides. In the contact-righting test examining their behavior when placed supine on a horizontal surface, the control mice-righted themselves, whereas the BL mice lay supine and did not right themselves. The BL mice were observed moving in circles, swayed their head, and curled up when pulled up by the tail. These vestibular symptoms have severely occurred the first 2 days postsurgery; after that, BL mice could stand unaided on a tilt platform and walk. Considering this natural recovery course, we conducted all the subsequent behavioral investigations beginning on POD 3, when all mice were free from the limitations of motor coordination problems (**Figure 1**).

Galvanic Vestibular Stimulation Effect on Locomotion in BL Mice

Bilateral labyrinthectomy caused a locomotion impairment that was indicated by a significant decrease in the total path length in the OF test. The values of the BVD_non-GVS group were lower than those of the control group on PODs 3 ($p < 0.001$, Bonferroni test), 7 ($p < 0.001$, Bonferroni test), and 14 ($p < 0.001$, Bonferroni test). GVS improved the total path length during OF activity on PODs 7 ($p = 0.031$, LSD test) and 14 ($p = 0.027$, LSD test) (**Figure 2A**).

We also used the OF task to quantify the effects of anxiety on this experimental findings by using an indicator, the percentage of time spent in the outer zone (31, 39, 40). Because of there being no significant differences among the groups in this metric, we could likely exclude the effects of anxiety on locomotor and spatial cognition results in this study (**Figure 2B**).

Spatial Cognition in BL Mice and GVS Effects

The alterations of spontaneous alternation performance (SAP) and same arm return (SAR) scores of the Y maze test have partially demonstrated the deficits of the short-term visuospatial cognitive alternation performance following BL. For instance, playing as an indicator of both the locomotor activity and spatial working memory, SAP was lower in the BVD_non-GVS group than in the control group on PODs 3 ($p < 0.001$, Bonferroni test), 7 ($p < 0.001$, Tamhane test), and 14 ($p < 0.001$, Bonferroni

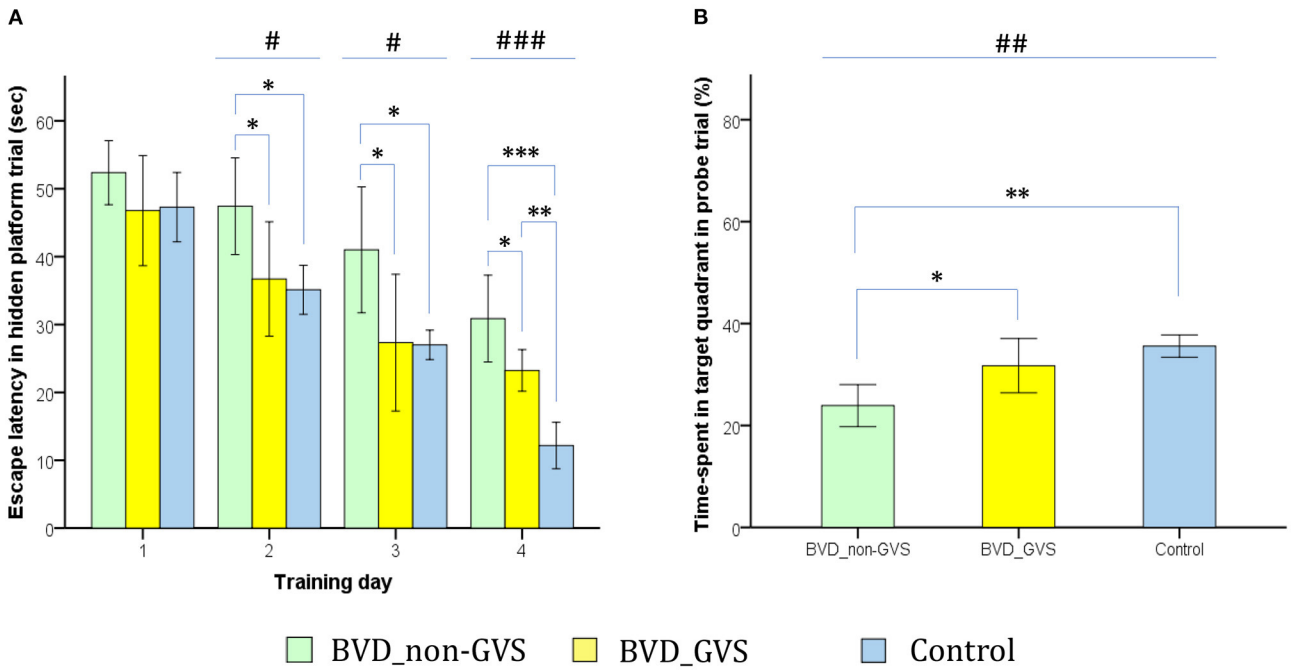

FIGURE 4 | Evaluation of long-term spatial reference memory using the Morris water maze (MWM). The escape latencies to find the hidden platform gradually decreased through the training sessions, indicating ongoing learning. Longer values of escape latency to find the hidden platform indicate an inadequate acquisition of spatial memory and navigation. Differences between the groups were observed on training days (TDs) 2 ($p = 0.012$, ANOVA), 3 ($p = 0.013$, ANOVA), and 4 ($p < 0.001$, ANOVA). The BVD_non-GVS group had longer escape latency than the control group on TDs 2 ($p = 0.022$, Bonferroni test), 3 ($p = 0.032$, Bonferroni test), and 4 ($p < 0.001$, Bonferroni test). The BVD_GVS group had shorter escape latency than the BVD_non-GVS group on TDs 2 ($p = 0.037$, Bonferroni test), 3 ($p = 0.028$, Bonferroni test), and 4 ($p = 0.024$, Bonferroni test) **(A)**. Residual impairments in long-term spatial memory were also indicated by a lower percentage of time spent in the target quadrant (probe trial) on POD 14 in the BVD_non-GVS compared with both the control ($p = 0.001$, Bonferroni test) and BVD_GVS groups ($p = 0.012$, Bonferroni test) ($p = 0.001$, ANOVA) **(B)**. The values are indicated as the mean ± SD. Statistical significance was calculated using one-way ANOVA with post-hoc tests. *Significant differences between two groups; #significant differences among three groups: *, #$p < 0.05$; **, ##$p < 0.01$; ***, ###$p < 0.001$.

test). The values of the BVD_GVS group were better than that of the BVD_non-GVS group on PODs 3 ($p = 0.018$, LSD test), 7 ($p = 0.049$, Tamhane test), and 14 ($p = 0.02$, Bonferroni test) (**Figure 3A**). Meanwhile, the values of SARs, reflected the degree of attentional difficulty during an active working-memory task, were significantly higher in the BVD_non-GVS group than in the control group on PODs 3 [3 (2.06–3.94) turns, Z = −2.79, $p = 0.005$, Mann-Whitney *U* test], 7 [5 (3.58–5.75) turns, Z = −2.796, $p = 0.005$, Mann-Whitney *U* test], and 14 [6.5 (3.49–10.51) turns, Z = −2.798, $p = 0.005$, Mann-Whitney *U* test]. The BVD_GVS group showed better values than the BVD_non-GVS group on PODs 3 (Z = −2.776, $p = 0.006$, Mann-Whitney *U* test), 7 (Z = −2.879, $p = 0.004$, Mann-Whitney *U* test), and 14 (Z = −2.929, $p = 0.003$, Mann-Whitney *U* test) (**Figure 3B**).

Serving as an indicator of spatial reference memory, the PRT was significantly lower in the BVD_non-GVS group than in the control mice on PODs 3 (24.66 ± 3.91% vs. 39.56 ± 5.66%, $p < 0.001$, Bonferroni test), 7 (26.41 ± 5.93% vs. 39.03 ± 3.66%, $p = 0.002$, Bonferroni test), and 14 (29.19 ± 4.84% vs. 39.6 ± 4.78%, $p = 0.017$, Bonferroni test). The mean time spent in the newly unblocked arm increased significantly in the BVD_GVS group compared with the BVD_non-GVS group on PODs 3 ($p = 0.033$, LSD test), 7 ($p = 0.038$, Bonferroni test), and 14 ($p = 0.031$, LSD test) (**Figure 3C**).

Morris water maze task was sought to assess long-term visuospatial memory and learning process (20, 35–37). Accordingly, the ongoing learning was indicated by the progressive decrease across the training sessions of the escape latencies to find the hidden platform. Longer escape latency values in finding the hidden platform reflected an impairment of spatial memory and navigation. We noticed the differences among the groups on training days (TDs) 2 ($p = 0.012$, ANOVA), 3 ($p = 0.013$, ANOVA), and 4 ($p < 0.001$, ANOVA). The BVD_non-GVS group had higher escape latency values than the control group on TDs 2 (47.43 ± 6.79 s vs. 35.12 ± 2.9 s, $p = 0.022$, Bonferroni test), 3 (41 ± 8.84 s vs. 27 ± 1.75 s, $p = 0.032$, Bonferroni test), and 4 (30.87 ± 6.09 s vs. 12.17 ± 2.76 s, $p < 0.001$, Bonferroni test). The escape latency was shortened in the BVD_GVS group compared with the BVD_non-GVS group on TDs 2 ($p = 0.037$, Bonferroni test), 3 ($p = 0.028$, Bonferroni test), and 4 ($p = 0.024$, Bonferroni test) (**Figure 4A**).

The residual impairments in long-term spatial memory exhibited in the MWM task were also indicated by a worse probe trial performance on POD 14, that is a lower percentage of time spent in the target quadrant in the BVD_non-GVS group (23.9 ± 3.93%) compared with the control (35.57 ± 1.76%, $p = 0.001$, Bonferroni test) and BVD_GVS groups (31.73 ± 5.08%, $p = 0.012$, Bonferroni test) ($p = 0.001$, ANOVA)

(**Figure 4B**). Meanwhile, the BVD_GVS group displayed a negligible difference from the control group ($p = 0.131$, LSD test). The differences in the MWM learning activities were not derived from motor deficits (41, 42) because the groups did not differ significantly in mean swim velocity ($p > 0.05$, LSD test).

DISCUSSION

Our data demonstrated the effects of the early GVS intervention on the short-term and long-term spatial memory, navigation, and locomotion deficits induced by acute BVD in a mouse model.

Locomotion and Spatial Cognition Impairments in BVD

Given its crucial role in integrating and converging multisensory information between the ipsi- and contralateral sides of multilevel brain regions, the relationship between bilateral impairment of vestibular system (BVD) and deficits of visuospatial cognitive performance has fascinated scientific interests for the past decades (17–19). Our experimental-based current findings could add an evidence that the BVD induces dysfunctions in spatial memory and navigation from the acute phase to at least 2 weeks after BL (17–19). Other neurophysiological investigations have suggested multiple pathways in which the vestibular signals project to the hippocampus along with other medial temporal lobe regions, to build up maps of 3D space for the development of spatial memory during learning tasks (43, 44).

In the Y maze, the SAP is driven by the innate curiosity and exploratory behavior of mice for the novel surroundings and requires good spatial working memory to recognize which arms have recently been visited (45). During the PRT, mice need to memorize the relationship between distal spatial cues and the arm that had previously been blocked to recognize it as novel, and thus, visit it more frequently than the other arms (33). Both the SAP and PRT have previously been used to measure spatial working and reference memory (32), especially short-term memory. The MWM is also designed to assess hippocampal-dependent spatial navigation and reference memory, especially in the place learning, and extensive evidence of its validity is available (20, 41, 46). Compared to the Y maze, the MWM is more specialized for hippocampal-dependent spatial navigation than the PRT since it eliminates the use of non-spatial or proximal cues, such as odor trail interference, to solve the maze (46). Furthermore, the 24-h interval between the training session and the probe trial session allows the MWM to reflect long-term memory or the consolidation process in the hippocampus rather than the immediate and short-term effects of bilateral vestibular loss (20, 35–37). It has been shown that short-term spatial memory is not sequentially linked with the different stages of long-term spatial memory, even though there was a time-dependent consolidation of the newly established memory into the long-term memory (35, 47).

In line with our findings, deficiencies in gait, locomotor activity, and spatial memory following BVD have been extensively described in both humans and other animals (17, 48–51). Vestibular signals make major contributions to balance and spatial memory functions *via* multisensory convergent and multimodal signaling pathways (1, 2, 11, 12). Concerned to the physiological formation of spatial memory and navigation, there were two major underlying components: (i) a continuous representation of the location and motion of the individual whose coordinates are provided mainly by vestibular and visual cues, and (ii) spatial memory processing in the hippocampal formation (20). As a result, inhibiting the vestibular signals in the pathways to the hippocampus, such as peripheral vestibular lesions, likely led to disrupt the function of hippocampal cells *in vivo* and hippocampal field potentials *in vitro* and cause long-term changes in hippocampal neurochemistry (18). Patients with chronic BVD experience bilateral hippocampal atrophy (20), particularly a reduction in hippocampal gray matter volume in the Cornu ammonis 3, which plays an important role in the formation of episodic memory and the acquisition of spatial information within short-term memory in tasks that require rapid encoding, novelty detection, working memory, and recall of primarily spatial information (21). Hippocampal atrophy predominantly impaired complex forms of visuospatial memory processing, even as non-spatial functions, which additionally rely on the surrounding medial temporal lobe and prefrontal tissue, remain well preserved (20). Morphometric changes in BVD subjects have also been shown to be time-dependent and take place in parallel with adaptive mechanisms (21). Alternatively, in some recent behavioral studies, BL was found to disrupt spatial learning, primarily in the absence of visual signals, because of oscillopsia (52), which is thought to be the result of difficulties in localization caused by problems with self-movement monitoring (53), a function ascribed to the hippocampus.

Galvanic Vestibular Stimulation Effects on Locomotion and Spatial Cognition in BVD Mouse Model

Intriguingly, this work has shown that a short-term GVS intervention conferred benefits on balance control, locomotion, and short- and long-term spatial memory following acute BL, which resulted in better behavioral outcomes more than a week after the cessation of the intervention. Our findings are consistent with previous studies, which also revealed that GVS had positive effects on postural control and locomotion in BVD (28, 29, 54–56). Meanwhile, one study revealed that 6-sessions of GVS induced changes in tactile extinction that lasted up to 1-year follow-up (57).

In this study, the significant increases we found in the total path length during the OF test and SAP of the Y maze task after the GVS intervention imply that the GVS positively affected the recovery of locomotor and postural control deficits following BL. The GVS affected the vestibulo-spinal and other non-dopaminergic pathways probably through a neuromodulation mechanism of facilitating effect on the vestibular nuclei (VN). Neuronal sensitivity to GVS increases with discharge variability, whereby the thick, fast-conducting irregularly firing afferents are more sensitive than the thin, slower-conducting regularly firing

vestibular afferents for both the cathode and anode (26, 58–60). Contrast to the slower-conducting regularly firing afferents are prevalent in the input of the VOR pathway, the fast-conducting irregularly firing afferent predominates in the VSR pathway (26, 61) that underlie postural dysfunction after BL (62–64). Therefore, the GVS intervention can restore locomotor function by modulating type I hair cells (58, 60), which show an irregular phasic signal (65, 66), and can accelerate vestibulo-motor compensation during the acute period after BL.

The beneficial effects of GVS on the recovery of visuospatial memory deficits following BL could be explained with the implications of the reestablishment of four proposed vestibular-hippocampal signaling pathways: vestibulo-thalamo-cortical, vestibulo-cerebello-cortical, head direction, and theta pathways (5, 6). Previous studies revealed that the electrical stimulation excited the medial VN and increased the firing rates of hippocampal CA1 complex spike cells, which correspond to place cells (67). Similarly, GVS at the ampulla of the SCCs generated the initiation of theta activity in the numerous areas of the hippocampal formation (44), and it can be speculated that GVS improves neuronal activity for spatial orientation (68). It has been also known that the critical involvement of the hippocampal theta rhythm in visuospatial information processing and regulating self-movement signals (68, 69). Furthermore, GVS enhances the neuronal activation demonstrated *via* an increase in c-Fos positive cells in the hippocampus following the multiple-session administration (29, 70). Besides, based on the concept of sensory substitution, strengthening the function of other sensory systems, such as visual (30, 71) and somatosensory functions (72) and boosting reciprocal intersensory interactions could be considered a beneficial influence of the GVS to enhance efficiency in the spatial memory and navigation activities (73). All the aforementioned mechanisms just assist us somewhat in imagining the explanation of the GVS effects on strengthening the function of spatial navigation. To acquire a comprehensive understanding, further in-depth investigations are required.

Although GVS has been shown to be effective in ameliorating both the motor impairments and short- and long-term spatial memory deficits induced by BVD that recovery did not appear to approach the baseline level. Expanding the number of GVS sessions to more than five might improve the effectiveness. A second strategy to maximize the effect of GVS could be the use of different modes of stimulation, such as subthreshold noisy GVS, which is based on the principle of stochastic resonance, in which a subthreshold sensory input can be upgraded to exceed a specified threshold when being augmented by a considerably higher-frequency noise signal (74). Therefore, further investigations should be conducted to find the optimal stimulating parameter for GVS in each disease model.

In conclusion, our data demonstrate that the early administration of sinusoidal GVS accelerated the recovery of both locomotion and spatial memory and navigation deficiencies, although the efficacy remained limited. Nonetheless, our promising early results allow us to hope that GVS can be used to treat patients with bilateral vestibulopathies who suffer from motor coordination and spatial cognitive difficulties.

DATA AVAILABILITY STATEMENT

The original contributions presented in the study are included in the article/supplementary material, further inquiries can be directed to the corresponding author/s.

ETHICS STATEMENT

The animal study was reviewed and approved by the Animal Care Committee of the Gachon University of Medicine and Science (IRB MRI2019-0008).

AUTHOR CONTRIBUTIONS

TTN: writing the article, analyzing the data and making the figures. G-SN: analyzing the data and conducting the experiment. GCH: analyzing the data and conducting the experiment. CL: analyzing the data. S-YO: conceptualizing the study and interpretation the data and writing the article.

FUNDING

This work was supported by a National Research Foundation of Korea (NRF) Grant funded by the Korean Government (Ministry of Science and ICT) (No. 2022R1A2B5B01001933) and by the Fund of Biomedical Research Institute, Jeonbuk National University Hospital.

REFERENCES

1. Vidal P-P, Cullen K, Curthoys IS, Du Lac S, Holstein G, Idoux E, et al. *The Vestibular System. The Rat Nervous System*. Amsterdam: Elsevier (2015). p. 805-864.
2. Angelaki DE, Cullen KE. Vestibular system: the many facets of a multimodal sense. *Annu. Rev. Neurosci.* (2008) 31:125–50. doi: 10.1146/annurev.neuro.31.060407.125555
3. Herdman SJ, Clendaniel RA. *Vestibular Rehabilitation*. Philadelphia, PA: FA Davis (2014).
4. Paterson JM, Menzies JR, Bergquist F, Dutia MB. Cellular mechanisms of vestibular compensation. *Neuroembryol. Aging.* (2004) 3:183–93. doi: 10.1159/000096796
5. Shinder ME, Taube JS. Differentiating ascending vestibular pathways to the cortex involved in spatial cognition. *J Vestib Res.* (2010) 20:3–23. doi: 10.3233/ves-2010-0344
6. Hitier M, Besnard S, Smith PF. Vestibular pathways involved in cognition. *Front Integr Neurosci.* (2014) 8:59. doi: 10.3389/fnint.2014.00059
7. Aitken P, Zheng Y, Smith PF. The modulation of hippocampal theta rhythm by the vestibular system. *J Neurophysiol.* (2018) 119:548–62. doi: 10.1152/jn.00548.2017
8. Bird CM, Burgess N. The hippocampus and memory: insights from spatial processing. *Nat Rev Neurosci.* (2008) 9:182–94. doi: 10.1038/nrn2335
9. Andersen P, Morris R, Amaral D, Bliss T, O'Keefe J. *The Hippocampus Book*. Oxford: Oxford university press (2006).
10. Hüfner K, Strupp M, Smith P, Brandt T, Jahn K. Spatial separation of visual and vestibular processing in the human hippocampal formation. *Ann N Y Acad Sci.* (2011) 1233:177–86. doi: 10.1111/j.1749-6632.2011.06115.x
11. Wijesinghe R, Protti DA, Camp AJ. Vestibular interactions in the thalamus. *Front Neural Circuits.* (2015) 9:79. doi: 10.3389/fncir.2015.00079
12. Dieterich M, Brandt T. Functional brain imaging of peripheral and central vestibular disorders. *Brain.* (2008) 131:2538–52. doi: 10.1093/brain/awn042

13. Lacour M, Bernard-Demanze L. Interaction between vestibular compensation mechanisms and vestibular rehabilitation therapy: 10 recommendations for optimal functional recovery. *Front Neurol.* (2015) 5:285. doi: 10.3389/fneur.2014.00285
14. Nguyen TT, Nam G-S, Kang J-J, Han GC, Kim JS, Dieterich M, et al. Galvanic vestibular stimulation improves spatial cognition after unilateral labyrinthectomy in mice. *Front Neurol.* (2021) 2021:1261. doi: 10.3389/fneur.2021.716795
15. Nguyen TT, Nam G-S, Kang J-J, Han GC, Kim JS, Dieterich, et al. The differential effects of acute right-vs. left-sided vestibular deafferentation on spatial cognition in unilateral labyrinthectomized mice. *Front Neurol.* (2021) 2021:2175. doi: 10.3389/fneur.2021.789487
16. Hüfner K, Hamilton DA, Kalla R, Stephan T, Glasauer S, Ma J, et al. Spatial memory and hippocampal volume in humans with unilateral vestibular deafferentation. *Hippocampus.* (2007) 17:471–85. doi: 10.1002/hipo.20283
17. Baek JH, Zheng Y, Darlington CL, Smith PF. Evidence that spatial memory deficits following bilateral vestibular deafferentation in rats are probably permanent. *Neurobiol Learn Mem.* (2010) 94:402–13. doi: 10.1016/j.nlm.2010.08.007
18. Russell NA, Horii A, Smith PF, Darlington CL, Bilkey DK. Bilateral peripheral vestibular lesions produce long-term changes in spatial learning in the rat. *J Vestib Res.* (2003) 13:9–16. doi: 10.3233/VES-2003-13102
19. Zheng Y, Balabhadrapatruni S. Baek J-h, Chung P, Gliddon C, Zhang M, et al. The effects of bilateral vestibular loss on hippocampal volume, neuronal number, and cell proliferation in rats. *Front Neurol.* (2012) 3:20. doi: 10.3389/fneur.2012.00020
20. Brandt T, Schautzer F, Hamilton DA, Brüning R, Markowitsch HJ, Kalla R, et al. Vestibular loss causes hippocampal atrophy and impaired spatial memory in humans. *Brain.* (2005) 128:2732–41. doi: 10.1093/brain/awh617
21. Göttlich M, Jandl NM, Sprenger A, Wojak JF, Münte TF, Krämer UM, et al. Hippocampal gray matter volume in bilateral vestibular failure. *Hum Brain Mapp.* (2016) 37:1998–2006. doi: 10.1002/hbm.23152
22. Lacour M, Helmchen C, Vidal P-P. Vestibular compensation: the neuro-otologist's best friend. *J Neurol.* (2016) 263:54–64. doi: 10.1007/s00415-015-7903-4
23. Zingler VC, Weintz E, Jahn K, Mike A, Huppert D, Rettinger N, et al. Follow-up of vestibular function in bilateral vestibulopathy. *J Neurol Neurosurg Psychiatry.* (2008) 79:284–8. doi: 10.1136/jnnp.2007.122952
24. Ossenkopp K-P, Hargreaves EL. Spatial learning in an enclosed eight-arm radial maze in rats with sodium arsanilate-induced labyrinthectomies. *Behav Neural Biol.* (1993) 59:253–7. doi: 10.1016/0163-1047(93)91034-K
25. Zheng Y, Goddard M, Darlington CL, Smith PF. Long-term deficits on a foraging task after bilateral vestibular deafferentation in rats. *Hippocampus.* (2009) 19:480–6. doi: 10.1002/hipo.20533
26. Dlugaiczyk J, Gensberger KD, Straka H. Galvanic vestibular stimulation: from basic concepts to clinical applications. *J Neurophysiol.* (2019) 121:2237–55. doi: 10.1152/jn.00035.2019
27. Dilda V, MacDougall HG, Curthoys IS, Moore ST. Effects of Galvanic vestibular stimulation on cognitive function. *Exp Brain Res.* (2012) 216:275–85. doi: 10.1007/s00221-011-2929-z
28. Shaabani M, Lotfi Y, Karimian SM, Rahgozar M, Hooshmandi M. Short-term galvanic vestibular stimulation promotes functional recovery and neurogenesis in unilaterally labyrinthectomized rats. *Brain Res.* (2016) 1648:152–62. doi: 10.1016/j.brainres.2016.07.029i
29. Ghahraman MA, Zahmatkesh M, Pourbakht A, Seifi B, Jalaie S, Adeli S, et al. Noisy galvanic vestibular stimulation enhances spatial memory in cognitive impairment-induced by intracerebroventricular-streptozotocin administration. *Physiol Behav.* (2016) 157:217–24. doi: 10.1016/j.physbeh.2016.02.021
30. Nam G-S, Nguyen TT, Kang J-J, Han GC, Oh S-Y. Effects of galvanic vestibular stimulation on vestibular compensation in unilaterally labyrinthectomized mice. *Front Neurol.* (2021) 12:736849. doi: 10.3389/fneur.2021.736849
31. Belzung C. *Open-Field Test*: Heidelberg: Springer (2014)
32. Lalonde R. The neurobiological basis of spontaneous alternation. *Neurosci Biobehav Rev.* (2002) 26:91–104. doi: 10.1016/S0149-7634(01)00041-0
33. Kraeuter A-K, Guest PC, Sarnyai Z. *The Y-Maze for Assessment of Spatial Working and Reference Memory in Mice. Pre-Clinical Models.* Berlin: Springer (2019). p. 105-111.
34. Thompson BL, Levitt P, Stanwood GD. Prenatal cocaine exposure specifically alters spontaneous alternation behavior. *Behav Brain Res.* (2005) 164:107–16. doi: 10.1016/j.bbr.2005.06.010
35. McGaugh JL. Memory-a century of consolidation. *Science.* (2000) 287:248–51. doi: 10.1126/science.287.5451.248
36. Sharma S, Rakoczy S, Brown-Borg H. Assessment of spatial memory in mice. *Life Sci.* (2010) 87:521–36. doi: 10.1016/j.lfs.2010.09.004
37. Dudchenko PA. An overview of the tasks used to test working memory in rodents. *Neurosci Biobehav Rev.* (2004) 28:699–709. doi: 10.1016/j.neubiorev.2004.09.002
38. Barnhart CD, Yang D, Lein PJ. Using the Morris water maze to assess spatial learning and memory in weanling mice. *PLoS ONE.* (2015) 10:e0124521. doi: 10.1371/journal.pone.0124521
39. Lipkind D, Sakov A, Kafkafi N, Elmer GI, Benjamini Y, Golani I. New replicable anxiety-related measures of wall vs. center behavior of mice in the open field. *J Appl Physiol.* (2004) 97:347–59. doi: 10.1152/japplphysiol.00148.2004
40. Seibenhener ML, Wooten MC. Use of the open field maze to measure locomotor and anxiety-like behavior in mice. *JoVE.* (2015) 2015:e52434. doi: 10.3791/52434
41. Vorhees CV, Williams MT. Morris water maze: procedures for assessing spatial and related forms of learning and memory. *Nat Protoc.* (2006) 1:848–58. doi: 10.1038/nprot.2006
42. Fitzgerald LW, Dokla CP. Morris water task impairment and hypoactivity following cysteamine-induced reductions of somatostatin-like immunoreactivity. *Brain Res.* (1989) 505:246–50. doi: 10.1016/0006-8993(89)91450-9
43. Chapuis N, Krimm M, de Waele C, Vibert N, Berthoz A. Effect of post-training unilateral labyrinthectomy in a spatial orientation task by guinea pigs. *Behav Brain Res.* (1992) 51:115–26. doi: 10.1016/s0166-4328(05)80205-0
44. Cuthbert PC, Gilchrist DP, Hicks SL, MacDougall HG, Curthoys IS. Electrophysiological evidence for vestibular activation of the guinea pig hippocampus. *Neuroreport.* (2000) 11:1443–7. doi: 10.1097/00001756-200005150-00018
45. Hughes RN. The value of spontaneous alternation behavior (SAB) as a test of retention in pharmacological investigations of memory. *Neurosci Biobehav Rev.* (2004) 28:497–505. doi: 10.1016/j.neubiorev.2004.06.006
46. D'Hooge R, De Deyn PP. Applications of the Morris water maze in the study of learning and memory. *Brain Res Rev.* (2001) 36:60–90. doi: 10.1016/S0165-0173(01)00067-4
47. Emptage NJ, Carew TJ. Long-term synaptic facilitation in the absence of short-term facilitation in Aplysia neurons. *Science.* (1993) 262:253–6. doi: 10.2307/2882342
48. Schöberl F, Pradhan C, Grosch M, Brendel M, Jostes F, Obermaier K, et al. Bilateral vestibulopathy causes selective deficits in recombining novel routes in real space. *Sci Rep.* (2021) 11:1–16. doi: 10.1038/s41598-021-82427-6
49. Schautzer F, Hamilton D, Kalla R, Strupp M, Brandt T. Spatial memory deficits in patients with chronic bilateral vestibular failure. *Ann NY Acad Sci.* (2003) 1004:316–24. doi: 10.1196/annals.1303.029
50. Dobbels B, Mertens G, Gilles A, Moyaert J, van de Berg R, Fransen E, et al. The virtual morris water task in 64 patients with bilateral vestibulopathy and the impact of hearing status. *Front Neurol.* (2020) 11:710. doi: 10.3389/fneur.2020.00710
51. Zheng Y, Goddard M, Darlington CL, Smith PF. Bilateral vestibular deafferentation impairs performance in a spatial forced alternation task in rats. *Hippocampus.* (2007) 17:253–6. doi: 10.1002/hipo.20266
52. Stackman RW, Herbert AM. Rats with lesions of the vestibular system require a visual landmark for spatial navigation. *Behav Brain Res.* (2002) 128:27–40. doi: 10.1016/S0166-4328(01)00270-4
53. Wallace DG, Hines DJ, Pellis SM, Whishaw IQ. Vestibular information is required for dead reckoning in the rat. *J Neurosci.* (2002) 22:10009–17. doi: 10.1523/jneurosci.22-22-10009.2002
54. Schniepp R, Boerner J, Decker J, Jahn K, Brandt T, Wuehr M. Noisy vestibular stimulation improves vestibulospinal function in patients with bilateral vestibulopathy. *J Neurol.* (2018) 265:57–62. doi: 10.1007/s00415-018-8814-y
55. Iwasaki S, Fujimoto C, Egami N, Kinoshita M, Togo F, Yamamoto Y, et al. Noisy vestibular stimulation increases gait speed in normals and in bilateral vestibulopathy. *Brain Stimul.* (2018) 11:709–15. doi: 10.1016/j.brs.2018.03.005

56. Fujimoto C, Egami N, Kawahara T, Uemura Y, Yamamoto Y, Yamasoba T, et al. Noisy galvanic vestibular stimulation sustainably improves posture in bilateral vestibulopathy. *Front Neurol.* (2018) 9:900. doi: 10.3389/fneur.2018.00900
57. Kerkhoff G, Hildebrandt H, Reinhart S, Kardinal M, Dimova V, Utz KS, et al. long-lasting improvement of tactile extinction after galvanic vestibular stimulation: two Sham-stimulation controlled case studies. *Neuropsychologia.* (2011) 49:186–95. doi: 10.1016/j.neuropsychologia.2010.11.014
58. Goldberg J, Smith CE, Fernandez C. Relation between discharge regularity and responses to externally applied galvanic currents in vestibular nerve afferents of the squirrel monkey. *J Neurophysiol.* (1984) 51:1236–56. doi: 10.1152/jn.1984.51.6.1236
59. Goldberg J, Ferna C, Smith C. Responses of vestibular-nerve afferents in the squirrel monkey to externally applied galvanic currents. *Brain Res.* (1982) 252:156–60. doi: 10.1016/0006-8993(82)90990-8
60. Kim J, Curthoys IS. Responses of primary vestibular neurons to galvanic vestibular stimulation (GVS) in the anaesthetised guinea pig. *Brain Res Bull.* (2004) 64:265–71. doi: 10.1016/j.brainresbull.2004.07.008
61. Goldberg JM. Afferent diversity and the organization of central vestibular pathways. *Exp Brain Res.* (2000) 130:277–97. doi: 10.1007/s002210050033
62. Highstein SM, Goldberg J, Moschovakis A, Fernandez C. Inputs from regularly and irregularly discharging vestibular nerve afferents to secondary neurons in the vestibular nuclei of the squirrel monkey. II Correlation with output pathways of secondary neurons. *J Neurophysiol.* (1987) 58:719–38. doi: 10.1152/jn.1987.58.4.719
63. Smith PF, Curthoys IS. Mechanisms of recovery following unilateral labyrinthectomy: a review. *Brain Res Rev.* (1989) 14:155–80. doi: 10.1016/0165-0173(89)90013-1
64. Lambert FM, Malinvaud D, Gratacap M, Straka H, Vidal P-P. Restricted neural plasticity in vestibulospinal pathways after unilateral labyrinthectomy as the origin for scoliotic deformations. *J Neurosci.* (2013) 33:6845–56. doi: 10.1523/jneurosci.4842-12.2013
65. Kwan A, Forbes PA, Mitchell DE, Blouin J-S, Cullen KE. Neural substrates, dynamics and thresholds of galvanic vestibular stimulation in the behaving primate. *Nat Commun.* (2019) 10:1–15. doi: 10.1038/s41467-019-09738-1
66. Vignaux G, Chabbert C, Gaboyard-Niay S, Travo C, Machado ML, Denise P, et al. Evaluation of the chemical model of vestibular lesions induced by arsanilate in rats. *Toxicol Appl Pharmacol.* (2012) 258:61–71. doi: 10.1016/j.taap.2011.10.008
67. Horii A, Russell NA, Smith PF, Darlington CL, Bilkey DK. Vestibular influences on CA1 neurons in the rat hippocampus: an electrophysiological study in vivo. *Exp Brain Res.* (2004) 155:245–50. doi: 10.1007/s00221-003-1725-9
68. Ringo JL, Sobotka S, Diltz MD, Bunce CM. Eye movements modulate activity in hippocampal, parahippocampal, and inferotemporal neurons. *J Neurophysiol.* (1994) 71:1285–8. doi: 10.1152/jn.1994.71.3.1285
69. Huxter J, Burgess N, O'Keefe J. Independent rate and temporal coding in hippocampal pyramidal cells. *Nature.* (2003) 425:828–32. doi: 10.1038/nature02058
70. Holstein GR, Friedrich Jr VL, Martinelli GP, Ogorodnikov D, Yakushin SB, Cohen B. Fos expression in neurons of the rat vestibulo-autonomic pathway activated by sinusoidal galvanic vestibular stimulation. *Front Neurol.* (2012) 3:4. doi: 10.3389/fneur.2012.00004
71. Voros JL, Sherman SO, Rise R, Kryuchkov A, Stine P, Anderson AP, et al. Galvanic vestibular stimulation produces cross-modal improvements in visual thresholds. *Front Neurosci.* (2021) 15:311. doi: 10.3389/fnins.2021.640984
72. Best C, Lange E, Buchholz H-G, Schreckenberger M, Reuss S, Dieterich M. Left hemispheric dominance of vestibular processing indicates lateralization of cortical functions in rats. *Brain Struct Funct.* (2014) 219:2141–58. doi: 10.1007/s00429-013-0628-1
73. Holschneider D, Givrad T, Yang J, Stewart SB, Francis SR, Wang Z, et al. Cerebral perfusion mapping during retrieval of spatial memory in rats. *Behav Brain Res.* (2019) 375:112116. doi: 10.1016/j.bbr.2019.112116
74. Moss F, Ward LM, Sannita WG. Stochastic resonance and sensory information processing: a tutorial and review of application. *Clin Neurophysiol.* (2004) 115:267–81. doi: 10.1016/j.clinph.2003.09.014

Conflict of Interest: The authors declare that the research was conducted in the absence of any commercial or financial relationships that could be construed as a potential conflict of interest.

Publisher's Note: All claims expressed in this article are solely those of the authors and do not necessarily represent those of their affiliated organizations, or those of the publisher, the editors and the reviewers. Any product that may be evaluated in this article, or claim that may be made by its manufacturer, is not guaranteed or endorsed by the publisher.

Copyright © 2022 Nguyen, Nam, Han, Le and Oh. This is an open-access article distributed under the terms of the Creative Commons Attribution License (CC BY). The use, distribution or reproduction in other forums is permitted, provided the original author(s) and the copyright owner(s) are credited and that the original publication in this journal is cited, in accordance with accepted academic practice. No use, distribution or reproduction is permitted which does not comply with these terms.

frontiers in Neurology

REVIEW
published: 18 March 2022
doi: 10.3389/fneur.2022.850337

Vestibular Cochlear Manifestations in COVID-19 Cases

Kathiravan Kaliyappan[1], *Yu-Chen Chen*[2*] *and Vijaya Prakash Krishnan Muthaiah*[1*]

[1] *Department of Rehabilitation Sciences, School of Public Health and Health Professions, State University of New York at Buffalo, Buffalo, NY, United States,* [2] *Department of Radiology, Nanjing First Hospital, Nanjing Medical University, Nanjing, China*

The severe acute respiratory syndrome coronavirus 2 (SARS-CoV-2) is a high transmissible infectious disease that primarily impacts the respiratory system and leads to death as it worsens. Ever since the World Health Organization declared the disease as a global pandemic, the pathophysiology, clinical manifestations, and disease prognosis has been discussed in various literature. In addition to impaired respiratory health, the symptoms also indicated the involvement of the cardiovascular and neurological system after SARS-CoV-2 infection. Despite the pulmonary, cardiovascular, and neurological complications, many reports also revealed the prevalence of vestibulocochlear symptoms like dizziness, vertigo, vestibular neuritis, sudden sensorineural hearing loss, and tinnitus. Though many clinical reports and scientific reviews reported the vestibular and cochlear impairments associated with coronavirus disease 2019 (COVID-19) infection, the underlying pathological mechanisms are still unclear and unexplored. In this review, we discussed the published clinical reports, research articles, and literature reviews related to vestibulocochlear manifestations following SARS-CoV-2 infections. We also summarized the current knowledge about the prevalence, epidemiological and clinical features, and potential pathological mechanisms related to vestibular and cochlear manifestations resulting from COVID-19 infections.

Keywords: auditory symptoms, vestibular symptoms, COVID-19, hearing loss, tinnitus

OPEN ACCESS

Edited by:
Arianna Di Stadio,
University of Catania, Italy

Reviewed by:
Zhenyu Xiong,
University of Texas Southwestern Medical Center, United States
Marije de Jong,
Hadassah Medical Center, Israel

****Correspondence:***
Yu-Chen Chen
chenyuchen1989@126.com
Vijaya Prakash Krishnan Muthaiah
vijayapr@buffalo.edu

Specialty section:
This article was submitted to Neuro-Otology, a section of the journal Frontiers in Neurology

Received: *07 January 2022*
Accepted: *15 February 2022*
Published: *18 March 2022*

Citation:
Kaliyappan K, Chen Y-C and Krishnan Muthaiah VP (2022) Vestibular Cochlear Manifestations in COVID-19 Cases. Front. Neurol. 13:850337. doi: 10.3389/fneur.2022.850337

INTRODUCTION

The novel coronavirus disease 2019 (COVID-19) infection caused by severe acute respiratory syndrome coronavirus 2 (SARS-CoV-2), severely impairs the human respiratory system and its clinical manifestation includes cough, fever, and fatigues (1). In December 2019, the outbreak was identified as pneumonia cases with an unknown cause in Wuhan, China, the WHO declared the infection as a pandemic in March 2020 (2). As of March 2022, the pandemic has caused 440 million confirmed cases with 5.9 million deaths worldwide and is still persistent (https://covid19.who.int/).

Many countries are developing vaccines that mainly target the SARS-CoV-2 spike protein (S protein), a viral surface protein that enters the human cells (3). Even with significant protective measures, the disease is spreading relentlessly worldwide and causing health and socioeconomic burden. The COVID-19 pandemic also impacts the mental health of a larger population due to lockdowns and lifestyle modification-mediated stress, anxiety, depression, and insomnia (4).

The majority of COVID-19 infected cases are asymptomatic in the early stage of disease progression and affected predominantly with respiratory or extrapulmonary symptoms in subsequent stages (5). It is becoming apparent through clinical observations that patients with

COVID-19 infection also exhibit neurological and otological symptoms (6, 7). With a high prevalent rate along with its asymptomatic and atypical nature, the COVID-19 is posing a huge burden and challenge to the healthcare communities. So there is a critical need for a detailed understanding of its demographics, transmission risk, symptoms, clinical outcomes, and manifestations in a broader manner.

In this review, we summarize the research reports and findings related to neurological, vestibular, and auditory complications in the patients affected with COVID-19 and discuss the potential pathological mechanisms.

REVIEW METHODS

Case reports, case series, and multicentral studies were sought from PubMed and Google using keywords, "coronavirus or COVID and neurological symptoms, audiological symptoms including hearing loss, tinnitus, vestibular symptoms including dizziness and vertigo" were included for this review. Self-reported case reports and observational studies without any clinical examination or tests were excluded from this review.

NEUROLOGICAL MANIFESTATIONS IN COVID-19 PATIENTS

While COVID-19 infections primarily affect the respiratory system, many clinical observations and symptoms demonstrate its extrapulmonary involvement in cardiovascular, digestive, hematological, endocrine, excretory, and neurological systems (5, 8, 9). Recent evidence are indicating the increasing neurological manifestations in central and peripheral nervous systems with symptoms, including headaches, dizziness, fatigue, and loss of consciousness (10). In addition, other neurological manifestations like meningitis (11), encephalitis (12), encephalopathy (13), myelitis (14), and Guillain Barre syndrome (15), in patients with COVID-19, suggesting its neuroinfectious properties. Many clinical cases demonstrated the potential involvement of COVID-19 in acute ischemic stroke (AIS) (16–19). It is predicted that the stroke risk is increased to 3.2- to 7.8-fold after the first three days of COVID-19 infection (20, 21). Evidence also implied that COVID-19 infection may lead to arterial thrombosis through endothelial dysfunction, thrombin formation, and platelet activation (22). The neurological symptoms are identified as an initial COVID-19 presentation in many patients and the prevalence increases with the severity of the disease. The neurological manifestations and symptoms associated with COVID-19 are listed in **Table 1**.

TABLE 1 | Neurological manifestations and symptoms in patients with COVID-19.

Authors	Manifestations and symptoms
Wang et al. (6)	Headaches, Dizziness, Fatigue
Bénézit et al. (23)	Hyposmia/anosmia and Hypogeusia/ageusia
Niazkar et al. (10)	Loss of consciousness
Liang et al. (11)	Meningitis
Ye et al. (12)	Encephalitis
Zhao et al. (14)	Myelitis
Filatov et al. (13)	Encephalopathy
Nannoni et al. (19)	Cerebrovascular disease
Sedaghat and Karimi (15)	Guillain Barre syndrome

OTOLOGICAL MANIFESTATIONS IN COVID-19 PATIENTS

The COVID-19 infection also presented with many early otolaryngological symptoms, like throat infections, dyspnoea, cough, along the sudden onset of anosmia and ageusia (23, 24). In addition, few case reports have documented the adverse otologic (25–28) and vestibular manifestations (29–31) after COVID-19 infection. The detailed otological information in each report was shown in **Table 2**.

AUDITORY MANIFESTATIONS

Hearing loss after viral infections are conductive or sensorineural types caused and being hypothesized to cause direct or indirect damage to inner ear structures. Studies have highlighted the neurotropic and neuroinvasive nature of the COVID-19 virus (54), and the infection has been considered a plausible cause for hearing loss. Auditory symptoms, including hearing loss and tinnitus, are being frequently reported along with other usual symptoms in patients with COVID-19 (32, 55, 56). Being a neglected symptom, screening for hearing is being encouraged in the patients with COVID-19. The first case of sensorineural hearing loss (SNHL), in a COVID-19-recovered elderly female patient, was reported in Thailand (26). Following this, a few other reports also stated the association between the SNHL and COVID-19 infection (33–36). Similarly, a case report demonstrated a unilateral conductive hearing loss and tinnitus in a 35-year-old female asymptomatic patient with COVID-19. The otoscopic examination revealed the acute otitis media mediated bulging tympanic membrane (37). In another study, asymptomatic patients with COVID-19 have significantly worsened high-frequency pure tone thresholds and transient evoked otoacoustic emission (TEOAE) amplitudes when compared to control subjects (25). In addition, a recent also study confirmed hearing impairment especially at 1,000 Hz through TEOAE tests (39).

Tinnitus is another significant clinical symptom additional to hearing loss, vertigo, and dizziness in patients with COVID-19 infection. Chirakkal et al. (38) have reported that unilateral tinnitus was observed at 4 kHz at 10 dB using frequency and intensity matching evaluation in a 35-year-old female patient with COVID-19. This study also demonstrated the detrimental effects of COVID-19 infection on cochlea outer hair cells, which was evident through TEOAE and distortion-product otoacoustic emissions amplitudes. Many case reports and reviews have reported sudden hearing loss and disabling tinnitus in a patient with severe COVID-19 infection (27, 40–42, 57). Furthermore,

TABLE 2 | The detailed otological information in each report.

Authors	Study design	Total patients	Age (Years)	Sex	Test	Symptoms
Dharmarajan et al. (32)	Case series	100	21–60	Both	PTA & TEOAE	Tinnitus, Hearing loss & Otalgia
Sriwijitalai and Wiwanitkit (26)	Case report	1	NA	NA	NA	Neurosensory hearing loss
Abdel Rhman and Abdel Wahid (33)	Case report	1	52	Male	Audiometry	SNHL
Degen et al. (34)	Case report	1	60	Male	MRI	Acute SNHL
Edwards et al. (35)	Case report	1	68	Female	Audiogram	Bilateral SNHL
Koumpa et al. (36)	Case report	1	45	Male	PTA	Hearing loss
Fidan (37)	Case report	1	35	Female	Tympanometry & audiometry	Conductive hearing loss
Mustafa (25)	Case series	20	20-50	NA	Tympanometry & TEOAE	Mild hearing loss
Chirakkal et al. (38)	Case report	1	35	Female	PTA, Tuning fork test, Impedance audiometry, OAE & Tinnitus pitch matching	Tinnitus
Kokten et al. (39)	Case series	30	NA	NA	PTA & TEOAE	Hearing loss
Lamounier et al. (40)	Case report	1	67	Female	Audiometry & MRI	Hearing loss
Pokharel et al. (41)	Case report	1	27	Male	Audiometry & MRI	SNHL
Ricciardiello et al. (42)	Case series	5	18–65	Male & female	PTA, acoustic immittance test, ABR, Acufenometry, THI & DHI	SNHL & Tinnitus
Daher et al. (43)	Case report	1	49	Male	Tympanometry & audiometry	Severe tinnitus & Mild Hearing loss
Javanbakht and Babaee (44)	Case report	1	27	Male	Tympanometry & audiometry	Tinnitus
Sun et al. (45)	Case report	1	38	Male	Tympanometry	Bilateral hearing loss & tinnitus
Viola et al. (46)	Multicentral study	185	NA	NA	Questionnaire	Tinnitus, Vestibular disorders, Dizziness & Vertigo
Liotta et al. (47)	Case series	509	NA	NA	Clinical examination	Neurologic manifestations & encephalopathy
Sari et al. (48)	Case report	2	12–13	Boy & Girl	NA	Headache & Dizziness
Vanaparthy et al. (49)	Case report	1	63	Female	Dix-Hallpike maneuver	Vertigo and vestibular neuritis
Maslovara and Košec (50)	Case report	2	29 & 41	Female	The Romberg test & Dix–Hallpike test	Vertigo, dizziness, and nausea
Mat et al. (51)	Case report	1	13	Female	Vestibulo-ocular reflex	Vestibular Neuritis
Motawea and Monib (52)	Case report	1	60	Female	Physical examination	Vertigo
Malayala and Raza (53)	Case report	1	29	Female	Self-report & Clinical examination	Vestibular Neuritis

PTA, pure tone audiometry; TEOAE, transient evoked otoacoustic emissions; ABR, auditory brainstem response; THI, tinnitus handicap inventory; DHI, dizziness handicap inventory; VOR, vestibulo-ocular reflex; NA, not applicable.

sudden unilateral hearing loss with worsening tinnitus was observed in a 52-year-old male physician affected with COVID-19 without any history of head trauma or ototoxic medications (33). Another study has reported bilateral tinnitus in a 60-year-old patient with COVID-19 having signs of inflammation in both cochleae through MRI findings (34). Multiple case reports and meta-analysis reviews have shown the prevalence of tinnitus in patients with COVID-19 (43–46, 56, 58, 59).

A case of sensorineural hearing loss and tinnitus was reported in the unilateral ear 2 days after administration of the Oxford-AstraZeneca (VAXZEVRIA) vaccine in a 57-year-old male patient (60). In another case study, the SSHL was demonstrated through pure tone audiometry 2 days after the second dose of Oxford-AstraZeneca vaccine in a 61-year-old female (61). But the hearing loss was recovered after 15 days with a treatment of glucocorticoids and acetylsalicylic acid. Furthermore, a 37-year-old male patient was diagnosed with tinnitus and cochleopathy after receiving his first AstraZeneca COVID-19 vaccine dose, which was reversed by dexamethasone and prednisolone treatment (62). Another case series have reported the transient sudden unilateral tinnitus after BNT162b2 mRNA-vaccine (e.g., *pfizer*), which resolved rapidly in 2 out of 3 cases (63). Recently, many case reports have reported a prevalence of sudden hearing loss and tinnitus after the COVID-19 vaccinations (64–68).

VESTIBULAR MANIFESTATIONS

Though the involvement of COVID-19 infection in otologic manifestations has not been confirmed yet, many case reports are providing preliminary evidence to emphasize the potential association between the COVID-19 infection and ear disorders. Along with auditory manifestations, a few vestibular symptoms like dizziness, vertigo, and tinnitus are described as the common clinical manifestations in patients with COVID-19 (47, 69). Many case studies have reported dizziness as a prevalent neurological symptom post-COVID-19 infection (47, 69, 70). In addition, many other reviews also reported dizziness as a common clinical manifestation along with other vertigo, hearing loss, and tinnitus (56, 71). A recent case report has stated the manifestation of

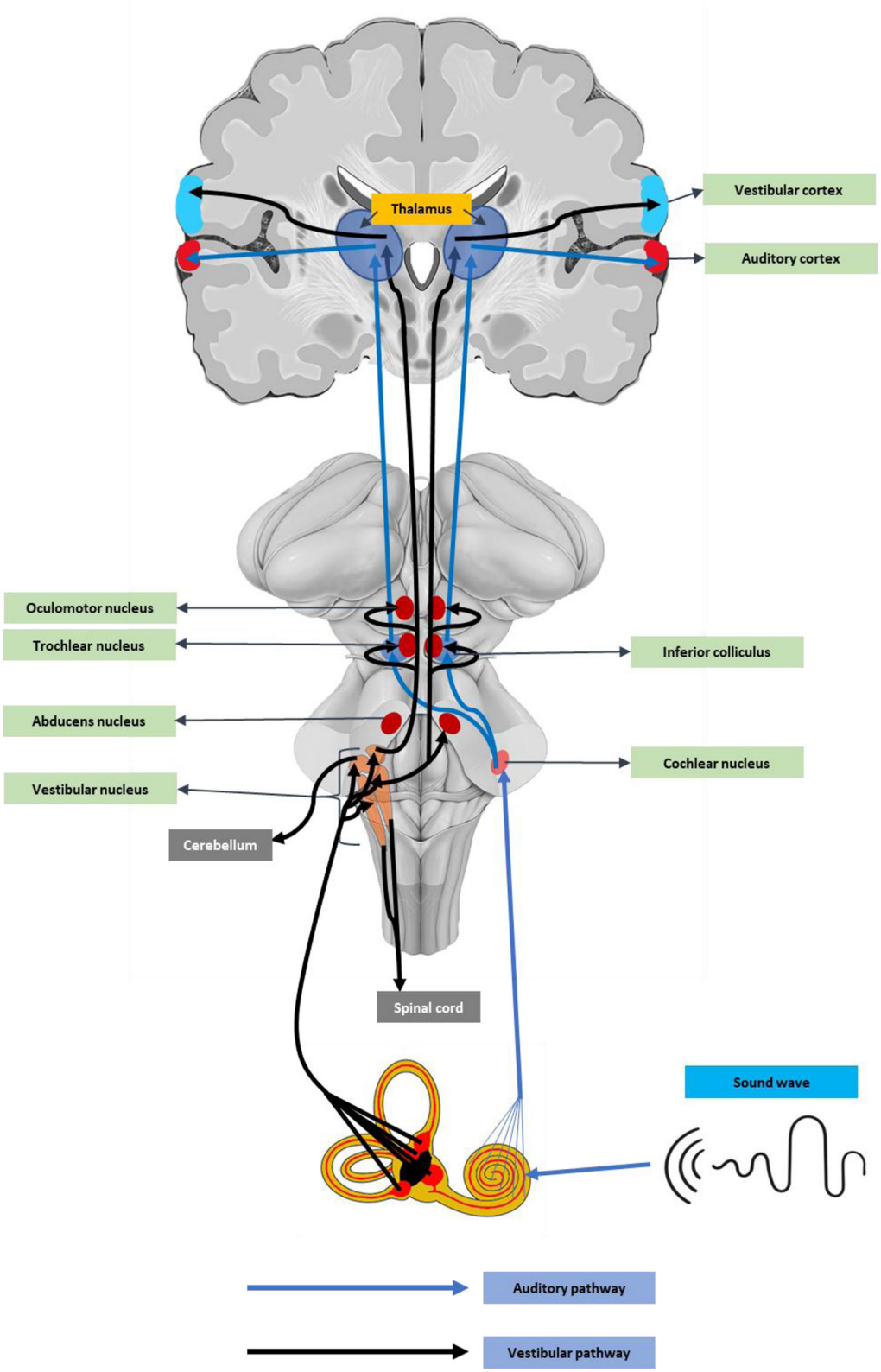

FIGURE 1 | Vestibulocochlear pathway.

dizziness in two COVID-19-affected children (12–13 years), which resolved in a week (48). Vestibular neuritis is a vestibular disorder that causes vertigo, dizziness, and balance problems, and is diagnosed in patients with COVID-19 (49). In addition, a few case reports also demonstrated vertigo as an important clinical manifestation of COVID-19 (50–53).

DISCUSSION

Association between various types of viral infections and hearing loss have been implied for years. Hearing loss is a well-known complication of bacterial and viral meningitis (72) and some viral infections can cause SNHL (73, 74).

Many researchers have discussed the neuroinvasive and neurotropic properties of SARS-CoV-2 (54, 75, 76), which has been linked the post-COVID neurological manifestations. Almost every coronavirus variant has a similar structure and infection mechanisms. Earlier reports have confirmed the presence of SARS-CoV in cerebrospinal fluid of infected patients (77, 78).

SARS-CoV-2 primarily enters the body through the angiotensin-converting enzyme-2 receptor (ACE2) in the respiratory epithelium. The virus is replicated and enters the circulation by attaching to the β chain of hemoglobin in erythrocytes, and transported and binds to several organs (79).

Angiotensin-converting enzyme-2 receptor (ACE2) receptors are abundant in neurons and glial cells of various brain regions like the cortex, striatum, substantia nigra, and the brainstem (80), suggesting the neuronal damage potential of SARS-CoV-2. In addition, the ACE2 receptors, including the medulla oblongata and temporal lobe (81), are key auditory regions. These auditory centers could be affected by cytokine release-mediated inflammatory responses (82). Recent reports also stated that SARS-CoV-2 can directly enter the brain through the olfactory epithelium or the cribriform bone (83). An earlier experimental study using a human ACE2 overexpressed mouse model, the intranasal SARS, SARS-CoV-1 infection caused neuronal death in the brainstem regions (84, 85). As the brainstem contains vital components of the auditory pathway (**Figure 1**), damage to these regions can cause hearing complications and deafness.

The blood-brain barrier is a physical barrier that prevents the entry of any harmful and infectious substances. Recent evidence also demonstrated that the spike protein of SARS-CoV-2 was able to cross the blood-brain barrier in male mice when it is administrated intravenously and intranasally (86). Adding to this, many research reports and review articles also cite the evidence of blood-brain barrier disruption caused by SARS-CoV-2 infection through upregulation of proinflammatory mediators (87–90). With a compromised blood-brain barrier, the SARs-CoV-2 can easily enter the brain parenchyma and lead to exacerbated brain pathology and neurological manifestations, including hearing and vestibular complications.

Another possible hypothesis of hearing loss and vestibular complications is hypoxia caused by the hyperfusion-mediated ischemia in the inner ear structures. Numerous clinical and experimental reports have confirmed that the SARS-CoV-2 infection enhances the chances of thrombus formation in the circulation and leads to increased risk for cerebrovascular diseases (91–96). SARS-CoV-2 can cause hypoxia by deoxygenating the binding erythrocytes. As vascular smooth muscles contain ACE2 receptors, the SARS-CoV-2 infection can form a blood clot in the blood vessels supplying the inner ear, thus leading to ischemic damage and subsequent hearing loss and vestibular impairments. According to the ischemia theory, the geriatric population is mainly prone to SARS-CoV-2-mediated otological complications (97).

A recent research finding has demonstrated the involvement of direct viral infections in the inner ear tissues as a potential cause for auditory and vestibular dysfunctions after COVID-19 infection (98). Varying degree of hearing impairment by direct or indirect damage to inner ear components following viral infections can be reversed with antiviral drugs. But, ototoxicity by specific drugs to treat SARS-CoV-2 infection, could be a potential cause for negative auditory and vestibular manifestations of COVID-19 treatments. Drugs like hydroxychloroquine used in early pandemics were proved to be ototoxic and cause SNHL, tinnitus, and balance issues (99). In addition, other drugs like azithromycin (100), Remdesivir, Favipiravir (101), and Lopinavir (102) used to combat COVID-19 have been proved to cause ototoxicity.

CONCLUSION

The novel coronavirus disease 2019 (COVID-19) pandemic became the major healthcare challenge in recent human history. Although respiratory and cardiovascular are identified as characteristic features, neurological and otological manifestations are being frequently reported in patients with COVID-19. These atypical symptoms can severely affect the long-term outcomes and impair the post-COVID-19 life quality. However, current data available on inner ear disorders associated with COVID-19 and studies describing the possible pathophysiology remain unclear and limited. Thus, there is a critical need for early screening and clinical laboratory diagnosis to identify the auditory and vestibular disorders to manage the disease effectively. Furthermore, it is crucial to ascertain the potential ototoxic properties of the drug used to manage COVID-19 to avoid permanent hearing and vestibular disorders.

AUTHOR CONTRIBUTIONS

KK checked the references and wrote the manuscript. Y-CC and VK contributed to the discussion and manuscript revision. All authors contributed to the article and approved the submitted version.

FUNDING

This work was supported by the Natural Science Foundation of Jiangsu Province (No. BK20211008) and Medical Science and Technology Development Foundation of Nanjing Department of Health (No. ZKX20037).

REFERENCES

1. Huang C, Wang Y, Li X, Ren L, Zhao J, Hu Y, et al. Clinical features of patients infected with 2019 novel coronavirus in Wuhan, China. *Lancet.* (2020) 395:497–506. doi: 10.1016/S0140-6736(20)30183-5
2. Cucinotta D, Vanelli M. WHO declares COVID-19 a pandemic. *Acta Bio Medica: Atenei Parmensis.* (2020) 91:157. doi: 10.23750/abm.v91i1.9397
3. Huang Y, Yang C, Xu Xf, Xu W, Liu S. Structural and functional properties of SARS-CoV-2 spike protein: potential antivirus drug development for COVID-19. *Acta Pharmacologica Sinica.* (2020) 41:1141–1149. doi: 10.1038/s41401-020-0485-4
4. Torales J, O'Higgins M, Castaldelli-Maia JM, Ventriglio A. The outbreak of COVID-19 coronavirus and its impact on global mental health. *Int J Soc Psychiatry.* (2020) 66:317–20. doi: 10.1177/0020764020915212
5. Gupta A, Madhavan MV, Sehgal K, Nair N, Mahajan S, Sehrawat TS, et al. Extrapulmonary manifestations of COVID-19. *Nat Med.* (2020) 26:1017–32. doi: 10.1038/s41591-020-0968-3
6. Wang D, Hu B, Hu C, Zhu F, Liu X, Zhang J, et al. Clinical characteristics of 138 hospitalized patients with 2019 novel coronavirus–infected pneumonia in Wuhan, China. *Jama.* (2020) 323:1061–9. doi: 10.1001/jama.2020.1585
7. Korkmaz MÖ, Egilmez OK, Özçelik MA. Otolaryngological manifestations of hospitalised patients with confirmed COVID-19 infection. *Euro Archiv Oto-Rhino-Laryngol.* (2021) 278:1675–85. doi: 10.1007/s00405-020-06396-8
8. Guan W, Ni Z, Hu Y, Liang W, Ou C, He J, et al. Clinical characteristics of coronavirus disease 2019 in China. *New Engl J Med.* (2020) 382:1708–20. doi: 10.1056/NEJMoa2002032
9. Zhou F, Yu T, Du R, Fan G, Liu Y, Liu Z, et al. Clinical course and risk factors for mortality of adult inpatients with COVID-19 in Wuhan, China: a retrospective cohort study. *Lancet.* (2020) 395:1054–62. doi: 10.1016/S0140-6736(20)30566-3
10. Niazkar HR, Zibaee B, Nasimi A, Bahri N. The neurological manifestations of COVID-19: a review article. *Neurologic Sci.* (2020) 41:1667–71. doi: 10.1007/s10072-020-04486-3
11. Liang W, Jia CAI, Huating LUO, Hongzhi G, Hongzhi W, Huang C, et al. A case of coronavirus disease 2019 with tuberculous meningitis. *Chinese J Neurol.* (2020) 20:E004. doi: 10.3760/cma.j.cn113694-20200302-00134
12. Ye M, Ren Y, Lv T. Encephalitis as a clinical manifestation of COVID-19. *Brain Behav Immun.* (2020) 88:945–6. doi: 10.1016/j.bbi.2020.04.017
13. Filatov A, Sharma P, Hindi F, Espinosa PS. Neurological complications of coronavirus disease (COVID-19): encephalopathy. *Cureus.* (2020) 12. doi: 10.7759/cureus.7352
14. Zhao K, Huang J, Dai D, Feng Y, Liu L, Nie S. Acute myelitis after SARS-CoV-2 infection: a case report. *MedRxiv*. (2020). doi: 10.1101/2020.03.16.20035105
15. Sedaghat Z, Karimi N. Guillain Barre syndrome associated with COVID-19 infection: a case report. *J Clinic Neurosci.* (2020) 76:233–5. doi: 10.1016/j.jocn.2020.04.062
16. Beyrouti R, Adams ME, Benjamin L, Cohen H, Farmer SF, Goh YY, et al. Characteristics of ischaemic stroke associated with COVID-19. *J Neurol Neurosurg Psychiatr.* (2020) 91:889–91. doi: 10.1136/jnnp-2020-323586
17. Oxley TJ, Mocco J, Majidi S, Kellner CP, Shoirah H, Singh IP, et al. Large-vessel stroke as a presenting feature of Covid-19 in the young. *New Engl J Med.* (2020) 382:e60. doi: 10.1056/NEJMc2009787
18. Yaghi S, Ishida K, Torres J, Mac Grory B, Raz E, Humbert K, et al. SARS-CoV-2 and stroke in a New York healthcare system. *Stroke.* (2020) 51:2002–11. doi: 10.1161/STROKEAHA.120.030335
19. Nannoni S, de Groot R, Bell S, Markus HS. Stroke in COVID-19: a systematic review and meta-analysis. *Int J Stroke.* (2021) 16:137–49. doi: 10.1177/1747493020972922
20. Smeeth L, Thomas SL, Hall AJ, Hubbard R, Farrington P, Vallance P. Risk of myocardial infarction and stroke after acute infection or vaccination. *New Engl J Med.* (2004) 351:2611–8. doi: 10.1056/NEJMoa041747
21. Warren-Gash C, Blackburn R, Whitaker H, McMenamin J, Hayward AC. Laboratory-confirmed respiratory infections as triggers for acute myocardial infarction and stroke: a self-controlled case series analysis of national linked datasets from Scotland. *Euro Respirat J.* (2018) 18:51. doi: 10.1183/13993003.01794-2017
22. Bikdeli B, Madhavan MV, Jimenez D, Chuich T, Dreyfus I, Driggin E, et al. COVID-19 and thrombotic or thromboembolic disease: implications for prevention, antithrombotic therapy, and follow-up: JACC state-of-the-art review. *J Am Coll Cardiol.* (2020) 75:2950–73. doi: 10.1016/j.jacc.2020.04.031
23. Bénézit F, Le Turnier P, Declerck C, Paillé C, Revest M, Dubée V, et al. Utility of hyposmia and hypogeusia for the diagnosis of COVID-19. *Lancet Infect Dis.* (2020) 20:1014–5. doi: 10.1016/S1473-3099(20)30297-8
24. Lechien JR, Chiesa-Estomba CM, De Siati DR, Horoi M, Le Bon SD, Rodriguez A, et al. Olfactory and gustatory dysfunctions as a clinical presentation of mild-to-moderate forms of the coronavirus disease (COVID-19): a multicenter European study. *Euro Archiv Oto-Rhino-Laryngol.* (2020) 277:2251–61. doi: 10.1007/s00405-020-05965-1
25. Mustafa MWM. Audiological profile of asymptomatic Covid-19 PCR-positive cases. *Am J Otolaryngol.* (2020) 41:102483. doi: 10.1016/j.amjoto.2020.102483
26. Sriwijitalai W, Wiwanitkit V. Hearing loss and COVID-19: A note. *Am J Otolaryngol.* (2020) 41:102473. doi: 10.1016/j.amjoto.2020.102473
27. Chern A, Famuyide AO, Moonis G, Lalwani AK. Bilateral Sudden Sensorineural Hearing Loss and Intralabyrinthine Hemorrhage in a Patient With COVID-19. *Otol Neurotol.* (2021) 42:e10–4. doi: 10.1097/MAO.0000000000002860
28. Zahran M, Ghazy R, Ahmed O, Youssef A. Atypical otolaryngologic manifestations of COVID-19: a review. *Egypt J Otolaryngol.* (2021) 37:1–4. doi: 10.1186/s43163-021-00075-z
29. Giannantonio S, Scorpecci A, Montemurri B, Marsella P. Case of COVID-19-induced vestibular neuritis in a child. *BMJ Case Reports CP.* (2021) 14:e242978. doi: 10.1136/bcr-2021-242978
30. Malayala SV, Mohan G, Vasireddy D, Atluri P. A case series of vestibular symptoms in positive or suspected COVID-19 patients. *Infez Med.* (2021) 29:117–22.
31. Tan M, Cengiz DU, Demir I, Demirel S, Çolak SC, Karakaş O, et al. Effects of Covid-19 on the audio-vestibular system. *Am J Otolaryngol.* (2021) 43:103173. doi: 10.1016/j.amjoto.2021.103173
32. Dharmarajan S, Bharathi M, Sivapuram K, Prakash B, Madhan S, Madhu A, et al. Hearing Loss-a Camouflaged Manifestation of COVID 19 Infection. *Indian J Otolaryngol Head Neck Surg.* (2021) 11:1–5. doi: 10.1007/s12070-021-02581-1
33. Abdel Rhman S, Abdel Wahid A. COVID−19 and sudden sensorineural hearing loss, a case report. *Otolaryngology Case Reports.* (2020) 16:100198–100198. doi: 10.1016/j.xocr.2020.100198
34. Degen C, Lenarz T, Willenborg K. Acute Profound Sensorineural Hearing Loss After COVID-19 Pneumonia. *Mayo Clin Proc.* (2020) 95:1801–3. doi: 10.1016/j.mayocp.2020.05.034
35. Edwards M, Muzaffar J, Naik P, Coulson C. Catastrophic bilateral sudden sensorineural hearing loss following COVID-19. *BMJ Case Rep.* (2021) 14:2315. doi: 10.1136/bcr-2021-243157
36. Koumpa FS, Forde CT, Manjaly JG. Sudden irreversible hearing loss post COVID-19. *BMJ Case Rep.* (2020) 13. doi: 10.1136/bcr-2020-238419
37. Fidan V. New type of corona virus induced acute otitis media in adult. *Am J Otolaryngol.* (2020) 41:102487. doi: 10.1016/j.amjoto.2020.102487
38. Chirakkal P, Al Hail AN, Zada N, Vijayakumar DS. COVID-19 and Tinnitus. *Ear, Nose and Throat J.* (2021) 100:160S-162S. doi: 10.1177/0145561320974849
39. Kokten N, Celik S, Mutlu A, Pektas E, Icten S, Kalcioglu MT. Does COVID-19 have an impact on hearing? *Acta Otolaryngol.* (2022) 142:48–51. doi: 10.1080/00016489.2021.2020897
40. Lamounier P, Franco Gonçalves V, Ramos HVL, Gobbo DA, Teixeira RP, Dos Reis PC, et al. A 67-Year-Old Woman with Sudden Hearing Loss Associated with SARS-CoV-2 Infection. *Am J Case Rep.* (2020) 21:e927519. doi: 10.12659/AJCR.927519
41. Pokharel S, Tamang S, Pokharel S, Mahaseth RK. Sudden sensorineural hearing loss in a post-COVID-19 patient. *Clinical Case Rep.* (2021) 9:e04956. doi: 10.1002/ccr3.4956
42. Ricciardiello F, Pisani D, Viola P, Cristiano E, Scarpa A, Giannone A, et al. Sudden sensorineural hearing loss in mild covid-19: case series and analysis of the literature. *Audiol Res.* (2021) 11:313–26. doi: 10.3390/audiolres11030029
43. Daher GS, Nassiri AM, Vanichkachorn G, Carlson ML, Neff BA, Driscoll CLW. New onset tinnitus in the absence of hearing changes

following COVID-19 infection. *Am J Otolaryngol.* (2022) 43:103208. doi: 10.1016/j.amjoto.2021.103208
44. Javanbakht M, Babaee S. Tinnitus in COVID-19 Patients; a Case Study. *Iran J War Public Health.* (2021) 13:79—83. doi: 10.29252/acadpub.ijwph.13.1.79
45. Sun R, Liu H, Wang X. Mediastinal emphysema, giant bulla, and pneumothorax developed during the course of COVID-19 pneumonia. *Korean J Radiol.* (2020) 21:541. doi: 10.3348/kjr.2020.0180
46. Viola P, Ralli M, Pisani D, Malanga D, Sculco D, Messina L, et al. Tinnitus and equilibrium disorders in COVID-19 patients: preliminary results. *Euro Archiv Oto-Rhino-Laryngol.* (2021) 278:3725–30. doi: 10.1007/s00405-020-06440-7
47. Liotta EM, Batra A, Clark JR, Shlobin NA, Hoffman SC, Orban ZS, et al. Frequent neurologic manifestations and encephalopathy-associated morbidity in Covid-19 patients. *Ann Clinic Translat Neurol.* (2020) 7:2221–30. doi: 10.1002/acn3.51210
48. Sari E, Külcü NU, Erdede O, Yalçin EU, Yamanel RGS. New-Onset Dizziness Associated With COVID-19. *Pediatr Neurol.* (2021) 115:72. doi: 10.1016/j.pediatrneurol.2020.11.007
49. Vanaparthy R, Malayala SV, Balla M. COVID-19-induced vestibular neuritis, hemi-facial spasms and Raynaud's phenomenon: a case report. *Cureus.* (2020) 12. doi: 10.7759/cureus.11752
50. Maslovara S, Košec A. Post-COVID-19 benign paroxysmal positional vertigo case reports. *Medicine.* (2021) 221:555. doi: 10.1155/2021/9967555
51. Mat Q, Noël A, Loiselet L, Tainmont S, Chiesa-Estomba CM, Lechien JR, et al. Vestibular neuritis as clinical presentation of COVID-19. *Ear, Nose and Throat Journal.* (2021) 0145561321995021. doi: 10.1177/0145561321995021
52. Motawea KR, Monib FA. New Onset Vertigo After COVID-19 infection. a case report. *Indian J Otolaryngol Head Neck Surg.* (2021) 21:1–3. doi: 10.1007/s12070-021-02715-5
53. Malayala SV, Raza A. A case of COVID-19-induced vestibular neuritis. *Cureus.* (2020) 12. doi: 10.7759/cureus.8918
54. Sahin A-R, Erdogan A, Agaoglu PM, Dineri Y, Cakirci A-Y, Senel M-E, et al. 2019 novel coronavirus (COVID-19) outbreak: a review of the current literature. *EJMO.* (2020) 4:1–7. doi: 10.14744/ejmo.2020.12220
55. De Luca P, Scarpa A, Ralli M, Tassone D, Simone M, Cassandro C, et al. Auditory Disturbances and SARS-CoV-2 infection: brain inflammation or cochlear affection? systematic review and discussion of potential pathogenesis. *Front Neurol.* (2021) 12:1234. doi: 10.3389/fneur.2021.707207
56. Jafari Z, Kolb BE, Mohajerani MH. Hearing loss, tinnitus, and dizziness in COVID-19: a systematic review and meta-analysis. *Canadian J Neurologic Sci.* (2021) 21:1–33. doi: 10.1017/cjn.2021.63
57. McIntyre KM, Favre NM, Kuo CC, Carr MM. Systematic Review of Sensorineural Hearing Loss Associated With COVID-19 Infection. *Cureus.* (2021) 13. doi: 10.7759/cureus.19757
58. Cui C, Yao Q, Zhang D, Zhao Y, Zhang K, Nisenbaum E, et al. Approaching Otolaryngology Patients During the COVID-19 Pandemic. *Otolaryngol Head Neck Surg.* (2020) 163:121–31. doi: 10.1177/0194599820926144
59. Lechien JR, Chiesa-Estomba CM, Place S, Van Laethem Y, Cabaraux P, Mat Q, et al. Clinical and epidemiological characteristics of 1420 European patients with mild-to-moderate coronavirus disease 2019. *J Intern Med.* (2020) 288:335—44. doi: 10.1111/joim.13089
60. Pisani D, Leopardi G, Viola P, Scarpa A, Ricciardiello F, Cerchiai N, et al. Sudden sensorineural hearing loss after covid-19 vaccine; A possible adverse reaction? *Otolaryngol Case Rep.* (2021) 21:100384. doi: 10.1016/j.xocr.2021.100384
61. Tsetsos N, Poutoglidis A, Vlachtsis K, Kilmpasanis A, Gougousis S. Sudden Sensorineural Hearing Loss Following the Second Dose of COVID-19 Vaccine. *Cureus.* (2021) 13. doi: 10.7759/cureus.17435
62. Tseng PT, Chen TY, Sun YS, Chen YW, Chen JJ. The reversible tinnitus and cochleopathy followed first-dose AstraZeneca COVID-19 vaccination. *QJM: Int J Med.* (2021) 21:210. doi: 10.1093/qjmed/hcab210
63. Parrino D, Frosolini A, Gallo C, De Siati RD, Spinato G, de Filippis C. Tinnitus following COVID-19 vaccination: report of three cases. *Int J Audiol.* (2021) 21:1–4. doi: 10.1080/14992027.2021.1931969
64. Briggs SE, Brenner MJ, Chandrasekhar SS. Sudden Sensorineural Hearing Loss and COVID-19 Vaccination. *JAMA Otolaryngol Head Neck Surg.* (2021) 21:3384. doi: 10.1001/jamaoto.2021.3384
65. Ciorba A, Bianchini C, Caranti A, Skarzyński PH, Pelucchi S, Hatzopoulos S. Incidence of audiological adverse effects induced by COVID-19 Vaccines: a preliminary study. *Ear Nose Throat J.* (2021) 21:01455613211048975. doi: 10.1177/01455613211048975
66. Formeister EJ, Chien W, Agrawal Y, Carey JP, Stewart CM, Sun DQ. Preliminary Analysis of Association Between COVID-19 Vaccination and Sudden Hearing Loss Using US Centers for Disease Control and Prevention Vaccine Adverse Events Reporting System Data. *JAMA Otolaryngol Head Neck Surg.* (2021) 21:869. doi: 10.1001/jamaoto.2021.0869
67. Jeong J, Choi HS. Sudden sensorineural hearing loss after COVID-19 vaccination. *Int J Infectious Dis.* (2021) 113:341–3. doi: 10.1016/j.ijid.2021.10.025
68. Wichova H, Miller ME, Derebery MJ. Otologic manifestations after COVID-19 vaccination: the house ear clinic experience. *Otol Neurotol.* (2021) 42:e1213. doi: 10.1097/MAO.0000000000003275
69. Mao L, Jin H, Wang M, Hu Y, Chen S, He Q, et al. Neurologic manifestations of hospitalized patients with coronavirus disease 2019 in Wuhan, China. *JAMA Neurol.* (2020) 77:683–90. doi: 10.1001/jamaneurol.2020.1127
70. Chen T, Wu D, Chen H, Yan W, Yang D, Chen G, et al. Clinical characteristics of 113 deceased patients with coronavirus disease 2019: retrospective study. *Bmj.* (2020) 368:m1091. doi: 10.1136/bmj.m1091
71. Saniasiaya J, Kulasegarah J. Dizziness and COVID-19. *Ear, Nose Throat J.* (2021) 100:29–30. doi: 10.1177/0145561320959573
72. Rosenhall U, Kankkunen A. Hearing alterations following meningitis. 1. Hearing improvement. *Ear Hear.* (1980) 1:185–90. doi: 10.1097/00003446-198007000-00002
73. Cohen BE, Durstenfeld A, Roehm PC. Viral causes of hearing loss: a review for hearing health professionals. *Trends Hear.* (2014) 18:2331216514541361. doi: 10.1177/2331216514541361
74. Young Y-H. Contemporary review of the causes and differential diagnosis of sudden sensorineural hearing loss. *Int J Audiol.* (2020) 59:243–53. doi: 10.1080/14992027.2019.1689432
75. Desforges M, Le Coupanec A, Dubeau P, Bourgouin A, Lajoie L, Dubé M, et al. Human coronaviruses and other respiratory viruses: underestimated opportunistic pathogens of the central nervous system? *Viruses.* (2020) 12:14. doi: 10.3390/v12010014
76. Li YC, Bai WZ, Hashikawa T. The neuroinvasive potential of SARS-CoV2 may play a role in the respiratory failure of COVID-19 patients. *J Med Virol.* (2020) 92:552–5. doi: 10.1002/jmv.25728
77. Hung EC, Chim SS, Chan PK, Tong YK, Ng EK, Chiu RW, et al. Detection of SARS coronavirus RNA in the cerebrospinal fluid of a patient with severe acute respiratory syndrome. *Clin Chem.* (2003) 49:2108. doi: 10.1373/clinchem.2003.025437
78. Lau K-K, Yu W-C, Chu C-M, Lau S-T, Sheng B, Yuen K-Y. Possible central nervous system infection by SARS coronavirus. *Emerg Infect Dis.* (2004) 10:342. doi: 10.3201/eid1002.030638
79. Baig AM, Khaleeq A, Ali U, Syeda H. Evidence of the COVID-19 virus targeting the CNS: tissue distribution, host–virus interaction, and proposed neurotropic mechanisms. *ACS Chem Neurosci.* (2020) 11:995–8. doi: 10.1021/acschemneuro.0c00122
80. Chen R, Wang K, Yu J, Howard D, French L, Chen Z, et al. The spatial and cell-type distribution of SARS-CoV-2 receptor ACE2 in the human and mouse brains. *Front Neurol.* (2021) 11:1860. doi: 10.3389/fneur.2020.573095
81. Krasniqi S, Daci A. Role of the angiotensin pathway and its target therapy in epilepsy management. *Int J Mol Sci.* (2019) 20:726. doi: 10.3390/ijms20030726
82. Saniasiaya J. Hearing loss in SARS-CoV-2: what do we know? *Ear, Nose Throat J.* (2021) 100:152S-154S. doi: 10.1177/0145561320946902
83. Butowt R, von Bartheld CS. <? covid19?> Anosmia in COVID-19: Underlying Mechanisms and Assessment of an Olfactory Route to Brain Infection. *The Neuroscientist.* (2020) 20:1073858420956905. doi: 10.1177/1073858420956905
84. McCray PBJr, Pewe L, Wohlford-Lenane C, Hickey M, Manzel L, Shi L, et al. Lethal infection of K18-hACE2 mice infected with severe acute respiratory syndrome coronavirus. *J Virol.* (2007) 81:813–21. doi: 10.1128/JVI.02012-06
85. Netland J, Meyerholz DK, Moore S, Cassell M, Perlman S. Severe acute respiratory syndrome coronavirus infection causes neuronal death in the

absence of encephalitis in mice transgenic for human ACE2. *J Virol.* (2008) 82:7264–75. doi: 10.1128/JVI.00737-08
86. Rhea EM, Logsdon AF, Hansen KM, Williams LM, Reed MJ, Baumann KK, et al. The S1 protein of SARS-CoV-2 crosses the blood–brain barrier in mice. *Nat Neurosci.* (2021) 24:368–78. doi: 10.1038/s41593-020-00771-8
87. Achar A, Ghosh C. COVID-19-Associated neurological disorders: the potential route of CNS invasion and blood-brain barrier relevance. *Cells.* (2020) 9:2360. doi: 10.3390/cells9112360
88. Buzhdygan TP, DeOre BJ, Baldwin-Leclair A, Bullock TA, McGary HM, Khan JA, et al. The SARS-CoV-2 spike protein alters barrier function in 2D static and 3D microfluidic in-vitro models of the human blood–brain barrier. *Neurobiol Dis.* (2020) 146:105131. doi: 10.1016/j.nbd.2020.105131
89. Burks SM, Rosas-Hernandez H, Ramirez-Lee MA, Cuevas E, Talpos JC. Can SARS-CoV-2 infect the central nervous system *via* the olfactory bulb or the blood-brain barrier? *Brain, Behavior, and Immun*. (2021) 21:31. doi: 10.1016/j.bbi.2020.12.031
90. Welcome MO, Mastorakis NE. Neuropathophysiology of coronavirus disease 2019: neuroinflammation and blood brain barrier disruption are critical pathophysiological processes that contribute to the clinical symptoms of SARS-CoV-2 infection. *Inflammopharmacology.* (2021) 2:1–25. doi: 10.1007/s10787-021-00806-x
91. Aid M, Busman-Sahay K, Vidal SJ, Maliga Z, Bondoc S, Starke C, et al. Vascular disease and thrombosis in SARS-CoV-2-infected rhesus macaques. *Cell.* (2020) 183:1354–66. e1313. doi: 10.1016/j.cell.2020.10.005
92. Helms J, Tacquard C, Severac F, Leonard-Lorant I, Ohana M, Delabranche X, et al. High risk of thrombosis in patients with severe SARS-CoV-2 infection: a multicenter prospective cohort study. *Intensive Care Med.* (2020) 46:1089–98. doi: 10.1007/s00134-020-06062-x
93. Kashi M, Jacquin A, Dakhil B, Zaimi R, Mahé E, Tella E, et al. Severe arterial thrombosis associated with Covid-19 infection. *Thromb Res.* (2020) 192:75–7. doi: 10.1016/j.thromres.2020.05.025
94. Mackman N, Antoniak S, Wolberg AS, Kasthuri R, Key NS. Coagulation abnormalities and thrombosis in patients infected with SARS-CoV-2 and other pandemic viruses. *Arterioscler Thromb Vasc Biol.* (2020) 40:2033–44. doi: 10.1161/ATVBAHA.120.314514
95. Mowla A, Shakibajahromi B, Shahjouei S, Borhani-Haghighi A, Rahimian N, Baharvahdat H, et al. Cerebral venous sinus thrombosis associated with SARS-CoV-2; a multinational case series. *J Neurol Sci.* (2020) 419:117183. doi: 10.1016/j.jns.2020.117183
96. Nougier C, Benoit R, Simon M, Desmurs-Clavel H, Marcotte G, Argaud L, et al. Hypofibrinolytic state and high thrombin generation may play a major role in SARS-COV2 associated thrombosis. *J Thrombosis Haemostasis.* (2020) 18:2215–9. doi: 10.1111/jth.15016
97. Cure E, Cure MC. Comment on "Hearing loss and COVID-19: a note". *Am J Otolaryngol.* (2020) 41:102513. doi: 10.1016/j.amjoto.2020.102513
98. Jeong M, Ocwieja KE, Han D, Wackym PA, Zhang Y, Brown A, et al. Direct SARS-CoV-2 infection of the human inner ear may underlie COVID-19-associated audiovestibular dysfunction. *Commun Med.* (2021) 1:1–14. doi: 10.1038/s43856-021-00044-w
99. Bortoli R, Santiago M. Chloroquine ototoxicity. *Clin Rheumatol.* (2007) 26:1809–10. doi: 10.1007/s10067-007-0662-6
100. Cianfrone G, Pentangelo D, Cianfrone F, Mazzei F, Turchetta R, Orlando MP, et al. Pharmacological drugs inducing ototoxicity, vestibular symptoms and tinnitus: a reasoned and updated guide. *Eur Rev Med Pharmacol Sci.* (2011) 15:601–36.
101. Kakuda TN. Pharmacology of nucleoside and nucleotide reverse transcriptase inhibitor-induced mitochondrial toxicity. *Clin Ther.* (2000) 22:685–708. doi: 10.1016/S0149-2918(00)90004-3
102. Thein P, Kalinec GM, Park C, Kalinec F. In vitro assessment of antiretroviral drugs demonstrates potential for ototoxicity. *Hear Res.* (2014) 310:27–35. doi: 10.1016/j.heares.2014.01.005

Conflict of Interest: The authors declare that the research was conducted in the absence of any commercial or financial relationships that could be construed as a potential conflict of interest.

Publisher's Note: All claims expressed in this article are solely those of the authors and do not necessarily represent those of their affiliated organizations, or those of the publisher, the editors and the reviewers. Any product that may be evaluated in this article, or claim that may be made by its manufacturer, is not guaranteed or endorsed by the publisher.

Copyright © 2022 Kaliyappan, Chen and Krishnan Muthaiah. This is an open-access article distributed under the terms of the Creative Commons Attribution License (CC BY). The use, distribution or reproduction in other forums is permitted, provided the original author(s) and the copyright owner(s) are credited and that the original publication in this journal is cited, in accordance with accepted academic practice. No use, distribution or reproduction is permitted which does not comply with these terms.

frontiers in Neurology

ORIGINAL RESEARCH
published: 21 March 2022
doi: 10.3389/fneur.2022.856472

Patterns of Vestibular Impairment in Bilateral Vestibulopathy and Its Relation to Etiology

Lisa van Stiphout[1†], Maksim Pleshkov[1,2*†], Florence Lucieer[1], Bieke Dobbels[3], Vergil Mavrodiev[4], Nils Guinand[5], Angelica Pérez Fornos[5], Josine Widdershoven[1,3], Michael Strupp[4], Vincent Van Rompaey[3] and Raymond van de Berg[1]*

[1] Division of Balance Disorders, Department of Otorhinolaryngology and Head and Neck Surgery, School for Mental Health and Neuroscience, Maastricht University Medical Center, Maastricht, Netherlands, [2] Faculty of Physics, Tomsk State University, Tomsk, Russia, [3] Department of Otorhinolaryngology and Head and Neck Surgery, Faculty of Medicine and Health Sciences, Antwerp University Hospital, University of Antwerp, Antwerp, Belgium, [4] Department of Neurology and German Center for Vertigo, Ludwig-Maximilians University, Munich, Germany, [5] Service of Otorhinolaryngology Head and Neck Surgery, Department of Clinical Neurosciences, Geneva University Hospitals, Geneva, Switzerland

OPEN ACCESS

Edited by:
Leonardo Manzari,
MSA ENT Academy Center, Italy

Reviewed by:
Alexander A. Tarnutzer,
University of Zurich, Switzerland
Nicolas Perez-Fernandez,
University Clinic of Navarra, Spain
Chisato Fujimoto,
The University of Tokyo, Japan

****Correspondence:***
Lisa van Stiphout
lisa.van.stiphout@mumc.nl
Maksim Pleshkov
pankerams@gmail.com

† These authors share first authorship

Specialty section:
This article was submitted to Neuro-Otology, a section of the journal Frontiers in Neurology

Received: *17 January 2022*
Accepted: *17 February 2022*
Published: *21 March 2022*

Citation:
van Stiphout L, Pleshkov M, Lucieer F, Dobbels B, Mavrodiev V, Guinand N, Pérez Fornos A, Widdershoven J, Strupp M, Van Rompaey V and van de Berg R (2022) Patterns of Vestibular Impairment in Bilateral Vestibulopathy and Its Relation to Etiology. Front. Neurol. 13:856472. doi: 10.3389/fneur.2022.856472

Objective: This study aimed to investigate (1) the patterns of vestibular impairment in bilateral vestibulopathy (BVP) and subsequently, the implications regarding patient eligibility for vestibular implantation, and (2) whether this pattern and severity of vestibular impairment is etiology dependent.

Methods: A total of one hundred and seventy-three subjects from three tertiary referral centers in Europe were diagnosed with BVP according to the Bárány Society diagnostic criteria. The subjects underwent vestibular testing such as the caloric test, torsion swing test, video Head Impulse Test (vHIT) in horizontal and vertical planes, and cervical and/or ocular vestibular evoked myogenic potentials (c- and oVEMPs). The etiologies were split into idiopathic, genetic, ototoxicity, infectious, Menière's Disease, (head)trauma, auto-immune, neurodegenerative, congenital, and mixed etiology.

Results: The caloric test and horizontal vHIT more often indicated horizontal semicircular canal impairment than the torsion swing test. The vHIT results showed significantly higher gains for both anterior canals compared with the horizontal and posterior canals ($p < 0.001$). The rates of bilaterally absent oVEMP responses were higher compared to the bilaterally absent cVEMP responses ($p = 0.010$). A total of fifty-four percent of the patients diagnosed with BVP without missing data met all three Bárány Society diagnostic test criteria, whereas 76% of the patients were eligible for implantation according to the vestibular implantation criteria. Regarding etiology, only horizontal vHIT results were significantly lower for trauma, neurodegenerative, and genetic disorders, whereas the horizontal vHIT results were significantly higher for Menière's Disease, infectious and idiopathic BVP. The exploration with hierarchical cluster analysis showed no significant association between etiology and patterns of vestibular impairment.

Conclusion: This study showed that caloric testing and vHIT seem to be more sensitive for measuring vestibular impairment, whereas the torsion swing test is more suited for measuring residual vestibular function. In addition, no striking patterns of vestibular impairment in relation to etiology were found. Nevertheless, it was demonstrated

that although the implantation criteria are stricter compared with the Bárány Society diagnostic criteria, still, 76% of patients with BVP were eligible for implantation based on the vestibular test criteria. It is advised to carefully examine every patient for their overall pattern of vestibular impairment in order to make well-informed and personalized therapeutic decisions.

Keywords: bilateral vestibulopathy, etiology, vestibular implantation, preclinical implantation criteria, Bárány Society diagnostic criteria, vestibular impairment, patterns

INTRODUCTION

Bilateral vestibulopathy (BVP) is a chronic disease which is characterized by bilaterally reduced or absent vestibular function due to deficits of the vestibular organs, the vestibular nerves, and/or the brain (1–3). Patients typically suffer from imbalance, worsening in the dark and/or on uneven ground, and movement-induced blurred vision (oscillopsia) (4). BVP also leads to additional symptoms such as an increased risk of falling, cognitive deficits, impairment of navigation and spatial memory, autonomic dysfunction, anxiety, and depression (4–11). Consequently, BVP leads to reduced quality of life and imposes a significant socioeconomic burden on society (12–14). BVP appears to be a heterogeneous disorder with various clinical characteristics and multiple identified etiologies, such as ototoxicity (e.g., gentamicin exposure), genetic disorders (e.g., DFNA9), Menière's Disease, infectious causes (e.g., meningitis), neurodegenerative and inherited syndromes (e.g., CANVAS), autoimmunity (e.g., Cogan's syndrome), or trauma (2, 15–23). Nonetheless, the reported percentages of idiopathic BVP vary between 20-75%, indicating that identifying the etiology can be challenging (2, 13, 15, 18, 24).

To date, the prognosis for the recovery of vestibular function is poor and the effective treatment for BVP is missing (18, 25–27). However, different research groups are in the process of developing a clinically applicable vestibular implant that might be able to address at least the major symptoms of BVP (28–35). Despite reaching important milestones in the development of the vestibular implant, many questions remain, and in order to develop a clinically useful device, it is crucial to gain a better understanding of the underlying disease BVP.

So far, it remains unclear which factors contribute to the severity of the vestibular impairment. The current diagnostic criteria for BVP are primarily based on the function of the horizontal semicircular canals (e.g., caloric test, video Head Impulse Test (vHIT), and torsion swing test) (3). However, recent studies have highlighted the varying pattern of impairment of the other vestibular sensors in patients with BVP (i.e., the otolith organs and the anterior and posterior semicircular canals) (24, 36–42). For example, anterior semicircular canal sparing was found in aminoglycoside-related BVP due to bilateral Menière's Disease and in idiopathic BVP (24, 39, 42). Ocular vestibular evoked myogenic potentials, most likely reflecting utricular function, showed to be the most impaired in aminoglycoside-related BVP and the least impaired in BVP due to bilateral Menière's Disease (38). An evidently rare subtype of idiopathic BVP was proposed in which the saccular function was impaired in the presence of normal functioning horizontal semicircular canals (37), while another study showed that horizontal semicircular canal function was more often affected than saccular function in aminoglycoside-related BVP (41).

All studies mentioned above either included small patient groups, retrospectively analyzed the data, did not always include patients with BVP according to the Bárány Society criteria, or investigated only one or two of the vestibular sensors. To date, no studies investigated the pattern of vestibular impairment of all vestibular sensors with relatively large patient groups, while recently published vestibular implantation criteria developed for research settings take all vestibular sensors into consideration. According to these criteria, for instance, all vestibular tests (i.e., caloric test, horizontal and vertical vHIT, and torsion swing test) need to show a significantly impaired function in order to qualify as a vestibular implant candidate (43).

This study provides a description of vestibular function, in a large cohort of patients with BVP diagnosed according to the Bárány Society criteria. The objective was to 1) investigate the patterns of vestibular impairment in BVP in general, and subsequently, the implications regarding patient eligibility for vestibular implantation, and 2) investigate whether the pattern and severity of vestibular impairment depend on the etiology.

METHODS

Subjects

Study subjects were recruited from three tertiary referral centers in The Netherlands, Belgium, and Germany: The Department of Otorhinolaryngology and Head and Neck surgery from Maastricht University Medical Center (MUMC+, center 1) and Antwerp University Hospital (UZA, center 2), and the Department of Neurology and the German Center for Vertigo and Balance Disorders, Ludwig Maximilians University Munich (LMU, center 3). Enrolled subjects were diagnosed with BVP in accordance with the BVP diagnostic criteria, which included unsteadiness and/or oscillopsia during walking or head movements, and a reduced bithermal caloric response (sum of the bithermal maximal peak slow phase velocity $<6°$/s bilaterally) and/or a bilaterally reduced horizontal vHIT gain of <0.6, and/or a vestibulo-ocular reflex (VOR) gain <0.1 during torsion swing test at 0.1 Hz (3). In center 1 and center 2, all patients diagnosed with BVP at the outpatient clinic of the Department of Otorhinolaryngology were asked to participate in the study. These studies consisted of a full day of clinical testing [e.g., caloric

test, horizontal and vertical vHIT, torsion swing test, ocular vestibular evoked myogenic potentials (oVEMP), and/or cervical vestibular evoked myogenic potentials (cVEMP)]. In center 3, all patients presented with BVP at the outpatient clinic of the Department of Neurology within the study period were included in the study. Subjects below the age of 18 and subjects who were not able to stop vestibulosuppressive medication were excluded from participation in this study.

Vestibular Testing

All centers performed vestibular testing to confirm a BVP diagnosis, although the number of tests performed differed between centers. In center 1, vestibular testing included electronystagmography with caloric and rotatory chair testing, as well as horizontal and vertical vHIT and c- and oVEMPs. In center 2, subjects underwent electronystagmography with caloric and rotatory chair testing, horizontal and vertical vHIT, and cVEMPs. In center 3, videonystagmography with caloric testing was performed, together with a horizontal vHIT. An overview of different tests performed in each center is shown in **Supplementary Table 1** of the supplementary materials (SM).

The Caloric Test

An extensive description of caloric testing was described previously (44). To summarize, in all centers, bithermal caloric testing was performed in both ears whilst patients were in supine position with a forward head inclination of 30°. Each irrigation lasted 30 s with a volume of at least 250 ml of water in centers 1 and 2 and at least 100 ml of water in center 3, for both cold (30°C) and warm (44°C) irrigations with a 5-min stimulus interval between irrigations (Variotherm Plus device, Atmos Medizin Technik GmbH, Lenzkirch, Germany for all three centers). Eye movements were recorded using electronystagmography with self-adhesive electrodes at centers 1 and 2 (Blue sensor, Ambu, Denmark) and with videonystagmography at center 3 (Interacoustics, Munich, Germany). The maximum peak slow phase eye velocity at the culmination phase (°/s) was measured (KingsLab 1.8.1, Maastricht University, Maastricht, The Netherlands at center 1; Nystagliner, Toennies, Germany at center 2; Interacoustics, Munich, Germany at center 3).

Torsion Swing Test

During the torsion swing test, patients were seated in a servo-controlled rotatory chair in complete darkness with their eyes open (Ekida GmbH, Buggingen, Germany at center 1 and ServoMed AB, Varberg, Sweden at center 2). Sinusoidal rotatory stimulation was performed at 0.1 Hz at center 1 and 0.05 Hz at center 2 with a peak velocity of 60°/s. Again, eye movements were recorded with electronystagmography with self-adhesive electrodes (Blue sensor, Ambu, Denmark in both center 1 and 2) and the VOR gain was calculated as the ratio between peak eye velocity and peak head velocity (KingsLab 1.8.1, Maastricht University, Maastricht, The Netherlands at center 1; Nystagliner, Toennies, Germany at center 2).

Video Head Impulse Test

The horizontal vHIT and the vHIT in the Right-Anterior-Left-Posterior (RALP) and Left-Anterior-Right-Posterior (LARP) canal planes were performed using the Video-Head Impulse Test device from Otometrics at center 1 and 2 (Otometrics, Taastrup, Denmark). At center 3, horizontal vHIT was performed using the Eye-SeeCam (Interacoustics, Munich, Germany). The testing method was described previously (45, 46). In brief, the technician stood behind the subject (who was sitting on a static chair) and held their head firmly without touching the goggles. The subject was instructed to maintain visual fixation on an earth-fixed target at a distance of 2 m at centers 1 and 2 and 1.8 m at center 3. Head impulses comprised fast unpredictable, low-amplitude (±20°) head movements in the horizontal plane (all three centers, peak head velocity >150°/s) and in the RALP and LARP planes (center 1 and 2, peak head velocity >100°/s). The Otometrics system defines the VOR gain as the ratio of the area under the eye velocity curve to the area under the head velocity curve from the impulse onset until the head velocity drops to zero again (47). The inter-acoustics system divides the eye and head velocity at a certain point in time (around 60 ms after impulse onset) (46).

Vestibular-Evoked Myogenic Potentials

Both centers 1 and 2 used the Neuro-Audio system with electromyographic software (v2010, Neurosoft, Ivanovo, Russia) and self-adhesive electrodes (Blue sensor, Ambu, Denmark) to record the o- and/or c-VEMPS. cVEMPs were measured over the sternocleidomastoid muscle after stimulating the ipsilateral vestibular organ with air-conducted tone bursts of 500 Hz, provided via inserted earphones at a stimulation rate of 13 Hz. oVEMPs were measured over the inferior oblique muscle after stimulating the contralateral vestibular organ with the same stimulation parameters as for cVEMPs. Details on the procedure have been published previously (44, 48, 49). In brief, for cVEMPS, subjects were in a supine position with their back tilted at an angle of 30° from the horizontal plane and were instructed to turn their head away from the stimulus and to lift their head up slightly. A total of 200 EMG traces with a minimum rectified voltage of 65 μv and a maximum rectified voltage of 205 μv were accepted. A visual feedback system (v2010, Neurosoft, Ivanovo, Russia) provided patient feedback to maintain correct muscle contraction. For oVEMPS, subjects were in a supine position and were instructed to keep their gaze fixed on a focus point 30 degrees behind the head to achieve superomedial gaze. A minimum of 300 EMG traces were accepted.

Vestibular-evoked myogenic potentials (VEMPs) were first recorded starting at maximum stimulus intensities of 130 dB sound pressure level (SPL) (center 1) or 95 dB hearing level (HL) (center 2). Then recordings were attempted again using stimulus amplitudes successively decreasing by 5 dB at each step. Thresholds were determined in consensus between two independent technicians at the level where a biphasic wave response was present. When no typical biphasic wave was found at 130 dB SPL at center 1 or 95 dB HL at center 2, a patient was considered to have an absent c- or oVEMP response.

Data Collection, Processing, and Analysis

The caloric test was performed in all three centers. The torsion swing test was performed in centers 1 and 2, but at different frequencies (0.1 and 0.05 Hz respectively). Since the frequency of sinusoidal rotatory stimulation at center 2 differed from the frequency stated in the BVP diagnostic criteria, the patients from center 2 were not included in this analysis based on their VOR gain measured during the torsion swing test alone. As described above, the horizontal vHIT was performed in all three centers, vertical vHIT and cVEMPs in centers 1 and 2, and oVEMPs only in center 1. Therefore, the amount of data available for analysis differed between tests.

IBM SPSS Statistics version 25 (Armonk, NY: IBM Corp.) and R version 3.5.2 (R Foundation for Statistical Computing, Vienna, Austria) were used for data analysis. Descriptive statistics were used to describe the basic features of the data (e.g., percentages). Non-parametric methods were applied to determine the significant differences between the test results (e.g., Kruskal Wallis H test with *post hoc* Dunn's test and Mann-Whitney *U* test). *P*-values ≤ 0.05 were considered significant and were adjusted and reported with Benjamini-Hochberg correction for multiple testing. Fisher's exact test and the Chi-squared test were used to compare proportions of categorical outcomes.

Before the data was analyzed extensively, it was checked whether the data between the centers could be pooled. Caloric test results differed between the three centers ($\chi 2(2) = 40.8$, $p < 0.001$), therefore, the data could not be pooled. The torsion swing test results from center 1 and center 2 could not be pooled since the frequency of sinusoidal rotatory stimulation at center 1 (0.1 Hz) differed from center 2 (0.05 Hz) and the results were significantly different (Mann-Whitney U = 1,954.5, $p = 0.002$). No significant differences for vHIT results between centers for five out of six semicircular canals were found (Kruskal-Wallis H test, $p > 0.05$). The left horizontal canal showed a significant difference between centers ($\chi 2(2) = 7.2$, $p = 0.029$), however the Levene's test for homogeneity of variance did not show a significant difference ($F = 1.32$, $p = 0.192$). Therefore, the vHIT results of all centers were pooled per canal.

The VEMP results were categorized in absent vs. present responses (i.e., when no typical biphasic wave was found at 130 dB SPL at center 1 or 95 dB HL at center 2, a patient was considered to have an absent c- or oVEMP response). cVEMPs were analyzed for each center separately since 1) the decibel measurement level differed between center 1 (dB SPL) and center 2 (dB HL) and 2) the Chi-squared test showed that there was a significant association between centers and absent vs. present cVEMP responses ($\chi(2) = 8.57$, $p = 0.014$).

To investigate the patterns of vestibular impairment in BVP in general, the vestibular test results were first analyzed using descriptive statistics to describe the basic features of the data. Subsequently, the results were interpreted according to the Bárány diagnostic criteria for BVP, which included a reduced bithermal caloric response (sum of bithermal maximal peak slow phase velocity $<6°$/s bilaterally) and/or a VOR gain <0.1 during the torsion swing test at 0.1 Hz and/or a bilaterally reduced horizontal vHIT gain of <0.6 (3). To investigate patient eligibility for vestibular implantation regarding the results from vestibular reflex testing, vestibular test results were interpreted according to the vestibular implantation criteria, which included a bilaterally reduced or absent angular VOR function documented by at least one of the major criteria and all minor criteria (i.e., in case only one or two major criteria were met, the remaining tests should comply the minor criteria). The major criteria included a reduced bithermal caloric response (sum of bithermal maximal peak slow phase velocity $\leq 6°$/s bilaterally), a reduced horizontal VOR gain ≤ 0.1 during the torsion swing test at 0.1 Hz, and a pathological horizontal VOR gain ≤ 0.6 bilaterally with at least one vertical VOR gain <0.7 bilaterally, measured with vHIT. The minor criteria included a reduced bithermal caloric response (sum of bithermal maximal peak slow phase velocity $<10°$/s bilaterally), a reduced horizontal VOR gain <0.2 during torsion swing test at 0.1 Hz, and pathological VOR gains of at least two semicircular canals <0.7 bilaterally, measured by vHIT (43).

Hierarchical cluster analysis was applied to explore and visualize patterns of vestibular impairment with respect to etiology. Cluster analysis requires complete cases (i.e., no missing data), therefore, only patients with complete data for caloric testing, torsion swing test, horizontal and vertical vHIT, cVEMPs, and oVEMPS were included (i.e., 45 patients from center 1). Before clustering, the data were standardized in Z-scores (i.e., the individual scores minus the mean, divided by the standard deviation), in order to have the variables weigh equally in the cluster analysis. Ward's method with the distance measure squared Euclidian distance was used since Ward's method has the highest agglomerative coefficient compared with the other hierarchical clustering methods. The silhouette method was used to determine the optimum number of clusters (50). Hierarchical cluster analysis resulted in two dendrograms with etiology on the x-axis and vestibular tests results on the y-axis. A heatmap was created. Each column represented one subject and each row represented the output of a specific vestibular test. A "relatively bad (vestibular) score" was illustrated by lower Z scores in the color red. A "relatively good (vestibular) score" was illustrated by higher Z scores in the color blue. After performing the analysis, etiology and patient characteristics, and vestibular test results were compared between clusters.

Ethical Considerations

The study was approved by the local ethical committee of center 1 (protocol number NL52768.068.15 / METC 151027), the local ethical committee of center 2 (protocol number 16/42/426), and the local ethical committee of center 3 (project number 20-174). The study was registered on trialregister.nl [center 1, Trial NL5446 (NTR5573)]and ClinicalTrials.gov [center 2, (NCT03690817)]. All study participants gave their written informed consent prior to inclusion in the study.

RESULTS

Patient Characteristics

A total of 173 patients (50 from center 1, 58 from center 2, and 65 from center 3, 53% males) were included in this study with a mean age of 60 ± 15 years (range 19–91 years). A diagnosis of the underlying etiology of BVP could be identified

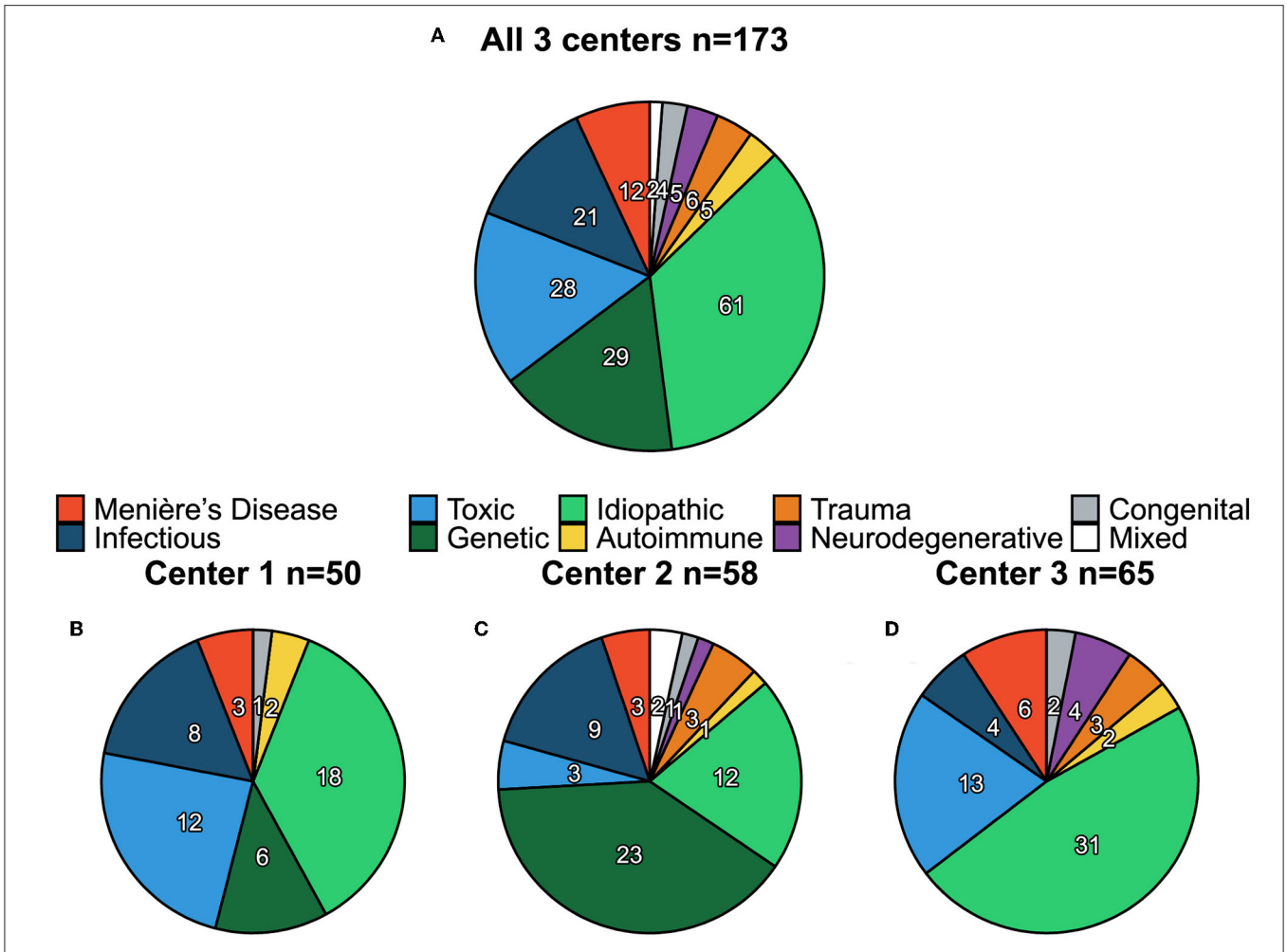

FIGURE 1 | Distribution of etiology of bilateral vestibulopathy (BVP) for all three centers combined **(A)** and per center separately **(B–D)**. Numbers shown in each pie chart represent the count (*n*) of each etiology.

in 112 out of the 173 patients. Genetic disorders ($n = 29$, 17%), ototoxicity ($n = 28$, 16%) and infectious disorders ($n = 21$, 12%) were the most common etiologies. Less frequently, the cause of BVP was due to Menière's Disease ($n = 12$, 7%), (head)trauma ($n = 6$, 4%), auto-immune disease ($n = 5$, 3%), neurodegenerative disorders ($n = 5$, 3%), or congenital disorders ($n = 4$, 2%). Two patients presented with a mixed etiology (vestibular schwannoma on one side and idiopathic etiology on the other side). In approximately one-third of the cases ($n = 61$, 35%), no underlying etiology could be identified. The distribution of etiology (**Figure 1**) was significantly different between centers (Fisher's Exact Test $p < 0.01$). A detailed overview of all etiologies is shown in **Supplementary Table 2**.

Vestibular Function

Vestibular Test Results

Median caloric test results were significantly higher for center 3 (6.2°/s) compared with centers 1 and 2 (both 0°/s) ($\chi 2(2) = 39.6$, $p < 0.001$, **Figure 2**). No significant differences were found between the median caloric test results for centers 1 and 2. The torsion swing test results from center 1 (0.1Hz) were significantly higher compared with center 2 (0.05 Hz) (Mann-Whitney $U = 1{,}954.5$, $p = 0.002$, **Figure 2**).

The vHIT results showed a median VOR gain below 0.5 for all semicircular canals, with the lowest VOR gain measured at the horizontal canals and the highest VOR gain measured at the anterior canals ($\chi 2(5) = 35.5$, $p < 0.001$, **Figure 3**). After analyzing the data separately per center, this trend was detectable in both centers 1 and 2 but only significant in center 2 after correction for multiple comparisons ($\chi 2(5) = 35.7$, $p < 0.001$, **Supplementary Figures 1, 2** and **Supplementary Table 3**).

The percentage of bilaterally absent cVEMP responses was higher in center 2 compared with center 1 (66 and 44% respectively, $\chi(2) = 8.57$, $p = 0.014$). When looking at the cVEMP and oVEMP responses at center 1, the rates of bilaterally absent oVEMP responses were higher compared to bilaterally absent cVEMP responses (74 vs. 44% respectively, $\chi(2) = 9.30$, $p = 0.010$) (**Figure 4**).

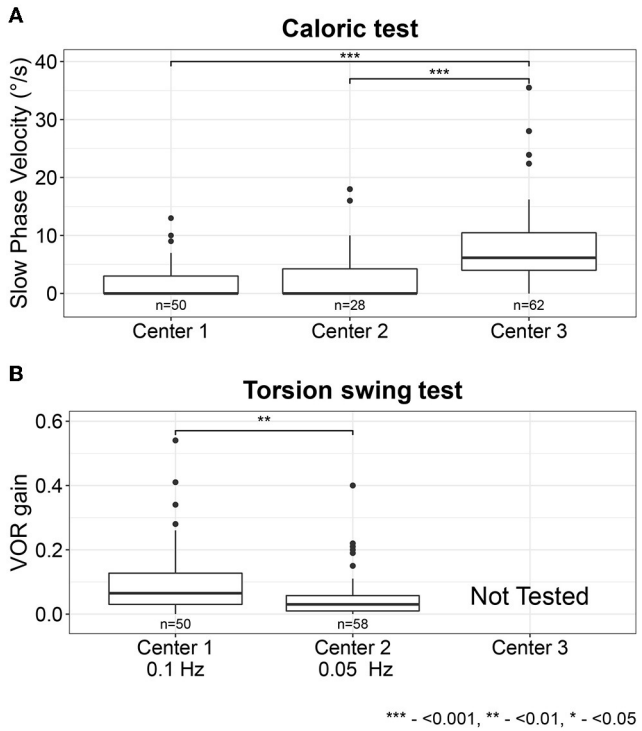

FIGURE 2 | Vestibular test results for the caloric test (sum of the bithermal maximal peak slow phase velocity bilaterally) **(A)** and torsion swing test (VOR gain) **(B)** per center. Each box plot represents the 25 to 75 percentiles, bold black lines the median, dots the outliers, and asterisks (*) illustrate statistically significant differences. Statistical significance levels: ***$p < 0.001$, **$p < 0.01$, *$p < 0.05$.

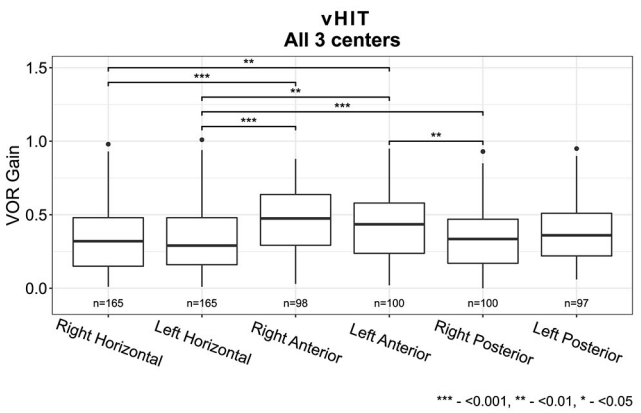

FIGURE 3 | Vestibulo-ocular reflex (VOR) gain for all six semi-circular canals measured with video Head Impulse Test for all three centers combined (Horizontal canals: center 1, 2 and 3, Vertical canals: center 1 and 2). Each box plot represents the 25 to 75 percentiles, bold black lines the median, dots the outliers, and asterisks (*) illustrate statistically significant differences.

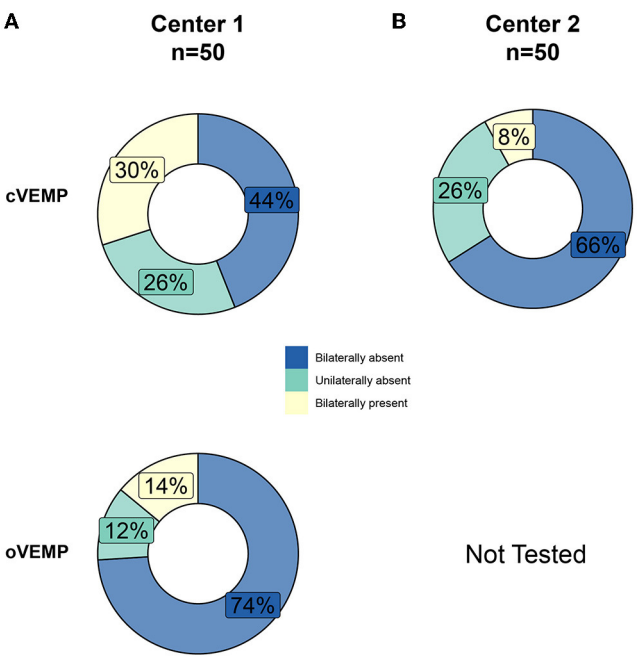

FIGURE 4 | Percentages of bilaterally absent, unilaterally absent, and bilaterally present cervical and ocular vestibular evoked myogenic potentials (cVEMPs, oVEMPs) of patients with BVP at center 1 **(A)** and center 2 **(B)**.

Vestibular Impairment According to the Bárány Diagnostic Criteria for BVP

Regarding the cases without missing data for caloric testing, torsion swing test, and horizontal vHIT, the majority of the patients (54%) met three of the criteria of the Bárány Society described earlier, whereas 21% met two of the Bárány criteria, and 25% only met one criterion. In the group of patients who met two out of three Bárány criteria, an impaired VOR gain measured with vHIT combined with a reduced caloric response was most prevalent (19%). In the group of patients who only met one of the Bárány criteria, a reduced caloric response was most prevalent (17%), followed by an impaired VOR gain measured with vHIT (6%) and torsion swing test (2%) (**Figure 5**).

When considering the total study population, the caloric test and horizontal vHIT more often indicated horizontal semicircular canal impairment than the torsion swing test (**Figure 6**). For example, in center 1 only one patient was diagnosed with BVP according to the Bárány criteria based on the torsion swing test alone, whereas the rest of the population was diagnosed with the caloric test or horizontal vHIT or both.

Patient Eligibility for Vestibular Implantation According to the Implantation Criteria

Regarding the cases without missing data for caloric testing, torsion swing test, and horizontal and vertical vHIT ($n = 45$), the majority of the patients ($n = 34$, 76%) met the implantation criteria. A total of 71% of this group met three of the major criteria, whereas 24% met two major criteria, and 6% only met one major criterion. In the group of patients who met two out of three major implantation criteria, an impaired VOR gain measured with vHIT combined with a reduced caloric response was most prevalent. In the group of patients who only met one of the major implantation criteria, a reduced

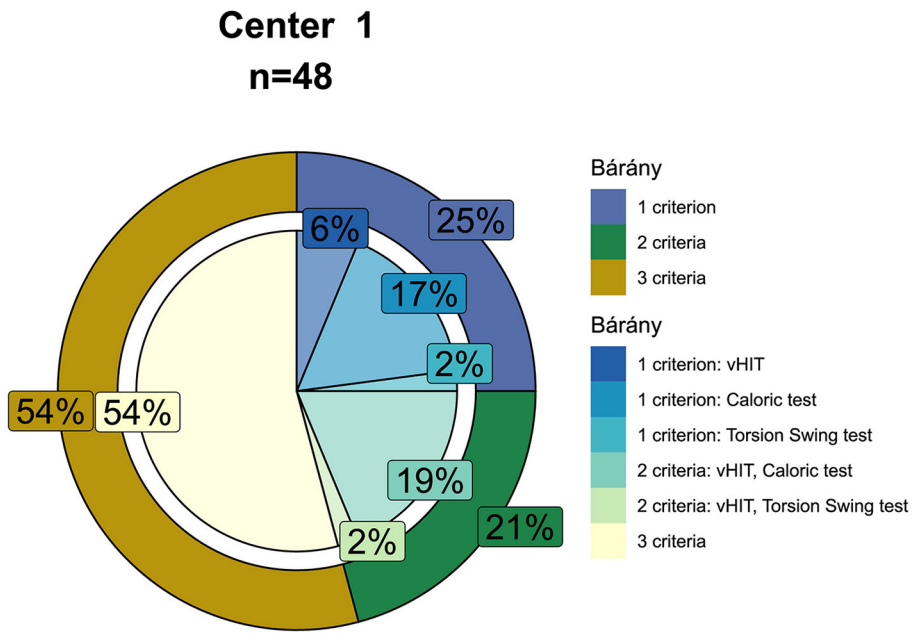

FIGURE 5 | Percentages of patients with BVP meeting one, two or three of the diagnostic criteria of the Bárány Society (shown in the outer circle, i.e., a reduced bithermal caloric response with a sum of the bithermal maximal peak slow phase velocity <6°/s bilaterally and/or a VOR gain <0.1 during torsion swing test at 0.01 Hz and/or a bilaterally reduced horizontal video Head Impulse Test gain of <0.6). The inner-circle shows the percentages of which tests are met by patients meeting one or two of the diagnostic criteria. Only cases without missing data for caloric testing, torsion swing test, and horizontal video Head Impulse Test were included (center 1, $n = 48$).

caloric response and an impaired VOR gain measured with vHIT were equally common. None of the patients only met the major implantation criteria for the torsion swing test (**Figure 7**).

Vestibular Function and Possible Relations to Underlying BVP Etiology

The median vestibular test results for caloric testing and torsion swing test did not differ between different etiologies (Kruskal-Wallis H test with *post hoc* Dunn test and Benjamini Hochberg correction $p > 0.05$, **Supplementary Tables 4, 5**). The vHIT results did not differ between etiologies for the anterior and posterior canals in the total group (Kruskal Wallis H test, $p > 0.05$, **Supplementary Table 4**). However, the horizontal vHIT results were significantly lower in the total group for neurodegenerative disorders compared with the idiopathic group, infectious disorders, Menière's Disease, and the mixed etiology group. The horizontal vHIT results were also significantly lower for genetic disorders compared with the idiopathic group and Menière's Disease. Lastly, horizontal vHIT results were significantly lower for (head)trauma compared with the idiopathic group, Menière's Disease and mixed etiology (Kruskal-Wallis H test with *post hoc* Dunn test and Benjamini Hochberg correction $p < 0.05$, **Figure 8** and **Supplementary Tables 4, 5**). After analyzing the data separately per center, some trends were detectable per center (e.g., lower horizontal vHIT results for genetic disorders in center 1 and lower horizontal vHIT results for (head)trauma in center 2), however, no significant differences were found except for lower horizontal vHIT results for neurodegenerative disorders compared with the idiopathic group and Menière's Disease in center 3 (Kruskal-Wallis H test with *post hoc* Dunn test and Benjamini Hochberg correction, **Supplementary Table 5**, **Supplementary Figure 3**).

Regarding VEMPs, the highest fraction (≥50%) of bilaterally absent cVEMP responses in center 1 was found in patients with ototoxic, infectious, autoimmune, and congenital etiologies, whereas in center 2 almost all etiologies showed high fractions (>60%) of bilaterally absent cVEMP responses (except neurodegenerative disorders). Next to this, all etiologies showed high fractions (≥50%) of bilaterally absent oVEMP responses (center 1) (**Supplementary Figures 4, 5**). No significant differences were found between the different etiologies and the proportion of patients with pathologic VEMP responses (Fisher's exact test $p = 0.52$ and $p = 0.99$ for cVEMPs centers 1 and 2 respectively and Fisher's exact test, $p = 0.36$ for oVEMPs center 1).

To investigate the pattern of vestibular impairment and its relation with etiology, hierarchical cluster analysis was performed, which resulted according to the silhouette method in two clusters (**Figure 9**). The first cluster "severe BVP" ($n = 30$; 47% female; mean age 58 years) showed overall lower median vestibular test results compared with the second cluster "moderate BVP" ($n = 15$; 60% female; mean age 60 years), which is illustrated by lower Z scores in the color red for relatively low vestibular scores and in the color blue for

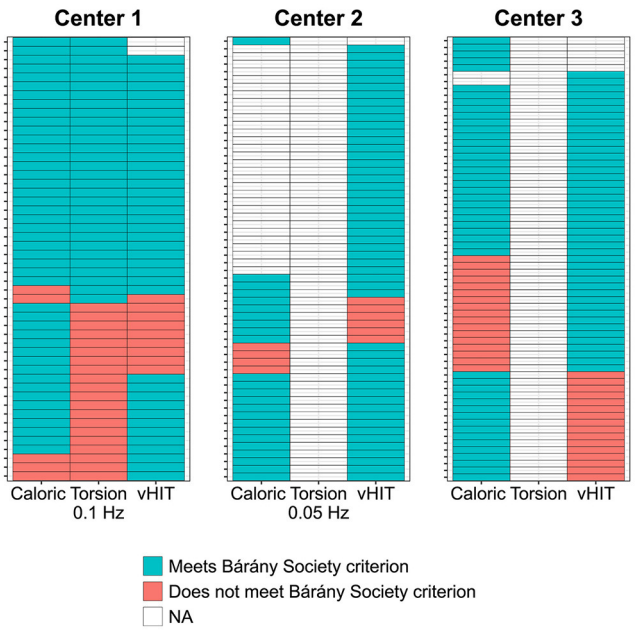

FIGURE 6 | Distribution of patients with BVP meeting the diagnostic criteria of the Bárány Society, presented for each test separately in the color blue (i.e., for the caloric test a reduced response with a sum of bithermal maximal peak slow phase velocity <6°/s bilaterally; for the torsion swing test (0.1 Hz) an impaired VOR gain <0.1; for horizontal video Head Impulse Test (vHIT) a bilaterally reduced VOR gain <0.6). Patients not meeting the diagnostic criteria for each test separately are indicated with the color red. Each column represents one of the diagnostic criteria per center; each row represents one subject per center. NA, no data available.

relatively high vestibular scores compared with the study group in **Figure 9**. This was significant for the caloric test, torsion swing test, horizontal vHIT, vertical vHIT (Mann-Whitney *U*, $p < 0.001$), and cVEMP (Fisher's Exact Test $p = 0.04$). A detailed overview of all median test results and statistics can be found in **Supplementary Tables 6, 7**. Next to this, the distribution of the amount of Bárány criteria met, was significantly different among clusters: cluster 1 "severe BVP" consisted of patients who predominantly met three criteria, whereas cluster 2 "moderate BVP" mainly included patients who only met one criterion (**Supplementary Figure 6**).

Some etiologies were more prevalent in one of the two clusters. For example, genetic disorders were more prevalent in the first cluster "severe BVP", whereas Menière's Disease was more prevalent in the second cluster "moderate BVP" (**Supplementary Figure 7**). However, no significant association between etiology and clusters was found (Fisher's Exact Test $p = 0.854$, **Supplementary Table 8**).

Next to this, some similarities in vestibular reflex tests were found in the cluster analysis (**Figure 9**, left dendrogram). It was observed that the horizontal and anterior vHITs were arranged close to each other and to caloric testing; the posterior vHIT was located close to the torsion swing test; and oVEMPs and cVEMPs formed a pair.

DISCUSSION

This study provided a description of patterns of vestibular impairment and its relation to BVP etiology in a cohort of 173 patients with BVP from 3 centers, diagnosed according to the Bárány Society criteria. Vestibular function was measured using the caloric test, torsion swing test, horizontal and vertical vHIT, cVEMPs, and/or oVEMPs. Etiologies were split into 10 separate groups (i.e., idiopathic, genetic disorders, ototoxicity, infectious disorders, Menière's Disease, (head)trauma, auto-immune disease, neurodegenerative disorders, congenital disorders, and mixed etiology). The patterns of the vestibular impairment and their relation to BVP etiology are discussed below.

Patterns of Vestibular Impairment

Overall, this study demonstrated that more than half of patients diagnosed with BVP according to the Bárány Society diagnostic criteria met all three criteria regarding vestibular testing. In patients who only met one or two of the criteria, the caloric test and horizontal vHIT criteria were most often met, in contrast to the torsion swing test criterion. The same trend was found when adhering to the vestibular implantation criteria. However, since the implantation criteria also include the vertical semicircular canals, the percentage of patients meeting the horizontal and vertical vHIT implantation criterion was lower compared with the percentage of patients meeting the horizontal vHIT diagnostic (Bárány Society) criterion. Despite the fact that the Bárány Society diagnostic criteria and vestibular implantation criteria seem to be, to some extent, similar to each other, they set different goals and have therefore several substantial differences. As stated above, the vestibular implantation criteria include all three semicircular canals. As a consequence, the vertical canal function should be considered next to the horizontal canal function. Additionally, although the major and especially the minor implantation criteria are less strict in terms of cut-off values for the caloric test, torsion swing test, and horizontal vHIT compared with the Bárány Society diagnostic criteria, a potential implant candidate must meet all the implantation criteria (**Figure 5** vs. **Figure 7**). Therefore, 76% of the patients diagnosed with BVP according to the Bárány Society diagnostic criteria were eligible for implantation according to the vestibular implantation criteria. Furthermore, apart from vestibular reflex testing, the vestibular implantation criteria also include assessment of comorbidities and eligibility to undergo surgery (43). Therefore, only a subgroup of the BVP population will be eligible for implantation.

When investigating vestibular test results per test and per center separately, it was observed that the slow phase eye velocities measured during the caloric test were significantly higher in center 3 compared with centers 1 and 2 (**Figure 2**). This can be explained by different factors, varying from differences in caloric testing methods used (namely electronystagmography at center 1 and 2 and videonystagmography at center 3) which can result in different phase velocities values due to different blink detection and image processing algorithms used (51), to different patient populations included in each center (2). Next to this, torsion swing test results were significantly higher in center

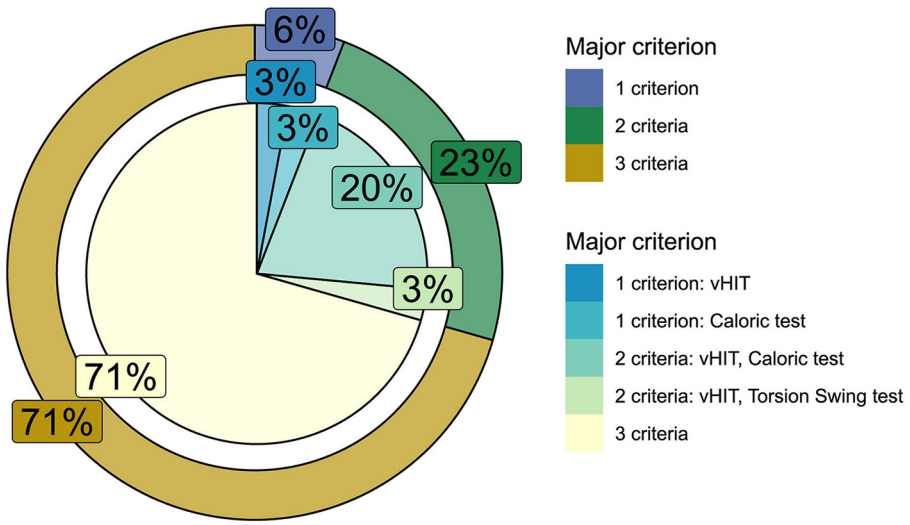

FIGURE 7 | Seventy-six percent of the patients met the criteria for vestibular implantation ($n = 34$). For this group, the outer circle shows the percentages of patients meeting one, two, or three of the major implantation criteria (i.e., for caloric testing bilateral impaired caloric responses with a sum of bithermal maximal peak slow phase velocity $\leq 6°/s$, for torsion swing test a reduced VOR gain ≤ 0.1 and for vHIT a bilaterally reduced horizontal VOR gain ≤ 0.6 combined with at least bilaterally one vertical VOR gain < 0.7). The inner-circle shows the percentages of which tests are met by patients meeting one or two of the major implantation criteria.

1 compared with center 2, which can be explained by the differences in the used frequency (0.1 Hz at center 1 and 0.05 Hz at center 2): the vestibular system is more sensitive for rotations at 0.1 Hz than 0.05 Hz, leading to a higher response (i.e., VOR gain) (2, 52, 53). This sensitivity might also account for the fact that the diagnostic torsion swing test criterion was less often met than the criteria of the caloric test. After all, since the vestibular system has its optimum sensitivity around the frequencies tested by the torsion swing test at 0.1 Hz (in contrast to the frequencies tested by the caloric test), a uniform decrease in semicircular canal function across all frequencies might result in losing responses to caloric testing first. Although frequencies tested with vHIT are also within the optimum frequency range of the vestibular system, vHIT more often indicated horizontal semicircular canal impairment than the torsion swing test. Therefore, it might be hypothesized that the vestibular system shows an impairment for conditions earlier that demand a relatively large vestibular output in response to high accelerations and velocities. This hypothesis needs further investigation. Nevertheless, the results of this study showed that the response to torsion swing testing might be preserved the longest (53). Therefore, the torsion swing test is least sensitive in detecting BVP, but most sensitive in measuring residual vestibular function, whereas caloric testing and vHIT seem to be more sensitive for measuring vestibular impairment (2).

The variability of VEMP responses in this study is in line with results from previous studies, which also demonstrated the wide range of otolith function (as measured with c- and oVEMPs) in patients with BVP (36, 38, 54). This variability could be explained by the large range of VEMP responses present in normal subjects, the heterogeneous nature of BVP, and the nature of VEMP testing itself (e.g., it is still unknown how much residual otolith function needs to be present to produce a synchronous motor discharge) (54). Furthermore, because of the diagnostic inclusion criteria, all of the included patients have horizontal semicircular canal impairment, whereas the function of the other vestibular end organs can have variable degrees of (dys)function. Since the utricle (tested with oVEMPs) projects into the superior branch of the vestibular nerve together with the horizontal semicircular canal, it can be hypothesized that patients included based on horizontal canal impairment also show bilaterally absent oVEMP responses (55). This might explain why rates of bilaterally absent oVEMP responses were higher compared to bilaterally absent cVEMP responses in center 1 (**Figure 4**) since there is possibly an intact inferior vestibular nerve function on which the saccule projects. Currently, it is not known whether isolated bilateral dysfunction of both otolith organs also causes significant disability (54). Therefore, all vestibular end organs should be evaluated before and after vestibular implantation in order to create awareness about potential damage to intact vestibular structures.

Contribution of Etiology to Vestibular Impairment

The distribution of etiologies (**Figure 1**) was significantly different among the three centers, indicating the inhomogeneity

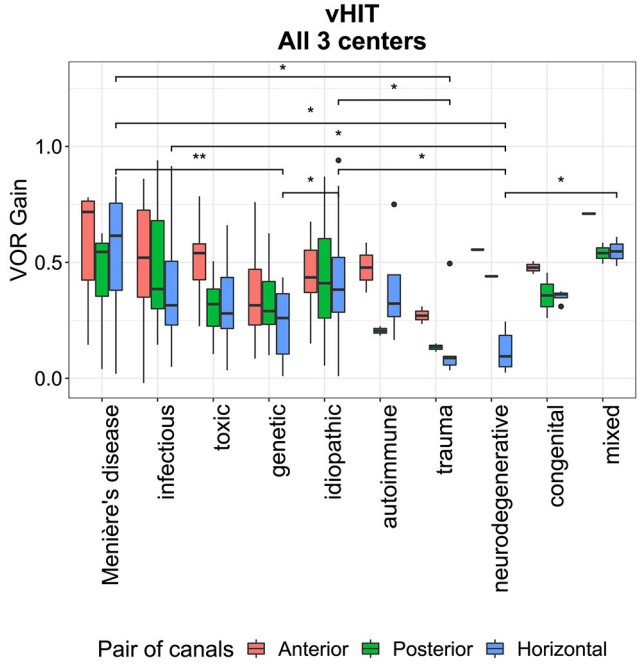

FIGURE 8 | Vestibular Ocular Reflex (VOR) gain per etiology for all three pairs of semi-circular canals (i.e., horizontal, anterior, and posterior canals) measured with video Head Impulse Test, presented for all three centers combined. Each box plot represents the 25–75 percentiles, bold black lines the median, dots the outliers and asterisks (*) illustrate statistically significant differences.

of the data. This can potentially be caused by differences in clinical settings, namely ENT clinics (center 1 and center 2) compared with a neurological clinic (center 3). This fact can explain the trend that among all 3 centers the biggest fraction of neurodegenerative and idiopathic patients was observed in center 3, whereas the biggest fraction of infectious and genetic disorders were observed in centers 1 and 2.

The distribution of the vHIT VOR gains between different etiologies indicated several trends, although not every trend proved to be statistically significant (**Figure 9**). Overall, the vHIT results showed significantly better gains for both anterior canals compared with the horizontal and posterior canals, which corresponds with previous literature (24). The vHIT results did not differ significantly between etiologies for anterior and posterior canals although trends of anterior canal sparing were observed for Menière's Disease, infectious disorders, ototoxicity, trauma, and idiopathic BVP. This is congruent with previous literature (24). Next to this, horizontal vHIT results were significantly lower for neurodegenerative disorders, genetic disorders, and trauma, whereas horizontal vHIT results were significantly higher for Menière's disease and infectious disorders.

Cluster analysis identified two separate clusters of patients with BVP in center 1 (which was the center with the most available vestibular test data) with significant differences in residual vestibular function according to vestibular testing. This was also reflected by the amount of diagnostic and vestibular implantation criteria met between clusters. Cluster 1 "severe BVP" consisted of patients who predominantly met 3 criteria, whereas cluster 2 "moderate BVP" mainly included patients who met only 1 criterion (**Supplementary Figure 6**). Although, no statistically significant differences were found in the etiology distribution between clusters (**Figure 9**), a slightly higher prevalence of Menière's Disease was observed in cluster 2 "moderate BVP" that performed "better" in all vestibular tests, whereas the idiopathic and ototoxicity etiologies prevailed in cluster 1 "severe BVP" and performed "worse" (**Supplementary Figure 4**). This could imply that the contribution of etiology to specific patterns of vestibular impairment might be limited and would eventually result in an overall better or worse vestibular function. Despite some patterns being found for a few BVP etiologies, one should consider every case individually and investigate every part of the vestibular system separately to obtain a full understanding of the vestibular impairment.

Order of Vestibular Test Outcomes According to Cluster Analysis

The cluster analysis showed similarities in the vestibular reflex tests used in center 1 (**Figure 9**, left dendrogram). For example, horizontal and anterior vHITs were arranged close to each other and to caloric testing; posterior vHIT was located close to torsion swing test; and oVEMPs and cVEMPs formed a pair. It is quite intuitive for VEMP results to be correlated to each other since the two otolith organs are located next to each other. However, the opposite was found when testing the semicircular canal function. The caloric test, torsion swing test, and horizontal vHIT are aimed to measure horizontal canal function and it could be hypothesized that they would closely correlate to each other. However, this was not observed in the cluster analysis, which showed the close correlation of the anterior and horizontal vHIT results together with the caloric test, and the close correlation of posterior vHIT results with the torsion swing test. The proximity of the horizontal and anterior vHIT in the cluster analysis can be partly explained in terms of anatomy. The horizontal and anterior canals ampullae are located close to each other and project into the same superior vestibular nerve division, whereas the inferior vestibular nerve division receives input from the posterior canals (56). Next to this, as stated before, vHIT and the caloric test seem to be able to indicate vestibular impairment, whereas the torsion swing test is more sensitive to measure the residual vestibular function (53). This could explain why the torsion swing test is not in close proximity to the horizontal vHIT and caloric test in the cluster analysis. The trends found in this cluster analysis differed from the trends described by a previous study (40). For example, differences in the arrangement of the variables after clustering [e.g., horizontal and posterior canals in close proximity to the utriculus according to the previous study (40)]. Furthermore, in contrast to the study presented here, no differences in vestibular impairment were found. This could be the result of different approaches used, namely: (1) Normalization of data using single test results across patient groups (this study) compared with

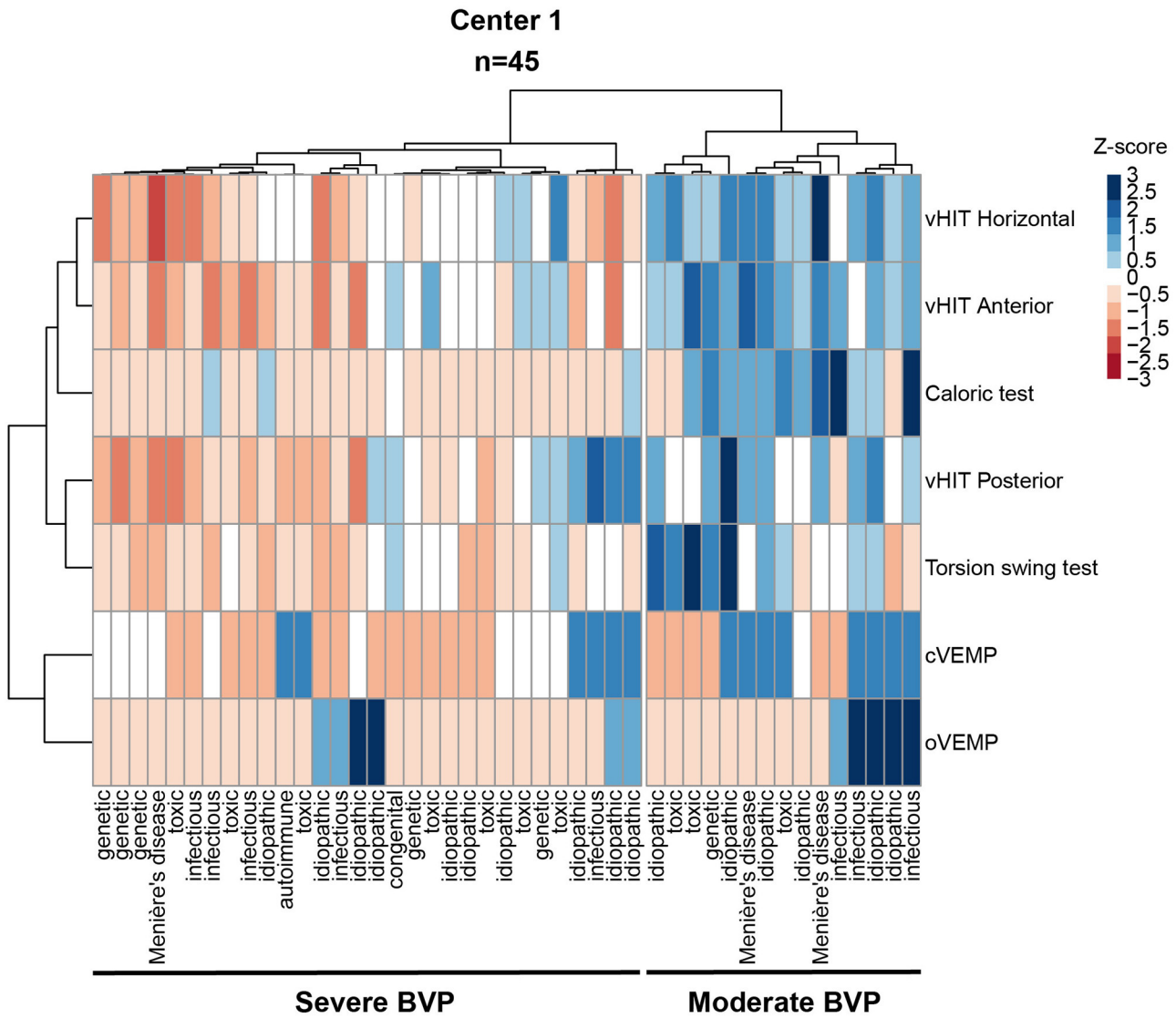

FIGURE 9 | Heatmap as a result of hierarchical cluster analysis with two dendrograms; Each column represents one subject; each row represents the results of a specific vestibular test. A "bad (vestibular) score" (i.e., low scores on tests of vestibular reflexes) is illustrated by lower Z scores in the color red. A "relatively good (vestibular) score" (i.e., relative high scores on tests of vestibular reflexes) is illustrated by higher Z scores in the color blue. Bold underlining indicates the 2 clusters; "Cluster 1, severe BVP" and "Cluster 2, moderate BVP". Only cases without missing data for caloric testing, torsion swing test, and horizontal and vertical vHIT, and o- and c-VEMPs ($n = 45$). vHIT, video Head Impulse Test; oVEMP, ocular Vestibular Evoked Myogenic Potential; cVEMP, cervical Vestibular Evoked Myogenic Potentials.

using all vestibular test results within one single patient (40); (2) scoring of vestibular function using results from separate vestibular reflex tests (this study) compared with considering separate vestibular organs [canals and otoliths, (40)]. To sum up, the different study goals could result in a different distribution of patients among clusters and different interpretations regarding etiology, despite the implementation of the same analysis. Therefore, it is advised to investigate all vestibular end organs separately to appreciate the vestibular impairment as a whole.

Limitations

Most importantly, some etiology groups included small amounts of patients ($n < 5$), which complicated statistical analysis. Next to this, the vestibular implantation criteria include a number of items that are not related to the vestibular reflex testing, which were not considered in this study (e.g., psychological or psychiatric disorders or an ability to undergo surgery). This could imply that the number of patients eligible for implantation in this study is an overestimation. Due to the study setting in centers 1 and 2, it cannot be ruled out that this study potentially

suffered from selection bias due to the inclusion of a relative "healthy" BVP population (i.e., patients with severe symptoms would potentially not want to participate in a full day of clinical testing). However, when comparing centers 1 and 2 with center 3, the results indicate that this might not be the case. A potential risk of referral bias in center 1 could not be excluded, since center 1 is involved in research regarding future vestibular implant therapy (43). This could lead to specific referrals or third opinion consultations in this center. Finally, the torsion swing test phase, being the 4th criterion according to Bárány criteria, was not used in this study, because either it was not measured or the automatic calculation algorithm was not considered reliable.

Future Perspectives

In order to gather a much bigger dataset from different sources that can be pooled and analyzed together, an international standardized approach for vestibular testing will be crucial (57). In particular, (1) different VEMP devices should be compared to each other in order to obtain the relation between stimuli and the threshold values; (2) the same torsion swing frequency and velocity should be used; and (3) raw traces of eye movements in both vHIT [obtained from different devices (46)] and caloric testing (electronystagmography vs. videonystagmography) should be analyzed, since different processing algorithms may lead to a significant difference in results of gain and SPV. In the case of a larger dataset, etiologies can be defined more specifically and at a more pathophysiological and morphological level (e.g., etiologies that lead to fibrosis). Next to this, future research between objective vestibular reflex test results and self-reported symptom severity could provide more insight into the effect of different patterns of vestibular impairment and degree of specific BVP symptoms (e.g., anterior canal sparing and self-reported oscillopsia severity).

CONCLUSION

This study provided a description of vestibular function in a large cohort of patients with BVP diagnosed according to the Bárány Society criteria. Overall, this study showed differences in the degree of vestibular impairment measured with different vestibular tests such as caloric test, vHIT, torsion swing test, and VEMPs. More specifically, some tests (i.e., caloric testing and horizontal vHIT) seem to be more sensitive for detecting vestibular impairment, whereas other tests (e.g., torsion swing test) are more suited for measuring residual vestibular function. In addition, no striking patterns of vestibular impairment in relation to etiology were found. Nevertheless, when comparing the Bárány Society diagnostic and vestibular implantation criteria, it was shown that although the implantation criteria are more strict, still 76% of the patients with BVP were eligible for implantation based on vestibular test criteria. It is advised, especially in the research setting, to carefully examine every patient for their overall pattern of vestibular impairment (i.e., all five vestibular end organs), in order to make well-informed and personalized therapeutic decisions.

DATA AVAILABILITY STATEMENT

The raw data supporting the conclusions of this article will be made available by the authors, without undue reservation.

ETHICS STATEMENT

The studies involving human participants were reviewed and approved by the Medical Ethics Committee of Maastricht, Antwerp and Munich. The patients/participants provided their written informed consent to participate in this study.

AUTHOR CONTRIBUTIONS

MP and LS conducted the analysis and wrote the manuscript. FL, BD, and VM ensured data acquisition. RB supervised the writing and edited the manuscript. MS, NG, AP, and JW reviewed the manuscript. All authors contributed to the article and approved the submitted version.

FUNDING

LS and FL were supported through funding of MED-EL (Innsbruck, Austria). RB, AP, and NG received funding for travel from MED-EL. MP was supported by the Tomsk State University Development Program (≪Priority-2030≫). MS receives support for clinical studies from Decibel, U.S.A., Cure within Reach, U.S.A. and Heel, Germany. MS distributes M-glasses and Positional vertigo App. The funders had no role in study design, data collection, data analysis, interpretation of data, decision to publish, or preparation of the manuscript.

SUPPLEMENTARY MATERIAL

The Supplementary Material for this article can be found online at: https://www.frontiersin.org/articles/10.3389/fneur.2022.856472/full#supplementary-material

REFERENCES

1. Hain TC, Cherchi M, Yacovino DA. Bilateral vestibular loss. *Semin Neurol.* (2013) 33:195–203. doi: 10.1055/s-0033-1354597
2. Lucieer F, Vonk P, Guinand N, Stokroos R, Kingma H, van de Berg R. Bilateral vestibular hypofunction: insights in etiologies, clinical subtypes, and diagnostics. *Front Neurol.* (2016) 7:26. doi: 10.3389/fneur.2016.00026
3. Strupp M, Kim JS, Murofushi T, Straumann D, Jen JC, Rosengren SM, et al. Bilateral vestibulopathy: diagnostic criteria consensus document of the classification committee of the barany society. *J Vestib Res.* (2017) 27:177–89. doi: 10.3233/VES-170619
4. Lucieer F, Duijn S, Van Rompaey V, Perez Fornos A, Guinand N, Guyot JP, et al. Full spectrum of reported symptoms of bilateral vestibulopathy needs further investigation-a systematic review. *Front Neurol.* (2018) 9:352. doi: 10.3389/fneur.2018.00352

5. Brandt T, Schautzer F, Hamilton DA, Brüning R, Markowitsch HJ, Kalla R, et al. Vestibular loss causes hippocampal atrophy and impaired spatial memory in humans. *Brain.* (2005) 128:2732–41. doi: 10.1093/brain/awh617
6. Kremmyda O, Hüfner K, Flanagin VL, Hamilton DA, Linn J, Strupp M, et al. Beyond dizziness: virtual navigation, spatial anxiety and hippocampal volume in bilateral vestibulopathy. *Front Human Neurosci.* (2016) 10. doi: 10.3389/fnhum.2016.00139
7. Dobbels B, Mertens G, Gilles A, Claes A, Moyaert J, van de Berg R, et al. Cognitive function in acquired bilateral vestibulopathy: a cross-sectional study on cognition, hearing, and vestibular loss. *Front Neurosci.* (2019) 13:340. doi: 10.3389/fnins.2019.00340
8. Dobbels B, Peetermans O, Boon B, Mertens G, Van de Heyning P, Van Rompaey V. Impact of bilateral vestibulopathy on spatial and nonspatial cognition: a systematic review. *Ear Hear.* (2019) 40:757–65. doi: 10.1097/AUD.0000000000000679
9. Dobbels B, Lucieer F, Mertens G, Gilles A, Moyaert J, van de Heyning P, et al. Prospective cohort study on the predictors of fall risk in 119 patients with bilateral vestibulopathy. *PLoS ONE.* (2020) 15:e0228768. doi: 10.1371/journal.pone.0228768
10. Lucieer FMP, Van Hecke R, van Stiphout L, Duijn S, Perez-Fornos A, Guinand N, et al. Bilateral vestibulopathy: beyond imbalance and oscillopsia. *J Neurol.* (2020) 267:241–55. doi: 10.1007/s00415-020-10243-5
11. Paredis S, van Stiphout L, Remmen E, Strupp M, Gerards M-C, Kingma H, et al. (2021). DISCOHAT: an acronym to describe the spectrum of symptoms related to bilateral vestibulopathy. *Front. Neurol.* 12:1949. doi: 10.3389/fneur.2021.771650
12. Guinand N, Boselie F, Guyot JP, Kingma H. Quality of life of patients with bilateral vestibulopathy. *Ann Otol Rhinol Laryngol.* (2012) 121:471–7. doi: 10.1177/000348941212100708
13. Sun DQ, Ward BK, Semenov YR, Carey JP, Della Santina CC. Bilateral vestibular deficiency: quality of life and economic implications. *JAMA Otolaryngology–Head & Neck Surgery.* (2014) 140:527–34. doi: 10.1001/jamaoto.2014.490
14. Kovacs E, Wang X, Grill E. Economic burden of vertigo: a systematic review. *Health Econ Rev.* (2019) 9:1–14. doi: 10.1186/s13561-019-0258-2
15. Rinne T, Bronstein AM, Rudge P, Gresty MA, Luxon LM. Bilateral loss of vestibular function: clinical findings in 53 patients. *J Neurol.* (1998) 245:314–21. doi: 10.1007/s004150050225
16. Ishiyama G, Ishiyama A, Kerber K, Baloh RW. Gentamicin ototoxicity: clinical features and the effect on the human vestibulo-ocular reflex. *Acta Otolaryngol.* (2006) 126:1057–61. doi: 10.1080/00016480600606673
17. Cushing SL, Papsin BC, Rutka JA, James AL, Blaser SL, Gordon KA. Vestibular end-organ and balance deficits after meningitis and cochlear implantation in children correlate poorly with functional outcome. *Otol Neurotol.* (2009) 30:488–95. doi: 10.1097/MAO.0b013e31819bd7c8
18. Zingler VC, Weintz E, Jahn K, Huppert D, Cnyrim C, Brandt T, et al. Causative factors, epidemiology, and follow-up of bilateral vestibulopathy. *Ann N Y Acad Sci.* (2009) 1164:505–8. doi: 10.1111/j.1749-6632.2009.03765.x
19. Bovo R, Ciorba A, Martini A. Vertigo and autoimmunity. *Eur Arch Otorhinolaryngol.* (2010) 267:13–9. doi: 10.1007/s00405-009-1122-5
20. Clemmens C, Ruckenstein M. Characteristics of patients with unilateral and bilateral Ménière's disease. *Otol Neurotol.* (2012) 33:1266–9. doi: 10.1097/MAO.0b013e31826426b9
21. Greco A, Gallo A, Fusconi M, Magliulo G, Turchetta R, Marinelli C, et al. Cogan's syndrome: an autoimmune inner ear disease. *Autoimmun Rev.* (2013) 12:396–400. doi: 10.1016/j.autrev.2012.07.012
22. de Varebeke SP, Termote B, Van Camp G, Govaerts PJ, Schepers S, Cox T, et al. Focal sclerosis of semicircular canals with severe DFNA9 hearing impairment caused by a P51S COCH-mutation: is there a link? *Otol Neurotol.* (2014) 35:1077–86. doi: 10.1097/MAO.0000000000000283
23. Szmulewicz DJ, McLean CA, MacDougall HG, Roberts L, Storey E, Halmagyi GM. CANVAS an update: clinical presentation, investigation and management. *J Vestib Res.* (2014) 24:465–74. doi: 10.3233/VES-140536
24. Tarnutzer AA, Bockisch CJ, Buffone E, Weiler S, Bachmann LM, Weber KP. Disease-specific sparing of the anterior semicircular canals in bilateral vestibulopathy. *Clin Neurophysiol.* (2016) 127:2791–801. doi: 10.1016/j.clinph.2016.05.005
25. Porciuncula F, Johnson CC, Glickman LB. The effect of vestibular rehabilitation on adults with bilateral vestibular hypofunction: a systematic review. *J Vestib Res.* (2012) 22:283–98. doi: 10.3233/VES-120464
26. Ward BK, Agrawal Y, Hoffman HJ, Carey JP, Della Santina CC. Prevalence and impact of bilateral vestibular hypofunction: results from the 2008 US National Health Interview Survey. *JAMA Otolaryngol Head Neck Surg.* (2013) 139:803–10. doi: 10.1001/jamaoto.2013.3913
27. Kingma H, Felipe L, Gerards MC, Gerits P, Guinand N, Perez-Fornos A, et al. Vibrotactile feedback improves balance and mobility in patients with severe bilateral vestibular loss. *J Neurol.* (2019) 266:19–26. doi: 10.1007/s00415-018-9133-z
28. Della Santina CC, Migliaccio AA, Patel AH. A multichannel semicircular canal neural prosthesis using electrical stimulation to restore 3-d vestibular sensation. *IEEE Trans Biomed Eng.* (2007) 54:1016–30. doi: 10.1109/TBME.2007.894629
29. Golub JS, Ling L, Nie K, Nowack A, Shepherd SJ, Bierer SM, et al. Prosthetic implantation of the human vestibular system. *Otol Neurotol.* (2014) 35:136–47. doi: 10.1097/MAO.0000000000000003
30. Perez Fornos A, Guinand N, van de Berg R, Stokroos R, Micera S, Kingma H, et al. Artificial balance: restoration of the vestibulo-ocular reflex in humans with a prototype vestibular neuroprosthesis. *Front Neurol.* (2014) 5. doi: 10.3389/fneur.2014.00066
31. Guinand N, Van de Berg R, Cavuscens S, Stokroos R, Ranieri M, Pelizzone M, et al. Restoring visual acuity in dynamic conditions with a vestibular implant. *Front Neurosci.* (2016) 10. doi: 10.3389/fnins.2016.00577
32. Perez Fornos A, Cavuscens S, Ranieri M, van de Berg R, Stokroos R, Kingma H, et al. The vestibular implant: A probe in orbit around the human balance system. *J Vestib Res.* (2017) 27:51–61. doi: 10.3233/VES-170604
33. Ramos de Miguel A, Falcon Gonzalez JC, Ramos Macias A. Vestibular Response to electrical stimulation of the otolith organs. implications in the development of a vestibular implant for the improvement of the sensation of gravitoinertial accelerations. *J Int Adv Otol.* (2017) 13, 154–161. doi: 10.5152/iao.2017.4216
34. Guyot JP, Perez Fornos A. Milestones in the development of a vestibular implant. *Curr Opin Neurol.* (2019) 32:145–53. doi: 10.1097/WCO.0000000000000639
35. Chow MR, Ayiotis AI, Schoo DP, Gimmon Y, Lane KE, Morris BJ, et al. Posture, gait, quality of life, and hearing with a vestibular implant. *N Engl J Med.* (2021) 384:521–32. doi: 10.1056/NEJMoa2020457
36. Zingler VC, Weintz E, Jahn K, Botzel K, Wagner J, Huppert D, et al. Saccular function less affected than canal function in bilateral vestibulopathy. *J Neurol.* (2008) 255:1332–6. doi: 10.1007/s00415-008-0887-6
37. Fujimoto C, Murofushi T, Chihara Y, Suzuki M, Yamasoba T, Iwasaki S. Novel subtype of idiopathic bilateral vestibulopathy: bilateral absence of vestibular evoked myogenic potentials in the presence of normal caloric responses. *J Neurol.* (2009) 256:1488–92. doi: 10.1007/s00415-009-5147-x
38. Agrawal Y, Bremova T, Kremmyda O, Strupp M. Semicircular canal, saccular and utricular function in patients with bilateral vestibulopathy: analysis based on etiology. *J Neurol.* (2013) 260:876–83. doi: 10.1007/s00415-012-6724-y
39. Hermann R, Ionescu EC, Dumas O, Tringali S, Truy E, Tilikete C. Bilateral vestibulopathy: vestibular function, dynamic visual acuity and functional impact. *Front Neurol.* (2018) 9:555. doi: 10.3389/fneur.2018.00555
40. Tarnutzer AA, Bockisch CJ, Buffone E, Weber KP. Hierarchical cluster analysis of semicircular canal and otolith deficits in bilateral vestibulopathy. *Front Neurol.* (2018) 9:244. doi: 10.3389/fneur.2018.00244
41. Fu TS, Carr SD, Douglas-Jones P, Dillon W, Ilan O, Syed IM, et al. Gentamicin vestibulotoxicity: further insights from a large clinical series. *Otol Neurotol.* (2020). doi: 10.1097/MAO.0000000000002698
42. Lee JY, Kim MB. Change of VOR gain and pure-tone threshold after single low-dose intratympanic gentamicin injection in Meniere's disease. *Acta Otolaryngol.* (2020) 140:314–8. doi: 10.1080/00016489.2019.1708457
43. Van De Berg R, Ramos A, Van Rompaey V, Bisdorff A, Perez-Fornos A, Rubinstein JT, et al. The vestibular implant: Opinion statement on implantation criteria for research. *J Vestibul Res.* (2020) 1–11. doi: 10.3233/VES-200701
44. van Stiphout L, Lucieer F, Pleshkov M, Van Rompaey V, Widdershoven J, Guinand N, et al. Bilateral vestibulopathy decreases self-motion perception. *J Neurol.* (2021). doi: 10.1007/s00415-021-10695-3

45. van Dooren TS, Lucieer FMP, Janssen AML, Kingma H, van de Berg R. The video head impulse test and the influence of daily use of spectacles to correct a refractive error. *Front Neurol.* (2018) 9:125. doi: 10.3389/fneur.2018.00125
46. Van Dooren TS, Starkov D, Lucieer FMP, Vermorken B, Janssen AML, Guinand N, et al. Comparison of three video head impulse test systems for the diagnosis of bilateral vestibulopathy. *J Neurol.* (2020). doi: 10.1007/s00415-020-10060-w
47. Macdougall HG, McGarvie LA, Halmagyi GM, Curthoys IS, Weber KP. The video head impulse test (vHIT) detects vertical semicircular canal dysfunction. *PLoS ONE.* (2013) 8:e61488. doi: 10.1371/journal.pone.0061488
48. Colebatch JG, Halmagyi GM, Skuse NF. Myogenic potentials generated by a click-evoked vestibulocollic reflex. *J Neurol Neurosurg Psychiatry.* (1994) 57:190–7. doi: 10.1136/jnnp.57.2.190
49. Vanspauwen R, Weerts A, Hendrickx M, Buytaert KI, Blaivie C, Jorens PG, et al. No effects of anti-motion sickness drugs on vestibular evoked myogenic potentials outcome parameters. *Otol Neurotol.* (2011) 32:497–503. doi: 10.1097/MAO.0b013e31820d94d0
50. Rousseeuw PJ. Silhouettes: A graphical aid to the interpretation and validation of cluster analysis. *J Comput Appl Math.* (1987) 20:53–65. doi: 10.1016/0377-0427(87)90125-7
51. Pietkiewicz P, Pepaś R, Sułkowski WJ, Zielińska-Blizniewska H, Olszewski J. Electronystagmography versus videonystagmography in diagnosis of vertigo. *Int J Occup Med Environ Health.* (2012) 25:59–65. doi: 10.2478/s13382-012-0002-1
52. Baloh RW, Sills AW, Honrubia V. Impulsive and sinusoidal rotatory testing: a comparison with results of caloric testing. *Laryngoscope.* (1979) 89:646–54. doi: 10.1288/00005537-197904000-00013
53. Kingma H, van de Berg R. Anatomy, physiology, and physics of the peripheral vestibular system. *Handb Clin Neurol.* (2016) 137:1–16. doi: 10.1016/B978-0-444-63437-5.00001-7
54. Rosengren SM, Welgampola MS, Taylor RL. Vestibular-evoked myogenic potentials in bilateral vestibulopathy. *Front Neurol.* (2018) 9:252. doi: 10.3389/fneur.2018.00252
55. Bordoni B, Mankowski NL, Daly DT. Neuroanatomy, cranial nerve 8 (vestibulocochlear). Treasure Island, FL: StatPearls Publishing (2019).
56. Khan S, Chang R. Anatomy of the vestibular system: a review. *NeuroRehabilitation.* (2013) 32:437–43. doi: 10.3233/NRE-130866
57. Strupp M, Grimberg J, Teufel J, Laurell G, Kingma H, Grill E. Worldwide survey on laboratory testing of vestibular function. *Neurol Clin Pract.* (2020) 10:379–87. doi: 10.1212/CPJ.0000000000000744

Conflict of Interest: MS acts as a consultant for Abbott, AurisMedical, Heel, IntraBio, and Sensorion. MS has received speaker's honoraria from Abbott, Auris Medical, Biogen, Eisai, Grünenthal, GSK, Henning Pharma, Interacoustics, J & J, MSD, NeuroUpdate, Otometrics, Pierre-Fabre, TEVA, UCB, and Viatris.

The remaining authors declare that the research was conducted in the absence of any commercial or financial relationships that could be construed as a potential conflict of interest.

Publisher's Note: All claims expressed in this article are solely those of the authors and do not necessarily represent those of their affiliated organizations, or those of the publisher, the editors and the reviewers. Any product that may be evaluated in this article, or claim that may be made by its manufacturer, is not guaranteed or endorsed by the publisher.

Copyright © 2022 van Stiphout, Pleshkov, Lucieer, Dobbels, Mavrodiev, Guinand, Pérez Fornos, Widdershoven, Strupp, Van Rompaey and van de Berg. This is an open-access article distributed under the terms of the Creative Commons Attribution License (CC BY). The use, distribution or reproduction in other forums is permitted, provided the original author(s) and the copyright owner(s) are credited and that the original publication in this journal is cited, in accordance with accepted academic practice. No use, distribution or reproduction is permitted which does not comply with these terms.

frontiers | Frontiers in Neurology

CLINICAL TRIAL
published: 14 April 2022
doi: 10.3389/fneur.2022.868976

A Randomized, Double-Blind, Sham-Controlled Trial of Transcranial Direct Current Stimulation for the Treatment of Persistent Postural-Perceptual Dizziness (PPPD)

Jooyeon Jamie Im[1], Seunghee Na[2], Sanghoon Kang[3], Hyeonseok Jeong[4], Eek-Sung Lee[5], Tae-Kyeong Lee[5], Woo-Young Ahn[1], Yong-An Chung[4] and In-Uk Song[2]*

[1] Department of Psychology, Seoul National University, Seoul, South Korea, [2] Department of Neurology, Incheon St. Mary's Hospital, The Catholic University of Korea, Seoul, South Korea, [3] Department of Psychiatry, Yale University, New Haven, CT, United States, [4] Department of Nuclear Medicine, Incheon St. Mary's Hospital, The Catholic University of Korea, Seoul, South Korea, [5] Department of Neurology, Soonchunhang University Bucheon Hospital, Bucheon, South Korea

OPEN ACCESS

Edited by:
Sun-Young Oh,
Jeonbuk National University,
South Korea

Reviewed by:
Yuka Morita,
Niigata University, Japan
Jeffrey P. Staab,
Mayo Clinic, United States
Yoon-Hee Cha,
University of Minnesota Twin Cities,
United States

***Correspondence:**
Seunghee Na
seunghee.na@gmail.com

Specialty section:
This article was submitted to Neuro-Otology, a section of the journal Frontiers in Neurology

Received: *03 February 2022*
Accepted: *14 March 2022*
Published: *14 April 2022*

Citation:
Im JJ, Na S, Kang S, Jeong H, Lee E-S, Lee T-K, Ahn W-Y, Chung Y-A and Song I-U (2022) A Randomized, Double-Blind, Sham-Controlled Trial of Transcranial Direct Current Stimulation for the Treatment of Persistent Postural-Perceptual Dizziness (PPPD). Front. Neurol. 13:868976. doi: 10.3389/fneur.2022.868976

Background: Persistent postural-perceptual dizziness (PPPD) is a functional vestibular disorder that causes chronic dizziness interfering with daily activities. Transcranial direct current stimulation (tDCS) has reportedly improved dizziness in patients with phobic postural vertigo in an open-label trial. However, no randomized, double-blind, sham-controlled study has been conducted on its therapeutic efficacy in PPPD.

Objective: This study was conducted to investigate the efficacy and safety of tDCS as an add-on treatment to pharmacotherapy in patients with PPPD. In addition, functional neuroimaging was used to identify the neural mechanisms underlying the effects of tDCS.

Materials and Methods: In a randomized, double-blind, sham-controlled trial, 24 patients diagnosed with PPPD were randomized to receive active (2 mA, 20 min) or sham tDCS to the left dorsolateral prefrontal cortex (DLPFC), administered in 15 sessions over 3 weeks. The clinical measures that assess the severity of dizziness, depression, and anxiety were collected at baseline, immediate follow-up, 1-month follow-up, and 3-month follow-up. Adverse events were also observed. The effect of tDCS on regional cerebral blood flow (rCBF) was evaluated with single photon emission tomography before and after tDCS sessions.

Results: For the primary outcome measure of the Dizziness Handicap Inventory (DHI) score, a significant main effect of time was found, but neither the treatment-by-time interaction effect nor the main effect of treatment was significant. For the Hamilton Depression Rating Scale (HDRS) score, there was a statistical significance for the treatment-by-time interaction effect and the main effect of time, but not for the main effect of treatment. However, the treatment-by-time interaction effect and the main effect of time on HDRS score appear to be due to one data point, an increase in depressive symptoms reported by the sham group at the 3-month follow-up. For the Activities-specific Balance

Confidence (ABC) Scale and the Hamilton Anxiety Rating Scale scores, there were no significant main effects of time, treatment, and treatment-by-time interaction. In a comparison with the changes in rCBF between the groups, a significant treatment-by-time interaction effect was found in the right superior temporal and left hippocampus, controlling for age and sex.

Conclusion: Active tDCS was not found to be significantly more efficacious than sham tDCS on dizziness symptoms in patients with PPPD. It is conceivable that tDCS targeting the DLPFC may not be an optimal treatment option for reducing dizziness symptoms in PPPD. Our findings encourage further investigation on the effects of tDCS in PPPD, which considers different stimulation protocols in terms of stimulation site or the number of sessions.

Clinical Trial Registration: cris.nih.go.kr, identifier: KCT0005068.

Keywords: dizziness, persistent postural-perceptual dizziness, neuromodulation, transcranial direct current stimulation, single photon emission computed tomography

INTRODUCTION

Persistent postural-perceptual dizziness (PPPD) is a chronic functional vestibular disorder that is characterized by waxing and waning non-spinning dizziness for more than 3 months (1). PPPD is a common disorder, which comprises about one-fifth of patients who visited the tertiary care dizziness clinic (2, 3). Prior to being established as a new diagnostic term, there were several clinical syndromes of functional dizziness such as chronic subjective dizziness (CSD) (4, 5), phobic postural vertigo (PPV) (6), visual vertigo (VV) (7), and space-motion discomfort (SMD) (8, 9). The unifying diagnosis of PPPD was established incorporating several descriptions of these syndromes by the Bárány Society in 2017, and it is now included in the International Classification of Diseases 11th Revision (ICD-11) (10).

While there are available treatments with some evidence of benefit including pharmacology, vestibular rehabilitation, and cognitive behavioral therapy, there are currently no gold standard guidelines for the treatment of PPPD (11, 12). Regarding pharmacological treatment, selective serotonin reuptake inhibitors (SSRIs) or serotonin norepinephrine reuptake inhibitors (SNRIs) are the first line of treatment options and are most commonly used. It has been reported that SSRI may indirectly interfere with dizziness symptoms by reducing anxiety and depressive symptoms, which are often observed in patients with PPPD (12). Moreover, it remains a possibility that SSRI may directly have effects on the vestibular nuclear complex, which is related to motion-sensitive neural pathways (13). Nonetheless, among patients who properly received SSRI treatment, more than 30% of them reported no significant benefits (14, 15). Therefore, developing another treatment option is a priority.

Transcranial direct current stimulation (tDCS) is a neuromodulation technique that applies a weak current to the scalp for modulating neuronal activity (16). tDCS has been shown to have therapeutic effects in various neurologic and psychiatric disorders (17). An open-label pilot study conducted in patients with PPV, which administers 5 daily sessions of tDCS, has shown to have acute effects on dizziness symptoms (18). However, this trial did not include sham controls and only observed short-term treatment effects.

Furthermore, while neuroimaging studies of PPPD have shown dysfunctional brain activities in regions related to balance and postural control (19), no studies have applied neuroimaging methods to study neural mechanisms associated with treatment effects in PPPD. Hence, the goal of this study was to investigate the therapeutic efficacy of tDCS combined with the medications in patients with PPPD using a double-blind, sham-controlled design. In addition, single photon computed tomography (SPECT) was used before and after the treatment to investigate the changes in regional cerebral blood flow (rCBF) associated with treatment effects.

MATERIALS AND METHODS

Participants

Patients with PPPD between the ages of 18 and 69 years were recruited from the neurology outpatient clinic. The diagnosis of PPPD was made by a licensed neurologist (SN) according to the diagnostic criteria of PPPD, established by the Classification Committee of the Bárány Society (10). All patients were tDCS naive and it was predetermined that patients who receive at least 80% of tDCS treatment (12 out of 15 sessions) were considered adherent. To minimize the possible confounds of side effects, patients were recommended to start and continue maintenance treatment with SSRIs for at least 3 weeks prior to and during the study period. Exclusion criteria were neurological disorders other than PPPD, psychiatric disorders (e.g., generalized anxiety disorder or major depressive disorder), contraindications to tDCS (e.g., metallic implants in the head or history of seizure), history of head trauma with loss of consciousness, and pregnancy. The study was approved by the Institutional Review Board of the Incheon St. Mary's Hospital and was conducted in

accordance with the Declaration of Helsinki. The study protocol was registered in the Clinical Research Information Service (Registration Number: KCT0005068).

Study Protocol

This study was a clinical trial that used a randomized, double-blind, sham-controlled design. Following screening evaluation, patients were randomized to receive active tDCS or sham tDCS. Randomization was performed using a computer-based random number-producing algorithm by a research staff who was not involved in the data collection (HJ). A neurological examination, clinical interview, self-report measures, and brain perfusion SPECT were performed at the baseline and within 1 week after completing the 3-week treatment (immediate follow-up). Additionally, a neurological examination, clinical interview, and self-report measures were collected at 1 and 3 months after the end of treatment. At the baseline, a research staff (JJI) provided training on tDCS self-administration and ensured that participants could independently set up and use the tDCS device, so they can safely perform tDCS at home.

Transcranial Direct Current Stimulation

Active or sham tDCS was administered for a total of 15 sessions (20 min per session) over 3 weeks *via* two surface electrodes with saline-soaked sponges (6 cm in diameter) using the YDS-301 N device (YBrain Inc, South Korea). The anodal electrode was placed over the left dorsolateral prefrontal cortex (DLPFC) (F3; International 10–20 EEG system) and the cathodal electrode over the right DLPFC (F4). For the active condition, the current was ramped up to 2.0 mA (current density, 0.07 mA/cm^2) over 30 s, remained at 2.0 mA for 19 min, and ramped down to 0 mA over 30 s. For the sham condition, the current was ramped up to 2 mA over 30 s and ramped down over the next 30 s. The tDCS device was set to be used only one time a day, and the usage logs were automatically stored after each session. Compliance was checked based on the usage logs when the device was returned at the immediate follow-up. During stimulation, patients were instructed not to fall asleep and they were allowed to go about their regular activities. Participants were asked to fill out a survey on side effects after each session. The side effects survey included 13 items, namely burning sensation, dizziness, fatigue, headache, itchiness, nausea, neck pain, pain at the stimulation site, redness of the skin, reduced concentration, sleepiness, tingling sensation, and others. Adequacy of blinding to treatment condition was assessed at the immediate follow-up by asking the participants to guess the treatment condition (active, sham, or do not know) that they were assigned to.

Clinical Measures

All patients underwent a detailed neurologic examination including neuro-otologic assessment with Frenzel glasses including various positional maneuvers, head-shaking test, bedside head impulse test, and oculomotor tests. Dizziness was rated with self-report measures including the Dizziness Handicap Inventory (DHI), which was the primary outcome measure, and the Activities-specific Balance Confidence (ABC) scale. Handedness was measured using the Edinburgh Handedness Inventory. The severity of depressive and anxiety symptoms was measured with the clinician-administered 17-item Hamilton Depression Rating Scale (HDRS) and the 14-item Hamilton Anxiety Rating Scale (HARS), respectively.

Brain SPECT Imaging Acquisition and Analysis

The SPECT images were obtained with a dual-headed gamma camera (Discovery NM630; GE Healthcare, Milwaukee, WI, USA) equipped with a low-energy fan-beam collimator. Prior to scanning, patients were injected with 555–740 MBq of technetium-99m ethyl cysteinate dimer (99mTc-ECD) and rested for about 40 min. The images were taken by rotating the camera a total of 720° at 6-degree intervals at a rate of 12 s per frame. Using a filtered back-projection technique, the images were corrected for attenuation and reconstructed into a 128 x 128 matrix with a pixel size of 1.95 mm^3 × 1.95 mm^3 × 2.08 mm^3.

Statistical Parametric Mapping 12 (SPM12; Wellcome Department of Cognitive Neurology, London, UK) implemented in MATLAB R2021 (MathWorks, Natick, MA, USA) was used for preprocessing and analysis. The SPECT images were spatially normalized to the SPM-provided standard SPECT template, which is based on the Montreal Neurological Institute (MNI) template. After spatial normalization, each voxel count was standardized to the mean voxel count of the whole brain using proportional scaling. The normalized SPECT images were then smoothed with a 16-mm full-width half-maximum Gaussian kernel.

Voxel-wise comparisons were performed using (1) a two-sample *t*-test model to investigate rCBF difference between groups at baseline, (2) a flexible factorial model to identify treatment (anode and sham) × time (baseline and immediate follow-up) interaction effects on rCBF, and (3) as a *post hoc* analysis, a paired *t*-test model to investigate rCBF changes within each group before and after the treatment. Statistical significance level was defined as a *p*-value threshold of 0.001 and a minimum cluster size of 50 contiguous voxels.

Statistical Analysis

Baseline characteristics of groups were compared using independent *t*-test for normally distributed continuous variables, Wilcoxon rank-sum test for non-normally distributed continuous variables, and chi-square test for categorical variables. A mixed-effects linear regression model was conducted to assess the interaction effect of treatment (anode and sham) and time (baseline, immediate, 1-month, and 3-month follow-ups) for each outcome measure. To better understand the interaction effects between group and time, a two-sample *t*-test was performed between active and sham groups at each visit. Reported side effects were compared between groups using the chi-square test. All statistical analyses were performed using R software (version 4.0.5).

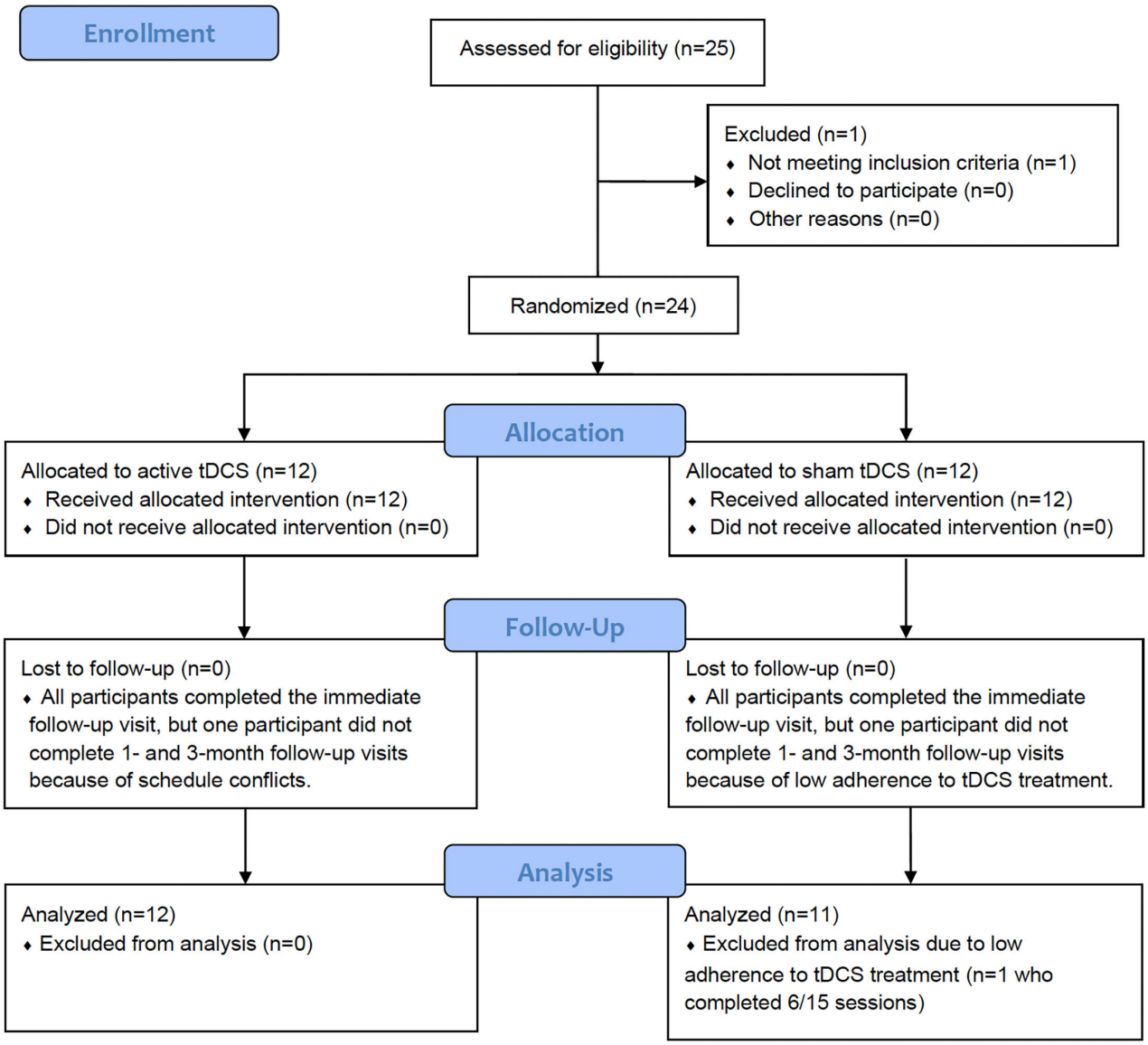

FIGURE 1 | Flow diagram for study participants.

RESULTS

Participants

Among 24 participants who were randomized into active ($n = 12$) or sham ($n = 12$) groups, 23 participants were included in the final analysis after excluding one participant in the sham group due to low adherence to tDCS treatment (**Figure 1**). The baseline demographic and clinical characteristics of the participants did not differ between active and sham groups (**Table 1**).

Neurologic examinations at the baseline and follow-ups revealed no abnormal findings except for subtle positional nystagmus in 1 patient and transient head-shaking nystagmus in 4 patients. Precipitating events of PPPD were reported as benign paroxysmal postural vertigo ($n = 8$), vestibular neuritis ($n = 5$), other systemic diseases such as flu ($n = 1$) or cardiovascular symptoms ($n = 3$), emotional stress ($n = 3$), mild head trauma without loss of consciousness ($n = 1$), and none ($n = 2$).

Prior to study entry, all participants started taking either SSRI [20 participants with escitalopram (8.82 ± 4.52 mg per day) and 1 with sertraline (25 mg per day)] or herbal medicine (2 participants with hypericum extracts known for antidepressant effects). Then, four out of 20 participants taking escitalopram discontinued the medication due to the side effects ($n = 3$ for gastrointestinal effects and $n = 1$ for loss of libido), and all other participants took their respective medication during tDCS treatment and the dosage did not change during the trial.

Regarding the validity of the blinding procedure, most participants from both groups (21/23) either guessed that the treatment they received was active treatment or was unsure. In the active group, 6 participants (50%) answered that they received active treatment (correctly guessing their treatment group) and 6 participants (50%) answered, "don't know." In the sham group, 7 participants (63.63%) answered that they received active treatment (incorrectly guessing their treatment group), 2 participants (18.18%) answered that they received sham treatment (correctly guessing their treatment group), and 2 participants (18.18%) answered, "don't know." Two participants ($n = 1$ in active and n = 1 in sham groups) were left-handed, and the rest were right-handed. The number of participants who experienced the side effects during tDCS treatment for each group is reported in **Table 4**.

TABLE 1 | Baseline demographic and clinical characteristics of the study participants.

Characteristic	Active group ($n = 12$)	Sham group ($n = 11$)	*p*-value
Age (years)	47.8 (13.0)	51.7 (13.1)	0.48
Sex (male:female)	4:8	4:7	1.00
Education (years)	11.6 (3.9)	11.9 (3.1)	0.90
Disease duration (months)	17.6 (396.3)	14.8 (348.0)	0.65
Medication	10 (8 with Escitalopram, 2 with Hypericum extracts), 2 with no medication	9 (8 with Escitalopram, 1 with Sertraline), 2 with no medication	0.99
DHI score	34.3 (15.9)	35.3 (14.2)	0.88
ABC score	77.3 (21.0)	77.6 (17.5)	0.90
HDRS score	5.4 (3.2)	5.8 (5.6)	0.81
HARS score	6.6 (3.2)	7.6 (6.4)	0.63

Data are presented as mean (standard deviation) or numbers.
ABC, activities-specific balance confidence; DHI, dizziness handicap inventory; HARS, hamilton anxiety rating scale; HDRS, hamilton depression rating scale.

Clinical Outcomes

Results for the clinical outcomes are illustrated in **Table 2** and **Figure 2**. For the primary outcome measure of DHI score, a significant main effect of time was found ($p < 0.001$), but neither the main effect of treatment ($p = 0.79$) nor the treatment-by-time interaction effect ($p = 0.58$) was significant. *Post hoc* analysis revealed no significant group difference in the DHI score at each time point. For the ABC score, there was no significant main effect of time ($p = 0.44$), treatment ($p = 0.45$), and treatment-by-time interaction effect ($p = 0.35$).

For the HDRS score, the treatment-by-time interaction effect ($p = 0.005$) and the main effect of time ($p = 0.02$) were significant,

TABLE 2 | Summary of clinical variables across time and group.

Measures	Anode	Sham	Treatment (active vs. sham)		Time		Treatment x Time	
			F	*p*-value	*F*	*p*-value	*F*	*p*-value
DHI								
Baseline	34.33 (15.9)	35.27 (14.2)	0.07	0.79	14.79	<0.001	0.66	0.58
Immediate F/U	29.17 (20.6)	25.64 (12.8)						
1-month F/U	23.1 (14.7)	21.8 (16.1)						
3-month F/U	25.1 (13.6)	19.1 (14.3)						
ABC								
Baseline	77.34 (21.0)	77.61 (17.5)	0.59	0.45	0.91	0.44	1.10	0.35
Immediate F/U	72.03 (26.6)	81.82 (15.9)						
1-month F/U	75.57 (21.9)	82.84 (16.4)						
3-month F/U	75.34 (24.7)	85.00 (15.1)						
HDRS								
Baseline	5.42 (3.20)	5.82 (5.56)	0.29	0.60	3.75	0.02	4.65	0.005
Immediate F/U	5.17 (4.30)	4.36 (2.87)						
1-month F/U	6.0 (3.58)	5.0 (4.84)						
3-month F/U	5.36 (3.59)	9.73 (6.80)						
HARS								
Baseline	6.58 (3.18)	7.64 (6.44)	0.54	0.47	0.48	0.70	0.66	0.58
Immediate F/U	5.92 (5.11)	6.82 (5.34)						
1-month F/U	6.55 (3.75)	7.09 (6.12)						
3-month F/U	6.09 (4.23)	8.91 (7.65)						

Data are presented as mean (standard deviation). Statistical test results are from linear mixed-effects models with each clinical variable as dependent variables and time and treatment (active vs. sham) as the predictors.
Treatment, main effect of treatment; Time, main effect of time; Treatment X Time, interaction effect of treatment and time.
ABC, activities-specific balance confidence; DHI, dizziness handicap inventory; F/U, follow-up; HARS, hamilton anxiety rating scale; HDRS, hamilton depression rating scale.

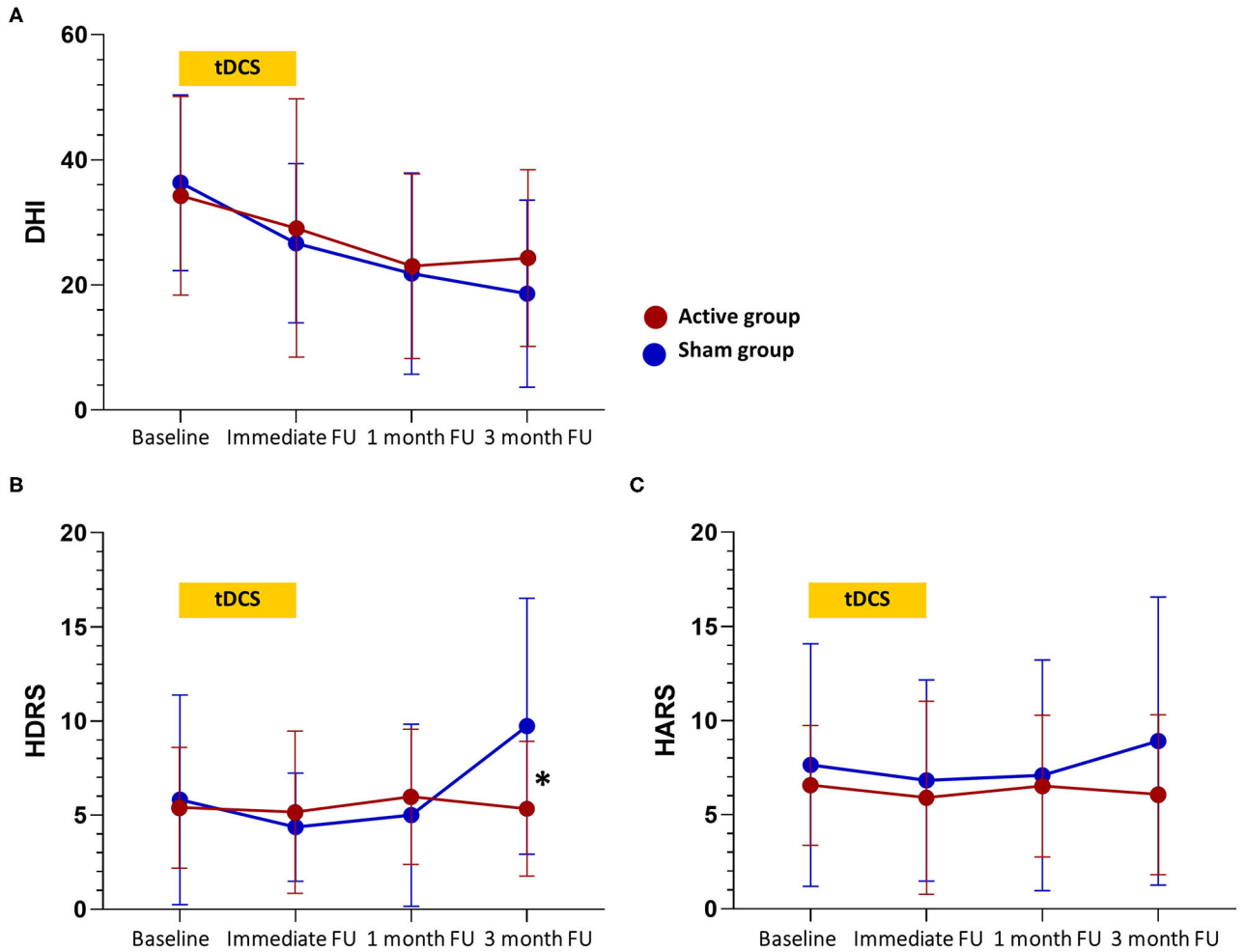

FIGURE 2 | Changes in clinical scores over time. **(A)** Changes in the Dizziness Handicap Inventory (DHI) total score. **(B)** Changes in the Hamilton Depression Rating Scale (HDRS) score. **(C)** Changes in the Hamilton Anxiety Rating Scale (HARS) score. tDCS sessions were between baseline and immediate follow-up. Values are mean scores and error bars indicate 95% confidence intervals. Significant differences at the $p < 0.05$ level between groups at a time point are denoted with a "*". FU, follow-up.

but the main effect of treatment ($p = 0.60$) was not significant. *Post hoc* analysis showed that the HDRS score was lower in the active group compared to the sham group at the 3-month follow-up (5.36 vs. 9.73, $p = 0.02$). Notably, the treatment-by-time interaction effect and the main effect of time on HDRS score appear to be due to an increase in depressive symptoms reported by the sham group at the 3-month follow-up. Considering that the minimal clinically important difference (MCID) is 4–6 points for the HDRS-17, there was no clinically meaningful difference in the HDRS score within or between groups at any other time point (20). For the HARS score, there were no significant main effect of time ($p = 0.70$), main effect of treatment ($p = 0.47$), and treatment-by-time interaction effect ($p = 0.58$).

Brain SPECT Imaging

Before testing models of interest, a two-sample *t*-test model was conducted to compare the baseline SPECT images between the active and sham groups and found that there was no significant difference in rCBF between groups at the baseline. In comparison with the changes in rCBF between the groups, a flexible factorial model identified a significant treatment-by-time interaction effect in the right superior temporal gyrus and left hippocampus or parahippocampus, controlling for age and sex (**Table 3** and **Figure 3**). *Post hoc* analysis of a paired *t*-test showed that the rCBF from the left superior frontal gyrus and left hippocampus was significantly decreased in the active group between the baseline and immediate follow-up, but no changes were observed in the sham group (**Table 3**).

Safety Outcomes

All participants filled out a survey on side effects after each session. The number of participants who reported side effects is summarized by groups in **Table 4**. The most reported side effects were transient dizziness and itchiness in both active and sham

groups. No significant group differences were observed for all side effects.

DISCUSSION

To the best of our knowledge, this was the first randomized, double-blind, sham-controlled trial that investigated the effects of tDCS in patients with PPPD. Our study found no significant beneficial effects of tDCS on dizziness symptoms and balance confidence, measured by DHI and ABC scale, respectively. Regarding psychiatric symptoms, there was no clinically meaningful effect of anodal tDCS on depressive and anxiety symptoms measured by HDRS and HARS, respectively.

The demographic characteristics of the participants were typical of PPPD. Mean age was middle-aged and female predominance was noted. Most patients reported that precipitating events were peripheral vestibular disorder but two patients could not identify any specific trigger. The failure to identify precipitants could be attributed in part to the patients regarding the triggers as trivial or having difficulty linking the seemingly unrelated triggers to the development of their symptoms.

The absence of tDCS effects on dizziness symptoms in PPPD patients contradicts the previous open-label study, which reported a significant reduction of DHI scores on the last day of the 5-day tDCS treatment in patients with PPV; however, these effects were transient and were not observed during the 1, 2, and 4-week follow-ups (18). In addition, although not statistically significant, this previous study showed a tendency for decreased depression and anxiety symptoms after the treatment compared to the baseline. Due to the absence of a control group

TABLE 3 | Information on the significant clusters for both the interaction contrast and the within-group contrast.

Region	*t*	*p*	Coordinates (x, y, z)	Cluster size (voxels)
Interaction				
Anode < sham				
Right superior temporal gyrus	4.78	<0.001	66, −2, 2	75
Left hippocampus	4.3	<0.001	−20, −32, −10	127
Within-Anode				
Baseline > immediate follow-up				
Left hippocampus	6.55	<0.001	−20, −32, 4	61
Left superior frontal gyrus	6.14	<0.001	−24, 54, 10	95
Within-Sham				
No significant findings				

All analyses used models with age and sex as covariates. The coordinates refer to the Montreal Neurological Institute coordinate system.

TABLE 4 | Reported side effects between treatment groups.

Side effects	Active group (*n* = 11)*	Sham group (*n* = 11)	*p*-value
Dizziness (*n*)	6	6	1.00
Itchiness (*n*)	6	4	0.81
Headache (*n*)	5	3	0.66
Tingling sensation (*n*)	5	3	0.66
Pain at the stimulation site (*n*)	3	3	1.00
Sleepiness (*n*)	3	2	1.00
Neck pain (*n*)	3	1	0.58
Redness of skin (*n*)	3	1	0.58
Reduced concentration (*n*)	3	1	0.58
Fatigue (*n*)	3	2	1.00
Nausea (*n*)	1	2	1.00
Burning sensation (*n*)	1	2	1.00

**Side effects records for 1 participant from the active group were missing.*

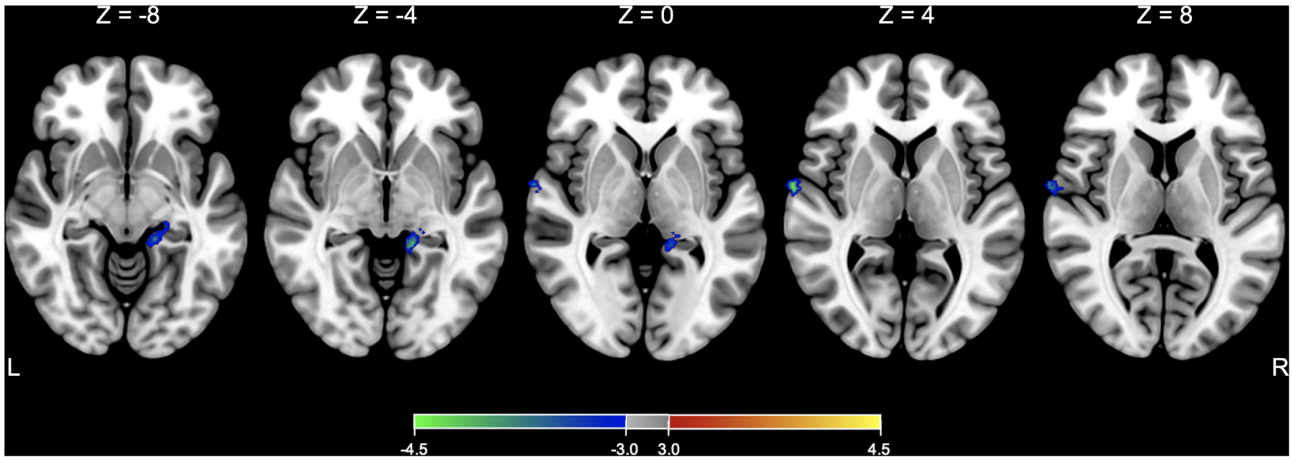

FIGURE 3 | SPECT analysis results. Significant areas with treatment (active vs. sham) x time (baseline vs. immediate follow-up) interaction effects of rCBF are overlaid on the Montreal Neurological Institute (MNI) 152 template. Color bar represents the voxel-level *t*-values.

and the small sample size, the results from this previous study should be interpreted with caution. For the DHI, our study revealed that there was a significant main effect of time. The gradually decreased dizziness symptoms with time in both groups could be due to the effects of SSRIs, as the treatment efficacy of serotonergic medication in PPPD has been proven in the previous studies (4, 14, 21).

Unexpectedly in our study, the severity of depressive symptoms increased at the 3-month follow-up in the patients of the sham group, whereas the severity of depressive symptoms remained stable in the patients of the active group. These results were not due to the outliers as the baseline HDRS scores were increased at the 3-month follow-up in 6 patients in the sham group, which is almost half of the patients in the group. The reasons for this isolated increase in the HDRS score in the sham group at the 3-month follow-up are unclear but may be due to the clinical outcome not meeting patients' expectations, frustration or anger with sustained dizziness symptoms, or initially underestimated baseline symptom (17, 22).

In our study, the brain SPECT analysis revealed a significant treatment-by-time effect on rCBF in the left hippocampus and right superior temporal areas. The *post hoc* analysis showed that the rCBF was decreased at the immediate follow-up compared to the baseline only in the active group. Considering that these regions are regarded as the components of multimodal vestibular cortical areas (22), this tDCS protocol might have unintentionally exacerbated the maladapted brain function to the extent that clinical symptoms did not worsen.

Several assumptions could be made concerning the absence of tDCS effects in patients with PPPD. First, it is possible that the target area for stimulation might be inappropriate. The left DLPFC was chosen as the target area based on the previous tDCS studies in PPV (18) and also in various neurological and psychiatric disorders including major depression disorder, addiction or craving, tinnitus, and neurodegenerative disorders (23). We expected that anodal tDCS would have positive effects on chronic dizziness by ameliorating various cognitive functions related to the high-risk postural control strategies, stimulating the functionally decreased prefrontal regions (24), and improving possibly coexisting psychiatric symptoms such as depressive or anxious mood in patients with PPPD. Contrary to the expectations, anodal tDCS did not improve dizziness symptoms compared to sham tDCS. In functional neuroimaging studies in PPPD, it was reported that the local activity and connectivity in the multimodal vestibular area are usually decreased and the connectivity between the prefrontal and primary visual areas is usually increased, which is related to the over-reliance on the visual stimuli (19, 24). In neurological disorders with chronic pain, the M1 (the primary motor cortex) area is adopted as the target area other than the dorsolateral prefrontal region (25). Patients with fibromyalgia and diabetic polyneuropathy who received tDCS stimulation on the M1 area showed efficacy on various pain measures but studies targeting the DLPFC were failed to show such effects (25, 26). Like these cases, changing the stimulation target might have therapeutic effects and should be tested in future studies. For example, tDCS stimulation on the multimodal vestibular cortical areas could enhance the local activity and connectivities to other relevant regions and may directly induce the improvement of dizziness symptoms.

The lack of tDCS efficacy may also be due to the suboptimal parameters of the tDCS protocol for PPPD. Whereas the tDCS protocol used in this study consists of 15 tDCS sessions, the pilot study of tDCS on PPV was conducted with only 5 sessions (18). In the previous studies of major depressive disorder and fibromyalgia, about 10 sessions were commonly conducted (25, 27). On the other hand, a much greater number of sessions with longer periods have been used in several previous studies (28, 29). In addition, other treatment modalities of PPPD such as vestibular rehabilitation or medications are needed up to 12 weeks to achieve sustained benefit. Thus, the number of sessions in this study might be inappropriate. Finally, the interaction with medication also could be another reason for the lack of tDCS effects (30, 31).

This study has strengths in that, in spite of a relatively small sample size, it utilized a larger sample size than the only existing study regarding the effects of tDCS on PPV (18) and is the first double-blind study with a sham-controlled condition. Moreover, this study demonstrated the feasibility of home-based treatment, of which its importance is being acknowledged especially in this pandemic era. Considering the reported adverse events in our study and the dropout rate of the enrolled patients, the home-based tDCS appears to be safe and easy to apply. This study has several limitations. We did not perform any prior power analysis. Therefore, due to the underpowered design, it cannot be ruled out that we may not detect the true effect of tDCS. Moreover, in spite of possible drug-induced effects over the tDCS effects, our study was not a monotherapy trial as it was difficult to conduct a study that would restrict patients from receiving SSRI/SNRIs, medications in which early studies have shown some benefits for treating PPPD, for more than 3 months in a clinical setting.

In conclusion, active tDCS targeting the left DLPFC was not found to be significantly more efficacious than sham tDCS on dizziness symptoms in patients with PPPD. Considering the high incidence of PPPD and the overall response rate of serotonergic medication, developing an alternative treatment option is needed. Our findings encourage further investigation on the effects of tDCS in PPPD, which considers different stimulation protocols in terms of stimulation site or the number of sessions.

DATA AVAILABILITY STATEMENT

The raw data supporting the conclusions of this article will be made available by the authors, without undue reservation.

ETHICS STATEMENT

The studies involving human participants were reviewed and approved by the Institutional Review Board of the Incheon St. Mary's Hospital. The patients/participants provided their written informed consent to participate in this study. Written informed consent was obtained from the individual(s) for the

publication of any potentially identifiable images or data included in this article.

AUTHOR CONTRIBUTIONS

JI, SN, Y-AC, and I-US: conceived and designed the study. JI and Y-AC: obtained the funding. Y-AC, I-US, T-KL, and W-YA: provided supervision. JI, E-SL, and SN: collected the data. HJ: independently performed the randomization process. JI, SK, and SN: performed data analysis and wrote the first draft of the manuscript. All authors contributed to manuscript revisions and read and approved the final version of the manuscript for submission.

FUNDING

This research was supported by the Basic Science Research Program through the National Research Foundation of Korea (NRF) and funded by the Ministry of Science and ICT (2018R1A6A3A11041118).

ACKNOWLEDGMENTS

We thank the patients who participated in the study and Seunghee Kim for her assistance with data entry and management.

REFERENCES

1. Popkirov S, Staab JP, Stone J. Persistent postural-perceptual dizziness (PPPD): a common, characteristic and treatable cause of chronic dizziness. *Pract Neurol.* (2018) 18:5–13. doi: 10.1136/practneurol-2017-001809
2. Staibano P, Lelli D, Tse D. A retrospective analysis of two tertiary care dizziness clinics: a multidisciplinary chronic dizziness clinic and an acute dizziness clinic. *J Otolaryngol Head Neck Surg.* (2019) 48:1–8. doi: 10.1186/s40463-019-0336-9
3. Kim H-J, Lee J-O, Choi J-Y, Kim J-S. Etiologic distribution of dizziness and vertigo in a referral-based dizziness clinic in South Korea. *J Neurol.* (2020) 267:2252–9. doi: 10.1007/s00415-020-09831-2
4. Staab JP, Ruckenstein MJ, Amsterdam JD, A. prospective trial of sertraline for chronic subjective dizziness. *Laryngoscope.* (2004) 114:1637–41. doi: 10.1097/00005537-200409000-00025
5. Staab JP, Ruckenstein MJ. Expanding the differential diagnosis of chronic dizziness. *Arch Otolaryngol Head Neck Surg.* (2007) 133:170–6. doi: 10.1001/archotol.133.2.170
6. Brandt T. Phobic postural vertigo. *Neurology.* (1996) 46:1515–9. doi: 10.1212/WNL.46.6.1515
7. Bronstein AM. Visual vertigo syndrome: clinical and posturography findings. *J Neurol Neurosurg Psychiatry.* (1995) 59:472–6. doi: 10.1136/jnnp.59.5.472
8. Jacob RG, Lilienfeld SO, Furman JM, Durrant JD, Turner SM. Panic disorder with vestibular dysfunction: further clinical observations and description of space and motion phobic stimuli. *J Anxiety Disord.* (1989) 3:117–30. doi: 10.1016/0887-6185(89)90006-6
9. Jacob RG, Woody SR, Clark DB, Lilienfeld SO, Hirsch BE, Kucera GD, et al. Discomfort with space and motion: a possible marker of vestibular dysfunction assessed by the situational characteristics questionnaire. *J Psychopathol Behav Assess.* (1993) 15:299–324. doi: 10.1007/BF00965035
10. Staab JP, Eckhardt-Henn A, Horii A, Jacob R, Strupp M, Brandt T, et al. Diagnostic criteria for persistent postural-perceptual dizziness (PPPD): consensus document of the committee for the classification of vestibular disorders of the Bárány Society. *J Vestib Res.* (2017) 27:191–208. doi: 10.3233/VES-170622
11. Popkirov S, Stone J, Holle-Lee D. Treatment of persistent postural-perceptual dizziness (PPPD) and related disorders. *Curr Treat Options Neurol.* (2018) 20:50. doi: 10.1007/s11940-018-0535-0
12. Staab JP. Persistent postural-perceptual dizziness. *Semin Neurol.* (2020) 40:130–7. doi: 10.1055/s-0039-3402736
13. Soto E, Vega R, Seseña E. Neuropharmacological basis of vestibular system disorder treatment. *J Vestib Res.* (2013) 23:119–37. doi: 10.3233/VES-130494
14. Staab JP, Ruckenstein MJ. Chronic dizziness and anxiety: effect of course of illness on treatment outcome. *Arch Otolaryngol Head Neck Surg.* (2005) 131:675–9. doi: 10.1001/archotol.131.8.675
15. Min S, Kim JS, Park HY. Predictors of treatment response to pharmacotherapy in patients with persistent postural-perceptual dizziness. *J Neurol.* (2021) 268:2523–32. doi: 10.1007/s00415-021-10427-7
16. Brunoni AR, Nitsche MA, Bolognini N, Bikson M, Wagner T, Merabet L, et al. Clinical research with transcranial direct current stimulation (tDCS): challenges and future directions. *Brain Stimul.* (2012) 5:175–95. doi: 10.1016/j.brs.2011.03.002
17. Utz KS, Dimova V, Oppenländer K, Kerkhoff GJN. Electrified minds: transcranial direct current stimulation (tDCS) and galvanic vestibular stimulation (GVS) as methods of non-invasive brain stimulation in neuropsychology—a review of current data and future implications. *Neuropsychologia.* (2010) 48:2789–810. doi: 10.1016/j.neuropsychologia.2010.06.002
18. Palm U, Kirsch V, Kübler H, Sarubin N, Keeser D, Padberg F, et al. Transcranial direct current stimulation (tDCS) for treatment of phobic postural vertigo: an open label pilot study. *Eur Arch Psychiatry Clin Neurosci.* (2019) 269:269–72. doi: 10.1007/s00406-018-0894-2
19. Im JJ, Na S, Jeong H, Chung Y-A. A review of neuroimaging studies in persistent postural-perceptual dizziness (PPPD). *Nucl Med Mol Imaging.* (2021) 55:53–60. doi: 10.1007/s13139-020-00675-2
20. Rush AJ, South C, Jain S, Agha R, Zhang M, Shrestha S, et al. Clinically significant changes in the 17- and 6-item hamilton rating scales for depression: a STAR*D report. *Neuropsychiatr Dis Treat.* (2021) 17:2333–45. doi: 10.2147/NDT.S305331
21. Yu YC, Xue H, Zhang YX, Zhou J. Cognitive behavior therapy as augmentation for sertraline in treating patients with persistent postural-perceptual dizziness. *Biomed Res Int.* (2018) 2018:8518631. doi: 10.1155/2018/8518631
22. Brandt T, Dieterich M. The vestibular cortex: its locations, functions, and disorders. *Ann N Y Acad Sci.* (1999) 871:293–312. doi: 10.1111/j.1749-6632.1999.tb09193.x
23. Lefaucheur J-P, Antal A, Ayache SS, Benninger DH, Brunelin J, Cogiamanian F, et al. Evidence-based guidelines on the therapeutic use of transcranial direct current stimulation (tDCS). *Clinical Neurophysiology.* (2017) 128:56–92. doi: 10.1016/j.clinph.2016.10.087
24. Indovina I, Passamonti L, Mucci V, Chiarella G, Lacquaniti F, Staab JP. Brain Correlates of persistent postural-perceptual dizziness: a review of neuroimaging studies. *Journal of Clinical Medicine.* (2021) 10:4274. doi: 10.3390/jcm10184274
25. Brighina F, Curatolo M, Cosentino G, De Tommaso M, Battaglia G, Sarzi-Puttini PC, et al. Brain modulation by electric currents in fibromyalgia: a structured review on non-invasive approach with transcranial electrical stimulation. *Front Human Neurosci.* (2019) 13:40. doi: 10.3389/fnhum.2019.00040
26. Kim YJ, Ku J, Kim HJ, Im DJ, Lee HS, Han KA, et al. Randomized, sham controlled trial of transcranial direct current stimulation for painful diabetic polyneuropathy. *Ann Rehabil Med.* (2013) 37:766–76. doi: 10.5535/arm.2013.37.6.766
27. Razza LB, Palumbo P, Moffa AH, Carvalho AF, Solmi M, Loo CK, et al. A systematic review and meta-analysis on the effects of transcranial direct current stimulation in depressive episodes. *Depress Anxiety.* (2020) 37:594–608. doi: 10.1002/da.23004

28. Aparicio LV, Rosa V, Razza LM, Sampaio-Junior B, Borrione L, Valiengo L, et al. Transcranial direct current stimulation (tDCS) for preventing major depressive disorder relapse: results of a 6-month follow-up. *Depress Anxiety.* (2019) 36:262–8. doi: 10.1002/da.22878
29. Im JJ, Jeong H, Bikson M, Woods AJ, Unal G, Oh JK, et al. Effects of 6-month at-home transcranial direct current stimulation on cognition and cerebral glucose metabolism in Alzheimer's disease. *Brain Stimul.* (2019) 12:1222–8. doi: 10.1016/j.brs.2019.06.003
30. Brunoni AR, Ferrucci R, Bortolomasi M, Scelzo E, Boggio P, Fregni F, et al. Interactions between transcranial direct current stimulation (tDCS) and pharmacological interventions in the major depressive episode: findings from a naturalistic study. *European Psychiatry.* (2013) 28:356–61. doi: 10.1016/j.eurpsy.2012.09.001
31. McLaren ME, Nissim NR, Woods AJ. The effects of medication use in transcranial direct current stimulation: a brief review. *Brain Stimul.* (2018) 11:52–8. doi: 10.1016/j.brs.2017.10.006

Conflict of Interest: The authors declare that the research was conducted in the absence of any commercial or financial relationships that could be construed as a potential conflict of interest.

Publisher's Note: All claims expressed in this article are solely those of the authors and do not necessarily represent those of their affiliated organizations, or those of the publisher, the editors and the reviewers. Any product that may be evaluated in this article, or claim that may be made by its manufacturer, is not guaranteed or endorsed by the publisher.

Copyright © 2022 Im, Na, Kang, Jeong, Lee, Lee, Ahn, Chung and Song. This is an open-access article distributed under the terms of the Creative Commons Attribution License (CC BY). The use, distribution or reproduction in other forums is permitted, provided the original author(s) and the copyright owner(s) are credited and that the original publication in this journal is cited, in accordance with accepted academic practice. No use, distribution or reproduction is permitted which does not comply with these terms.

frontiers | Frontiers in Neurology

ORIGINAL RESEARCH
published: 15 April 2022
doi: 10.3389/fneur.2022.877342

Purification of Fibroblasts From the Spiral Ganglion

*Annett Anacker[1], Karl-Heinz Esser[2], Thomas Lenarz[1,3] and Gerrit Paasche[1,3]**

[1] Department of Otolaryngology, Hannover Medical School, Hannover, Germany, [2] Stiftung Tierärztliche Hochschule Hannover, Hannover, Germany, [3] Cluster of Excellence Hearing4all, Hannover Medical School, Hannover, Germany

Using cultures of freshly isolated spiral ganglion cells (SGC) is common to investigate the effect of substances on spiral ganglion neurons (SGN) *in vitro*. As these cultures contain more cell types than just neurons, and it might be beneficial to have cochlear fibroblasts available to further investigate approaches to reduce the growth of fibrous tissue around the electrode array after cochlear implantation, we aimed at the purification of fibroblasts from the spiral ganglion in the current study. Subcultivation of the primary SGC culture removed the neurons from the culture and increased the fibroblast to glial cell ratio in the preparations, which was revealed by staining for vimentin, the S100B-protein, and the 200-kD neurofilament. We performed direct immunolabeling for the Thy1-glycoprotein and the p75NGFR-enabled fluorescence-based cell sorting. This procedure resulted in a cell culture of cochlear fibroblasts with a purity of more than 99%. The received fibroblasts can be subcultivated for up to 10 passages before proliferation rates drop. Additionally, 80% of the cells survived the first attempt of cryopreservation and exhibited a fibroblast-specific morphology. Using the described approach provides a purified preparation of cochlear fibroblasts, which can now be used *in vitro* for further investigations.

Keywords: inner ear, spiral ganglion cells, cochlear fibroblasts, Thy1, vimentin, cell sorting

OPEN ACCESS

Edited by:
In Seok Moon, Yonsei University Health System, South Korea

Reviewed by:
Alexsandra Fernandes Pereira, Federal University Rural Semi-Arid, Brazil
Anandhan E. Dhanasingh, MED-EL, Austria

***Correspondence:**
Gerrit Paasche
paasche.gerrit@mh-hannover.de

Specialty section:
This article was submitted to Neuro-Otology, a section of the journal Frontiers in Neurology

Received: *16 February 2022*
Accepted: *21 March 2022*
Published: *15 April 2022*

Citation:
Anacker A, Esser K-H, Lenarz T and Paasche G (2022) Purification of Fibroblasts From the Spiral Ganglion. Front. Neurol. 13:877342. doi: 10.3389/fneur.2022.877342

INTRODUCTION

Fibroblasts are the main cells of the loose fibrous tissue and are responsible for the formation of the extracellular matrix (1). Besides fibroblasts, fibrous tissue contains also other cells such as lymphocytes, granulocytes, macrophages, and mast cells, which are a part of the immune defense. The morphology of the fibroblasts can be variable and appears to be tissue-specific (1). Fibroblasts are involved in wound healing and encapsulation of foreign bodies (2, 3). In the cochlea, this is of special importance in connection to cochlear implantation. After the insertion of the cochlear implant (CI) electrode array into scala tympani, an increase in electrical impedance at the stimulating contacts can be observed (4, 5). Even though not all authors agree, this was shown to be connected to the formation of fibrous tissue around the electrode array (6, 7).

Potentially, there are at least three possible sources where fibroblasts could be recruited for this process. The first option is that the fibroblasts are derived from pieces of tissue (muscle or fascia) that are typically used to seal the entrance of the electrode array into the cochlea, which can be a cochleostomy or the round window (8). Indication for this was found in earlier studies showing that the increase in impedance starts at the basal electrodes (5). But this study also showed that the impedance increase can be higher in the apical contacts than in the middle contacts. This might indicate that there are additionally other sources of the fibroblasts. As the electrode arrays

have to be inserted into the spiral of the scala tympani, they will most likely touch the cochlear walls during insertion or when taking its final position. This might, depending on the electrode type (straight or perimodiolar) and insertion technique, injure either the lateral wall or/and the modiolar wall close to Rosenthal's canal and could include bleeding, which is known to enhance tissue formation (9). These regions are considered the other two possible sources of fibroblasts.

Despite huge efforts to reduce tissue growth after cochlear implantation (10), this problem is not solved yet and needs further attention. To facilitate further *in vitro* tests in this direction, organ-specific cell cultures might be helpful. There is one report on an immortalized fibroblast cell line originating from type I fibrocytes of the spiral ligament (11). The authors considered this cell line a research tool for investigating homeostasis and inflammation in the ear and it was used in several reports in this context. According to Yian et al. (11), type I fibrocytes can mainly be found next to stria vascularis, far away from scala tympani.

In our lab, the preparation of spiral ganglion cells (SGC) was established for many years to investigate the effects of drugs and electrical stimulation on spiral ganglion neurons (SGN) (12, 13). But this is a mixed culture containing more of other cells than neurons. Besides neurons, the spiral ganglion contains mainly glial cells of the peripheral nervous system and endoneural fibroblasts, which are embedded in the endoneural fibrous tissue. The spiral ganglion is surrounded by a fibrous capsule, which extends into the epi- and perineurium of the nerve fibers (14). Therefore, it is to be expected that at least glial cells and fibroblasts are part of the dissociated SGC culture. Enrichment and purification of Schwann cells from these cultures using either different adhesion properties to surfaces (15) or an immune-magnetic purification procedure (16) was described, but there was no purification of fibroblasts. Both authors used the p75NGF-receptor staining to identify the Schwann cells of the spiral ganglion, as described by Whitlon et al. (17).

The aim of the current study was to purify cochlear fibroblasts from the existing mixed culture of SGC and make them available for other investigations *in vitro*.

MATERIALS AND METHODS

Ethics Statement

All experiments were carried out according to the German "Law on Protecting Animals" (§4) and with the European Directive 2010/63/EU for the protection of animals used for experimental purposes. These experiments were registered (2013/44 and TVT-2017-V-95) with the local authorities.

Animals

Sprague–Dawley rats (postnatal days 2–4) of both sexes were used for the experiments with one exception (postnatal day 1). Animals were kept at room temperature with 50–60% relative humidity. They had access to food and water *ad libitum*. Day–night cycle was automatically regulated with 12 h each. Rat pups were separated from their mothers about 30 min before cell preparation and kept in groups at 37°C.

Preparation of Spiral Ganglion Cells

Spiral ganglion cells were prepared as described by Wefstaedt et al. (12). Briefly, the rats were decapitated, skull opened, and subsequently the cochlea removed from the temporal bone and transferred into ice-cold phosphate-buffered saline (PBS). Under a stereomicroscope (Leica-MZ6) and by means of fine forceps (Dumont), the cochlea was opened by removing

TABLE 1 | Overview on conditions for the different cell preparations.

Preparation/sort number	Age of the animals [d]	Time to subcultivation [d]	Confluence in T25 [%]	Amount of trypsin [%]	Duration of trypsin incubation [min]	Harvested cells [%]
1	3–4	8	100	0.05	7	70
2	3	6	90	0.05	7	80
3	2	4	90	0.05	7	90
4	2	4	70	0.25	5	95
5	3–4	8	100	0.05	7	70
6	1	6	100	0.05	7	70
7	3	5	95	0.15	4	90
8	2–4	5	100	0.15	4	90
9	3	8	100	0.15	4	95
10	2–3	11	100	0.15	4	95
11	2–4	8	100	0.15	4	95
12	2–4	9	100	0.15	4	95
13	2–4	7	100	0.15	4	95

the outer shell. In the next step, the spiral ligament, organ of Corti, and spiral ganglion were disconnected from the modiolus before the spiral ganglion was separated from the other parts and transferred to ice–cold Hank's buffered salt solution (HBSS) without calcium and magnesium. The spiral ganglia were enzymatically and mechanically dissociated. They were transferred to HBSS solution containing 0.1% trypsin (BIOCHROM, Berlin, Germany), 0.1% DNase I (ROCHE, Basel, Switzerland), and 0.01% collagenase and then incubated for 17–20 min at 37°C, 5% CO_2, and 95% humidity. Dissociation was stopped by adding pre-warmed fetal calf serum, and the cells were transferred to a serum-free medium. Mechanical dissociation was performed by gentle trituration. Dissociated cells were then transferred into fibroblast specific medium containing 89% DMEM + L-glutamine, 10% FCS, and 1% penicillin/streptomycin.

Cell Culture

Spiral ganglion cells were seeded at densities of 3×10^5 cells per T25 culture flask, kept at 37°C, 5% CO_2, and 95% humidity. The medium was exchanged every 2–4 days. When the cells reached confluence, they were detached by the addition of trypsin (concentrations between 0.05 and 0.25%)/0.02% EDTA solution. To stop the enzyme action, 3–5 ml pre-warmed medium with FCS was added. Cells were counted in a Neubauer counting chamber after adding 10 µl trypan blue (0.5%) to 10 µl of cell suspension. An overview of the different conditions used to prepare the cells for sorting is provided in **Table 1**.

Immunolabeling

For immunolabeling, 1×10^4 cells were seeded on coverslips positioned in 24-well plates and fixed after 72 h. Cells on coverslips were washed twice with PBS before fixation by the addition of 300 µl PFA (4%) to the wells for 10 min. After the removal of PFA, cells were again washed twice with Tris-buffered saline (TBS) and additionally incubated with TBS for 5 min. Then TBS was removed, 600 µl PBS

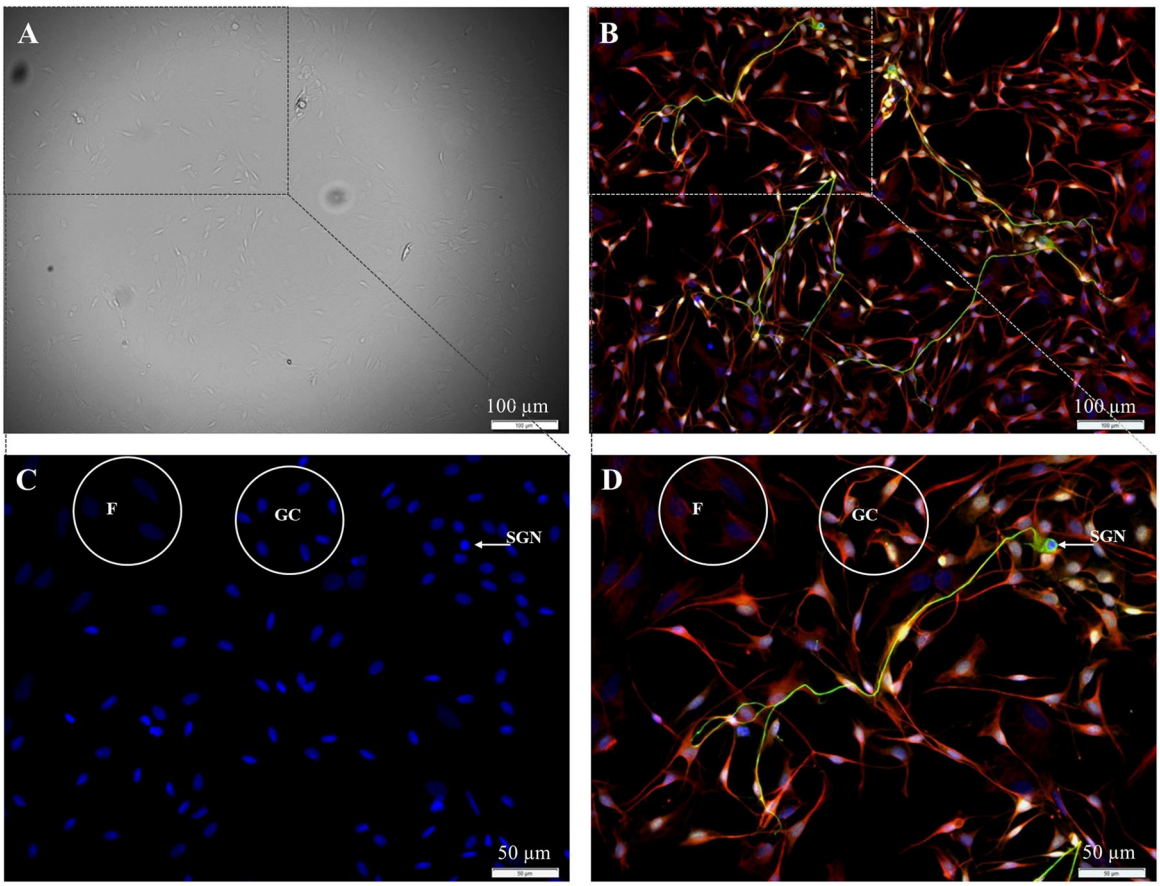

FIGURE 1 | Isolated cells from the spiral ganglion after 72 h cultivation. **(A)** DIC-image, exposure time 40 ms. **(B–D)** Fluorescence images: 200 kD-NF (DL488, green), S100B-protein (Cy3, yellow), vimentin, *clone V9* (Cy5, red), DAPI (blue). Exposure times: **(B)** DL488 1 s, Cy3 500 ms, Cy5 500 ms, DAPI 800 ms. **(C,D)** Higher magnification of the marked section in B. DL488 1 s, Cy3 200 ms, Cy5 1 s, DAPI 800 ms. **SGN:** 200kD-NF-positive spiral ganglion neuron. **GC:** S100B- and vimentin-positive glial cells. **F:** Vimentin-positive fibroblasts.

For indirect immunocytochemistry, the following primary antibodies were used.

Antibody against	Type	Source	Catalog-number	Dilution
Intracellular:				
200kD-NF	polyclonal, chicken-IgY	Abcam, Cambridge, UK	Ab4680	1:10,000
S100, *astrocyte marker*	polyclonal, rabbit-IgG	Abcam	Ab868	1:100
Vimentin, *clone V9*	monoclonal, mouse-IgG	DakoCytomation, Wiesentheid, Germany	M0725	1:75
carbonic-anhydrase II	polyclonal, rabbit-IgG	Abcam	Ab6621	1:50
Connexin-26 (Cx26)	monoclonal, mouse-IgG	Invitrogen, Karlsruhe, Germany	13-8100	1:50
S100	polyclonal, rabbit-IgG	Sigma-Aldrich GmbH, Steinheim, Germany	S2644	1:100
Extracellular:				
Thy1.1, *clone Ox-7*	monoclonal, mouse-IgG	Merck Millipore, Darmstadt, Germany	MAB 1406	1:100
p75NGFR	polyclonal, rabbit-IgG	Abcam	Ab8874	1:400
As secondary antibodies were used:				
rabbit-IgG, *Cy3-conjugated*	polyclonal, goat-IgG	JacksonImmunoResearch Laboratories, Hamburg, Germany	111-165-045	1:500
chicken-IgY, *DL488-conjugated*	polyclonal, goat-IgG	Abcam	Ab96947	1:250
mouse-IgG, *Cy5-conjugated*	polyclonal, goat-IgG	Abcam	Ab97037	1:250
Direct immunolabeling of the cells for sorting was performed using:				
Thy1 (CD90.1), *clone Ox-7*, *FITC-conjugated*	monoclonal, mouse-IgG	Merck Millipore	CBL1500F	10 μl/1 × 10^6 cells
p75NGFR (192-IgG), *PE-conjugated*	monoclonal, mouse-IgG	Santa Cruz Biotechnology, Inc., Heidelberg, Germany	Sc - 71691	1 μg/1 × 10^6 cells

was added to each well, and the cells were stored at 4°C until staining.

Antibodies were diluted by adding a solution containing 10 ml PBS and 0.858 ml bovine serum albumin (BSA) solution (0.7 g BSA in 2 ml aqua dest). For intracellular staining, the cells were permeabilized by the addition of 300 μl of 0.1% PBT (0.5 g Triton X-100 in 500 ml PBS) per well for 5 min at room temperature (RT). After washing with PBS (3×), the cells were first incubated for 1 h at RT in 20 μl of the solution containing the primary antibody followed by further washing steps. Then incubation with 20 μl of the secondary antibody followed by washing in PBS was performed. The cells were then covered using ProLong-Gold-Antifade reagent with DAPI (Life Technologies GmbH, Darmstadt, Germany). For this, 5 μl of the reagent was added on a slide and the coverslip with the cells was put on it such that no air bubbles were entrapped. The slides were dried for at least 12 h and then stored at 4°C while keeping them in the dark.

Cell Sorting

The harvested cells were counted and transferred to the buffer solution for cell sorting consisting of 12.5 ml PBS and 1.79 ml BSA solution. A total of 1 × 10^6 cells was re-suspended in 1 ml buffer solution. Staining for Thy1 (FITC-conjugated, fibroblasts) or p75NGFR (PE-conjugated, glial cells) was done at the concentrations recommended by the manufacturers by the addition of 10 μl Thy1-antibody and 20 μl p75NGFR antibody per 100 μl buffer solution with cells for 30 min and subsequent washing of the cell preparation. In addition, at least 5 × 10^4 cells remained unlabeled as the negative control.

Cell sorting was done using a MoFlo^{TM}-XDP Upgrade high-speed sorter (Beckman Coulter GmbH, Krefeld, Germany) equipped with a 488-nm solid-state laser. Before the sort, cells were filtered through a 70-μm nylon filter. The nozzle used had a diameter of 100 μm. The process was controlled and the data was analyzed by Summit-software 5.1.0, which is running the system. The negative controls were always investigated first to check and optimize settings.

To confirm the purity of each preparation, the collected fibroblasts were re-analyzed. Finally, collected fibroblasts were centrifuged at 800 rpm for 5 min, the supernatant removed, and the cells re-suspended in 5 ml warm medium before culturing the cells again.

Microscopy

Immunolabeled cells were documented using an Olympus-Bx51 fluorescence microscope (Olympus, Hamburg, Germany) equipped with 4×, 10×, 20×, and 40× optics and the following filter sets: F41-017 (DL488), U-MWIG3 (Cy3), U-M41024 (Cy5), and U-MWU2 (DAPI). Image acquisition was done via a cooled color camera (CAM-XC10) and a 1.4 MPixel CCD chip using

CellSense software (Olympus), which controlled all the settings for image acquisition. Individual settings are provided in the figure legends.

Cryoconservation

After subcultivation to 80% confluence in T75 flasks, the cells were trypsinized for 6 min by the addition of 3 ml of 0.05% trypsin solution. The process was stopped by adding 10 ml of pre-warmed medium. The cell suspension was transferred to a 15-ml Falcon tube and the number of cells were determined. After centrifugation at 800 rpm for 4 min, the cell pellet was resuspended in a freezing medium (95% FCS, 5% DMSO) such that a cell concentration of 1.4×10^6 cells per ml was achieved. Cells were then transferred into cryovials at 1-ml aliquots and frozen at −80°C. Two days later, the vials were stored in liquid nitrogen at −196°C.

After 3 weeks, cells were thawed again, taken into cell culture, and further subcultivated.

RESULTS

In the first step, the preparation of spiral ganglion cells was modified in a way that the fibroblast-specific medium was used for all preparation steps. Using this medium, SGN, glial cells, and fibroblasts were still found in the culture after 72 h of cultivation (**Figure 1**).

To increase the number of available cells, SGC were seeded in culture flasks (25 cm²) at densities of 1×10^5 to 5×10^5 cells and subcultivated after confluence was achieved. Starting with 3×10^5 cells, the time until confluence remained constant from passage P0 to P2 whereas for lower cell densities more time was necessary with each subcultivation to reach confluence (**Figure 2**). For all further subcultivation steps, a cell density of 3×10^5 cells per flask was used.

Subcultivation of the cell preparation removed the neuronal cells, and the number of glial cells in the preparations was reduced to about 30%. Additionally, the distribution of cells within the cultures appeared altered. Glial cells seem to arrange in clusters, whereas fibroblasts are widely spread (**Figure 3**). These results were independent of the amount of trypsin used and the duration of incubation with trypsin.

With this approach, only a fibroblast-enriched culture was achieved, and cells were now prepared for fluorescence-based cell sorting. To distinguish between neurons, fibroblasts, and glial cells, indirect labeling with fluorescent antibodies against the p75NGF receptor (glial cells), 200 kD neurofilament (SGN), and Thy1-glycoprotein (fibroblasts) was established with P0 preparations (**Figures 4A–D**) and later applied to P2 preparations (**Figure 4E**). Thy1 and p75NGFR were then used for direct immunofluorescence labeling of vital cells, which enabled cell sorting (**Figure 4F**). The neuron in **Figure 4** appears to be stained not only for the 200 kD neurofilament but also for p75NGFR and Thy1. Thy1 positive fibroblasts can have either a weak or intense staining (**Figures 4D–F**). Additionally, few cells without staining were found (**Figure 4E**, white arrowhead). As the neurons were removed by subcultivation, cells were either positive for Thy1 (fibroblasts) or p75NGFR (glial cells), but no coexpression was detected.

From each cell preparation, a negative control was tested first and the gates were defined. The first gate should remove cell debris and cell cluster. In gate 3, cells were classified according to their autofluorescence (**Figure 5**). Regions R4 (FITC-fluorescence) and R5 (PE) should still be empty. Intensity values below $10^{2.3}$ (FITC-channel) and below $10^{2.7}$ (PE-channel) were defined as autofluorescence. Investigating negative controls, no counts were detected in R4 and R5 for all the samples.

An example of the results of a stained preparation is presented in **Figure 6**, where cells were also found in R4 and R5. The number of counts in both regions is given in G4 with the R9 region comprising all cells counted in R4, which are the FITC-labeled fibroblasts.

Parts of the collected fibroblasts were re-analyzed (**Figure 7**). This confirmed a very high purity of fibroblasts. Only in two out of 13 preparations, a single cell was detected in R5 (glial cells). In all other preparations, only fibroblasts (R4) were detected. This results in a purity of 99.9% cochlear fibroblasts, when averaged over all preparations. Some cells were damaged during the sorting procedure in all experiments.

An overview of the counted cell numbers for all preparations is provided in **Figure 8**. The total number of counted cells was between 3.3×10^5 (prep 5) and 1.2×10^7 (prep 12) with an average number of $3.6 \times 10^6 \pm 3.3 \times 10^6$ cells (mean ± SD). On average, the number of collected fibroblasts was 1.2×10^6, which is 33% of the total cell number before the sorting process. The number of counted glial cells was 1.2×10^5 (3.3% of total cells), far lower than the fibroblasts. Only in preparations 4 and 6 more glial cells than fibroblasts were detected.

The collected fibroblasts were cultured and subcultivated again. Intracellular staining revealed that all cells (100%) were Vimentin-positive and S100B negative (**Figure 9A**), indicating that (nearly) only fibroblasts were in the culture. This was confirmed by staining for p75NGFR and Thy1, where only Thy1 fluorescence was detected (**Figure 9B**). Additionally, all cells showed the typical morphology of fibroblasts. Again, cells with strong and weak fluorescence signals were detected.

The received fibroblast preparations were subcultivated for up to 16 passages. A relatively slow growth of cells was observed between P3 and P5 followed by P6 to P8 with the highest proliferation rates. Starting with P9 or P10, cell growth slowed down again before it stopped between P13 and P16. First morphological changes (granules were observed) could be observed starting from P5, which became more pronounced (nuclei appeared homogenous) around P10.

A first attempt was made for cryoconservation of the received cochlear fibroblast preparations (P5). After 3 weeks, cells were thawed and subcultivated for at least three more passages. After 24 h, about 80% of the cells adhered to the surface and after 3 days of culture, no differences to the non-frozen fibroblasts were found morphologically. Only the growth rate was slightly diminished from P2 after thawing.

Different populations of fibroblasts from the spiral ligament were distinguished according to their immunhistochemical

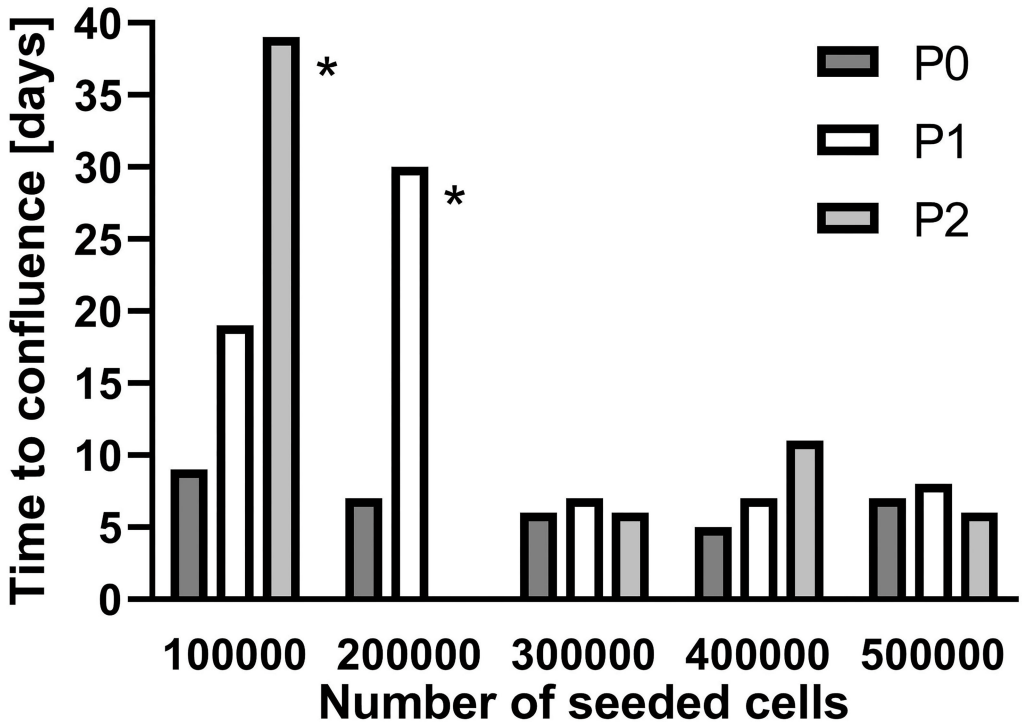

FIGURE 2 | Subcultivation of isolated spiral ganglion cells in T25 flasks. Growth until confluence is provided in days for different seeded cell numbers. **P0:** Primary cell culture. **P1:** First passage. **P2:** Second passage. *subcultivated at 60–65% coverage.

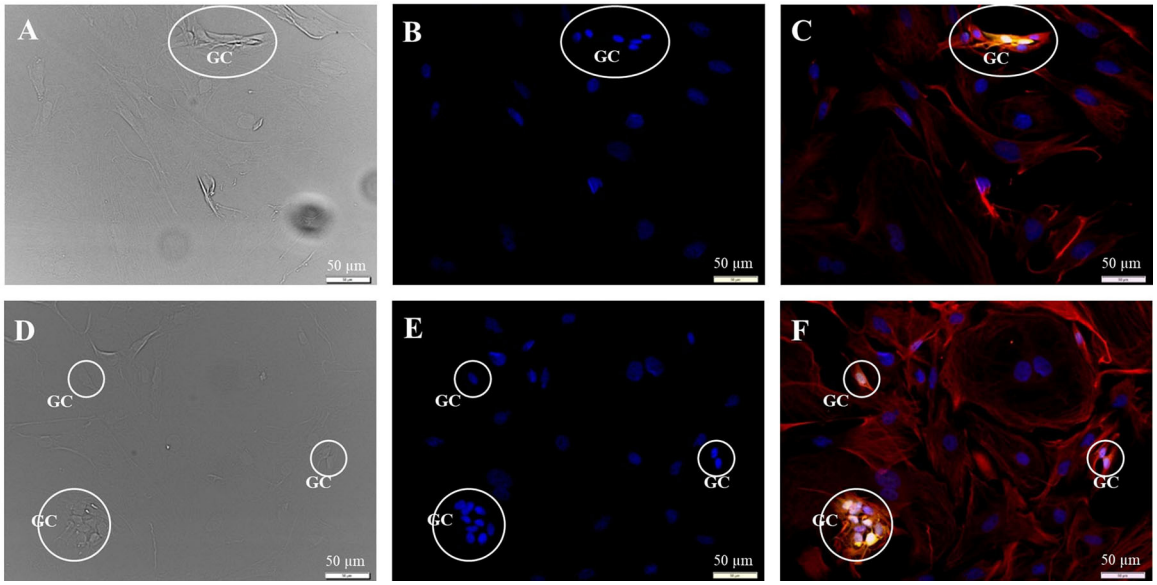

FIGURE 3 | Subcultivation of the SGC culture in fibroblast specific medium 72 h after seeding. Fluorescence images: 200kD-NF (DL488, green), S100B-protein (Cy3, yellow), vimentin, *clone V9* (Cy5, red), DAPI (blue). **(A–C)** Passage P1, exposure times: DIC 100 ms, DAPI 1 s, DL488 40 ms, Cy5 1 s, Cy3 50 ms. **(D–F)** Passage P2, exposure times: DIC 100 ms, DAPI 1 s, DL488 50 ms, Cy5 1 s, Cy3 137 ms. **GC:** S100B- and vimentin-positive glial cells.

profile (18–23). To be able to compare our fibroblasts from Rosenthal's canal with these published results, additional staining against S100, Connexin-26, and carbonic anhydrase II was performed. The fibroblasts from the current study were found to be positive for S100, vimentin, CAII, and Cx-26 (**Figure 10**).

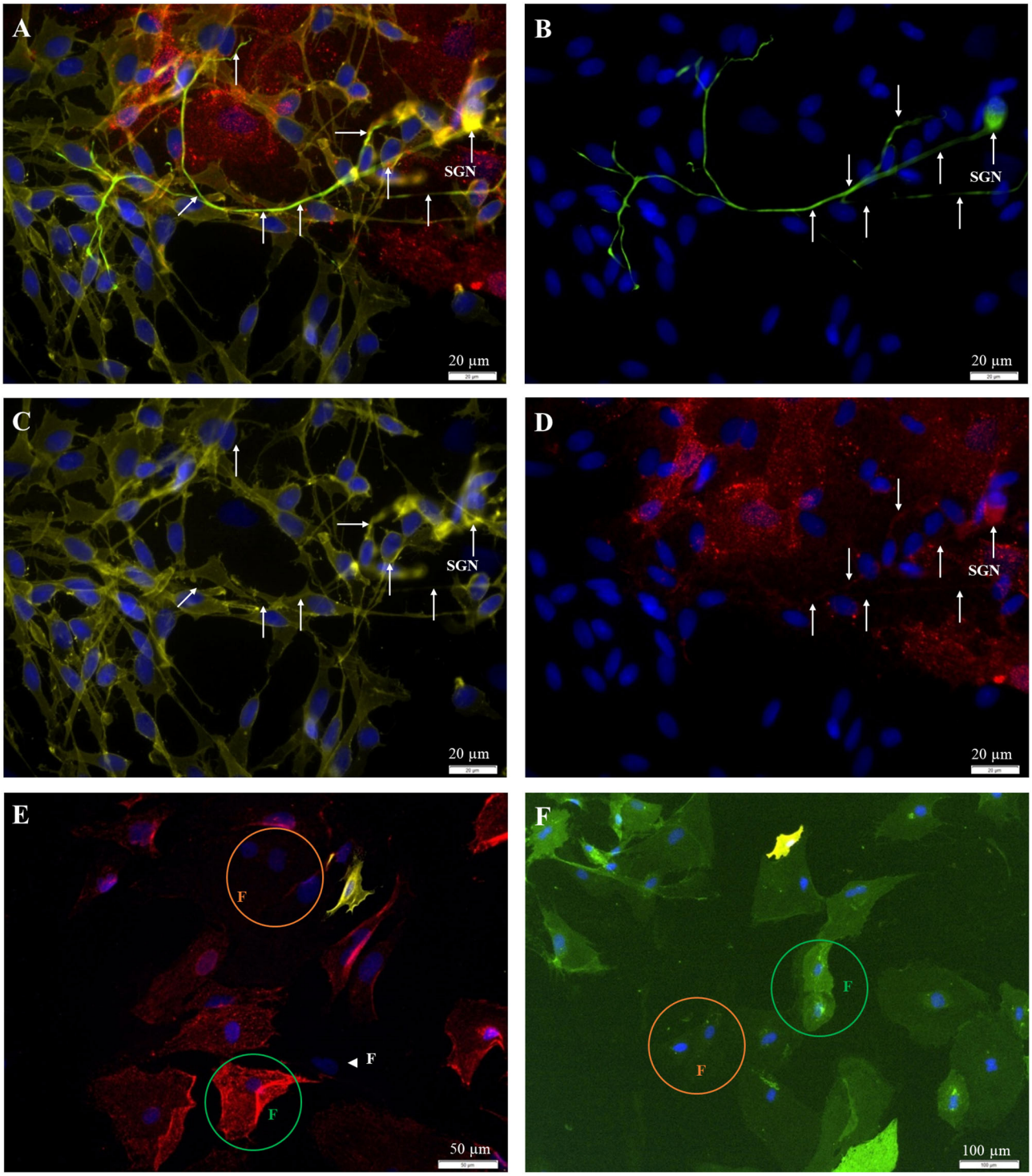

FIGURE 4 | Fluorescent staining of cultures [**(A**–**D)** P0; **(E,F)** P2]. **(A)** 200kD-NF (DL488, green, exposure time: 1 s), Thy1.1, *clone Ox-7* (Cy5, red, 5 s), p75NGFR (Cy3, yellow, 250 ms), DAPI (blue, 500 ms). **(B)** 200kD-NF of the SGN **(C)** p75NGFR-receptor (glial cells). **(D)** Thy1-protein (fibroblasts). **(E)** Indirect staining: Thy1.1, *clone Ox-7* (Cy5, red, 5 s), p75NGFR (Cy3, yellow, 600 ms), DAPI (blue, 1 s). **(F)** Direct staining: Thy1 (CD90.1), *clone Ox-7*, *FITC-conjugated* (green, 1 s), p75NGFR (192-IgG), *PE-conjugated* (yellow, 1 s), DAPI- (blue, 1 s). **White arrows:** SGN with neurites. **Green circle:** Strong Thy1-fluorescence. **Orange circle:** weak Thy1-fluorescence, **Arrowhead:** p75NGFR- und Thy1-negative cell with fibroblast-like morphology.

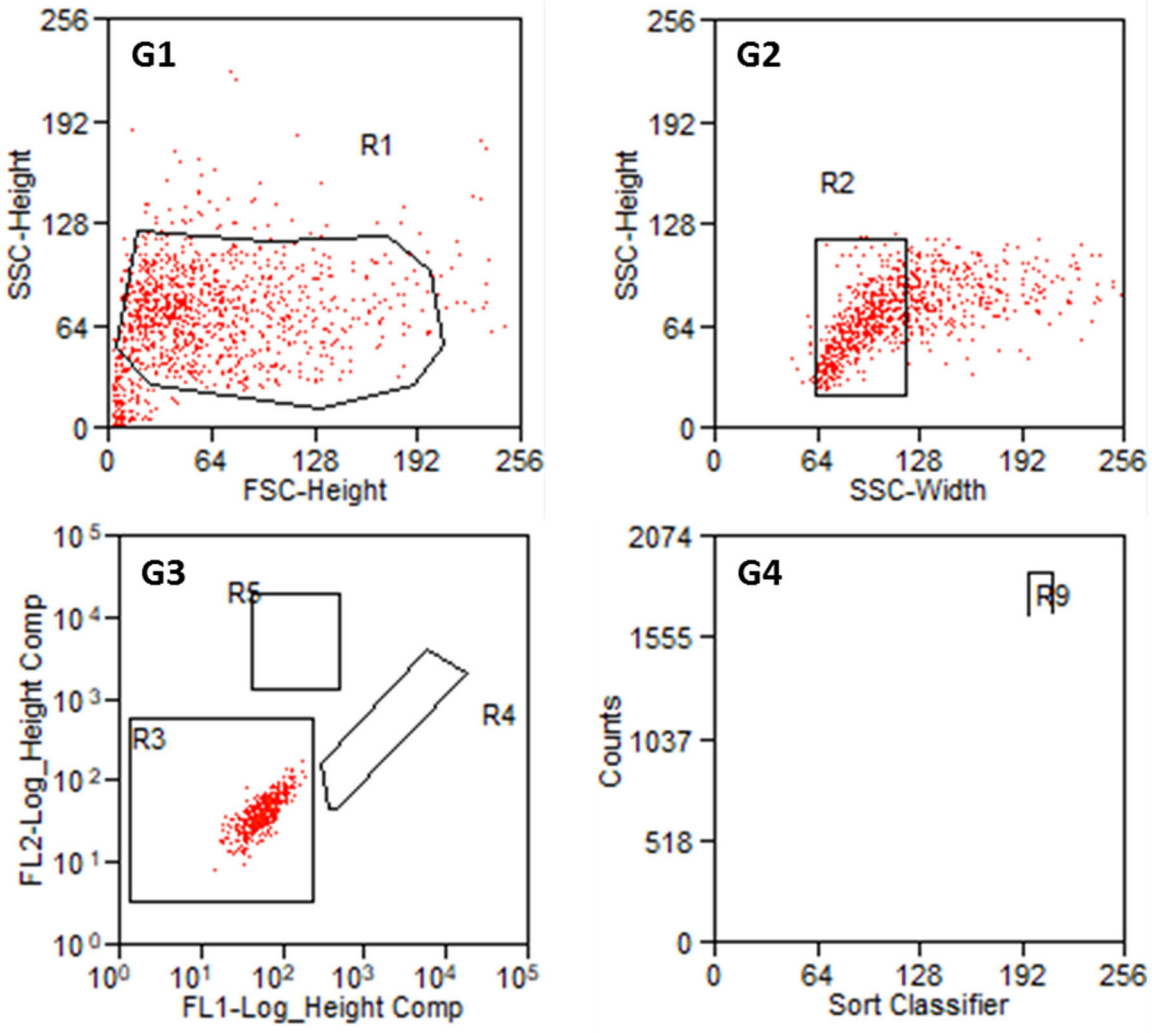

FIGURE 5 | Results of the sorting process with non-labeled cells from P2. **G1:** Entire cell population in side scatter (SSC-Height) and forward scatter (FSC-Height). R1 is set to exclude cell debris. **G2:** Cell population from R1 in SSC (Width and Heights). **G3:** Autofluorescence of the cell population in R2. FL1 serves as FITC-channel (green) and FL2 as PE-channel (yellow). R3 is set such that FL1- values below $10^{2.3}$ and FL2-values below $10^{2.7}$ are taken as autofluorescence. R4: FITC positive cells. R5: PE positive cells. **G4:** Counts of detected cells within R4 and R5. R9 contains Thy1-FITC positive fibroblasts.

DISCUSSION

Freshly prepared spiral ganglion cells (SGC) are typically used to investigate the effects of drugs or electrical stimulation on spiral ganglion neurons (SGN) (12, 13). When addressing the growth of fibrous tissue in *in vitro* experiments, immortalized cells lines, such as NIH/3T3 or L929, are used (24). Here, it might be beneficial to have organ-specific primary fibroblasts available. When preparing the SGC culture, apart from spiral ganglion neurons, glial cells and fibroblasts are also part of the culture (25, 26). Based on the SGC culture, enrichment and purification of Schwann cells has already been described (15, 16). Therefore, in the current study, we isolated fibroblasts from the SGC culture.

When establishing the staining protocol for our SGC preparation, it was first observed that all 200-kD neurofilament negative cells were positive for vimentin but no neurons expressed vimentin. Studying the human spiral ganglion (SG) (27) and the SG of 3–4 months old Wistar rats (28), all neurons were negative for vimentin. Furthermore, for cells from the spinal ganglion and the Ischias nerve of 10-week-old rats, it was documented that glial cells in the PNS and fibroblasts express vimentin (29), which is in accordance with the current results. The 200-kD neurofilament could only be detected in type II SGN (27, 30) when using mature cochleae, whereas in early developmental stages it is found in type I and type II neurons (31). Therefore, we can expect that in our preparations from postnatal days 2–4 both types of neurons are detected. Additional staining against the glial cell-specific S100B protein revealed that some of the vimentin-positive cells were also positive for the S100B protein. As Schwann

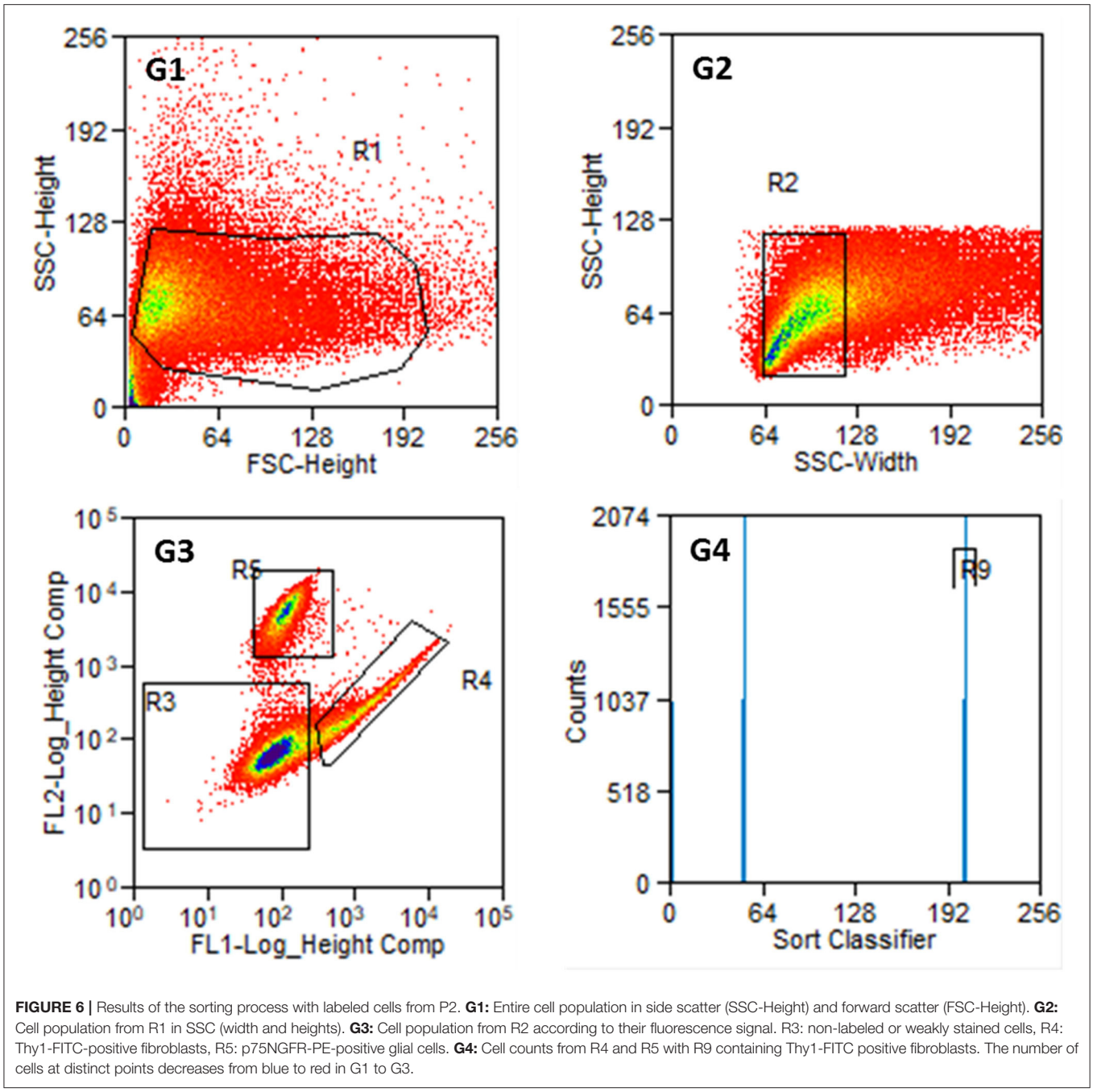

FIGURE 6 | Results of the sorting process with labeled cells from P2. **G1:** Entire cell population in side scatter (SSC-Height) and forward scatter (FSC-Height). **G2:** Cell population from R1 in SSC (width and heights). **G3:** Cell population from R2 according to their fluorescence signal. R3: non-labeled or weakly stained cells, R4: Thy1-FITC-positive fibroblasts, R5: p75NGFR-PE-positive glial cells. **G4:** Cell counts from R4 and R5 with R9 containing Thy1-FITC positive fibroblasts. The number of cells at distinct points decreases from blue to red in G1 to G3.

cells are the main glial cells in the PNS (25, 32, 33), we expect that the S100B positive cells are mainly Schwann cells. But also satellite cells were described as vimentin- and S100-positive (28, 29, 34). Van Neerven et al. (29) reported that fibroblasts in the PNS were S100B negative and vimentin-positive whereas Schwann cells and satellite cells were S100B- and vimentin-positive. Regarding the SGC, more than 50% of the non-neural cells in the culture were other cells than glial (Schwann) cells (16). In our study, more glial cells than fibroblasts were found in P0 preparations, and only after subcultivation, the number of fibroblasts increased to more than 50 %.

In contrast to the published procedure of preparing SGC (12), a fibroblast-specific medium was used in the current study. Using DMEM plus FCS should enhance the proliferation rate of fibroblasts but not glial cells (25, 35). As other authors reported that after 72 h the proliferation rate of fibroblasts was enhanced whereas after 48 h Schwann cells were still outnumbering the fibroblasts; cells were cultured on coverslips for 72 h. Before seeding the cells (except for P0), cells grew in culture flasks and

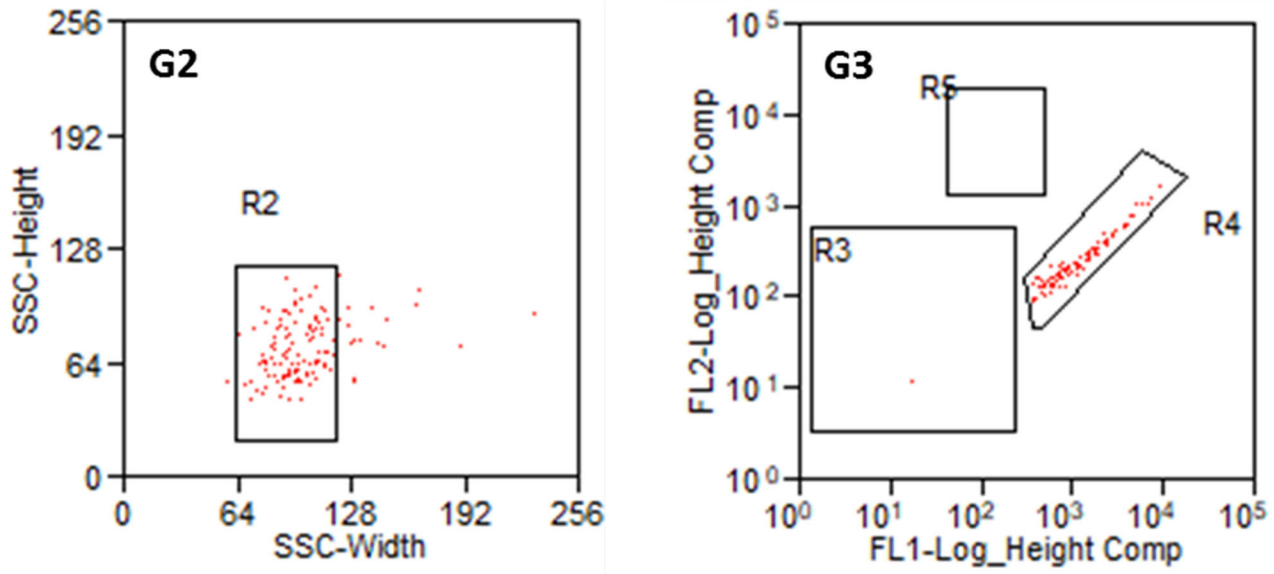

FIGURE 7 | Reanalysis of collected fibroblasts. **G2:** Cell population from R1 in SSC (Width and Heights). **G3:** Cell population from R2 according to their fluorescence signal. R3: non-labeled or weakly stained cells, R4: Thy1-FITC-positive fibroblasts, R5: p75NGFR-PE-positive glial cells.

had to be trypsinized. Incubation in 0.25% trypsin 0.02% EDTA for 4 min resulted in the detachment of 100% of the cells. Already after the first passage no SGN was observed and the number of glial cells was reduced to about 20–30% in the culture. The reduction in glial cells could be explained by the lack of SGN (16) or the use of a fibroblast-specific medium (35).

To separate fibroblasts and glial cells by cell sorting, immunolabeling of the cells has to be done using extracellular marker proteins. From other studies, it was known that fibroblasts express the surface protein Thy1 (CD90) and glial cells the p75NGF receptor (p75NGFR) (33, 36, 37). For the spiral ganglion, neurons and fibroblasts were shown to be Thy1 positive (38, 39). Furthermore, satellite cells and neurons express p75NGFR (40). Staining of the p75NGFR was also used die purify Schwann cells from the spiral ganglion (16). These authors additionally report that some neurons were also collected using their approach. These findings perfectly match with the immunolabeling pattern in the current study where non-neuronal cells were either Thy1- or p75NGFR-positive and neurons were stained for both the proteins. As discussed above, neuronal cells were removed from the culture after the first passage. Therefore, we can be sure to have only fibroblasts and glial cells in our preparations for cell sorting when using cells of the second passage.

Altogether, 13 preparations were used for cell sorting, some of them with slightly modified protocols (compare **Table 1**). All the collected Thy1 positive fractions were re-analyzed. Some counts were always outside the regions defined for fibroblasts and glial cells. This could potentially be explained by a reduced fluorescence intensity due to first exposure to the LASER (41) or some (mechanical) damage to the cells during the process. More than 99% purity of the collected fibroblasts, as determined by the device, was confirmed while immunolabeling the cells after the sort. Nearly no glial cells were detected at P3. In most preparations, the number of counted fibroblasts was relatively low compared to the original cell number. On average, 74.5% of the cells were lost during the procedure. This is larger than described for the separation of Schwann cells and fibroblasts using magnetic-activated cell sorting (35) for cells from rat sciatic nerve. One of the reasons for this might be the settings used for the sorting process. To receive a fibroblast preparation as pure as possible it might be that with the settings chosen weaker labeled cells were not detected. In all of our preparations, strong and weakly labeled cells were found. This observation was already described by Fields et al. (38) for antibodies against the Thy1 protein. It could also be that some unlabeled cells were still in the culture as macrophages are described for the PNS (42), and these cells were negative for Thy1. Furthermore, it is also known that fibroblasts are a heterogeneous group within a population and not all sub-groups might be Thy1 positive (43). The latter explanation appears to be unlikely in our investigation as nearly no unlabeled cells were detected before cell sorting.

As the ratio of counted fibroblasts and glial cells differed between preparations, some damage to the epitopes during trypsinization cannot be excluded, especially with long incubation times or high concentrations (44). With 0.25% trypsin in the solution, the total loss of cells was with 83.7% very high, and much more glial cells than fibroblasts were counted. Using only 0.05% trypsin in the solution, which is the standard for weakly adherent cells (44), cell loss was reduced and the number of fibroblasts increased. Here, maybe not all fibroblasts were detached from the culture flasks. Best results were achieved with 0.15% trypsin in the solution. Using this approach, cell loss was about 60%, which is in the range of the reported cell loss for

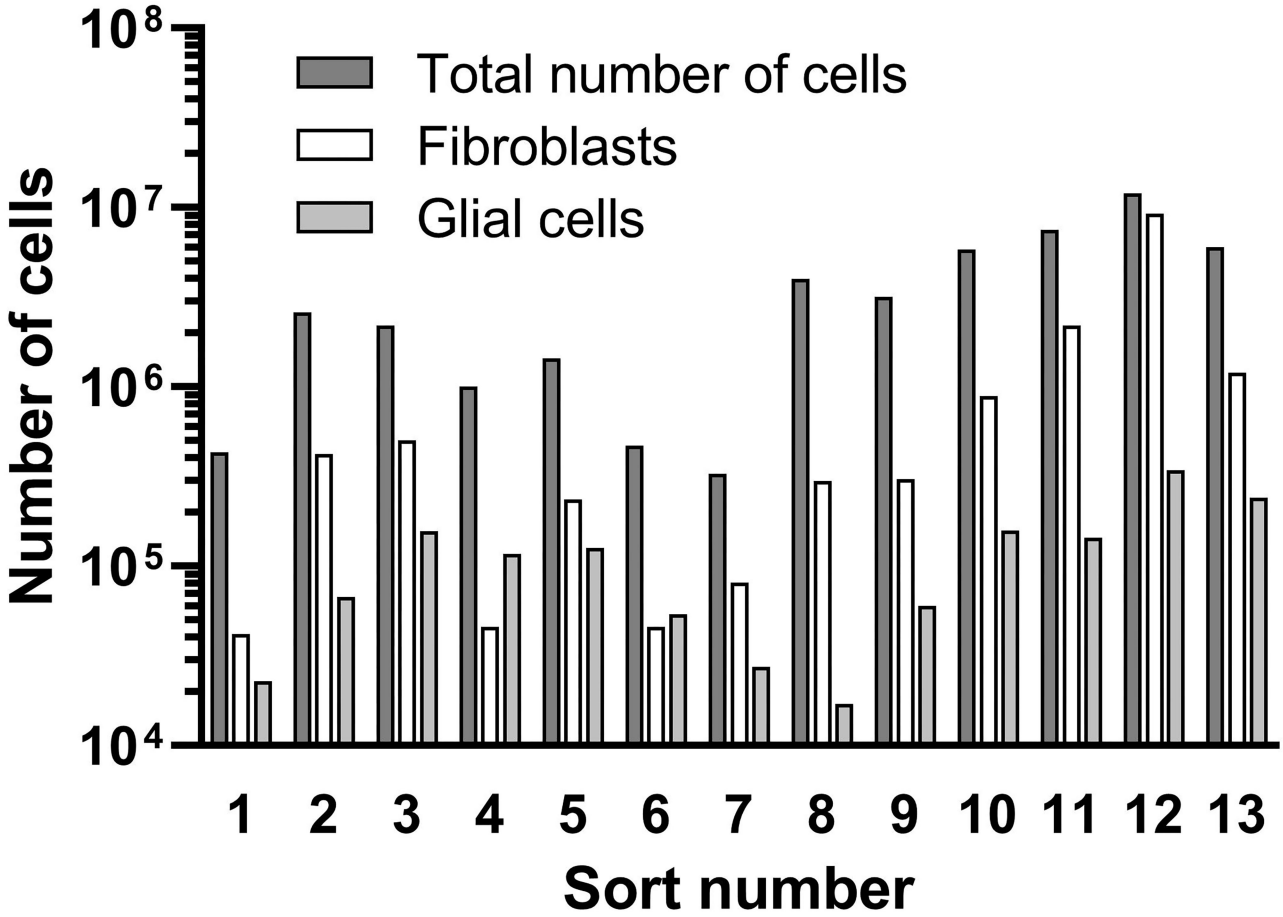

FIGURE 8 | Results of the cell sorting procedure. Total cell numbers, received fibroblasts and glial cells are presented.

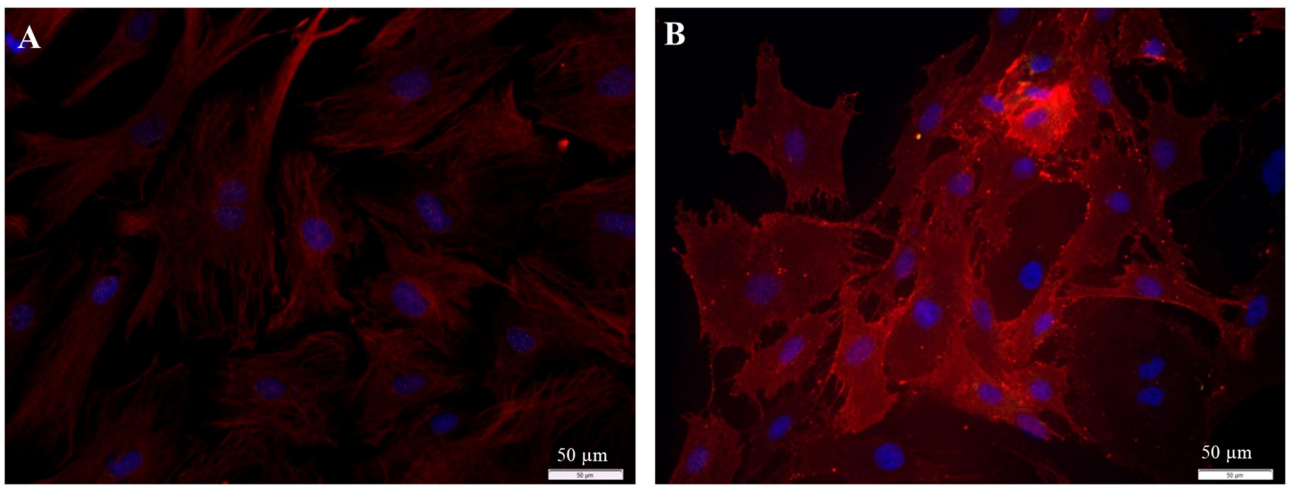

FIGURE 9 | Staining of collected fibroblasts after the sorting process (P3 after 72 h cultivation). **(A)** Intracellular staining: vimentin, *clone V9* (Cy5, red, 5 s), S100B-protein (Cy3, yellow, 100 ms), DAPI (blue, 1 s). **(B)** Staining of surface proteins: Thy1.1, *clone Ox-7* (Cy5, red, 1 s), p75NGFR (Cy3, yellow, 1 s), DAPI (blue, 1 s).

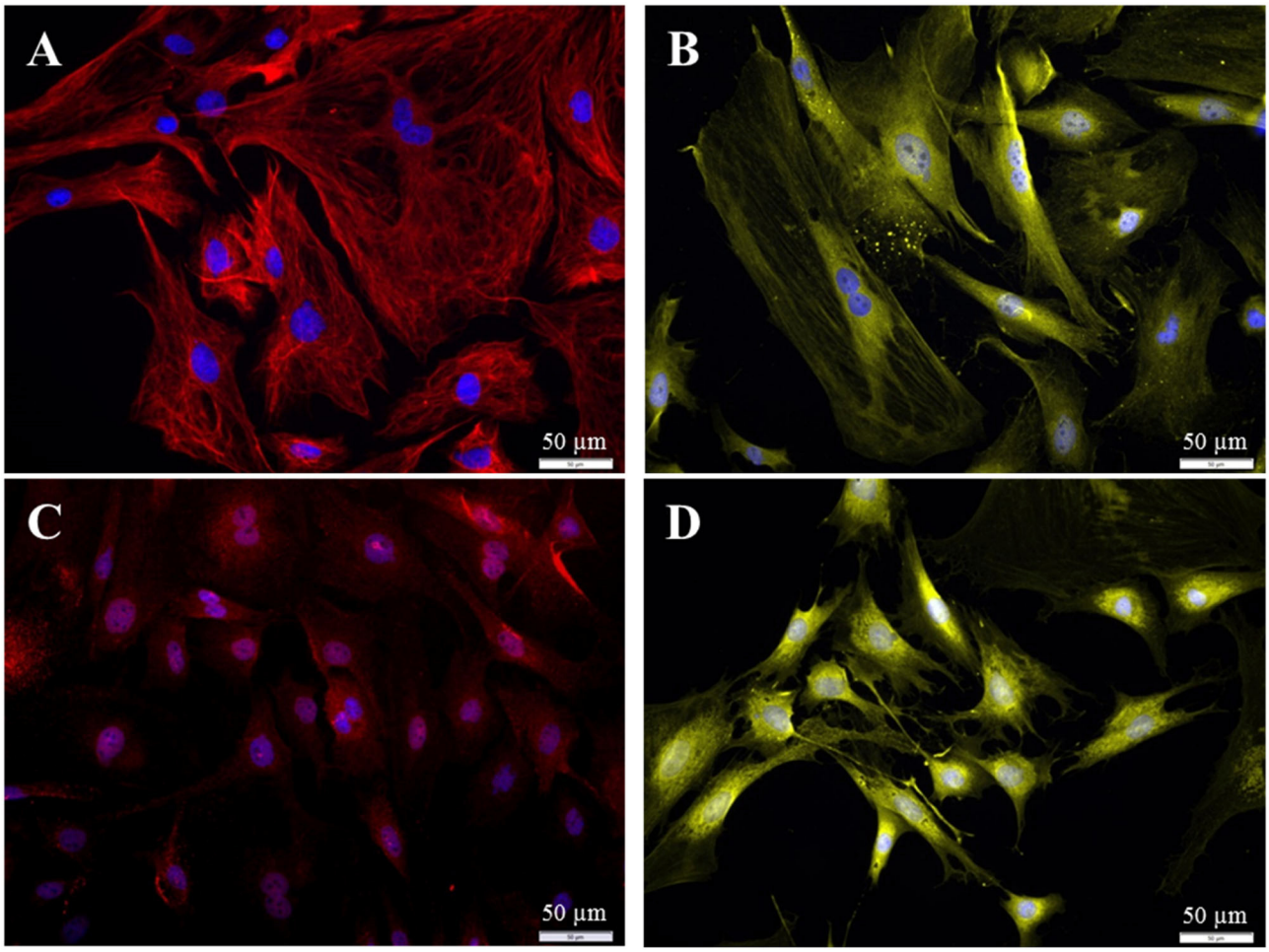

FIGURE 10 | Immuncytochemical characterization of the purified fibroblasts (P3 after 72 h cultivation). **(A)** *Anti-Vimentin, clone V9* (Cy5, red, 3 s) . **(B)** *Anti-S100* (Cy3, yellow, 400 ms). **(C)** *Anti-Cx26* (Cy5, red, 5 s). **(D)** *Anti-carbonic-anhydrase II* (Cy3, yellow, 100 ms). All preparations were additionally stained for DAPI (blue, 1 s).

magnetic-activated cell sorting (35). Besides preparation 4 (high trypsin), there was one more preparation with more counted glial cells than fibroblasts. This preparation (sort 6) was the only preparation where the animals were only 1 day old instead of 2–4 days. This might be the reason for the different result in this preparation.

Compared to immortalized cell lines, primary cells and their subcultures have the advantage of keeping most characteristics from their host tissue, also *in vitro* (3). The purified cochlear fibroblasts were further subcultivated until P16. The observed changes in cell growth correspond to the phases described by Hayflick and Moorhead (45). Phase I (Lag-phase) is the primary cell culture until a confluent monolayer is reached. This is followed by phase II (Log-phase) with good proliferation rates and phase III with a decreasing proliferation rate and finally death of the cell culture. The cochlear fibroblasts seem to enter the latter phase after 9–10 passages, at least with the seeding density used in this study.

The purified fibroblasts were analyzed according to the immunohistochemical profile that is described for fibroblasts of the spiral ligament (18–23). They were positive not only for vimentin but also for carbonic anhydrase II, connexin 26, and the S100 protein. The expression pattern of the fibroblasts from Rosenthal's canal appears to be similar to that of type I fibroblasts of the spiral ligament, which can be found predominantly in the spiral ligament distal from scala tympani (11). Here, a more detailed characterization would be necessary.

Finally, and as not all cells might be suitable for cryoconservation, purified fibroblasts were frozen and thawed again. Cells with a survival rate of about 80% and an unchanged morphology are considered suitable for cryconservation (46). Therefore, we conclude that the described purified fibroblasts from Rosenthal's canal are also suitable for cryoconservation.

With the described procedure, fibroblasts could be purified from the SGC preparation and are now available for further *in vitro* experiments. As the cells can be subcultivated and frozen, cells from one preparation could be used for experiments for days and weeks without frequent new preparation from the animals.

DATA AVAILABILITY STATEMENT

The original contributions presented in the study are included in the article/supplementary material, further inquiries can be directed to the corresponding author/s.

ETHICS STATEMENT

Ethical review and approval was not required for the animal study in accordance with the local legislation and institutional requirements.

AUTHOR CONTRIBUTIONS

AA: investigation, formal analysis, and writing—original draft. K-HE: methodology, validation, and writing—review and editing. TL: funding and writing—review and editing. GP: conceptualization, supervision, and writing—review and editing. All authors contributed to the article and approved the submitted version.

FUNDING

This study was supported by BMBF Innovationswettbewerb Medizintechnik (FKZ: 13EZ1001B) and BMBF RESPONSE "Partnerschaft für Innovation in der Implantattechnologie" (FKZ 03ZZ0925A).

ACKNOWLEDGMENTS

The authors wish to thank Dr. Matthias Ballmaier and his team from the Sorter Lab of Hannover Medical School and Miriam Behrendt and Jasmin Bohlmann for technical support. Presented results are part of the doctoral thesis of AA (47).

REFERENCES

1. Egger G. *Die akute Entzündung: Grundlagen, Pathophysiologie und klinische Erscheinungsbilder der unspezifischen Immunität*. 1. ed., Wien: Springer (2005). pp. 225–9. doi: 10.1007/3-211-29899-1
2. Schubert T, Friede RL. The role of endoneurial fibroblasts in myelin degradation. *J Neuropathol Exp Neurol.* (1981) 40:134–54. doi: 10.1097/00005072-198103000-00006
3. Schmitz S. *Der Experimentator: Zellkultur*. 3. ed., Heidelberg: Spektrum (2011). p. 82–4. doi: 10.1007/978-3-8274-2573-7
4. Busby PA, Plant KL, Whitford LA. Electrode impedance in adults and children using the nucleus 24 cochlear implant system. *Cochlear Implants Int.* (2002) 3:87–103. doi: 10.1179/cim.2002.3.2.87
5. Paasche G, Bockel F, Tasche C, Lesinski-Schiedat A, Lenarz T. Changes of postoperative impedances in cochlear-implant patients: the short-term effects of modified electrode surfaces and intracochlear corticosteroids. *Otol Neurotol.* (2006) 27:639–47. doi: 10.1097/01.mao.0000227662.88840.61
6. Xu J, Shepherd RK, Millard RE, Clark GM. Chronic electrical stimulation of the auditory nerve at high stimulus rates: a physiological and histopathological study. *Hear Res.* (1997) 105:1–29. doi: 10.1016/S0378-5955(96)00193-1
7. Wilk M, Hessler R, Mugridge K, Jolly C, Fehr M, Lenarz T, et al. Impedance changes and fibrous tissue growth after cochlear implantation are correlated and can be reduced using a dexamethasone eluting electrode. *PLoS One.* (2016) 11:e0147552. doi: 10.1371/journal.pone.0147552
8. Lenarz T. Cochlear implants: what can be achieved? *Am J Otol.* (1997) 18:2–3.
9. Ryu KA, Lyu AR, Park H, Choi JW, Hur GM, Park YH. Intracochlear bleeding enhances cochlear fibrosis and ossification: an animal study. *PLoS ONE.* (2015) 10:e0136617. doi: 10.1371/journal.pone.0136617
10. Lenarz T, Pau HW, Paasche G. Cochlear implants. *Curr Pharm Biotechnol.* (2013) 14:112–23. doi: 10.2174/1389201011314010014
11. Yian C, Moon SK, Jin S, Webster P, Rhim JS, Andalibi A, et al. Characterization of rat spiral-ligament-cell line immortalized by Adenovirus 12-Simian virus 40 hybrid-virus. *Ann Otol Rhinol Laryngol.* (2006) 115:930–8. doi: 10.1177/000348940611501213
12. Wefstaedt P, Scheper V, Lenarz T, Stöver T. Brain-derived-neurotrophic-factor/glial-cell-line-derived-neurotrophic factor survival effects on auditory neurons are not limited by dexamethasone. *Neuroreport.* (2005) 16:2011–4. doi: 10.1097/00001756-200512190-00008
13. Peter MN, Warnecke A, Reich U, Olze H, Szczepek AJ, Lenarz T, et al. Influence of *in-vitro*-electrical stimulation on survival of spiral-ganglion neurons. *Neurotox Res.* (2019) 36:204–16. doi: 10.1007/s12640-019-00017-x
14. Liebich H-G. *Funktionelle Histologie der Haussäugetiere*. 5. ed., Stuttgart: Schattauer-Verlag (2010). p. 109–27. doi: 10.1055/b-005-148994
15. Niapour A, Karamali F, Karbalaie K, Kiani A, Mardani M, Nasr-Esfahani MH, et al. Novel method to obtain highly enriched cultures of adult rat Schwann cells. *Biotechnol Lett.* (2010) 32:781–6. doi: 10.1007/s10529-010-0230-z
16. Whitlon DS, Tieu D, Grover M. Purification and transfection of cochlear Schwann cells. *Neuroscience.* (2010) 171:23–30. doi: 10.1016/j.neuroscience.2010.08.069
17. Whitlon DS, Tieu D, Grover M, Reilly B, Coulson MT. Spontaneous association of glial cells with regrowing neurites in mixed cultures of dissociated spiral ganglia. *Neuroscience.* (2009) 161:227–35. doi: 10.1016/j.neuroscience.2009.03.044
18. Spicer SS, Schulte BA. Differentiation of inner ear fibrocytes according to their ion transport related activity. *Hear Res.* (1991) 56:53–64. doi: 10.1016/0378-5955(91)90153-Z
19. Gratton MA, Schulte BA, Hazen-Martin DJ. Characterization and development of an inner ear type-I-fibrocyte-cell culture. *Hear Res.* (1996) 99:71–8. doi: 10.1016/S0378-5955(96)00080-9
20. Suko T, Ichimiya I, Yoshida K, Suzuki M, Mogi G. Classification and culture of spiral-ligament fibrocytes from mice. *Hear Res.* (1999) 140:137–44. doi: 10.1016/S0378-5955(99)00191-4
21. Liu Y-P, Zhao H-B. Cellular characterization of Connexin-26 and Connnexin-30 expression in the cochlear lateral wall. *Cell Tissue Res.* (2008) 333:395–403. doi: 10.1007/s00441-008-0641-5
22. Sun G-W, Fujii M, Matsunaga T. Functional interaction between mesenchymal-stem cells and spiral-ligament fibrocytes. *J Neurosci Res.* (2012) 90:1713–22. doi: 10.1002/jnr.23067
23. Wu X, Tang W, Muly EC, Zhang L, Lin X. Expression pattern of Connexin-26 and Connexin-30 in mature cochlea of the monkey. *Biochem Biophys Res Commun.* (2019) 518:357–61. doi: 10.1016/j.bbrc.2019.08.063
24. Reich U, Müller PP, Fadeeva E, Chichkov BN, Stöver T, Fabian T, et al. Differential fine-tuning of cochlear implant material-cell interactions by femtosecond laser microstructuring. *J Biomed Mater Res B Appl Biomater.* (2008) 87:146–53. doi: 10.1002/jbm.b.31084
25. Brockes JP, Fields KL, Raff MC. Studies on cultured rat Schwann cells. I Establishment of purified populations from cultures of peripheral nerve. *Brain Res.* (1979) 165:105–18. doi: 10.1016/0006-8993(79)90048-9
26. Pannunzio ME, Jou IM, Long A, Wind TC, Beck G, Balian G. A new method of selecting Schwann cells from adult mouse sciatic nerve. *J Neurosci Meth.* (2005) 149:74–81. doi: 10.1016/j.jneumeth.2005.05.004
27. Anniko M, Arnold W, Stigbrand TT, Ström A. The human spiral ganglion. *ORL.* (1995) 57:68–77. doi: 10.1159/000276714

28. Nascimento RS, Santiago MF, Marques SA, Allodi S, Martinez AMB. Diversity among satellite-glial cells in dorsal-root ganglia of the rat. *Braz J Med Biol Res.* (2008) 41:1011–7. doi: 10.1590/S0100-879X2008005000051
29. Van Neerven SGA, Pannaye P, Bozkurt A, van Nieuwenhoven F, Joosten E, Hermans E, et al. Schwann-cell migration and neurite outgrowth are influenced by media conditioned by epineurial fibroblasts. *Neuroscience.* (2013) 252:144–53. doi: 10.1016/j.neuroscience.2013.08.009
30. Berglund AM, Ryugo DK. A monoclonal antibody labels type-II neurons of the spiral ganglion. *Brain Res.* (1986) 383:327–32. doi: 10.1016/0006-8993(86)90034-X
31. Romand M-R, Romand R. Development of spiral-ganglion cells in mammalian cochlea. *J Microsc Res Tech.* (1990) 15:144–54. doi: 10.1002/jemt.1060150206
32. Jessen KR. Glial cells. *Int J Biochem Cell Biol.* (2004) 36:1861–7. doi: 10.1016/j.biocel.2004.02.023
33. Jin YQ, Liu W, Hong TH, Cao Y. Efficient Schwann cell purification by differential cell detachment using multiplex collagenase treatment. *J Neurosci Meth.* (2008) 170:140–8. doi: 10.1016/j.jneumeth.2008.01.003
34. Hanani M. Satellite-glial cells in sensory ganglia: from form to function. *Brain Res Brain Res Rev.* (2005) 48:457–76. doi: 10.1016/j.brainresrev.2004.09.001
35. Mauritz C, Grothe C, Haastert K. Comparative study of cell culture and purification methods to obtain highly-enriched cultures of proliferating adult rat SCHWANN cells. *J Neurosci.* (2004) 77:453–61. doi: 10.1002/jnr.20166
36. Haastert K, Seef P, Stein VM, Tipold A, Grothe C. A new cell-culture protocol for enrichment and genetic modification of adult canine SCHWANN cells suitable for peripheral nerve tissue engineering. *Res Vet Sci.* (2009) 87:140–2. doi: 10.1016/j.rvsc.2009.01.001
37. Schmitte R, Tipold A, Stein VM, Schenk H, Flieshardt C, Grothe C, et al. Genetically modified canine SCHWANN cells—*In vitro* and *in vivo* evaluation of their suitability for peripheral nerve tissue engineering. *J Neurosci.* (2010) 186:202–8. doi: 10.1016/j.jneumeth.2009.11.023
38. Fields KL, Brockes JP, Mirsky R, Wendon LMB. Cell surface markers for distinguishing different types of rat dorsal root ganglion cells in culture. *Cell.* (1978) 14:43–51. doi: 10.1016/0092-8674(78)90299-4
39. Raff MC, Fields KL, Hakomori SI, Mirsky R, Pruss RM, Winter J. Cell-type-specific markers for distinguishing and studying neurons and the major classes of glial cells in culture. *Brain Res.* (1979) 174:283–308. doi: 10.1016/0006-8993(79)90851-5
40. Pannese E, Procacci P. Ultrastructural localization of NGF receptors in satellite cells of the rat spinal ganglia. *J Neurocytol.* (2002) 31:755–63. doi: 10.1023/A:1025708132119
41. Welsch U, Mulisch M. *Romeis: Mikroskopische Technik*. 19. ed., Berlin/Heidelberg: Springer. (2015). p. 19–21, 283–92.
42. Richard L, Vedrenne N, Vallat J-M, Funalot B. Characterisation of endoneurial fibroblast-like cells from human and rat peripheral nerves. *J Histochem Cytochem.* (2014) 62:424–35. doi: 10.1369/0022155414530994
43. Baglole CJ, Ray DM, Bernstein SH, Feldon SE, Smith TJ, Sime PJ, et al. More than structural cells, fibroblasts create and orchestrate the tumor microenvironment. *Immunol Invest.* (2006) 35:297–325. doi: 10.1080/08820130600754960
44. Gstraunthaler G, Lindl T. *Zell- und Gewebekultur: Allgemeine Grundlagen und spezielle Anwendungen*. 7. ed., Berlin/Heidelberg: Springer (2013). p. 69–193.
45. Hayflick L, Moorhead PS. The serial cultivation of human diploid cell strains. *Exp Cell Res.* (1961) 25:585–621. doi: 10.1016/0014-4827(61)90192-6
46. Ganten D, Ruckpaul K. *Molekular- und zellbiologische Grundlagen.* 1. ed., Berlin/Heidelberg: Springer (1997). pp. 168–9. doi: 10.1007/978-3-662-08822-7
47. Anacker A. *Isolation, Aufreinigung und Kultivierung von Fibroblasten aus dem Spiralganglion. Dissertation*. Hannover: Stiftung Tierärztliche Hochschule Hannover (2021). Available online at: https://elib.tiho-hannover.de/receive/tiho_mods_00005978

Conflict of Interest: The authors declare that the research was conducted in the absence of any commercial or financial relationships that could be construed as a potential conflict of interest.

Publisher's Note: All claims expressed in this article are solely those of the authors and do not necessarily represent those of their affiliated organizations, or those of the publisher, the editors and the reviewers. Any product that may be evaluated in this article, or claim that may be made by its manufacturer, is not guaranteed or endorsed by the publisher.

Copyright © 2022 Anacker, Esser, Lenarz and Paasche. This is an open-access article distributed under the terms of the Creative Commons Attribution License (CC BY). The use, distribution or reproduction in other forums is permitted, provided the original author(s) and the copyright owner(s) are credited and that the original publication in this journal is cited, in accordance with accepted academic practice. No use, distribution or reproduction is permitted which does not comply with these terms.

frontiers | Frontiers in Neurology

ORIGINAL RESEARCH
published: 18 April 2022
doi: 10.3389/fneur.2022.868144

Heading Direction Is Significantly Biased by Preceding Whole-Body Roll-Orientation While Lying

Alexander Andrea Tarnutzer[1,2]*, *Vasco Duarte da Costa*[3], *Denise Baumann*[3] and *Simone Hemm*[3]

[1] Department of Neurology, Cantonal Hospital of Baden, Baden, Switzerland, [2] Faculty of Medicine, University of Zurich, Zurich, Switzerland, [3] School of Life Sciences, Institute for Medical Engineering and Medical Informatics, University of Applied Sciences and Arts Northwestern Switzerland, Muttenz, Switzerland

Background: After a prolonged static whole-body roll-tilt, a significant bias of the internal estimates of the direction of gravity has been observed when assessing the subjective visual vertical.

Objective: We hypothesized that this post-tilt bias represents a more general phenomenon, broadly affecting spatial orientation and navigation. Specifically, we predicted that after the prolonged roll-tilt to either side perceived straight-ahead would also be biased.

Methods: Twenty-five healthy participants were asked to rest in three different lying positions (supine, right-ear-down, and left-ear-down) for 5 min ("adaptation period") prior to walking straight-ahead blindfolded for 2 min. Walking was recorded with the inertial measurement unit sensors attached to different body locations and with sensor shoe insoles. The raw data was segmented with a gait–event detection method. The Heading direction was determined and linear mixed-effects models were used for statistical analyses.

Results: A significant bias in heading into the direction of the previous roll-tilt position was observed in the post-adaptation trials. This bias was identified in both measurement systems and decreased again over the 2-min walking period.

Conclusions: The bias observed further confirms the influence of prior knowledge on spatial orientation and navigation. Specifically, it underlines the broad impact of a shifting internal estimate of direction of gravity over a range of distinct paradigms, illustrating similar decay time constants. In the broader context, the observed bias in perceived straight-ahead emphasizes that getting up in the morning after a good night's sleep is a vulnerable period, with an increased risk of falls and fall-related injuries due to non-availability of optimally tuned internal estimates of the direction of gravity and the direction of straight-ahead.

Keywords: prior knowledge, spatial orientation and navigation, post-tilt bias, perceived straight-ahead, inertial measurement unit, sensor shoe insoles

OPEN ACCESS

Edited by:
Stefano Ramat,
University of Pavia, Italy

Reviewed by:
Vito Enrico Pettorossi,
University of Perugia, Italy
Luc Vereeck,
University of Antwerp, Belgium

***Correspondence:**
Alexander Andrea Tarnutzer
alexander.tarnutzer@ksb.ch

Specialty section:
This article was submitted to Neuro-Otology, a section of the journal Frontiers in Neurology

Received: *02 February 2022*
Accepted: *18 March 2022*
Published: *18 April 2022*

Citation:
Tarnutzer AA, Duarte da Costa V, Baumann D and Hemm S (2022) Heading Direction Is Significantly Biased by Preceding Whole-Body Roll-Orientation While Lying. Front. Neurol. 13:868144. doi: 10.3389/fneur.2022.868144

INTRODUCTION

For the spatial orientation and navigation in 3-dimensional space, accurate and precise estimates of self-motion and orientation relative to gravity are important. To keep track of the current body positions with reference to previous locations and surroundings (1, 2), input from several, partially redundant sensory systems are computationally combined within the central nervous system in a weighted fashion based on their reliability. Thereby, optimal internal estimates of the direction of gravity (3), self-motion (1, 4) and heading direction (5) are achieved.

Such awareness of one's spatial orientation and movement in the environment has been referred to as "spatial cognition" (6) and it is used to achieve a variety of goals, including navigation through space, maintaining postural control and identifying and acting on objects (2). Sensory input signals emerge from the peripheral–vestibular organs (measuring rotational and linear accelerations), the visual system and proprioception.

The perceptual estimates of the self-orientation relative to the gravity provide a straightforward means to quantify graviception at the level of the cortex. Due to their widespread availability and easy-to-understand instructions, visual line adjustments indicating the "subjective visual vertical" (SVV) are preferentially used to assess graviception. In behavioral studies investigating prolonged whole-body roll-tilt, concomitant drifts of the SVV (7, 8) and a bias (i.e., deviations of SVV) upon return to upright position (9), termed "post-tilt bias" were observed.

We have previously characterized this post-tilt bias using an SVV paradigm, demonstrating that it is usually toward the direction of previous whole-body roll-tilt (termed "adaptation position") and that it decays exponentially [time constant = ∼70 s (10)]. We favored the central mechanisms to explain the post-tilt bias and proposed a perceptual shift of perceived vertical toward the recent (roll-tilted) position based on prior knowledge (10). This concept describes a strategy relying on the assumption that an earth–vertical (upright) position is most likely and therefore assumes that the subject's recent whole-body orientation was approximately parallel to gravity. Accordingly, this prior knowledge is combined with sensory input in a Bayesian framework to estimate the most likely roll position (11–13). As a result, the perceived direction of gravity will be shifted toward the body-longitudinal axis. A similar effect was observed for vision-independent paradigms of verticality perception as the subjective haptic vertical, again showing significant post-tilt biases (14).

Internal estimates of the direction of gravity are not only important for verticality perception, but also for postural control and ambulation. Specifically, a significant post-tilt bias toward the adaptation position has been demonstrated for self-positioning in space relative to gravity after prolonged static roll tilt (15). In the patients with acute or persistent unilateral peripheral–vestibular deficits, both heading direction and self-alignment relative to straight-ahead have been shown to be biased toward the affected ear when removing vision. With eyes closed, strong ipsilesional walking deviations (16, 17) and ipsilesional whole-body rotational deviations when walking on the spot (18) have been observed. Furthermore, it has been shown that the repetitive one side predominant asymmetric (off-vertical axis) stimulation of the vestibular system influences the spatial representation of the subjective straight-ahead (SSA) and self-motion perception in the opposite direction of the most rapid stimulus (19, 20), emphasizing a significant otolithic component in this paradigm.

Thus, in analogy to the observed post-tilt bias in perceived direction of vertical, we hypothesized that after prolonged static roll-tilt a shift in the internal estimate of direction of gravity will bias heading direction during ambulation. Specifically, we predicted walking straight-ahead while blindfolded to be biased toward the adaptation side, resulting in a curved walking pattern. The magnitude of this effect is expected to decay exponentially. Alternatively, preserved straight-ahead walking would suggest that the post-tilt bias is a more restricted phenomenon, limited to verticality perception and self-positioning relative to gravity. To test this hypothesis, we measured walking with vision removed after prolonged static whole-body roll-tilt in different body positions relative to gravity in healthy human subjects using two different gait–assessment systems.

MATERIALS AND METHODS

Ethical Approval

All subjects provided written informed consent after a full explanation of the experimental procedure. The study was approved by the Ethikkommission Nordwest- und Zentralschweiz (EKNZ, ID = 2020–01712) on the research involving humans. The research project was conducted in accordance with the university policies, the Federal Act on Data Protection, the Declaration of Helsinki (except for registration in a database), the principles of Good Clinical Practice, the Human Research Act (HRA) and the Human Research Ordinance (HRO). The data will be made available on request from the authors.

Subjects

Twenty-five healthy, adult human subjects (9 females, 16 males, age [mean ± 1 standard deviation (SD): 29.4 ± 8.7 years, range, 20–60 years] were recruited for the study. The subjects weighed between 50 and 121 kg with an average height of 163.5 and 178.6 cm for female and male subjects, respectively. The vast majority of participating subjects reported that they were right-handed (22 of 25).

Experimental Setup

The trials were performed in a double sports hall (length, 31 m; width, 26 m). One of the sports hall's corners was selected as the starting point, where subjects could rest on two vaulting boxes before walking. All trials were performed while the participant was equipped as shown in **Figure 1**. The subjects had to wear a sleeping mask and earmuffs to eliminate visual cues during walking and to reduce auditory feedback for orientation in space, respectively.

FIGURE 1 | The fully-equipped participant during the study; 9 IMUs (MTw Awinda, Xsens Technologies B.V., Enschede, Netherlands) were attached to the subject with Velcro® patches and bands at both ankles, both thighs, lower back, chest, both wrists, and at the forehead. Sensory shoe insoles (Insole3, Moticon ReGo AG, Munich, Germany) were laid in the subject's own shoes. Additionally, the subject wore a GoPro Hero 6 on a chest mount (GoPro Inc., San Mateo CA, USA), a sleeping mask and earmuffs.

Sensor Systems

Inertial Measurement Unit (IMU) Based Motion Tracking

Motion was measured with nine inertial motion trackers (MTw Awinda, Xsens Technologies B.V., Enschede, Netherlands). This motion tracker is composed of a three-dimensional (3D) accelerometer, 3D gyroscope, 3D magnetometer, barometer, and a thermometer (21). Inertial motion trackers were placed at both ankles, both thighs, lower back, chest, both wrists, and at the forehead with Velcro® patches and bands, resulting in a total of nine sensors attached. The individual sensors were placed at the same defined body parts for every participant. The forehead sensor was directly placed onto the sleeping mask at the height of the nasion. The chest sensor was either positioned on a chest mount (Chesty, GoPro Inc., San Mateo CA, USA) or on a Velcro® band, which was wrapped around the subject's chest. Signals were recorded at a sampling rate of 100 Hz. Before each individual measurement, the sensor orientation of all motion trackers was reset while the subjects stood in neutral pose.

Inertial Pressure Measurement Sensory Shoe Insoles

Foot pressure was measured using sensory shoe insoles (Insole3, Moticon ReGo AG, Munich, Germany). The Insole3 is a thin, wireless measuring insole with an integrated 16 MB flash storage. It contains 16 pressure sensors and 1 IMU with a 3D-accelerometer and a 3D-gyroscope. The area covered by pressure sensors in relation to the total area of the sensor insoles is between 62.5 and 67.4%, with a higher sensor coverage for larger insoles. The origin is defined as the center of the shoe insole. Consequently, center of pressure measurements during normal walking is subject dependent and can vary from zero. The posterior–anterior (PA) direction is set as the positive x-direction and the lateral–medial (LM) direction as the positive y-direction thus resulting in an opposite orientation between the

left and right foots. The shoe insoles were laid in the subject's own shoes. Before all measurements, the soles' pressure sensors were zeroed. Apart from pressure measurement data, the sensory shoe insoles also recorded data of an integrated inertial measurement unit sensor. The sensor insole data was recorded with a sample rate of 100 Hz.

Subjects were able to get used to the attached sensors by walking once with their eyes open and once with their eyes covered before data collection started. This acclimation phase lasted approximately 3 min to adjust the temperature of the sensory insoles to that of the shoe to reduce possible sensor drifts (22, 23). For later determination of eventual irregularities, the feet and floor were also filmed using a GoPro Hero 6 camera (GoPro Inc., San Mateo CA, USA).

Experimental Paradigm

The baseline measurements were recorded first. Therefore, the subjects remained in a sitting–upright position for 1 min before walking ("baseline trials"). Subsequently, the test trials were collected. Each test trial consisted of an *adaptation phase* in different resting (i.e., whole-body horizontal) positions and a *walking phase* directly following the adaptation phase (for description, see the following paragraphs). For each resting position, three runs per participant were performed.

During the adaptation phase, subjects had to rest in one of three different whole-body horizontal positions (eyes closed) for 5 min. To study the effect of gravity on perceived straight-ahead, and thus on the following walking direction, three distinct horizontal whole-body positions were defined (as illustrated in **Figure 2**): lying in supine position, lying on the right side (i.e., right-ear-down, RED) or lying on the left side (left-ear-down, LED). While lying, the head was positioned in reference to gravity. For the adaptation phase, a duration of 5 min was selected based on previous reports stating that adaption mechanisms during SVV adjustments occurred mostly during the first three to 5 min (7, 8, 10, 24).

At the beginning of the walking phase (before standing up from the vaulting boxes), subjects had to sit upright and slap their legs together. This event was used for later sensor-system synchronization. Next, the subjects were guided to the starting position, and they were realigned with the sports hall's diagonal. Briefly, the subjects took the neutral pose and started walking naturally and at a slow, comfortable pace. The neutral pose was defined as the subject standing upright with the feet parallel to the hips and the hands turned toward the body. The subjects were accompanied by the experimenter to allow interventions when needed. Whenever an end of the sports field was reached, the subjects were turned around (clockwise or counter-clockwise direction, direction selected randomly) and they could continue their walk. This procedure was continued until a total walking time of 2 min was reached. The ranges between the turning points are referred to as walking segments (WS). To avoid learning effects toward a straight walking direction, the subjects were guided back to the measurement starting area before removal of earmuffs and blindfolding at the end of each measurement (**Figure 2**, right panel).

The session started with three baseline trials in a row, which were followed by three repetitions of each of the adaptation trial conditions in random order to avoid learning effects (**Figure 2**, left panel).

Data Analysis

The measurements from both sensor systems were processed with MATLAB (version R2020a; The MathWorks Inc., Massachusetts, USA). A schematic overview of both sensor systems' signal processing is shown in **Figure 3**. The statistical analyses were performed with RStudio Version 1.4 (RStudio, Boston, USA) and R Version 4.03 (R Core Team, Vienna, Austria). Statistical comparisons were conducted with the R libraries *car* (25), *nlme* (26), *emmeans* (27) and *rstatix* (28).

Sensor System Synchronization

Both sensor systems were synchronized in time by detection of the leg slapping event, which was performed at the beginning of every trial. The event was detected in the signals of the left ankle motion tracker and the left sensory shoe insole. The synchronization points were identified by a threshold peak identification algorithm on the absolute medial–lateral (ML) acceleration signals.

Signal Scaling and Equalization

The signals of both measurement systems were scaled to standardized measurement units and equalized in time. The missing data from the measurements of both sensor systems were interpolated using modified Akima Cubic Hermite interpolation.

Gait–Event Detection

For the later extraction of gait–cycle dependent parameters, individual gait events (strides) were determined. Due to a timely drift between both sensor systems, the gait–event detection was performed on both systems individually. For both measurement systems, smoothed angular velocity signals of the sagittal plane were used. For the motion tracking sensors, the signals from both ankle sensors were used, for the sensory insoles, signals of the integrated IMU sensor were analyzed. Signal smoothing was obtained by a fourth-order Butterworth filter with a cut-off frequency of 12 Hz.

As a first step, mid-swing phases were determined. It was shown that positive peaks of the angular velocity around the frontal axis denote the mid-swing phases of every step (29–31). Therefore, positive peak detection was used to determine the mid-swing phases of every gait cycle in the smoothed angular velocities around the participant's frontal axis. The peak thresholds were determined for every trial and sensor system individually. The mid-swing peaks were detected to define search windows in the signals for heel strike (following zero-crossing) and toe-off (previous valley) identification (29–32). **Figure 4** shows an example of the resulting gait–event detection.

The WS were defined as phases of walking separated by passively turning subjects after reaching the border of the sports hall. The WS were determined for both sensor systems separately. The first step of every WS was found by comparing the events of both legs. The last step was defined with the same conditions

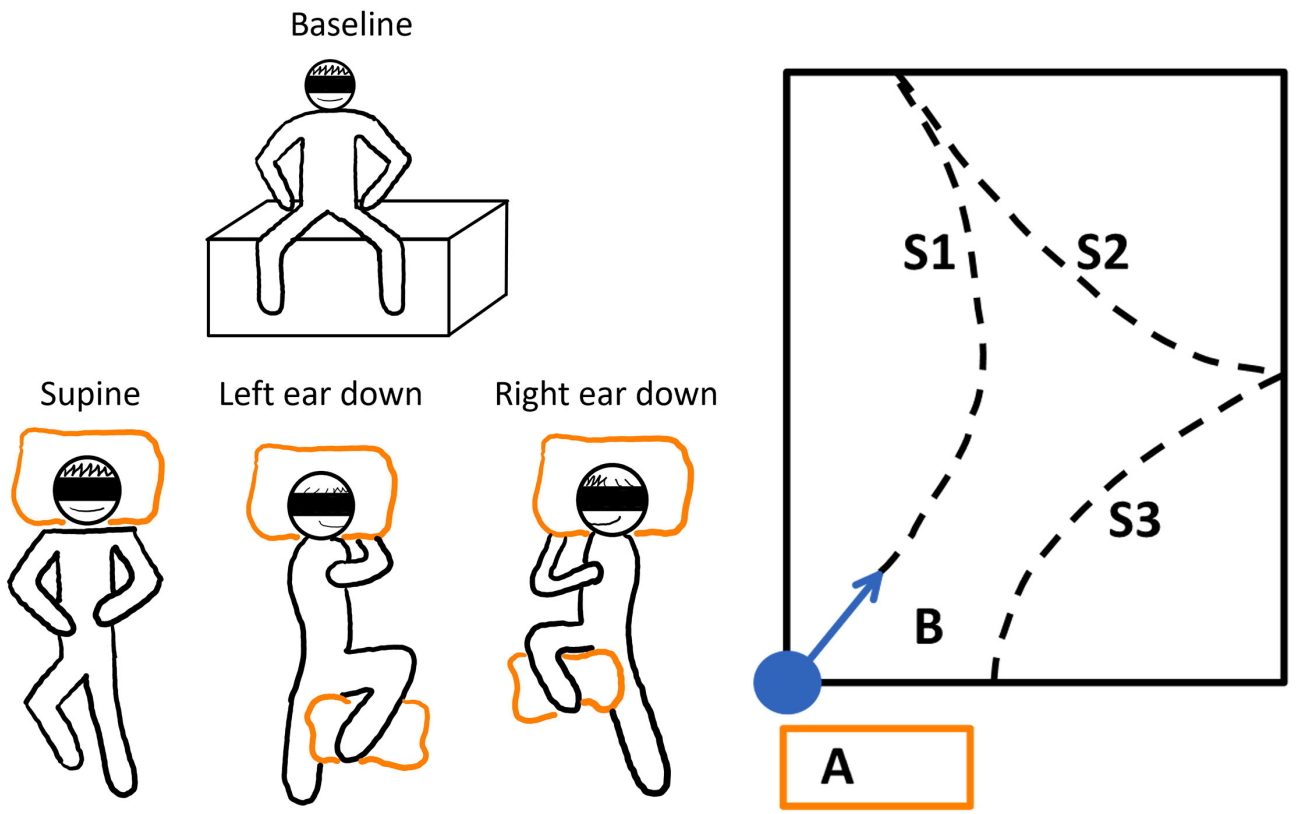

FIGURE 2 | The schematic illustration of the experimental paradigm. Left panel: The baseline resting position and the three different whole-body horizontal positions are depicted. To stabilize the subjects while lying, pillows were used (orange boxes). Each trial was repeated three times. The adaptation trials were performed in randomized order after the baseline trials. Right panel: The adaptation or resting phase was conducted on vaulting boxes at position A. The subjects were guided to the starting position, and they were realigned with the sports hall's diagonal (B). The dashed lines show how a subject could have walked during the trials; WS1-3 denote the different WS.

but in reverse direction. Larger time differences (≥2 sec) between detected gait cycles were used to separate WS. The first and last steps were performed with high variability and thus could not be defined with an equal peak detection threshold.

Gait Measure Extraction

The different gait measures with the aim to describe postural control and walking direction of the participants were analyzed. Ideally, a possible trial effect would be described by both sensor systems. Two measures were calculated for every WS.

Linear Regression of the Yaw

The heading direction or yaw (rotation of the sagittal plane around the cranio–caudal axis) of the subjects was estimated from data of the chest motion tracker, as this sensor has shown the steadiest behavior in terms of body orientation during walking in the initial data analysis. Orientation of the chest sensor was estimated by fusing acceleration (accelerometer) and angular velocity (gyroscope) data using a Kalman filter (MATLAB function imufilter). No magnetometer data were considered. In the resulting coordinate system *x*-, *y*-, and *z*-axes were oriented in cranio–caudal, medio-lateral and PA direction respectively. Orientation was transformed to Euler angles relating to the rotations around the medio-lateral (pitch), anterior–posterior (AP, roll) and the cranio–caudal (yaw) body axes. The linear regression of the orientation of the chest around the cranio–caudal axis (yaw) was computed for each WS. The inclination of the determined regression line is further being referred to as "yaw slope." In accordance with the IMU coordinate system, chest rotations to the left and the right were assigned positive and negative values, respectively.

Centre of Pressure (CoP)

The CoP sensory insole data in LM and AP was averaged for each step and each WS. To increase the separability of the results, only data recorded during the stance phase were considered.

Statistical Investigations

For the statistical analysis of walking patterns, yaw slope and CoP in medio–lateral direction (CoP_{LM}) of the first three WS were considered. As it was found that the averaged CoP_{LM} is more separable when observing the difference between the left ($CoP_{LM\ left}$), and the right leg ($CoP_{LM\ right}$), the investigations

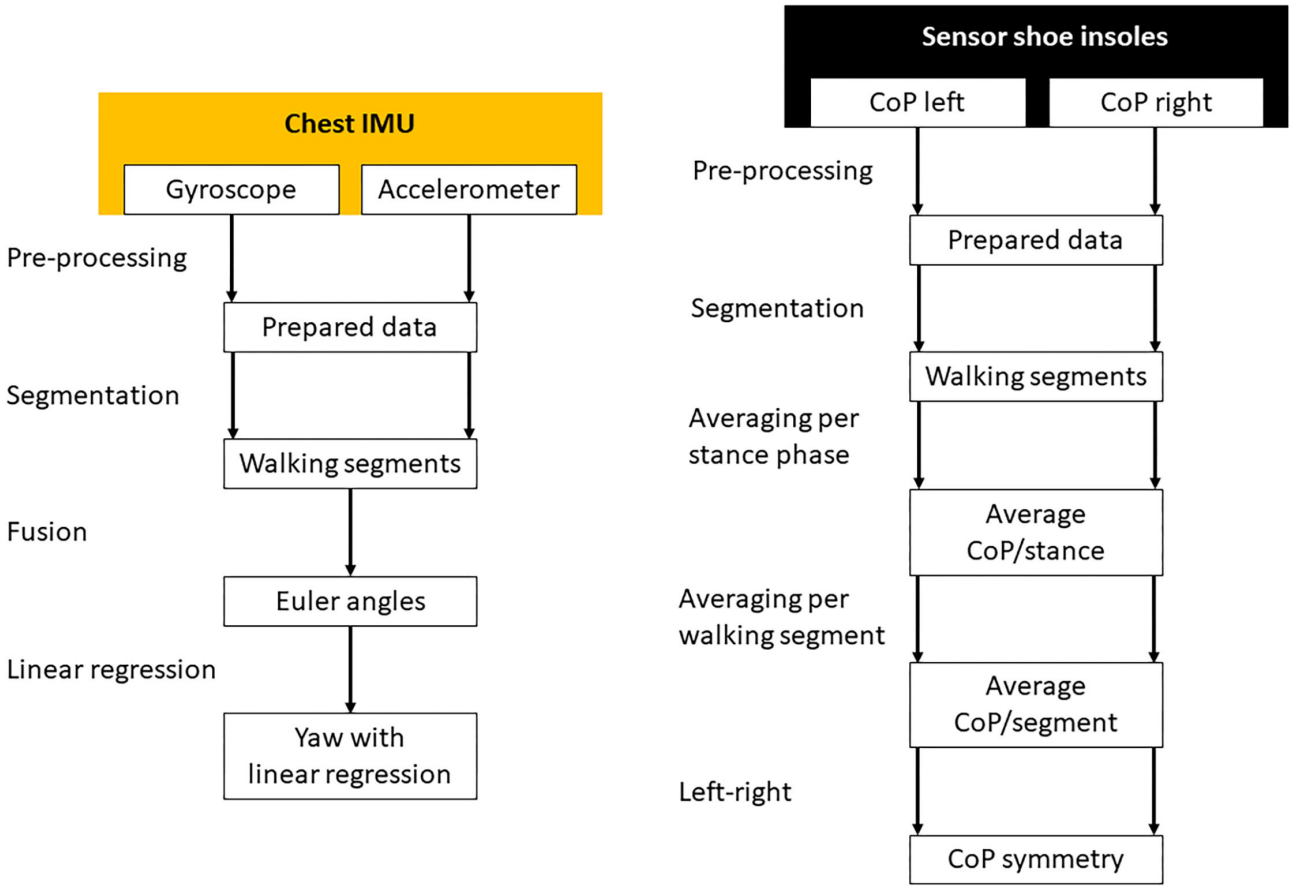

FIGURE 3 | The signal processing of the chest inertial measurement unit (left) and the sensory shoe insoles (right). Missing data was interpolated and both sensor systems were synchronized during the pre-processing phase. The measurements were separated in time to different WS. Gyroscope and accelerometer data were fused to calculate Euler angles in three-dimensional space. In the resulting yaw signal, linear regressions were calculated for every WS separately. The CoP of each leg was averaged for every stance phase of each step. Afterward the CoP was averaged for every WS separately and the difference between the left and right foot calculated.

were performed based on the symmetries ($CoP_{LM\ Sym}$), with

$$CoP_{LM\ Sym} = CoP_{LM\ left} - CoP_{LM\ right}. \quad (1)$$

Consequently, a disequilibrium to the left side would result in a negative value, to right in a positive value.

The distribution of yaw slope and $CoP_{LM\ Sym}$ was tested for equal variance using Bartlett's and Levene's tests and for normality in Shapiro–Wilk tests and quantile–quantile plots.

For the correlation analysis between yaw slope and $CoP_{LM\ Sym}$ in the first WS, the average was calculated for each trial condition for both variables and the baseline average was subtracted (baseline-corrected average data). The distribution of all the resulting data together was tested for normality using the Shapiro–Wilk test and visual histogram analysis. Correlation was analysed with the Pearson's correlation coefficient.

Linear Mixed Effect Models

The statistical investigation of the results was performed using linear effects models. The models were created as shown in Eq. (2) (26).

$$data.lme = lme(slope \sim trial + trial^{*}\ walkingSegment, \quad (2)$$
$$random = \sim 1 \mid \frac{participant}{walkingSegment},$$
$$data = slope.data$$

The *slope* is described by the fixed effects *trial* and *walkingSegment*, which interact with each other. The interaction was included since any effect of the adaptation phases could potentially decrease over time. Testing the model with an ANOVA showed significance in the interaction term (25, 26, 33). The main random effect *participant* was included to consider subject-dependent deviations in walking direction. The random term was nested with *walkingSegment* because any decay of a possible effect would take different lengths of time for individual subjects. The R library emmeans (27) was used to calculate estimated marginal means from the linear mixed effect models. The pairwise comparisons between trials were performed and

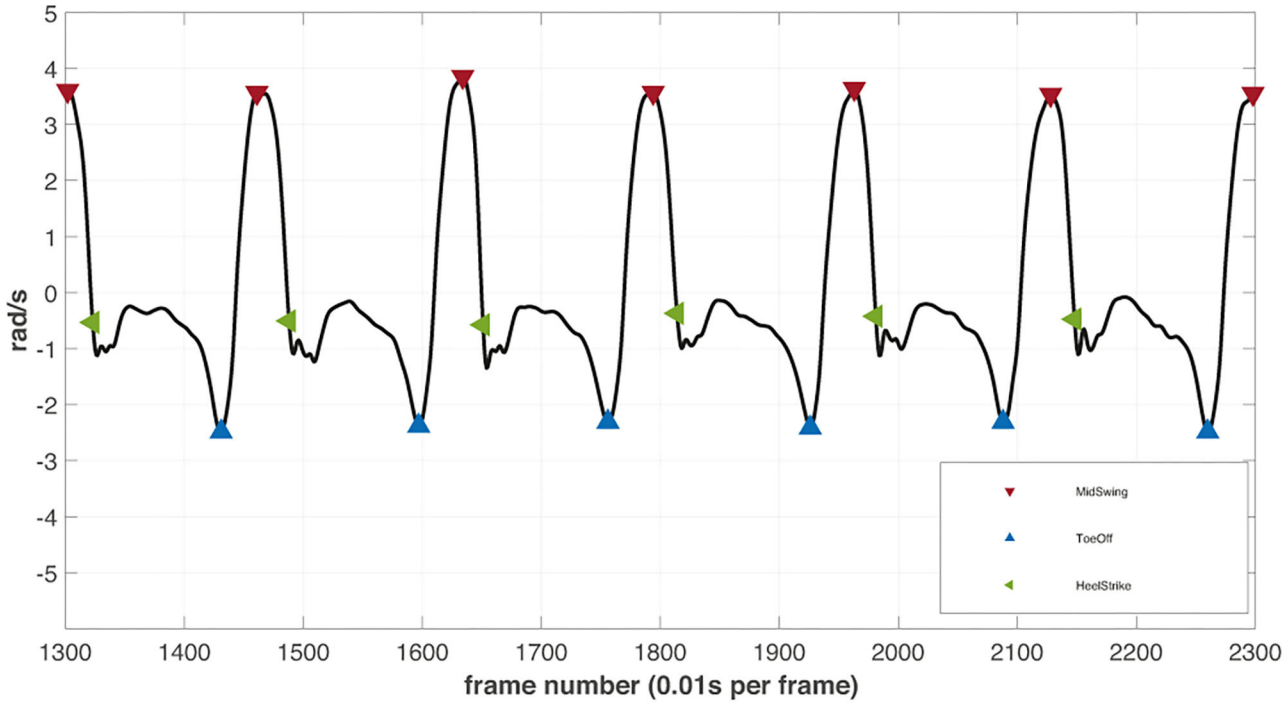

FIGURE 4 | The illustrative example of filtered angular velocity signal from the right ankle inertial motion tracker with detected gait events. The detected peaks (red) in the signals are defined as mid-swing phases of every step. The lowest valley right before the mid-swing peaks are assumed to depict the toe-off events (blue). The datapoint at the zero-crossing event after every mid-swing peak determines the heel strike (green) of the next step.

p-values were calculated, using the Tukey method to adjust for the multiple testing (27).

RESULTS

On average, the subjects completed 4.5 ± 0.8 WS within the 2-min time limit. One subject (#3) had to repeat a single supine and one LED trial on a second examination day due to information loss during data transfer. To adjust for possible changes in the elementary drift between the test days in this subject, all three baseline attempts were repeated as well. Noteworthy, no change in the elementary drift was observed in this subject. For two subjects (#10 and #21) one RED trial was omitted for the CoP-measurements because of missing data of one foot.

Single Subject Data for Both Sensory Systems

The calculated chest heading orientations ("yaw") from the IMUs with fitted linear regressions are shown in **Figure 5** for all four resting positions studied for a single participant (#25). For the baseline trial, the subject showed a tendency to walk to the left side (**Figure 5**, upper left). In this example, the deviation to the left side decreased during the supine trial (**Figure 5**, upper right). The subject turned more to the right-hand side during RED trials and more to the left-hand side during LED trials (**Figure 5**, bottom left and right). Comparing the WS during the LED trial shows that the slope decreases for subsequent WS.

Using the sensory shoe inlets, the CoP-coordinates of each leg during the first segment are shown in **Figure 6**. The subject and trials are the same as shown for chest heading orientation (**Figure 5**). The CoP in this example generally spreads on a larger area for the right foot indicated as well as by a higher standard deviation of the average CoP_{LM}. The anterior and medial tail (toe-off) is more pronounced in the right foot. Generally, the medial borders are sharper on the right foot. The LM distribution is highest during the RED trial for the right foot. Observations of the left foot show that the dispersion is lowest during the LED trials. Average CoPs show a very small difference between left and right foot during baseline and supine positions resulting in very small $CoP_{LM\ Sym}$ values. During RED and LED conditions the Avg CoP values become more negative for the right and left foot respectively indicating a weight shift to the lateral side. Average values for the foot opposite to the ear-down direction remain the same compared to baseline for the left foot (RED condition) and shows a slight weight shift to the left for the right foot (LED condition). $CoP_{LM\ Sym}$ values indicate this shift by a positive value for the RED condition and a negative value for the LED condition.

Inter-Individual Variability in Walking Performance

The yaw slopes derived from the IMU sensors of every participant and trial for the first WS are shown in **Figure 7A**. During the

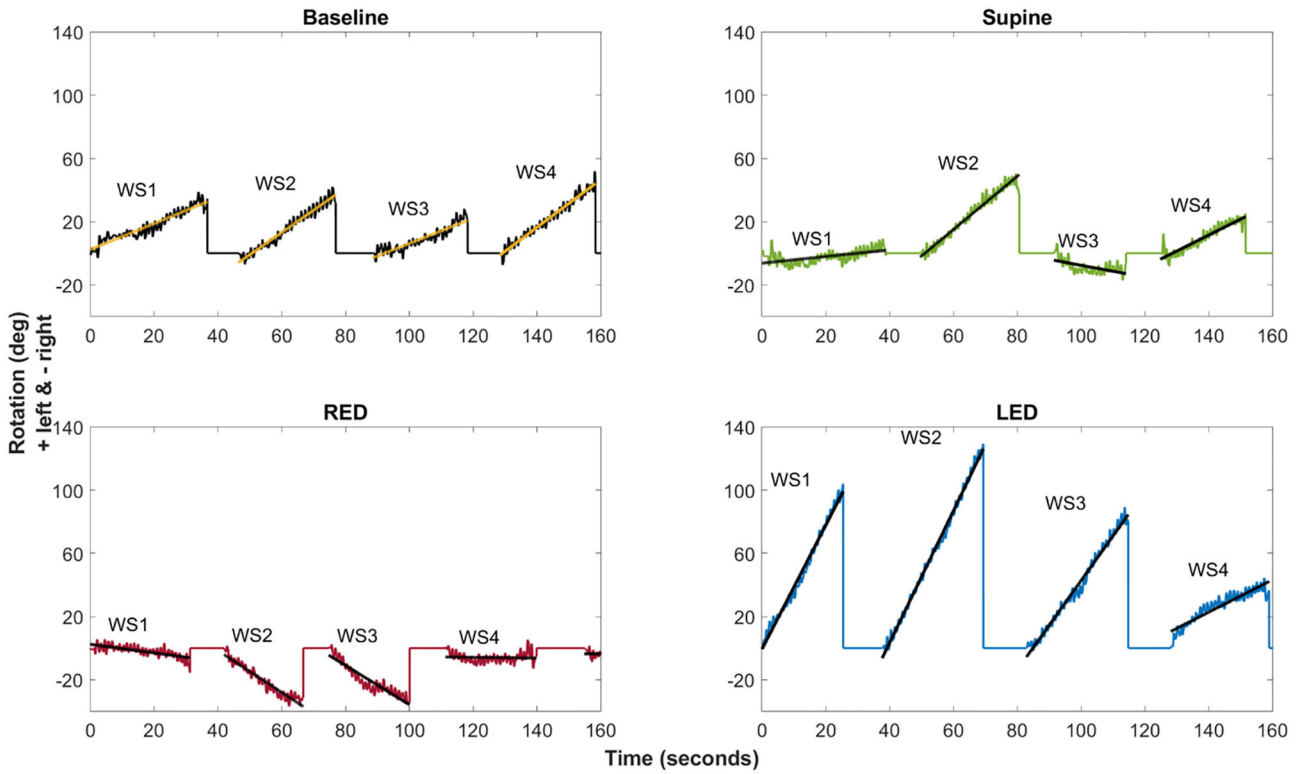

FIGURE 5 | The example of the chest heading orientation (yaw) with linear regression lines for all four resting positions of a single subject (#25). The oscillations in the yaw result from upper body twists while walking. Linear regression of the yaw was computed for each WS (WS1–WS4) separately. The slope of the fitted linear regression lines ("yaw slope") was used in statistical investigations as an estimate of heading direction. Upper left: Baseline trial showing tendency to walk to the left side. Upper right: deviation decrease to the left side during the supine trial. Bottom left: Turn to the right-hand side during RED trials. Bottom right: Turn to the left-hand side during LED trials.

baseline trials, the investigated population generally deviated to the left side when walking blindfolded, resulting in positive yaw slope values. The yaw slopes are mostly more positive for supine than for baseline trials. Even if the extent of the deviations varies between patients, the LED and RED conditions led in most cases to a deviation to the left and right side, respectively.

Using the sensory shoe inlets, the differences between the averaged LM–CoP symmetries are shown in **Figure 7B**. Absolute values for the LM–CoP symmetries differ between subjects and are though subject specific. Averaged LM–CoP symmetries (left–right foot) of the baseline and supine trials seem to be similar. During the RED condition the weight was more shifted to the right, during the LED condition more to the left compared to the baseline. The general tendencies of changes in LM–CoP symmetry between the conditions are opposite to the yaw slopes as depicted in **Figure 7A**, which means that the direction of the deviation is identical when comparing to the baseline data.

Effect of Adaptation Position on Walking Direction

In a next step, we compared individual walking patterns and focused on the impact of the previous adaptation position. Bartlett's and Levene's tests showed that the yaw slopes do not have equal variance between the trials while $CoP_{LM\ Sym}$ is distributed with equal variance. Shapiro–Wilk tests and quantile–quantile plots showed that both measures are normally distributed except for the RED trials. In **Figure 8A** results are depicted as boxplots per trial and WS for the IMU sensors. The general deviation of the investigated population to the left, in form of a positive shift, can also be observed in this figure. For the first WS, all trials significantly differ from each other. The deviation to the left side was larger for the supine laying trials compared to baseline trials and was highest when subjects rested LED. The only distribution with a median heading rotation toward the right side can be observed for the RED trials. The difference between the trials was largest when comparing yaw slopes from RED trials with those from LED trials.

The boxplots and significance values show decreasing differences between the trials for subsequent WS. In the third WS, results significantly differed only between the LED trials and the baseline trials, and between the LED trials and the RED trials.

In **Figure 8B** results are depicted as boxplots per trial and WS for the sensory shoe inlets. The distributions of the difference between both feet of the averaged LM–CoP symmetry show that, except for the baseline compared to the supine trials, all trials

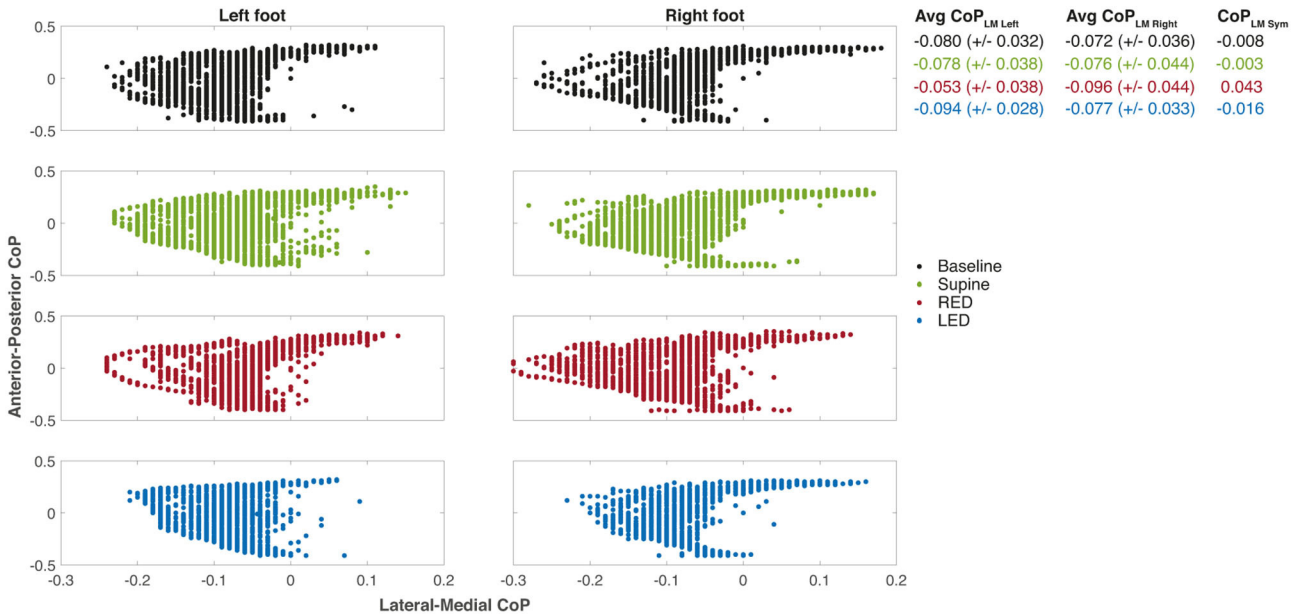

FIGURE 6 | The CoP coordinates of each leg during the first WS for each resting position of the same subject. The examples depict the same measurements of subject #25 as shown in **Figure 5**. The positive x-axis values are medial, and the positive y-axis values are anterior CoP displacements. The CoP output of the sensory insoles on both axes ranges from −0.5 to 0.5 and is related to the corresponding insole length or width, respectively. Some values appeared more than once which is not illustrated in the figure. Averaged CoP_{LM} values are presented next to each plot for left and right foot as well as well as the $CoP_{LM\,Sym}$ all together with their standard deviations.

significantly differ to each other for the first WS. Compared to the baseline, a shift in the positive direction can be observed for the RED trials and in the negative direction for the LED trials. The distribution difference between the trials is highest when comparing RED and LED trials. The difference between the trials decreases for subsequent WS. In the third WS, results only significantly differ between the RED and LED trials. For the baseline and supine trials, no significant difference was found for any WS.

The correlation analysis of the baseline corrected and averaged yaw slope and CoPLM Sym per trial condition during the first walking revealed a moderate negative correlation ($R = -0.518$; $p < 0.001$) (34), as shown in **Figure 9**.

DISCUSSION

Asking healthy human subjects to walk straight-ahead blindfolded after prolonged whole-body roll-tilt to either side, we observed a significant bias in post-adaptation walking in darkness into the direction of the previous roll-tilt position. This bias was observed in two independent measurement systems for gait tracking and decreased again over the time.

An Overall Leftward Bias in Perceived Straight-Ahead

Yaw data showed a tendency to deviate toward the left side while walking blindfolded both in the baseline trials and in the "neutral" adaptation trials (i.e., in supine position) in the majority of subjects. This leftward bias was significantly stronger for the supine adaptation condition than the baseline condition in the first two WS as recorded by the IMU motion tracking system, while this difference disappeared again in the third WS, possibly indicating a decay in adaptational mechanisms due to prolonged supine roll position. This overall leftward tendency could also be depicted on the adaptation trials with preceding RED or LED resting position. While subjects deviated significantly more toward the left after adaptation in LED position, the overall walking direction was still slightly leftward after adaptation in RED position.

The reason for this overall leftward bias when walking blindfolded remains unclear. Previously, lateralized cortical processing of vestibular input has been reported. Perception of straight-ahead was studied in patients with unilateral vestibular deficits (UVD), indicating side-specific deviations in subjective straight-ahead (SSA). While patients with left-sided UVD demonstrated a contralesional shift in SSA, the SSA remained accurate in patients with right-sided UVD (35). Thus, the authors concluded that their data support the hypothesis of an asymmetric vestibular function in healthy human subjects. Others have demonstrated an overall right-hemispheric dominance of the vestibular cortex as well (36, 37). With regards to the observed overall tendency to deviate toward the left side in the post-adaptation trials, this could be linked to such asymmetric representation of higher cortical vestibular properties. Lack of reporting of such an effect in the literature on blindfolded walking could be related to the total walking distance, being much shorter (5–8 m) in previous

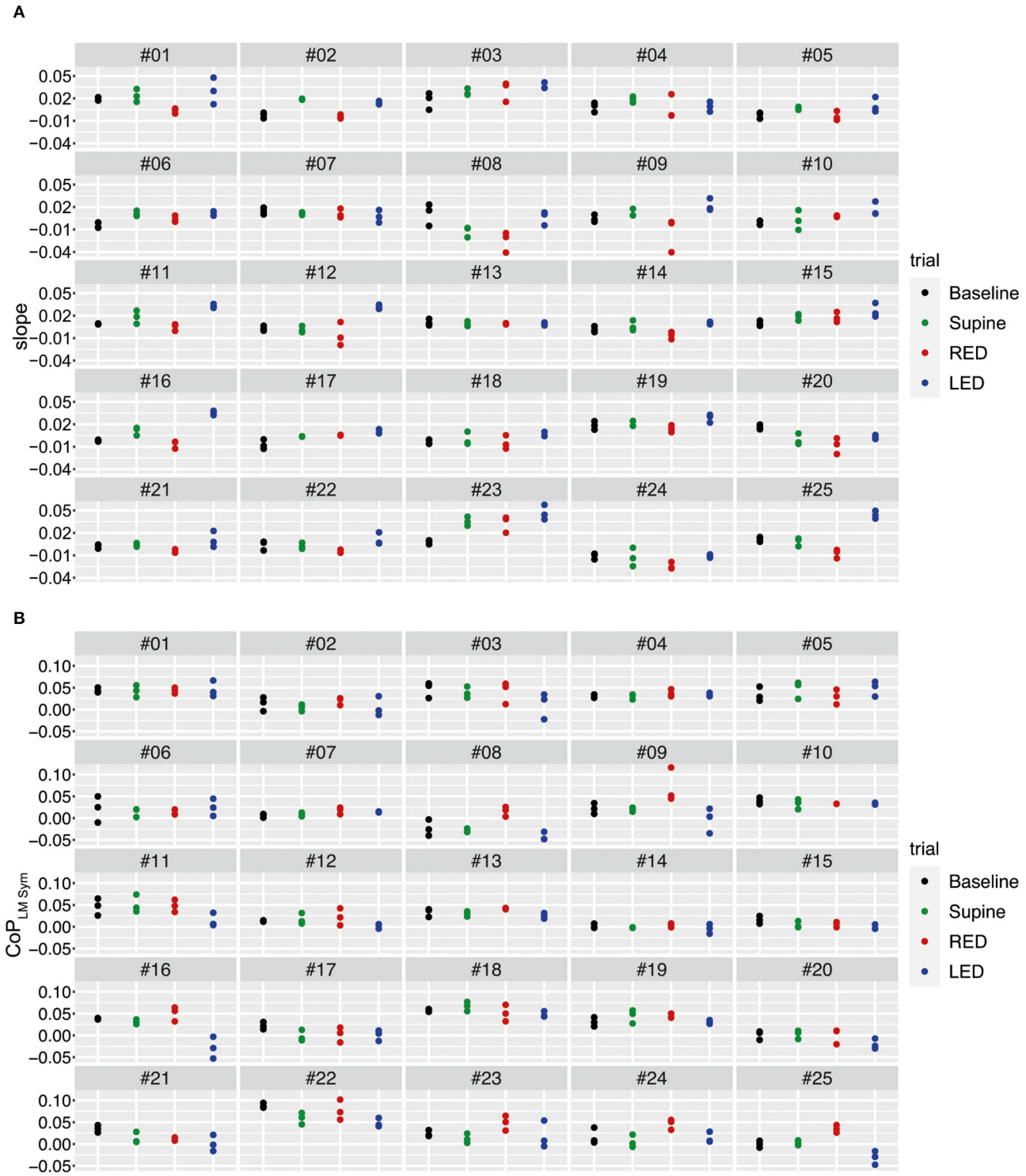

FIGURE 7 | The yaw slope (slope of the linear regression of the chest heading orientation) **(A)** and differences of the averaged $LMCoP_{LM\ Sym}$ (left–right) **(B)** per trial for the first WS for all 25 subjects. For **(A)**, positive slope values correspond to a rotation to the left. For **(B)**, positive differences of LM–CoP symmetries to the baseline indicate a pressure shift to the right, negative ones to the left.

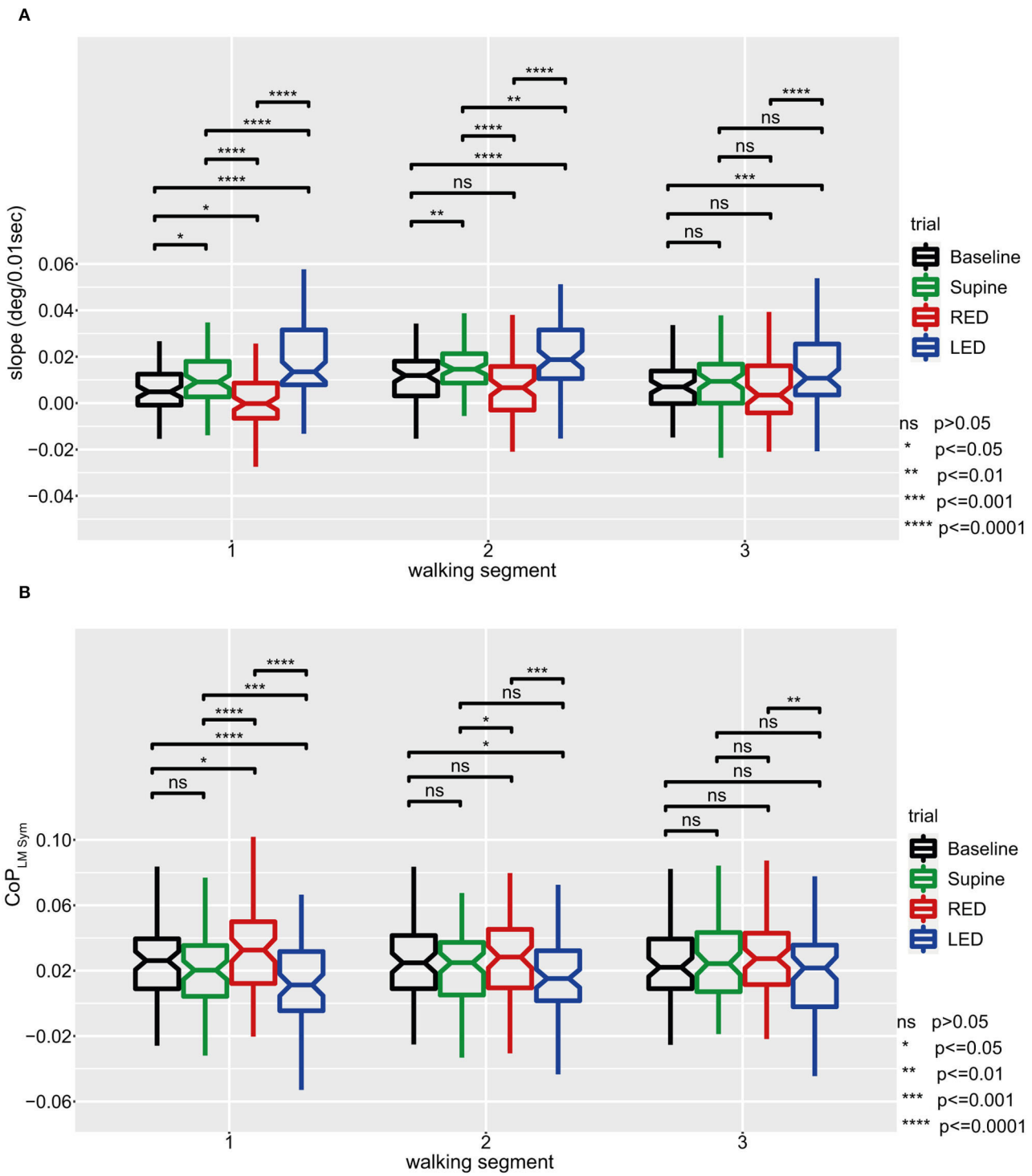

FIGURE 8 | The yaw slope **(A)** and averaged LM–CoP symmetries ($CoP_{LM\ Sym}$, left to right foot) **(B)** and for all subjects and trials with pairwise comparisons between trials for the first three WS. For **(A)**, positive slopes indicate yaw rotations to the left side, negative slopes to the right side. For **(B)**, the results were calculated by subtracting the averaged CoP of the right foot from those of the left foot. Baseline values are hardware related and subject specific and should not be interpreted but used as a reference value. Positive changes between two measurement conditions or WS represent a shift of weight to the right side, negative changes to the left side. For both panels, linear mixed-effects models were calculated for every WS in which all trials were compared pairwise. Comparisons and *p*-value adjustments according to Tukey are displayed on top of the boxplots according to the legend on the lower right. Boxplot details: Lower and upper edges of the boxes depict the boundaries between the 25th and the 75th percentile of the data. The lines inside the boxes represent the median for every trial. Each whisker has at most a length of 1.5 times the interquartile range (box length). Data points outside of this limit are marked as separate points. Extreme points (i.e., further apart than 3*IQR) were classified as outliers and disregarded for the analysis. An inlet (placed right to the figure) provides the level of significance by using different numbers of * symbols.

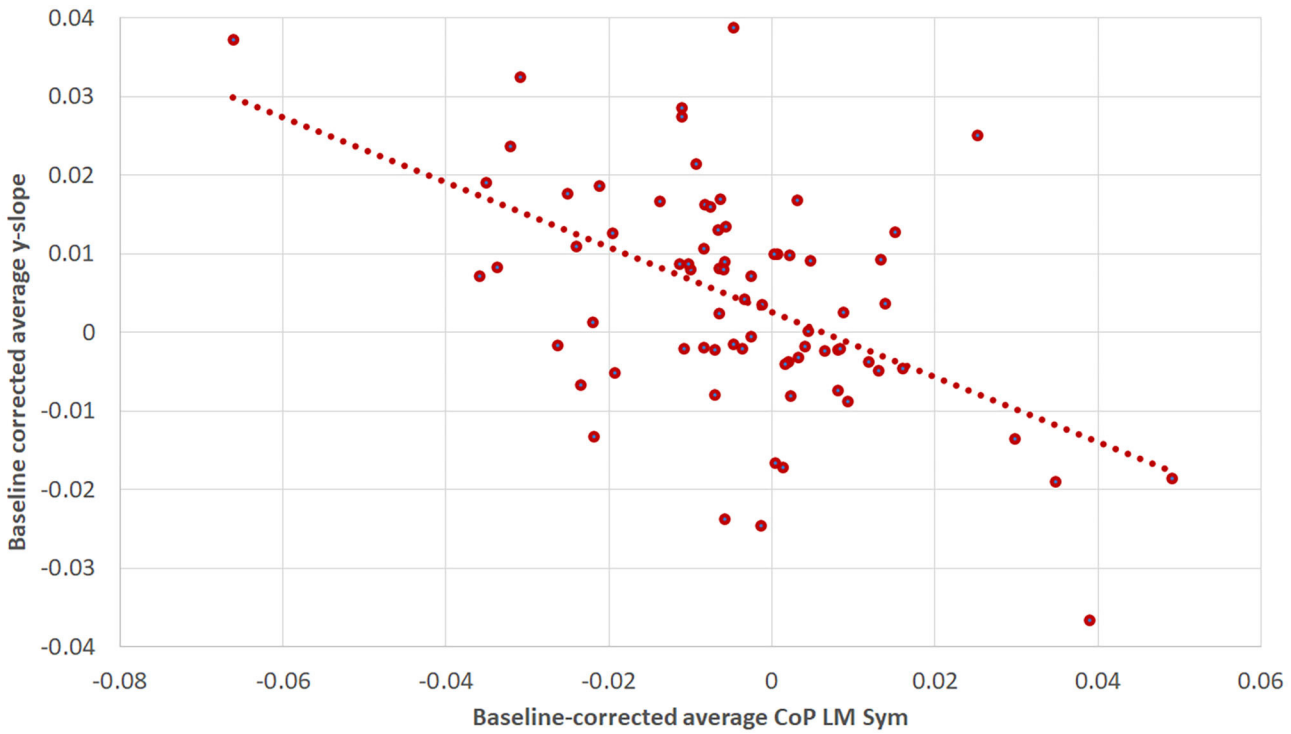

FIGURE 9 | The correlation between baseline-corrected average yaw slope and baseline-corrected average $CoP_{LM\ Sym}$ for the first WS. The Pearson correlation coefficient was R = −0.518 ($p < 0.001$). The figure is composed of three data points per subject: one for the supine, one for the RED and one for the LED condition.

publications, the specific experimental paradigms applied or the patient populations studied.

When investigating larger walking distances when blindfolded, healthy human subjects tend to walk in sometimes surprisingly small circles (<20 m diameter), though rarely in a systematic direction (38). The authors proposed accumulating noise in all components of the sensory system to explain such non-systematic deviations from straight-ahead. Noteworthy, no correlations between the laterality of these deviations and functional asymmetries (handedness/footedness) were found. Thus, on top of a systematic post-tilt bias, accumulating noise may have affected the precision of walking in our study. Noteworthy, the duration of walking blindfolded was much longer in the study by Souman and colleagues (38) than in the work presented here, possibly triggering different walking patterns over larger time scales.

The Pathophysiology of the Observed Post-Tilt Walking Bias

Five minutes of the whole-body static roll-tilt to either side were sufficient to induce significant shifts in walking direction compared to lying on the back during the adaptation period. Over the time, the effect of the adaptation in ear-down position on walking direction decreased, indicating partial re-adaptation to the current (non-biased) condition. Thus, over a period of 2 min walking a decrease, but not complete cessation of the adaptation effect can be noted. While in the current paradigm no decay time constant of the post-tilt bias can be calculated, the pattern observed suggests a decay time constant in the range of a few minutes. Noteworthy, using the pressure measurement sensory shoe insoles, observed differences in walking direction in the adaptation trials disappeared faster, but were still significant for RED *vs.* LED post-adaptation trials in WS 3.

We have previously discussed the pathophysiological bases for such a post-tilt bias on the SVV (10, 14) and SHV (14). In brief, we have proposed a shift in the internal estimate of direction of gravity based on recent experience (prior knowledge) in the context of Bayesian optimal observer theory (see introduction). As a result, the perceived direction of gravity will be shifted toward the body-longitudinal axis, thus immediately after returning back upright shows a shift toward the previous static whole-body roll-tilted position. We predicted that a shift in perceived earth–vertical in the roll-plane affects walking direction as well, which was confirmed in our study demonstrating a clear bias in perceived straight-ahead toward the previous adaptation position.

A potential mechanism to explain an effect of prolonged static roll-tilt on translational responses could be related to the continuous otolith stimulation while lying on the side. Thus, in left/right ear-down position gravity pulls down the otoliths of the utricles and activates them continuously. This stimulus for the receptors is identical to an ongoing linear translational acceleration. Consequently, an adaptive process to this acceleration could occur that is maintained for a certain

amount of time after returning to the upright position. In this position, the adaptive response would be reoriented in a latero-lateral adaptation, that, in turn, would influence the SSA and thus translatory motor activity. While this mechanism emphasizes adaptational effects of body resting position on central coordinates, alternatively, prolonged whole-body roll tilt could act on the motor system of gait by changing directly one side otolithic descending motor output. Thus, the walking directional shift observed in our study cannot be directly related with a shift of the SSA. However, taking into account previous studies emphasizing adaptational mechanisms on both perceived direction of gravity (10, 14) and self-motion perception (19, 20) by prolonged (asymmetric) otolith stimulation, such a direct mechanism seems less likely.

The path integration in both healthy human subjects and patients with either acute or chronic vestibular deficits has been extensively studied [see (39) for review]. Previously, the galvanic vestibular stimulation has been applied to study the role of the vestibular organs in path integration (40), demonstrating significantly increased arrival errors and angular errors in a virtual triangle completion task. Likewise, the repetitive transcranial magnetic stimulation (rTMS) has been used to disrupt path integration in a vestibular navigation task, demonstrating deteriorated perceived contralateral spatial displacement after rTMS in the area of the right posterior parietal cortex (41).

In patients with UVD, veering has been noted in non-visually guided walking tasks (42, 43), with walking trajectories deviating toward the lesioned side when walking straight-ahead over short distances (5.5 m) (17) and significantly larger final arrival errors in a triangular-path walking task have been reported (44).

Comparison of Two Independent Gait Analysis Systems

Whereas we measured trunk yaw rotation in the first setup, distribution of pressure on the feet was assessed in the second setup. Both systems detected significant deviations in heading while walking blindfolded toward the side of the adaptation position during the first WS in the post-adaptation trials, with results from both setups correlating significantly. Thus, our findings were confirmed using two independent gait measurement systems that monitored distinct parameters of heading simultaneously. Specifically, when biasing internal estimates of perceived straight-ahead, walking patterns in participants were modified in such a way that both the difference in distribution of pressure between the left and the right foot and the yaw rotation of the trunk were pointing toward the adapted side.

However, when assessing the temporal evolvement of the deviations over the whole walking distance, the dynamics were distinct. Overall, the level of significance was higher when comparing the different post-adaptation test conditions and more frequently found also in the 3rd WS when assessing the body-fixed accelerometers/gyroscopes compared to the pressure sensors placed in the participant's shoes. Thus, the first system was superior in detecting deviations in walking direction for the paradigm studied here. These discrepancies are most likely related to the selection of the parameters to be monitored, the signal-to-noise ratio of the sensors implemented and inter-individually varying walking habits, foot shape and type of shoes used. Based on these observations, with the proposed parameters, the use of trunk-fixed gyroscopes/accelerometers currently seems more suitable to detect deviations in walking direction accurately and precisely in future studies than pressure sensors located in shoe inlets. On the other side, the handling of the inlets was less demanding, thus selection of devices for recordings depends also on the requirements (temporal/spatial resolution, signal-to-noise ratio) of the specific paradigm to be implemented.

Clinical Implications of a Heading Bias

While none of our healthy young participants showed signs of truncal instability or even demonstrated (near) falls, this post-tilt bias may become clinically relevant in the elderly and in patients with pre-existing gait disorders. Taking into account the sleeping habits, lying on the side at night may increase the risk of falls and fall-related injuries when getting up in the morning or during the night, especially if vision is impaired. Furthermore, besides building up a directional bias during a good night's sleep, internal estimates may also be less precise in the morning. It has been demonstrated that immediately after getting up in the morning the trial-to-trial variability of perceived earth–vertical is significantly larger than in the evening (45). Thus, special attention should be paid in the morning when getting up to minimize the risk of falls and fall-related injuries.

Limitations

The size of the indoor walking hall requiring splitting up the entire walking over 2 min into several segments with experimenter-guided rotations of the participant's orientation before continuing walking, resulting in potential clues while repositioning. Importantly, we controlled for direction of rotation-specific effects between WS and did not find any significant differences. Thus, we do not think that this segmented walking significantly biased our findings.

Deviations from straight-ahead while walking were determined indirectly from parameters indicating uneven pressure distribution (shoe soles) or yaw trunk rotation. We have chosen this strategy as due to growing offsets over time of the sensory input obtained from both systems, performing a path integration was not feasible. Nonetheless, using two independent measurement systems, comparable results in heading patterns after whole-body roll-tilt adaptation could be obtained, strongly supporting the existence of such a post-tilt bias.

CONCLUSIONS

In summary, a significant bias in perceived straight-ahead after static whole-body roll-tilt in either left-ear-down or right-ear-down position over periods as short as 5 min further confirms the impact of prior knowledge on spatial orientation and navigation. Specifically, it emphasizes the broad impact of a shifting internal estimate of direction of gravity over a range of distinct paradigms, illustrating similar decay time constants of

this bias. For tracking changes in walking direction, a set of body-fixed accelerometers/gyroscopes seems superior to foot pressure measurements when considering averaged data, which should be taken into account for future studies. The observed bias in perceived straight-ahead likely has also implications in daily life and especially in the context of fall-prevention. It emphasizes that getting up in the morning after a good night's sleep is a vulnerable period, with an increased risk of falls and fall-related injuries due to not optimally tuned internal estimates of direction of gravity and direction of straight-ahead.

DATA AVAILABILITY STATEMENT

The raw data supporting the conclusions of this article will be made available by the authors, without undue reservation.

ETHICS STATEMENT

The studies involving human participants were reviewed and approved by Ethikkommission Nordwest- und Zentralschweiz (EKNZ, ID=2020-01712). The patients/participants provided their written informed consent to participate in this study.

AUTHOR CONTRIBUTIONS

AT: conception of the work, interpretation of data for the work, drafting the work, and revising it critically for important intellectual content. VD: acquisition, analysis and interpretation of data for the work, drafting the work, and revising it critically for important intellectual content. DB: interpretation of data for the work and revising the work critically for important intellectual content. SH: conception of the work, interpretation of data for the work, and revising the work critically for important intellectual content. All authors approved the final version of the manuscript and agreed to be accountable for all aspects of the work in ensuring that questions related to the accuracy or integrity of any part of the work are appropriately investigated and resolved. The authors confirm that all persons designated as authors qualify for authorship, and all those who qualify for authorship are listed.

FUNDING

VD was financially supported by the Cantonal Hospital of Baden (Grant #009192).

REFERENCES

1. Cullen KE, Taube JS. Our sense of direction: progress, controversies and challenges. *Nat Neurosci.* (2017) 20:1465–73. doi: 10.1038/nn.4658
2. Ekstrom AD, Spiers HJ, Bohbot VD, Rosenbaum RS. *Human Spatial Navigation*. Princeton, New Jersey, USA: Princeton University Press (2018).
3. Angelaki DE, Gu Y, Deangelis GC. Multisensory integration: psychophysics, neurophysiology, and computation. *Curr Opin Neurobiol.* (2009) 19:452–8. doi: 10.1016/j.conb.2009.06.008
4. Noel JP, Angelaki DE. Cognitive, Systems, and Computational Neurosciences of the Self in Motion. *Annu Rev Psychol.* (2021) 73:103–29. doi: 10.1146/annurev-psych-021021-103038
5. Mcnaughton BL, Battaglia FP, Jensen O, Moser EI, Moser MB. Path integration and the neural basis of the 'cognitive map'. *Nat Rev Neurosci.* (2006) 7:663–78. doi: 10.1038/nrn1932
6. Shinder ME, Taube JS. Differentiating ascending vestibular pathways to the cortex involved in spatial cognition. *J Vestib Res.* (2010) 20:3–23. doi: 10.3233/VES-2010-0344
7. Schoene H, Udo De Haes H. Perception of gravity-vertical as a function of head and trunk position. *Zeitschrift für vergleichende Physiologie.* (1968) 60:440–4. doi: 10.1007/BF00297938
8. Wade NJ. Effect of prolonged tilt on visual orientation. *Q J Exp Psychol.* (1970) 22:423–39. doi: 10.1080/14640747008401916
9. Day RH, Wade NJ. Visual spatial aftereffect from prolonged head-tilt. *Science.* (1966) 154:1201–2. doi: 10.1126/science.154.3753.1201
10. Tarnutzer AA, Bertolini G, Bockisch CJ, Straumann D, Marti S. Modulation of internal estimates of gravity during and after prolonged roll-tilts. *PLoS ONE.* (2013) 8:e78079. doi: 10.1371/journal.pone.0078079
11. Kording KP, Wolpert DM. Bayesian integration in sensorimotor learning. *Nature.* (2004) 427:244–7. doi: 10.1038/nature02169
12. Laurens J, Droulez J. Bayesian processing of vestibular information. *Biol Cybern.* (2007) 96:405. doi: 10.1007/s00422-006-0133-1
13. Macneilage PR, Banks MS, Berger DR, Bulthoff HH. A Bayesian model of the disambiguation of gravitoinertial force by visual cues. *Exp Brain Res.* (2007) 179:263–90. doi: 10.1007/s00221-006-0792-0
14. Wedtgrube A, Bockisch CJ, Tarnutzer AA. Effects of prolonged roll-tilt on the subjective visual and haptic vertical in healthy human subjects. *J Vestib Res.* (2020) 30:1–16. doi: 10.3233/VES-200690
15. Wedtgrube A, Bockisch CJ, Straumann D, Tarnutzer AA. Prolonged Static Whole-Body Roll-Tilt and Optokinetic Stimulation Significantly Bias the Subjective Postural Vertical in Healthy Human Subjects. *Front Neurol.* (2020) 11:595975. doi: 10.3389/fneur.2020.595975
16. Cohen HS. Vestibular disorders and impaired path integration along a linear trajectory. *J Vestib Res.* (2000) 10:7–15. doi: 10.3233/VES-2000-10102
17. Borel L, Harlay F, Lopez C, Magnan J, Chays A, Lacour M. Walking performance of vestibular-defective patients before and after unilateral vestibular neurotomy. *Behav Brain Res.* (2004) 150:191–200. doi: 10.1016/S0166-4328(03)00257-2
18. Zhang YB, Wang WQ. Reliability of the Fukuda stepping test to determine the side of vestibular dysfunction. *J Int Med Res.* (2011) 39:1432–7. doi: 10.1177/147323001103900431
19. Pettorossi VE, Panichi R, Botti FM, Kyriakareli A, Ferraresi A, Faralli M, et al. Prolonged asymmetric vestibular stimulation induces opposite, long-term effects on self-motion perception and ocular responses. *J Physiol.* (2013) 591:1907–20. doi: 10.1113/jphysiol.2012.241182
20. Panichi R, Occhigrossi C, Ferraresi A, Faralli M, Lucertini M, Pettorossi VE. Adaptive Changes in the Perception of Fast and Slow Movement at Different Head Positions. *Aerosp Med Hum Perform.* (2017) 88:463–8. doi: 10.3357/AMHP.4595.2017
21. Paulich M, Schepers M, Rudigkeit N, Bellusci G. *Xsens MTw Awinda: Miniature Wireless Inertial-Magnetic Motion Tracker for Highly Accurate 3D Kinematic Applications* (2018). Available online at: https://www.xsens.com/hubfs/3446270/Downloads/Manuals/MTwAwinda_WhitePaper.pdf
22. Oerbekke MS, Stukstette MJ, Schutte K, De Bie RA, Pisters MF, Vanwanseele B. Concurrent validity and reliability of wireless instrumented insoles measuring postural balance and temporal gait parameters. *Gait Posture.* (2017) 51:116–24. doi: 10.1016/j.gaitpost.2016.10.005
23. Price FT. *Validation of a Wearable Sensor Insole Device for Analysis of Postural Control* (MSc thesis). Miami University, Oxford, Ohio (2018). Available online at: https://etd.ohiolink.edu/apexprod/rws_etd/send_file/send?accession=miami152517168199145&disposition=inline
24. Tarnutzer AA, Bockisch CJ, Straumann D, Marti S, Bertolini G. Static roll-tilt over 5 minutes locally distorts the internal estimate of direction of gravity. *J Neurophysiol.* (2014) 112:2672–9. doi: 10.1152/jn.00540.2014
25. Fox J, Weisberg S. *An R Companion to Applied Regression, third edition*. Thousand Oaks, CA: Sage Publications Inc (2019).

26. Pinheiro J, Bates D, Debroy S, Sarkar D. *Team RC. Nlme: Linear and Nonlinear Mixed Effects Models; version 3.1-152*. (2021). Available online at: https://cran.r-project.org/web/packages/nlme/nlme.pdf (accessed October 1, 2021).
27. Lenth RV. *Emmeans: Estimated Marginal Means, Aka Least-Squares Means; version 1.5.4*. (2021). Available online at: https://cran.r-project.org/web/packages/emmeans/emmeans.pdf (accessed October 1, 2021).
28. Kassambara A. *Rstatix: Pipe-Friendly Framework for Basic Statistical Tests; version 0.7.0*. (2021). Available online at: https://cran.r-project.org/web/packages/rstatix/rstatix.pdf (accessed October 1, 2021).
29. Gouwanda D, Gopalai AA. A Robust Real-Time Gait Event Detection Using Wireless Gyroscope and Its Application on Normal and Altered Gaits. *Med Eng Phys.* (2015) 37:219–25. doi: 10.1016/j.medengphy.2014.12.004
30. Behboodi A, Zahradka N, Wright H, Alesi J, Lee SCK. Real-Time Detection of Seven Phases of Gait in Children with Cerebral Palsy Using Two Gyroscopes. *Sensors (Basel).* (2019) 19:2517. doi: 10.3390/s19112517
31. Fadillioglu C, Stetter BJ, Ringhof S, Krafft FC, Sell S, Stein T. Automated gait event detection for a variety of locomotion tasks using a novel gyroscope-based algorithm. *Gait Posture.* (2020) 81:102–8. doi: 10.1016/j.gaitpost.2020.06.019
32. Rueterbories J, Spaich EG, Larsen B, Andersen OK. Methods for Gait Event Detection and Analysis in Ambulatory Systems. *Med Eng Phys.* (2010) 32:545–52. doi: 10.1016/j.medengphy.2010.03.007
33. Field A, Miles J, Field Z. *Discovering Statistics Using R*. Thousand Oaks, CA: Sage Publishing Ltd (2012).
34. Schober P, Boer C, Schwarte LA. Correlation Coefficients: Appropriate Use and Interpretation. *Anesth Analg.* (2018) 126:1763–8. doi: 10.1213/ANE.0000000000002864
35. Saj A, Honore J, Bernard-Demanze L, Deveze A, Magnan J, Borel L. Where is straight ahead to a patient with unilateral vestibular loss? *Cortex.* (2013) 49:1219–28. doi: 10.1016/j.cortex.2012.05.019
36. Fasold O, Von Brevern M, Kuhberg M, Ploner CJ, Villringer A, Lempert T, et al. Human vestibular cortex as identified with caloric stimulation in functional magnetic resonance imaging. *Neuroimage.* (2002) 17:1384–93. doi: 10.1006/nimg.2002.1241
37. Karnath HO, Dieterich M. Spatial neglect–a vestibular disorder? *Brain.* (2006) 129:293–305. doi: 10.1093/brain/awh698
38. Souman JL, Frissen I, Sreenivasa MN, Ernst MO. Walking straight into circles. *Curr Biol.* (2009) 19:1538–42. doi: 10.1016/j.cub.2009.07.053
39. Borel L, Lopez C, Peruch P, Lacour M. Vestibular syndrome: a change in internal spatial representation. *Neurophysiol Clin.* (2008) 38:375–89. doi: 10.1016/j.neucli.2008.09.002
40. Karn T, Cinelli ME. The effect of galvanic vestibular stimulation on path trajectory during a path integration task. *Q J Exp Psychol (Hove).* (2019) 72:1550–60. doi: 10.1177/1747021818798824
41. Seemungal BM, Rizzo V, Gresty MA, Rothwell JC, Bronstein AM. Posterior parietal rTMS disrupts human Path Integration during a vestibular navigation task. *Neurosci Lett.* (2008) 437:88–92. doi: 10.1016/j.neulet.2008.03.067
42. Cohen HS, Sangi-Haghpeykar H. Walking speed and vestibular disorders in a path integration task. *Gait Posture.* (2011) 33:211–3. doi: 10.1016/j.gaitpost.2010.11.007
43. Arthur JC, Kortte KB, Shelhamer M, Schubert MC. Linear path integration deficits in patients with abnormal vestibular afference. *Seeing Perceiving.* (2012) 25:155–78. doi: 10.1163/187847612X629928
44. Glasauer S, Amorim MA, Viaud-Delmon I, Berthoz A. Differential effects of labyrinthine dysfunction on distance and direction during blindfolded walking of a triangular path. *Exp Brain Res.* (2002) 145:489–97. doi: 10.1007/s00221-002-1146-1
45. Schwarz AJ, Straumann D, Tarnutzer AA. Diurnal Fluctuations of Verticality Perception - Lesser Precision Immediately after Waking up in the Morning. *Front Neurol.* (2015) 6:195. doi: 10.3389/fneur.2015.00195

Conflict of Interest: The authors declare that the research was conducted in the absence of any commercial or financial relationships that could be construed as a potential conflict of interest.

Publisher's Note: All claims expressed in this article are solely those of the authors and do not necessarily represent those of their affiliated organizations, or those of the publisher, the editors and the reviewers. Any product that may be evaluated in this article, or claim that may be made by its manufacturer, is not guaranteed or endorsed by the publisher.

Copyright © 2022 Tarnutzer, Duarte da Costa, Baumann and Hemm. This is an open-access article distributed under the terms of the Creative Commons Attribution License (CC BY). The use, distribution or reproduction in other forums is permitted, provided the original author(s) and the copyright owner(s) are credited and that the original publication in this journal is cited, in accordance with accepted academic practice. No use, distribution or reproduction is permitted which does not comply with these terms.

frontiers | Frontiers in Neurology

ORIGINAL RESEARCH
published: 11 May 2022
doi: 10.3389/fneur.2022.881682

B81 Bone Vibrator-Induced Vestibular-Evoked Myogenic Potentials: Normal Values and the Effect of Age

Yuzhong Zhang[1†], Zichen Chen[1†], Huandi Zhao[1], Jiali Shen[2,3,4], Bo Zhong[5], Qiong Wu[2,3,4], Jun Yang[2,3,4], Yulian Jin[2,3,4], Qing Zhang[1,2,3,4*] and Pengyu Ren[1*]*

[1] Department of Otorhinolaryngology, Head and Neck Surgery, Second Affiliated Hospital of Xi'an Jiaotong University, Xi'an, China, [2] Department of Otorhinolaryngology, Head and Neck Surgery, Xinhua Hospital, Shanghai Jiao Tong University School of Medicine, Shanghai, China, [3] Institute of Ear Science, School of Medicine, Shanghai Jiao Tong University, Shanghai, China, [4] Shanghai Key Laboratory of Otolaryngology and Translational Medicine, Shanghai, China, [5] Division of Mechanics and Acoustics, National Institute of Metrology, Beijing, China

OPEN ACCESS

Edited by:
Toshihisa Murofushi,
Teikyo University Mizonokuchi Hospital, Japan

Reviewed by:
Tatiana Rocha Silva,
Federal University of Minas Gerais, Brazil
Erin Gillikin Piker,
James Madison University, United States

***Correspondence:**
Pengyu Ren
reaping2006@126.com
Qing Zhang
zhangqing03@xinhuamed.com.cn
Yulian Jin
yulianjin66@163.com

[†] These authors have contributed equally to this work and share first authorship

Specialty section:
This article was submitted to Neuro-Otology, a section of the journal Frontiers in Neurology

Received: 22 February 2022
Accepted: 04 April 2022
Published: 11 May 2022

Citation:
Zhang Y, Chen Z, Zhao H, Shen J, Zhong B, Wu Q, Yang J, Jin Y, Zhang Q and Ren P (2022) B81 Bone Vibrator-Induced Vestibular-Evoked Myogenic Potentials: Normal Values and the Effect of Age. Front. Neurol. 13:881682. doi: 10.3389/fneur.2022.881682

Objective: To define the normal values and examine the influence of aging on B81 bone vibrator-induced cervical vestibular-evoked myogenic potentials (B81-cVEMPs) and ocular vestibular-evoked myogenic potentials (B81-oVEMPs).

Methods: Seventy healthy subjects, divided into seven groups according to their ages, were enrolled in this study. The 4–9-, 10–19-, 20–29-, 30–39-, 40–49-, 50–59-, and 60–70-year-old participants were divided into groups I–VII, respectively. B81-cVEMP and B81-oVEMP were recorded in each group.

Results: The B81-cVEMP response rates for groups I–VII were 100, 100, 100, 100, 95, 95, and 75%, respectively, with significant differences only between groups I–VI and group VII ($p = 0.047$, $p < 0.05$). The B81-oVEMP response rates for groups I–VII were 100, 100, 100, 100, 70, 65, and 40%, respectively, with significant differences only between groups I–IV and groups V–VII ($p = 0.020$, $p = 0.008$, $p = 0.000$; $p < 0.05$). The threshold, P13, and N23 latencies of B81-cVEMP positively correlated with age ($r = 0.756$, $p = 0.000$; $r = 0.357$, $p = 0.003$; $r = 0.316$, $p = 0.009$; $p < 0.05$). The raw amplitudes and corrected amplitudes negatively correlated with age ($r = -0.641$, $p = 0.000$; $r = -0.609$, $p = 0.000$, $p < 0.05$). For B81-oVEMP, the corrected amplitudes negatively correlated with age ($r = -0.638$, $p = 0.000$, $p<0.05$), but the threshold and N10 latency positively correlated with age ($r = 0.768$, $p = 0.000$; $r = 0.334$, $p = 0.009$, $p < 0.05$). Moreover, the interaural asymmetry ratio did not significantly correlate with age for B81-cVEMP and B81-oVEMP.

Conclusion: As age increased, the B81-cVEMP response rate decreased, the thresholds increased, P13 and N23 latencies were prolonged, and the raw amplitude and corrected amplitude decreased. The B81-oVEMP response rate and corrected amplitude decreased, the thresholds increased, and N10 latency was prolonged with age. These changes are probably due to the occurrence of morphological and functional changes in

the vestibular system with aging. Therefore, we suggest establishing different reference values according to different age groups when evaluating the VEMP results in patients with vestibular diseases.

Keywords: B81 bone vibrator, aging, cervical vestibular-evoked myogenic potential, ocular vestibular-evoked myogenic potential, vestibular function

INTRODUCTION

The vestibular-evoked myogenic potential (VEMP) is a non-invasive, objective, and easily accepted clinical test that is now widely used to assess otolithic function (1–3). The potentials recorded on the surface of the sternocleidomastoid (SCM) muscles are called cervical VEMPs (cVEMPs), and those recorded on the surface of the extraocular muscles are called ocular VEMPs (oVEMPs) (4–7). Therefore, cVEMP is a manifestation of the vestibulocollic reflex and predominantly reflects saccular function, while oVEMP is a manifestation of the vestibulo-ocular reflex (VOR) and reflects utricular function (1, 3, 8).

Currently, there are three types of stimulation used to detect VEMPs: air-conducted sound (ACS), bone-conducted vibration (BCV), and galvanic vestibular stimulation (2, 3, 8, 9). VEMP elicited by ACS stimulation is widely used. However, there are some drawbacks to the use of ACS as a stimulus delivery method for VEMPs. First, high-intensity ACS stimuli increase hazardous sound exposure when the equivalent ear canal volumes are less than or equal to 0.8 ml. Additionally, patients with conductive hearing loss or air–bone gaps may not generate VEMPs in response to ACS (10). BCV is a viable alternative mode of stimulation for eliciting VEMP responses. Various bone vibrators have been used to elicit VEMPs, such as tap hammer (9, 11), mini-shaker 4810 (3, 12), B-70B (13), V201 (14), Radioear B71 (6, 15), and Radioear B81 (16, 17). Radioear B71 and B81 are universal components for the testing of hearing levels using the bone conduction method. It has been reported that relative to the B71, the B81 vibrator has higher maximum output levels and lower distortion to be used in pure-tone audiometry (18). However, Clinard et al. (16) reported that the maximum output levels of the B81 vibrator were equivalent to B71 at 500 Hz (stimuli were tone bursts with a fixed duration of 8 ms). Romero et al. (19) used the same frequency and duration of stimuli (500 Hz, rise-plateau-fall times: 4-0-4 ms), as Clinard et al. showed no statistically significant differences between the amplitudes of the B71- and B81-cVEMP. Hence, whether the B81 vibrator can be effectively used for c/oVEMP response requires further study.

Age-related morphological changes may occur in the vestibular system from the end organs to the central nuclei, including loss of hair cells, decreased numbers of vestibular nerve cells, and loss of neurons in the vestibular nucleus (20–23). Therefore, the effects of advancing age on the response rate, latency, and amplitude of ACS-VEMPs have been well explored (24, 25). However, the age-related impact on the B81-VEMPs remains unclear. Therefore, this study aimed to establish normal values and examine the effect of age on c- and oVEMP responses using the B81 vibrator.

MATERIALS AND METHODS

Subjects

Healthy subjects with no hearing or vestibular deficits were recruited from the Second Affiliated Hospital of Xi'an Jiaotong University. Pure tone audiometry, acoustic immittance, and otoscope tests were performed on all subjects to exclude those with hidden hearing loss (pure tone average threshold $\geq$ 20 dB), asymmetric hearing loss, an air–bone gap larger than 10 dB, and abnormal tympanic pressure. Finally, 70 subjects ranging from 4 to 70 years were divided into seven groups by decade. Each group consisted of 10 subjects (five men and five women). Group I included subjects aged 4–9 years, Group II subjects aged 10–19 years, Group III subjects aged 20–29 years, Group IV subjects aged 30–39 years, Group V subjects aged 40–49 years, Group VI subjects aged 50–59 years, and Group VII subjects aged 60–70 years. The study protocol was reviewed and approved by Xi'an Jiaotong University (approval number: 2016205). All participants were informed and volunteered to participate in this study.

BCV Stimuli and Recording Parameters

The cVEMP and oVEMP tests were performed using the Interacoustics Eclipse system (Interacoustics, Middelfart, Denmark). BCV stimuli were delivered using a Radioear B81 bone vibrator (housing dimensions: height, 16 mm; length, 31.7 mm; width, 18.2 mm; weight, 20 g). The stimulus level was measured in decibels of peak force level (dB peFL) (re: 1 μN) using an artificial mastoid 4930 (Brüel & Kjær, Denmark) (**Figure 1**). Stimuli with the alternating polarity of 500 Hz tone bursts with a fixed duration of 6 ms (rise/fall time: 2 ms, plateau time: 2 ms) were delivered. For subjects $\geq$20 years, the stimulation started from a maximum intensity of 134.5 dB peFL (5.3 N), and for subjects $<$20 years, the stimulation intensity started from 129.5 dB peFL (3.0 N). The stimulation rate was 5.1/s, and 80 responses were averaged for each run. The electromyogram (EMG) signals were amplified and bandpass filtered between 10 and 1,000 Hz. The recording window was 0 ms to 80 ms. To measure background muscle activity for cVEMP, subjects were provided feedback on the level of activity in their SCM muscles during data collection. They were required

Abbreviations: B81-cVEMP, B81 bone vibrator-induced cervical vestibular-evoked myogenic potentials; B81-oVEMP, B81 bone vibrator-induced ocular vestibular-evoked myogenic potentials; VEMP, vestibular-evoked myogenic potential; SCM, sternocleidomastoid; cVEMP, cervical VEMP; oVEMP, ocular VEMP; VOR, vestibulo-ocular reflex; ACS, air-conducted sound; BCV, bone-conducted vibration; peFL, peak force level; EMG, electromyogram.

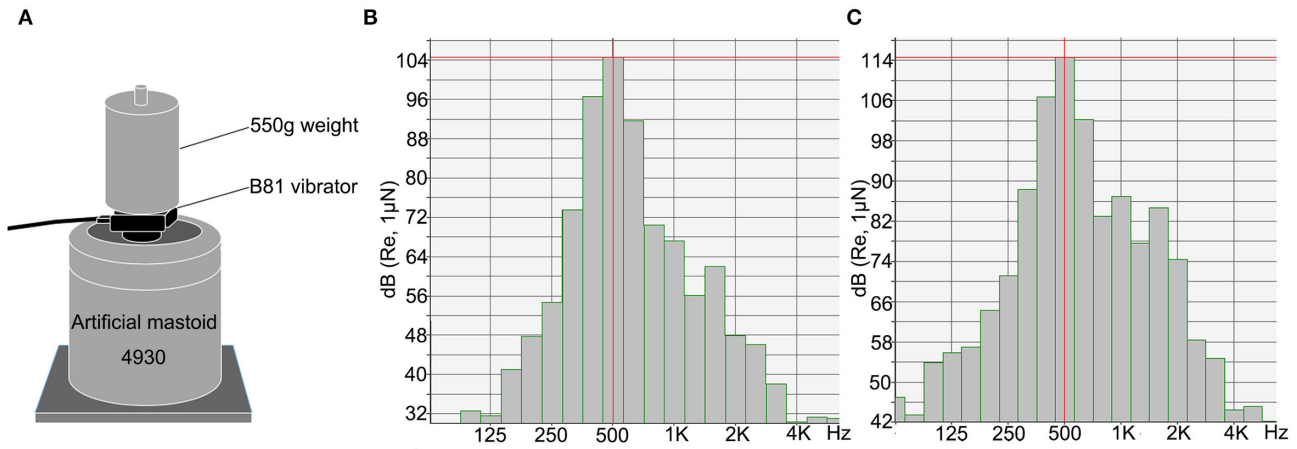

FIGURE 1 | The Radioear B81 bone vibrator was calibrated using an artificial mastoid. **(A)** Artificial mastoid 4930 (Brüel & Kjær, Denmark) was used to calibrate the B81 bone vibrator. A constant force was maintained by adding a 550 g weight to the artificial mastoid when calibrating. **(B,C)** The spectra show energy distribution of 500 Hz tone burst of the B81 bone vibrator at the output of 119.5 dB peFL (stimuli were delivered at 50 dB nHL) **(B)** and 129.5 dB peFL (stimuli were delivered at 60 dB nHL) **(C)**. The central energy is at 500 Hz.

to maintain a background muscle activity of 50–200 μV. Electrode impedance was maintained below 5 kΩ.

B81-cVEMP and B81-oVEMP Recording

The subjects remained in a sitting position. The B81 bone vibrator was placed on the mastoid (3 cm behind and 2 cm above the external acoustic meatus) on the stimulation side (**Figures 2A,B**) (15).

The cVEMP recording electrodes were positioned on the upper half of the bilateral SCM muscles, with a common reference electrode placed on the upper sternum. One ground electrode was placed in the middle of the forehead (**Figure 2A**). The subject sat with the head rotating sideways toward one shoulder to activate the SCM muscles for the recording duration (26).

The oVEMP recording electrodes were placed on the face inferior to each eye, approximately 1 cm below the center of the lower eyelid. A common reference electrode was positioned on the jaw. One ground electrode was placed in the middle of the forehead (**Figure 2B**). During recording, the subject was instructed to look upward, with a vertical visual angle of ∼30–35° above the horizon (14).

When a typical cVEMP and oVEMP waveform (**Figures 2C,D**) appeared, it was decremented by 10 dB each time until the waveform disappeared or the reproducibility was poor, and then increased by 5 dB until the waveform appeared. The threshold for B81-VEMPs was the lowest level in dB peFL at which VEMPs could be reliably recorded. The initial peak-to-peak amplitude indicated the raw amplitude. To compensate for uneven SCM muscle contractions, raw amplitudes were divided by the mean rectified EMG activity during the 20 ms before the onset of the stimulus (corrected amplitudes) (27). The raw interaural asymmetry ratio (IAR) was calculated as IAR =100 (larger amplitude – smaller amplitude) / larger amplitude + smaller amplitude). The corrected IAR was calculated based on the corrected amplitudes. Subjects with unilaterally or bilaterally absent responses were not included in the IAR calculation. For B81-oVEMP, the corrected amplitudes and corrected IAR were calculated in the same way as B81-cVEMP. The threshold, P13(N10) latency, N23(P15) latency, P13–N23 (N10-P15) interval latency, raw amplitudes, raw IAR, corrected amplitudes, and corrected IAR of the maximum stimulation intensity (≥ 20 years old: 134.5 dB peFL, < 20 years old: 129.5 dB peFL) were measured.

Statistical Analyses

All the statistical analyses were performed using SPSS 22.0 (IBM, Armonk, NY). The chi-square test or Fisher's exact test was used to compare the response rate of B81-VEMPs between each age group (categorical variables). Kruskal–Wallis one-way analysis of variance was performed for the multiple comparisons of P13 (N10) latency, N23 (P15) latency, P13- N23 (N10-P15) interval latency, amplitudes, and IAR (continuous variables). Bonferroni (homogeneity of variance) or Tamhane's (heterogeneity of variance) adjusted multiple comparisons were used as *post-hoc* tests. Spearman's correlation analyses were used to determine the relationship between age and B81-VEMP parameters. Using Spearman's correlation analysis, linear regression curves were computed only when a statistically significant correlation was observed. The curves were constructed with Prism 8.0 (GraphPad, La Jolla, CA). For all comparisons, $p < 0.05$ were considered statistically significant.

RESULTS

Response Rate of B81-cVEMP

The response rate of B81-cVEMP in all subjects was 95% (133/140). The rate was 100% for groups I–IV, 95% for groups V and VI, and 75% for group VII. There were statistically significant differences among the age groups ($p = 0.026$, $p < 0.05$, chi-square

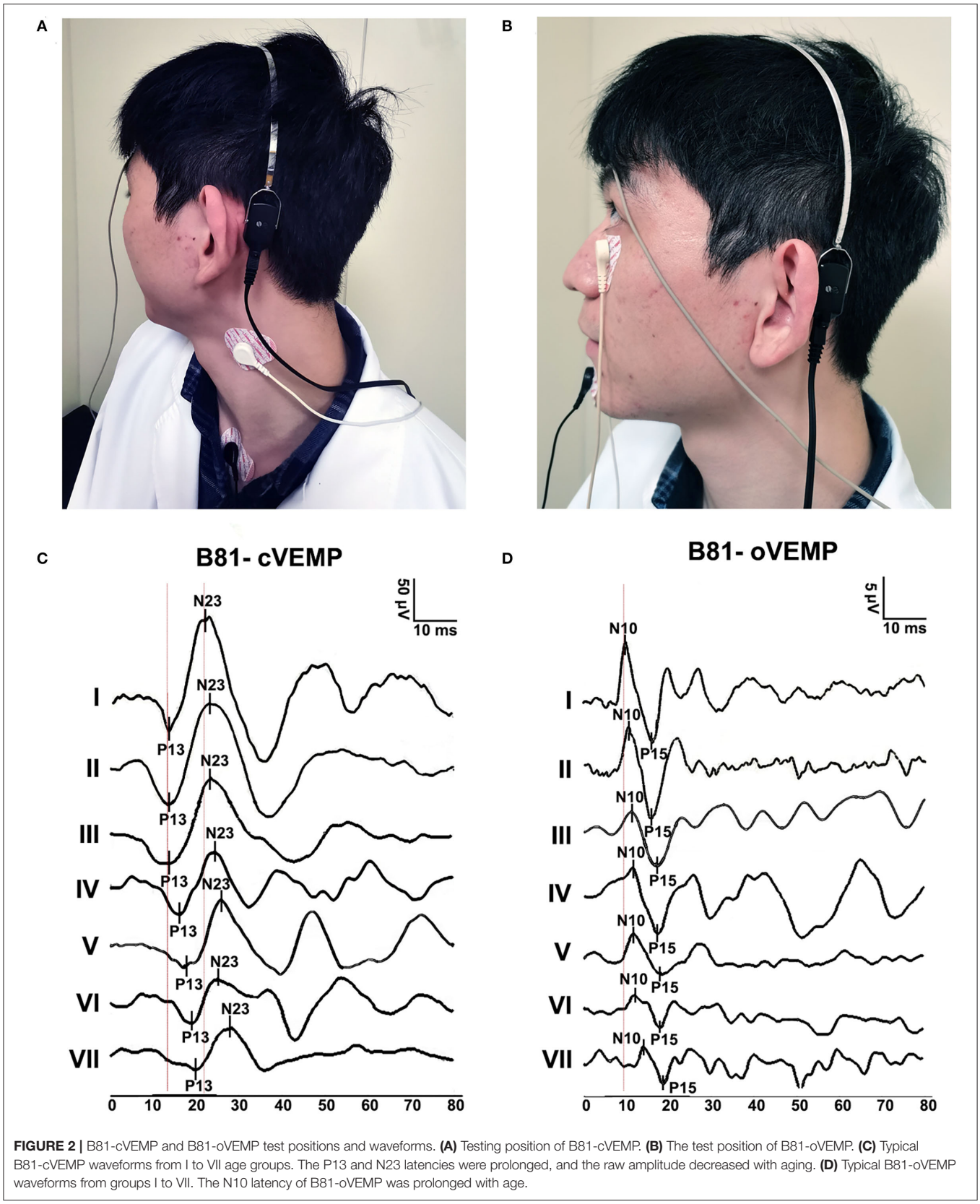

FIGURE 2 | B81-cVEMP and B81-oVEMP test positions and waveforms. **(A)** Testing position of B81-cVEMP. **(B)** The test position of B81-oVEMP. **(C)** Typical B81-cVEMP waveforms from I to VII age groups. The P13 and N23 latencies were prolonged, and the raw amplitude decreased with aging. **(D)** Typical B81-oVEMP waveforms from groups I to VII. The N10 latency of B81-oVEMP was prolonged with age.

TABLE 1 | The response rate and threshold of B81-cVEMP with increasing age.

Age groups	Response rate	Threshold (dB peFL)		
		Mean ± SD	Median	IQR
I	100% (20/20)	111.75 ± 5.50	114.50	104.50–114.50
II	100% (20/20)	113.75 ± 5.45	114.50	109.50–119.50
III	100% (20/20)	112.50 ± 3.77	114.50	109.50–114.50
IV	100% (20/20)	121.25 ± 6.34	119.50[b]	115.75–124.50
V	95% (19/20)	125.55 ± 4.88	124.50[b]	124.50–129.50
VI	95% (19/20)	125.55 ± 3.15	124.50[b]	124.50–129.50
VII	75% (15/20)[a]	129.83 ± 3.52	129.50[b,c,d]	129.50–134.50
p-value	0.026	/	0.000	/

p-value, chi-square test and Kruskal–Wallis one-way analysis of variance; [a]p < 0.05, Fisher's exact test, compared with groups I–IV; [b]p < 0.01, compared with groups I–III; [c]p < 0.01, compared with group IV; [d]p < 0.05, compared with group VI (Tamhane-adjusted t-test). B81-cVEMP, B81 bone vibrator-induced cervical vestibular-evoked myogenic potential; IQR, interquartile range; peFL, peak force level; SD, Standard deviation.

test; **Table 1**). Further analyses showed statistically significant differences between groups I–IV and VII ($p = 0.047$, $p < 0.05$, Fisher's exact test; **Table 1**). There was no statistically significant difference between the other groups.

Threshold of B81-cVEMP

The median of the threshold of B81-cVEMP for groups I–VII was 114.50, 114.50, 114.50, 119.50, 124.50, 124.50, and 129.50 dB peFL, respectively, with significant differences in the threshold between groups I–III and IV–VII ($p = 0.000$, $p < 0.01$, Tamhane-adjusted *t*-test; **Table 1**). In addition, there was also a significant difference for group VII compared to groups IV and VI ($p = 0.000$, $p < 0.05$; $p = 0.019$, $p < 0.05$, Tamhane-adjusted *t*-test; **Table 1**). The B81-cVEMP threshold showed an increase with age ($r = 0.756$, $p < 0.01$, Spearman's correlation analysis). **Figure 3A** shows that the linear regression curve depicts the relationship between age and the B81-cVEMP threshold ($y = 0.3344x + 108.7$).

P13 and N23 Latencies and P13-N23 Interval of B81-cVEMP

The mean, standard deviation, median, and interquartile range (IQR) of the descriptive statistics across ages are summarized in **Table 2**. The Kruskal–Wallis test revealed significant differences in the P13 latency ($p = 0.003$, $p < 0.01$) and N23 latency ($p = 0.008$, $p < 0.01$) of B81-cVEMP among the seven groups (**Table 2**). For the P13 latency of B81-cVEMP, there were statistically significant differences between groups I–III and VII ($p = 0.001$, $p = 0.018$, $p = 0.012$, $p < 0.05$, Tamhane-adjusted *t*-test; **Table 2**). There was no statistically significant difference between groups I–VI. The N23 latency of B81-cVEMP was significantly different between group VI and groups I and II ($p = 0.004$, $p = 0.035$, $p < 0.05$, Bonferroni-adjusted *t*-test; **Table 2**); there was no significant difference between the other groups. For the P13-N23 interval of B81-cVEMP, there were no statistically significant differences between groups I–VII ($p = 0.390$, $p > 0.05$, Kruskal–Wallis test; **Table 2**). Spearman's correlation analysis revealed that significant correlations existed between the age factor and the P13 latency ($r = 0.357$, $p = 0.003$, $p < 0.01$) and N23 latency ($r = 0.316$, $p = 0.009$, $p < 0.01$), but not with the P13–N23 interval ($r = -0.017$, $p = 0.839$, $p > 0.05$). The P13 and N23 latencies of B81-cVEMP waveforms from I to VII groups are shown in **Figure 2C**. **Figure 3B** shows the relationship between age and the P13 latency of B81-cVEMP using a linear regression curve ($y = 0.03388x + 15.57$). **Figure 3C** shows the relationship between age and the N23 latency of B81-cVEMP ($y = 0.03264x + 24.36$).

Raw Amplitudes, Corrected Amplitudes, Raw IAR, and Corrected IAR of B81-cVEMP

There was a statistically significant difference both in the raw amplitudes and corrected amplitudes of B81-cVEMP ($p = 0.000$, $p < 0.01$, Kruskal–Wallis test; **Table 3**). No significant differences were found for the raw IAR among the seven groups ($p = 0.919$, $p > 0.05$, **Table 3**), while the corrected IAR was statistically significantly different ($p = 0.015$, $p < 0.05$; **Table 3**). The IAR of group VII was larger than group III. The Tamhane-adjusted *t*-test showed no significant change in amplitude up to group III, whereas a significant reduction in peak-to-peak amplitude was observed beyond this group. Using Spearman's analysis, both the raw and corrected amplitudes showed a significant negative correlation with age ($r = -0.641$, $p = 0.000$, $p < 0.01$; $r = -0.609$, $p = 0.000$, $p < 0.01$). The raw and corrected IAR showed no correlation with age ($r = -0.089$, $p = 0.483$, $p > 0.05$; $r = 0.072$, $p = 0.601$, $p > 0.05$). **Figure 2C** shows the raw amplitudes of B81-cVEMP gradually decrease from I to VII age groups. **Figures 3D,E** show an inverse relationship between age and the raw/corrected amplitude of B81-cVEMP ($y = -3.116x + 237.7$; $y = -0.03044x + 2.956$).

Response Rate for B81-oVEMP

Using B81 stimuli, the response rate of oVEMP for all subjects was 82% (115/140). The response rate was 100% in groups I–IV, whereas it was 70% in group V, 65% in group VI, and 40% in group VII, exhibiting significant differences between groups I–IV and V–VII ($p = 0.02$, $p = 0.008$, $p = 0.000$, $p < 0.05$, Fisher's exact test; **Table 4**). There were no statistically significant differences

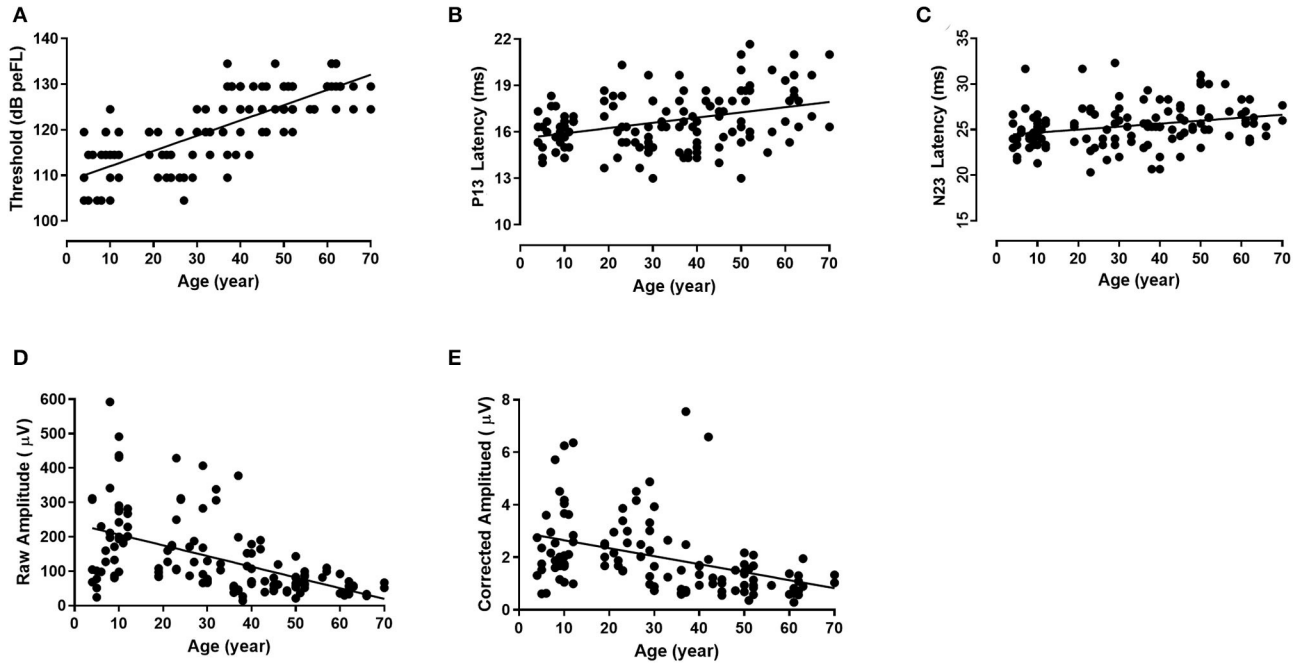

FIGURE 3 | The relationship between age and individual B81-cVEMP parameters (linear regression). The threshold ($r^2 = 0.571$, $p = 0.000$, $p < 0.01$) **(A)**, P13 latency ($r^2 = 0.143$, $p = 0.001$, $p < 0.01$) **(B)**, and N23 latency ($r^2 = 0.096$, $p = 0.010$, $p < 0.05$) **(C)** are positively correlated with age, whereas the raw amplitude ($r^2 = 0.288$, $p = 0.000$, $p < 0.01$) **(D)** and corrected amplitude ($r^2 = 0.246$, $p = 0.000$, $p < 0.01$) **(E)** are negatively correlated with age.

TABLE 2 | The latencies and P13-N23 interval of B81-cVEMP with increasing age.

Age groups	P13 latency (ms)			N23 latency (ms)			P13-N23 interval (ms)		
	Mean ± SD	Median	IQR	Mean ± SD	Median	IQR	Mean ± SD	Median	IQR
I	15.97 ± 1.18	16.00	15.08–16.59	24.58 ± 2.22	24.00	23.08–25.50	8.62 ± 1.59	8.34	7.67–9.24
II	16.27 ± 1.16	16.50	15.67–16.92	24.73 ± 1.29	25.00	23.75–25.67	8.47 ± 1.45	8.84	7.08–9.33
III	16.24 ± 1.76	15.84	15.08–17.34	25.28 ± 2.99	24.50	23.33–26.91	9.03 ± 2.09	8.84	8.00–10.26
IV	16.43 ± 1.68	16.50	14.75–17.83	25.25 ± 2.23	25.33	23.42–26.33	8.82 ± 1.97	9.00	8.00–10.42
V	16.44 ± 1.44	16.67	15.00–17.67	25.26 ± 2.09	25.33	24.33–27.00	8.82 ± 1.70	9.00	7.33–9.67
VI	17.58 ± 2.30	18.00	16.00–19.00	27.16 ± 2.37	26.33[b]	25.00–30.00	9.58 ± 2.72	10.00	7.00–11.33
VII	18.22 ± 1.70	18.00[a]	16.67–19.67	25.91 ± 1.54	26.00	24.33–27.00	7.69 ± 2.11	7.67	5.67–9.67
p-value	/	0.003	/	/	0.008	/	/	0.390	/

p-value, Kruskal–Wallis one-way analysis of variance. [a]p < 0.05, compared with groups I–III (Tamhane-adjusted t-test); [b]p < 0.05, compared with groups I and II (Bonferroni-adjusted t-test); B81-cVEMP, B81 bone vibrator-induced cervical vestibular-evoked myogenic potential; IQR, interquartile range; SD, Standard deviation.

among groups V, VI, and VII (V vs. VI: $p = 0.741$; V vs. VII: $p = 0.111$; VI vs VII: $p = 0.205$; $p > 0.05$, chi-square test).

Threshold of B81-oVEMP

The thresholds of B81-oVEMP exhibited significant differences between groups I–III and IV–VII ($p = 0.000$, $p < 0.01$, Bonferroni-adjusted *t*-test; **Table 4**). There was no statistically significant difference between the other groups. Spearman's correlation analysis revealed a significant positive correlation between age and the threshold ($r = 0.768$, $p = 0.000$, $p < 0.01$). **Figure 4A** shows that the linear regression curve depicts the increase of B81-oVEMP threshold with age ($y = 0.2744x + 115.3$).

N10 and P15 Latencies and N10-P15 Interval of B81-oVEMP

The descriptive statistics (mean, standard deviation, median, and IQR) of latencies and intervals across the age groups are shown in **Table 5**. There were significant differences in N10 latency, P15 latency, and N10-P15 interval among the seven groups ($p = 0.000$, $p = 0.001$, $p = 0.005$, $p < 0.01$, Kruskal–Wallis test; **Table 5**). Groups IV and VI showed significantly longer N10 latencies than group III ($p = 0.007$, $p = 0.004$, $p < 0.01$,

TABLE 3 | Raw amplitudes, corrected amplitudes, raw IAR, and corrected IAR of B81-cVEMP with increasing age.

Age groups	Raw amplitudes (μV)			Corrected amplitudes			Raw IAR (%)			Corrected IAR (%)		
	Mean ± SD	Median	IQR	Mean± SD	Median	IQR	Mean± SD	Median	IQR	Mean± SD	Median	IQR
I	173.85 ± 133.61	130.05	81.94-225.42	2.26 ± 1.30	1.94	1.46–2.81	21.00 ± 13.62	23.00	9.00–33.75	34.74 ± 20.08	35.00	15.50–54.50
II	233.13 ± 117.57	215.20	126.68–281.28	2.79 ± 1.50	2.29	1.81–3.66	17.40 ± 14.62	13.50	5.00–27.25	27.30 ± 13.91	29.00	17.50–36.00
III	191.09 ± 106.29	169.80	104.38–274.28	2.67 ± 1.11	2.52	1.73–3.37	16.40 ± 10.96	17.00	7.75–26.75	9.80 ± 5.65	9.00	5.50–14.50
IV	119.39 ± 106.19	74.33[a]	47.35–146.63	1.86 ± 1.91	1.06[e]	0.71–2.52	14.40 ± 10.97	11.00	4.75–26.25	35.39 ± 22.27	36.00	10.00–51.00
V	86.31 ± 50.32	68.94[b]	43.86–119.60	1.57 ± 1.50	1.19[e]	0.89–1.68	14.67 ± 10.70	8.00	5.50–25.00	30.33 ± 14.50	28.50	20.75–40.00
VI	73.96 ± 27.86	68.31[c]	56.95–88.94	1.23 ± 0.54	1.14[e]	0.83–1.68	21.11 ± 16.82	17.00	5.00–38.00	32.43 ± 20.11	29.00	15.00–56.00
VII	47.72 ± 18.75	42.07[d]	33.09–57.51	0.97 ± 0.45	0.89[f]	0.61–1.31	14.14 ± 13.57	11.00	7.00–13.00	31.67 ± 10.01	34.50[g]	25.75–38.50
p-value	/	0.000	/	/	0.000	/	/	0.919	/	/	0.015	/

p-value, Kruskal–Wallis one-way analysis of variance; [a]p < 0.05, compared with group I (Tamhane-adjusted t-test); [b]p < 0.01, compared with groups II and III (Tamhane-adjusted t-test); [c]p < 0.05, compared with groups I–III; [d]p < 0.05, compared with groups I–IV and VI; [e]p < 0.05, compared with groups II and III (Bonferroni-adjusted t-test); [f]p < 0.01, compared with groups I–III (Bonferroni-adjusted t-test); [g]p < 0.05, compared with group III (Bonferroni-adjusted t-test). B81-cVEMP, B81 bone vibrator-induced cervical vestibular-evoked myogenic potential; IAR, interaural asymmetry ratio; IQR, interquartile range; SD, Standard deviation.

TABLE 4 | The response rate and threshold of B81-oVEMP with increasing age.

Age groups	Response rate	Threshold (dB peFL)		
		Mean ± SD	Median	IQR
I	100% (20/20)	116.00 ± 5.40	114.50	114.50–119.50
II	100% (20/20)	119.75 ± 6.17	119.50	114.50–124.50
III	100% (20/20)	120.00 ± 4.56	119.50	119.50–124.50
IV	100% (20/20)	128.00 ± 4.32	129.50[b]	124.50–129.50
V	70% (14/20)[a]	127.36 ± 5.79	127.00[b]	123.25–134.50
VI	65% (13/20)[a]	129.88 ± 4.31	129.50[b]	124.50–134.50
VII	40% (8/20)[a]	129.50 ± 3.78	129.50[b]	129.50–134.50
p-value	0.001	/	0.000	/

p-value, chi-square test and Kruskal–Wallis one-way analysis of variance; [a]p < 0.05, Fisher's exact test, compared with groups I–IV; [b]p < 0.01, Bonferroni-adjusted t-test, compared with groups I–III; B81-oVEMP, B81 bone vibrator-induced ocular vestibular-evoked myogenic potential; IQR, interquartile range; peFL, peak force level; SD, Standard deviation.

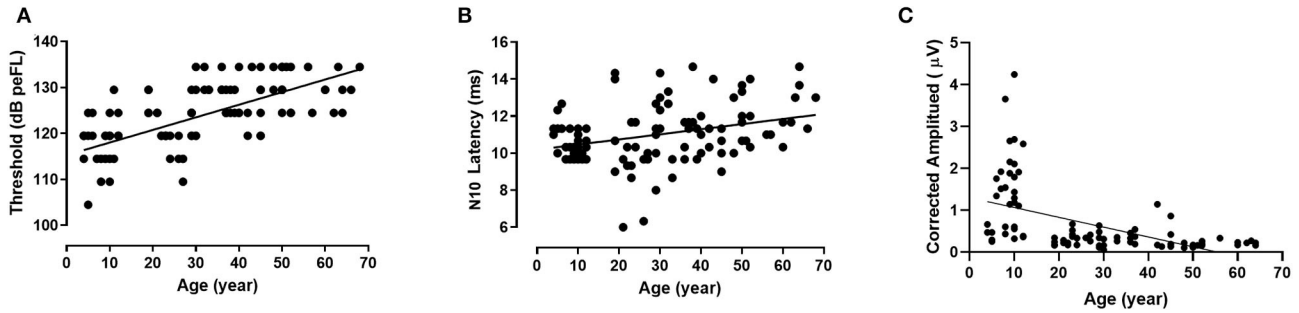

FIGURE 4 | Relationship between age and individual B81-oVEMP parameters (linear regression). The threshold ($r^2 = 0.470$, $p = 0.000$, $p < 0.01$) **(A)** and N10 latency ($r^2 = 0.107$, $p = 0.000$, $p < 0.01$) **(B)** of B81-oVEMP are positively correlated with age, whereas the corrected amplitude ($r^2 = 0.266$, $p = 0.000$, $p < 0.01$) **(C)** is negatively correlated with age.

Bonferroni-adjusted *t*-test). Group VII showed significantly longer N10 latencies than groups II and III ($p = 0.018$, $p = 0.001$, $p < 0.05$, Bonferroni-adjusted *t*-test). For the P15 latency, group III showed significantly shorter latencies than groups IV and VI ($p = 0.004$, $p = 0.000$, $p < 0.01$, Bonferroni-adjusted *t*-test). For the N10-P15 interval, group III showed significantly shorter latencies than group I ($p = 0.041$, $p < 0.05$, Tamhane-adjusted *t*-test), and group VII showed significantly shorter latencies than

TABLE 5 | The latencies and N10-P15 interval of B81-oVEMP with increasing age.

Age groups	N10 latency (ms)			P15 latency (ms)			N10-P15 interval (ms)		
	Mean ± SD	Median	IQR	Mean ± SD	Median	IQR	Mean ± SD	Median	IQR
I	10.77 ± 0.86	10.66	10.00–11.33	16.12 ± 0.84	15.83	15.67–16.91	5.35 ± 0.81	5.34	5.00–6.00
II	10.68 ± 1.32	10.33	10.00–10.92	16.10 ± 1.56	16.00	15.33–16.92	5.42 ± 1.26	5.67	4.08–6.25
III	9.86 ± 1.70	10.00	9.33–11.25	14.03 ± 2.39	14.17[c]	12.42–15.50	4.17 ± 1.38	4.17[d]	3.00–5.25
IV	11.58 ± 1.54	11.50[a]	10.58–12.59	16.35 ± 2.11	16.67	14.58–18.00	4.77 ± 1.40	4.84	3.75–5.92
V	11.05 ± 1.30	10.84	10.00–11.50	15.67 ± 1.50	16.00	14.83–17.00	4.62 ± 1.25	5.00	3.25–5.67
VI	11.77 ± 1.23	11.67[a]	10.67–12.67	17.05 ± 1.26	17.33	15.67–18.00	5.28 ± 0.80	5.33	4.50–6.00
VII	12.42 ± 1.41	12.34[b]	11.42–13.50	16.54 ± 1.80	16.50	15.17–18.34	4.12 ± 0.73	4.00[e]	3.42–4.83
p-value	/	0.000	/	/	0.001	/	/	0.005	/

p-value, Kruskal–Wallis one-way analysis of variance; [a]$p < 0.01$, compared with group III (Bonferroni-adjusted t-test); [b]$p < 0.05$, compared with groups II and III (Bonferroni-adjusted t-test); [c]$p < 0.01$, compared with groups IV and VI (Bonferroni-adjusted t-test); [d]$p < 0.05$, compared with group I (Tamhane-adjusted t-test); [e]$p < 0.05$, compared with groups I, II, and VI (Tamhane-adjusted t-test). B81-oVEMP, B81 bone vibrator-induced ocular vestibular-evoked myogenic potential; IQR, interquartile range; SD, Standard deviation.

groups I, II, and VI ($p = 0.007$, $p = 0.019$, $p = 0.039$, $p < 0.05$, Tamhane-adjusted *t*-test). Except for the above-mentioned results, there was no significant difference between the age groups for the N10 latency, P15 latency, and N10-P15 interval. Analyses between the age factor and latencies revealed a significant positive correlation between age and the N10 latency ($r = 0.334$, $p = 0.009$, $p < 0.01$, Spearman's correlation analysis) but not between age and the P15 latency and N10-P15 interval. The changes in the latencies of B81-oVEMP in each age group are shown in **Figure 2D**. **Figure 4B** shows the relationship between age and the N10 latency of B81-oVEMP using a linear regression curve ($y = 0.02762x + 10.19$).

Raw Amplitudes, Corrected Amplitudes, Raw IAR, and Corrected IAR of B81-oVEMP

There was a significant difference in the corrected amplitudes between the different age groups ($p = 0.000$, $p < 0.01$), but no significant difference was found in the raw amplitudes, raw IAR, and corrected IAR ($p = 0.320$, $p = 0.738$, $p = 0.218$, $p > 0.05$, Kruskal–Wallis test; **Table 6**). The corrected amplitudes of groups III, IV, VI, and VII were smaller than that of group I ($p = 0.000$, $p < 0.01$, Tamhane-adjusted *t*-test), those of groups IV, VI, and VII were smaller than that of group II ($p = 0.000$, $p < 0.01$, Tamhane-adjusted *t*-test), and that of group VI was smaller than that of group III ($p = 0.005$, $p < 0.01$, Tamhane-adjusted *t*-test). The corrected amplitudes of B81-oVEMP were significantly correlated with age ($r = -0.683$, $p = 0.000$, $p < 0.01$, Spearman's correlation analysis). **Figure 4C** shows the negative correlation between age and corrected amplitudes of B81-oVEMP using a linear regression curve ($y = -0.02343x + 1.297$).

DISCUSSION

The VEMP test elicited by ACS is a classical method that is widely employed in clinical settings. Compared to the ACS, BCV has some advantages that overcome the limitations of ACS in the VEMP test. Therefore, it is indispensable to establish the normal range of BCV-induced VEMP for different age groups. Several previous studies have reported the influence of age on oVEMP and cVEMP parameters (17, 24, 25, 27–31). Most studies showed a significant decline in the response rates, prolongation of latencies, and reduction of oVEMP and cVEMP amplitudes with increasing age (24, 33). The association of cVEMP with age has been studied more extensively than that of oVEMP with age. Besides, VEMP parameters are usually affected by position, stimulating method, and setting of the output and record. The results of the studies are not entirely consistent. This study used a Radioear B81 bone vibrator to evoke VEMPs on the mastoids and observed the changes in B81-VEMP parameters with increasing age.

Effects of Age on the Parameters of B81-cVEMP

The total response rate of B81-cVEMP was 95% (133/140) in our study. The result was similar to that reported by Patterson et al. (92%, 144/156), who used the B81 bone vibrator (17), and Rosengren et al. (93%, 113/122), who used B71 bone vibrator (28). In all the studies, the bone vibrator was applied on the mastoid; however, we used the sitting position, while Patterson et al. and Rosengren et al. used the reclined position. Therefore, both the sitting and reclined positions are suitable for the cVEMP test. In this study, the response rate of B81-cVEMP was 100% up to the age group of 40–49 years and declined to 75% in the group of individuals older than 60 years. The results revealed an increase in threshold values and a decrease in raw and corrected amplitudes in individuals ≥30 years. In addition, the study showed prolongation of the B81-cVEMP P13 and N23 latencies with increasing age.

The reduction in the response rate and both raw and corrected amplitudes with advancing age has been consistently reported across studies. It might be related to the morphological changes and reduced saccular hair cells and neuroepithelia in Scarpa's ganglion and the brainstem vestibular nuclei (31). The prolongation in the P13 and N23 latencies of B81-cVEMP with age can also be explained by age-related changes in the otolith-cervical reflexes based on the alterations in the processing of otolithic signals by the central nervous systems.

TABLE 6 | Raw amplitudes, corrected amplitudes, raw IAR, and corrected IAR of B81-oVEMP with increasing age.

Age groups	Raw amplitudes (μV)			Corrected amplitudes			Raw IAR (%)			Corrected IAR (%)		
	Mean ± SD	Median	IQR	Mean ± SD	Median	IQR	Mean ± SD	Median	IQR	Mean ± SD	Median	IQR
I	9.16 ± 6.77	6.71	3.05–11.46	1.29 ± 0.94	1.24	0.47–1.89	18.70 ± 16.53	15.00	4.00–34.00	21.00 ± 10.02	17.00	13.00–28.00
II	10.40 ± 6.23	8.99	4.70–14.39	1.19 ± 1.09	0.85	0.34–1.88	22.90 ± 16.94	22.00	13.00–25.50	36.70 ± 28.34	29.50	9.75–68.00
III	9.80 ± 5.22	7.60	6.66–10.19	0.34 ± 0.15	0.34[a]	0.22–0.41	16.70 ± 14.36	12.00	7.50–25.25	18.40 ± 8.67	17.00	13.00–24.25
IV	7.82 ± 4.13	6.85	4.63–10.17	0.27 ± 0.14	0.29[a,b]	0.18–0.35	19.20 ± 11.56	18.00	10.75–27.75	15.57 ± 12.45	14.00	6.00–31.00
V	11.68 ± 9.21	7.87	6.08–17.66	0.37 ± 0.37	0.19	0.13–0.64	30.00 ± 18.57	23.50	17.50–51.75	41.25 ± 23.27	36.00	23.00–64.75
VI	6.47 ± 2.81	5.56	4.50–8.33	0.17 ± 0.07	0.16[a,b,c]	0.11–0.20	22.50 ± 15.70	15.00	14.00–38.50	21.33 ± 3.22	20.00	19.00–/
VII	9.15 ± 3.79	8.38	6.40–10.27	0.21 ± 0.04	0.22[a,b]	0.17–0.24	17.00 ± 18.39	17.00	4.00–/	14.50 ± 0.71	14.50	14.00–/
p-value	/	0.320	/	/	0.000	/	/	0.738	/	/	0.218	/

p-value, Kruskal–Wallis one-way analysis of variance; [a]p < 0.01, compared with group I (Tamhane-adjusted t-test); [b]p < 0.05, compared with group II (Tamhane-adjusted t-test); [c]p < 0.01, compared with group III (Tamhane-adjusted t-test); B81-oVEMP, B81 bone vibrator-induced ocular vestibular-evoked myogenic potential; IAR, interaural asymmetry ratio; IQR, interquartile range; SD, Standard deviation.

Effects of Age on the Parameters of B81-oVEMP

In the present study, the total response rate of B81-oVEMP was 82% (115/140). Our results were lower than those reported by Patterson et al. (89%, 139/156), who used the B81 bone vibrator (17), but higher than that of Rosengren et al. (65%, 79/122), who used B71 bone vibrator (28). The main difference between the studies was that we placed the vibrator on the mastoid. Rosengren et al. (3) showed that slight displacement of the B81 or B71 vibrator on the mastoid could result in the absence or reduced responses when recording the VEMPs, which was also shown in our VEMP test recording. Another reason may be that Patterson et al. (17) increased the stimulation intensity to 75 dB nHL (138 dB peFL) when oVEMP could not be elicited with 70 dB nHL (136 dB peFL) stimulation. However, in our study, we calibrated the B81 vibrator using artificial mastoid 4,930, and the output was distorted when it was above 65 dB nHL. Hence, we used the maximum stimulus intensity of 65 dB nHL (134.5 dB peFL). It should be noted that the response rates using the B81 outperformed those using the B71, which cannot be attributed to output. This equals the force output of the B81 when the frequency is 500 Hz (16, 17, 28). We believe that forehead stimulation may be the best location for the oVEMP response instead of the mastoid (17, 28, 32). Our results showed that the response rate of B81-oVEMP was 100% up to the age group of 40–49 years and progressively declined afterward to only 40% in the group of individuals ≥60 years. These findings agree with those reported in the literature (14). However, these findings contradicted those reported by a previous study, which showed 100% response rates in both the younger and older groups (12). This may be attributed to the different stimulation conditions. Iwasaki et al. used a Brüel and Kjaer 4810 Mini-shaker or a light tap with a tendon hammer in the middle at the hairline to provide BCV stimuli.

Few studies have explored the effect of age on the oVEMP threshold. Our study showed that the threshold of B81-oVEMP gradually increased with age. A morphological study of the vestibular neuroepithelium revealed that degenerative changes in the vestibular organs occurred after the age of 40 years. Approximately, 20% loss of the hair cell population was noted in the utricular macula with increasing age, consistent with a significant decline in the response rates and increase in the threshold of B81-oVEMP in individuals ≥40 years (14, 20). In addition to age-related changes in the vestibular hair cells, depletion of the vestibular ganglion cells and vestibular afferent neurons are also noted during the aging process. Richter et al. reported a decrease in the number of vestibular hair cells after the age of 20 years and a decrease in vestibular ganglia after the age of 50 years (21). Merchant also reported a gradual loss in vestibular hair cells in all the end organs (three cristae and two maculae) with increasing age (23). A previous study identified significant age-related loss of neurons in the medial vestibular nucleus (33), a well-documented VOR relay center. The prolonged N10 latency of B81-oVEMP may degrade the central vestibular processing of otolithic signals with age.

Our results showed that the P15 latency and raw amplitude of B81-oVEMP were not significantly correlated with age, contradicting the results of previous studies (14, 28). However, the corrected amplitude decreased with increasing age. These data indicate the importance of stimulus parameters (testing position, electrode montage position, vibrator position, force, etc.) in the oVEMP test (3, 34).

Raw IAR and Corrected IAR of B81-cVEMP and B81-oVEMP

For B81-cVEMP and B81-oVEMP, our results revealed no correlation between the raw IAR and corrected IAR with increasing age. These results are consistent with previous reports (14, 25, 27). The lack of change in the IAR with advancing age could be attributed to the bilateral and usually symmetrical nature of the aging process, which has been reported most often in the studies conducted on the effect of aging on hearing and balance (31).

We also observed the raw IAR and corrected IAR in each group. The corrected amplitude did not reduce the IAR values in our study. Instead, the maximum value of the corrected IAR increased by using the corrected amplitude in most age groups, being more apparent for B81-cVEMP.

During VEMP testing, we found that some subjects had a reduced IAR, but the IAR of other subjects increased using the corrected amplitude. McCaslin et al. found similar results. However, they suggested that the cVEMP test is best performed using optimal EMG activation with amplitude normalization techniques (35). Lee et al. reported that rectified data can produce a more reliable IAR and may help diagnose some vestibular disorders according to amplitude-associated parameters (36). As we only included 10 subjects in each group in this study, the results of our study need to be further explored.

The Response Rate of B81-oVEMP Decreases More Significantly With Age

This study showed that when patients were older than 60 years, the response rate of B81-cVEMP was 75%, while that of B81-oVEMP was only 40%. B81-oVEMP is an excitatory postsynaptic potential that is not affected by muscle contraction. Still, the recording potential is small, and many interference factors, such as stimulus artifacts, electromagnetic interference, head size, stimulation location, and lower eyelid thickness, could affect its record (37). Besides, the B81 bone vibrator placed on the mastoid typically produces good cVEMP but poorer oVEMP because forehead stimulation may be the best location for the oVEMP response (17, 28). Therefore, when recording oVEMP, the influencing factors need to be carefully controlled. The disappearance of the waveform does not necessarily indicate utricular dysfunction and should be considered comprehensively.

Limitations

Finally, several limitations to the present study should be considered. First, BCV stimulations have several advantages compared to ACS stimulation. BCV stimulations can be used in patients with conductive hearing loss, decrease the sound exposure in children with small external auditory canal volumes, and produce large oVEMP responses. But BCV stimulation activates the utricle and saccule of both ears, rendering their interpretation more difficult in patients with unilateral vestibular loss (3). Second, BCV stimulation is less sensitive and specific than ACS stimulation when diagnosing third-window diseases (38). Third, the B81 vibrator was placed on the mastoid because it is difficult to attach it firmly to the forehead. VEMPs are sometimes sensitive to small variations in vibrator placement. The vibrator locations should be moved slightly if B81-VEMPs are very small or absent (3). Furthermore, based on a small sample size in this study, the results of patients with vestibular diseases using different BCV stimulations are needed for future research.

CONCLUSION

Age significantly affects B81-cVEMP and B81-oVEMP responses, particularly the response rate of B81-oVEMP. Hence, we suggest establishing reference values according to different age groups when evaluating the VEMP responses in patients with vestibular diseases.

DATA AVAILABILITY STATEMENT

The original contributions presented in the study are included in the article/supplementary material, further inquiries can be directed to the corresponding author/s.

ETHICS STATEMENT

The studies involving human participants were reviewed and approved by Xi'an Jiaotong University. Written informed consent to participate in this study was provided by the participants' legal guardian/next of kin. Written informed consent was obtained from the individual(s) for the publication of any potentially identifiable images or data included in this article.

AUTHOR CONTRIBUTIONS

YZ and ZC wrote the manuscript. PR, QZ, and YJ provided the idea for the study, reviewed, and edited the manuscript. JY reviewed and edited the manuscript. HZ, JS, and QW collected the clinical data. All authors contributed to the article and approved the submitted version.

FUNDING

This work was supported by the National Natural Science Foundation of China (Grant Nos: 81970891, 82171137, and 81971766) and the Key International Cooperation Project of Shaanxi Province (Grant No: 2020-KWZ-019) and the Science and Technology Project of Shanghai Science and Technology Commission (Grant No: 21S31900600).

ACKNOWLEDGMENTS

The authors thank the healthy volunteers who participated in this study.

REFERENCES

1. Curthoys IS, Grant JW, Burgess AM, Pastras CJ, Brown DJ, Manzari L. Otolithic receptor mechanisms for vestibular-evoked myogenic potentials: a review. *Front Neurol.* (2018) 9:e366. doi: 10.3389/fneur.2018.00366
2. Curthoys IS, Grant JW, Pastras CJ, Brown DJ, Burgess AM, Brichta AM, et al. review of mechanical and synaptic processes in otolith transduction of sound and vibration for clinical VEMP testing. *J Neurophysiol.* (2019) 122:259–76. doi: 10.1152/jn.00031.2019
3. Rosengren SM, Colebatch JG, Young AS, Govender S, Welgampola MS. Vestibular evoked myogenic potentials in practice: methods, pitfalls and clinical applications. *Clin Neurophysiol Pract.* (2019) 4:47–68. doi: 10.1016/j.cnp.2019.01.005
4. Colebatch JG, Halmagyi GM. Vestibular evoked potentials in human neck muscles before and after unilateral vestibular deafferentation. *Neurology.* (1992) 42:1635–6. doi: 10.1212/WNL.42.8.1635
5. Colebatch JG, Halmagyi GM, Skuse NF. Myogenic potentials generated by a click-evoked vestibulocollic reflex. *J Neurol Neurosurg Psychiatry.* (1994) 57:190–7. doi: 10.1136/jnnp.57.2.190
6. Rosengren SM, McAngus Todd NP, Colebatch JG. Vestibular-evoked extraocular potentials produced by stimulation with bone-conducted sound. *Clin Neurophysiol.* (2005) 116:1938–48. doi: 10.1016/j.clinph.2005.03.019
7. Rosengren SM, Welgampola MS, Colebatch JG. Vestibular evoked myogenic potentials: past, present and future. *Clin Neurophysiol.* (2010) 121:636–51. doi: 10.1016/j.clinph.2009.10.016
8. Curthoys IS. A critical review of the neurophysiological evidence underlying clinical vestibular testing using sound, vibration and galvanic stimuli. *Clin Neurophysiol.* (2010) 121:132–44. doi: 10.1016/j.clinph.2009.09.027
9. Halmagyi GM, Yavor RA, Colebatch JG. Tapping the head activates the vestibular system: a new use for the clinical reflex hammer. *Neurology.* (1995) 45:1927–9. doi: 10.1212/WNL.45.10.1927
10. Han P, Zhang R, Chen Z, Gao Y, Cheng Y, Zhang Q, et al. Evaluation of ocular and cervical vestibular evoked myogenic potentials in a conductive hearing loss model. *J Otol.* (2016) 11:192–7. doi: 10.1016/j.joto.2016.12.002
11. Iwasaki S, McGarvie LA, Halmagyi GM, Burgess AM, Kim J, Colebatch JG, et al. Head taps evoke a crossed vestibulo-ocular reflex. *Neurology.* (2007) 68:1227–9. doi: 10.1212/01.wnl.0000259064.80564.21
12. Iwasaki S, Smulders YE, Burgess AM, McGarvie LA, MacDougall HG, Halmagyi GM, et al. Ocular vestibular evoked myogenic potentials to bone conducted vibration of the midline forehead at Fz in healthy subjects. *Clin Neurophysiol.* (2008) 119:2135–47. doi: 10.1016/j.clinph.2008.05.028
13. Basta D, Todt I, Ernst A. Characterization of age-related changes in vestibular evoked myogenic potentials. *J Vestib Res.* (2007) 17:93–8. doi: 10.3233/VES-2007-172-304
14. Tseng CL, Chou CH, Young YH. Aging effect on the ocular vestibular-evoked myogenic potentials. *Otol Neurotol.* (2010) 31:959–63. doi: 10.1097/MAO.0b013e3181e8fb1a
15. Welgampola MS, Rosengren SM, Halmagyi GM, Colebatch JG. Vestibular activation by bone conducted sound. *J Neurol Neurosurg Psychiatry.* (2003) 74:771–8. doi: 10.1136/jnnp.74.6.771
16. Clinard CG, Piker EG, Thorne AP, Surface EN, Anderson AE, Beacham VA, et al. Maximum output and low-frequency limitations of B71 and B81 clinical bone vibrators: implications for vestibular evoked potentials. *Ear Hear.* (2020) 41:847–54. doi: 10.1097/AUD.0000000000000808
17. Patterson JN, Rodriguez AI, Gordon KR, Honaker JA, Janky KL. Age effects of bone conduction vibration vestibular-evoked myogenic potentials (VEMPs) using B81 and impulse hammer stimuli. *Ear Hear.* (2021) 42:1328–37. doi: 10.1097/AUD.0000000000001024
18. Jansson KJ, Håkansson B, Johannsen L, Tengstrand T. Electro-acoustic performance of the new bone vibrator radioear B81: a comparison with the conventional radioear B71. *Int J Audiol.* (2015) 54:334–40. doi: 10.3109/14992027.2014.980521
19. Romero DJ, Piker EG, Thorne A, Clinard C. Comparison of bone-conducted cervical VEMPs elicited by B71 and B81 bone vibrators. *Ear Hear.* (2021) 42:596–605. doi: 10.1097/AUD.0000000000000978
20. Rosenhall U. Degenerative patterns in the aging human vestibular neuro-epithelia. *Acta Otolaryngol.* (1973) 76:208–20. doi: 10.3109/00016487309121501
21. Richter E. Quantitative study of human Scarpa's ganglion and vestibular sensory epithelia. *Acta Otolaryngol.* (1980) 90:199–208. doi: 10.3109/00016488009131716
22. Merchant SN, Velázquez-Villaseñor L, Tsuji K, Glynn RJ, Wall C III, Rauch SD. Temporal bone studies of the human peripheral vestibular system normative vestibular hair cell data. *Ann Otol Rhinol Laryngol Suppl.* (2000) 181:3–13. doi: 10.1177/00034894001090S502
23. Velázquez-Villaseñor L, Merchant SN, Tsuji K, Glynn RJ, Wall C III, Rauch SD. Temporal bone studies of the human peripheral vestibular system normative Scarpa's ganglion cell data. *Ann Otol Rhinol Laryngol Suppl.* (2000) 181:14–9. doi: 10.1177/00034894001090S503
24. Macambira YKD, Carnauba ATL, Fernandes LCBC, Bueno NB, Menezes PD. Aging and wave-component latency delays in oVEMP and cVEMP: a systematic review with meta-analysis. *Braz J Otorhinolar.* (2017) 83:475–87. doi: 10.1016/j.bjorl.2016.12.006
25. Singh NK, Firdose H. Characterizing the impact of advancing age on 500 Hz tone-burst evoked ocular-vestibular evoked myogenic potentials. *Eur Arch Otorhinolaryngol.* (2021) 278:4259–68. doi: 10.1007/s00405-020-06542-2
26. Tseng CC, Wang SJ, Young YH. Comparison of head elevation versus rotation methods for eliciting cervical vestibular-evoked myogenic potentials via bone-conducted vibration. *Int J Audiol.* (2013) 52:200–6. doi: 10.3109/14992027.2012.754108
27. Welgampola MS, Colebatch JG. Vestibulocollic reflexes: normal values and the effect of age. *Clin Neurophysiol.* (2001) 112:1971–9. doi: 10.1016/S1388-2457(01)00645-9
28. Rosengren SM, Govender S, Colebatch JG. Ocular and cervical vestibular evoked myogenic potentials produced by air- and bone-conducted stimuli: comparative properties and effects of age. *Clin Neurophysiol.* (2011) 122:2282–9. doi: 10.1016/j.clinph.2011.04.001
29. Colebatch JG, Govender S, Rosengren SM. Two distinct patterns of VEMP changes with age. *Clin Neurophysiol.* (2013) 124:2066–8. doi: 10.1016/j.clinph.2013.04.337
30. Su HC, Huang TW, Young YH, Cheng PW. Aging effect on vestibular evoked myogenic potential. *Otol Neurotol.* (2004) 25:977–80. doi: 10.1097/00129492-200411000-00019
31. Singh NK, Kashyap RS, Supreetha L, Sahana V. Characterization of age-related changes in sacculocolic response parameters assessed by cervical vestibular evoked myogenic potentials. *Eur Arch Otorhinolaryngol.* (2014) 271:1869–77. doi: 10.1007/s00405-013-2672-0
32. Rodriguez AI, Marler E, Fitzpatrick D, Creutz T, Cannon SA, Thomas MLA, et al. Optimization of cervical and ocular vestibular evoked myogenic potential testing using an impulse hammer in adults, adolescents, and children. *Otol Neurotol.* (2020) 41:817–27. doi: 10.1097/MAO.0000000000002632
33. Tang Y, Lopez I, Baloh RW. Age-related change of the neuronal number in the human medial vestibular nucleus: a stereological investigation. *J Vestib Res.* (2001-2002) 11:357–63. doi: 10.3233/VES-2002-11602
34. Govender S, Colebatch JG. Effects of midline sagittal location on bone-conducted cervical and ocular vestibular evoked myogenic potentials. *J Appl Physiol (1985).* (2017) 122:1470–84. doi: 10.1152/japplphysiol.01069.2016
35. McCaslin DL, Jacobson GP, Hatton K, Fowler AP, DeLong AP. The effects of amplitude normalization and EMG targets on cVEMP interaural amplitude asymmetry. *Ear Hear.* (2013) 34:482–90. doi: 10.1097/AUD.0b013e31827ad792
36. Lee KJ, Kim MS, Son EJ, Lim HJ, Bang JH, Kang JG. The usefulness of rectified VEMP. *Clin Exp Otorhinolaryngol.* (2008) 1:143–7. doi: 10.3342/ceo.2008.1.3.143
37. Curthoys IS, Manzari L, Smulders YE, Burgess AM. A review of the scientific basis and practical application of a new test of utricular function – ocular vestibular-evoked myogenic potentials to bone-conducted vibration. *Acta Otorhinolaryngol Ital.* (2009) 29:179–86.
38. Janky KL, Nguyen KD, Welgampola M, Zuniga MG, Carey JP. Air-conducted oVEMPs provide the best separation between intact

and superior canal dehiscent labyrinths. *Otol Neurotol.* (2013) 34:127–34. doi: 10.1097/MAO.0b013e318271c32a

Conflict of Interest: The authors declare that the research was conducted in the absence of any commercial or financial relationships that could be construed as a potential conflict of interest.

Publisher's Note: All claims expressed in this article are solely those of the authors and do not necessarily represent those of their affiliated organizations, or those of the publisher, the editors and the reviewers. Any product that may be evaluated in this article, or claim that may be made by its manufacturer, is not guaranteed or endorsed by the publisher.

Copyright © 2022 Zhang, Chen, Zhao, Shen, Zhong, Wu, Yang, Jin, Zhang and Ren. This is an open-access article distributed under the terms of the Creative Commons Attribution License (CC BY). The use, distribution or reproduction in other forums is permitted, provided the original author(s) and the copyright owner(s) are credited and that the original publication in this journal is cited, in accordance with accepted academic practice. No use, distribution or reproduction is permitted which does not comply with these terms.

frontiers | Frontiers in Neurology

ORIGINAL RESEARCH
published: 17 May 2022
doi: 10.3389/fneur.2022.881411

The Role of Neck Input in Producing Corrective Saccades in the Head Impulse Test

Shinichi Iwasaki[1], Teru Kamogashira[2], Chisato Fujimoto[2], Kayoko Kabaya[1], Makoto Kinoshita[2] and Tatsuya Yamasoba[2]*

[1] Department of Otolaryngology & Head and Neck Surgery, Nagoya City University Graduate School of Medicine, Nagoya, Japan, [2] Department of Otolaryngology and Head and Neck Surgery, Faculty of Medicine, The University of Tokyo, Tokyo, Japan

Background: The head impulse test is a valuable clinical test that can help identify peripheral vestibular dysfunction by observing corrective saccades that return the eyes to the target of interest. Corrective saccades have been classified as covert if the onset occurs before the end of the head impulse and as overt if they occur afterwards. However, the mechanism that trigger these saccades remain unclear.

Objective: The objective of this study was to examine the role of neck input in generating overt as well as covert saccades.

Methods: Sixteen patients (9 males and 7 females: age 35-80 years, average 62.7 years old) who showed corrective saccades during the head impulse test were included. Twelve patients had unilateral vestibular dysfunction, and 4 patients had bilateral vestibular dysfunction. Patients underwent both the head impulse test (HIT) and the body impulse test (BIT) in a randomized order. While the head is rotated horizontally in HIT, the body is rotated horizontally in BIT. During BIT, the neck is fixed by a cervical collar (neck lock extrication collar) to reduce somatosensory input from the neck. The head movements and eye movements were recorded and analyzed by the video HIT recording system.

Results: In all 16 patients, corrective saccades were observed in HIT as well as in BIT. While there were no significant differences in peak head velocities between HIT and BIT ($p = 0.33$, paired t-test), the VOR gain in BIT was significantly smaller than that in HIT ($p = 0.011$, paired t-test). The number of overt saccades per trial in BIT was significantly decreased compared to that in HIT ($p < 0.001$, paired t-test) whereas there were no significant differences in the number of covert saccades between the two tests. The proportion of overt saccades among all corrective saccades in BIT was significantly lower than the proportion in HIT ($p < 0.001$, paired t-test).

Conclusions: Somatosensory input from the neck contributes to the generation of overt saccades and reinforces the vestibulo-ocular reflex complementing the retinal slip during high frequency head movements.

Keywords: vestibular, head impulse test, neck input, overt saccades, covert saccades

OPEN ACCESS

Edited by:
Sun-Young Oh,
Jeonbuk National University,
South Korea

Reviewed by:
Sun-Uk Lee,
Korea University Medical Center,
South Korea
John Allum,
University of Basel, Switzerland

****Correspondence:***
Shinichi Iwasaki
iwashin@med.nagoya-cu.ac.jp

Specialty section:
This article was submitted to Neuro-Otology, a section of the journal Frontiers in Neurology

Received: *22 February 2022*
Accepted: *03 May 2022*
Published: *17 May 2022*

Citation:
Iwasaki S, Kamogashira T, Fujimoto C, Kabaya K, Kinoshita M and Yamasoba T (2022) The Role of Neck Input in Producing Corrective Saccades in the Head Impulse Test. Front. Neurol. 13:881411. doi: 10.3389/fneur.2022.881411

INTRODUCTION

The head impulse test (HIT) is a valuable clinical test to identify peripheral vestibular dysfunction (1, 2). When clinicians turn the head briskly in the plane of the semicircular canals, healthy subjects can stabilize their gaze with the angular vestibulo-ocular reflex (VOR) that compensates for the head rotation with an equal eye rotation in the direction opposite to the head. In patients with vestibular dysfunction, the eyes move with the head, requiring corrective saccades to return the gaze to the earth-fixed target. Detecting these corrective saccades is the clinical sign of VOR hypofunction in clinical HIT (2).

Objective eye movement measurement during HIT using the scleral search coil technique as well as high-speed video imaging has revealed that corrective saccades occur not only after the end of the eye response defined as the zero crossing of eye velocity but also during the head rotation (3, 4). The latter is called a covert saccade, since it is difficult to perceive them without recording equipment. The former is called an overt saccade since it is easily observed by the clinician without recording.

The mechanisms of how corrective saccades are generated are still unclear. Previous studies have suggested that they are triggered by retinal slip (5), visual input (6), residual vestibular function (7), or internal models created in the central nervous system (8). However, the role of somatosensory input from cervical movement in the generation of corrective saccades is still unclear.

Previous studies have shown that while the contribution of the somatosensory input from cervical movement to VOR is minimal in normal conditions, it potentiates after bilateral vestibular loss (9, 10). After unilateral labyrinthectomy, somatosensory input can be used to change activity in the vestibular afferents in frogs (11), but not in primates (12, 13).

To investigate the role of cervical input in generating corrective saccades in HIT, we performed both HIT and the body impulse test (BIT), in which the examiner quickly rotates the patient's body with their neck fixed using a cervical collar, in patients with peripheral vestibular dysfunction. We compared the differences in the generation of corrective saccades between HIT and BIT and revealed that the sensory input from the neck mainly contributes to the generation of overt saccades.

METHODS

Experimental Procedure

All procedures were in accordance with the Helsinki declaration and were approved by the University of Tokyo Human Ethics Committee (No. 2487). All patients gave written informed consent.

Patients

Sixteen patients (9 males and 7 females; age 35–80 years, mean age 62.7 ± 14.6 years) were recruited from the Balance Disorder Clinic, Department of Otolaryngology at the University of Tokyo Hospital. All the patients received a detailed history taking and neuro-otological tests including the head impulse test, caloric test (4°C ice water). The methods of these vestibular function tests have been described previously (14). The inclusion criteria were (1) unilateral or bilateral vestibular hypofunction shown with the caloric test (canal paresis calculated using Jongkee's formula >20%, or maximum slow phase eye velocity < 10°/s bilaterally) (14), (2) corrective saccades present with decreased VOR gain (< 0.8) on at least on one side in the lateral canal using vHIT (15), and (3) free from any disease of the central nervous system. The clinical characteristics of the patients are listed in **Table 1**. The vestibular schwannomas in patients #10 and #11 were located in the internal auditory meatus without any compression of the brainstem. The tumors sizes were 6.2 and 4.7 mm, respectively.

Head Impulse Test (HIT)

Subjects were seated on a chair in a light room, and were instructed to visualize an eye level target on the wall at a distance of 1 m. The examiner stood behind the subject and held the subject's head. Horizontal head impulses were manually applied to each side with unpredictable timing and direction by the examiner (**Figure 1A**). The amplitude of the head rotation was 15-20°, and the head velocity of the impulse was 110-220°/s. At least 20 accepted head impulses were collected for each horizontal semicircular canal.

Body Impulse Test (BIT)

Subjects were seated on a rotating stool, the seat of which could rotate freely in the horizontal plane, and were instructed to visualize an eye level target on the wall at a distance of 1 m in a light room. They wore a cervical collar (Ossur Miami-J Neck Brace; Ossur Japan, Tokyo) to stabilize the head. To minimize neck movement, particular care was taken to secure the neck brace tightly around the neck. The examiner stood behind the subject and held both shoulders. Impulsive horizontal body rotations were manually applied to each side with unpredictable timing and direction by the examiner (**Figure 1B**). The amplitude of the rotation was 15-20°. The head velocity of the impulse was 110-220°/s. At least 20 accepted head impulses were collected for each horizontal semicircular canal.

HIT and BIT were performed in a randomized order.

Data Collection and Analysis

Eye velocity and head velocity were recorded for each head rotation using an Otometrics Impulse device (Otometrics, Denmark). Subjects wore a lightweight goggle frame with a built-in camera to record eye movements from the right eye and an accelerometer to record head movement at a sampling frequency of 250 Hz. The values of VOR gain were calculated as the ratio of mean eye velocity over mean head velocity during a 40-ms window centered at peak head acceleration (3).

Corrective saccades were analyzed off-line with custom SciLab 6.1.1 software (SciLab, ESI Group). Saccades were identified by their peak velocity. We only analyzed corrective saccades that brought the eye toward the target. Compensatory saccades that occurred during the head movement were classified as "covert." Saccades appearing after the head movement had finished were classified as "overt" (4). The beginning of a head impulse was defined as the first time point when the head velocity exceeded 2% of the peak prior to peak head velocity. The end of a head

TABLE 1 | Clinical characteristics of the 16 patients with vestibular dysfunction.

Patient No.	Age	Sex	Affected side	Etiologies	Duration from onset	vHIT gain		Caloric (deg/s)	
						Deficit	Normal	Deficit	Normal
1	36	F	R	Vestibular neuritis	3 months	0.27	0.46	0	25
2	51	M	R	Vestibular neuritis	38 days	0.22	0.83	0	11
3	53	M	R	Vestibular neuritis	10 days	0.37	0.98	4.8	29
4	54	F	L	Vestibular neuritis	1 year	0.32	0.81	3.9	15
5	75	F	R	Vestibular neuritis	40 days	0.53	1.06	3.4	23
6	75	F	L	Vestibular neuritis	8 months	0.57	0.84	3.3	50
7	80	M	L	Vestibular neuritis	2.6 years	0.52	1.18	4.3	21
8	77	F	R	Meniere's disease	4 years	0.73	0.83	4	18
9	78	F	L	Meniere's disease	2 months	0.67	1.11	22	41
10	35	M	L	Vestibular schwannoma	>10 years	0.27	0.77	0	24.8
11	64	F	L	Vestibular schwannoma	>10 years	0.76	1.1	3.6	15
12	67	M	L	Labyrinthitis	1.5 years	0.55	0.97	0	14
						R	**L**	**R**	**L**
13	51	M	Bilateral	Aminoglycoside	2.2 years	0.53	0.51	1.3	0.5
14	61	M	Bilateral	Aminoglycoside	10 months	0.72	0.69	0	2.5
15	70	M	Bilateral	Unknown	10 months	0.23	0.25	0	0
16	76	M	Bilateral	A3243G	Unknown	0.5	0.62	1.4	2.2

R, right; L, left; vHIT, video head impulse test; A3243G, mitochondrial A3243G mutation.

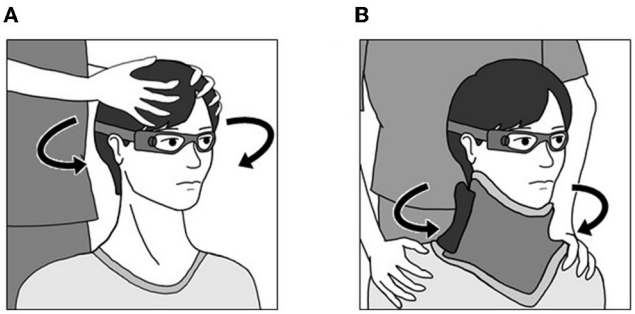

FIGURE 1 | Methods for the head impulse test and body impulse test. **(A)** Head Impulse Test. The examiner stood behind the subject and held the subject's head. Horizontal head impulses were manually applied to each side with unpredictable timing and direction by the examiner. **(B)** Body Impulse Test. Subjects were seated on a rotating stool, and wore a cervical collar to minimize neck movements. The examiner held both shoulders. Impulsive horizontal body rotation was manually applied to each side with unpredictable timing and direction by the examiner.

impulse was defined as the first time when head velocity had a zero crossing after the peak velocity. The amplitude of the saccade was measured at the peak. Covert saccade amplitude was adjusted such that velocity of the VOR was removed (16). The latency of the saccade was the difference between the beginning of the head impulse and the time of the peak velocity of the saccade.

Statistical Analysis

Data are expressed as mean ± SD. Statistical analysis of the data was done using SPSS software version 21 (IBM Corp., Armonk, NY, USA). The peak head velocity, VOR gain, and the number, latency and amplitude of corrective saccades between HIT and BIT were compared using a paired *t*-test. The correlation between the decrease in the proportion of overt saccades and various parameters (duration from the onset, HIT gain, differences in gain between HIT and BIT, difference in head velocities between HIT and BIT, and age) were examined using a Pearson's correlation coefficient analysis. A difference was considered significant at $p < 0.05$.

RESULTS

Figure 2 shows the results of HIT and BIT in a representative patient with vestibular neuritis on the right side (Patient #2 in **Table 1**). While both overt and covert saccades were observed in HIT to the right side, almost all saccades were covert in BIT to the same side.

We performed HIT as well as BIT in 12 patients with unilateral vestibulopathy and 4 patients with bilateral vestibulopathy. Disruptive artifacts such as a large bounce or multiple peaks (17) were not observed either in HIT or BIT. Since there were no significant differences in the decrease in the proportion of overt saccades in BIT compared to HIT between patients with unilateral vestibular dysfunction and bilateral vestibular dysfunction ($p = 0.079$, unpaired *t*-test), we combined the data of the patients with unilateral and bilateral vestibular dysfunction.

Table 2 shows the summarized results of HIT and BIT in 20 affected sides in total. While there were no significant differences in peak head velocities between HIT and BIT ($p = 0.33$, paired *t*-test), the VOR gain in BIT was significantly smaller than that in HIT ($p = 0.011$, paired *t*-test). The number of corrective

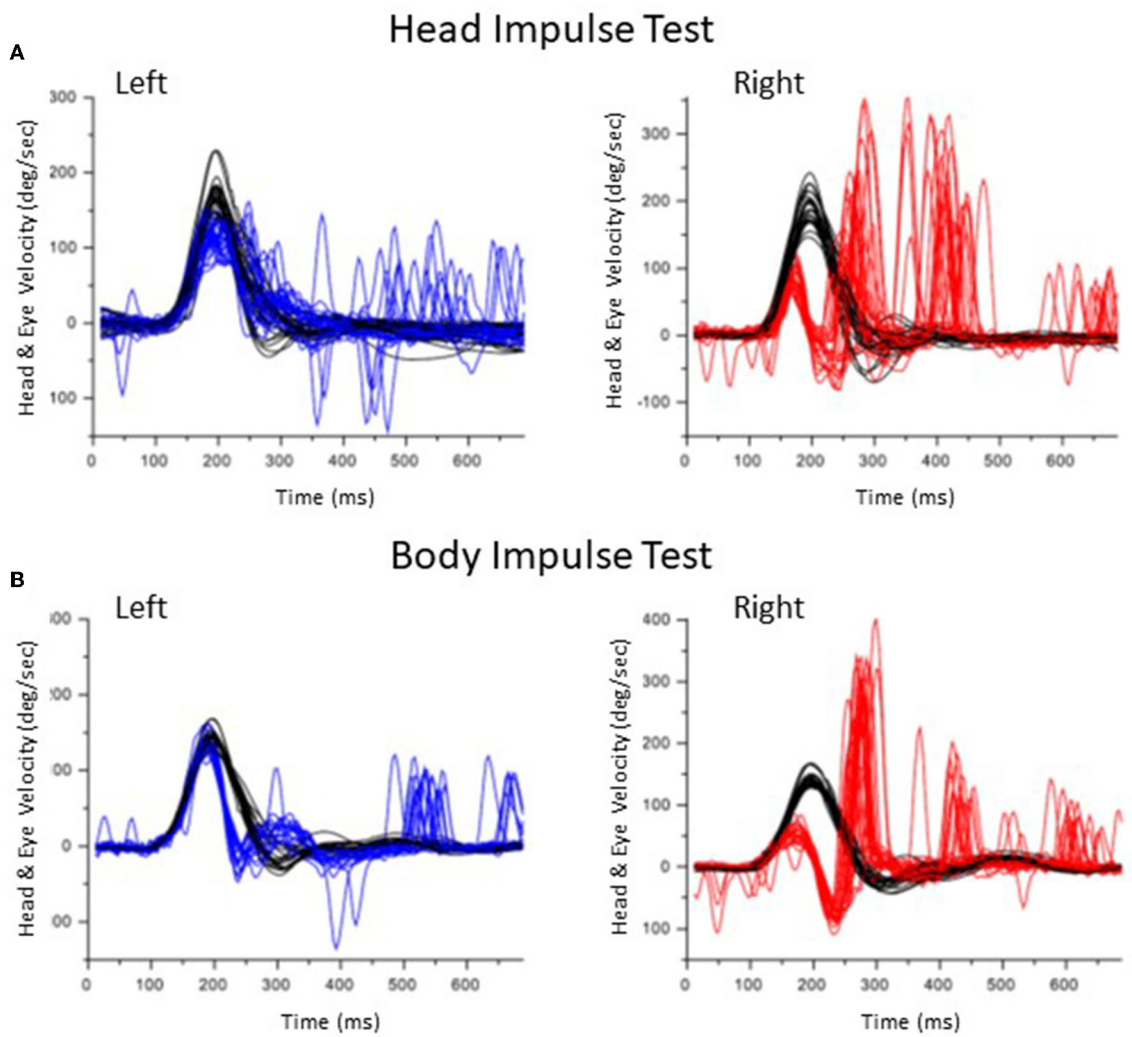

FIGURE 2 | Results of the head impulse test and body impulse test in a patient with a right vestibular neuritis (Patient #2). **(A)** Head Impulse test. Head velocity is black. Eye velocity is blue in the left lateral rotation and red in the right lateral rotation. In the right lateral rotation, both covert and overt saccades were observed. **(B)** Body Impulse Test. In the right lateral rotation, overt saccades decreased.

saccades in BIT was significantly smaller than that in HIT ($p = 0.0011$, paired t-test). There were no significant differences in the number of covert saccades per trial between HIT and BIT ($p = 0.81$, paired t-test). However, the number of overt saccades in BIT was significantly decreased compared to that in HIT ($p < 0.001$, paired t-test). The proportion of covert saccades among all corrective saccades in HIT was $54.3 \pm 11.4\%$ whereas in BIT it was significantly greater at $74.2 \pm 14.9\%$ ($p < 0.001$, paired t-test). The latency of all corrective saccades in BIT was significantly smaller than that in HIT ($p = 0.0065$, paired t-test).

Since we included patients with a variety of diseases, we also analyzed the results of HIT and BIT limited to patients with vestibular neuritis (Patients #1-#7; **Supplementary Table 1**). While there were no significant differences in peak head velocities between HIT and BIT ($p = 0.34$, paired t-test), the VOR gain in BIT was significantly smaller than that in HIT ($p = 0.028$, paired t-test). The proportion of covert saccades among all corrective saccades in BIT ($67.3 \pm 11.4\%$) significantly increased compared to than that in HIT ($57.3 \pm 14.1\%$; $p = 0.038$, paired t-test).

To investigate the factors that have an association with the decrease in the proportion of overt saccades in BIT in comparison with HIT, we examined its correlation with several factors (**Supplementary Figure 1**). There were no significant correlations between the decrease in the rate of overt saccades in BIT and the duration from the onset of the disease ($r = 0.039$, $p = 0.89$, Pearson's correlation coefficient analysis), the gain in HIT ($r = 0.13$, $p = 0.58$, Pearson's correlation coefficient analysis), differences in gain in between HIT and BIT ($r = -0.057$, $p = 0.81$, Pearson's correlation coefficient analysis) or the difference in head velocity between HIT and BIT ($r = 0.31$, $p = 0.19$, Pearson's correlation coefficient analysis). Only patient age had a weak

TABLE 2 | Results of head impulse test and body impulse test.

	Head impulse test (n = 20 ears)	Body impulse test (n = 20 ears)	p-value
Peak head velocity (deg/s)	166.4 ± 46.5	155.7 ± 36.9	0.33
Gain	0.50 ± 0.19	0.42 ± 0.17	0.011*
Number of all corrective saccades (per trial)	2.14 ± 0.53	1.59 ± 0.49	0.0011**
Number of covert saccades (per trial)	1.15 ± 0.35	1.13 ± 0.23	0.81
Number of overt saccades (per trial)	0.99 ± 0.38	0.46 ± 0.37	<0.001***
Proportion of covert saccades (%)	54.3 ± 11.4	74.2 ± 14.9	<0.001***
Proportion of overt saccades (%)	45.7 ± 11.4	25.8 ± 14.9	<0.001***
Latency of all corrective saccades (ms)	244.7 ± 25.0	214.1 ± 50.9	0.0065**
Velocity of all corrective saccades (deg/s)	127.1 ± 27.4	122.3 ± 33.0	0.49
Velocity of covert saccades (deg/s)	123.0 ± 19.4	125.1 ± 35.9	0.76
Velocity of overt saccades (deg/s)	130.5 ± 37.4	117.0 ± 29.3	0.081

*$p < 0.05$, **$p < 0.01$, ***$p < 0.001$.

correlation with the decrease in the rate of overt saccades in BIT ($r = -0.453$, $p = 0.045$, Pearson's correlation coefficient analysis).

DISCUSSION

In the present study, we performed HIT as well as BIT in patients with peripheral vestibular dysfunction, and showed that the proportion of overt saccades significantly decreased in BIT compared to HIT, suggesting that input from the neck contributes to the production of overt saccades in HIT.

During each head impulse, corrective saccades are induced to bring the eyes back on target, and they have been accepted as a clinical sign of vestibular dysfunction. Corrective saccades have been suggested to have a role in facilitating patient recovery (9). Visual processing is suppressed during saccades, so that neither the motion of the eye nor the blur of the retinal image during inadequate VOR is perceived. This saccadic suppression can reduce oscillopsia and improve visual performance during high-velocity head movements (9, 10).

The mechanism of how corrective saccades are generated is still unclear. Retinal slip during head rotation has been suggested as the main trigger of corrective saccades (5, 6). However, the presence of corrective saccades in darkness indicates that there are triggers other than the retinal slip during head movement (6). The remaining vestibular function and the somatosensory input from the neck have been proposed as possible triggers of corrective saccades (18). Another possible explanation might be generation through internal models in the central nervous system (8). This hypothesis is consistent with previous findings that corrective saccades are triggered earlier when the head turns are active (19, 20), and when they are predictable (21).

We have addressed the question of whether the somatosensory input from the neck contributes to the generation of corrective saccades during high-velocity head rotations. When the head is rotated on the body, neck joints and muscle proprioceptors are also activated, generating the slow phase eye movement through the cervico-ocular reflex (COR) pathway. While the contribution of the COR to gaze stabilization is very small under normal conditions, it has been shown that the COR potentiates after bilateral vestibular loss (22, 23). Since this potentiated COR mainly compensates for head velocity at lower frequencies, the slow phase eye movement generated by the COR may contribute to improving the slow compensatory eye responses to passive low-acceleration head turns but not to generating the slow eye movements to passive head turns with naturally high accelerations. However, it is possible that the potentiated COR enhances oculomotor responses to low frequency stimuli and serves to trigger covert saccadic responses for high-acceleration head rotations. In fact, it has been reported that a patient with absent labyrinthine function was able to make both the slow and quick phases of nystagmus during rotation of the body with the head stationary in darkness (24). In the present study, BIT showed slightly but significantly reduced gain in comparison with HIT, suggesting that the somatosensory input from the neck can contribute to generating compensatory eye movements to the high-frequency head movement.

During head rotation, gaze shifts are achieved by eye-head saccades to bring the image of an object to the fovea (25, 26). The eye-head saccades are composed of eye and head components which show distinct properties. The head component lags the eye component by ∼40 ms although this latency can be affected by the shape of the driving neural signal (27). The waveform of the head component is different from that of the eye component and its velocity increases with the amplitude of the head movement. The generator of the head component is considered to be distinct from that of the eye component, and includes the superior colliculus in the brainstem (25). It is possible that the head component of eye-head saccades may contribute to the generation of overt saccades in HIT since the proportion of overt saccades was significantly reduced in BIT compared to HIT.

There are several limitations in the present study. First, the sample size was relatively small, which might make it difficult to analyze the factors that have an association with the decrease in the proportion of overt saccades in BIT in comparison with HIT. Second, we included patients with wide range of duration from the onset of disease. It has been reported that the gain of the COR continues to increase

after making vestibular lesions (23). However, there were no significant correlations between the duration from the onset of the disease and the decrease in the proportion of overt saccades in BIT compared to HIT. Third, the body rotation in BIT was not measured. There is a possibility that there are differences in velocities of body movement and that of head movement in BIT. Additionally, it is possible that the cervical collar used while performing BIT may not completely eliminate the somatosensory input from the neck. We carefully secured the collar to stabilize the head on the body to reduce the movement of the neck during the body rotation. It is possible that the pressure of the collar to the neck skin and muscle might affect the COR and the generation of corrective saccades.

In conclusion, we have performed BIT and HIT in patients with unilateral and bilateral vestibular dysfunction, and shown that stabilization of the neck resulted in a reduction of overt saccades and a slight decrease in the VOR gain. These results suggest that the somatosensory input from the neck contributes to the generation of overt saccades and reinforces the VOR, complementing the retinal slip trigger during high frequency head movements.

DATA AVAILABILITY STATEMENT

The raw data supporting the conclusions of this article will be made available by the authors, without undue reservation.

ETHICS STATEMENT

The studies involving human participants were reviewed and approved by the University of Tokyo Human Ethics Committee. The patients/participants provided their written informed consent to participate in this study.

AUTHOR CONTRIBUTIONS

SI, TK, CF, KK, and TY conceived and designed the experiments, wrote, and revised the manuscript. SI, TK, CF, and MK performed and analyzed the experiments. All authors contributed to the article and approved the submitted version.

FUNDING

This work was supported by the Ministry of Education, Culture, Sports, Science and Technology (18K09370, 21H03088) and the Japan Agency for Medical Research and Development (AMED).

SUPPLEMENTARY MATERIAL

The Supplementary Material for this article can be found online at: https://www.frontiersin.org/articles/10.3389/fneur.2022.881411/full#supplementary-material

Supplementary Figure 1 | Correlation of the decrease in the proportion of overt saccades in BIT in comparison with HIT with various parameters. **(A)** Correlation between the decrease in the proportion of overt saccades in BIT in comparison with HIT and the duration from the onset of disease. **(B)** Correlation between the decrease in the proportion of overt saccades in BIT in comparison with HIT and VOR gain in HIT. **(C)** Correlation between the decrease in the proportion of overt saccades in BIT in comparison with HIT and the differences in gain between HIT and BIT. **(D)** Correlation between the decrease in the proportion of overt saccades in BIT in comparison with HIT and the differences in head velocities between HIT and BIT. **(E)** Correlation between the decrease in the proportion of overt saccades in BIT in comparison with HIT and the patient's age.

Supplementary Table 1 | Results of head impulse test and body impulse test in patients with vestibular neuritis.

REFERENCES

1. Halmagyi GM, Chen L, MacDougall HG, Weber KP, McGarvie LA, Curthoys IS. The video head impulse test. *Front Neurol.* (2017) 8:258. doi: 10.3389/fneur.2017.00258
2. Halmagyi GM, Curthoys IS, A. clinical sign of canal paresis. *Arch Neurol.* (1988) 45:737–9. doi: 10.1001/archneur.1988.00520310043015
3. MacDougall HG, Weber KP, McGarvie LA, Halmagyi GM, Curthoys IS. The video head impulse test: diagnostic accuracy in peripheral vestibulopathy. *Neurology*. (2009) 73:1134–41. doi: 10.1212/WNL.0b013e3181bacf85
4. Weber KP, Aw ST, Todd MJ, McGarvie LA, Curthoys IS, Halmagyi GM. Head impulse test in unilateral vestibular loss: vestibulo-ocular reflex and catch-up saccades. *Neurology.* (2008) 70:454–63. doi: 10.1212/01.wnl.0000299117.48935.2e
5. Scherer M, Schubert MC. High-velocity angular vestibulo-ocular reflex adaptation to position error signals. *J Neurol Phys Ther.* (2010) 34:82–6. doi: 10.1097/NPT.0b013e3181dde7bc
6. Van Nechel C, Bostan A, Duquesne U, Hautefort C, Toupet M. Visual input is the main trigger and parametric determinant for catch-up saccades during video head impulse test in bilateral vestibular loss. *Front Neurol.* (2018) 9:1138. doi: 10.3389/fneur.2018.01138
7. Tian J, Crane BT, Demer JL. Vestibular catch-up saccades in labyrinthine deficiency. *Exp Brain Res.* (2000) 131:448–57. doi: 10.1007/s002219900320
8. Colagiorgio P, Versino M, Colnaghi S, Quaglieri S, Manfrin M, Zamaro E, et al. New insights into vestibular-saccade interaction based on covert corrective saccades in patients with unilateral vestibular deficits. *J Neurophysiol.* (2017) 117:2324–38. doi: 10.1152/jn.00864.2016
9. Leigh RJ, Zee DS. *The Saccadic System. The Neurology of Eye Movement*. 5 ed. Oxford University Press (2015). p. 169-288.
10. Matin E. Saccadic suppression: a review and an analysis. *Psychol Bull.* (1974) 81:899–917. doi: 10.1037/h0037368
11. Precht W, Llinás R, Clarke M. Physiological responses of frog vestibular fibers to horizontal angular rotation. *Exp Brain Res.* (1971) 13:378–407. doi: 10.1007/bf00234338
12. Cullen KE, Minor LB, Beraneck M, Sadeghi SG. Neural substrates underlying vestibular compensation: contribution of peripheral versus central processing. *J Vestib Res.* (2009) 19:171–82. doi: 10.3233/ves-2009-0357
13. Sadeghi SG, Minor LB, Cullen KE. Dynamics of the horizontal vestibuloocular reflex after unilateral labyrinthectomy: response to high frequency, high acceleration, and high velocity rotations. *Exp Brain Res.* (2006) 175:471–84. doi: 10.1007/s00221-006-0567-7
14. Fujimoto C, Suzuki S, Kinoshita M, Egami N, Sugasawa K, Iwasaki S. Clinical features of otolith organ-specific vestibular dysfunction. *Clin Neurophysiol.* (2018) 129:238–45. doi: 10.1016/j.clinph.2017.11.006
15. McGarvie LA, MacDougall HG, Halmagyi GM, Burgess AM, Weber KP, Curthoys IS. The video head impulse test (vHIT) of semicircular canal function - age-dependent normative values of vor gain in healthy subjects. *Front Neurol.* (2015) 6:154. doi: 10.3389/fneur.2015.00154
16. Anson ER, Bigelow RT, Carey JP, Xue QL, Studenski S, Schubert MC, et al. Aging increases compensatory saccade amplitude in the video

head impulse test. *Front Neurol.* (2016) 7:113. doi: 10.3389/fneur.2016.00113
17. Mantokoudis G, Saber Tehrani AS, Kattah JC, Eibenberger K, Guede CI, Zee DS, et al. Quantifying the vestibulo-ocular reflex with video-oculography: nature and frequency of artifacts. *Audiol Neuro otol.* (2015) 20:39–50. doi: 10.1159/000362780
18. Macdougall HG, Curthoys IS. Plasticity during vestibular compensation: the role of Saccades. *Front Neurol.* (2012) 3:21. doi: 10.3389/fneur.2012.00021
19. Black RA, Halmagyi GM, Thurtell MJ, Todd MJ, Curthoys IS. The active head-impulse test in unilateral peripheral vestibulopathy. *Arch Neurol.* (2005) 62:290–3. doi: 10.1001/archneur.62.2.290
20. Peng GC, Minor LB, Zee DS. Gaze position corrective eye movements in normal subjects and in patients with vestibular deficits. *Ann. N Y Acad. Sci.* (2005) 1039:337–48. doi: 10.1196/annals.1325.032
21. Mantokoudis G, Agrawal Y, Newman-Toker DE, Xie L, Saber Tehrani AS, Wong A, et al. Compensatory saccades benefit from prediction during head impulse testing in early recovery from vestibular deafferentation. *Eur Arch Otorhinolaryngol.* (2016) 273:1379–85. doi: 10.1007/s00405-015-3685-7
22. Bronstein AM. Plastic changes in the human cervicoocular reflex. *Ann. N Y Acad Sci.* (1992) 656:708–15. doi: 10.1111/j.1749-6632.1992.tb25248.x
23. Yakushin SB, Kolesnikova OV, Cohen B, Ogorodnikov DA, Suzuki J, Della Santina CC, et al. Complementary gain modifications of the cervico-ocular (COR) and angular vestibulo-ocular (aVOR) reflexes after canal plugging. *Exp Brain Res.* (2011) 210:549–60. doi: 10.1007/s00221-011-2558-6
24. Kasai T, Zee DS. Eye-head coordination in labyrinthine-defective human beings. *Brain Res.* (1978) 144:123–41. doi: 10.1016/0006-8993(78)90439-0
25. Guitton D. Control of eye-head coordination during orienting gaze shifts. *Trends Neurosci.* (1992) 15:174–9. doi: 10.1016/0166-2236(92)90169-9
26. Proudlock FA, Gottlob I. Physiology and pathology of eye-head coordination. *Prog Retin Eye Res.* (2007) 26:486–515. doi: 10.1016/j.preteyeres.2007.03.004
27. Zangemeister WH, Stark L. Gaze latency: variable interactions of head and eye latency. *Exp Neurol.* (1982) 75:389–406. doi: 10.1016/0014-4886(82)90169-8

Conflict of Interest: The authors declare that the research was conducted in the absence of any commercial or financial relationships that could be construed as a potential conflict of interest.

Publisher's Note: All claims expressed in this article are solely those of the authors and do not necessarily represent those of their affiliated organizations, or those of the publisher, the editors and the reviewers. Any product that may be evaluated in this article, or claim that may be made by its manufacturer, is not guaranteed or endorsed by the publisher.

Copyright © 2022 Iwasaki, Kamogashira, Fujimoto, Kabaya, Kinoshita and Yamasoba. This is an open-access article distributed under the terms of the Creative Commons Attribution License (CC BY). The use, distribution or reproduction in other forums is permitted, provided the original author(s) and the copyright owner(s) are credited and that the original publication in this journal is cited, in accordance with accepted academic practice. No use, distribution or reproduction is permitted which does not comply with these terms.

frontiers | Frontiers in Neurology

BRIEF RESEARCH REPORT
published: 20 May 2022
doi: 10.3389/fneur.2022.897012

Is There an "Acquired Idiopathic Head-Shaking Nystagmus"?—A Discussion of Mechanisms and Clinical Implications Based on a Case Report

Filipp M. Filippopulos[1,2]*, *Andreas Zwergal*[1,2] *and Doreen Huppert*[1,2]

[1] German Center for Vertigo and Balance Disorders (DSGZ), University Hospital LMU Munich, Munich, Germany,
[2] Department of Neurology, University Hospital Ludwig-Maximilians-Universität (LMU) Munich, Munich, Germany

Background: Head-shaking nystagmus (HSN) occurs in both peripheral and central vestibular disorders. In most cases, HSN can be attributed to an asymmetric peripheral vestibular input or a structural lesion mostly in the cerebellum affecting the central velocity storage mechanism. An isolated HSN is very rare.

Case Presentation: We report on a young female patient with the clinical picture of recurrent episodes of vertigo, which were induced by fast head movements and were accompanied by a severe right-beating HSN with a long time constant of 60 s. There was no other clinical and instrument-based evidence of peripheral vestibular dysfunction (including video head impulse test, caloric test, vestibular-evoked myogenic potentials) or indication of a structural lesion in the nodulus, uvula or pontomedullary brainstem on fine-slice magnetic resonance imaging. She had no previous history of migraine, hearing deficits, or other focal neurological symptoms. Diagnostic criteria for vestibular paroxysmia, vestibular migraine, benign peripheral paroxysmal vertigo, or any other known vestibular disorders were not fulfilled. Chart review in the database of the German Center for Vertigo and Balance Disorders indicated eight additional patients with a similar clinical phenotype between 2018 and 2022.

Conclusion: We propose a clinical entity called acquired idiopathic head shaking nystagmus (aiHSN) as a rare cause of episodic vertigo induced by fast head movements. Nystagmus characteristics suggest a subtle functional pathology of the central velocity storage mechanism in the nodulus and uvula, which is exacerbated during symptomatic episodes.

Keywords: head-shaking nystagmus, oculomotor disturbances, vertigo, dizziness, peripheral vestibular system, central vestibular system

OPEN ACCESS

Edited by:
Sun-Young Oh,
Jeonbuk National University,
South Korea

Reviewed by:
Gabor Michael Halmagyi,
The University of Sydney, Australia
Diego Kaski,
University College London,
United Kingdom

***Correspondence:**
Filipp M. Filippopulos
filipp.filippopulos@
med.uni-muenchen.de

Specialty section:
This article was submitted to
Neuro-Otology,
a section of the journal
Frontiers in Neurology

Received: *15 March 2022*
Accepted: *03 May 2022*
Published: *20 May 2022*

Citation:
Filippopulos FM, Zwergal A and Huppert D (2022) Is There an "Acquired Idiopathic Head-Shaking Nystagmus"?—A Discussion of Mechanisms and Clinical Implications Based on a Case Report. Front. Neurol. 13:897012. doi: 10.3389/fneur.2022.897012

INTRODUCTION

Head-shaking nystagmus (HSN) is a distinct ocular motor finding, which is considered to occur in cases with an imbalance in the bilateral peripheral and/or central vestibular system (1, 2). In the case of a reduced unilateral peripheral vestibular input, HSN occurs during head-shaking in accordance with Ewald's second law. HSN is modulated by mechanisms of central velocity storage

located mainly in the nodulus and uvula (1, 3). In consequence, lesions of the central vestibular system can also cause HSN, which does not necessarily follow Ewald's second law and appears as so-called perverted HSN (pHSN) (the direction of HSN differs from the direction of the head shaking) (2). The mechanisms leading to pHSN though are not fully understood and lesions to different central structures have been reported to induce pHSN (4–7).

Overall, HSN may occur in a broad spectrum of diseases of the vestibular system including central vestibular disorders (e.g., stroke), vestibular migraine, and diseases mainly affecting the peripheral vestibular organs such as unilateral vestibulopathy or Menière disease (2, 8, 9). Recently, a disorder was characterized by recurrent spontaneous vertigo of unknown etiology and interictal head-shaking nystagmus (RSV-HSN) in the broader spectrum of patients with benign recurrent vertigo (BRV) (10). Patients with RSV-HSN showed recurring episodes of vertigo with no accompanying symptoms indicative of vestibular migraine or Menière's disease and with an interictal presence of HSN. Furthermore, these patients showed no evidence of peripheral or central vestibular deficits. Cases in which HSN occurs as an isolated symptom are extremely rare, but might indicate a more severe underlying cause (6), so that a broad diagnostic approach is merited.

We present a case of a young female patient with isolated recurrent HSN without evidence of any underlying cause after an extensive diagnostic workup including neurologic examination, neuro-orthoptic examination, instrument-based vestibular diagnostics (e.g., video head impulse test, caloric stimulation, vestibular evoked myogenic potentials), and magnetic resonance imaging (MRI). We discuss the potential clinical impact and the diagnostic approach, as well as therapeutic options. Furthermore, we hypothesize the existence of a distinct clinical entity for a subgroup of patients with "acquired idiopathic head-shaking nystagmus".

CASE DESCRIPTION

A 31-year-old female presented to the German Center for Vertigo and Balance Disorders, (DSGZ) at the University Hospital of the Ludwig-Maximilians-Universität (LMU), Munich, Germany with recurrent episodes of vertigo exclusively trigger by fast head movements. Symptoms initially occurred 2 years prior to the first presentation at the DSGZ during a pregnancy. Since then, she had four episodes lasting for 2–6 weeks each. During these episodes, the patient described vertigo lasting between 20 and 60 s, that was consistently triggered only by head movements. No accompanying symptoms, including symptoms indicative for migraine (e.g., focal neurological symptoms, headache, photo-/phonophobia, aural fullness, hearing loss, tinnitus) were reported. Regarding a possible migraine triggered by hormonal changes during pregnancy, the patient reported no symptoms that might suggest a migrainous predisposition such as motion sickness, reoccurring headaches, or association with menstruation, weather changes, or certain foods. The further patient history and family history, especially regarding migraine, were completely unremarkable. She took no regular medication and had no history of nicotine, drug, or alcohol abuse. Two prior outpatient neurological evaluations during symptomatic episodes suspected unilateral vestibulopathy as an underlying cause, although no peripheral vestibular deficit in the head-impulse test (HIT) or caloric stimulation had been documented.

In the initial clinical evaluation at our center, the patient was awake and fully oriented. The examination of the cranial nerves, motor and sensory function was completely normal. There were no deficits of fine motor skills, nor evidence of ataxia or walking difficulties. Speech and higher cognitive functions were also normal. The ocular motor testing, however, revealed a fast, right-beating HSN with a peak intensity of 13 degrees per second and a frequency of 3 Hz that persisted for up to 60 s after head shaking (see **Supplementary Material**). The nystagmus was not suppressed by visual fixation and no nystagmus reversal was present at any time-point. The nystagmus was induced by head-shaking with a frequency of at least 2–3 Hz and head excursions of 20–25 deg. Further ocular motor testing, including saccade function and HIT, as well as the Dix-Hallpike maneuver and supine roll test were without pathological findings. No head-bending or lying-down nystagmus was noted. A complete neuro-otological workup including orthoptic evaluation, vestibular hot-/cold-water caloric testing, video-oculography, video HIT, hearing test, posturography, as well as cervical and ocular vestibular evoked myogenic potentials (c/oVEMPs) was conducted. A summary of the findings can be found in **Table 1**. Besides the aforementioned right-beating HSN, the only pathological finding was a 3-degree deviation of the subjective visual vertical (SVV) to the left.

Magnetic resonance imaging (MRI) including 1 mm slices of the brainstem and cerebellum, as well as a CISS (constructive interference in steady state) sequence was normal with no evidence of structural abnormalities of the vestibular organ or evidence of a vascular compression of the 8th cranial nerve. Laboratory workup, including complete blood count, renal and liver function tests, vitamin B1 and B6, as well as basic immunologic workup (antinuclear antibodies, antimitochondrial antibodies, antineutrophil cytoplasmic antibodies, rheumatoid factor, and cardiolipin antibodies), was normal with no evidence of a vitamin deficiency, autoimmune or infectious disease.

In 6 years of follow-up, episodes of HSN occurred every 3–12 months and lasted for 1–2 weeks. Documentation by the patient and the general practitioner revealed a right-beating HSN in the majority of episodes without other accompanying symptoms. Follow-up visits in our center revealed no SVV deviation, peripheral vestibular dysfunction or central neuro-orthoptic deficit, despite a slight vertical saccadic smooth pursuit (**Table 1**). In the attack-free interval, no HSN, SVV deviation, or other peripheral or central vestibular deficit (despite the above-mentioned vertical saccadic smooth pursuit) was detected. Several therapeutic trials, including physical therapy, exercise, regular magnesium intake (300 mg/d), and transient administration of the sodium channel blocker carbamazepine, had no effect on the recurrence of vertigo episodes.

A revision of cases with HSN at our center revealed eight additional patients since 2018 with very similar symptoms of

TABLE 1 | Summary of the findings of broad neuro-orthoptic and instrument-based examinations over a follow-up period of 6 years.

Time point			Initial presentation *(within episode)*	After 1 week *(out of episode)*	After 4 years *(out of episode)*	After 5 years *(within episode)*
Neuro-orthoptic examinations	Head-shaking nystagmus	Direction	Right-beating	None	None	Right-beating
		deg/sec	13			14
		Frequency (Hz)	3			3–4
	Positional maneuvers (Dix-Hallpike, supine roll test)		No nystagmus	No nystagmus	No nystagmus	No nystagmus
	Head impulse test right/left		Normal/normal	Normal/normal	Normal/normal	Normal/normal
	Visual acuity right/left		1.0/1.0	1.0/1.0	1.0/1.0	1.0/1.0
	Eye alignment	near	Orthophoria	Orthophoria	Orthophoria	Orthophoria
		distance	Orthophoria	Orthophoria	Orthophoria	Orthophoria
	Convergence		Normal	Normal	Normal	Normal
	Gaze-holding		Normal	Normal	Normal	Normal
	Optokinetic nystagmus		Normal	Normal	Normal	Normal
	Fixation suppression		Normal	Normal-	Normal-	Normal
	Hyperventilation		No nystagmus	No nystagmus	No nystagmus	No nystagmus
	Politzer balloon		No nystagmus	-	-	-
	Smooth pursuit	Horizontal	Smooth	Smooth	Smooth	Smooth
		Vertical	Smooth	Slightly saccadic	Slightly saccadic	Slightly saccadic
	Saccades		Metric	Metric	Metric	Metric
Instrument-based examinations	Video head impulse test gain	Right	0.84	-	0.95	0.88
		Left	0.94	-	0.90	0.91
	Subjective visual vertical deviation (hemispherical dome method)		3° to the left	None	None	None
	Eye fundus (Scanning laser ophthalmoscope)		No torsion	No torsion	No torsion	
	Caloric stimulation (deg/sec)	Left	10.9	-	13.8	14.6
		Right	11.5		15.0	12.4
	Audiometry		Normal hearing	-	Normal hearing	-
	Posturography		Normal sway pattern	-	-	-
	AC-cVEMPs and BC-oVEMPs		Normal	-	-	-

deg, degrees, sec, seconds, Hz, Hertz, AC-cVEMPs, Air -Conducted cervical Vestibular Evoked Myogenic Potentials, BC-oVEMPs, Bone-Conducted ocular Vestibular Evoked Myogenic Potentials.

isolated HSN, which could not be explained by any other peripheral or central vestibular disorder. These patients were 41 ± 14.5 years old. Men and women were equally represented.

DISCUSSION

We present a rare case of episodically occurring, isolated HSN in a young female patient, followed up over a period of 6 years. Besides the right-beating HSN and a slight transient SVV deviation to the left, no neurological, neuro-otological, or neuro-orthoptic deficits were found. The presentation was not consistent with another vestibular disorders (such as vestibular migraine, or vestibular paroxysmia).

HSN or pHSN are found in different peripheral and central vestibular disorders, but almost never occur without any other ocular motor signs at symptom onset or without any pathological findings in the peripheral or central vestibular system. HSN of suspected peripheral vestibular origin is most commonly present in vestibular neuritis, Menière disease (MD) and benign paroxysmal positional vertigo (especially of the horizontal semicircular canal) (8). Furthermore, HSN has been shown to be present in vestibular paroxysmia (11). In the case of peripheral HSN, the direction of the nystagmus beats in most cases toward the side of the unaffected vestibular organ (monophasic HSN) but may change direction over time (biphasic HSN), or more rarely beats toward the affected side first (reversed biphasic HSN) (8, 12, 13). In central disorders, HSN occurs less frequently and may also manifest as perverted HSN (pHSN) (2). The most frequent central causes of HSN are brainstem or cerebellar infarction and vestibular migraine (2, 14). Regarding cerebral stroke, lesions involving the nodulus, uvula, and inferior tonsil, as well as infarction of the lateral medulla have been shown

to cause HSN/pHSN (4, 9). The neural mechanisms underlying HSN in central disorders are widely unknown. One common hypothesis is that the nodulus and uvula play an important role in central vestibular velocity storage that becomes asymmetrical in the case of unilateral infarction of the nodulus/uvula or their projections to the brainstem (i.e., pons and medulla), resulting in ipsilesional HSN (4, 9, 15). pHSN is further explained by a cross-coupling between horizontal and vertical velocity storage pathways (5, 6). In vestibular migraine, where HSN or pHSN can be observed within or between attacks, amplification of a peripheral vestibular asymmetry by the central velocity storage mechanism is assumed (14).

In the present case, a peripheral cause for the episodic HSN can be broadly excluded, especially since in 6 years of follow up no peripheral deficit was ever noted in head impulse or caloric testing. Contrast-enhanced MRI showed no vestibular schwannoma. Furthermore, there was no evidence for a pathological irrigation of peripheral vestibular afferents (e.g., in the context of BPPV or vestibular paroxysmia). The long time constant of the HSN in our case is not compatible with a peripheral HSN type, as previous systematic investigations in patients with unilateral peripheral vestibulopathies revealed a maximum HSN time constant of 20 s (16). A few cases have previously been described with a peripheral syndrome labeled "head-jolting nystagmus", where rapid head-shaking induced horizontal nystagmus lasting up to 45 s (17, 18). The authors attributed the long-lasting nystagmus to dislodged material within the horizontal semicircular canal. In contrast to the present case the symptoms of these patients could be elicited continuously (not episodically), were suppressed by visual fixation (nystagmus lasted significantly shorter in light vs. dark) and showed evidence of peripheral vestibular dysfunction (e.g., by caloric hypofunction). Thus, "head-jolting nystagmus" seems an unlikely cause in the present case.

Regarding the central vestibular system, an MRI with 1 mm slices of the brainstem and cerebellum did not reveal any structural abnormalities, especially in the nodulus, uvula, medulla, and pons. Accordingly, neuro-orthoptic examination revealed no evidence for a focal central ocular motor disorder indicative of a structural lesion.

In 1979 Slater (19) suggested the term benign recurrent vertigo (BRV) for patients with recurrent vertigo attacks in the absence of any additional otological or neurological symptoms such as hearing loss or headache, and without evidence of peripheral or central vestibular deficits. Since then, there have been attempts to better classify these patients and evaluate possible causes (20–22), but the etiology broadly remains unknown. Most commonly, BRV is thought to be in the spectrum of migraine or MD, although only few patients with BRV have been shown to develop migraine or MD over time (20, 23, 24). One study found HSN in the attack-free period of about 10% of BRV patients and suggested a disorder characterized by recurrent spontaneous vertigo of unknown etiology and interictal head-shaking nystagmus (RSV-HSN) (10). In contrast to the patients described as RSV-HSV, in the present case study the patient only showed HSN during certain, recurring periods and not in the interictal interval. Furthermore, the patient presented here did not exhibit spontaneous vertigo attacks without any apparent trigger such as weather change, menstruation, certain foods, medication. Vertigo, which was only elicited by head-shaking, lasted as long as the HSN persisted, and only occurred in the ictal period. Therefore, we argue that our patient does not entirely fit the concept of BRV or RSV-HSV. To our knowledge, there are no similar cases described in literature. Based on the current case and a cohort of patients with similar clinical presentations, seen in our center, we suggest a distinct disorder characterized by an "acquired idiopathic head-shaking nystagmus" (aiHSN). Our experience shows that patients in the third and fourth decade of life are affected most by aiHSN. Due to the clinical and instrument-based findings, a peripheral cause can widely be excluded. Therefore, based on the nystagmus characteristics (long time constant) and the current literature on HSN/pHSN, we hypothesize that a recurrent functional asymmetry of the central velocity storage might be the most likely cause, despite a missing central structural lesion. The underlying etiology for this is unknown. From a theoretical perspective, the following possibilities may be considered: (1) Temporary decompensation of a slight (undetectable) peripheral vestibular deficit that under normal circumstances is fully centrally compensated. The temporary decompensation might be due to a transient imbalance of neurotransmitters at the level of the nodulus and uvula or vestibular nuclei. Factors leading to such a transient decompensation are only speculative (e.g., hormones). (2) Transient imbalance of the central velocity storage possibly also due to a neurotransmitter imbalance. Mechanisms leading to the imbalance might be related to migraine pathophysiology. (3) An undetectable central microlesion (e.g., at the vestibular nuclei, nodulus, cerebellar peduncles) that might lead to recurrent excitations. Overall, none of these theories can be supported sufficiently with evidence from the here presented cases. Even after extensive and repeated evaluation, there was no evidence of vestibular migraine, a central or peripheral vestibular lesion, or vestibular paroxysmia. From a therapeutic perspective, a specific treatment does not seem to be available. Nevertheless, we suggest habituation and balance exercises to suppress the vertigo sensation induced by HSN.

Future research on patients with aiHSN should focus on experimental testing of the central velocity storage function using established paradigms such as tilt-suppression of the post-rotatory nystagmus (25, 26).

DATA AVAILABILITY STATEMENT

The raw data supporting the conclusions of this article will be made available by the authors, without undue reservation.

ETHICS STATEMENT

Ethical review and approval was not required for the study on human participants in accordance with the local legislation and institutional requirements. The patients/participants provided their written informed consent to participate in this study. Written informed consent was obtained from the individual(s)

for the publication of any potentially identifiable images or data included in this article.

AUTHOR CONTRIBUTIONS

FF: patient treatment, acquisition and interpretation of data, and drafting the manuscript. AZ: interpretation of data and revising the manuscript. DH: patient treatment, acquisition and interpretation of data, and drafting the manuscript. All authors approved the final version of the manuscript.

SUPPLEMENTARY MATERIAL

The Supplementary Material for this article can be found online at: https://www.frontiersin.org/articles/10.3389/fneur.2022.897012/full#supplementary-material

REFERENCES

1. Takahashi S, Fetter M, Koenig E, Dichgans J. The clinical significance of head-shaking nystagmus in the dizzy patient. *Acta Otolaryngol.* (1990) 109:8–14. doi: 10.3109/00016489009107409
2. Yang TH, Lee JH, Oh SY, Kang JJ, Kim JS, Dieterich M. Clinical implications of head-shaking nystagmus in central and peripheral vestibular disorders: is perverted head-shaking nystagmus specific for central vestibular pathology? *Eur J Neurol.* (2020) 27:1296–303. doi: 10.1111/ene.14161
3. Fetter M, Zee DS, Koenig E, Dichgans J. Head-shaking nystagmus during vestibular compensation in humans and rhesus monkeys. *Acta Otolaryngol.* (1990) 110:175–81. doi: 10.3109/00016489009122534
4. Huh YE, Kim JS. Patterns of spontaneous and head-shaking nystagmus in cerebellar infarction: imaging correlations. *Brain.* 134:3662–3671. doi: 10.1093/brain/awr269
5. Kim H-A, Lee H, Sohn S-I, Kim JS, Baloh RW. Perverted head shaking nystagmus in focal pontine infarction. *J Neurol Sci.* (2011) 301:93–5. doi: 10.1016/j.jns.2010.11.009
6. Kim J, Ahn K, Moon S, Choi K, Park S, Koo J. Isolated perverted head-shaking nystagmus in focal cerebellar infarction. *Neurology.* (2005) 64:575–6. doi: 10.1212/01.WNL.0000150729.87682.79
7. Minagar A, Sheremata WA, Tusa RJ. Perverted head-shaking nystagmus: a possible mechanism. *Neurology.* (2001) 57:887–9. doi: 10.1212/WNL.57.5.887
8. Kim M-B, Huh SH, Ban JH. Diversity of head shaking nystagmus in peripheral vestibular disease. *Otol Neurotol.* (2012) 33:634–9. doi: 10.1097/MAO.0b013e31824950c7
9. Choi KD, Kim JS. Head-shaking nystagmus in central vestibulopathies. *Ann N Y Acad Sci.* (2009) 1164:338–43. doi: 10.1111/j.1749-6632.2008.03737.x
10. Lee S-U, Choi J-Y, Kim H-J, Kim J-S. Recurrent spontaneous vertigo with interictal headshaking nystagmus. *Neurology.* (2018) 90:e2135–e45. doi: 10.1212/WNL.0000000000005689
11. Hüfner K, Barresi D, Glaser M, Linn J, Adrion C, Mansmann U, et al. Vestibular paroxysmia: diagnostic features and medical treatment. *Neurology.* (2008) 71:1006–14. doi: 10.1212/01.wnl.0000326594.91291.f8
12. Spindler J, Schiff M. Variations of biphasic head shake response: physiology and clinical significance. *Clinical Testing of the Vestibular System*. Basel: Karger Publishers (1988). 95–103. doi: 10.1159/000416086
13. Lee YJ, Shin JE, Park MS, Kim JM, Na BR, Kim C-H, et al. Comprehensive analysis of head-shaking nystagmus in patients with vestibular neuritis. *Audiol Neurotol.* (2012) 17:228–34. doi: 10.1159/000336958
14. Beh SC, Masrour S, Smith SV, Friedman DI. The spectrum of vestibular migraine: clinical features, triggers, and examination findings. *Headache.* (2019) 59:727–40. doi: 10.1111/head.13484
15. Choi K-D, Oh S-Y, Park S-H, Kim J-H, Koo J-W, Kim J. Head-shaking nystagmus in lateral medullary infarction: patterns and possible mechanisms. *Neurology.* (2007) 68:1337–44. doi: 10.1212/01.wnl.0000260224.60943.c2
16. Kamei T, Takegoshi T, Matsuzaki M, A. Quantitative analysis of head-shaking nystagmus of peripheral vestibular origin. *Acta Otolaryngol.* (1995) 115:216–9. doi: 10.3109/00016489509125233
17. Bronstein AM, Kaski D, Cutfield N, Buckwell D, Banga R, Ray J, et al. Head-jolting nystagmus: occlusion of the horizontal semicircular canal induced by vigorous head shaking. *JAMA Otolaryngol Head Neck Surg.* (2015) 141:757–60. doi: 10.1001/jamaoto.2015.0711
18. Welgampola MS, Croxson GR, McGarvie LA, Halmagyi GM. Head-shaking nystagmus and vertigo cured by lateral semicircular canal occlusion. *J Neurol.* (2016) 263:588–90. doi: 10.1007/s00415-016-8027-1
19. Slater R. Benign recurrent vertigo. *J Neurol Neurosurg Psychiatry.* (1979) 42:363–7. doi: 10.1136/jnnp.42.4.363
20. Pan Q, Zhang Y, Zhang S, Wang W, Jiang H, Fan Y, et al. Clinical features and outcomes of benign recurrent vertigo: a longitudinal study. *Acta Neurol Scand.* (2020) 141:374–9. doi: 10.1111/ane.13214
21. Kentala E, Pyykkö I. Benign recurrent vertigo—true or artificial diagnosis? *Acta Otolaryngol.* (1997) 117:101–3. doi: 10.3109/00016489709124095
22. Oh AK, Lee H, Jen JC, Corona S, Jacobson KM, Baloh RW. Familial benign recurrent vertigo. *Am J Med Genet.* (2001) 100:287–91. doi: 10.1002/ajmg.1294
23. Lee HK, Ahn SK, Jeon SY, Kim JP, Park JJ, Hur DG, et al. Clinical characteristics and natural course of recurrent vestibulopathy: a long-term follow-up study. *Laryngoscope.* (2012) 122:883–6. doi: 10.1002/lary.23188
24. Van Leeuwen R, Bruintjes T. Recurrent vestibulopathy: natural course and prognostic factors. *J Laryngol Otol.* (2010) 124:19–22. doi: 10.1017/S0022215109991009
25. Hain T, Zee D, Maria B. Tilt suppression of vestibulo-ocular reflex in patients with cerebellar lesions. *Acta Otolaryngol.* (1988) 105:13–20. doi: 10.3109/00016488809119440
26. Lee S-U, Choi J-Y, Kim H-J, Park J-J, Zee DS, Kim J-S. Impaired tilt suppression of post-rotatory nystagmus and cross-coupled head-shaking nystagmus in cerebellar lesions: image mapping study. *Cerebellum.* (2017) 16:95–102. doi: 10.1007/s12311-016-0772-2

Conflict of Interest: The authors declare that the research was conducted in the absence of any commercial or financial relationships that could be construed as a potential conflict of interest.

Publisher's Note: All claims expressed in this article are solely those of the authors and do not necessarily represent those of their affiliated organizations, or those of the publisher, the editors and the reviewers. Any product that may be evaluated in this article, or claim that may be made by its manufacturer, is not guaranteed or endorsed by the publisher.

Copyright © 2022 Filippopulos, Zwergal and Huppert. This is an open-access article distributed under the terms of the Creative Commons Attribution License (CC BY). The use, distribution or reproduction in other forums is permitted, provided the original author(s) and the copyright owner(s) are credited and that the original publication in this journal is cited, in accordance with accepted academic practice. No use, distribution or reproduction is permitted which does not comply with these terms.

frontiers | Frontiers in Neurology

OPINION
published: 22 June 2022
doi: 10.3389/fneur.2022.955081

Commentary: Is There an "Acquired Idiopathic Head-Shaking Nystagmus?": A Discussion of Mechanisms and Clinical Implications Based on a Case Report

Sun-Uk Lee[1] *and Ji-Soo Kim*[2,3]*

[1] Department of Neurology, Korea University Medical Center, Seoul, South Korea, [2] Department of Neurology, Seoul National University College of Medicine, Seoul, South Korea, [3] Department of Neurology, Dizziness Center, Clinical Neuroscience Center, Seoul National University Bundang Hospital, Seongnam, South Korea

Keywords: vertigo, nystagmus, benign recurrent vertigo, head-shaking nystagmus, dizziness

OPEN ACCESS

Edited by:
Sun-Young Oh,
Jeonbuk National University,
South Korea

Reviewed by:
Michael C. Schubert,
Johns Hopkins University,
United States

Correspondence:
Ji-Soo Kim
jisookim@snu.ac.kr

Specialty section:
This article was submitted to Neuro-Otology, a section of the journal Frontiers in Neurology

Received: *28 May 2022*
Accepted: *03 June 2022*
Published: *22 June 2022*

Citation:
Lee S-U and Kim J-S (2022) Commentary: Is There an "Acquired Idiopathic Head-Shaking Nystagmus?": A Discussion of Mechanisms and Clinical Implications Based on a Case Report. Front. Neurol. 13:955081. doi: 10.3389/fneur.2022.955081

We read the article by Filippopulos and his colleagues with great interest (1). This report described a patient with recurrent episodes of vertigo prompted by fast head movement (1). The vertigo was accompanied by a severe right-beating head-shaking nystagmus (HSN) with an increased time constant of 60 s. Despite scrutinized neurotologic and radiologic evaluation, there was no evidence of peripheral or central vestibulopathy, except prominent HSN. The patient had no prior history or subsequent development of any associated symptoms during the 6 years of follow-up, which may exclude the diagnosis of vestibular migraine, Meniere's disease, or vestibular paroxysmia. The authors insisted that this patient represents a distinct clinical entity with an unstable velocity storage mechanism (VSM), thereby assigning a new disorder termed "acquired idiopathic head-shaking nystagmus" (aiHSN).

As the authors noted, we previously reported a group of patients with recurrent spontaneous vertigo with interictal HSN (BRV-HSN) in the absence of peripheral vestibulopathy as was documented by caloric, head-impulse, or rotatory chair tests. Even though we could not assess HSN in those patients with BRV-HSN during the attacks, the only difference between the BRV-HSN and aiHSN appears to be the absent HSN between the attacks in aiHSN. Given the (1) increased time constants of the HSN and rotatory nystagmus, (2) emergence of the HSN even with a short duration of head-shaking, and (3) good responses to baclofen, we proposed that unstable and asymmetric VSM may be the cause for vertigo and BRV-HSN (2). Apparently, the characteristics of HSN observed in the patient reported by Filippopulos et al. (1) do not seem to differ from those observed in our patients with BRV-HSN. Thus, the BRV-HSN and aiHSN may lie on the same spectral line due to a common pathomechanism (unstable and asymmetric VSM), rather than distinct disease entities. In addition, the clinical presentation does not escape from the umbrella term of BRV.

AUTHOR CONTRIBUTIONS

S-UL analyzed and interpreted the data and wrote the manuscript. J-SK designed and conceptualized the study, interpreted the data, and revised the manuscript. Both authors contributed to the article and approved the submitted version.

FUNDING

This study was supported by the Korea Health Technology R&D Project through the Korea Health Industry Development Institute (KHIDI), funded by the Ministry of Health and Welfare (HI14C3477), and the Basic Science Research Program through the National Research Foundation of Korea (NRF) funded by the Ministry of Education, Science and Technology (no. NRF-2016R1D1A1B04935568).

REFERENCES

1. Filippopulos F, Zwergal A, Huppert D. Is there an "acquired idiopathic head-shaking nystagmus"?-A discussion of mechanisms and clinical implications based on a case report. *Front Neurol.* (2022) 13:897012. doi: 10.3389/fneur.2022.897012
2. Lee SU, Choi JY, Kim HJ, Kim JS. Recurrent spontaneous vertigo with interictal headshaking nystagmus. *Neurology.* (2018) 90:e2135–45. doi: 10.1212/WNL.0000000000005689

Conflict of Interest: J-SK serves as an Associate Editor of Frontiers in Neuro-Otology and on the editorial boards of the Journal of Clinical Neurology, Frontiers in Neuro-Ophthalmology, Journal of Neuro-Ophthalmology, Journal of Vestibular Research, Medicine, and Clinical and Translational Neuroscience.

The remaining author declares that the research was conducted in the absence of any commercial or financial relationships that could be construed as a potential conflict of interest.

Publisher's Note: All claims expressed in this article are solely those of the authors and do not necessarily represent those of their affiliated organizations, or those of the publisher, the editors and the reviewers. Any product that may be evaluated in this article, or claim that may be made by its manufacturer, is not guaranteed or endorsed by the publisher.

Copyright © 2022 Lee and Kim. This is an open-access article distributed under the terms of the Creative Commons Attribution License (CC BY). The use, distribution or reproduction in other forums is permitted, provided the original author(s) and the copyright owner(s) are credited and that the original publication in this journal is cited, in accordance with accepted academic practice. No use, distribution or reproduction is permitted which does not comply with these terms.

frontiers | Frontiers in Neurology

ORIGINAL RESEARCH
published: 24 May 2022
doi: 10.3389/fneur.2022.880714

Comparison of Clinical Balance and Visual Dependence Tests in Patients With Chronic Dizziness With and Without Persistent Postural-Perceptual Dizziness: A Cross-Sectional Study

Charlotte De Vestel[1,2]*, *Willem De Hertogh*[1,2], *Vincent Van Rompaey*[3,4] and *Luc Vereeck*[1,2]

[1] Department of Rehabilitation Sciences and Physiotherapy/Movant, Faculty of Medicine and Health Sciences, University of Antwerp, Antwerp, Belgium, [2] Multidisciplinary Motor Centre Antwerp (M2OCEAN), Antwerp University Hospital, Antwerp, Belgium, [3] Department of Otorhinolaryngology and Head & Neck Surgery, Antwerp University Hospital, Antwerp, Belgium, [4] Department of Translational Neurosciences, Faculty of Medicine and Health Sciences, University of Antwerp, Antwerp, Belgium

OPEN ACCESS

Edited by:
Jeffrey P. Staab,
Mayo Clinic, United States

Reviewed by:
Arata Horii,
Niigata University, Japan
Mark Gregory Carpenter,
University of British Columbia, Canada

***Correspondence:**
Charlotte De Vestel
charlotte.devestel@uantwerpen.be

Specialty section:
This article was submitted to Neuro-Otology, a section of the journal Frontiers in Neurology

Received: 21 February 2022
Accepted: 19 April 2022
Published: 24 May 2022

Citation:
De Vestel C, De Hertogh W, Van Rompaey V and Vereeck L (2022) Comparison of Clinical Balance and Visual Dependence Tests in Patients With Chronic Dizziness With and Without Persistent Postural-Perceptual Dizziness: A Cross-Sectional Study. Front. Neurol. 13:880714. doi: 10.3389/fneur.2022.880714

Background: The diagnosis of persistent postural-perceptual dizziness (PPPD) is primarily based on medical history taking. Research on the value of clinical balance and visual dependence tests in identifying PPPD is scarce.

Objectives: (1) to contrast clinical balance and visual dependence tests between PPPD patients, dizzy non-PPPD patients, and healthy persons; and (2) to evaluate whether these clinical tests can help to identify PPPD in patients with chronic dizziness.

Methods: Consecutive patients with chronic dizziness (38 PPPD and 21 non-PPPD) and 69 healthy persons underwent Static Balance tests, the Timed Up and Go test, the Tandem Gait test, and the Functional Gait Assessment (FGA). Visual dependence tests included the Visual Vertigo Analog Scale (VVAS), the Rod-and-Disc test (RDT), and postural sway while facing rotating dots. Groups were compared using ANOVA with *post-hoc* Tukey, or independent samples *t*-tests. The value of the clinical tests for PPPD identification was evaluated through logistic regression and Partial Least Squares Discriminant (PLS-DA) analyses.

Results: PPPD patients had significantly higher VVAS scores than dizzy non-PPPD patients ($p = 0.006$). Facing rotating dots, PPPD and dizzy non-PPPD patients had increased postural sway compared to healthy persons (PPPD vs. healthy: center of pressure (COP) velocity $p < 0.001$, and COP area $p < 0.001$; but non-PPPD vs. healthy: COP velocity $p = 0.116$ and COP area $p = 0.207$). PPPD patients had no significantly increased postural sway compared to dizzy non-PPPD patients. PPPD and dizzy non-PPPD patients also scored significantly worse on balance tests compared to healthy persons (PPPD vs. healthy: for all balance tests $p < 0.001$; non-PPPD vs. healthy: FGA $p < 0.001$, for all other tests $p < 0.05$). Differences were insignificant in balance scores between PPPD and dizzy non-PPPD patients, or in RDT scores between the three study groups. In patients with chronic dizziness, a higher VVAS score was most associated with

PPPD [odds ratio 1.04; 95% CI (1.01; 1.07); $p = 0.010$]. The cross-validated (CV) PLS-DA model with all clinical tests included, had fair discriminative ability (CVerror = 47%).

Conclusion: PPPD patients were more visually dependent, but did not have worse postural balance compared to dizzy non-PPPD patients. Elevated VVAS scores characterized PPPD most in patients with chronic dizziness.

Keywords: persistent postural-perceptual dizziness, chronic dizziness, vestibular diseases, balance, visual dependence

INTRODUCTION

With a prevalence of up to 20%, persistent postural-perceptual dizziness (PPPD) is among the top five most common causes of vestibular complaints reported in tertiary care hospitals (1–3). PPPD is designated by the Bárány Society as a separate vestibular disorder and an umbrella term for four subtypes: Phobic Postural Vertigo, Space-Motion Discomfort, Visual Vertigo, and Chronic Subjective Dizziness (4).

Patients with PPPD clinically present with non-rotatory vertigo and postural imbalance, which are present almost on a daily basis. The symptoms are worsened by upright posture, active or passive movements, and visual stimuli (4). Visual stimulation is the most characteristic aggravating factor for PPPD (5).

The pathophysiological mechanism of PPPD and its four subtypes is still uncertain (6). It is thought to result from maladaptation to a condition that caused vestibular symptoms (e.g., a peripheral or central vestibular disorder, vestibular migraine, or psychogenic dizziness) (6). Previous research identified altered functional brain connectivity (7, 8): i.e. reduced between the (pre)cuneus and the premotor cortex (8), and increased in the visual cortices (9). The former impairs the regulation of body posture and movement (10, 11), while the latter leads to increased visual dependence (12). Excessive reliance on visual information often causes dizziness and/or postural instability in visually disturbing situations (13).

The diagnosis of PPPD is currently primarily based on medical history taking (4). The often vague symptoms in patients with chronic dizziness tend to correlate weakly with the results of standard vestibular tests, making diagnosis difficult (14).

Several clinical tests exist in the literature that allow for evaluation of postural balance and visual dependence in patients with a vestibular disorder (13, 15). However, it is not yet clear whether these clinical tests can be used for identifying PPPD in patients with chronic dizziness.

The aim of this study was 2 fold: (1) to contrast clinical balance and visual dependence tests between PPPD patients, dizzy non-PPPD patients, and healthy persons; and (2) to evaluate whether these clinical tests can help to identify PPPD in patients with chronic dizziness.

MATERIALS AND METHODS

Design and Setting

This study is a cross-sectional study consisting of consecutive patients enrolled between March 2019 and July 2020, either at the Department of Otolaryngology of the Antwerp University Hospital or in one of the two participating general hospitals (AZ Klina, Brasschaat and AZ Sint-Jozef, Malle). The control group consisted of healthy persons from the direct (employees) or indirect environment (family and friends) of the MOVANT research team. The study was performed in the M2OCEAN laboratory (Multidisciplinary Motor Centre Antwerp) of the Antwerp University Hospital.

The study report is drafted conform the "Strengthening the Reporting of Observational studies in Epidemiology (STROBE)" guidelines for cross-sectional studies (16).

Ethical Considerations

Ethical approval was obtained from the Medical Ethics Committees of the Antwerp University Hospital (reference number 18/586).

Participants

Patients' eligibility was assessed by an Ear-Nose-Throat (ENT) specialist through medical history taking [using the SO STONED method (17)], and through a micro-otoscopic, a vestibular (including video head impulse, sinusoidal harmonic acceleration, and binaural bithermal caloric testing) and an audiometric assessment. The inclusion criteria were: (1) speaking the Dutch language; (2) being at least 18 years old; and (3) suffering of chronic non-rotatory vertigo and/or unsteadiness for at least 15 days per month for a minimum of 3 months. The exclusion criteria were: (1) presence of an acute vestibular disorder; (2) balance problems not due to dizziness (e.g., neurological, orthopedic, or other medical conditions); (3) dizziness due to untreated metabolic or cardiac disease, hormonal disturbances, vasovagal syncope, hyperventilation, acute mental problems, or substance abuse; and (4) severe visual impairment, not correctable by e.g., wearing glasses.

Eligibility of healthy persons was verified by the researcher. Their inclusion criteria were (1) speaking the Dutch language; and (2) being at least 18 years old. The exclusion criteria were: (1) history of or currently suffering from rotatory vertigo; (2) frequent episodes of non-rotatory vertigo (more than one episode in 3 months); (3) balance problems; and (4) severe visual impairment, not correctable by e.g., wearing glasses.

Diagnosis of PPPD

A patient was diagnosed with PPPD if he or she met all five diagnostic criteria for PPPD as established by the Committee for Classification of Vestibular Disorders of the Bárány Society (4). These are: (1) presence of chronic ($\geq$ 3 months) non-spinning

(rotatory) vertigo, dizziness or unsteadiness; (2) symptoms are aggravated by an upright position, active/passive body movements, and visual stimuli; (3) prior presence of a condition that caused dizziness or instability; (4) symptoms have a major impact on patients' mental or physical functioning; and (5) symptoms cannot be explained by another existing condition.

Outcome Variables

Descriptive Variables

Age (years), gender, dizziness duration (years), and *ENT diagnosis* were collected from the electronic patient record.

The *Dizziness Handicap Inventory (DHI)* evaluates the physical, functional and emotional handicap experienced by patients as a result of their vestibular symptoms. For 25 statements, patients were asked to indicate the extent to which they applied to them ("no" = 0; "sometimes" = 2; "yes" = 4 points). The total DHI score was recorded, ranging from 0 (no impairment) to 100 (maximal impairment) (18, 19).

The *Hospital Anxiety and Depression Scale (HADS)* evaluates patients' emotional state by means of 7 anxiety-related (HADS-A) and 7 depression-related (HADS-D) questions answered on a 4-level ordinal scale. The total HADS-A and HADS-D scores, both ranging from 0 (no anxiety/depression) to 21 (maximal anxiety/depression), were retained (20).

The *Subjective Visual Vertical (SVV) test* measures patients' perception of verticality in the absence of visual reference points. The experimental setup is shown in **Figure 1**. The patient was asked to reposition a red line (6 cm length) on a black background until they felt it matched the true vertical. This was done using a handheld remote control and without moving the head or body. The test was done twice with the line initially tilted 20 degrees to the left, and twice with the line tilted 20 degrees to the right. More information on the test conditions can be found in the (**Supplementary Table 1**). Performance was expressed as the mean absolute misalignment (in degrees) with the gravitational vertical (0°) for these four tests.

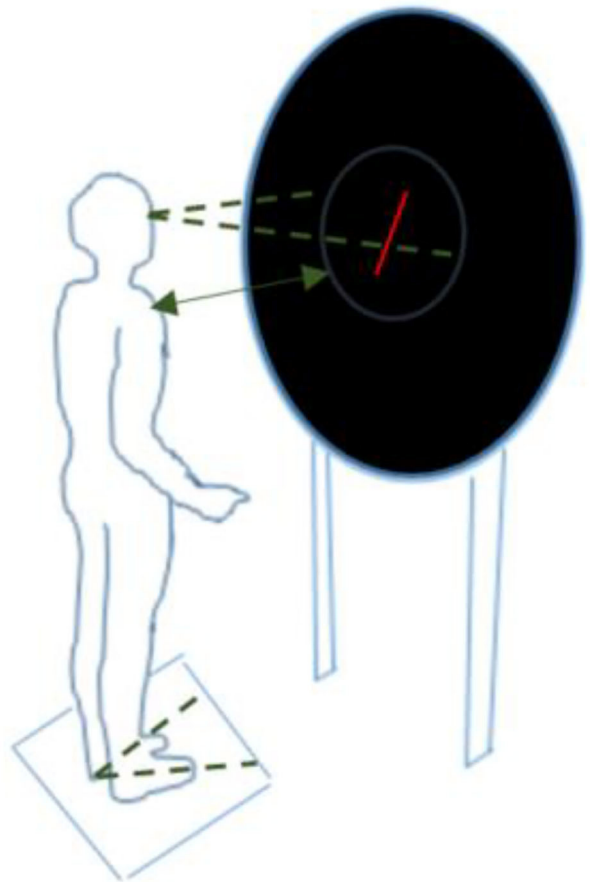

FIGURE 1 | Experimental setup for the Subjective Visual Vertical test, Rod-and-Disc test, and postural sway while facing rotating dots (screen display varied depending on the test condition) [a,b]. [a]The participant stood upright, barefoot, with arms alongside the body, in a completely dark room. A television screen was placed at eye level at a distance of 40 cm, providing an almost full-field stimulus of 80%. A ring with an inner diameter of 54.5 was mounted on the television set to prevent the edges of the television screen from acting as a frame of reference. [b]The feet were placed at an angle of 20 degrees with the inner malleoli 10 cm apart.

Clinical Balance Variables

The *Static Balance tests* measures the patients' balance while they were standing still and upright in four different foot positions with eyes closed: (1) feet together, combined with Jendrassik maneuver (i.e., fingers were interlocked with arms in abduction, and tension was created by pulling the hands apart); (2) feet 5 cm apart standing on a foam plate (NeuroCom International Inc., Clackamas, USA; 60 kg/cm^3 medium density; 45 × 45 × 12 cm), combined with Jendrassik maneuver (i.e., the same hand grip as described above); (3) heel-to-toe tandem stance; and (4) standing on one leg. For each condition, the patient had three attempts to maintain the respective condition 30 s. Only the best score (in seconds) out of these three attempts was retained. The sum of these best scores for each of the four conditions constitutes the total static balance score, which ranges from 0 (markedly reduced balance) to 120 (excellent balance) (15).

The *Timed Up and Go test* evaluates how quickly a person can get up from a chair, walk 3 m, turn around, walk back and sit back down on the chair. The fastest performance time (in seconds) of three attempts was retained (15).

The *Tandem Gait test* measures the number of correctly performed steps when walking heel-to-toe on a straight line. The highest number of steps of three attempts was retained. The maximal score was 20 steps (15).

The *Functional Gait Assessment (FGA)* evaluates balance control during ten different walking tasks (e.g., walking fast, or walking with head movements). The total FGA score ranges between 0 (markedly reduced balance) and 30 (normal balance) (21).

Clinical Visual Dependence Variables

The *Visual Vertigo Analog Scale (VVAS)* is a questionnaire consisting of nine statements describing different situations in daily life where disturbing visual stimuli are present (e.g., supermarket, or traffic at a busy intersection). For each statement, patients were asked to mark the extent to which they experienced dizziness on a 10 cm visual analog scale. If a situation was not

applicable for the patient, it was not marked and not included in the final score. The total VVAS score is the sum of the marks for each relevant situation, rescaled to a percentage where 100% indicates maximal visually induced dizziness (22).

The *Rod-and-Disc test (RDT)* measures the influence of visual disturbance on the perception of verticality. The experimental setup and the four test conditions were the same as for the SVV test, but for the RDT each test had to be performed twice with dots rotating clockwise (CW) and twice with dots rotating counter-clockwise (CCW) on the black screen. More information on the test conditions can be found as **Supplementary Table 1**. The mean misalignment for the SVV test was used as baseline and subtracted from the differences in misalignment with the gravitational vertical (0°) for each of the CW and CCW rotating dots tests. These adjusted differences were then averaged out (after inverting the sign of the data for the CCW rotating dots, as the directions were mirrored), resulting in an indication of the overall impact of visual disturbance on the perception of verticality. A positive value means that the patient placed the line more in the direction of the rotating dots compared to the SVV, a negative value more opposite to the direction of the rotating dots.

Preliminary analyses showed that the Rod-and-Frame test-which was equivalent to the RDT, except that the dots were replaced by a frame tilted left or right-yielded less pronounced results than the RDT, and is therefore not retained for discussion. The test conditions and data are available as **Supplementary Tables 2**, **3**.

Postural sway while facing rotating dots was evaluated by measuring the displacement of patients' center of pressure (COP) first while looking at a black screen, and then during exposure to dots rotating CW and dots rotating CCW. The experimental setup differed from the SVV and RDT that no line was shown in any of the three tests, and that the patient stood on a force plate (AMTI type OR 6; 1,000 fps, 46 × 50 × 8 cm). More information on the test conditions can be found as **Supplementary Table 1**. Postural sway parameters for COP lean, COP velocity, and COP area were computed. The degree of visual dependence was calculated by subtracting the baseline value (black screen condition) from the values obtained during the CW and CCW rotating dots tests. More information is provided in **Table 1**.

Preliminary analyses showed that the postural sway while facing a tilted frame–which was equivalent to the postural sway while facing rotating dots, except that the dots were replaced by a frame tilted left or right-yielded less pronounced postural sway results compared to the rotating dots conditions, and are therefore not retained for discussion. The test conditions and data are available as **Supplementary Tables 2**, **3**.

TABLE 1 | Parameters of the postural sway while facing rotating dots[a].

Postural sway parameters	Description
COP lean (mediolateral; mm)	Average deviation of the COP in mediolateral direction in relation to the starting position. Data were reversed for CCW rotating dots to average the data for CW and CCW rotating dots, resulting in an indication of the overall impact of visual disturbance on the COP lean. A positive value means that the body leaned in the direction of the rotating dots, a negative value indicates leaning in the opposite direction.
COP velocity (mediolateral; mm/s)	Average velocity of the COP in mediolateral direction. A positive value means that the COP velocity was larger during the rotating dots conditions compared to the baseline condition (black screen), while a negative value means the opposite.
COP area (mm^2)	Ellipse that contains 85% of the COP data. A positive value means that the COP area was larger during the rotating dots conditions compared to the baseline condition (black screen), while a negative value means the opposite.

[a]*COP, center of pressure; mm, millimeters; s, seconds.*

Data Sources and Measurement

The researcher is an accredited physiotherapist (Master's degree). The study took 2.5 h per participant, using the following strict assessment order: first the questionnaires, then the clinical balance tests, and finally the visual dependence tests. The visual dependence tests (except the VVAS) were performed in a different randomized order for every participant to avoid a habituation effect on the results. Breaks were allowed between and during the different tests. The next test was only started when the dizziness symptoms had returned to participant's baseline level. The data were collected pseudonymised in an IBM SPSS Statistics data file stored on a secure server of the University of Antwerp.

Blinding

During data collection, the researcher was blinded to the ENT diagnosis of each patient. Blinding to whether a participant was a patient or healthy person was not possible, as the healthy persons were recruited from the environment of the research team.

Statistical Analyses

Descriptive statistics included means and standard deviations for quantitative variables, and frequencies and percentages for categorical variables. Shapiro-Wilk tests indicated whether quantitative variables were normally distributed (23).

Inter-group comparison of quantitative variables was carried out through one-way analysis of variance (ANOVA), using a Bonferroni-corrected significance level of $p < 0.006$ accounting for 9 comparisons, followed by *post-hoc* analysis with Tukey correction for multiple testing. For inter-group comparison of the categorical variables, chi-square ($\chi 2$) tests were used. Two-group comparison of dizziness-related variables was carried out through independent samples *t*-tests.

Univariable logistic regression and Partial Least Squares Discriminant Analysis (PLS-DA) models were fitted to determine the predictors of PPPD in patients with chronic dizziness. The relation between the clinical tests and PPPD was expressed as odds ratios [95% confidence interval (CI)], area under the receiver operating characteristic curve (AUC), and optimal cut-off with corresponding sensitivity and specificity (according to maximization of the Youden index). For the PLS-DA model, the potential of each of the clinical tests to discriminate between PPPD and dizzy non-PPPD patients was evaluated through their

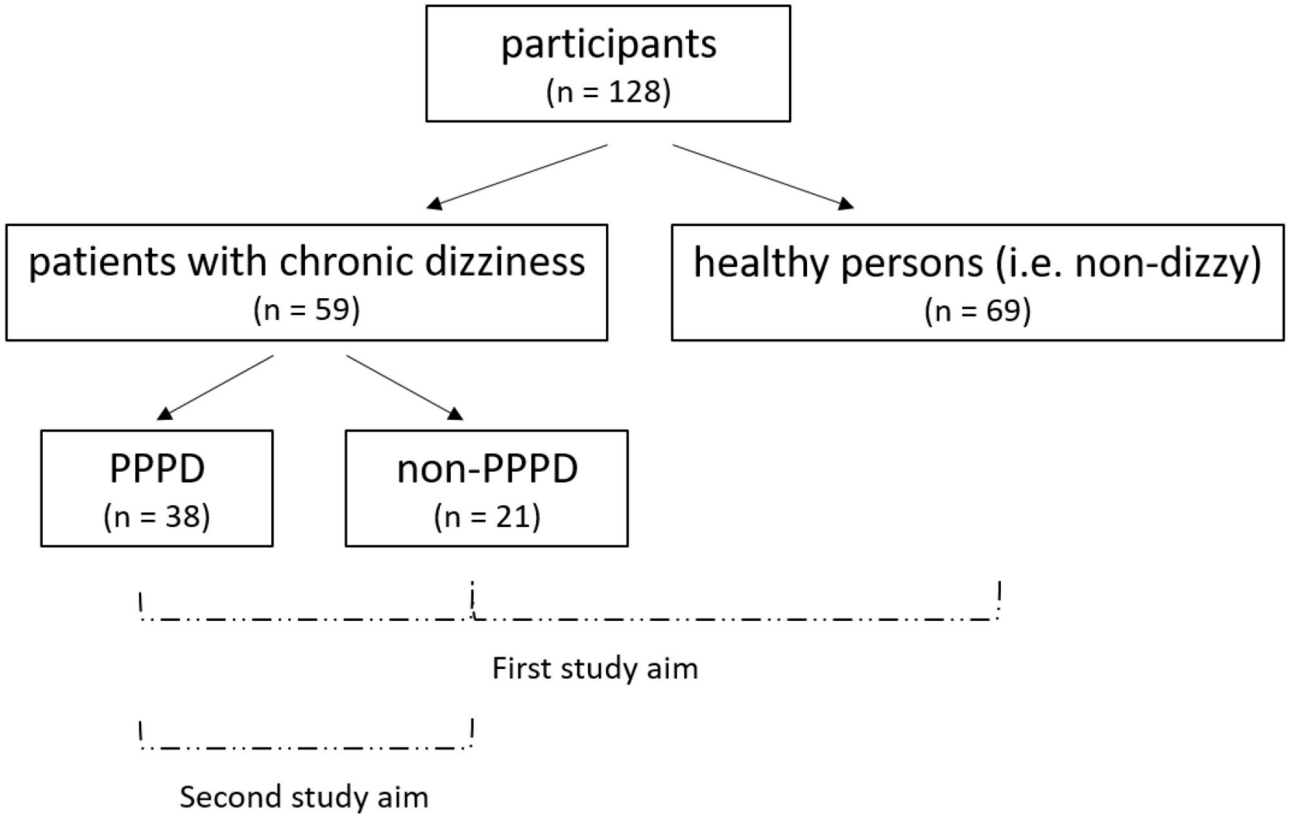

FIGURE 2 | Overview of the recruited samples and study aims[a]. First study aim: comparison of the clinical balance and visual dependence tests between PPPD patients, dizzy non-PPPD patients, and healthy persons. Second study aim: evaluation whether these clinical tests can help to identify PPPD in patients with chronic dizziness. [a]PPPD, persistent postural-perceptual dizziness.

loading values. The overall discriminative value of the PLS-DA model was 5-fold cross-validated (CV) (24). In brief, for each fold we included 80% of the observations in the training set and 20% in the validation set. The training set was used to fit the PLS-DA models, with the number of components ranging from 2 to 10. Subsequently, these models predicted the outcome from the observations in the validation set, and the percentage of error (CVerror) was registered. This was carried out in 5-fold, with each individual observation belonging to the validation set exactly one time. The 5-fold CV was repeated 500 times to obtain the standard error of the CVerror.

Significance was set at $p < 0.05$, unless otherwise stated. Statistical analyses were performed using the SPSS software version 27.0 (25). The PLS-DA was fitted with the R software (26).

RESULTS

Participants

Seventy patients with chronic dizziness met the predefined study eligibility criteria as listed in the method section. Nine patients decided not to participate because of reduction of dizziness complaints with medication and/or physical therapy (2 patients), personal reasons (3 patients), or COVID outbreak (4 patients). The results of two other patients had to be excluded after the study because of unreliable test results due to disturbing background noise near the laboratory during the testing.

Of the 59 patients (mean age 57.34 ± 12.96) that successfully participated, 38 were diagnosed with PPPD. The 21 patients without PPPD were primarily diagnosed with vestibular hypofunction (4 patients), bilateral vestibulopathy (1 patient), proprioceptive cervicogenic dizziness (8 patients), multiple sensory deficits (3 patients), and mal de débarquement syndrome (1 patient). In four patients no cause could be found.

The control group consisted of 69 healthy non-dizzy persons (mean age 51.71 ± 17.24).

An overview of the recruited samples and the study aims are shown in **Figure 2**.

Sample Characteristics

Gender numbers ($p = 0.453$) were not significantly different between the three study groups.

All patients with chronic dizziness had significantly higher HADS-A (PPPD vs. healthy, $p < 0.001$; dizzy non-PPPD vs. healthy, $p = 0.020$) and HADS-D scores (PPPD vs. healthy, $p < 0.001$; dizzy non-PPPD vs. healthy, $p < 0.001$) compared to healthy persons. PPPD patients had significantly higher

TABLE 2 | Results on descriptive variables of the included participants [a,b].

Measurement tool (unit)	Mean ± SD or number (%)			Statistical analyses (*p*-values)			
	Chronic dizziness		Healthy (*n* = 69)	3-group comparison	With PPPD vs. without PPPD	With PPPD vs. healthy	Without PPPD vs. healthy
	With PPPD (*n* = 38)	Without PPPD (*n* = 21)					
Age (years)	55.18 ± 12.31	61.23 ± 13.49	51.71 ± 17.24	**0.045**[†*]	0.320	0.503	**0.037**[¶*]
Female	24 (63.2)	10 (47.6)	34 (49.3)	0.453[§]			
Dizziness duration (years)	7.84 ± 6.50	3.91 ± 3.24	N/A		**0.003**[‡*]		
DHI (0–100)	46.32 ± 18.18	36.95 ± 18.59	N/A		0.065[‡]		
$HADS_{anxiety}$ (0–21)	7.21 ± 3.89	5.86 ± 4.00	3.32 ± 2.25	**<0.001**[†**]	0.308[¶]	**<0.001**[¶**]	**0.020**[¶*]
$HADS_{depression}$ (0–21)	5.68 ± 3.43	5.67 ± 3.62	1.57 ± 1.63	**<0.001**[†**]	1.000[¶]	**<0.001**[¶**]	**<0.001**[¶**]
SVV (°)	1.73 ± 1.17	1.38 ± 0.90	1.18 ± 0.84	**0.022**[†*]	0.406 [¶]	**0.016**[¶*]	0.707[¶]

[a]*ANOVA test (†), Independent samples t-test (‡), Chi-squared test (§), post-hoc analysis with Tukey correction (¶).*
ANOVA: p < 0.05 (*) and p < 0.001 (**).
[b] *°, degrees; DHI, Dizziness Handicap Inventory; HADS, Hospital Anxiety and Depression Scale; PPPD, persistent postural-perceptual dizziness; SD, standard deviation; SVV, Subjective Visual Vertical; vs, versus.*

TABLE 3 | Results on clinical balance tests of the included participants [a,b].

Measurement tool (unit)	Mean ± SD			Statistical analyses (*p*-values)			
	Chronic dizziness		Healthy (*n* = 69)	3-group comparison	With PPPD vs. without PPPD	With PPPD vs. healthy	Without PPPD vs. healthy
	With PPPD (*n* = 38)	Without PPPD (*n* = 21)					
Static balance test (0–120 s)	64.22 ± 33.07	70.32 ± 27.09	93.30 ± 22.49	**<0.001**[†**]	0.680[¶]	**<0.001**[¶***]	**0.002**[¶*]
Timed Up and Go test (s)	8.07 ± 2.70	7.78 ± 2.57	6.34 ± 1.13	**<0.001**[†**]	0.846[¶]	**<0.001**[¶***]	**0.012**[¶*]
Tandem gait (# steps)	13.47 ± 7.95	13.95 ± 8.23	18.84 ± 3.60	**<0.001**[†**]	0.954[¶]	**<0.001**[¶***]	**0.004**[¶*]
FGA (0–30)	23.24 ± 4.38	23.81 ± 5.17	28.25± 1.82	**<0.001**[†**]	0.813[¶]	**<0.001**[¶***]	**<0.001**[¶***]

[a]*ANOVA test (†), post-hoc analysis with Tukey correction (¶).*
ANOVA Bonferroni cut-off: p < 0.006 (**); other tests: p < 0.05 (*) and p < 0.001 (***).
[b] *#, amount; FGA, Functional Gait Assessment; PPPD, persistent postural-perceptual dizziness; SD, standard deviation; TUG, Timed Up and Go test; vs, versus.*

SVV scores ($p = 0.016$) and dizzy non-PPPD patients were significantly older ($p = 0.037$), both compared to healthy persons.

PPPD patients had significantly higher duration of dizziness complaints ($p = 0.003$), but not significantly higher DHI ($p = 0.065$), HADS (HADS-A, $p = 0.308$; HADS-D, $p = 1.00$) and SVV scores ($p = 0.406$), compared to dizzy non-PPPD patients.

Data are provided in **Table 2**.

Comparison of the Clinical Balance Tests Between PPPD Patients, Dizzy Non-PPPD Patients, and Healthy Persons

All patients with chronic dizziness had significantly worse static (PPPD vs. healthy, $p < 0.001$; dizzy non-PPPD vs. healthy, $p = 0.002$) and dynamic balance scores (Timed Up and Go, Tandem Gait, and FGA, PPPD vs. healthy, $p < 0.001$; dizzy non-PPPD vs. healthy, $p < 0.05$) compared to healthy persons.

Between PPPD and dizzy non-PPPD patients, no significant differences were found in either static ($p = 0.680$) or dynamic balance scores (Timed Up and Go, $p = 0.846$; Tandem Gait, $p = 0.954$; and FGA, $p = 0.813$).

Data are provided in **Table 3**.

Comparison of the Clinical Visual Dependence Tests Between PPPD Patients, Dizzy Non-PPPD Patients, and Healthy Persons

There was no significant difference in RDT results ($p = 0.431$) between the three study groups. The RDT values were positive in all three groups, indicating that in all cases the perceived vertical had an larger offset in the same direction of the rotation of the dots compared to the SVV tests. The COP lean results ($p = 0.800$) were not significantly different between the three study groups either. The COP lean values were small (≤ 1 mm), indicating that the visual disturbance did not cause the participant to tilt more to one side.

Patients suffering from chronic dizziness had larger COP velocity values (PPPD vs. healthy, $p < 0.001$; dizzy non-PPPD vs. healthy, $p = 0.116$) compared to healthy persons.

TABLE 4 | Results on clinical visual dependence tests of the included participants [a,b].

Measurement tool (unit)	Mean ± SD			Statistical analyses (*p*-values)			
	Chronic dizziness		Healthy (*n* = 69)	3-group comparison	With PPPD vs. without PPPD	With PPPD vs. healthy	Without PPPD vs. healthy
	With PPPD (*n* = 38)	Without PPPD (*n* = 21)					
VVAS (0–100%)	33.87 ± 20.65	18.13 ± 20.08	N/A		**0.006**[‡*]		
RDT (degrees)	6.05 ± 3.96	6.09 ± 3.80	5.07 ± 4.21	0.431[†]			
Postural sway analysis with rotating dots							
COP lean (mm)	−0.05 ± 10.92	−0.32 ± 6.28	−1.01 ± 4.95	0.800[†]	0.475[¶]	**<0.001**[¶***]	0.116[¶]
COP velocity (mm/s)	11.04 ± 15.32	7.68 ± 11.75	2.36 ± 5.12	**<0.001**[†**]	0.116[¶]	**<0.001**[¶***]	0.207[¶]
COP area (mm^2)	648.44 ± 1009.44	302.91 ± 648.15	31.38 ± 132.36	**<0.001**[†**]			

[a]*ANOVA test (†), Independent samples t-test (‡), post-hoc analysis with Tukey correction (¶).*
ANOVA Bonferroni cut-off: p<0.006 (**); other tests: p<0.05 (*) and p<0.001 (***).
[b]*COP, center of pressure; mm, millimeters; PPPD, persistent postural-perceptual dizziness; RDT, Rod-and-Disc test; s, seconds; SD, standard deviation; vs, versus; VVAS, Visual Vertigo Analog Scale.*

TABLE 5 | Univariable logistic regression of the clinical tests for the prediction of PPPD in patients with chronic dizziness [a,b].

Measurement tools	Estimate	Standard error	OR (95% CI)	*p*-value
Static Balance tests (0–120 s)	−0.007	0.009	0.99 [0.98; 1.01]	0.467
Timed Up and Go test (s)	0.045	0.109	1.05 [0.85; 1.29]	0.678
Tandem Gait (# steps)	−0.008	0.035	0.99 [0.93; 1.06]	0.824
FGA (0–30)	−0.027	0.060	0.97 [0.87; 1.10]	0.648
VVAS (0–100%)	0.039	0.015	1.04 [1.01; 1.07]	**0.010***
RDT (°)	−0.003	0.076	1.00 [0.87; 1.16]	0.968
Postural sway while facing rotating dots				
COP lean (mm)	0.003	0.030	1.00 [0.95; 1.06]	0.918
COP velocity (mm/s)	0.019	0.023	1.02 [0.97; 1.07]	0.404
COP area (mm^2)	0.001	<0.001	1.00 [1.00; 1.001]	0.197

[a]*$p < 0.05$ (*).*
[b]*COP, center of pressure; FGA, Functional Gait Assessment; mm, millimeters; OD, odds ratio; PPPD, persistent postural-perceptual dizziness; RDT, Rod-and-Disc test; s, seconds; TUG, Timed Up and Go test; vs, versus; VVAS, Visual Vertigo Analog Scale.*

The COP velocity values were positive in all three study groups, indicating larger mediolateral sway in visually disturbing conditions compared to the SVV tests. Next to this, PPPD patients also showed a significantly higher COP area ($p < 0.001$) compared to healthy persons. The COP area values were positive in all three study groups, indicating that the COP displacement was larger in visually disturbing conditions compared to the SVV condition.

PPPD patients had significantly higher VVAS scores ($p = 0.006$), but not significantly larger COP velocity values ($p = 0.475$) and COP area values ($p = 0.116$), compared to dizzy non-PPPD patients.

Data are provided in **Table 4**.

Evaluation of the Value of the Clinical Tests for PPPD Identification in Patients With Chronic Dizziness

Univariable logistic regression analyses of the clinical tests, displayed in **Table 5**, revealed that a higher VVAS score was associated most with PPPD [odds ratio 1.04; 95% CI (1.01; 1.07); $p = 0.010$].

The ROC analysis of the VVAS showed fair discriminative accuracy [AUC = 0.72, 95% CI (0.57; 0.86)]. The cut-off value for the VVAS (through maximization of the Youden index) was 21.01 which resulted in a sensitivity of 0.74 and a specificity of 0.67 for identification of PPPD.

In addition, a PLS-DA model was built to classify patients with chronic dizziness into PPPD and non-PPPD based upon all clinical tests listed in **Table 5**. The highest loading in the first component of the PLS-DA model was observed for VVAS, which is in line with the result from the logistic regression analysis where VVAS showed the strongest positive association with PPPD. Loadings are graphically shown in **Figure 3**.

The first two components of the PLS-DA accounted for 51% of the variance in the data (Kappa coefficient = 0.32; AUC of the ROC curve = 0.70). However, since the same observations were used to build the model and to test its predictive power, the prediction error is probably underestimated. To obtain an unbiased estimate of the prediction error of the PLS-DA model, and to find the optimal number of components to be included,

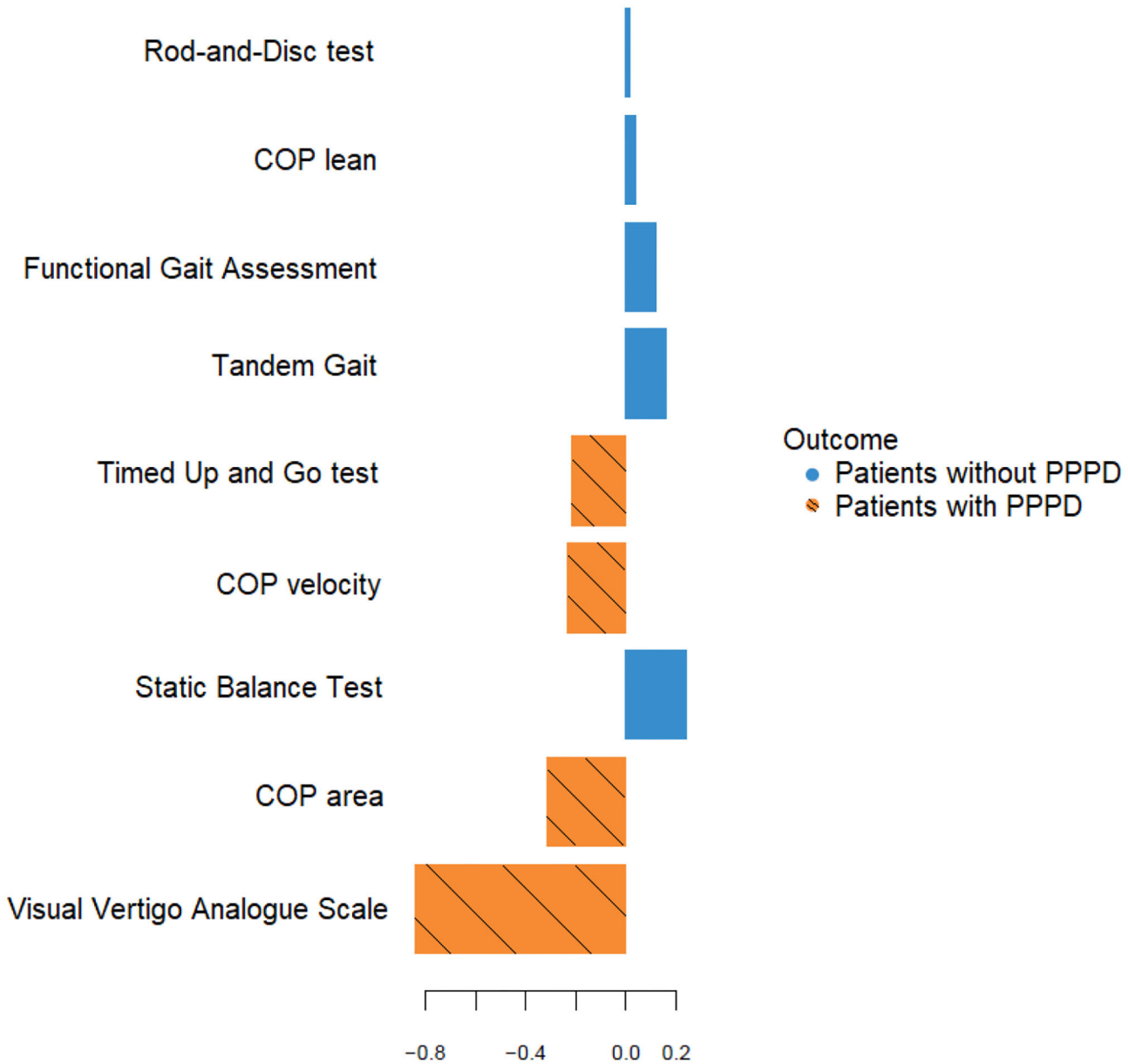

FIGURE 3 | Loading plot of the first component of the PLS-DA model [a,b]. [a]Loadings of the original variables for the first PLS-DA component are represented on the X-axis. The color of the horizontal bars shows in which of the two groups (patients with or without PPPD) the mean value of the original variable is the largest. In this dataset, the original variables with a negative loading on the first PLSDA component all have a larger mean value in the patients with PPPD. [b]COP, center of pressure; PPPD, persistent postural-perceptual dizziness.

5-fold cross validation (CV) was carried out. The CVerror was 47%, as presented in **Figure 4**, which indicates that the PLS-DA model performs fairly in distinguishing between PPPD patients and dizzy non-PPPD patients.

DISCUSSION

Our results show significantly reduced static and dynamic balance scores in patients with chronic dizziness compared to healthy subjects. However, no significant difference in any balance test results could be demonstrated between patients with and without PPPD. The literature indeed confirms reduced balance in all forms of chronic dizziness (6, 27–29). This is attributed to ongoing sensory conflict between the visual, vestibular and proprioceptive systems that are responsible for maintaining postural balance (30). Additionally, emotions (e.g., fear can cause conditioned avoidance) (31, 32) and musculoskeletal pain or dysfunction (33) are known triggers for balance problems. None of these triggers are specific to PPPD.

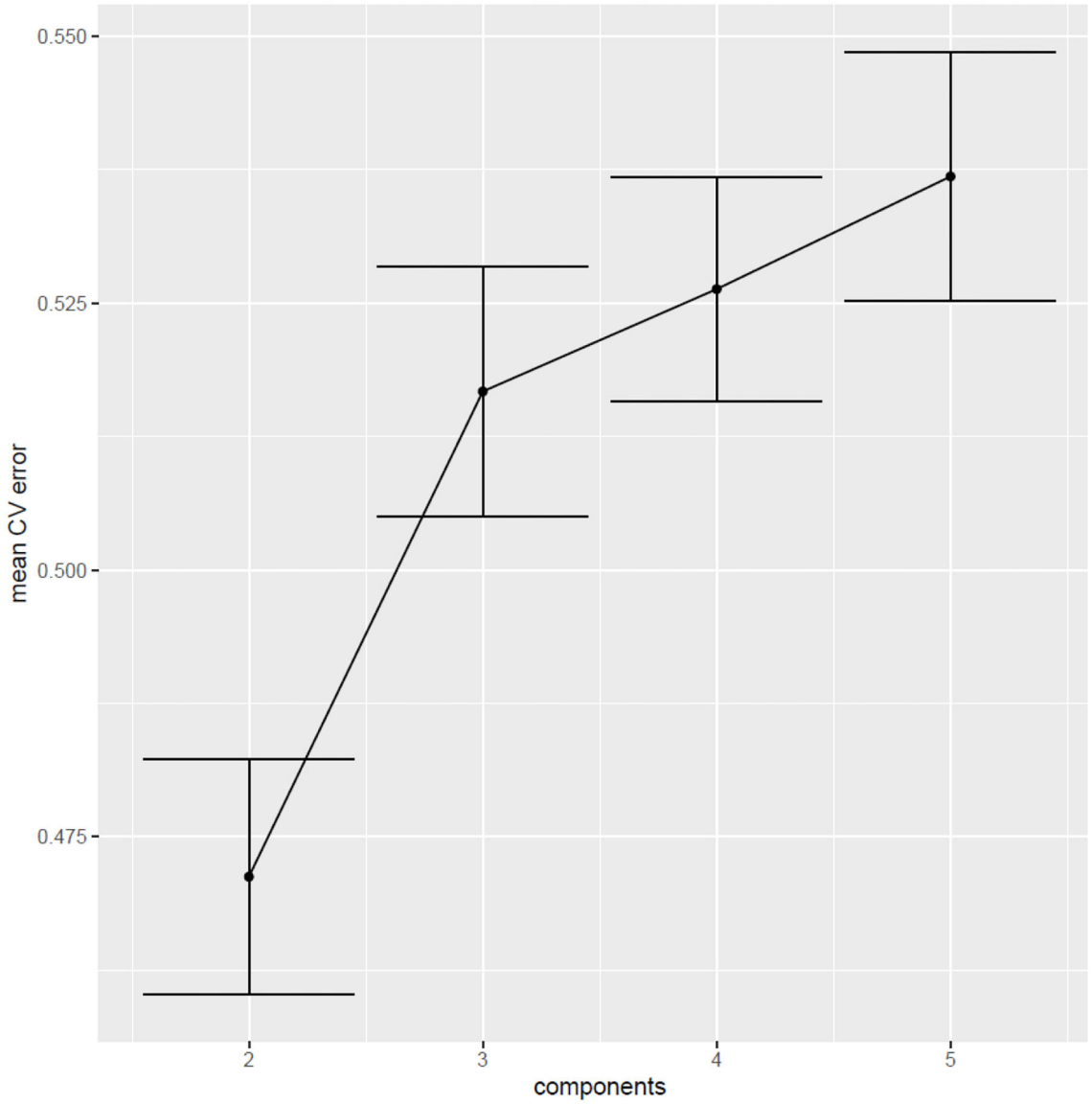

FIGURE 4 | Cross-validation error (5-fold) of 500 iterations [a,b]. [a]This figure shows the cross-validation error of the models vs. the number of components. The error bars represent the 95% confidence interval around the mean CVerror (across 500 runs of 5-fold CV). The best performance is observed in the models with 2 components, with a CVerror of 47% [95% CI (0.46; 0.48)].[b] CV, cross-validation.

Furthermore, our results show increased postural sway while facing rotating dots compared to the baseline condition (black screen) in all three study groups, as indicated by the positive values for COP velocity and COP area. The largest increase in postural sway was found in PPPD patients. These results are in line with the literature which states that disturbing visual stimuli can reduce balance control, especially in persons who are less able to rely on their vestibular and proprioceptive systems in visually challenging conditions (i.e., increased visual dependence) (34). In PPPD patients, this increased visual dependence can be expected as it is one of the diagnostic criteria of PPPD (4). Increased visual dependence also occurs in patients with chronic dizziness of non-PPPD origin as it is a frequently used coping mechanism for reduced vestibular function, aimed at restoring postural balance (35–37). On top of this, there is an inter-individual variability in visual susceptibility in the general population, which explains why participants without dizziness or balance complaints can have increased postural sway in visually challenging conditions (38).

The COP lean deviations were very limited ($\leq$ 1 mm), but in line with the low values reported in the literature (13), and not significantly different between the three groups. The lean effect could be strengthened in future research by: (1) only showing rotating dots in the peripheral field while keeping the center of

the screen empty (13, 34), or (2) by showing more realistic visual materials (e.g., fairground carousel, passing traffic) (39).

Another finding was the larger SVV deviations in all patients with chronic dizziness (both PPPD and non-PPPD patients) compared to healthy persons, although in none of the three study groups the SVV values were pathological [i.e., they were within the normal limit of 2.5° (40–43)]. The literature indicates that the upright SVV is sufficiently compensated in the chronic vestibular phase (44–46).

In our results, the SVV misalignment of RDT was not significantly different in PPPD patients compared to non-PPPD patients. This result agrees with earlier findings indicating that SVV misalignment of RDT is independent of the subtype of chronic dizziness, e.g., no significant differences in scores were found between visual vertigo and labyrinth-defective subjects (13), or between patients with vestibular neuritis with high vs. low DHI scores (35). In contrast to other studies, we could not observe significant differences in SVV misalignment of RDT between dizzy patients and healthy subjects (13, 35). The higher SVV errors for healthy subjects in our study may be due to interindividual variability (34), resulting in a slightly higher visual sensitivity in our sample group. Lastly, the SVV misalignment of RDT of our results was always in the direction of the visual stimuli, which corresponds with previous results (47, 48).

Preliminary results showed that participants had less postural sway disturbances in presence of a tilted frame compared to the black screen condition. This adds to the literature that any reference frame, even if it deviates from the earth gravitational as in this study, provides the participant with a visual aid to maintain a more stable upright position. The perception of verticality was more disturbed in the RFT than in the SVV test, but less so than in the RDT. The literature confirms that rotating dots are a stronger visually disturbing stimulus than a tilted frame (38).

Lastly, this study aimed to identify PPPD in chronic dizziness patients by means of commonly used clinical tests. Balance and visual dependence tests were chosen, since poor balance and increased visual dependence have been reported in previous studies as indicators of PPPD (4, 6). The results show that VVAS had the most, yet limited, discriminative value. These results complement the literature which already indicates duration of momentary worsening of dizziness, head roll-tilt SVV, and the Niigata PPPD questionnaire as useful tools in identifying PPPD. More specifically, duration of momentary worsening of dizziness can distinguish between PPPD and psychogenic chronic dizziness (49), the head roll-tilt SVV can help diagnosing PPPD in chronic vestibular disorders (50), and the Niigata PPPD questionnaire is useful in patients with other vestibular disorders (not specified as chronic) to detect PPPD (5).

Analysis of Study Strengths and Weaknesses

Strengths of this study include (1) the meticulous elimination of visual fixation points during the visual dependence tests (e.g., completely darkened room, edges of the television screen covered by a ring), (2) preliminary analysis of the RFT, RDT and postural sway while facing a tilted frame vs. rotating dots, and (3) the randomization of the visual dependence tests to eliminate a habituation effect on the results. Limitations of the study are (1) the limited sample size, (2) not having performed vestibular tests to confirm the absence of vestibular deficits in healthy persons, (3) the slightly younger age of the healthy persons, (4) the use of "best of three attempts" for the Timed Up and Go and Tandem Gait tests which may have induced a ceiling effect, and (4) the administration time of the test protocol (2.5 h) which may have caused fatigue in some patients.

Implications for Clinical Practice and Future Research

The VVAS was the most useful clinical test for the detection of PPPD of the balance and visual dependence tests examined in this study. Both PPPD and dizzy non-PPPD patients had significantly impaired balance and increased visual dependence compared to healthy persons. This shows the importance of evaluating balance and visual dependence in patients with chronic dizziness. The clinical tests can be useful to chart the patient's individual complaint profile. This profile can then be used to accentuate certain therapy elements, for example the degree of visual desensitization training.

Further research can investigate the discriminative value of other clinical tests not discussed in this article, preferably in combination with the VVAS results.

CONCLUSION

PPPD patients were more visually dependent, but did not have worse postural balance compared to dizzy non-PPPD patients. The VVAS had the most, but limited, discriminative value for identifying PPPD in chronic dizziness. In clinical practice, evaluation of balance control and visual dependence is indicated in patients with chronic dizziness, and corresponding exercises should be integrated into their exercise program in a patient-tailored way.

DATA AVAILABILITY STATEMENT

The datasets presented in this study can be found in online repositories. The name of the repository and accession number can be found at: Zenodo, https://zenodo.org/, doi: 10.5281/zenodos.6077074.

ETHICS STATEMENT

The studies involving human participants were reviewed and approved by Medical Ethics Committees of the Antwerp University Hospital (reference number 18/586). The patients/participants provided their written informed consent to participate in this study.

AUTHOR CONTRIBUTIONS

All authors contributed to the outline of the research goals, the analysis/interpretation of data or editing of the manuscript, and the final reviewing and approval of the manuscript. All authors contributed to the article and approved the submitted version.

FUNDING

This work was supported by the University of Antwerp (Faculty of Medicine and Health Sciences), Antwerp, Belgium.

ACKNOWLEDGMENTS

We would like to thank the University of Antwerp for funding this study.

SUPPLEMENTARY MATERIAL

The Supplementary Material for this article can be found online at: https://www.frontiersin.org/articles/10.3389/fneur.2022.880714/full#supplementary-material

REFERENCES

1. Brandt T, Dieterich M. Phobischer attacken-schwankschwindel, ein neues syndrom. *Munchener medizinische Wochenschrift.* (1986) 128:247–50.
2. Staab JP, Ruckenstein MJ. Expanding the differential diagnosis of chronic dizziness. *Arch Otolaryngol Head Neck Surg.* (2007) 133:170–6. doi: 10.1001/archotol.133.2.170
3. Xue H, Chong Y, Jiang ZD, Liu ZL, Ding L, Yang SL, et al. [Etiological analysis on patients with vertigo or dizziness]. *Zhonghua yi xue za zhi.* (2018) 98:1227–30. doi: 10.3760/cma.j.issn.0376-2491.2018.16.008
4. Staab JP, Eckhardt-Henn A, Horii A, Jacob R, Strupp M, Brandt T, et al. Diagnostic Criteria for Persistent Postural-Perceptual Dizziness (Pppd): Consensus Document of the Committee for the Classification of Vestibular Disorders of the Barany Society. *Journal of vestibular research: equilibrium & orientation.* (2017) 27:191–208. doi: 10.3233/VES-170622
5. Yagi C, Morita Y, Kitazawa M, Nonomura Y, Yamagishi T, Ohshima S, et al. A Validated questionnaire to assess the severity of persistent postural-perceptual dizziness (Pppd): the niigata Pppd questionnaire (Npq). *Otol Neurotol.* (2019) 40:e747–e52. doi: 10.1097/MAO.0000000000002325
6. Popkirov S, Staab JP, Stone J. Persistent postural-perceptual dizziness (Pppd): a common, characteristic and treatable cause of chronic dizziness. *Pract Neurol.* (2018) 18:5–13. doi: 10.1136/practneurol-2017-001809
7. Van Ombergen A, Heine L, Jillings S, Roberts RE, Jeurissen B, Van Rompaey V, et al. Altered functional brain connectivity in patients with visually induced dizziness. *NeuroImage Clinical.* (2017) 14:538–45. doi: 10.1016/j.nicl.2017.02.020
8. Li K, Si L, Cui B, Ling X, Shen B, Yang X. Altered intra- and inter-network functional connectivity in patients with persistent postural-perceptual dizziness. *NeuroImage Clinical.* (2020) 26:102216. doi: 10.1016/j.nicl.2020.102216
9. Lee JO, Lee ES, Kim JS, Lee YB, Jeong Y, Choi BS, et al. Altered brain function in persistent postural perceptual dizziness: a study on resting state functional connectivity. *Hum Brain Mapp.* (2018) 39:3340–53. doi: 10.1002/hbm.24080
10. Cavanna AE, Trimble MR. The precuneus: a review of its functional anatomy and behavioural correlates. *Brain.* (2006) 129:564–83. doi: 10.1093/brain/awl004
11. Margulies DS, Vincent JL, Kelly C, Lohmann G, Uddin LQ, Biswal BB, et al. Precuneus shares intrinsic functional architecture in humans and monkeys. *Proc Natl Acad Sci U S A.* (2009) 106:20069–74. doi: 10.1073/pnas.0905314106
12. Sohsten E, Bittar RS, Staab JP. Posturographic profile of patients with persistent postural-perceptual dizziness on the sensory organization test. *J Vestib Res.* (2016) 26:319–26. doi: 10.3233/VES-160583
13. Guerraz M, Yardley L, Bertholon P, Pollak L, Rudge P, Gresty MA, et al. Visual vertigo: symptom assessment, spatial orientation and postural control. *Brain.* (2001) 124:1646–56. doi: 10.1093/brain/124.8.1646
14. Bronstein AM, Lempert T, Seemungal BM. Chronic dizziness: a practical approach. *Pract Neurol.* (2010) 10:129–39. doi: 10.1136/jnnp.2010.211607
15. Vereeck L, Wuyts F, Truijen S, Van de Heyning P. Clinical assessment of balance: normative data, and gender and age effects. *Int J Audiol.* (2008) 47:67–75. doi: 10.1080/14992020701689688
16. Cuschieri S. The strobe guidelines. *Saudi J Anaesth.* (2019) 13:S31–S4. doi: 10.4103/sja.SJA_543_18
17. Wuyts FL, Van Rompaey V, Maes LK. "So stoned": common sense approach of the dizzy patient. *Front Surg.* (2016) 3:32. doi: 10.3389/fsurg.2016.00032
18. Vereeck L, Truijen S, Wuyts F, Van de Heyning PH. Test-retest reliability of the dutch version of the dizziness handicap inventory. *B-ENT.* (2006) 2:75–80.
19. Vereeck L, Truijen S, Wuyts FL, Van De Heyning PH. Internal consistency and factor analysis of the dutch version of the dizziness handicap inventory. *Acta Otolaryngol.* (2007) 127:788–95. doi: 10.1080/00016480601075464
20. Bjelland I, Dahl AA, Haug TT, Neckelmann D. The Validity of the hospital anxiety and depression scale. An updated literature review. *J Psychosom Res.* (2002) 52:69–77. doi: 10.1016/S0022-3999(01)00296-3
21. Wrisley DM, Marchetti GF, Kuharsky DK, Whitney SL. Reliability, internal consistency, and validity of data obtained with the functional gait assessment. *Phys Ther.* (2004) 84:906–18. doi: 10.1093/ptj/84.10.906
22. Dannenbaum E, Chilingaryan G, Fung J. Visual vertigo analogue scale: an assessment questionnaire for visual vertigo. *J Vestib Res.* (2011) 21:153–9. doi: 10.3233/VES-2011-0412
23. Mishra P, Pandey CM, Singh U, Gupta A, Sahu C, Keshri A. Descriptive statistics and normality tests for statistical data. *Ann Card Anaesth.* (2019) 22:67–72. doi: 10.4103/aca.ACA_157_18
24. Ruiz-Perez D, Guan H, Madhivanan P, Mathee K, Narasimhan G. So you think you can pls-da? *BMC Bioinformatics.* (2020) 21:2. doi: 10.1186/s12859-019-3310-7
25. *Ibm Corp. Released 2020. Ibm Spss Statistics for Windows; Version 27.0* Armonk, NY.
26. R Core Team (2020). *R: A Language and Environment for Statistical Computing*. R Foundation for Statistical Computing, Vienna, Austria. Available online at: Https://Www.R-Project.Org/.
27. Herssens N, Verbecque E, McCrum C, Meijer K, van de Berg R, Saeys W, et al. A systematic review on balance performance in patients with bilateral vestibulopathy. *Phys Ther.* (2020) 100:1582–94. doi: 10.1093/ptj/pzaa083
28. Giray M, Kirazli Y, Karapolat H, Celebisoy N, Bilgen C, Kirazli T. Short-term effects of vestibular rehabilitation in patients with chronic unilateral vestibular dysfunction: a randomized controlled study. *Arch Phys Med Rehabil.* (2009) 90:1325–31. doi: 10.1016/j.apmr.2009.01.032
29. Balci B, Akdal G. Imbalance, motion sensitivity, anxiety and handicap in vestibular migraine and migraine only patients. *Auris Nasus Larynx.* (2020) 47:747–51. doi: 10.1016/j.anl.2020.02.015
30. Bronstein AM. Multisensory integration in balance control. *Handb Clin Neurol.* (2016) 137:57–66. doi: 10.1016/B978-0-444-63437-5.00004-2
31. Balaban CD, Thayer JF. Neurological bases for balance–anxiety links. *J Anxiety Disord.* (2001) 15:53–79. doi: 10.1016/S0887-6185(00)00042-6
32. Goto F, Kabeya M, Kushiro K, Ttsutsumi T, Hayashi K. Effect of anxiety on antero-posterior postural stability in patients with dizziness. *Neurosci Lett.* (2011) 487:204–6. doi: 10.1016/j.neulet.2010.10.023
33. Haukanes L, Knapstad MK, Kristiansen L, Magnussen LH. Association between Musculoskeletal Function and Postural Balance in Patients with Long-Lasting Dizziness. A cross-sectional study. *Physiother Res Int.* (2021) 26:e1916. doi: 10.1002/pri.1916
34. Lee SC. Relationship of visual dependence to age, balance, attention, and vertigo. *J Phys Ther Sci.* (2017) 29:1318–22. doi: 10.1589/jpts.29.1318

35. Cousins S, Cutfield NJ, Kaski D, Palla A, Seemungal BM, Golding JF, et al. Visual dependency and dizziness after vestibular neuritis. *PLoS ONE.* (2014) 9:e105426. doi: 10.1371/journal.pone.0105426
36. Agarwal K, Bronstein AM, Faldon ME, Mandala M, Murray K, Silove Y. Visual Dependence and Bppv. *J Neurol.* (2012) 259:1117–24. doi: 10.1007/s00415-011-6311-7
37. Bisdorff AR. Management of vestibular migraine. *Ther Adv Neurol Disord.* (2011) 4:183–91. doi: 10.1177/1756285611401647
38. Pavlou M, Quinn C, Murray K, Spyridakou C, Faldon M, Bronstein AM. The effect of repeated visual motion stimuli on visual dependence and postural control in normal subjects. *Gait Posture.* (2011) 33:113–8. doi: 10.1016/j.gaitpost.2010.10.085
39. Meyer GF, Shao F, White MD, Hopkins C, Robotham AJ. Modulation of visually evoked postural responses by contextual visual, haptic and auditory information: a 'virtual reality check'. *PLoS ONE.* (2013) 8:e67651. doi: 10.1371/journal.pone.0067651
40. Dieterich M, Brandt T. Ocular torsion and tilt of subjective visual vertical are sensitive brainstem signs. *Ann Neurol.* (1993) 33:292–9. doi: 10.1002/ana.410330311
41. Zwergal A, Rettinger N, Frenzel C, Dieterich M, Brandt T, Strupp M, et al. Bucket of static vestibular function. *Neurology.* (2009) 72:1689–92. doi: 10.1212/WNL.0b013e3181a55ecf
42. Friedmann G. The judgement of the visual vertical and horizontal with peripheral and central vestibular lesions. *Brain.* (1970) 93:313–28. doi: 10.1093/brain/93.2.313
43. Habs M, Strobl R, Grill E, Dieterich M, Becker-Bense S. Primary or secondary chronic functional dizziness: does it make a difference? a dizzyreg study in 356 patients. *J Neurol.* (2020) 267:212–22. doi: 10.1007/s00415-020-10150-9
44. Vibert D, Hausler R. Long-term evolution of subjective visual vertical after vestibular neurectomy and labyrinthectomy. *Acta Otolaryngol.* (2000) 120:620–2. doi: 10.1080/0001648007500 00432
45. Cnyrim CD, Rettinger N, Mansmann U, Brandt T, Strupp M. Central compensation of deviated subjective visual vertical in wallenberg's syndrome. *J Neurol Neurosurg Psychiatry.* (2007) 78:527–8. doi: 10.1136/jnnp.2006.100727
46. Kumagami H, Saino Y, Baba A, Fujiyama D, Takasaki K, Takahashi H. Subjective visual vertical test in patients with chronic dizziness without abnormal findings in routine vestibular function tests. *Acta oto-laryngologica Supplementum.* (2009) 129:46—9. doi: 10.1080/00016480902926456
47. Mittelstaedt H. A new solution to the problem of the subjective vertical. *Naturwissenschaften.* (1983) 70:272–81. doi: 10.1007/BF00404833
48. Merfeld DM, Zupan LH. Neural Processing of Gravitoinertial Cues in Humans. III modeling tilt and translation responses. *J Neurophysiol.* (2002) 87:819–33. doi: 10.1152/jn.00485.2001
49. Ishizuka K, Shikino K, Yamauchi Y, Yanagita Y, Yokokawa D, Ikegami A, et al. The clinical key features of persistent postural perceptual dizziness in the general medicine outpatient setting: a case series study of 33 patients. *Intern Med.* (2020) 59:2857–62. doi: 10.2169/internalmedicine.5172-20
50. Yagi C, Morita Y, Kitazawa M, Nonomura Y, Yamagishi T, Ohshima S, et al. Head roll-tilt subjective visual vertical test in the diagnosis of persistent postural-perceptual dizziness. *Otol Neurotol.* (2021) 42:e1618–e24. doi: 10.1097/MAO.0000000000003340

Conflict of Interest: The authors declare that the research was conducted in the absence of any commercial or financial relationships that could be construed as a potential conflict of interest.

Publisher's Note: All claims expressed in this article are solely those of the authors and do not necessarily represent those of their affiliated organizations, or those of the publisher, the editors and the reviewers. Any product that may be evaluated in this article, or claim that may be made by its manufacturer, is not guaranteed or endorsed by the publisher.

Copyright © 2022 De Vestel, De Hertogh, Van Rompaey and Vereeck. This is an open-access article distributed under the terms of the Creative Commons Attribution License (CC BY). The use, distribution or reproduction in other forums is permitted, provided the original author(s) and the copyright owner(s) are credited and that the original publication in this journal is cited, in accordance with accepted academic practice. No use, distribution or reproduction is permitted which does not comply with these terms.

frontiers | Frontiers in Neurology

CASE REPORT
published: 09 June 2022
doi: 10.3389/fneur.2022.874451

Case Report: Diagnosis of Petrous Apex IgG4-Related Disease by Middle Cranial Fossa Craniotomy and Temporal Bone Biopsy

Louis Hofmeyr[1,2], Gerrida Herbst[3], Elias Pretorius[4], Brian Sarembock[1], Kathryn Taylor[5] and David Roytowski[1,6]*

[1] Netcare Christiaan Barnard Memorial Hospital, Cape Town, South Africa, [2] Division of Otorhinolaryngology, Tygerberg Academic Hospital, University of Stellenbosch, Cape Town, South Africa, [3] Netcare Blaauwberg Hospital, Cape Town, South Africa, [4] Morton and Partners Radiologists, Cape Town, South Africa, [5] Pathcare, Cape Town, South Africa, [6] Division of Neurosurgery, Tygerberg Academic Hospital, University of Stellenbosch, Cape Town, South Africa

OPEN ACCESS

Edited by:
Michael Strupp,
Ludwig Maximilian University of Munich, Germany

Reviewed by:
Takeshi Tsutsumi,
Tokyo Medical and Dental University, Japan
Albert Sufianov,
Federal Center of Neurosurgery, Russia

***Correspondence:**
Louis Hofmeyr
louishofmeyr@me.com

Specialty section:
This article was submitted to Neuro-Otology, a section of the journal Frontiers in Neurology

Received: 12 February 2022
Accepted: 20 April 2022
Published: 09 June 2022

Citation:
Hofmeyr L, Herbst G, Pretorius E, Sarembock B, Taylor K and Roytowski D (2022) Case Report: Diagnosis of Petrous Apex IgG4-Related Disease by Middle Cranial Fossa Craniotomy and Temporal Bone Biopsy. Front. Neurol. 13:874451. doi: 10.3389/fneur.2022.874451

Introduction: Primary IgG4-related disease (IgG4-RD) of the temporal bone is a rare condition. Unlike typical petrous apicitis or Gradenigo syndrome, our patient presented exclusively with unilateral cranial nerve VI palsy and symptoms of diplopia. Skull base imaging demonstrated a destructive bony lesion in the petrous apex. Imaging and systemic investigations were insufficient to support a diagnosis. The diagnosis was achieved histologically after acquiring the specimen by middle cranial fossa craniotomy and temporal bone biopsy. This case report is thought to be the first published description of a diagnosis of IgG4-RD proven with the middle cranial fossa approach.

Case Report: We describe a 29-year-old female with primary IgG4-RD of the petrous apex of the temporal bone. This patient presented with a few-month history of left-sided headache and recent-onset diplopia due to paralysis of cranial nerve VI. Imaging demonstrated a petrous apex lesion, and comprehensive systemic investigations could not reach a diagnosis. A middle cranial fossa craniotomy and a biopsy of the temporal bone lesion were undertaken to establish the diagnosis. Histological confirmation of IgG4-RD was proven. Following treatment with corticosteroids, the patient experienced complete recovery and resolution of her symptoms.

Conclusion: This study describes a case of primary IgG4-RD of the petrous apex of the temporal bone that presented with diplopia and was diagnosed by middle fossa craniotomy and temporal bone biopsy. To the best of our knowledge, this is the first case description where primary diagnosis was made based on middle cranial fossa craniotomy and temporal bone biopsy.

Keywords: IgG4-related disease, temporal bone, middle cranial fossa, diplopia, case report, Gradenigo syndrome

INTRODUCTION

IgG4-related disease (IgG4-RD) is a chronic immune-mediated fibro-inflammatory disorder (1). Perhaps, it is more common than anticipated, Although it was initially described in the context of autoimmune pancreatitis, it has now been described in nearly all parts of the body (2–4). It appears that IgG infiltration causes organ enlargement. Kuttner's tumor, Mikulicz's syndrome, and Riedel's

thyroiditis are diseases that fall in the IgG4-RD spectrum (5–7). In the head and neck region, IgG4-RD of the thyroid, lymph nodes, nasal cavity, paranasal sinuses, lacrimal glands, orbits, and salivary glands have all been described (8–14).

Skull base involvement of IgG4-RD is less commonly noted, with most accounts being an extension from paranasal disease. IgG4-RD should be a consideration when a lesion involves the temporal bone in patients presenting with otalgia and diplopia (15–17).

Recently, a rare case of a patient with IgG4-RD of the temporal bone who presented with otalgia and diplopia due to cranial nerve VI palsy was described (18). Unsurprisingly, the presentation was considered Gradenigo syndrome, where otitis media and mastoiditis lead to temporal bone apicitis with otalgia and cranial nerve VI palsy (19). In this case, the diagnosis was made after a biopsy of the middle ear, mastoid, and sinus cavity (18). In another case, a patient with visual loss, facial nerve paralysis, and diplopia was diagnosed with IgG4-RD after obtaining histology via a mastoidectomy (20).

In this report, we present a young patient who had primarily diplopia as a symptom. This case is unique, as to the best of our knowledge, it is the first case of IgG4-RD diagnosed from a biopsy acquired with the middle cranial fossa approach. The serum IgG4 level in this patient was normal.

FIGURE 1 | Axial high-resolution computed tomography (HRCT) of the skull base shows a destructive process in the petrous apex (arrow) with regional sclerosis involving the petroclival fissure (asterisk) and clivus (arrowhead).

CASE REPORT

An otherwise healthy 29-year-old female presented to the emergency room with diplopia from isolated cranial nerve VI palsy on the left and a history of left-sided headaches of several-month duration. Associated symptoms included pressure in the left ear and a "blocked" sensation. The patient did not complain of any vestibular symptoms. Otoscopy revealed normal tympanic membranes with no signs of middle ear pathology. Diagnostic audiometry revealed normal hearing and middle ear function. Normal blood investigation findings included fasting glucose, corrected calcium, magnesium, liver functions, thyroid functions, and a complete blood and platelet count. Serological testing, including human immunodeficiency virus (HIV) testing, treponema pallidum antibodies, anti-nuclear antibody (ANA) titers, and antineutrophil cytoplasmic antibody (ANCA) titres, was negative. Erythrocyte sedimentation rate (ESR) was 29, and C-reactive protein (CRP) was 14, mildly raised in both instances.

High-resolution computed tomography (HRCT) of the skull base demonstrated an aggressive erosive disease process centered on the left petrous apex involving the petroclival fissure and inferolateral clivus (**Figure 1**). Subsequent magnetic resonance imaging (MRI) revealed a trans-spatial marrow-replacing tumor-like soft tissue lesion of low T1/T2 signal (**Figure 2A**) and mild apparent diffusion coefficient (ADC) reduction. The lesion was enhanced avidly following gadolinium contrast administration (**Figure 2B**). Focal pachymeningeal thickening of the retroclival dura and enhancement of the cisternal segment of the left abducens nerve as it enters Dorello's canal were present.

The initial diagnosis favored Gradenigo syndrome, otomastoiditis, lateral rectus palsy, and deep facial pain, with a differential diagnosis of cholesteatoma, cholesterol granuloma, tuberculosis, mucocele formation, and petrous apex air cell effusion. The absence of signs of a systemic disease, clinically and later supported by pathology results, ruled out an infective process. Malignancies considered included chondrosarcoma, chordoma, plasmacytoma, multiple myeloma, paraganglioma, and meningioma. A tissue biopsy was required to make a definitive diagnosis.

Surgical access to the petrous apex includes the infracochlear, infralabyrinthine, middle fossa, and transsfenoid approaches. After studying the anatomy on the HRCT scans, the middle fossa approach was chosen as the most appropriate option.

Given the epicenter of the lesion, middle fossa craniotomy provided an elegant and effective means of approaching the lesion to obtain tissue for histological analysis. Nevertheless, the middle cranial fossa approach to the temporal bone can be considered invasive and is not without risks. However, by employing the transtemporal supralabyrinthine modification of the middle cranial fossa approach, described by Fisch, minimal retraction is placed on the temporal lobe (21, 22). In the author's experience of more than 150 cases, the risk of developing epilepsy with this modification is minimal. Following the craniotomy, the petrous apex was identified, image guidance utilized to confirm and diamond burr drilling of the distorted petrous bone performed to access the lesion. The macroscopic appearance of the tissue was pink, firm, and without a clear capsule or vascularity (**Figure 3**). Numerous tissue biopsies were taken. The patient recovered well after the surgery without complications.

The microscopic examination of the biopsy fragments showed a dense lymphoplasmacytic inflammatory infiltrate with a fibrous background. Strands and vague fascicles of collagen fibers were also seen, as well as regions of focal storiform-type fibrosis. There was no evidence of obliterative phlebitis or granulomata. Fungal, bacterial, and mycobacterial stains were negative. A lymphoproliferative disorder was excluded. Immunohistochemical stains for IgG4 showed greater than 50 IgG4-positive plasma cells in some high-power fields (**Figure 4**).

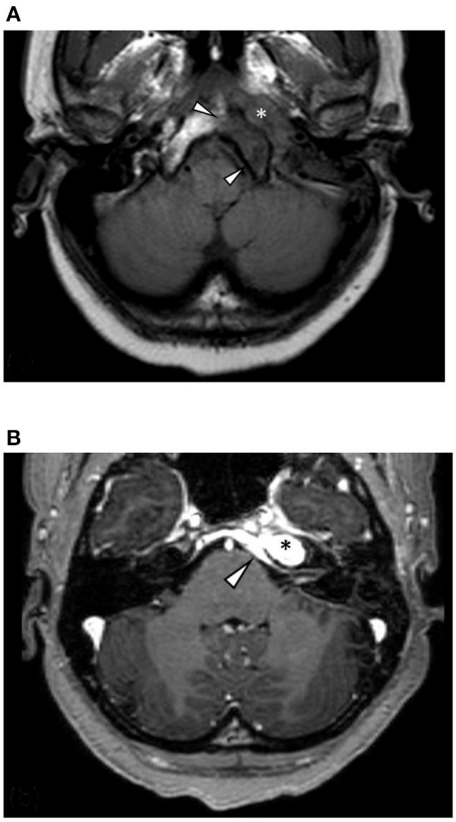

FIGURE 2 | (A) Axial T1-weighted MRI shows a hypointense mass centered on the left petrous apex (asterisk) and regional marrow hypointensity due to infiltration and marrow replacement (arrowheads). **(B)** Axial T1 following contrast administration shows avid homogenous enhancement of the lesion (asterisk) and intracranial disease extension with pachymeningeal enhancement and thickening of the retroclival dura (arrowhead).

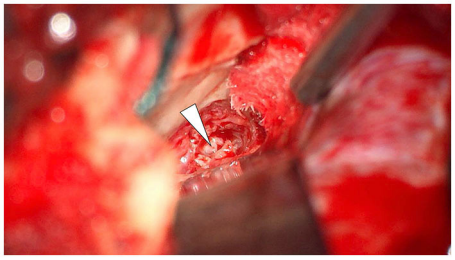

FIGURE 3 | Middle cranial fossa craniotomy demonstrating the lesion in the petrous apex (arrowhead).

IgG4/IgG ratio was greater than 20%. These features were highly suggestive of IgG4-related disease.

Once the diagnosis was made, the patient was commenced on oral prednisone at 40mg daily to taper over a 6-month interval.

One month post-surgery, the patient complained of hoarseness. She was diagnosed with left vocal cord paralysis, with the affected vocal cord in the paramedian position. MRI revealed an extension of the original disease process, and the MRI of the neck was normal. In the light of the MRI findings, the paralysis of the recurrent laryngeal nerve was thought to be due to IgG4-related peripheral axonal neuropathy.

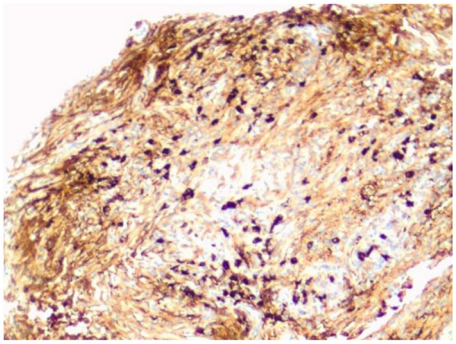

FIGURE 4 | IgG4 immunohistochemical stain highlights the IgG4-positive plasma cells. There are more than 50 IgG4-positive cells in this field (magnification ×200).

Three months after the post-procedure, the patient continued on prednisone. The left cranial nerve VI palsy and vocal cord paralysis have resolved entirely. The patient returned to work with an occasional complaint of blurred vision. Concerns exist that upon discontinuation of prednisone, she will experience symptom recurrence.

DISCUSSION

IgG4-RD is a recently described systemic fibro-inflammatory disease, although it was first diagnosed in salivary glands (Mikulicz's disease) more than 100 years ago (7). The etiology remains unclear, although the most likely mechanism is thought to be antigen-driven inflammation or infection (1, 5).

The head and neck region is the second most common site of IgG4-RD presentation (1). This case report is, to our knowledge, the first from the African continent. IgG4-RD involvement of the ear is thought to be rare. The sexual preponderance is roughly equal (2, 3, 5). It occurs mainly in patients in the 6th decade (1). Our case was somewhat unusual, as the patient was 29 years old.

Diagnosis is usually made by correlating clinical presentation, serological studies, imaging findings, and histopathological results (2). Histological confirmation of the diagnosis is the gold standard (4).

IgG4-RD may mimic many conditions, including infections, malignancies, and autoimmune diseases (5). Clinicians should cultivate a healthy index of suspicion in patients with atypical presentation.

Although the head and neck are often involved in systemic IgG4-related disease with frequent lacrimal and major salivary glands, primary skull base involvement is highly uncommon. The typical imaging features of a skull base disease are nonspecific and often mimic inflammatory and neoplastic entities. Focal lesions are frequently misinterpreted as nasopharyngeal carcinoma,

meningioma, or primary lymphoma and are usually included in the imaging differential diagnosis (22–24).

The typical imaging characteristics of IgG4-RD describe a focal mass-like and infiltrative lesion with iso- to hypointense signal intensity on T2 and correlative apparent diffusion coefficient (ADC) reduction. Imaging features may vary in intensity depending on the degree of fibrosis and lymphoplasmacytic cellular composition. Lesions are typically enhanced homogeneously following contrast administration. HRCT of the skull base is a helpful adjunct to MRI and superior in assessing osseous destruction and erosion (24–27).

IgG4-RD is an immune-mediated inflammatory disorder in multiple organs characterized by abundant infiltration of IgG4-positive plasmacytes and fibrosis in the involved organs. The precise pathogenic mechanism remains unclear. Aberrant innate and adaptive immunity is considered the primary pathogenesis of IgG4-RD.

Recent studies have shown that abnormal adaptive immune responses mediated by T-helper type 2 cells, regulatory T lymphocytes, CD4 -positive cytotoxic T lymphocytes, T follicular helper cells, and T follicular regulatory cells are involved in IgG4-RD (5, 28). In addition to adaptive immune responses, innate immune responses play pathogenic roles in IgG4-RD. Macrophages, mast cells, basophils, and complement and plasmacytoid dendritic cells are activated to produce various cytokines in IgG4-RD. There is increasing evidence that B cells play significant roles in the pathogenesis of IgG4-RD. The fact that B cell depletion has been shown to correlate with rapid improvement of tissue fibrosis in affected organs of patients with IgG4-RD raises the hypothesis that B lymphocytes may be involved in fibrogenesis.

Currently, the standard of care for IgG4-RD worldwide remains to be corticosteroids (prednisone). Treatment usually starts with 40 mg of prednisone daily for 1 month. This dose is then tapered to and maintained at 5 to 10 mg per day. Should the steroids fail, rituximab should be considered as a second-line treatment (29).

Making the diagnosis of IgG4-RD requires tissue sampling; if the petrous apex is the site of infiltration, middle cranial fossa craniotomy can be performed. The middle cranial fossa craniotomy approach may be considered invasive. Temporal lobe epilepsy is a known potential complication. It is based on the author's experience in performing over 150 cases of middle cranial fossa approaches that this is an infrequent occurrence when the modified transtemporal supralabyrinthine approach is employed, as described by Fisch. The technique involves drilling the temporal bone to access the petrous apex rather than retracting the temporal lobe. The technique has been described as "one-third temporal lobe retraction and two-third temporal bone drilling". The important takeaway message is that middle cranial fossa craniotomy with transtemporal supralabyrinthine modification, as described by Fisch, is a viable, safe, and practical approach to obtain access to the petrous apex (21, 22).

CONCLUSION

In summary, we describe, to our knowledge, the first case of primary temporal bone IgG4-RD causing cranial nerve VI palsy that has been proven histologically by a middle cranial fosssa craniotomy and temporal bone biopsy. This demonstrates that the middle cranial fossa approach, which is considered invasive, is a practical and viable option to diagnose petrous apex lesions.

DATA AVAILABILITY STATEMENT

The raw data supporting the conclusions of this article will be made available by the authors, without undue reservation.

ETHICS STATEMENT

Written informed consent was obtained from the individual(s) for the publication of any potentially identifiable images or data included in this article.

AUTHOR CONTRIBUTIONS

LH: otorhinolaryngologist involved in the middle cranial fossa biopsy, coordinator of contributions, submission, and contact for the manuscript. DR: neurosurgeon involved in the middle cranial fossa craniotomy, preparation, and grammar check of the manuscript. GH: primary treating otorhinolaryngologist. BS: treating rheumatologist. EP: reporting radiologist. KT: reporting histopathologist. All authors contributed to the article and approved the submitted version.

REFERENCES

1. Umehara H, Okazaki K, Nakamura T, Satoh-Nakamura T, Nakajima A, Kawano M, et al. Current approach to the diagnosis of IgG4related disease - combination of comprehensive diagnostic and organ-specific criteria. *Mod Rheumatol.* (2017) 27:381–91. doi: 10.1080/14397595.2017.1290911
2. Hamano H, Kawa S, Horiuchi A, Unno H, Furuya N, Akamatsu T, et al. High serum IgG concentrations in patients with sclerosing pancreatitis. *N Engl J Med.* (2001) 344:732–8. doi: 10.1056/NEJM200103083441005
3. Kamisawa T, Okamoto A. Autoimmune pancreatitis: proposal of IgG4-related sclerosing disease. *J Gastroenterol.* (2006) 41:613–25. doi: 10.1007/s00535-006-1862-6
4. Kamisawa T, Funata N, Hayashi Y, Eishi Y, Koike M, et al. A new clinicopathological entity of IgG4-related autoimmune disease. *J Gastroenterol.* (2003) 38:982–4. doi: 10.1007/s00535-003-1175-y
5. Stone JH, Zen Y, Deshpande V. IgG4-related disease. *N Engl J Med.* (2012) 366:539–51. doi: 10.1056/NEJMra1104650
6. Pieringer H, Parzer I, Wöhrer A, Reis P, Oppl B, Zwerina J. IgG4-related disease: an orphan disease with many faces. *Orphanet J Rare Dis.* (2014) 9:110. doi: 10.1186/s13023-014-0110-z
7. von Mikulicz-Radecki J. *Über eine eigenartige symmetrische Erkrankung der Thränen- und Mundspeicheldrüsen. Beiträge zur Chirurgie. Festschrift gewidmet Theodor Billroth.* Stuttgart: Verlag von Ferd (1892). 610–30.

8. Hong X, Sun ZP, Li W, Chen Y, Gao Y, Su JZ, et al. Comorbid diseases of IgG4-related sialadenitis in the head and neck. *Laryngoscope.* (2015) 125:2113–8. doi: 10.1002/lary.25387
9. WongWK, Morton RP. Immunoglobulin G4-related disease of the orbital cavity, cervical lymph nodes, and greater auricular nerve: case report. *Am J Otolaryngol.* (2016) 37:182–5. doi: 10.1016/j.amjoto.2016.01.010
10. Kubota T, Moritani S. Orbital IgG4-related disease: clinical features and diagnosis. *ISRN Rheumatol.* (2012) 2012:412896. doi: 10.5402/2012/412896
11. Hwang G, Jin SY, Kim HS. IgG4-related disease presenting as hypertrophic pachymeningitis and compressive optic neuropathy. *Joint Bone Spine.* (2016). doi: 10.1016/j.jbspin.2015.07.016
12. Mehta M, Jakobiec F, Fay A. Idiopathic fibroinflammatory disease of the face, eyelids, and periorbital membrane with immunoglobulin G4-positive plasma cells. *Arch Pathol Lab Med.* (2009) 133:1251–5. doi: 10.5858/133.8.1251
13. Takano K, Yamamoto M, Takahashi H, Himi T. Recent advances in knowledge regarding the head and neck manifestations of IgG4-related disease. *Auris Nasus Larynx.* (2017) 44:7–17. doi: 10.1016/j.anl.2016.10.011
14. Cain RB, Colby TV, Balan V, Patel NP, Lal D. Perplexing lesions of the sinonasal cavity and skull base: IgG4-related and similair inflammatory diseases. *Otolaryngol Head Neck Surg.* (2015) 151:496–502. doi: 10.1177/0194599814533648
15. Della-Torre E, Mattoo H, Mahajan VS, Deshpande V, Krause D, Song P, et al. IgG4-related midline destructive lesion. *Ann Rheum Dis.* (2014) 73:1434–6. doi: 10.1136/annrheumdis-2014-205187
16. Deshpande V, Zane NA, Kraft S, Stone JH, Faquin WC. Recurrent mastoiditis mimics IgG4 related disease: a potential diagnostic pitfall. *Head Neck Pathol.* (2016) 10:314–20. doi: 10.1007/s12105-016-0710-0
17. Lu P, Sha Y, Wang F, Wang S. IgG4-related sclerosing disease involving middle ear. *Otol Neurotol.* (2017) 38:e65–7. doi: 10.1097/MAO.0000000000001420
18. Chaiyasate S, Salee P, Sukapan K, Teeranoraseth T, Roongrotwattanasiri K. Temporal bone involvement of IgG4-related disease: a rare condition misleading to petrous apicitis causing lateral rectus palsy. *BMJ Case Rep.* (2019) 12:e228550. doi: 10.1136/bcr-2018-228550
19. Devic M, Boucher M, Raveau M. "[Some cases of Gradenigo-Lannois syndrome]". *J Méd Lyon.* (1966) 47:537–47.
20. Wick CC, Zacharia J, Manjila S, Brown WC, Malla P, Katirji B, et al. IgG4-related disease causing facial nerve and optic nerve palsies: Case report and literature review. *Am J Otolrangol.* (2016) 37:567–71. doi: 10.1016/j.amjoto.2016.08.005
21. Fisch U. *Transtemporal Surgery of the Internal Auditory Canal. Transtemporal Surgery of the Internal Auditory Canal.* Basel: Karger Publishers (1970). p. 203–40.
22. Fisch U, Mattox D. *Microsurgery of the Skull Base.* New York, NY: Thieme (1988).
23. Liu J, Zhang B, Sun H, Han J, Yang D. Immunoglobulin G4–Related disease in the skull base mimicking nasopharyngeal carcinoma. *J Craniofac Surg.* (2015) 26:e144–5. doi: 10.1097/SCS.0000000000001381
24. Thompson A, Whyte A. Imaging of IgG4-related disease of the head and neck. *Clin Radiol.* (2017) 73:106–20. doi: 10.1016/j.crad.2017.04.004
25. Li L, Ward B, Cocks M, Kheradmand A, Francis HW. IgG4-related disease of bilateral temporal bones. *Ann Otol Rhinol Laryngol.* (2017) 126:236e40. doi: 10.1177/0003489416672476
26. Dragan A D, Weller A, Ravi Kumar L. Imaging of IgG4-related disease in the extracranial head and neck. *Eur J Radiol.* (2021) 136:109560. doi: 10.1016/j.ejrad.2021.109560
27. Martínez-de-Alegría A, Baleato-González A, García-Figueiras R, Bermúdez-Naveira A, Abdulkader-Nallib I, Díaz-Peromingo J, et al. IgG4-related disease from head to Toe. *RadioGraphics.* (2015) 35:2007–25. doi: 10.1148/rg.357150066
28. Perugino CA, Kaneko N, Maehara T, Mattoo H, Kers J, Allard-Chamard H, et al. $CD4^+$ and $CD8^+$ cytotoxic T lymphocytes may induce mesenchymal cell apoptosis in IgG_4-related disease. *J Allergy Clin Immunol.* (2021) 147:368–82. doi: 10.1016/j.jaci.2020.05.022
29. Khosroshahi A, Wallace ZS, Crowe JL, Akamizu T, Azumi A, Carruthers MN, et al. International consensus guidance statement on the management and treatment of IgG4-related disease. *Arthritis Rheumatol.* (2015) 67:1688–99. doi: 10.1002/art.39132

Conflict of Interest: The authors declare that the research was conducted in the absence of any commercial or financial relationships that could be construed as a potential conflict of interest.

Publisher's Note: All claims expressed in this article are solely those of the authors and do not necessarily represent those of their affiliated organizations, or those of the publisher, the editors and the reviewers. Any product that may be evaluated in this article, or claim that may be made by its manufacturer, is not guaranteed or endorsed by the publisher.

Copyright © 2022 Hofmeyr, Herbst, Pretorius, Sarembock, Taylor and Roytowski. This is an open-access article distributed under the terms of the Creative Commons Attribution License (CC BY). The use, distribution or reproduction in other forums is permitted, provided the original author(s) and the copyright owner(s) are credited and that the original publication in this journal is cited, in accordance with accepted academic practice. No use, distribution or reproduction is permitted which does not comply with these terms.

frontiers | Frontiers in Neurology

ORIGINAL RESEARCH
published: 27 June 2022
doi: 10.3389/fneur.2022.879149

Description of a New Labyrinthine Dehiscence: Horizontal Semicircular Canal Dehiscence at the Tympanic Segment of the Facial Nerve

Gerard Gianoli[1], James Soileau[1] and Bradley Shore[2]*

[1] The Ear and Balance Institute, Covington, LA, United States, [2] Diagnostic Imaging Services, New Orleans, LA, United States

Objective: This report is a case series of patients with findings suspicious for a labyrinthine dehiscence syndrome not previously described in the medical literature. We describe the clinical and test findings in 16 patients with CT findings suspicious for dehiscence of the ampullated end of the horizontal semicircular canal at the tympanic segment of the facial nerve.

Study Design: Observational case series.

Setting: Neurotology vestibular referral center.

Patients: To be included in this study the patients were seen at our center in 2019 and had a high-resolution CT scan with a collimation of 0.6 mm. Patients who were identified as having findings suspicious for dehiscence of bone where the facial nerve crosses the ampullated end of the horizontal semicircular canal (HSC-FND) were identified and further analyzed.

Interventions: Case series retrospective record review of patient symptoms, physical findings, audiometry, vestibular testing, and CT scans was performed. CT findings of other dehiscent sites were noted. A comparison to surgically treated perilymph fistula (PLF) patients of the same period was performed.

Main Outcome Measures: History and physical exam were reviewed for auditory symptoms, vestibular symptoms, and exacerbating factors. and. Audiometry and vestibular testing were reviewed to determine which tests were most likely to be abnormal. CT scans were independently graded according to degree of suspicion for HSC-FND. Finally, patients with HSC-FND as the sole dehiscence identified were compared to those who had HSC-FND plus other dehiscent sites (HSC-FND+O) and to the group of surgically treated PLF patients.

Results: Of 18 patients, 16 met inclusion criteria. Nine (56%) of those suspicious for HSC-FND had dehiscences in other parts of the labyrinth. Additional dehiscent sites included: six superior semicircular canal dehiscences (SSCD), two cochlear facial dehiscences and one cochlear carotid dehiscence. The most common auditory symptoms were autophony followed by tinnitus and aural fullness. The most common vestibular symptoms were pulsion sensation (feeling of being pushed to one side)

OPEN ACCESS

Edited by:
P. Ashley Wackym,
The State University of New Jersey,
United States

Reviewed by:
Michael Thomas Teixido,
Thomas Jefferson University,
United States
Samuel Gubbels,
University of Colorado Denver,
United States

****Correspondence:***
Gerard Gianoli
ggianoli@gmail.com

Specialty section:
This article was submitted to Neuro-Otology, a section of the journal Frontiers in Neurology

Received: *18 February 2022*
Accepted: *31 May 2022*
Published: *27 June 2022*

Citation:
Gianoli G, Soileau J and Shore B (2022) Description of a New Labyrinthine Dehiscence: Horizontal Semicircular Canal Dehiscence at the Tympanic Segment of the Facial Nerve. Front. Neurol. 13:879149. doi: 10.3389/fneur.2022.879149

followed by vertigo spells. The most common exacerbating factors for vertigo were straining, and sound. The most commonly abnormal vestibular test was nasal Valsalva testing, which was positive in all but one patient. Anamnesis and examination observations were similar in both groups, but the HSC-FND group were less likely to demonstrate a caloric weakness or an abnormal ECOG compared to the HSC-FND+O group. Of note, cVEMP was more often found to have lower thresholds in the HSC-FND group compared to the HSC-FND+O group. An example case is highlighted. Comparison to the PLF patients revealed statistically significant difference in the presenting symptoms of autophony, fullness and pulsion sensation. When comparing testing, HSC-FND patients were more likely to have an abnormal cVEMP and PLF patients were more likely to have asymmetric hearing. The incidence of bilateral disease was also more common among the HSC-FND patients than the PLF patients.

Conclusions: A new labyrinthine dehiscence has been described to occur where the tympanic segment of the facial nerve crosses over the ampullated end of the horizontal semicircular canal. HSC-FND patients can present in a similar manner as HSC-FND+O patients with similar test findings except as mentioned above. The identification of one dehiscence such as SSCD does not preclude the presence of another dehiscence such as HSC-FND. HSC-FND could be the source of persistent symptoms post SSCD surgery as illustrated in the case presented. HSC-FND patients seem to identify themselves compared to PLF patients by a much more likely presenting symptoms of autophony, fullness, pulsion, abnormal cVEMP, bilaterality of disease, and symmetric hearing.

Keywords: third mobile window, dehiscence, horizontal semicircular canal, facial nerve, vertigo, Tullio phenomenon, perilymphatic fistula

INTRODUCTION

Superior Semicircular Canal Dehiscence (SSCD), first reported in 1998 (1), is a disorder defined as the absence of bone over the superior semicircular canal at the middle cranial fossa. The proposed pathophysiology is the Third Mobile Window Theory which posits abnormal compliance of the dehiscence (i.e., the third window) results in stimulation of the superior canal from egress of endolymph by changes in intracranial pressure or middle ear pressure. Its varying clinical presentations garnered it the nickname of the "Great Otologic Mimicker" (2). However, it has been most commonly characterized by the symptoms of Tullio's phenomenon, strain-induced vertigo/dizziness and autophony. Autophony to voice, heartbeat and eye movement are frequently reported with SSCD.

Since its identification it is being increasingly recognized that there are other bony dehiscences of the labyrinthine which can cause these same characteristic symptoms. Among these are posterior semicircular canal dehiscence (3), erosive processes into the horizontal semicircular canal, cochlear carotid dehiscence (4), cochlear facial dehiscence (5), enlarged vestibular aqueduct, X-linked gusher syndrome, cochlear-internal auditory canal defects (6), modiolar defects (7), and jugular bulb dehiscence into the vestibular aqueduct (8). Further, surgical repair or occlusion of SSCD has been shown to produce generally good outcomes for autophony and vestibular symptoms (9, 10). However, there are still some patients that have persistence of these symptoms in spite of what would seem to be successful surgery (11). This suggests an additional pathology or process in this subgroup of patients.

There are three elements to the diagnosis of Semicircular Canal Dehiscence Syndrome (SCD): (1) History consistent with SCD, namely Tullio's phenomenon, strain-induced vertigo and autophony, (2) Physiologic testing consistent with SCD (such as VEMP, ECOG, Tullio, Hennebert testing, etc.) and (3) CT imaging demonstrating a bony dehiscence of the superior semicircular canal (12). If the identifiable dehiscence is in another area of the otic capsule such as mentioned above, this is suspected to be the site of the pathology, i.e., Posterior Semicircular Canal Dehiscence, Cochlear Facial Dehiscence, etc. Many patients present with the first two elements of SCD syndrome but have no bony dehiscence of the labyrinth found on CT scan (13, 14).

In this paper we will describe a cohort of patients who meet criteria for labyrinthine dehiscence but have CT scan findings suspicious for a hitherto unreported bony dehiscence of the labyrinth. This dehiscence is located near the ampullated end of the horizontal semicircular canal bone at the crossover of the tympanic segment of the facial nerve (HSC-FND). We will present data on clinical presentation, audiovestibular test findings and imaging and compare to a group of patients with PLF. Our purpose is to help characterize what appears to be a newly identified labyrinthine dehiscence. We will also

highlight a case of SSCD with concomitant HSC-FND who had persistent problems with autophony and vestibular symptoms despite appropriate surgical repair of the SSCD.

METHODS

The setting for this case series retrospective review is a tertiary Neurotology referral center for vestibular disorders that receives a high case load of SCD patient referrals. For the calendar year 2019, charts were retrospectively reviewed for the observation of HSC-FND on CT scan. These patients were referred to the primary author due to persistent symptoms of a third mobile window disorder. Further scrutiny of the CT scans identified 18 patients with a possible HSC-FND. The charts were analyzed for clinical symptoms, physical findings, audiometric testing, vestibular testing, and CT findings. Additionally, all patients had undergone MRI scanning with unremarkable findings.

Patients were excluded if CT was not available for review, or if CT slice thickness was inappropriately large. Patients were also excluded if another pathology (with the exception of other bony dehiscences) was identified that could explain the patient's symptomatology. Lastly, patients were excluded if they had not undergone audio-vestibular testing.

Historical information extracted from the charts included antecedent events, auditory symptoms of hearing loss, fluctuation, fullness, tinnitus, noise intolerance, hearing sensitivity, and autophony. When we use the term autophony, we refer to an enhanced perception of any bodily sound, including voice, heartbeat, and eye movement. Vestibular symptoms extracted included the presence of unsteadiness and vertigo. Exacerbating factors for vertigo–sound, straining and position–were also recorded. Physical findings recorded were Fukuda stepping test and the presence of spontaneous nystagmus during infrared video examination. Treatment and outcomes were recorded.

Comprehensive audiometry, electrocochleography and cervical vestibular evoked myogenic potentials (cVEMP) were analyzed. Results for caloric testing, Tullio testing, fistula testing, Valsalva testing and Platform Pressure Testing were analyzed.

cVEMP testing was performed with 500 Hz toneburst via insert electrodes. Surface electrodes on the sternocleidomastoid muscles during active muscle contraction recorded P1/N1 latencies and peak to peak amplitudes as well as thresholds. A threshold search was performed.

Tullio testing, fistula testing, and Valsalva testing was performed with VNG recording. Tullio testing was performed with the use of a portable audiometer. Sequential stimulation of each ear with 500 Hz pulsing tone at 105 db for 10 s each. Fistula testing was accomplished using a Bruening Otoscope with direct visualization of the tympanic membrane. Alternating positive and negative pressure was applied while looking for eye deflections synchronized with the pressure application over a thirty second time period. Valsalva testing was done using both glottic and nasal Valsalva over a thirty second period for each. Valsalva testing was defined as abnormal if the patient developed nystagmus and/or vertigo during the test. Platform pressure testing was accomplished on an Equitest sensory organization test number 5 with alternating positive, negative or no pressure applied to each ear sequentially. Abnormal results were noted for >50% increase in sway energy over baseline. If a patient was unable to maintain balance on sensory organization test number 5, then the Platform Pressure Test was deferred.

For the CT studies we used the standard application (inner ear high-resolution program) as suggested by the manufacturer. The parameters used with the Hitachi Supria (Hitachi HeathCare Tokyo, Japan) system were as follows: 120 kV, 125 mAs, pitch 0.562, 2.5 × 0.6 mm collimation, matrix 512 × 512; reconstruction using the bone algorithm to yield 0.6-mm-thick sections with an increment of 0.06 mm; field of view 8 cm; image length 5 cm; imaging time 20 s; reconstruction with extended CT scale.

The CT protocols were intended to achieve the highest spatial resolution. The Poschl projection was obtained perpendicular to the long axis of the petrous bone, at an angle of 45 degrees with the sagittal and coronal planes. The superior semicircular canal was seen as a ring in a single plane in the Poschl projection. The Stenvers projection was obtained parallel to the petrous apex and perpendicular to the Poschl plane. Specifically, for analyzing the scans for HSC-FND the coronal and Poschl images were reviewed.

These CT scans of these patients were analyzed by two Neurotologists and one Neuroradiologist for the degree of certainty of HSC-FND on a scale of 0-3. A "0" represented findings of no bony dehiscence in this region. Whereas, a "3" represented a high degree of certainty for a bony dehiscence being present at the region of the horizontal semicircular canal where the tympanic segment of the facial nerve crosses it laterally with at least two slices demonstrating dehiscence. The scores were averaged between the three reviewers. For the purpose of our study, an average score below 1.5 was considered to not have HSC-FND, while score $\geq$1.5 was considered to have HSC-FND. The scans were reviewed for concomitant bony dehiscences in other parts of the labyrinth (HSC-FND+O). Findings for HSC-FND patients were compared to HSC-FND+O patients.

The HSC-FND patients were compared to a group of seven surgically treated PLF patients from the same time period. The PLF group had no evidence of otic capsule dehiscence on CT scan and were successfully treated with surgical repair. Chi square analysis was applied to compare symptom presentation, vestibular testing, auditory testing and bilaterality of disease.

The procedures followed were in accordance with the ethical standards of the responsible committee on human experimentation and with the Helsinki Declaration. The Salus Institutional Review Board approved this study.

RESULTS

There were 18 patients identified in our chart review. Of these, one patient was excluded because the CT scan was not available for review. Another patient was excluded because they had not undergone vestibular testing. Consequently, there were 16 patients available for analysis.

TABLE 1 | Auditory symptoms, vestibular symptoms and testing for HSC-FND patients ($N = 16$) compared to PLF patients ($N = 7$).

Findings	HSC-FND ($N = 16$)	PLF ($N = 7$)	
Age	43 (range 17–63)	54 (36–69)	
Male:Female	9:7	4:3	
Trauma history	10 (63)*	5 (71)	$p = 0.679$
Auditory symptoms			
Autophony	16 (100)	0 (0)	$p < 0.05$
Tinnitus	13 (81)	6 (86)	$p = 0.479$
Aural fullness	12 (75)	2 (29)	$p < 0.05$
Noise intolerance	10 (63)	3 (43)	$p = 0.382$
Otalgia	7 (44)	3 (43)	$p = 0.968$
Hearing loss	5 (31)	4 (57)	$p = 242$
Fluctuation of hearing	5 (31)	2 (29)	$p = 0.898$
Hearing hypersensitive	3 (19)	0 (0)	$p = 0.698$
Vestibular symptoms			
Positional vertigo/Dizziness	13 (81)	5 (71)	$p = 0.738$
Pulsion sensation	12 (75)	1 (14)	$p < 0.05$
Strain-induced vertigo/Dizziness	12 (75)	5 (71)	$p = 0.858$
Rotary vertigo (non-positional)	11 (69)	5 (71)	$p = 0.898$
Unsteadiness	9 (56)	6 (86)	$p = 0.172$
Tullio phenomenon	8 (50)	3 (43)	$p = 0.752$
Testing			
Valsalva (Nasal or Glottic) Test	15 (94)	6(86)	$p = 0.529$
Fistula test	14 (88)	7 (100)	$p = 0.743$
Platform pressure test	9 (82)**	5 (71)	$p = 0.605$
Tullio testing	11 (69)	2 (29)	$p = 0.074$
ECOG	6 (40)++	1 (14)	$p = 0.228$
Caloric testing (UW > 25%)	5 (31)	4 (57)	$p = 0.242$
cVEMP	10(63)	1 (14)	$p < 0.05$
Asymmetric HL	4 (25)	6 (86)	$p < 0.05$
Bilateral disease	13 (81)	2 (29)	$p < 0.05$

**Eight cases of direct head trauma and 2 cases of barotrauma. **N = 11, Four patients could not stand on SOT #5 and one patient surpassed the weight limit for testing. Consequently, a total of 5 patients could not complete Platform Pressure Testing. ++ N = 15, One patient could not be evaluated because of no measurable SP wave.*

Using our grading system, the presence of HSC-FND was noted to be bilateral in 13 cases and unilateral in 3 cases. The three reviewers were highly consistent with average score of 2.1, ranging from 1 to 3 (out of a possible 3) for all the areas analyzed. There was also highly consistent agreement on the scans that did not have an HSC-FND. The correlation coefficient comparing examiner 1 to examiner 2 was 0.61; for examiner 2 compared to examiner 3 it was 0.60; and for examiner 1 compared to examiner 3 it was 0.73.

Nine patients had findings of other dehiscent sites whereas seven had no other identifiable otic capsule dehiscences. The additional dehiscent sites included SSCD (six cases), Facial-Cochlear Dehiscence (FCD) (two cases) and one case of Cochlear Carotid Dehiscence (CCD). All patients had undergone MRI scan with no pathologic findings of note.

Of the 16 patients, 10 patients reported onset of symptoms immediately after trauma. Eight of these were after direct blunt head trauma. Two of these were subsequent to barotrauma–one during air travel and another with scuba diving.

Auditory and vestibular symptoms, as well as testing, are detailed in **Table 1**. The most common auditory symptoms included autophony (16, 100%), tinnitus (13, 81%), aural fullness (12, 75%) and noise intolerance (10, 63%). The most common vestibular symptoms were positional vertigo/dizziness (13, 81%), pulsion sensation (12, 75%), strain-induced vertigo/dizziness (12, 75%), non-positional rotary vertigo (11, 69%), unsteadiness (9, 56%) and Tullio phenomenon (8, 50%).

Physical exam demonstrated evidence of spontaneous nystagmus with infrared video exam in seven (44%) patients. An abnormal Fukuda test was found in 11 (69%) patients, but one patient (6%) was unable to stand to perform the Fukuda test. Three patients (19%) had no evidence of nystagmus and a normal Fukuda test. Audiometry was normal in 12 patients (75%). There were two patients (13%) who had bilateral asymmetric sensorineural hearing loss, one (13%) with a unilateral sensorineural hearing loss and one (13%) with symmetric sensorineural scores but had a unilateral conductive gap.

The most common vestibular test abnormalities were nasal and/or glottic Valsalva test (15, 94%), fistula test (14, 88%), Platform Pressure Test (9, 82%) and Tullio test (11, 69%). It should be noted that five patients could not perform the

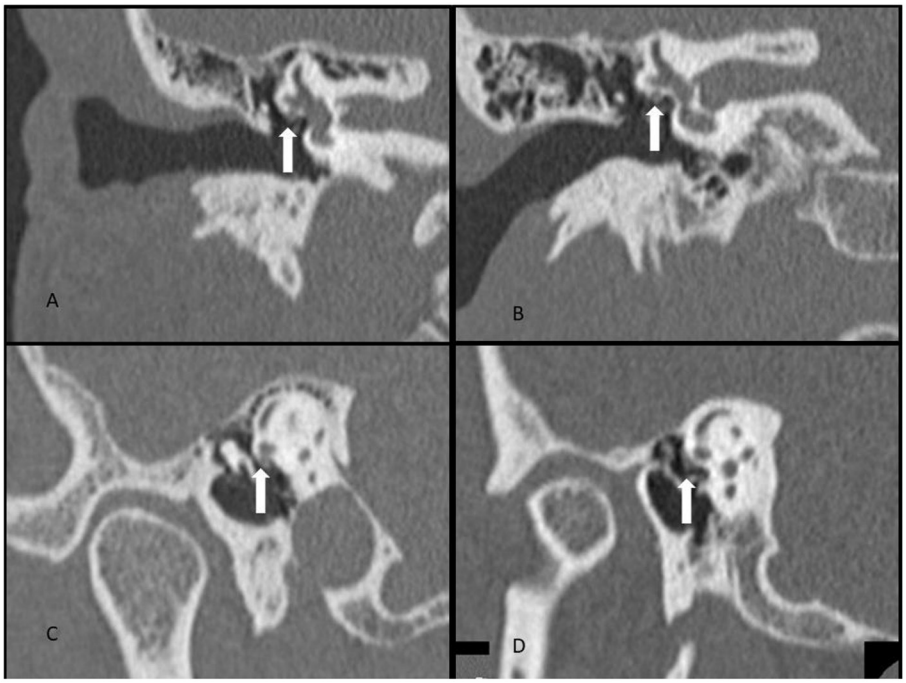

FIGURE 1 | CT scan demonstrating **(A)** HSC-FND on coronal imaging, **(B)** normal HSC and facial nerve anatomy on coronal imaging, **(C)** HSC-FND on Poschl imaging, and **(D)** normal HSC and facial canal on Poschl imaging.

Platform Pressure test because four could not stand on Sensory Organization Test #5 and one was over the weight limit for Platform Testing.

Comparison of HSC-FND to HSC-FND+O demonstrated similar historical and physical exam qualities. There were a few differences in the HSC-FND and HSC-FND+O groups when it came to testing. Most notable was a higher incidence of ECOG abnormalities (SP/AP ratio > 0.40) in the HSC-FND+O group (56%) vs. the HSC-FND group (17%). Unilateral caloric weakness was also more common among the HSC-FND+O group (44%) vs. HSC-FND (17%). However, reduced cVEMP thresholds were more common among the HSC-FND group (83% were $\leq$85 db) compared to the HSC-FND+O group (56% were $\leq$85 db); and abnormal Valsalva testing was similar in both groups−100% for HSC-FND vs. 89% for HSC-FND+O. None of these outcomes were statistically significant. However, this may be due to the small total number of cases involved in this study.

There were 6 of 16 with no nystagmus on Tullio testing (5 HSC-FND+O and 1 HSC-FND) although some had symptoms but no nystagmus. There were 6 of 16 with horizontal nystagmus (1 HSC-FND+O and 5 HSC-FND). There were 4 of 16 with vertical/torsional nystagmus (3 HSC-FND+O and 1 HSC-FND). Another way to view this is that among those with HSC-FND ($N = 7$), on Tullio testing 5 had horizontal nystagmus, one had vertical/torsional nystagmus and one had no nystagmus. Whereas, among HSC-FND+O ($N = 9$) patients, Tullio testing resulted in 3 with vertical/torsional nystagmus, one with horizontal nystagmus and 5 with no nystagmus.

The fistula testing was more inclined to demonstrated horizontal phase-locked eye movement regardless of the group. Among HSC-FND patients, horizontal eye movement was noted in 6 of 7 patients with 1 of 7 demonstrating no eye movement. Among HSC-FND+O patients, 5 of 9 demonstrated horizontal phase-locked eye movement, 3 of 9 demonstrated vertical/torsional eye movement and 1 of 9 demonstrated no eye movement.

Comparison to the surgically treated PLF patients as detailed in **Table 1**, demonstrated statistically significant differences for the symptoms of autophony (100 vs. 0%), aural fullness (75 vs. 29%), pulsion sensation (75 vs. 14%). Testing demonstrated significant differences in cVEMP (63 vs. 14%), and asymmetric hearing loss (25 vs. 86%). Lastly, PLF patients were less likely to have bilateral disease (29%) compared to HSC-FND patients (81%).

All 16 HSC-FND patients were given medical management which consisted of dietary restrictions (low salt and caffeine avoidance), physical restrictions (avoidance of abdominal/thoracic straining) and either diuretics or a carbonic anhydrase inhibitor. One patient was lost to follow up. Of the remaining 14 patients, 10 (71%) had resolution of their vestibular symptoms with medical management. Four underwent surgical reinforcement of the suspected area, inclusive of the oval window along with round window reinforcement. One had sequential bilateral surgical repair, and one had unilateral repair–both with complete resolution of their vestibular symptoms. The third patient who underwent surgery completed the first of planned bilateral sequential repairs noting significant improvement in

their symptoms at present. At the time of this writing, it is uncertain whether the contralateral procedure will be required. The fourth case is detailed below:

Case Report

A 36-year-old female experienced onset of autophony, Tullio phenomenon and strain-induced vertigo after a head injury seven years prior. She was evaluated and treated at an outside facility for SSCD identified on CT scan, supported by an abnormal cVEMP result with a 55 db threshold. A middle fossa craniotomy with SSCD occlusion was performed. Postoperatively the patient noted no change in symptoms, with persistent autophony, Tullio's and strain-induced vertigo. The following year she was referred to our facility for evaluation. Audiometry was normal. cVEMP testing demonstrated thresholds improved to 85 db. VNG demonstrated balanced caloric testing. Tullio testing and Valsalva testing were abnormal, producing nystagmus and the symptoms of vertigo. Fistula testing produced synchronous eye movement with positive and negative pressure application to the ear canal. vHIT testing revealed reduced function in the superior canal that had been surgically occluded, suggesting the occlusion was successful. An MRI scan demonstrated a filling defect of the superior canal, again suggesting successful surgical occlusion of the superior canal. CT scan demonstrated HSC-FND as well as the previously noted SSCD and middle fossa craniotomy postoperative changes. She was referred back to her referring physician with therapeutic recommendations. She underwent window reinforcement by the referring surgeon that included the HSC-FND, oval and round window reinforcement. This resulted in complete resolution of her vestibular symptoms and improvement in her autophony as of her last communication which was approximately 6 months postoperative.

DISCUSSION

Most commonly, dehiscence or fistula of the horizontal semicircular canal has been identified to occur secondary to erosion from cholesteatoma (15). While this has been extensively reported in the medical literature, dehiscence of the horizontal semicircular canal not caused by some erosive process is not. Only two case reports of horizontal semicircular canal dehiscence were identified in our review of PubMed.

In 2007, Bassim et al. (16) reported a case of bony dehiscence of the horizontal semicircular canal in a patient being evaluated for cochlear implantation. The dehiscence was located throughout the entire apex of the arch of the horizontal semicircular canal and included more than half of the semicircular canal. The patient had a history of radiation therapy for lymphoma of the palate, but the authors did not suspect this as the cause of the dehiscence because of its unilaterality. The contralateral side had normal bony coverage. No vestibular symptoms and no physiologic testing were reported in this paper.

In 2010, Zhang et al. (17) reported a case of a 76-year-old with vertigo, Tullio phenomenon and autophony. The patient exhibited nystagmus with sound application to the right ear. A CT scan demonstrated a 2.0 mm bony defect of the right horizontal semicircular canal. They recommended consideration of dehiscence of the horizontal semicircular canal be included in the differential diagnosis of sound- or pressure-induced vestibular symptoms. We could not find in PubMed any reports of horizontal semicircular canal dehiscence located at the tympanic segment of the facial nerve.

As noted in the introduction, the proposed pathophysiology of SSCD is due to the abnormal compliance of the inner system due to the dehiscence of the superior canal bone at the temporal lobe dura (1). This renders the superior canal (as well as the otolithic organs) susceptible to abnormal pressure changes from the middle ear and from the temporal lobe dura. In HSC-FND, the defect is qualitatively different from SSCD. It is a dehiscence that is covered by the facial nerve, which by itself should provoke no pressure changes such as seen with dural pressure transmission in SSCD. In our patient population, 63% developed symptoms after head trauma. This raises the question as to whether trauma played a role. There were no fractures identified on CT scan or intraoperative. We propose that the pressure wave from the head trauma could have caused a shift in the facial nerve or an increased compliance in this area resulting in the third mobile window symptoms in these patients.

The only clinical symptom seen in every patient of our case series was autophony. This is in striking contrast to the PLF patient group were there were no complaints of autophony. Beyond this, the most common auditory symptoms were tinnitus, aural fullness, and noise intolerance. Vestibular symptoms of rotary vertigo and disequilibrium were provoked by positional changes, straining and sound (Tullio's phenomenon). While most patients had normal or symmetric hearing, cVEMP testing and vestibular testing was frequently abnormal. Most notable was Valsalva testing with all but one patient having an abnormal Valsalva test. The fistula test was abnormal in all but two patients and the Tullio test was abnormal in almost two thirds of patients. The Platform Pressure Test was abnormal in 82% of the patients who completed the test. However, there were five patients who could not perform Platform Pressure Testing–four because they could not maintain their balance for baseline testing (SOT#5) and one because they were beyond the weight limit capacity for the platform. The above clinical profile of symptoms and test findings are suggestive of the SCD patients we have seen over the last 22 years and that have been reported in the literature.

A surprising number of patients (75%) reported pulsion sensation–a rocking/swaying feeling or feeling like being pushed to one side–suggesting abnormal otolithic stimulation, compared to only 14% ($p < 0.05$) among the PLF patients. The attribution to central pathology of the pulsion/rocking sensation has been longstanding and without any significant studies to back this up. More recently, these symptoms have been attributed to otolithic stimulation (18). Intuitively, this makes more sense, since isolated otolithic stimulation would result in a pulsion sensation rather than a rotary sensation; and this is something we have observed in our patient population as well. Given that the otoliths are located anatomically near this dehiscence, pulse waves from vascular pressure changes could theoretically be the cause for the rocking sensation experienced. In fact, some of the patients reported the rocking to be in concert with their heartbeat.

Clinical findings of HSC-FND compared with HSC-FND+O patients did not differ statistically. In fact, the HSC-FND group was slightly more likely to have lowered thresholds on cVEMP and abnormal Valsalva test results than the HSC-FND+O group. Compared to the PLF group, only 14% had an abnormal cVEMP compared to 63% among the HSC-FND group ($p < 0.05$). This further supports the theory that HSC-FND is an alternative otic capsule dehiscent instrumental in creating dehiscent symptoms/test findings.

What was notable in both the HSC-FND group and to a lesser extent, the HSC-FND+O group was the presence of horizontal nystagmus on Tullio testing and horizontal phase-locked eye movement on fistula testing. Overall, on Tullio testing 6 patients had horizontal nystagmus, 4 had vertical/torsional nystagmus, and 6 had no nystagmus. Three of the 4 patients with vertical/torsional nystagmus were among the HSC-FND+O group that included SSCD and other dehiscences. On fistula testing, 11 patients had horizontal phase-locked eye movements, 3 had vertical/torsional phase-locked eye movements and 2 had no eye movement. All three who had vertical/torsional eye movements were in the HSC-FND+O group and had SSCD. The finding of horizontal nystagmus on Tullio testing and horizontal phase-locked eye movement with fistula testing would implicate horizontal semicircular canal stimulation. This finding would seem to support HSC-FND as a cause for the patients' symptomatology.

The presence of similar symptoms in HSC-FND could explain what some authors have reported as oval window perilymphatic fistula. HSC-FND could result in labyrinthine fistula from the ampullated end of the horizontal semicircular canal, around the facial nerve canal and into the oval window niche. Theoretically, reinforcement of the oval window would potentially reinforce the HSC-FND deficient area resulting in cessation of symptoms.

Fallopian canal dehiscence was not systematically recorded, but it seems that all patients had fallopian canal dehiscence noted at surgery. We believe that fallopian canal dehiscence is a necessary part of the anatomy for HSC-FND to become "active." As noted in **Figure 1**, there are concomitant defects of the HSC and the fallopian canal at the Oval Window. The concept being the horizontal canal defect leads to pressure changes or an intermittent leak around the facial nerve. If there was no fallopian canal dehiscence, then there would be no means for fluid/pressure movement.

Our treatment paradigm for these patients with HSC-FND has been to begin medical management on all patients when feasible. This resulted in high symptoms resolution rate (71%). For many patients, understanding that straining was provoking many of their vestibular symptoms was revelatory. Educating the patients on how to avoid such provocations resulted in greatly improved quality of life. Further, additional medical measures including salt restriction, diuretics and titration dosing of acetazolamide lowered intracranial pressure and eventually allowed many of the medically treated patients to gradually increase their activity levels without return of vestibular symptoms. For those who continued to have persistent disabling symptoms, surgery was offered.

Of the four patients who did not have resolution on medical management, we offered surgical repair. The surgical repair included soft tissue reinforcement of the HSC-FND inclusive of the oval window and included round window reinforcement. This resulted in complete resolution of vestibular symptoms for three of the patients (one unilateral repair and one bilateral repair by us and one unilateral repair by the referring physician). The fourth patient had been scheduled for sequential bilateral repair and has completed one side as of this writing. This patient has noted significant improvement and we are unsure whether the contralateral surgery will be necessary at this time.

Evidence suggests that otic capsule volume is less and subsequent thickness of the bone surrounding the semicircular canals is thinner in SSCD cases compared with control cases. Park et al. (19) compared the thickness of otic capsule bone covering the semicircular canals in patients with SSCD compared to control cases. Not only did they find thinner bony coverage around the superior semicircular canal, but the bony coverage was also significantly thinner around the posterior and horizontal semicircular canals. Given the reduced volume of otic capsule bone and thinner bony coverage of all three semicircular canals, our study's finding of more than half the patients with other dehiscent sites is not surprising. In addition to HSC-FND, nine of the 16 CT scans reviewed demonstrated dehiscences at other locations in the otic capsule. These other sites included superior canal dehiscences, facial cochlear dehiscences and one case of cochlear carotid dehiscence.

The CT scans of our series of HSC-FND do not identify any erosive process such as cholesteatoma as the source for the dehiscence (see **Figure 1** for examples of HSC-FND compared to normal CT scans.). The overlying tympanic segment of the facial nerve suggests a probable anatomic defect that may be of congenital or developmental origin, perhaps due to the reduced otic capsule bone volume as noted by Park et al. (19). Among the 16 cases, 10 (63%) reported the onset of their symptoms immediately after trauma. This is consistent with the second event observation seen with many SSCD patients and suggests a similar pathogenic mechanism for the production of symptoms (12). However, the cause for this bony defect and symptoms onset awaits further investigation.

In the case presented, the patient had all three elements of the triad to make the diagnosis of SCD–history, physiologic testing, and CT scan findings of SSCD. The surgical occlusion would seem to have been performed successfully as demonstrated by improvement of the cVEMP threshold, reduction of the superior canal function on vHIT and absence of the superior canal signal on MRI scan. However, the patient's symptoms were unchanged and our test findings of positive fistula test, Tullio test and Valsalva test strongly pointed to an otic capsule dehiscence. While the abnormal test results could be the results of inadequate SSCD plugging in what appears to be a successful SSCD occlusion procedure, it was surprising to see no improvement in symptoms, especially given reduced anterior canal function on vHIT testing. Alternatively, a concomitant otic capsule dehiscence could explain these findings. Surgical reinforcement as we detailed in the methods section (round window reinforcement and oval window reinforcement inclusive of the adjacent facial nerve

segment) by the referring surgeon resulted in resolution of the patient's symptoms. The identification of HSC-FND in this patient provides the likely reason for the patient's persistent symptoms after SSCD surgery. When evaluating patients with SSCD (or any other labyrinthine dehiscence) syndrome, it behooves surgeons to scrutinize the CT scan for additional dehiscent sites. Others have also documented patients with more than one site of dehiscence (5). Proactive treatment of these areas could possibly help improve symptom resolution.

Alternative explanations for the symptomatology in our HSC-FND+O group could be due to the other dehiscences noted in these nine patients. However, the seven patients with no other identifiable dehiscences (HSC-FND group) had a nearly identical symptom and testing profile, consistent with labyrinthine dehiscence. This supports that HSC-FND, as a sole finding, can provoke a similar clinical presentation as other labyrinthine dehiscences.

In our series, the HSC-FND was most evident on both the coronal and Poschl view (a projection perpendicular to the long axis of the petrous bone, at an angle of 45 degrees with the sagittal and coronal planes). This orientation allowed visualization of a cross section of the facial nerve and the bony septum with the horizontal semicircular canal. The axial, sagittal, and Stenvers projections did not demonstrate the dehiscence with the same level of confidence.

Currently, multidetector CT (MDCT) is the mainstay of the diagnosis of a semicircular canal dehiscence. The accuracy in the detection of SSCD in one study was between 92.9% utilizing standard axial and coronal planes and 98.8% using planes parallel and perpendicular to the SSC, similar to the technique and imaging planes as used in this study (20). However, Sequeira et al. (21) caution that MDCT tends to overestimate the prevalence of SSCD in comparison with higher resolution CT techniques such as microCT.

The studies of CT detection for SSCD should alert us to the possibility of falsely positive CT scans. Findings of "dehiscence" on CT, even though not a guarantee of actual bony dehiscence is not without merit. As demonstrated by Ward et al. (14), "near" dehiscence can represent a physiologic phenomenon similar to a frank dehiscence. In our case series, we cannot be certain that all of the identified HSC-FND were bony dehiscences. However, given the patients' symptoms and physiologic test findings, we have a raised degree of confidence that the dehiscences were real or at the very least, represent "near" HSC-FND.

Newer imaging techniques such as microCT and flat panel CT (FPCT) should increase our sensitivity and specificity in detection of HSC-FND (22–24). MicroCT scanning is able to achieve much better resolution than conventional clinical computed tomographic scanning, reducing, or eliminating the chance for error, but cannot be performed on patients at this time because of high radiation dosage and long scanning times. FPCT which uses an area detector instead of detector rows, offers improved spatial resolution for complex anatomy such as the temporal bone, but is currently limited by price and accessibility.

The HSC-FND patients were more likely to have symmetric hearing and evidence of bilateral disease compared to the PLF patients. Bilateral disease was found in 81% of the HSC-FND patients compared to 29% of the PLF patients ($p < 0.05$). This may suggest a congenital/developmental etiology for HSC-FND compared to PLF patients. With regards to hearing, only 25% of HSC-FND patients had asymmetric hearing loss compared to 86% of PLF patients ($p < 0.05$).

This paper has obvious weaknesses, most notably the problems with being a retrospective cases series, which are level IV evidence lacking a good control comparison adding to bias. The inclusion criteria was any new pateint during 2019 who had a CT scan that had been noted in the medical record of possibly having an HSC-FND. Patients with third mobile window symptoms may have had their CT scans more heavily scrutinized for otic capsule defects than those who did not have third mobile window findings. This could potentially bias the selection process and we don't know how many patients with no third mobile window symptoms may have had HSC-FND. However, this could be analogous to finding an asymptomatic SSCD patient. The area in question–the facial nerve as it crosses over the horizontal semicircular canal–is an area where bone is normally thin and could be prone to overdiagnosis as has been seen in CT surveys of SSCD. Further, it is entirely possible that the HSC-FND is not the source of the third mobile window, but another area that has yet been identified could be the source of pathology. These results should be applied cautiously to patients with the above-mentioned clinical profile while carefully scrutinizing for other pathology. As mentioned earlier, the diagnosis of labyrinthine dehiscence requires three elements: (1) symptoms consistent with dehiscence, (2) physiologic test findings consistent with dehiscence and (3) radiographic confirmation of anatomic bony dehiscence. While this study supplies a patient population with all three of these elements, to confirm HSC-FND as a diagnostic entity, histologic studies should be performed to further detail this anatomic area of thin or dehiscent bone.

CONCLUSIONS

A newly described labyrinthine dehiscence is reported. This case series of 16 patients presented with symptoms suggestive of labyrinthine dehiscence–autophony, strain-induced vertigo and Tullio's phenomenon. A history of trauma that immediately preceded the onset of symptoms was seen in most patients. Test findings objectively confirmed the patients' reported symptoms–most commonly by Valsalva testing and less often by fistula testing, Tullio testing and Platform Pressure testing. Imaging with CT demonstrated absence of bone at the ampullated end of the horizontal semicircular canal at the tympanic segment of the facial nerve adjacent to the oval window niche. While nine of these patients had additional dehiscent sites (HSC-FND + O group), seven did not (HSC-FND group). Comparison of clinical symptoms and test findings were not materially different in these two groups, strongly suggesting a similar pathophysiologic process. Compared to a control group of surgical repaired PLF patients, the HSC-FND patients were more likely to have autophony, aural fullness, pulsion sensation, abnormal cVEMP, bilateral disease and symmetric hearing. Medical treatment was successful in

symptom resolution in most patients. Surgical reinforcement was successful in the few cases that did not respond to medical management. We recommend consideration of this entity when evaluating patients with symptoms and test findings consistent with labyrinthine dehiscence. We also recommend further confirmation of HSC-FND with temporal bone histologic studies.

DATA AVAILABILITY STATEMENT

The raw data supporting the conclusions of this article will be made available by the authors, without undue reservation.

ETHICS STATEMENT

The studies involving human participants were reviewed and approved by the Salus Institutional Review Board. Written informed consent for participation was not required for this study in accordance with the national legislation and the institutional requirements.

AUTHOR CONTRIBUTIONS

GG, JS, and BS contributed to the data analysis and writing of the paper. All authors contributed to the article and approved the submitted version.

REFERENCES

1. Minor LB, Solomon D, Zinreich JS, Zee DS. Sound- and/or pressure-induced vertigo due to bone dehiscence of the superior semicircular canal. *Arch Otolaryngol Head Neck Surg.* (1998) 124:249–58. doi: 10.1001/archotol.124.3.249
2. Zhou G, Gopen Q, Poe DS. Clinical and diagnostic characterization of canal dehiscence syndrome: a great otologic mimicker. *Otol Neurotol.* (2007) 28:920–6. doi: 10.1097/MAO.0b013e31814b25f2
3. Nomiya S, Cureoglu S, Kariya S, Morita N, Nomiya R, Schachern PA, et al. Posterior semicircular canal dehiscence: a histopathologic human temporal bone study. *Otol Neurotol.* (2010) 31:1122–7. doi: 10.1097/MAO.0b013e3181eb3309
4. Oliver JR, Chen DS, Pearl MS, Carey JP, Sun DQ. Carotid artery-cochlear dehiscence. *Otol Neurotol.* (2020) 41:e290–2. doi: 10.1097/MAO.0000000000002494
5. Wackym PA, Balaban CD, Zhang P, Siker DA, Hundal JS. Third window syndrome: surgical management of cochlea-facial nerve dehiscence. *Front Neurol.* (2019) 10:1281. doi: 10.3389/fneur.2019.01281
6. Varadarajan VV, DeJesus RO, Antonelli PJ. Novel computed tomography findings suggestive of perilymph gusher. *Otol Neurotol.* (2018) 39:1066–9. doi: 10.1097/MAO.0000000000001916
7. Antonelli PJ, Nall AV, Lemmerling MM, Mancuso AA, Kubilis PS. Hearing loss with cochlear modiolar defects and large vestibular aqueducts. *Am J Otol.* (1998) 19:306–12.
8. Park JJ, Shen A, Loberg C, Westhofen M. The relationship between jugular bulb position and jugular bulb related inner ear dehiscence: a retrospective analysis. *Am J Otolaryngol.* (2015) 36:347–51. doi: 10.1016/j.amjoto.2014.12.006
9. Smullen JL, Andrist EC, Gianoli GJ. Superior semicircular canal dehiscence: a new cause of vertigo. *J La State Med Soc.* (1999) 151:397–400.
10. Gianoli GJ, Soileau JS. Superior semicircular canal dehiscence: pathophysiology and surgical outcomes. *Curr Otorhinolaryngol Rep.* (2017) 5:153–9. doi: 10.1007/s40136-017-0156-2
11. Sharon JD, Pross SE, Ward BK, Carey JP. Revision surgery for superior canal dehiscence syndrome. *Otol Neurotol.* (2016) 37:1096–103. doi: 10.1097/MAO.0000000000001113
12. Ward BK, Carey JP, Minor LB. Superior canal dehiscence syndrome: lessons from the first 20 years. *Front Neurol.* (2017) 8:177. doi: 10.3389/fneur.2017.00177
13. Wackym PA, Wood SJ, Siker DA, Carter DM. Otic capsule dehiscence syndrome: Superior semicircular canal dehiscence syndrome with no radiographically visible dehiscence. *Ear Nose Throat J.* (2015) 94:E8–24. doi: 10.1177/014556131509400802
14. Ward BK, Wenzel A, Ritzl EK, Gutierrez-Hernandez S, Della Santina CC, Minor LB, et al. Near-dehiscence: clinical findings in patients with thin bone over the superior semicircular canal. *Otol Neurotol.* (2013) 34:1421–8. doi: 10.1097/MAO.0b013e318287efe6
15. Soda-Merhy A, Betancourt-Suárez MA. Surgical treatment of labyrinthine fistula caused by cholesteatoma. *Otolaryngol Head Neck Surg.* (2000) 122:739–42. doi: 10.1067/mhn.2000.99075
16. Bassim MK, Patel KG, Buchman CA. Lateral semicircular canal dehiscence. *Otol Neurotol.* (2007) 28:1155–6. doi: 10.1097/MAO0b013e31809ed965
17. Zhang LC, Sha Y, Dai CF. Another etiology for vertigo due to idiopathic lateral semicircular canal bony defect. *Auris Nasus Larynx.* (2011) 38:402–5. doi: 10.1016/j.anl.2010.11.003
18. Pelosi S, Schuster D, Jacobson GP, Carlson ML, Haynes DS, Bennett ML, et al. Clinical characteristics associated with isolated unilateral utricular dysfunction. *Am J Otolaryngol.* (2013) 34:490–5. doi: 10.1016/j.amjoto.2013.04.008
19. Park JH, Kang SI, Choi HS, Lee SY, Kim JS, Koo JW. Thickness of the bony otic capsule: etiopathogenetic perspectives on superior canal dehiscence syndrome. *Audiol Neurootol.* (2015) 20:243–50. doi: 10.1159/000371810
20. Sparcia G, Iaia A. The diagnostic performance of reformatted isotropic thin-section helical CT images in the detection of superior semicircular canal dehiscence. *Neuroradiol J.* (2017) 30:216–21. doi: 10.1177/1971400916689484
21. Sequeira SM, Whiting BR, Shimony JS, Vo KD, Hullar TE. Accuracy of computed tomography detection of superior canal dehiscence. *Otol Neurotol.* (2011) 32:1500–5 doi: 10.1097/MAO.0b013e318238280c
22. Tunkel AE, Carey JP, Pearl M. Flat panel computed tomography in the diagnosis of superior semicircular canal dehiscence syndrome. *Otol Neurotol.* (2019) 40:213–7. doi: 10.1097/MAO.0000000000002076
23. Conte G, Scola E, Calloni S, Brambilla R, Campoleoni M, Lombardi L, et al. Flat panel angiography in the cross-sectional imaging of the temporal bone: assessment of image quality and radiation dose compared with a 64-section multisection CT scanner. *AJNR Am J Neuroradiol.* (2017) 38:1998–2002. doi: 10.3174/ajnr.A5302
24. Lee JY, Shin KJ, Kim JN, Yoo JY, Song WC, Koh KS, et al. A morphometric study of the semicircular canals using micro-CT images in three-dimensional reconstruction. *Anat Rec.* (2013) 296:834–9. doi: 10.1002/ar.22664

Conflict of Interest: The authors declare that the research was conducted in the absence of any commercial or financial relationships that could be construed as a potential conflict of interest.

Publisher's Note: All claims expressed in this article are solely those of the authors and do not necessarily represent those of their affiliated organizations, or those of the publisher, the editors and the reviewers. Any product that may be evaluated in this article, or claim that may be made by its manufacturer, is not guaranteed or endorsed by the publisher.

Copyright © 2022 Gianoli, Soileau and Shore. This is an open-access article distributed under the terms of the Creative Commons Attribution License (CC BY). The use, distribution or reproduction in other forums is permitted, provided the original author(s) and the copyright owner(s) are credited and that the original publication in this journal is cited, in accordance with accepted academic practice. No use, distribution or reproduction is permitted which does not comply with these terms.

frontiers | Frontiers in Neurology

ORIGINAL RESEARCH
published: 11 July 2022
doi: 10.3389/fneur.2022.910062

Olfactory, Auditory, and Vestibular Performance: Multisensory Impairment Is Significantly Associated With Incident Cognitive Impairment

Jacob C. Lucas[1], Zack Arambula[1], Alexandra M. Arambula[1], Katherine Yu[1], Nathan Farrokhian[1], Linda D'Silva[2], Hinrich Staecker[1] and Jennifer A. Villwock[1]*

[1] *Department of Otolaryngology- Head and Neck Surgery, University of Kansas School of Medicine, Kansas City, MO, United States,* [2] *Department of Physical Therapy and Rehabilitation Science, University of Kansas Medical Center, Kansas City, MO, United States*

OPEN ACCESS

Edited by:
Michael Strupp, Ludwig Maximilian University of Munich, Germany

Reviewed by:
Juan Carlos Amor-Dorado, Hospital Can Misses, Spain
Alessandra Fioretti, European Hospital, Italy

****Correspondence:***
Jacob C. Lucas
jake.lucas.ent@gmail.com

Specialty section:
This article was submitted to Neuro-Otology, a section of the journal Frontiers in Neurology

Received: *31 March 2022*
Accepted: *21 June 2022*
Published: *11 July 2022*

Citation:
Lucas JC, Arambula Z, Arambula AM, Yu K, Farrokhian N, D'Silva L, Staecker H and Villwock JA (2022) Olfactory, Auditory, and Vestibular Performance: Multisensory Impairment Is Significantly Associated With Incident Cognitive Impairment. Front. Neurol. 13:910062. doi: 10.3389/fneur.2022.910062

Background: Dysfunction in the olfactory, auditory, and vestibular systems are commonly seen in aging and are associated with dementia. The impact of sensory loss(es) on cognition is not well understood. Our aim was to assess the relationships between performance on objective multisensory testing and quantify the impact of dysfunction on cognition.

Methods: Patients presenting with subjective hearing loss presenting to a tertiary care otologic/audiologic clinic were identified and underwent multisensory testing using the Affordable, Rapid Olfactory Measurement Array (AROMA), pure tone audiometric evaluations, and the Timed "Up and Go" test. Cognitive impairment (CI) was assessed *via* the Montreal Cognitive Assessment (MoCA) was also administered.

Key Results: 180 patients were enrolled. Thirty one percentage ($n = 57$) screened positive for cognitive impairment. When evaluating single sensory impairments, we found that olfactory dysfunction, gait impairment, and sensorineural hearing loss were all statistically significantly ($p < 0.05$) associated with a higher risk of cognitive impairment (ORs 3.89, 3.49, and 2.78, respectively) for CI. Multisensory impairment was significantly associated with cognitive impairment. Subjects with dysfunction in all domains were at the highest risk for cognitive impairment (OR 15.7, $p < 0.001$) vs. those with impairment in 2 domains (OR 5.32, $p < 0.001$).

Conclusion: Dysfunction of the olfactory, auditory, and vestibular systems is associated with a significantly increased risk of CI. The dramatically increased risk of CI with multisensory dysfunction in all three systems indicated that MSD may synergistically contribute to CI.

Keywords: multisensory impairment, age-related hearing impairment, vestibular impairment, olfactory impairment, cognitive impairment, AROMA, Montreal Cognitive Assessment (MoCA)

INTRODUCTION

Cognitive impairment (CI) and dementia have been linked to sensory impairments in multiple domains such as hearing loss, olfactory dysfunction, and vestibular dysfunction. Several large, epidemiologic studies suggest that impairments in more than one sensory domain may be additive with respect to subsequent risk of developing CI. Unlike other risk factors such as age and genetics, sensory deficits are potentially modifiable by techniques such as hearing amplification, olfactory training, and vestibular therapy. Emerging literature suggests that approaches to improve sensory processing, such as cochlear implantation, may reverse cognitive decline (1).

The concept of Multisensory Impairment has been broached in the literature and is an area of active study; several retrospective cohort studies have examined age-related sensory decline including the Epidemiology of Hearing Loss Study (EHLS) (2, 3), Health Aging and Body Composition (Health ABC) (4), National Social Life, Health and Aging Project (NSHAP) (5), and Baltimore Longitudinal Study of Aging (6). Dual impairments in hearing and vision have even been associated with increased risk of all-cause mortality (7). The additive effects of multiple sensory impairments is compounded when compared to loss of a single sense (2). Sensory domains examined include hearing, touch, taste, olfaction, and vision (4, 5, 7, 8). Balance, gait, and vestibular function are also implicated and associated with age-related cognitive decline (6, 8–10). In the context of multisensory impairment, no studies have examined the summative effects of hearing, balance and gait, and olfaction on incident cognitive impairment.

The objective of this study was to prospectively examine neurocognition, olfactory performance, and gait and balance in subjects presenting for audiologic evaluation to determine the incidence of multisensory impairment in this population and the correlation of sensory impairments with neurocognitive status.

METHODS

Institutional review board approval was obtained prior to commencement of any study activities (IRB #145682). This was a cross-sectional case-control study with initial recruitment occurring over a 6-month period from February 2021 through June 2021.

Subjects

Subjects were recruited from a patient pool presenting with chief complaint of "Hearing Loss" to an otology and audiology clinic. Subjects presenting for audiologic evaluation were screened for eligibility and provided with written informed consent to participate. Enrolled subjects underwent evaluation of hearing, gait and balance, olfaction, and cognitive function. Exclusion criteria were age <50, history of primary progressive neurological disease such as Parkinson's and Multiple Sclerosis, non-ambulatory patients, patients that were unable to follow instructions due to severe cognitive impairment, conductive hearing loss due to middle ear pathology, non-intact tympanic membrane, vestibular schwannoma or other central nervous system tumor, and recent COVID-19 infection. Hearing was assessed using a comprehensive audiologic evaluation including audiometric thresholds, pure tone average, speech discrimination, and tympanometry. Olfaction was assessed using the Affordable, Rapid, Olfactory Measurement Array (AROMA) test (11, 12). Gait and balance were assessed with the Timed Up-and Go assessment (13). Cognitive function was evaluated using the Montreal Cognitive Assessment (MoCA) (14). Baseline demographic data was also obtained.

Audiometric Data

Audiometry was performed in accordance with the American National Standards Institute ANSI/ASA S3.21-2004 (R 2019) standards (15) and the American Speech-Language-Hearing Association guidelines (16). Hearing level (HL) thresholds measured in decibels (dB) were obtained at 250, 500, 1,000, 2,000, 3,000, 4,000, 6,000, and 8,000 Hertz (Hz). Air and bone conduction thresholds were measured in both ears. Pure-tone averages (PTA) were calculated for each individually tested ear using 500, 1,000, 2,000, and 3,000 Hz, as recommended by the American Academy of Otolaryngology–Head and Neck Surgery (AAO-HNS) (17) and the American Medical Association (18). If no recording existed of the 3000 Hz threshold, the mean of the 2,000 and 4,000 Hz thresholds was utilized; a PTA valuation using this average is within +/- 5 dB of the PTA utilizing 3,000 Hz in 99% of audiograms in one previous series of 2170 patients (19). Word recognition scores were also obtained. A PTA > 25 dB HL was considered to have a sensorineural hearing impairment. For purposes of analysis, the best hearing ear was used for subject classification.

Timed Up-and-Go

The Timed "Up & Go" (13) test was chosen as a simple screening tool for balance impairment due to its ease of administration and well-established cut off scores for patients with vestibular dysfunction. It is a timed version of the older "Get Up and Go" test (20). The TUG consists of the average time of three trials: the patient is instructed to sit in a chair, a timer is started, the patient stands, walks 3 meters, then turns around and walks back to the chair, and finally sits back down (13). The TUG is well-studied and has excellent validity and reliability in a wide range of adult populations with various disabilities, including Parkinson's, cerebral palsy, and stroke. It has also been studied in otherwise "normal" elderly adult populations (21). It had a sensitivity of 80% in determining fall risk for patients with vestibular disorders, making it a reasonable choice for balance screening. Fall risk due to impairment was associated with a TUG score > 11 s (22). For this reason, subjects with TUG scores > 11 s were considered to have gait and balance impairment during analysis.

Affordable, Rapid, Olfactory Measurement Arrays Testing

AROMA (11) is an essential oil-based test that comprises 14 scents and one negative control at four concentrations: 1X, 2X, 4X, and 8X. It is administered by trained research personnel. The full battery consists of four rounds of 15 inhalant sticks. The number of odorants and concentrations included in olfactory

testing is dependent on each subject's baseline olfactory status; participants start at the 2X concentration and are presented all scents in randomized order. Patients select answers from a 4-item multiple-choice field. Incorrect responses trigger a higher concentration to be presented in the next round. Correct responses trigger the lower concentration to be presented. Due to this branching logic and the nested quality of the testing array, every test is unique, and requires administration on a tablet computer. All participants are asked to identify the 2X concentrations, but subsequent rounds are customized based on responses. This allows increased stratification of responses and development olfactory phenotypes. Preliminary data has identified unique testing phenotypes for normal, mild cognitive impairment, and Alzheimer's disease patients (12). Out of a total score of 100, patients were classified as normosmic (>75), hyposmic (< 75), and anosmic (<40). During multivariate modeling, anosmic and hyposmic patients were collapsed into a single category (Hyposmia) to allow for more straightforward interpretation of binary logistic regression. Related to cognitively impaired individuals, AROMA was validated in examining the relationship of olfactory dysfunction to Alzheimer's dementia, mild cognitive impairment, and cognitively unimpaired individuals. Other advantages of the AROMA are its re-usability, odorant levels that are dynamic, and ability to test both detection and identification of smell (11, 12).

Montreal Cognitive Assessment

The MoCA, as compared to the Mini Mental Status Exam (MMSE) is more sensitive in the detection of mild cognitive impairment (MCI) (23, 24). It is a multiple domain instrument that tests short term memory recall, working memory, visuospatial ability, abstraction, attention, concentration, and executive functioning (14). It has up to 90% sensitivity in MCI detection and takes ∼10 min to administer, making it an ideal cognitive function screening test in the clinical setting. A score of 26 was used as the cutoff for cognitive impairment; (14) subjects with scores <26 were considered CI. The overall score was corrected based on education level–one additional point was added for patients who did not complete high school.

Data Analysis

Ideal Sample Size and Power Analysis

Using previous literature that has estimated the prevalence of various sensory impairments among an aging population, an approximately 30% prevalence of olfactory dysfunction was expected in the control group. Prior prospective cohort studies (2, 3) have demonstrated a Hazard Ratio (HR) of 1.5 for hearing loss and incident dementia. The Odds Ratio (OR) for hearing loss in Alzheimer's dementia was found to be 2.0 in a case-control study with similar design considerations to the present study (25). Risk of fall in a 12-month period for adults aged 65 and older was calculated at 28.7% (26, 27). For the present case-control study comparing multisensory impairment and odds of incident CI; we estimated a likely 0.3 proportion of CI in the control group (28), a 2.0 OR for multisensory impairment and CI, 0.95 confidence level (alpha = 0.05), and 0.8 power level. With these estimates, we determined a conservative sample size of $n = 275$ to uncover a moderate effect size. Patients were actively recruited from a clinical pool of patients presenting with hearing loss. The first author (JCL) screened scheduled clinic lists the day before enrollment for eligible subjects based on chart review. Some initially eligible subjects were ineligible after additional in-person screening. Some subjects declined participation. Some were unable to complete the entirety of testing and so were excluded from analysis. Of the theoretical 585 eligible subjects on preliminary screening during the enrollment period, 180 were included. Enrollment rate based on initial eligibility screening was ∼31% and fell short of goal enrollment of 275 subjects.

Statistical Analysis

Data was cleaned and wrangled using R (29), RStudio, and the Tidyverse (30) suite of packages. Statistical analysis was performed using base R generalized linear model functions. Plots were generated using the R ggplot2 (31) and audiometry (32) packages.

Wilcoxon Rank Sum, Pearson's Chi-squared, and Fisher's exact test were used where appropriate to evaluate sociodemographic differences between patients with cognitive impairment (**Table 1**). Univariate analysis was performed for all predictor variables with cognitive status as the outcome variable (**Table 2**), again utilizing Wilcoxon Rank Sum and Chi-squared testing where appropriate.

Binary logistic regression was chosen for multivariate analysis. Results of multisensory testing, age, gender, and education levels were submitted to binary logistic regression analysis using a stepwise selection procedure. Only items that were related ($p < 0.10$) to the outcome after adjusting for all other items were retained. Odds ratios (OR) for incident cognitive impairment with confidence intervals were calculated for each of two models. Predictor values included hearing impairment, balance impairment, and olfactory impairment, along with control variables for age and education. Each predictor variable was categorized as a binary value and the response variable (cognitive impairment) was also coded as binary, with cases having a MoCA score <26 and controls having scores >26. A first model comparing the outcome for each of three sensory deficits was created, demonstrated in **Table 3**; a second model comparing the outcome for patients with multiple sensory deficits sought to define the influence of multiple sensory impairments on incident CI demonstrated in **Table 4**.

In demographic analysis, education level was found to have significant predictive value toward incident cognitive impairment. Additional stratification revealed significant differences between subjects with graduate-level education, and subjects without graduate-level education. Due to this finding, education was added as a control variable to the logistic regression model, with Odds Ratios reported separately. Age was also included as a control predictor variable, with patients stratified into either "50–65" and "65+" age categories.

RESULTS

One hundred and eighty subjects were enrolled after excluding 4 subjects with incomplete datasets. Fourteen subjects required

TABLE 1 | Demography of recruited subjects.

Characteristic	Normal, $N = 123^a$	CI, $N = 57^a$	p-value[b]
Age at Enrollment	66 (60, 72)	69 (63, 75)	0.064
Age category			0.3
50–65	50 (41%)	19 (33%)	
65+	73 (59%)	38 (67%)	
Sex			0.7
Female	67 (54%)	29 (51%)	
Male	56 (46%)	28 (49%)	
Black	8 (6.5%)	8 (14%)	0.10
Asian	2 (1.6%)	0 (0%)	>0.9
Native American	1 (0.8%)	0 (0%)	>0.9
White	111 (90%)	49 (86%)	0.4
Other	1 (0.8%)	1 (1.8%)	0.5
Education level			**<0.001**
Completed college	47 (38%)	18 (32%)	
Completed high school	34 (28%)	31 (54%)	
Completed graduate/professional degree	39 (32%)	6 (11%)	
Did not complete high school	3 (2.4%)	2 (3.5%)	
Employment status			0.12
Retired	68 (55%)	33 (58%)	
Work <40 h per week	15 (12%)	5 (8.8%)	
Work 40 or more h per week	37 (30%)	13 (23%)	
Unemployed	3 (2.4%)	6 (11%)	

[a]*Median (IQR); n (%).* [b]*Wilcoxon rank sum test; Pearson's Chi-squared test; Fisher's exact test. The bold values indicate the significant p values.*

an assistive device such as a cane or walker to perform the TUG examination. Subject demographic data are presented in **Table 1.** One hundred and twenty three subjects with normal cognition as defined on the MoCA were enrolled, and 57 subjects with CI were enrolled. The mean age at enrollment was 66 for normal subjects and 69 for CI subjects. Fifty four percentage of subjects were female with 46% male. Recruited subjects were predominantly Caucasian (89%). Education level and employment status were collected during enrollment. Education was found to be significantly associated with differences in incident cognitive impairment, as indicated by Fisher's exact test (two-tailed $p < 0.001$. Other sociodemographic data, including age, gender, race, and employment status were not associated with increased incidence of cognitive impairment.

Total MoCA scores from all subjects are demonstrated in **Figure 1**. Scores are ordinal and range from 0 to 30. The data is left-skewed with normal or near-normal scores heavily weighted. Cognitive impairment is defined as any score <26. Univariate analysis for all predictor variables on incident cognitive impairment is summarized in **Table 2**. All three sensory impairments demonstrated significant associations with incident cognitive impairment.

Hearing

Hearing-impaired subjects had higher proportions of CI, $\chi^2(1, N = 180) = 11.2$, $p < 0.001$. **Figure 2** shows aggregate audiometric data for all subjects, with a negative correlation noted between MoCA score and PTA ($R = -0.18$, $p = 0.018$); subjects with impaired hearing on audiometry were more likely to score lower on the MoCA ($p = 0.011$). Composite audiograms for both "Normal" and "CI" subjects are displayed in **Figure 2C**. **Figure 2D** displays the minimum standard for reporting hearing loss as prescribed by the AAO-HNS (17). Hearing severity was also significantly associated with cognition, although severity categories were collapsed across moderate, moderately severe, and severe hearing due to a scarcity of subjects with hearing worse than the "Mild" classification. "Normal" and "Mild" hearing loss were heavily weighted in the dataset. No patients with profound hearing loss in the better hearing ear were recruited.

Gait and Balance

A higher proportion of gait-impaired subjects had co-incident CI on Pearson's Chi Squared test, $\chi^2(1, N = 180) = 17.6$, $p < 0.001$. Gait impairment is depicted in **Figure 3**; impaired gait scores were associated with lower scores on the MoCA assessment ($R = -0.34$, $p < 0.001$).

Olfaction

Olfactory impairment was similarly associated with co-incident CI on Pearson's Chi Squared test, $\chi^2(1, N = 180) = 18.4$, $p < 0.001$. **Figure 4** shows the positive correlation between MoCA score and AROMA score ($R = 0.41$, $p < 0.001$). On univariate analysis of olfaction, distinct differences in MoCA score were noted between normosmic, hyposmic, and anosmic individuals; with anosmic individuals scoring lower than

TABLE 2 | Univariate analysis for all measured sensory impairments, with continuous and categorical variables analyzed with Wilcoxan rank-sum and Pearson's Chi-squared, respectively.

Characteristic	Normal, *N* = 123[a]	CI, N = 57[a]	*p*-value[b]
MoCA score	28.0 (27.0, 29.0)	24.0 (21.0, 25.0)	**<0.001**
Timed Up-and-Go	9.1 (8.1, 10.2)	10.4 (8.8, 13.3)	**0.003**
PTA (500, 1k, 2k, 3k Hz)	28 (21, 38)	38 (26, 46)	**0.002**
Gait status			**<0.001**
Normal gait	103 (84%)	31 (54%)	
Gait impairment	20 (16%)	26 (46%)	
Hearing status			**<0.001**
Normal hearing	58 (47%)	12 (21%)	
SNHL	65 (53%)	45 (79%)	
Hearing severity			**0.002**
Normal	58 (47%)	12 (21%)	
Mild	38 (31%)	22 (39%)	
Moderate-severe	27 (22%)	23 (40%)	
Olfactory status			**<0.001**
Normal olfaction	58 (47%)	8 (14%)	
Hyposmia	65 (53%)	49 (86%)	
Number of sensory			**<0.001**
Impairments			
0 or 1	75 (61%)	11 (19%)	
2	39 (32%)	27 (47%)	
3	9 (7.3%)	19 (33%)	

[a]*Median (IQR); n (%).* [b]*Wilcoxon rank sum test; Pearson's Chi-squared test. The bold values indicate the significant p values.*

hyposmic individuals on the MoCA instrument (**Figure 4B**). For multivariate modeling using binary logistic regression, anosmic and hyposmic individuals were collapsed into a single "Hyposmia" group to simplify interpretation in the context of other confounding variables.

Multivariate Modeling–Binary Logistic Regression

Analysis using binary logistic regression is shown in **Tables 3**, **4**. Within initial analysis of sociodemographic data, education level was found to have a significant correlation to cognitive status. Further breakdown demonstrated the stratification to be primarily between individuals with and without graduate-level education. Due to this, education was included as a control variable in the models.

The multivariate influence of three sensory domains on incident cognitive impairment was examined in two separate models.

Model 1: Influence of Individual Sensory Impairments

In the first model (**Table 3A**), the influence of each individual sensory impairment was examined on co-incident cognitive impairment. Hearing loss [OR = 2.78, 95% CI (1.25, 6.52), $p = 0.014$], gait and balance [OR = 3.49, 95% CI (1.57, 8.00), $p = 0.002$], and olfaction [OR = 3.89, 95% CI (1.67, 9.94), $p = 0.003$] were all significant predictors of co-incident cognitive impairment. Having a graduate-level education was associated with a lower odds of co-incident CI [OR = 0.22, 95% CI (0.07, 0.58), $p = 0.004$], while no statistical difference was seen between age groups. **Table 3B** reports coefficients for the model. **Figure 5** depicts the OR values graphically.

Model 2: Summative Influence of Multiple Sensory Impairments

The second model sought to examine the additive effects of multiple sensory impairments on co-incident cognitive impairment. To account for the small number of subjects with zero sensory impairments and incident CI ($n = 2$), 0 and 1 sensory impairment categories were collapsed into a single level "0 or 1 Sensory Impairments." Education and age were again included as control variables in the model. **Table 4A** displays odds ratios for increasing number of sensory impairments as predictors for co-incident CI. "0 or 1" sensory impairments were considered as the baseline condition. With 2 coexisting sensory impairments, the odds of CI increased [OR = 5.32, 95% CI (2.36, 12.8), $p < 0.001$]. When all 3 sensory impairments were present, the odds increased further [OR = 15.7, 95% CI (5.54, 48.8), $p < 0.001$]. **Table 4B** reports coefficients for the model.

DISCUSSION

Despite the well-established link between sensory deficits–many of which are potentially modifiable with training and targeted rehabilitation–and neurocognitive decline, the incidence and impact of multisensory impairments are not well understood. Sensorineural hearing loss increases the relative risk for dementia

TABLE 3 | Binary logistic regression model of all sensory impairments, age, and education level; **(A)** Odds Ratios (OR), 95% Confidence Intervals (CI), and p-values for each predictor variable. **(B)** Model coefficients with deviance values for the tested model.

A	**Model 1–binary logistic regression by sensory impairment**		
Characteristic	**OR**[a]	**95% CI**[a]	***p*-value**
Hearing loss			
Normal hearing	—	—	
SNHL	2.78	1.25, 6.52	**0.014**
Gait and Balance			
Normal gait	—	—	
Gait impairment	3.49	1.57, 8.00	**0.002**
Olfaction			
Normal olfaction	—	—	
Hyposmia	3.89	1.67, 9.94	**0.003**
Age category			
50–65	—	—	
65+	0.98	0.45, 2.15	>0.9
Holds graduate degree			
No graduate degree	—	—	
Graduate degree	0.22	0.07, 0.58	**0.004**

B	**Model 1–coefficients.**				
	Estimate	**Standard error**	**z value**	***p*-value**	**Signif.**
(Intercept)	−2.485	0.520	−4.775	0.0000	***
Hearing loss	1.023	0.418	2.446	0.0144	*
Gait and balance	1.251	0.413	3.029	0.0025	**
Olfaction	1.357	0.451	3.012	0.0026	**
Age category	−0.021	0.399	−0.053	0.9575	
Holds graduate degree	−1.495	0.515	−2.904	0.0037	**

[a]*OR, Odds Ratio; CI, Confidence Interval. Odds Ratios (OR), 95% Confidence Intervals (CI), and p-values for each predictor variable. Signif. codes: 0 <= "***" < 0.001 < "**" < 0.01 < "*" < 0.05 < "." < 0.1 < "" < 1. Null deviance: 224.8 on 179 degrees of freedom. Residual deviance: 177.6 on 174 degrees of freedom. The bold values indicate the significant p values.*

and has a weighted population attributable fraction of 8.2% among midlife (age 45–65) adults according to the recent Lancet Commission on Dementia Prevention (33), making it the number one modifiable risk factor in the prevention of dementia. Apart from hearing loss, there are no current guidelines related to the screening and treatment of sensory impairments in the context of cognitive decline. The objective of this study was to determine the incidence of hearing, olfactory, and/or balance impairment and determine the magnitude of the impact of single vs. multisensory dysfunction on cognitive performance. When evaluating single sensory impairments, we found that olfactory dysfunction, gait impairment, and sensorineural hearing loss were all statistically significantly associated with a higher incidence of cognitive impairment (OR 3.89, $p = 0.003$; 3.49, $p = 0.002$; and 2.78, $p = 0.014$, respectively) for cognitive impairment. Subjects with dysfunction in all domains were at the highest risk for cognitive impairment (OR 15.7, $p < 0.001$) vs. those with impairment in 2 domains (OR 5.32, $p < 0.001$). These findings underscore the need to comprehensively evaluate patients for multisensory impairment, particularly those who are at-risk for cognitive decline due to advancing age or other known risk factors. Additionally, the sensory domains studied are all amenable to rehabilitation. The dramatically increased risk of cognitive impairment in those with multisensory impairment highlights the potential of sensory rehabilitation, even if only in a single domain, to potentially improve outcomes.

The concept of multisensory impairment is a burgeoning area of active study. For example, several cohort studies have examined age-related sensory decline including the Epidemiology of Hearing Loss Study (EHLS), Beaver Dam Offspring Study (BOSS), Health Aging and Body Composition (Health ABC), National Social Life, Health and Aging Project (NSHAP), and Baltimore Longitudinal Study of Aging (2–6).

The Correlation Between Sensory Impairments and Cognitive Impairment

There are competing and parallel hypotheses for why sensory impairment contributes to the onset and trajectory of cognitive decline. Most of these use hearing loss as an illustrative example. The "cognitive load" theory postulates that loss of hearing places additional cognitive processing demands on the brain, resulting in diverting of limited neuroprocessing resources

TABLE 4 | Binary logistic regression model of *number* of sensory impairments, age, and education level; **(A)** Odds Ratios (OR), 95% Confidence Intervals (CI), and p-values for each predictor variable. **(B)** Model coefficients with deviance values for the tested model.

A	**Model 2–binary logistic regression by number of sensory impairments**		
Characteristic	**OR[a]**	**95% CI[a]**	***p*-value**
Number sensory impairments			
0 or 1	—	—	
2	5.32	2.36, 12.8	**<0.001**
3	15.7	5.54, 48.8	**<0.001**
Age category			
50–65	—	—	
65+	0.92	0.42, 1.99	0.8
Holds graduate degree			
No graduate degree	—	—	
Graduate degree	0.22	0.07, 0.57	**0.003**

B	**Model 2–coefficients**				
	Estimate	**Standard error**	**z value**	***p*-value**	**Signif.**
(Intercept)	−1.631	0.376	−4.336	0.0000	***
2 Sensory impairments	1.672	0.429	3.898	0.0001	***
3 Sensory impairments	2.753	0.551	4.994	0.0000	***
Age category	−0.086	0.394	−0.219	0.8264	
Holds graduate degree	−1.511	0.511	−2.959	0.0031	**

[a]*OR, Odds Ratio; CI, Confidence Interval. Signif. codes: 0 <= "***" < 0.001 < "**" < 0.01 < "*" < 0.05 < "." < 0.1 < "" < 1. Null deviance: 224.8 on 179 degrees of freedom. Residual deviance: 179.5 on 175 degrees of freedom. The bold values indicate the significant p values.*

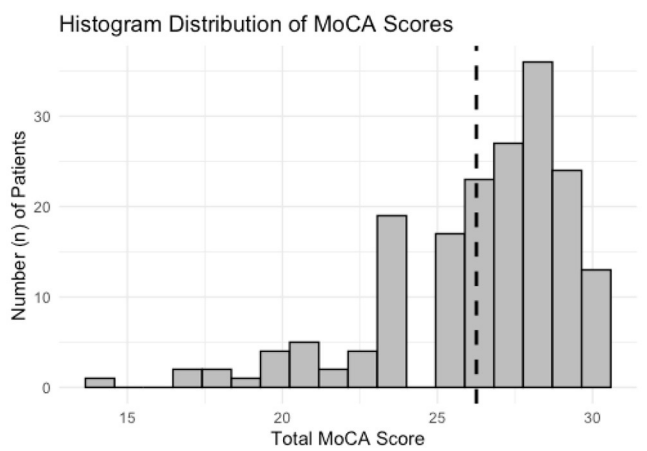

FIGURE 1 | Histogram distribution of MoCA scores for all subjects enrolled for analysis. The data is left-skewed with a heavier distribution of normal and near-normal scores. Dashed line corresponds to a score of 26, scores below which are considered for analysis to have "Cognitive Impairment."

toward auditory processing, and away from other cognitive processes such as working memory (34, 35). The cumulative strain may contribute to loss of cognitive function over time. Social isolation due to hearing loss may also contribute to cognitive decline. Self-reported measures such as depression and "fair or poor" overall mental health are seen with a higher frequency in the hearing impaired (36). A common pathophysiologic mechanism underpinning both hearing loss and dementia such as microvascular insult could explain the apparent linkage as well. However, multiple large cohort studies controlling for cardiovascular disease have repeatedly shown hearing loss to be an independent risk factor for the development of dementia (2–5).

Neuroanatomic Basis for Sensory and Cognitive Impairments

The neuroanatomy of sensory processing provides context for why multiple sensory impairments occur concomitantly in the context of cognitive impairment. Bilateral vestibular loss is linked to hippocampal atrophy detectable on MRI (37, 38). Olfaction and neurocognition are also linked anatomically and pathophysiologically, particularly concerning Alzheimer's disease and related dementias (39–41). Abnormal amyloid and tau proteins deposit in the olfactory bulb and tract prior to cognitive decline (42). As regional involvement increases, so does the extent of cognitive decline. As the disease progresses, additional neurofibrillary tangles develop in the entorhinal cortex and hippocampal-related structures (43). These are the same anatomic areas through which olfaction is processed. Olfactory identification deficits correlate with atrophy of the hippocampus, olfactory bulb, and entorhinal cortex (44, 45). Behavioral and functional data both indicate that activation of the primary olfactory cortex depends on attention (46, 47). The anterior cingulate cortex, which is activated when cognitive demand is

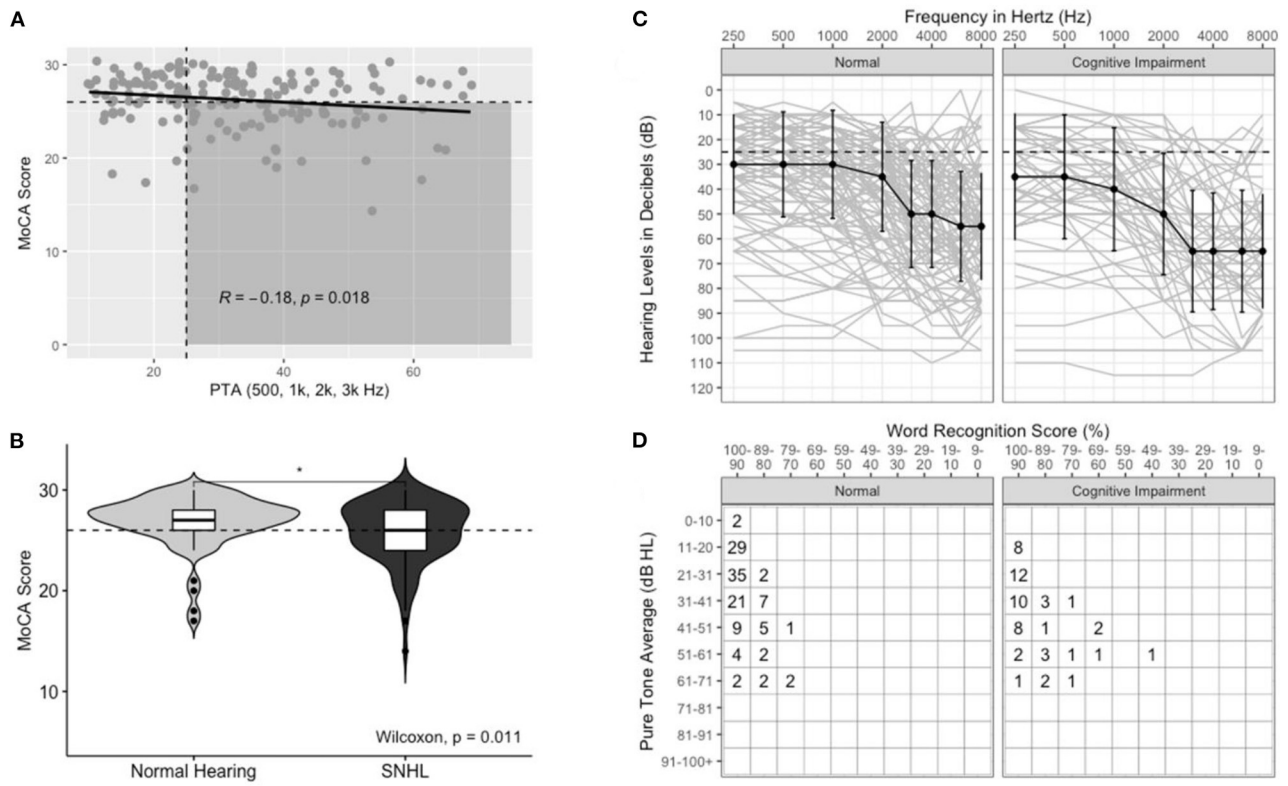

FIGURE 2 | Aggregate audiometric data for patients with Normal Cognition and Cognitive Impairment (CI). **(A)** Scatterplot of PTA versus MoCA score. Horizontal dashed line correlates to MoCA score of 26. Vertical dashed line correlates to PTA of 25. Shaded area includes patients with co-incident hearing loss and CI, line of best fit included with R- and *p*-values for Pearson's correlation. **(B)** Box- and violin-plots of Normal Hearing and Hearing-Impaired (SNHL) individuals and the distribution of MoCA scores in each group. **(C)** Composite audiometric data, median scores for each threshold correspond to the dark line, error bars correspond to 1 SD. **(D)** AAO-HNS minimum reporting standards for raw data of PTA plotted against word recognition scores (WRS) (17).

high (48), and during working memory tasks is also activated by olfactory stimuli (49). The increased workload of maintaining appropriate attention and memory as neurocognitive decline progresses may occur at the expense of specific aspects of olfactory and other sensory performance (50). In the context of hearing loss, loss of high-SR auditory fibers, as occurs in age-related hearing loss, is implicated in the development of imbalances in excitation and inhibition in ascending central pathways. This imbalance may lead to a decrease in central gain, dysregulation of the hypothalamic-pituitary axis, decrease in hippocampal long-term potentiation, and an overall decrease in signal-noise ratio (51).

Contextualizing With Prior Epidemiologic Research

Prior studies have investigated multiple sensory domains including hearing, touch, olfaction, vision, and even taste (52), and found that subjects with multiple sensory impairments have worse neurocognitive outcomes. Our data are consistent in demonstrating the individual associations of hearing, balance, and olfaction with cognitive impairment. Additionally, the highest risk of neurocognitive impairment was in subjects with deficits in all three of the sensory domains tested. This suggests that the effects of multiple sensory impairments may be additive toward odds of CI.

The Epidemiology of Hearing Loss Study (EHLS) demonstrated that olfactory dysfunction predicted the development of cognitive impairment in a cohort of patients prospectively followed for a 5-year period (2). In addition to cognitive impairment, studies of community-dwelling elders have also shown increased morbidity and mortality in subjects with olfactory dysfunction (53–56).

Vestibular dysfunction has been shown to correlate strongly with CI and dementia (9, 57–59). The vestibular system has been independently studied in the context of aging and cognition. Dysfunction is associated with an increased risk of cognitive impairment, dementia, and Alzheimer's disease. Vestibular loss–particularly impairment of the saccule–also predicts poorer spatial cognition in a subset of patients with Alzheimer's disease (57, 58). Cross-sectional analysis of 3 prospective cohort studies on aging populations demonstrated a link between vestibular decline and cognitive decline: the Baltimore Longitudinal

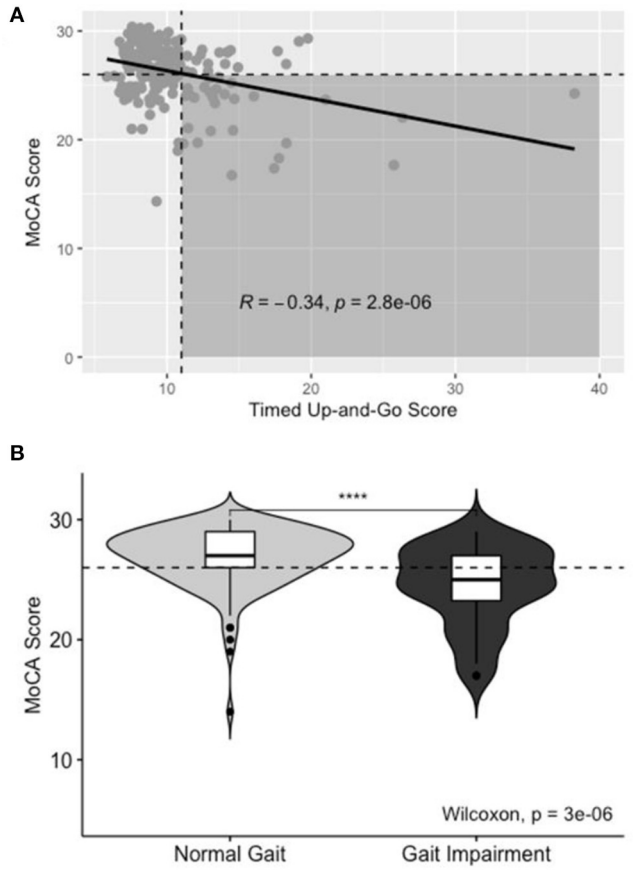

FIGURE 3 | Aggregate TUG data for Normal and Gait-impaired individuals. **(A)** Scatterplot of TUG score vs. MoCA score. Horizontal dashed line correlates to MoCA score of 26. Vertical dashed line correlates to TUG of 11. Shaded area includes patients with co-incident gait impairment and CI, line of best fit included with R- and *p*-values for Pearson's correlation. **(B)** Box- and violin-plots of Normal and Gait-Impaired individuals and the distribution of MoCA scores in each group.

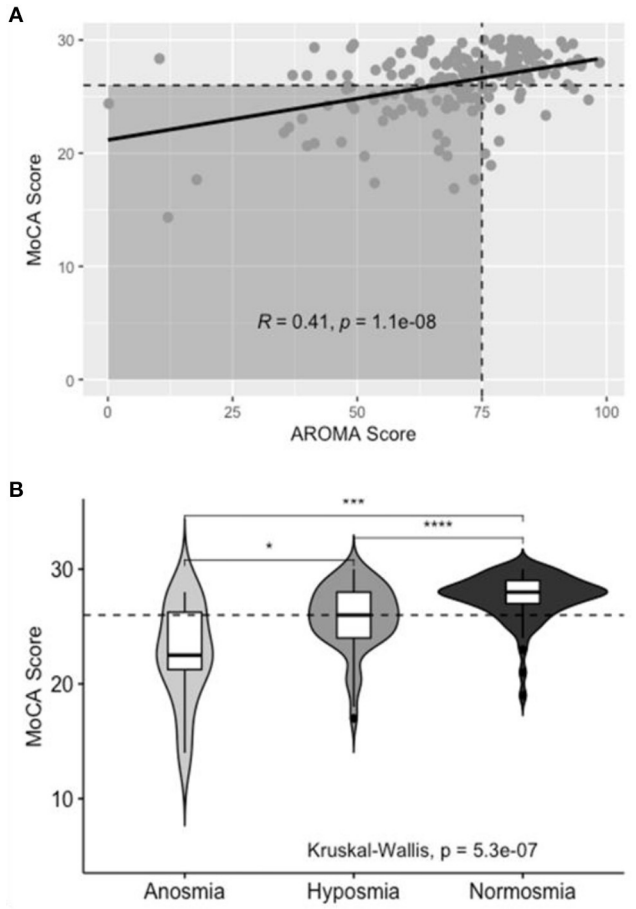

FIGURE 4 | Aggregate AROMA data for subjects with normal and impaired olfaction. **(A)** Scatterplot of AROMA vs. MoCA score. Horizontal dashed line correlates to MoCA score of 26. Vertical dashed line correlates to AROMA score of 75. Shaded area includes patients with co-incident olfactory impairment and CI, line of best fit included with R- and *p*-values for Pearson's correlation. **(B)** Box- and violin-plots of Normal, Hyposmic, and Anosmic individuals and the distribution of MoCA scores in each group.

Study on Aging (BLSA) (6), the National Health Interview Survey (8), and National Health and Nutrition Examination Survey (60). Within a cross-sectional analysis of the BLSA, an association between olfaction and motor function was identified (61).

A Link Between Olfactory Impairment and Cognitive Decline

Subjects with baseline olfactory impairment are more likely to develop cognitive impairment during longitudinal follow-up. Pooled analysis of 8 cohort studies (2, 62–68) encompassing 13,165 participants demonstrated a relative risk of 2.37 (95% CI = 1.91–2.94) for accelerated cognitive decline when subjects with olfactory impairment were followed longitudinally (69). Odor detection is associated with word recall and orientation scores on the Alzheimer's Disease Assessment Scale (70). Odor detection and identification is also correlated with blood flow to the left temporal lobe, entorhinal cortex, and frontal lobes; and activation of the right anterior piriform cortex on fMRI.

Gait, Balance, and a Testing Proxy for Vestibular Function

"Vestibular Cognition" as a concept is evolving (71) to encompass the peripheral end organs as well as projections through the brainstem to a widespread distribution in higher cortical centers. Low-level reflexes such as the vestibulo-ocular reflex (72) and vestibulospinal reflex (73) stabilize gaze and posture, respectively. These reflexes, along with proprioceptive and visual input interface with higher-order projections to the cerebellum and somatosensory cortex to provide a "sense" of balance. This complex interplay between lower brainstem reflexes and higher-order cortical processing makes contextualizing balance and cognition challenging. For this reason, the Timed-Up-and-Go test was felt to be a

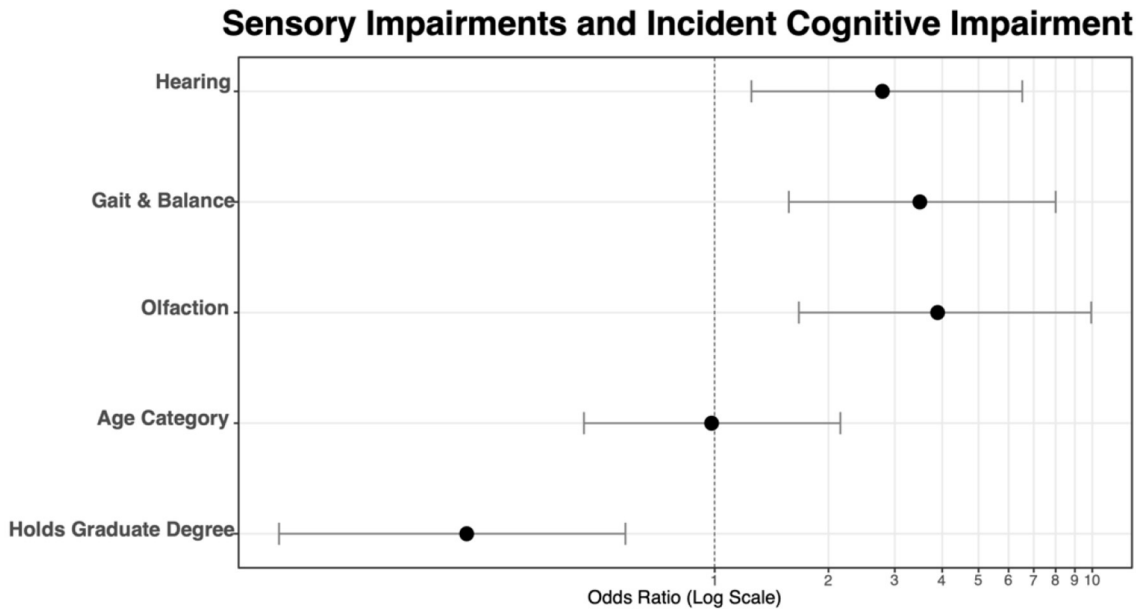

FIGURE 5 | Odds ratios visualized for each of three sensory components and two control variables, age, and education level.

simple, easily interpretable proxy for gait and balance function. Due to the need for visual, proprioceptive, and vestibular coordination, this single test was utilized in the present study (13). No studies to date have looked at balance in the context of multisensory impairment, and none of the previously mentioned prospective cohorts have included balance and vestibular dysfunction alongside hearing and olfaction during analyses. Our results show that individual sensory deficits are significantly correlated to co-incident cognitive impairment. More interesting, the effects of multiple sensory impairments appear to be additive in the odds of having CI.

The Potential for Sensory Rehabilitation

Hearing, olfactory, and vestibular impairments are critically important to recognize due to their potentially modifiable nature. Each of the sensory impairments represents a unique opportunity to intervene and improve outcomes. Our data demonstrate an OR for cognitive impairment of 15.7 in subjects with deficits in three sensory modalities vs. an OR of 5.32 for those with deficits in only two. This indicates that referring subjects with multisensory impairment for hearing restoration *via* hearing aids, vestibular therapy, and/or olfactory training may meaningfully modify the risk of neurocognitive decline. Hearing aids have been shown to potentially mitigate the risk for cognitive decline (74–76). Mertens et al. (77) showed that cochlear implantation in cognitively impaired patients could slow, and even reverse, cognitive changes associated with aging. Olfactory training has been shown to improve olfaction and increase neural connectivity within and between brain regions. When comparing performance on assessments of cognition, depression, overall brain health, and olfaction of non-cognitively impaired community-dwelling senior citizens, 6 months of olfactory training was superior to 6 months of sudokus (78). Olfactory stimulation with scent-impregnated patches placed on the sternum has also been shown to improve vestibular performance and decrease fall risk (79). Taken together, this evidence further highlights the importance of assessing and rehabilitating multisensory dysfunction.

Limitations of the Present Study

This study is not without limitations. Due to its cross-sectional nature, we are unable to comment on the long-term outcomes of the included subjects. There is an inherent risk of bias during subject recruitment as not all eligible subjects were willing to participate in the study. A degree of selection bias is present due to the exclusion of a large portion of eligible subjects; approximately 31% of initially screened subjects were included in the final cohort. Olfactory assessment utilized AROMA, a relatively novel objective test of olfactory performance, which could be viewed as a limitation. However, prior studies using AROMA have demonstrated high test-retest reliability and a significant correlation of AROMA results with more commonly used tests like the UPSIT (11, 12). Additionally, the study was underpowered to stratify hearing contribution by severity (Normal, Mild, Moderate, Moderately Severe, Severe, Profound), due to a low number of patients with hearing loss worse than "mild." Recent literature has suggested that central, rather than auditory processing may be more strongly tied to cognitive status (80), rather than PTA as measured here. Secondary analysis of the

Adult Changes in Thought (ACT) study (81) showed that decreased performance status on two dichotic central auditory processing tests predicted a higher likelihood of dementia and Alzheimer's disease.

Choice of Cognitive Screening Protocol

To assess cognitive status, the MoCA was utilized. The MoCA is commonly deployed in a screening capacity and is not capable of differentiating between etiologies of cognitive impairment. While a more robust neuropsychological battery would be preferable, adding a 1–2-h evaluation to each subject's clinical visit with the psychometricians needed to perform them was not logistically possible. The MoCA is supported in the literature as superior to other common tests like the Mini-Mental Status Exam because it includes measures of executive function (14). Educational status is known to confound MoCA performance with higher education levels positively correlated with MoCA score. Higher education status was found to be a contributing protective factor for the identification of CI in our study, with an OR of 0.22, 95% CI [0.07, 0.58], $p < 0.001$, and was controlled for during multivariate modeling. Future studies will include longitudinal data as well as the impact of sensory deficit-specific rehabilitation of cognitive outcomes. Patients with severe or profound hearing loss were planned to undergo the modified MoCA for the hearing impaired (MoCA-HI) that has previously been validated in this population (82). However, there were no patients with hearing levels worse than "Moderately Severe" recruited, when using the best hearing ear for classification purposes. On retrospective review of the study's recruitment practices, patients with more severe hearing were more commonly funneled into visits for cochlear implant evaluations and so were not as easily captured during enrollment. These subjects are now recruited in a more targeted fashion and are the topic of future study.

CONCLUSIONS

Multisensory impairment is common and associated with cognitive impairment. Deficits in hearing, balance, and olfaction significantly increase the odds of co-incident cognitive impairment vs. those with deficits in fewer domains. When considering single sensory deficits, olfactory dysfunction was the strongest predictor of cognitive impairment. The significance of these findings is in their immediate clinical applicability. These sensory impairments are testable in a point of care fashion and are amenable to rehabilitation. Assessment of multisensory impairment in patients presenting with subjective loss in any of these domains should be considered to facilitate subsequent therapeutic intervention to improve sensory impairments and potentially prevent cognitive decline.

DATA AVAILABILITY STATEMENT

The raw data supporting the conclusions of this article will be made available by the authors, without undue reservation.

ETHICS STATEMENT

The studies involving human participants were reviewed and approved by Institutional Review Board (IRB), University of Kansas Medical Center. The patients/participants provided their written informed consent to participate in this study.

AUTHOR CONTRIBUTIONS

JL conceived the study and coordinated study design, performed statistical analysis, wrote, and critically revised the manuscript. ZA designed data acquisition protocols and critically revised the manuscript. AA and KY critically revised the manuscript. NF performed statistical analysis and critically revised the manuscript. LD'S, HS, and JV conceived the study, participated in study design and data acquisition protocols, and critically revised the manuscript. JV conceived the study, participated in study design and data acquisition protocols, performed statistical analysis, wrote, and critically revised the manuscript. All authors contributed to the article and approved the submitted version.

FUNDING

Fees for open access publication are provided at the expense of the Department of Otolaryngology-Head and Neck Surgery at the University of Kansas Medical Center.

ACKNOWLEDGMENTS

The authors thank Scott Fassas, Emily Cummings, and Shaan Somani for their efforts in recruitment and testing of subjects. Special thank to Mark Villwock for consultation on statistical modeling.

REFERENCES

1. Claes AJ, Mertens G, Gilles A, Hofkens-Van den Brandt A, Fransen E, Van Rompaey V, et al. The repeatable battery for the assessment of neuropsychological status for hearing impaired individuals (RBANS-H) before and after cochlear implantation: a protocol for a prospective, longitudinal cohort study. *Front Neurosci.* (2016) 10:512. doi: 10.3389/fnins.2016.00512
2. Fischer ME, Cruickshanks KJ, Schubert CR, Pinto AA, Carlsson CM, Klein BEK, et al. Age-related sensory impairments and risk of cognitive impairment. *J Am Geriatr Soc.* (2016) 64:1981–7. doi: 10.1111/jgs.14308
3. Schubert CR, Cruickshanks KJ, Fischer ME, Pinto AA, Chen Y, Huang GH, et al. Sensorineural impairments, cardiovascular risk factors, and 10-year incidence of cognitive impairment and decline in midlife: the beaver dam offspring study. *J Gerontol A Biol Sci Med Sci.* (2019) 74:1786–92. doi: 10.1093/gerona/glz011

4. Brenowitz WD, Kaup AR, Lin FR, Yaffe K. Multiple sensory impairment is associated with increased risk of dementia among black and white older adults. *J Gerontol A Biol Sci Med Sci.* (2019) 74:890–6. doi: 10.1093/gerona/gly264
5. Correia C, Lopez KJ, Wroblewski KE, Huisingh-Scheetz M, Kern DW, Chen RC, et al. Global sensory impairment in older adults in the United States. *J Am Geriatr Soc.* (2016) 64:306–13. doi: 10.1111/jgs.13955
6. Bigelow RT, Semenov YR, Trevino C, Ferrucci L, Resnick SM, Simonsick EM, et al. Association between visuospatial ability and vestibular function in the baltimore longitudinal study of aging. *J Am Geriatr Soc.* (2015) 63:1837–44. doi: 10.1111/jgs.13609
7. Gopinath B, Schneider J, McMahon CM, Burlutsky G, Leeder SR, Mitchell P. Dual sensory impairment in older adults increases the risk of mortality: a population-based study. *PLoS ONE.* (2013) 8:e55054. doi: 10.1371/journal.pone.0055054
8. Bigelow RT, Semenov YR, du Lac S, Hoffman HJ, Agrawal Y. Vestibular vertigo and comorbid cognitive and psychiatric impairment: the 2008 national health interview survey. *J Neurol Neurosurg Psychiatry.* (2016) 87:367–72. doi: 10.1136/jnnp-2015-310319
9. Harun A, Oh ES, Bigelow RT, Studenski S, Agrawal Y. Vestibular impairment in dementia. *Otol Neurotol.* (2016) 37:1137–42. doi: 10.1097/MAO.0000000000001157
10. Lee HW, Lim YH, Kim SH. Dizziness in patients with cognitive impairment. *J Vestib Res Equilib Orientat.* (2020) 30:17–23. doi: 10.3233/VES-190686
11. Villwock JA, Li J, Moore C, Chiu AG, Sykes KJ. Affordable rapid olfaction measurement array: a novel, essential oil-based test strongly correlated with upsit and subjective outcome measures. *Ann Otol Rhinol Laryngol.* (2020) 129:39–45. doi: 10.1177/0003489419870833
12. Li J, Bur AM, Villwock MR, Shankar S, Palmer G, Sykes KJ, et al. Olfactory phenotypes differentiate cognitively unimpaired seniors from alzheimer's disease and mild cognitive impairment: a combined machine learning and traditional statistical approach. *J Alzheimers Dis JAD.* (2021) 81:641–50. doi: 10.3233/JAD-210175
13. Podsiadlo D, Richardson S. The timed "up & go": a test of basic functional mobility for frail elderly persons. *J Am Geriatr Soc.* (1991) 39:142–8. doi: 10.1111/j.1532-5415.1991.tb01616.x
14. Nasreddine ZS, Phillips NA, Bédirian V, Charbonneau S, Whitehead V, Collin I, et al. The montreal cognitive assessment, MoCA: a brief screening tool for mild cognitive impairment. *J Am Geriatr Soc.* (2005) 53:695–9. doi: 10.1111/j.1532-5415.2005.53221.x
15. Melnick W. American National Standard specifications for audiometers. *ASHA.* (1971) 13:203–6.
16. Campbell J, Graley J, Meinke D, Vaughan L, Aungst R, Madison T. Guidelines for manual pure-tone threshold audiometry. *ASHA.* (1978) 20:297–301. Available online at: https://www.asha.org/policy/gl2005-00014/
17. Gurgel RK, Jackler RK, Dobie RA, Popelka GR. A new standardized format for reporting hearing outcome in clinical trials. *Otolaryngol Head Neck Surg.* (2012) 147:803–7. doi: 10.1177/0194599812458401
18. Guide for the evaluation of hearing handicap. *JAMA.* (1979) 241:2055–9. doi: 10.1001/jama.241.19.2055
19. Gurgel RK, Popelka GR, Oghalai JS, Blevins NH, Chang KW, Jackler RK. Is it valid to calculate the 3-kilohertz threshold by averaging 2 and 4 kilohertz? *Otolaryngol Head Neck Surg.* (2012) 147:102–4. doi: 10.1177/0194599812437156
20. Mathias S, Nayak US, Isaacs B. Balance in elderly patients: the "get-up and go" test. *Arch Phys Med Rehabil.* (1986) 67:387–9.
21. Christopher A, Kraft E, Olenick H, Kiesling R, Doty A. The reliability and validity of the timed up and go as a clinical tool in individuals with and without disabilities across a lifespan: a systematic review. *Disabil Rehabil.* (2019) 26:1–15. doi: 10.1080/09638288.2019.1682066
22. Whitney SL, Marchetti GF, Schade A, Wrisley DM. The sensitivity and specificity of the Timed "Up & Go" and the dynamic gait index for self-reported falls in persons with vestibular disorders. *J Vestib Res Equilib Orientat.* (2004) 14:397–409. doi: 10.3233/VES-2004-14506
23. Pinto TCC, Machado L, Bulgacov TM, Rodrigues-Júnior AL, Costa MLG, Ximenes RCC, et al. Is the montreal cognitive assessment (MoCA) screening superior to the mini-mental state examination (MMSE) in the detection of mild cognitive impairment (MCI) and Alzheimer's disease (AD) in the elderly? *Int Psychogeriatr.* (2019) 31:491–504. doi: 10.1017/S1041610218001370
24. Ciesielska N, Sokołowski R, Mazur E, Podhorecka M, Polak-Szabela A, Kedziora-Kornatowska K. Is the montreal cognitive assessment (MoCA) test better suited than the mini-mental state examination (MMSE) in mild cognitive impairment (MCI) detection among people aged over 60? *Meta-analysis Psychiatr Pol.* (2016) 50:1039–52. doi: 10.12740/PP/45368
25. Uhlmann RF, Larson EB, Rees TS, Koepsell TD, Duckert LG. Relationship of hearing impairment to dementia and cognitive dysfunction in older adults. *JAMA.* (1989) 261:1916–9. doi: 10.1001/jama.261.13.1916
26. Bergen G. Falls and fall injuries among adults aged ≥65 Years — United States, 2014. *MMWR Morb Mortal Wkly Rep.* (2016) 65:993–8. doi: 10.15585/mmwr.mm6537a2
27. Cuevas-Trisan R. Balance problems and fall risks in the elderly. *Phys Med Rehabil Clin N Am.* (2017) 28:727–37. doi: 10.1016/j.pmr.2017.06.006
28. Ward A, Arrighi HM, Michels S, Cedarbaum JM. Mild cognitive impairment: disparity of incidence and prevalence estimates. *Alzheimers Dement J Alzheimers Assoc.* (2012) 8:14–21. doi: 10.1016/j.jalz.2011.01.002
29. R Core Team. *R: A Language and Environment for Statistical Computing.* Vienna: R Foundation for Statistical Computing (2021). Available online at: https://www.R-project.org/
30. Wickham H, Averick M, Bryan J, Chang W, McGowan LD, François R, et al. Welcome to the tidyverse. *J Open Source Softw.* (2019) 4:1686. doi: 10.21105/joss.01686
31. Wickham H. *ggplot2: Elegant Graphics for Data Analysis.* New York, NY: Springer-Verlag (2016).
32. Lehnert B. *Audiometry: Standard Conform Pure Tone Audiometry (PTA) Plots* (2020). Available online at: https://CRAN.R-project.org/package=audiometry
33. Livingston G, Huntley J, Sommerlad A, Ames D, Ballard C, Banerjee S, et al. Dementia prevention, intervention, and care: 2020 report of the lancet commission. *Lancet.* (2020) 396:413–46. doi: 10.1016/S0140-6736(20)30367-6
34. Tun PA, McCoy S, Wingfield A. Aging, hearing acuity, and the attentional costs of effortful listening. *Psychol Aging.* (2009) 24:761–6. doi: 10.1037/a0014802
35. Rabbitt P. Mild hearing loss can cause apparent memory failures which increase with age and reduce with IQ. *Acta Oto Laryngol Suppl.* (1990) 476:167–75. doi: 10.3109/00016489109127274
36. Strawbridge WJ, Wallhagen MI, Shema SJ, Kaplan GA. Negative consequences of hearing impairment in old age: a longitudinal analysis. *Gerontologist.* (2000) 40:320–6. doi: 10.1093/geront/40.3.320
37. Brandt T, Schautzer F, Hamilton DA, Brüning R, Markowitsch HJ, Kalla R, et al. Vestibular loss causes hippocampal atrophy and impaired spatial memory in humans. *Brain J Neurol.* (2005) 128:2732–41. doi: 10.1093/brain/awh617
38. Göttlich M, Jandl NM, Sprenger A, Wojak JF, Münte TF, Krämer UM, et al. Hippocampal gray matter volume in bilateral vestibular failure. *Hum Brain Mapp.* (2016) 37:1998–2006. doi: 10.1002/hbm.23152
39. Schmitt AL, Livingston RB, Reese EM, Davis KM. The relationship between the repeatable battery for the assessment of neuropsychological status (RBANS) and olfaction in patients referred for a dementia evaluation. *Appl Neuropsychol.* (2010) 17:163–71. doi: 10.1080/09084281003715667
40. Suzuki Y, Yamamoto S, Umegaki H, Onishi J, Mogi N, Fujishiro H, et al. Smell identification test as an indicator for cognitive impairment in Alzheimer's disease. *Int J Geriatr Psychiatry.* (2004) 19:727–33. doi: 10.1002/gps.1161
41. Rezek DL. Olfactory deficits as a neurologic sign in dementia of the Alzheimer type. *Arch Neurol.* (1987) 44:1030–2. doi: 10.1001/archneur.1987.00520220036012
42. Hummel T, Landis BN, Hüttenbrink KB. Smell and taste disorders. *GMS Curr Top Otorhinolaryngol Head Neck Surg.* (2011) 10:Doc04. doi: 10.3205/cto000077
43. Arriagada PV, Growdon JH, Hedley-Whyte ET, Hyman BT. Neurofibrillary tangles but not senile plaques parallel duration and severity of Alzheimer's disease. *Neurology.* (1992) 42:631–9. doi: 10.1212/WNL.42.3.631
44. Sánchez SM, Duarte-Abritta B, Abulafia C, De Pino G, Bocaccio H, Castro MN, et al. White matter fiber density abnormalities in cognitively normal adults at risk for late-onset Alzheimer's disease. *J Psychiatr Res.* (2020) 122:79–87. doi: 10.1016/j.jpsychires.2019.12.019

45. Gili T, Cercignani M, Serra L, Perri R, Giove F, Maraviglia B, et al. Regional brain atrophy and functional disconnection across Alzheimer's disease evolution. *J Neurol Neurosurg Psychiatry.* (2011) 82:58–66. doi: 10.1136/jnnp.2009.199935
46. Zelano C, Bensafi M, Porter J, Mainland J, Johnson B, Bremner E, et al. Attentional modulation in human primary olfactory cortex. *Nat Neurosci.* (2005) 8:114–20. doi: 10.1038/nn1368
47. Sela L, Sobel N. Human olfaction: a constant state of change-blindness. *Exp Brain Res.* (2010) 205:13–29. doi: 10.1007/s00221-010-2348-6
48. Pessoa L. On the relationship between emotion and cognition. *Nat Rev Neurosci.* (2008) 9:148–58. doi: 10.1038/nrn2317
49. Tabert MH, Steffener J, Albers MW, Kern DW, Michael M, Tang H, et al. Validation and optimization of statistical approaches for modeling odorant-induced fMRI signal changes in olfactory-related brain areas. *Neuroimage.* (2007) 34:1375–90. doi: 10.1016/j.neuroimage.2006.11.020
50. Nelson L, Tabet N. Slowing the progression of Alzheimer's disease; what works? *Ageing Res Rev.* (2015) 23:193–209. doi: 10.1016/j.arr.2015.07.002
51. Knipper M, Singer W, Schwabe K, Hagberg GE, Li Hegner Y, Rüttiger L, et al. Disturbed balance of inhibitory signaling links hearing loss and cognition. *Front Neural Circuits.* (2022) 15:785603. doi: 10.3389/fncir.2021.785603
52. Steinbach S, Hundt W, Vaitl A, Heinrich P, Förster S, Bürger K, et al. Taste in mild cognitive impairment and Alzheimer's disease. *J Neurol.* (2010) 257:238–46. doi: 10.1007/s00415-009-5300-6
53. Hinz A, Luck T, Riedel-Heller SG, Herzberg PY, Rolffs C, Wirkner K, et al. Olfactory dysfunction: properties of the Sniffin' sticks screening 12 test and associations with quality of life. *Eur Arch Otorhinolaryngol.* (2019) 276:389–95. doi: 10.1007/s00405-018-5210-2
54. Schubert CR, Cruickshanks KJ, Klein BEK, Klein R, Nondahl DM. Olfactory impairment in older adults: five-year incidence and risk factors. *Laryngoscope.* (2011) 121:873–8. doi: 10.1002/lary.21416
55. Talamo BR, Rudel R, Kosik KS, Lee VM, Neff S, Adelman L, et al. Pathological changes in olfactory neurons in patients with Alzheimer's disease. *Nature.* (1989) 337:736–9. doi: 10.1038/337736a0
56. Tian Q, Chastan N, Thambisetty M, Resnick SM, Ferrucci L, Studenski SA. Bimanual gesture imitation links to cognition and olfaction. *J Am Geriatr Soc.* (2019) 67:2581–6. doi: 10.1111/jgs.16151
57. Wei EX, Oh ES, Harun A, Ehrenburg M, Agrawal Y. saccular impairment in Alzheimer's disease is associated with driving difficulty. *Dement Geriatr Cogn Disord.* (2017) 44:294–302. doi: 10.1159/000485123
58. Wei EX, Oh ES, Harun A, Ehrenburg M, Agrawal Y. vestibular loss predicts poorer spatial cognition in patients with Alzheimer's disease. *J Alzheimers Dis JAD.* (2018) 61:995–1003. doi: 10.3233/JAD-170751
59. Agrawal Y, Smith PF, Rosenberg PB. Vestibular impairment, cognitive decline and Alzheimer's disease: balancing the evidence. *Aging Ment Health.* (2019) 29:1–4. doi: 10.1080/13607863.2019.1566813
60. Semenov YR, Bigelow RT, Xue QL, du Lac S, Agrawal Y. Association between vestibular and cognitive function in US adults: data from the national health and nutrition examination survey. *J Gerontol A Biol Sci Med Sci.* (2016) 71:243–50. doi: 10.1093/gerona/glv069
61. Tian Q, Resnick SM, Studenski SA. Olfaction is related to motor function in older adults. *J Gerontol A Biol Sci Med Sci.* (2017) 72:1067–71. doi: 10.1093/gerona/glw222
62. Graves AB, Bowen JD, Rajaram L, McCormick WC, McCurry SM, Schellenberg GD, et al. Impaired olfaction as a marker for cognitive decline: interaction with apolipoprotein E epsilon4 status. *Neurology.* (1999) 53:1480–7. doi: 10.1212/WNL.53.7.1480
63. Adams DR, Kern DW, Wroblewski KE, McClintock MK, Dale W, Pinto JM. Olfactory dysfunction predicts subsequent dementia in older U. S adults. *J Am Geriatr Soc.* (2018) 66:140–4. doi: 10.1111/jgs.15048
64. Devanand DP, Lee S, Luchsinger JA, Andrews H, Goldberg T, Huey ED, et al. *Intact Global Cognitive and Olfactory Ability Predicts Lack of Transition to Dementia. Alzheimers Dement.* (2019) Available online at: https://www.sciencedirect.com/science/article/pii/S1552526019353749 (accessed May 19, 2022).
65. Yaffe K, Freimer D, Chen H, Asao K, Rosso A, Rubin S, et al. Olfaction and risk of dementia in a biracial cohort of older adults. *Neurology.* (2017) 88:456–62. doi: 10.1212/WNL.0000000000003558
66. Lipnicki DM, Sachdev PS, Crawford J, Reppermund S, Kochan NA, Trollor JN, et al. Risk factors for late-life cognitive decline and variation with age and sex in the Sydney memory and ageing study. *PLoS ONE.* (2013) 8:e65841. doi: 10.1371/journal.pone.0065841
67. Roberts RO, Christianson TJH, Kremers WK, Mielke MM, Machulda MM, Vassilaki M, et al. Association between olfactory dysfunction and amnestic mild cognitive impairment and Alzheimer disease dementia. *JAMA Neurol.* (2016) 73:93–101. doi: 10.1001/jamaneurol.2015.2952
68. Stanciu I, Larsson M, Nordin S, Adolfsson R, Nilsson LG, Olofsson JK. Olfactory impairment and subjective olfactory complaints independently predict conversion to dementia: a longitudinal, population-based study. *J Int Neuropsychol Soc JINS.* (2014) 20:209–17. doi: 10.1017/S1355617713001409
69. Chen Z, Xie H, Yao L, Wei Y. Olfactory impairment and the risk of cognitive decline and dementia in older adults: a meta-analysis. *Braz J Otorhinolaryngol.* (2021) 87:94–102. doi: 10.1016/j.bjorl.2020.07.009
70. Kashibayashi T, Takahashi R, Fujita J, Fujito R, Kamimura N, Okutani F, et al. Correlation between cerebral blood flow and olfactory function in mild cognitive impairment and Alzheimer's disease. *Int J Geriatr Psychiatry.* (2021) 36:1103–9. doi: 10.1002/gps.5527
71. Mast FW, Ellis AW. Internal models, vestibular cognition, and mental imagery: conceptual considerations. *Multisensory Res.* (2015) 28:443–60. doi: 10.1163/22134808-00002503
72. Raphan T, Cohen B. The vestibulo-ocular reflex in three dimensions. *Exp Brain Res.* (2002) 145:1–27. doi: 10.1007/s00221-002-1067-z
73. Dichgans J, Diener HC. The contribution of vestibulo-spinal mechanisms to the maintenance of human upright posture. *Acta Otolaryngol.* (1989) 107:338–45. doi: 10.3109/00016488909127518
74. Maharani A, Dawes P, Nazroo J, Tampubolon G, Pendleton N, SENSE-Cog WP1 group. Longitudinal relationship between hearing aid use and cognitive function in older Americans. *J Am Geriatr Soc.* (2018) 66:1130–6. doi: 10.1111/jgs.15363
75. Jafari Z, Kolb BE, Mohajerani MH. Age-related hearing loss and tinnitus, dementia risk, and auditory amplification outcomes. *Ageing Res Rev.* (2019) 56:100963. doi: 10.1016/j.arr.2019.100963
76. Sarant J, Harris D, Busby P, Maruff P, Schembri A, Lemke U, et al. The effect of hearing aid use on cognition in older adults: can we delay decline or even improve cognitive function? *J Clin Med.* (2020) 9:E254. doi: 10.3390/jcm9010254
77. Mertens G, Andries E, Claes AJ, Topsakal V, Van de Heyning P, Van Rompaey V, et al. Cognitive improvement after cochlear implantation in older adults with severe or profound hearing impairment: a prospective, longitudinal, controlled, multicenter study. *Ear Hear.* (2020) 42:606-14. doi: 10.1097/AUD.0000000000000962
78. Birte-Antina W, Ilona C, Antje H, Thomas H. Olfactory training with older people. *Int J Geriatr Psychiatry.* (2018) 33:212–20. doi: 10.1002/gps.4725
79. Sakamoto Y, Ebihara S, Ebihara T, Tomita N, Toba K, Freeman S, et al. Fall prevention using olfactory stimulation with lavender odor in elderly nursing home residents: a randomized controlled trial. *J Am Geriatr Soc.* (2012) 60:1005–11. doi: 10.1111/j.1532-5415.2012.03977.x
80. Mohammed A, Gibbons LE, Gates G, Anderson ML, McCurry SM, McCormick W, et al. Association of performance on dichotic auditory tests with risk for incident dementia and Alzheimer dementia. *JAMA Otolaryngol Neck Surg.* (2022) 148:20–7. doi: 10.1001/jamaoto.2021.2716
81. Kukull WA, Higdon R, Bowen JD, McCormick WC, Teri L, Schellenberg GD, et al. Dementia and Alzheimer disease incidence: a prospective cohort study. *Arch Neurol.* (2002) 59:1737–46. doi: 10.1001/archneur.59.11.1737
82. Lin VYW, Chung J, Callahan BL, Smith L, Gritters N, Chen JM, et al. Development of cognitive screening test for the severely hearing impaired: hearing-impaired MoCA. *Laryngoscope.* (2017) 127:S4–11. doi: 10.1002/lary.26590

Conflict of Interest: JV discloses intellectual property and a filed patent (17/281121–"Olfactory Diagnostic and Training Kits and Methods") related to the objective olfactory testing methods used in this research.

The remaining authors declare that the research was conducted in the absence of any commercial or financial relationships that could be construed as a potential conflict of interest.

Publisher's Note: All claims expressed in this article are solely those of the authors and do not necessarily represent those of their affiliated organizations, or those of the publisher, the editors and the reviewers. Any product that may be evaluated in this article, or claim that may be made by its manufacturer, is not guaranteed or endorsed by the publisher.

Copyright © 2022 Lucas, Arambula, Arambula, Yu, Farrokhian, D'Silva, Staecker and Villwock. This is an open-access article distributed under the terms of the Creative Commons Attribution License (CC BY). The use, distribution or reproduction in other forums is permitted, provided the original author(s) and the copyright owner(s) are credited and that the original publication in this journal is cited, in accordance with accepted academic practice. No use, distribution or reproduction is permitted which does not comply with these terms.

frontiers | Frontiers in Neurology

MINI REVIEW
published: 11 July 2022
doi: 10.3389/fneur.2022.891536

Simultaneous Dual Recordings From Vestibular Hair Cells and Their Calyx Afferents Demonstrate Multiple Modes of Transmission at These Specialized Endings

Donatella Contini[1], *Gay R. Holstein*[2,3] *and Jonathan J. Art*[1]*

[1] Department of Anatomy & Cell Biology, University of Illinois College of Medicine, Chicago, IL, United States, [2] Department of Neurology, Icahn School of Medicine at Mount Sinai, New York, NY, United States, [3] Department of Neuroscience, Icahn School of Medicine at Mount Sinai, New York, NY, United States

In the vestibular periphery, transmission *via* conventional synaptic boutons is supplemented by post-synaptic calyceal endings surrounding Type I hair cells. This review focusses on the multiple modes of communication between these receptors and their enveloping calyces as revealed by simultaneous dual-electrode recordings. Classic orthodromic transmission is accompanied by two forms of bidirectional communication enabled by the extensive cleft between the Type I hair cell and its calyx. The slowest cellular communication low-pass filters the transduction current with a time constant of 10–100 ms: potassium ions accumulate in the synaptic cleft, depolarizing both the hair cell and afferent to potentials greater than necessary for rapid vesicle fusion in the receptor and potentially triggering action potentials in the afferent. On the millisecond timescale, conventional glutamatergic quantal transmission occurs when hair cells are depolarized to potentials sufficient for calcium influx and vesicle fusion. Depolarization also permits a third form of transmission that occurs over tens of microseconds, resulting from the large voltage- and ion-sensitive cleft-facing conductances in both the hair cell and the calyx that are open at their resting potentials. Current flowing out of either the hair cell or the afferent divides into the fraction flowing across the cleft into its cellular partner, and the remainder flowing out of the cleft and into the surrounding fluid compartment. These findings suggest multiple biophysical bases for the extensive repertoire of response dynamics seen in the population of primary vestibular afferent fibers. The results further suggest that evolutionary pressures drive selection for the calyx afferent.

Keywords: synaptic transmission, hair cell, calyx, ion accumulation, quantal transmission, ephaptic transmission, resistive coupling, vestibular

OPEN ACCESS

Edited by:
Hans Straka,
Ludwig Maximilian University of Munich, Germany

Reviewed by:
Daniel John Brown,
Curtin University, Australia

Correspondence:
Jonathan J. Art
jart@uic.edu

Specialty section:
This article was submitted to Neuro-Otology, a section of the journal Frontiers in Neurology

Received: *07 March 2022*
Accepted: *02 May 2022*
Published: *11 July 2022*

Citation:
Contini D, Holstein GR and Art JJ (2022) Simultaneous Dual Recordings From Vestibular Hair Cells and Their Calyx Afferents Demonstrate Multiple Modes of Transmission at These Specialized Endings. Front. Neurol. 13:891536. doi: 10.3389/fneur.2022.891536

INTRODUCTION

A persistent question in vestibular research is the functional significance of specialized calyx endings present on a subset of primary afferents in vestibular end organs. A majority of afferent and all efferent synapses involving hair cells (HCs) in the labyrinth and cochlea are mediated by conventional bouton endings. While the calyx represents a unique characteristic distinguishing

vestibular from auditory sensory epithelia, the function of this morphologically specialized synapse remains obscure. Recent dual simultaneous recordings from HCs and their associated calyx afferents demonstrate that there are three modes of intercellular communication between them. In addition to unidirectional quantal transmission from HCs to afferents, there are two bidirectional forms of transmission. The slower of the two results from potassium flux into the cleft from either HC or afferent over tens of milliseconds, which can elevate $[K^+]_{cleft}$ from a resting ∼8 to >28 mM. The corresponding $E_{(K)}$ for channels facing the cleft are depolarized from −71 to −38 mV. The more rapid form of bidirectional transmission results from HC and afferent channels open near their respective resting potentials. These allow current flowing into the cleft from either HC or afferent to divide between a component flowing out of the cleft near its apex at the neck of the Type I HC and a component flowing across the cleft into the synaptic partner. As yet, there is no compelling evidence that the calyx is uniquely associated with particular characteristics of afferent discharge regularity or dynamics.

ANATOMY, SYNAPTIC MORPHOLOGY, AND INNERVATION

Vestibular epithelia of amniotes contain two HC receptor subtypes. These were initially differentiated by HC cytology alone, and were subsequently defined by morphological differences in their associated afferent processes as well (1). Type I HCs are flask-shaped and are innervated by an afferent chalice surrounding the entire basolateral HC surface except the apical neck. The extensiveness and exclusivity of the cleft between the HC and its enveloping calyx, together with the tight junction seal protecting the endolymphatic space, creates a unique, diffusion-limited, femtoliter environment that is markedly different from perilymph. Type II HCs are cylindrical and participate in comparatively small synapses involving bouton-like endings of vestibular afferents that terminate on the receptor somata and the outer calyceal faces (2, 3).

Both vestibular HC subtypes utilize ribbon synapses for quantal transmission. These structures were originally recognized in retinal photoreceptors, where the ribbons were bedecked with synaptic vesicles, a few of which attached to the cell's plasma membrane (4–8). Subsequent studies revealed variability in their overall structure (9, 10), resulting in the adoption of the more general term "synaptic body" to describe synaptic vesicles tethered to a central structure with a minority docked at an active zone.

Synaptic bodies have been reported in retinal photoreceptors and bipolar cells, pinealocytes, electroreceptors, and auditory and vestibular HCs (9). Both the morphology of the synaptic body, and the number, density, tethering, and docking of the associated synaptic vesicles (10, 11) vary. In auditory HCs, this morphological diversity has been correlated with functional differences in peripheral auditory signal processing based on Ca^{2+}-dependent exocytosis (12, 13). In both vestibular and auditory HCs, ribbon synapse morphology is thought to underlie the ability of HCs to respond with graded, high rates of sustained quantal transmitter release (14, 15). This dual function is achieved by the orchestrated availability of docked vesicles for immediate exocytosis, and tethered vesicles (the "readily releasable pool") poised for imminent release (16, 17). As shown in **Figure 1**, ribbon synapses are present at Type I HC synapses with calyces, and Type II HC synapses with both boutons and calyx outer faces (2, 3, 25, 26). Efferent synapses with afferents and Type II HCs display conventional presynaptic membrane specializations and post-synaptic subsynaptic cisterns in the HCs. Despite this well-defined anatomy, however, the precise role of the calyx in shaping HC-afferent signaling is not known. In that context, it is noteworthy that Wersäll reportedly regretted his sequential naming of the HCs, deeming the Type I HC-calyx architecture more highly evolved (27).

MORPHOPHYSIOLOGY

Decades of effort has focused on mapping morphological attributes of vestibular end organs and correlating these maps with dynamics and statistics of afferent firing (28–36); [Review: (37)]. Based on intracellular recordings, dye injections, and light microscopic reconstructions (18, 22), the crista ampullaris in multiple species has been subdivided into concentrically or linearly organized zones that evince differences in HC demographics and afferent innervation patterns (38, 39) (**Figure 1D**). The posterior canal crista of turtles, for example, is organized into two symmetrical hemicristae separated by a central torus (21, 40). Each hemicrista has a central zone surrounded by a peripheral area that extends toward the torus and planum. All afferents in the central zone have calyces, manifest as either calyx-only fibers (18, 38) or dimorphic (41) fibers having both calyx and bouton endings. Afferents with bouton terminals are present in the peripheral zones throughout the crista, but more densely populate the zone with larger afferent fibers nearest the torus (18). Reflecting this, Type I HCs are more prevalent in the central zone while Type II HCs are present throughout the crista.

This differential localization of HCs and afferent endings across the crista underlies a coherent physiological and functional map of afferent activity (22, 38, 42–46). Specifically, the regularity of afferent fiber discharge, defined by the variability in time between sequential action potentials (APs) is reportedly a continuous variable correlating with the fiber's response to velocity or angular acceleration (47–50). Regular afferents have evenly spaced spontaneous firing rates and respond to low frequency angular motion with tonic discharge. In effect, this mathematically integrates the acceleration stimulus, transmitting signals that are proportional to head velocity. In contrast, the spontaneous firing of irregular afferents shows high variability in the timing between APs. Angular acceleration elicits phasic, dynamic responses from these fibers, which more closely resemble the accelerative stimulus. Moreover, regularly discharging fibers as a group have lower gain ($spikes^*sec^{-1}/degrees^*sec^{-1}$) than irregular afferents. In turtles, low gain, regularly-firing bouton afferent endings sensitive to

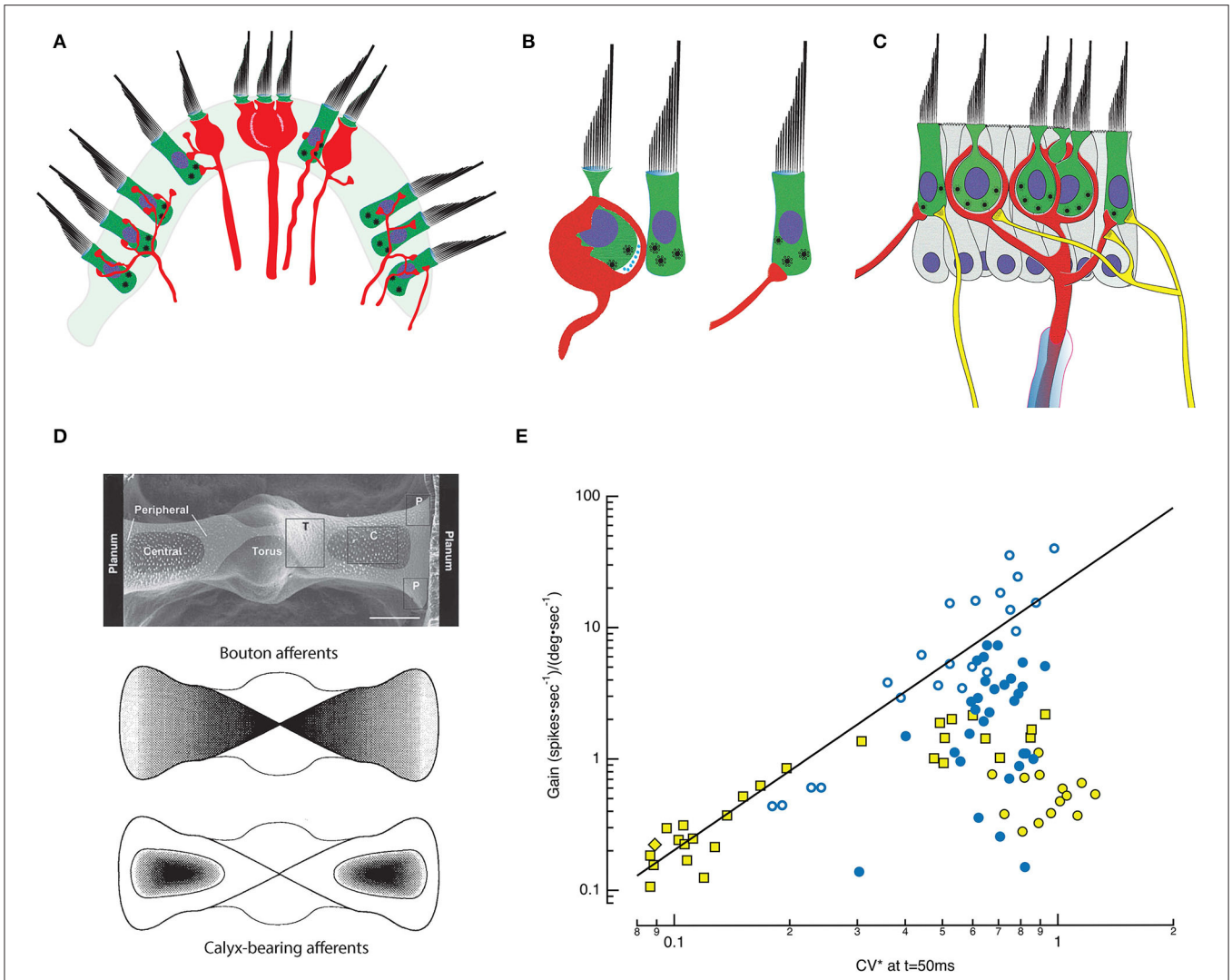

FIGURE 1 | Morphophysiology of the semicircular canal (SCC) epithelium. **(A)** Cross section through the saddle-shaped crista reveals distinct innervation patterns: boutons are found peripherally, with calyx and dimorphic afferents located centrally [adapted from (18)]. **(B)** Type I HCs are internal to an enveloping calyx that creates an extensive synaptic cleft in which ions accumulate. Type I HCs have synaptic bodies associated with quantal transmission onto the inner leaflet of the calyx. Type II HCs also have synaptic bodies indicative of quantal transmission, and synapse onto bouton endings (right) or onto the outer leaflet of an afferent calyx (middle and left). **(C)** A single myelinated afferent (center, red) may branch into several calyces, each containing one or more Type I HCs. Additional input from Type II HCs may occur *via* synapses onto the outer face of the afferent (left), or through bouton endings of fine collateral branches (right). Efferent fibers (yellow) from the brainstem synapse on HCs and on the outer faces of calyces (19). **(D)** Top: SEM plan view of the turtle posterior SCC (20). The epithelium is divided into two hemicristae with central and peripheral regions that extend bilaterally from the torus to the planum on either side. Middle: Map of the density of bouton afferents in each hemicrista. Bottom: Density map of the distribution of calyx-bearing afferents in the central regions of each hemicrista (21). **(E)** Afferent signaling dynamics and discharge statistics in the posterior SCC of chinchilla (yellow symbols) (22) and turtle (blue symbols) (18) are correlated and map systematically across the epithelia. CV*, a measure of the irregularity of the interval between successive APs, is a continuous variable with the most regular fibers on the left and the most irregular on the right. Typically, when either animal was examined with low-frequency, 0.3 or 2 Hz, rotations, low gain afferents sensitive to velocity are more regular, and high gain afferents are sensitive to accelerations. For the chinchilla, the low gain bouton (yellow diamond) and dimorphic (yellow square) afferents demonstrate that regular discharge can be achieved with either bouton or calyx endings. Data seen on the right side, including high gain bouton (turtle: blue, open circle) and dimorphic (turtle: blue, filled circle; chinchilla: yellow square) fibers demonstrate that irregular discharge can be achieved by afferents containing either type of ending. The irregular low gain "calyx only" afferents in chinchilla (yellow filled circle) remain a puzzle but may simply be afferents that respond maximally to stimulations at higher frequencies (23) or with vibration (24). CV* for chinchilla data transformed from 15 ms inter-spike interval (ISI) CV* to that at 50 ms ISI using a third-order polynomial fit to the CV* vs. ISI data at 50 ms in Figure 1 of (22), equivalent to the CV* and ISI used in the turtle data (18).

velocity are concentrated near the planum, while higher gain bouton afferents sensitive to acceleration terminate closer to the torus (51). In contrast, most calyx-bearing fibers, which end in the central zone, are irregular afferents. The sensitivity of these fibers to low-frequency rotation varies over two orders of magnitude and is not strictly correlated with the degree of

irregularity of the spontaneous discharge rate. Nevertheless, an integrated morphophysiological map of the crista emerges in which low gain, regularly discharging, velocity-sensitive bouton afferents terminate nearest the planum, bouton afferents of higher gain and more irregular discharge terminate nearest the torus, and calyx-bearing, irregularly-firing units terminate in the central zone of each hemicrista (**Figure 1D**). Functionally, the high gain fibers across species are particularly attuned to acceleration (51) or to jerks, the derivative of acceleration (52), and rapidly saturate as the amplitude of the stimulus increases. Medium gain afferents remain active over a wider motion spectrum, while low gain fibers are not prone to saturate, regardless of the magnitude of the head acceleration (**Figure 1E**). One caveat to this characterization is that the afferent gains were typically assessed at single low frequencies of stimulation (18, 22), although the most irregular fibers are often maximally responsive to higher frequencies and even vibrational or sound stimuli (23, 53, 54).

Based on the initial correlation of afferent terminal distribution with regularity of spontaneous firing and response dynamics, significant effort was directed toward identifying causality. It remained to be determined whether the regularity of a fiber's spontaneous firing derived from the geographical position of its terminals in the crista, or from the biophysical properties of HC inputs to trunk, branch, and twig segments of the parent process. Studies addressing this have been useful in highlighting the overall importance of regional localization in the crista and suggesting the type of HCs, three-dimensional terminal architecture and synapses contributing to individual afferent responses. However, efferent innervation (55–59), GABA-mediated modulation of glutamatergic transmission (60–62), ion accumulation in the synaptic cleft (19, 63–65), and Type II HC input to the external face of the calyx (3, 66) have not been incorporated into these analyses. Since each of these has the potential to markedly alter peripheral vestibular activity, conclusions from these studies are necessarily tentative.

SOLITARY CELLS

To supplement information gleaned by morphophysiology, currents were analyzed from HCs classified as Type I or II based on their amphoral or cylindrical profile (65, 67–85), from identified regions of the epithelia (20). This approach emulated a strategy used in lower vertebrates to demonstrate that the kinetics of voltage- and ion-sensitive basolateral channels imparted frequency selectivity to solitary auditory HCs (86–92). Typically, solitary vestibular HCs were bathed in artificial perilymph, an ionic environment appropriate for Type II cells, but of unknown propriety for the ionically dynamic milieu of a Type I HC and its calyx. In principle, such a bath would be apposite for isolating conductances based on their voltage ranges of activation, kinetics, ionic permeabilities, and pharmacological profiles. In an artificial perilymph however, analysis of fundamental metrics such as I-V curves would be altered by driving forces reflecting equilibrium potentials for each ion when bathed in high sodium and low potassium. The vestibular potassium channels characterized in this way have been reviewed (93). A startling discovery was that Type I HCs possess a low-voltage outward-rectifying potassium current, $IK_{(LV)}$, that activates at very hyperpolarized potentials. Its full activation near the HC resting potential was considered problematic, since enormous transduction currents would be required to depolarize a cell to potentials necessary for the calcium influx and vesicle fusion associated with quantal transmission. A solution to this paradox was proposed by Chen (94), who suggested that potassium accumulation in the synaptic cleft between the HC and calyx was analogous to the potassium accumulation in tissues surrounding the squid giant axon (95), and that potassium flowing from the HC would increase $[K^+]_{cleft}$ and depolarize E_K for HC and afferent conductances facing the cleft. As a result, the Type I HC would be depolarized, at least to potentials necessary for calcium influx and quantal transmission, but the increased $[K^+]_{cleft}$ would also depolarize the calyx.

THEORETICAL AND SINGLE-ELECTRODE STUDIES

Theoretical and experimental approaches were then used to examine the Chen conjecture. The theoretical analysis (96, 97) relied on equivalent circuits of the Type I HC, cleft, and calyx to analyze the problem primarily as ephaptic transmission (98–100) embellished by potassium accumulation. In general, this analysis concluded that the potential drops associated with current flow along the cleft from HC base to apex created only minor differences in the driving force for channels facing the cleft, and as a result were not likely to be a major source of coupling (97). The possibility that ion accumulation could have the effect suggested by Chen was also examined experimentally (101). Following blockade of quantal transmission, slow potentials that were phase-locked to the stimulus could be detected, a phenomenon consistent with ion accumulation. Two groups examined the potassium accumulation question by perforating the calyx and patch-recording from the enveloped Type I HCs *in situ* (102–104). These experiments demonstrated that depolarization of either the HC or the calyx caused a reversal of the HC potassium tail currents, suggesting an elevation of $[K^+]_{cleft}$ consistent with Chen's conjecture. Such studies, together with one suggesting a transmitter role for protons (64), yielded results in which the interactions/coupling between cells occurred over tens of milliseconds. However, experiments using mechanical stimulation of the HC bundle demonstrated that when quantal transmission was blocked, the HC-afferent coupling could be extremely rapid, which would facilitate transmission of high frequency information (105, 106). Such contradictory viewpoints evoke the Indian parable of blind men describing an elephant (107), where each detects and interprets a small part of the more complex whole. This led to a quest to discover underlying biophysical mechanisms that could reconcile the differing results.

DUAL-ELECTRODE STUDIES

The demonstration that $[K^+]_{cleft}$ can be increased by potassium fluxes from either synaptic partner is a reminder that

interpretations of single-electrode voltage-clamp studies of either HC or afferent alone can be problematic. The privileged ionic compartment created by the apposition between a HC and calyx means that any single-electrode study that voltage clamped one cell necessarily allowed the potential of the other cell to vary freely. Moreover, studies that patched onto Type I HCs *in situ* (102–106) did so by perforating the calyx, and there is ample evidence that this approach compromises the cleft environment and results in two types of recordings: those similar to solitary cells bathed in perilymph, and those in which reversal of the potassium tail currents demonstrate an increase in $[K^+]_{cleft}$ (102, 103).

To address this, we developed an approach to simultaneously patch the HC and calyx without breaching the inner calyceal membrane (19, 63). In essence, this requires patching the HC either on its apex or on the exposed 2–3 μm of its basolateral wall extending apically above the enveloping calyx. With this approach, the potentials of both cells can be interrogated or controlled in a current clamp or voltage clamp, leaving the cleft ionic environment intact.

SLOW POTASSIUM ACCUMULATION DEPOLARIZES BOTH HC AND AFFERENT TO FACILITATE QUANTAL TRANSMISSION

Our initial studies (19) focused on ion accumulation and used the reversal potential of the HC potassium tail currents following depolarization to track E_K and estimate $[K^+]_{cleft}$. Blocking HC potassium flux abolished low-pass coupling of the transducer current occurring over tens of milliseconds, but spared quantal transmission. Our subsequent study (63) demonstrated that HC potassium flux depended upon the activation of both voltage-activated and calcium-activated potassium channels, and that the voltage-activated conductance was sensitive to $[K^+]_{cleft}$ and $[Ca^{2+}]_{cleft}$. Clamping $[H^+]_{cleft}$ resulted in stronger coupling between the two, suggesting that H^+ was not a primary transmitter acting through acid-sensitive ion channels. Pharmacological experiments using an HCN channel blocker (19) demonstrated that, in addition to synaptic coupling acting through HC and afferent potassium channels, the elevated $[K^+]_{cleft}$ not only decreased outward K^+ flux through calyceal voltage-sensitive potassium channels, but also shifted the activation curve of G_{HCN} (84), creating a depolarizing inward flux of Na^+ and K^+ through the HCN channels. These potassium-sensitive effects were obtained regardless of whether the increased $[K^+]_{cleft}$ was due to HC or to afferent fluxes. Inward transduction currents would generate an outward flow of K^+ through the basolateral HC, elevate $[K^+]$, and shift E_K, causing depolarization of both HC and afferent (**Figure 2A**). Taken together, these results expand Chen's conjecture that potassium accumulation in the cleft facilitates classical quantal transmission between a Type I HC and calyx, and extend it to direct stimulation of the afferent as well. For complex calyces with more than one enveloped HC, the findings indicate that depolarization of one HC can depolarize the afferent, which would then depolarize neighboring receptors enveloped by the shared afferent (**Figure 2A**). In that light, slow potassium accumulation in the cleft, above that in perilymph, is the ongoing leaky integration of transduction currents or efferent excitation of the calyx, and thus can be interpreted as bidirectional intercellular communication that acts over tens of milliseconds.

HC AND AFFERENT DEPOLARIZATION CREATES RESISTIVE COUPLING THROUGH INCREASED OPEN-PROBABILITY OF HC AND AFFERENT CHANNELS FACING THE CLEFT

One remarkable result of these experiments (63) was a demonstration that there is also a rapid bidirectional coupling between the cells that allows currents to activate within microseconds of depolarization. With depolarization near the HC and calyx resting potentials, there are a significant number of ion channels with high open probabilities. Rapid inward transduction current would immediately flow out as potassium through HC channels, with much of the current flowing into the extensive synaptic cleft and a minority flowing into the calyx (**Figure 2B**). Such coupling can be analyzed using either Kirchhoff's current or voltage laws, and the conclusion is the same: there would be relatively small voltage gains or drops of a few mV along the cleft depending on the current direction and the precise resistance (97, 110). The impact of this on specific channels facing the cleft is unknown and would greatly depend on their position with respect to the apical gap between HC and calyx. The dual recordings allow us to measure the currents flowing out of one synaptic partner and into the other, or out through the cleft (19, 63) (**Figures 2B,C**). Such rapid current flow from HC into calyx, **Figure 2B**, may underlie the rapid transmission of high frequency mechanical stimuli (105, 106, 111), and may be the substrate for detection of sound and vibration (24, 33, 54, 112–117). As with slow potassium accumulation, this rapid ion flow through open channels is bidirectional, as evidenced by the retrograde transmission of calyx afferent APs into the HC (**Figure 2C**) (19). Thus, as depolarization persists, $[K^+]_{cleft}$ increases, and both the number of open channels and the amount of HC-afferent electrical coupling increase concomitantly.

Dual recordings also provided the incidental observation that in the central region, the EPSCs from Type I HCs onto the calyx inner leaflet were small (19, 118, 119), whereas those from Type II HCs onto the outer leaflet (19) were as large as those reported in the cochlea (14), and would be sufficient to trigger APs in afferents near the spike threshold. This highlights the risk of morphophysiological studies defining calyx-only afferents based on light microscopy alone.

CONCLUSIONS

During vertebrate evolution, selective pressures favored increased sensitivity and flawless encoding of three-dimensional

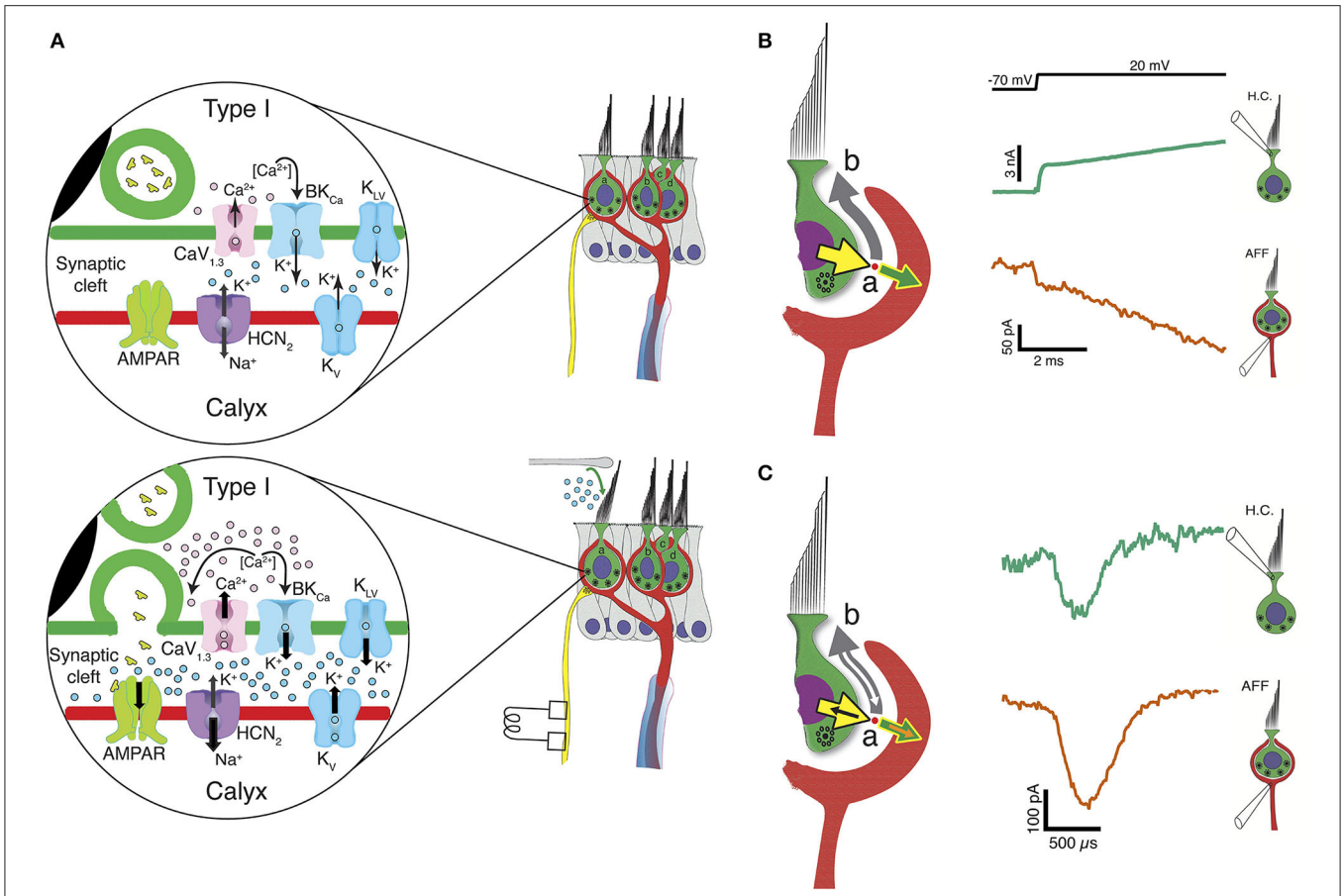

FIGURE 2 | Three forms of synaptic transmission between a Type I HC and calyx afferent. **(A)** In the absence of mechanical stimulation (upper panel), basolateral potassium currents activated at hyperpolarized potentials elevate the $[K^+]_{cleft}$ to concentrations near 8 mM, twice that found in perilymph. This results in a shift in E_K and depolarization of the HC to a resting potential between −60 and −50 mV, where $Ca_{1,3}$ channels are activated. At rest there is occasional vesicle fusion and the production of a background rate of afferent discharge. Upon mechanical stimulation (lower panel), the inward transduction current flows into the HC and out the basolateral conductances into the cleft as a potassium current. The further increase in $[K^+]_{cleft}$ is a low-pass integral of the transduction current and further depolarizes E_K for conductances in the HC and afferent membranes facing the cleft. The HC depolarization gates Ca^{2+} influx, resulting in fusion of synaptic vesicles and quantal transmission of glutamate to AMPARs on the calyx inner leaflet. The slow accumulation of potassium thereby facilitates quantal transmission near the resting potential, and for maintained depolarizations toward 0 mV, elevates $[K^+]_{cleft}$ to greater than 28 mM within 25 ms. It is likely that the irregularities of vesicle fusion and large quanta that initiate an AP are driven by neighboring Ca-channel noise (108), and as a consequence the degree of regularity of afferent discharge would be determined by the degree to which the post-synaptic afferent conductances have intrinsic memory and oscillatory behavior similar to those found in HCs of the turtle auditory papilla (90, 109). **(B)** Large conductances in the HC and calyx near the resting potential also create an open resistive pathway between the two that permits a fraction of the transduction current to be communicated across the cleft and into the calyx without synaptic delay. Outward current from the HC (yellow arrow) divides at point (a) into a large component (gray arrow) going along the cleft into the bath at point (b), and a smaller current flowing into the calyx (green arrow). The measured current for the HC (bluish-green current trace) and calyx (vermillion trace) show transmission within 10 μs. **(C)** Resistive coupling can also be demonstrated during large HC depolarizations that depolarize the calyx to potentials sufficient to generate an AP that travels into the calyx. Currents due to the invasion of an AP will sum with the primary currents illustrated in **(B)**. With an AP, an additional inward current (orange arrow) flows into the calyx, with an amplitude equal to the sum of the corresponding currents flowing into the HC (black arrow) and down the cleft (white arrow). The coupling between the calyx retrograde AP current (vermillion) and the induced HC current (bluish-green) is 12 μs [modified from (63)].

vestibular information. This correlated with a higher prevalence of Type I HCs and calyx afferents (120–123), which exhibit unidirectional quantal and two forms of bidirectional communication. Potassium accumulation in the synaptic cleft is a low-pass filter of HC transduction currents and afferent depolarizations by efferent fibers, and thus a leaky integrator of activity. At rest, $[K^+]_{cleft}$ is roughly 8 mM, or twice that found in perilymph, and is sufficient to depolarize E_K and facilitate conventional quantal transmission. Maintained low-frequency excitation elevates $[K^+]_{cleft}$ further to >28 mM, a value sufficient to trigger afferent APs even in the absence of quantal transmission. From an evolutionary perspective, the pressure to extend transmission to higher frequencies was best served by direct resistive coupling created by large HC and afferent cleft-facing conductances present at and depolarized from rest. In evolving from bouton, through

protocalyx to calyx, these conductances elevate $[K^+]_{cleft}$, depolarize E_K to facilitate quantal transmission, and provide a resistive path between synaptic partners that has minimal delay, is dynamic, and would increase as mechanical inputs become larger.

AUTHOR CONTRIBUTIONS

All authors listed have made a substantial, direct, and intellectual contribution to the work and approved it for publication.

FUNDING

This work was supported by NIH National Institute on Deafness and Other Communication Disorders grants R21 DC017292; R21 DC017577, R01 DC019953, and R01 DC008846.

ACKNOWLEDGMENTS

We would like to thank Professor A. Brichta for graciously allowing us to modify, reuse, and repurpose his figures in **Figure 1**.

REFERENCES

1. Wersäll J. Studies on the structure and innervation of the sensory epithelium of the cristae ampullares in the guinea pig. *Acta Otolaryngol Suppl.* (1956) 126:7–85. doi: 10.3109/00016485609120818
2. Goldberg JM, Lysakowski A, Fernández C. Morphophysiological and ultrastructural studies in the mammalian cristae ampullares. *Hear Res.* (1990) 49:89–102. doi: 10.1016/0378-5955(90)90097-9
3. Lysakowski A, Goldberg JM. Ultrastructural analysis of the cristae ampullares in the squirrel monkey (*Saimiri sciureus*). *J Comp Neurol.* (2008) 511:47–64. doi: 10.1002/cne.21827
4. Sjöstrand FS, editor. The ultrastructure of the innersegments of the retinal rods of the guinea pig eye as revealed by electron microscopy. *J Appl Phys.* (1953) 42:45–70. doi: 10.1002/jcp.1030420104
5. De Robertis E, Franchi CM. Electron microscope observations on synaptic vesicles in synapses of the retinal rods and cones. *J Biophys Biochem Cytol.* (1956) 2:307–18. doi: 10.1083/jcb.2.3.307
6. Carasso N. Etude au microscope électronique des synapses des cellules visuelles chez le têtard d'Alytes obstetricans. [Electron microscopy of the synapses of the visual cells in the tadpole of Alytes obstetricans]. *Comptes Rendus Hebdomadaires Séances Acad Sci D Sci Nat.* (1957) 245:216–9.
7. Polyak SL. *The Retina*. Chicago, IL: The University of Chicago Press (1941).
8. Sjostrand FS. Ultrastructure of retinal rod synapses of the guinea pig eye as revealed by three-dimensional reconstructions from serial sections. *J Ultrastruct Res.* (1958) 2:122–70. doi: 10.1016/S0022-5320(58)90050-9
9. Sterling P, Matthews G. Structure and function of ribbon synapses. *Trends Neurosci.* (2005) 28:20–9. doi: 10.1016/j.tins.2004.11.009
10. Moser T, Brandt A, Lysakowski A. Hair cell ribbon synapses. *Cell Tissue Res.* (2006) 326:347–59. doi: 10.1007/s00441-006-0276-3
11. Schmitz F. The making of synaptic ribbons: how they are built and what they do. *Neuroscientist.* (2009) 15:611–24. doi: 10.1177/1073858409340253
12. Johnson SL, Forge A, Knipper M, Munkner S, Marcotti W. Tonotopic variation in the calcium dependence of neurotransmitter release and vesicle pool replenishment at mammalian auditory ribbon synapses. *J Neurosci.* (2008) 28:7670–8. doi: 10.1523/JNEUROSCI.0785-08.2008
13. Meyer AC, Frank T, Khimich D, Hoch G, Riedel D, Chapochnikov NM, et al. Tuning of synapse number, structure and function in the cochlea. *Nature Neurosci.* (2009) 12:444–53. doi: 10.1038/nn.2293
14. Glowatzki E, Fuchs PA. Transmitter release at the hair cell ribbon synapse. *Nat Neurosci.* (2002) 5:147–54. doi: 10.1038/nn796
15. Fuchs PA, Glowatzki E, Moser T. The afferent synapse of cochlear hair cells. *Curr Opin Neurobiol.* (2003) 13:452–8. doi: 10.1016/S0959-4388(03)00098-9
16. von Gersdorff H, Matthews G. Electrophysiology of synaptic vesicle cycling. *Annu Rev Physiol.* (1999) 61:725–52. doi: 10.1146/annurev.physiol.61.1.725
17. Holt M, Cooke A, Neef A, Lagnado L. High mobility of vesicles supports continuous exocytosis at a ribbon synapse. *Curr Biol.* (2004) 14:173–83. doi: 10.1016/j.cub.2003.12.053
18. Brichta AM, Goldberg JM. Morphological identification of physiologically characterized afferents innervating the turtle posterior crista. *J Neurophysiol.* (2000) 83:1202–23. doi: 10.1152/jn.2000.83.3.1202
19. Contini D, Price SD, Art JJ. Accumulation of K+ in the synaptic cleft modulates activity by influencing both vestibular hair cell and calyx afferent in the turtle. *J Physiol.* (2017) 595.3:777–803. doi: 10.1113/JP273060
20. Brichta AM, Aubert A, Eatock RA, Goldberg JM. Regional analysis of whole cell currents from hair cells of the turtle posterior crista. *J Neurophysiol.* (2002) 88:3259–78. doi: 10.1152/jn.00770.2001
21. Brichta AM, Peterson EH. Functional architecture of vestibular primary afferents from the posterior semicircular canal of a turtle, *Pseudemys (Trachemys) scripta* elegans. *J Comp Neurol.* (1994) 344:481–507. doi: 10.1002/cne.903440402
22. Baird RA, Desmadryl G, Fernández C, Goldberg JM. The vestibular nerve of the chinchilla. II. Relation between afferent response properties and peripheral innervation patterns in the semicircular canals. *J Neurophysiol.* (1988) 60:182–203. doi: 10.1152/jn.1988.60.1.182
23. Dickman JD, Correia MJ. Responses of pigeon horizontal semicircular canal afferent fibers II. High-frequency mechanical stimulation. *J Neurophysiol.* (1989) 62:1102–12. doi: 10.1152/jn.1989.62.5.1102
24. Curthoys IS, Grant JW. How does high-frequency sound or vibration activate vestibular receptors? *Exp Brain Res.* (2015) 233:691–9. doi: 10.1007/s00221-014-4192-6
25. Lysakowski A, Goldberg JM. A regional ultrastructural analysis of the cellular and synaptic architecture in the chinchilla cristae ampullares. *J Comp Neurol.* (1997) 389:419–43.
26. Lysakowski A. Synaptic organization of the crista ampullaris in vertebrates. *Ann N Y Acad Sci.* (1996) 781:164–82. doi: 10.1111/j.1749-6632.1996.tb15700.x
27. Engström H. The first-order vestibular neuron. In: Graybiel A, editor. *Symposium on the Role of the Vestibular Organs in Space Exploration NASA SP-187*. Washington, DC: National Academies (1970). p. 123–35.
28. Goldberg JM, Fernández C. Vestibular mechanisms. *Annu Rev Physiol.* (1975) 37:129–62. doi: 10.1146/annurev.ph.37.030175.001021
29. Suzuki M, Harada Y. An experimental study on the frog semicircular canal–functions of cupula and vestibular ganglion. *J Otolaryngol.* (1985) 14:36–40.
30. Suzuki M, Harada Y. An experimental study on the physiological significance of the mode of cupular movement. *Arch Otorhinolaryngol.* (1985) 242:57–62. doi: 10.1007/BF00464407
31. Rabbitt RD, Boyle R, Highstein SM. Sensory transduction of head velocity and acceleration in the toadfish horizontal semicircular canal. *J Neurophysiol.* (1994) 72:1041–8. doi: 10.1152/jn.1994.72.2.1041
32. Hullar TE, Della Santina CC, Hirvonen T, Lasker DM, Carey JP, Minor LB. Responses of irregularly discharging chinchilla semicircular canal vestibular-nerve afferents during high-frequency head rotations. *J Neurophysiol.* (2005) 93:2777–86. doi: 10.1152/jn.01002.2004
33. Curthoys IS, Kim J, McPhedran SK, Camp AJ. Bone conducted vibration selectively activates irregular primary otolithic vestibular neurons in the guinea pig. *Exp Brain Res.* (2006) 175:256–67. doi: 10.1007/s00221-006-0544-1
34. Lasker DM, Han GC, Park HJ, Minor LB. Rotational responses of vestibular-nerve afferents innervating the semicircular canals in the C57BL/6 mouse. *J Assoc Res Otolaryngol.* (2008) 9:334–48. doi: 10.1007/s10162-008-0120-4

35. Jamali M, Sadeghi SG, Cullen KE. Response of vestibular nerve afferents innervating utricle and saccule during passive and active translations. *J Neurophysiol*. (2009) 101:141–9. doi: 10.1152/jn.91066.2008
36. Yu XJ, Dickman JD, Angelaki DE. Detection thresholds of macaque otolith afferents. *J Neurosci*. (2012) 32:8306–16. doi: 10.1523/JNEUROSCI.1067-12.2012
37. Paulin MG, Hoffman LF. Models of vestibular semicircular canal afferent neuron firing activity. *J Neurophysiol*. (2019) 122:2548–67. doi: 10.1152/jn.00087.2019
38. Fernández C, Baird RA, Goldberg JM. The vestibular nerve of the chinchilla. I. Peripheral innervation patterns in the horizontal and superior semicircular canals. *J Neurophysiol*. (1988) 60:167–81. doi: 10.1152/jn.1988.60.1.167
39. Fernandez C, Lysakowski A, Goldberg JM. Hair-cell counts and afferent innervation patterns in the cristae ampullares of the squirrel monkey with a comparison to the chinchilla. *J Neurophysiol*. (1995) 73:1253–69. doi: 10.1152/jn.1995.73.3.1253
40. Brichta AM, Peterson EH. Vestibular afferents innervating the posterior ampullae in a turtle, *Pseudemys scripta*. *Ann N Y Acad Sci*. (1992) 656:914–6. doi: 10.1111/j.1749-6632.1992.tb25293.x
41. Schessel DA, Highstein SM. Is transmission between the vestibular type I hair cell and its primary afferent chemical? *Ann N Y Acad Sci*. (1981) 374:210–4. doi: 10.1111/j.1749-6632.1981.tb30871.x
42. Schessel DA, Ginzberg R, Highstein SM. Morphophysiology of synaptic transmission between type I hair cells and vestibular primary afferents. An intracellular study employing horseradish peroxidase in the lizard, Calotes versicolor. *Brain Res*. (1991) 544:1–16. doi: 10.1016/0006-8993(91)90879-Z
43. Goldberg JM, Baird RA, Fernández C. Morphophysiological studies of the mammalian vestibular labyrinth. *Prog Clin Biol Res*. (1985) 176:231–45.
44. Fernández C, Goldberg JM, Baird RA. The vestibular nerve of the chinchilla. III. Peripheral innervation patterns in the utricular macula. *J Neurophysiol*. (1990) 63:767–80. doi: 10.1152/jn.1990.63.4.767
45. Goldberg JM, Desmadryl G, Baird RA, Fernández C. The vestibular nerve of the chinchilla. V. Relation between afferent discharge properties and peripheral innervation patterns in the utricular macula. *J Neurophysiol*. (1990) 63:791–804. doi: 10.1152/jn.1990.63.4.791
46. Goldberg JM, Desmadryl G, Baird RA, Fernández C. The vestibular nerve of the chinchilla. IV. Discharge properties of utricular afferents. *J Neurophysiol*. (1990) 63:781–90. doi: 10.1152/jn.1990.63.4.781
47. Fernández C, Goldberg JM. Physiology of peripheral neurons innervating semicircular canals of the squirrel monkey. II. Response to sinusoidal stimulation and dynamics of peripheral vestibular system. *J Neurophysiol*. (1971) 34:661–75. doi: 10.1152/jn.1971.34.4.661
48. Goldberg JM, Fernández C. Physiology of peripheral neurons innervating semicircular canals of the squirrel monkey. III. Variations among units in their discharge properties. *J Neurophysiol*. (1971) 34:676–84. doi: 10.1152/jn.1971.34.4.676
49. Goldberg JM, Fernández C. Physiology of peripheral neurons innervating semicircular canals of the squirrel monkey. I. Resting discharge and response to constant angular accelerations. *J Neurophysiol*. (1971) 34:635–60.
50. Curthoys IS. The response of primary horizontal semicircular canal neurons in the rat and guinea pig to angular acceleration. *Exp Brain Res*. (1982) 47:286–94. doi: 10.1007/BF00239388
51. Brichta AM, Goldberg JM. Responses to efferent activation and excitatory response-intensity relations of turtle posterior-crista afferents. *J Neurophysiol*. (2000) 83:1224–42. doi: 10.1152/jn.2000.83.3.1224
52. Art JJ. *Comparative physiology of primary afferents innervating semicircular canals in two species of plethodontid salamanders* (Dissertation). Chicago, IL: University of Chicago (1979).
53. McCue MP, Guinan JJ Jr. Acoustically responsive fibers in the vestibular nerve of the cat. *J Neurosci*. (1994) 14:6058–70. doi: 10.1523/JNEUROSCI.14-10-06058.1994
54. Curthoys IS, Burgess AM, Goonetilleke SC. Phase-locking of irregular guinea pig primary vestibular afferents to high frequency (>250Hz) sound and vibration. *Hear Res*. (2019) 373:59–70. doi: 10.1016/j.heares.2018.12.009
55. Poppi LA, Holt JC, Lim R, Brichta AM. A review of efferent cholinergic synaptic transmission in the vestibular periphery and its functional implications. *J Neurophysiol*. (2019). doi: 10.1152/jn.00053.2019
56. Holt JC, Jordan PM, Lysakowski A, Shah A, Barsz K, Contini D. Muscarinic acetylcholine receptors and m-currents underlie efferent-mediated slow excitation in calyx-bearing vestibular afferents. *J Neurosci*. (2017) 37:1873–87. doi: 10.1523/JNEUROSCI.2322-16.2017
57. Holt JC, Kewin K, Jordan PM, Cameron P, Klapczynski M, McIntosh JM, et al. Pharmacologically distinct nicotinic acetylcholine receptors drive efferent-mediated excitation in calyx-bearing vestibular afferents. *J Neurosci*. (2015) 35:3625–43. doi: 10.1523/JNEUROSCI.3388-14.2015
58. Jordan PM, Parks XX, Contini D, Holt JC. A review of synaptic mechanisms of vestibular efferent signaling in turtles: extrapolation to efferent actions in mammals. *J Vestib Res*. (2013) 23:161–75. doi: 10.3233/VES-130492
59. Raghu V, Salvi R, Sadeghi SG. Efferent inputs are required for normal function of vestibular nerve afferents. *J Neurosci*. (2019) 39:6922–35. doi: 10.1523/JNEUROSCI.0237-19.2019
60. Holstein GR, Rabbitt RD, Martinelli GP, Friedrich VL, Jr., Boyle RD, Highstein SM. Convergence of excitatory and inhibitory hair cell transmitters shapes vestibular afferent responses. *Proc Natl Acad Sci USA*. (2004) 101:15766–71. doi: 10.1073/pnas.0402824101
61. Holstein GR, Martinelli GP, Henderson SC, Friedrich VL, Jr., Rabbitt RD, Highstein SM. Gamma-aminobutyric acid is present in a spatially discrete subpopulation of hair cells in the crista ampullaris of the toadfish *Opsanus tau*. *J Comp Neurol*. (2004) 471:1–10. doi: 10.1002/cne.11025
62. Highstein SM, Rabbitt RD, Holstein GR, Boyle RD. Determinants of spatial and temporal coding by semicircular canal afferents. *J Neurophysiol*. (2005) 93:2359–70. doi: 10.1152/jn.00533.2004
63. Contini D, Holstein GR, Art JJ. Synaptic cleft microenvironment influences potassium permeation and synaptic transmission in hair cells surrounded by calyx afferents in the turtle. *J Physiology*. (2020) 598.4:853–89. doi: 10.1113/JP278680
64. Highstein SM, Holstein GR, Mann MA, Rabbitt RD. Evidence that protons act as neurotransmitters at vestibular hair cell-calyx afferent synapses. *Proc Natl Acad Sci USA*. (2014) 111:5421–6. doi: 10.1073/pnas.1319561111
65. Chen JW, Eatock RA. Major potassium conductance in type I hair cells from rat semicircular canals: characterization and modulation by nitric oxide. *J Neurophysiol*. (2000) 84:139–51. doi: 10.1152/jn.2000.84.1.139
66. Ross MD, Rogers CM, Donovan KM. Innervation patterns in rat saccular macula. A structural basis for complex sensory processing. *Acta Otolaryngol*. (1986) 102:75–86. doi: 10.3109/00016488609108649
67. Valat J, Devau G, Dulon D, Sans A. Vestibular hair cells isolated from guinea pig labyrinth. *Hear Res*. (1989) 40:255–60. doi: 10.1016/0378-5955(89)90166-4
68. Masetto S, Russo G, Taglietti V, Prigioni I. [K+ and Ca++ currents in hair cells isolated from the semicircular canals of the frog]. *Boll Soc Ital Biol Sper*. (1991) 67:493–500.
69. Rennie KJ, Ashmore JF. Ionic currents in isolated vestibular hair cells from the guinea-pig crista ampullaris. *Hear Res*. (1991) 51:279–92. doi: 10.1016/0378-5955(91)90044-A
70. Prigioni I, Masetto S, Russo G, Taglietti V. Calcium currents in solitary hair cells isolated from frog crista ampullaris. *J Vestib Res*. (1992) 2:31–9. doi: 10.3233/VES-1992-2103
71. Griguer C, Kros CJ, Sans A, Lehouelleur J. Potassium currents in type II vestibular hair cells isolated from the guinea-pig's crista ampullaris [published erratum appears in Pflugers Arch 1994 May;427:193]. *Pflugers Archiv Eur J Physiol*. (1993) 425:344–52. doi: 10.1007/BF00374185
72. Griguer C, Sans A, Lehouelleur J. Non-typical K(+)-current in cesium-loaded guinea pig type I vestibular hair cell. *Pflugers Archiv Eur J Physiol*. (1993) 422:407–9. doi: 10.1007/BF00374300
73. Griguer C, Sans A, Valmier J, Lehouelleur J. Inward potassium rectifier current in type I vestibular hair cells isolated from guinea pig. *Neurosci Lett*. (1993) 149:51–5. doi: 10.1016/0304-3940(93)90345-L
74. Lapeyre PN, Kolston PJ, Ashmore JF. GABAB-mediated modulation of ionic conductances in type I hair cells isolated from guinea-pig semicircular

canals. *Brain Res*. (1993) 609:269–76. doi: 10.1016/0006-8993(93)90882-N
75. Rennie KJ, Ashmore JF. Effects of extracellular ATP on hair cells isolated from the guinea-pig semicircular canals. *Neurosci Lett*. (1993) 160:185–9. doi: 10.1016/0304-3940(93)90409-E
76. Rennie KJ, Correia MJ. Potassium currents in mammalian and avian isolated type I semicircular canal hair cells. *J Neurophysiol*. (1994) 71:317–29. doi: 10.1152/jn.1994.71.1.317
77. Ricci AJ, Cochran SL, Rennie KJ, Correia MJ. Vestibular type I and type II hair cells. 2: morphometric comparisons of dissociated pigeon hair cells. *J Vestib Res*. (1997) 7:407–20. doi: 10.3233/VES-1997-7504
78. Ricci AJ, Rennie KJ, Cochran SL, Kevetter GA, Correia MJ. Vestibular type I and type II hair cells. 1: morphometric identification in the pigeon and gerbil. *J Vestib Res*. (1997) 7:393–406. doi: 10.3233/VES-1997-7503
79. Eatock RA, Rusch A, Lysakowski A, Saeki M. Hair cells in mammalian utricles. *Otolaryngol Head Neck Surg*. (1998) 119:172–81. doi: 10.1016/S0194-5998(98)70052-X
80. Marcotti W, Russo G, Prigioni I. Inactivating and non-activating delayed rectifier K+ currents in hair cells of frog crista ampullaris. *Hear Res*. (1999) 135:113–23. doi: 10.1016/S0378-5955(99)00097-0
81. Martini M, Rossi ML, Rubbini G, Rispoli G. Calcium currents in hair cells isolated from semicircular canals of the frog. *Biophys J*. (2000) 78:1240–54. doi: 10.1016/S0006-3495(00)76681-1
82. Rennie KJ, Weng T, Correia MJ. Effects of KCNQ channel blockers on K(+) currents in vestibular hair cells. *Am J Physiol Cell Physiol*. (2001) 280:C473–80. doi: 10.1152/ajpcell.2001.280.3.C473
83. Li GQ, Meredith FL, Rennie KJ. Development of K(+) and Na(+) conductances in rodent postnatal semicircular canal type I hair cells. *Am J Physiol Regul Integr Comp Physiol*. (2010) 298:R351–8. doi: 10.1152/ajpregu.00460.2009
84. Meredith FL, Benke TA, Rennie KJ. Hyperpolarization-activated current. (I(h)) in vestibular calyx terminals: characterization and role in shaping postsynaptic events. *J Assoc Res Otolaryngol*. (2012) 13:745–58. doi: 10.1007/s10162-012-0342-3
85. Mann SE, Johnson M, Meredith FL, Rennie KJ. Inhibition of K+ currents in type I vestibular hair cells by gentamicin and neomycin. *Audiol Neurootol*. (2013) 18:317–26. doi: 10.1159/000354056
86. Lewis RS, Hudspeth AJ. Voltage- and ion-dependent conductances in solitary vertebrate hair cells. *Nature*. (1983) 304:538–41. doi: 10.1038/304538a0
87. Lewis RS, Hudspeth AJ. Frequency tuning and ionic conductances in hair cells of the bullfrog's sacculus. In: Klinke R, Hartmann R, editors. *Hearing-Physiological Bases and Psychophysics*. Berlin: Springer-Verlag (1983). p. 17–24. doi: 10.1007/978-3-642-69257-4_3
88. Hudspeth AJ, Lewis RS. A model for electrical resonance and frequency tuning in saccular hair cells of the bull-frog, *Rana catesbeiana*. *J Physiol*. (1988) 400:275–97. doi: 10.1113/jphysiol.1988.sp017120
89. Hudspeth AJ, Lewis RS. Kinetic analysis of voltage- and ion-dependent conductances in saccular hair cells of the bull-frog, Rana catesbeiana. *J Physiol*. (1988) 400:237–74. doi: 10.1113/jphysiol.1988.sp017119
90. Art JJ, Fettiplace R. Variation of membrane properties in hair cells isolated from the turtle cochlea. *J Physiol*. (1987) 385:207–42. doi: 10.1113/jphysiol.1987.sp016492
91. Art JJ, Crawford AC, Fettiplace R. Electrical resonance and membrane currents in turtle cochlear hair cells. *Hear Res*. (1986) 22:31–6. doi: 10.1016/0378-5955(86)90073-0
92. Smotherman MS, Narins PM. The electrical properties of auditory hair cells in the frog amphibian papilla. *J Neurosci*. (1999) 19:5275–92. doi: 10.1523/JNEUROSCI.19-13-05275.1999
93. Meredith FL, Rennie KJ. Channeling your inner ear potassium: K(+) channels in vestibular hair cells. *Hear Res*. (2016). doi: 10.1016/j.heares.2016.01.015
94. Chen W-Y. *The properties and functions of a low-voltage activated K(+) current in type I hair cells of rat semicircular canal organs* (Dissertation). Rochester, NY: University of Rochester (1995).
95. Frankenhaeuser B, Hodgkin AL. The after-effects of impulses in the giant nerve fibres of Loligo. *J Physiol*. (1956) 131:341–76. doi: 10.1113/jphysiol.1956.sp005467
96. Goldberg JM. Transmission between the type I hair cell and its calyx ending. *Ann N Y Acad Sci N Direct Vestib Res*. (1996) 781:474–88. doi: 10.1111/j.1749-6632.1996.tb15721.x
97. Goldberg JM. Theoretical analysis of intercellular communication between the vestibular type I hair cell and its calyx ending. *J Neurophysiol*. (1996) 76:1942–57. doi: 10.1152/jn.1996.76.3.1942
98. Arvanitaki A. Effects evoked in an axon by the activity of a contiguous one. *J Neurophysiol*. (1942) 5:89–108. doi: 10.1152/jn.1942.5.2.89
99. Katz B, Schmitt OH. Electric interaction between two adjacent nerve fibres. *J Physiol*. (1940) 97:471–88. doi: 10.1113/jphysiol.1940.sp003823
100. Kramer RH, Davenport CM. Lateral inhibition in the vertebrate retina: the case of the missing neurotransmitter. *PLoS Biol*. (2015) 13:e1002322. doi: 10.1371/journal.pbio.1002322
101. Holt JC, Chatlani S, Lysakowski A, Goldberg JM. Quantal and nonquantal transmission in calyx-bearing fibers of the turtle posterior crista. *J Neurophysiol*. (2007) 98:1083–101. doi: 10.1152/jn.00332.2007
102. Contini D. *Intercellular K+ accumulation drives Type I hair cells into the activation range of voltage-gated Ca channels* (Dissertation). Pavia, Italy: University of Pavia (2011).
103. Contini D, Zampini V, Tavazzani E, Magistretti J, Russo G, Prigioni I, et al. Intercellular K(+) accumulation depolarizes Type I vestibular hair cells and their associated afferent nerve calyx. *Neuroscience*. (2012) 227:232–46. doi: 10.1016/j.neuroscience.2012.09.051
104. Lim R, Kindig AE, Donne SW, Callister RJ, Brichta AM. Potassium accumulation between type I hair cells and calyx terminals in mouse crista. *Exp Brain Res*. (2011) 210:607–21. doi: 10.1007/s00221-011-2592-4
105. Eatock RA, Songer JE. Vestibular hair cells and afferents: two channels for head motion signals. *Annu Rev Neurosci*. (2011) 34:501–34. doi: 10.1146/annurev-neuro-061010-113710
106. Songer JE, Eatock RA. Tuning and timing in mammalian type I hair cells and calyceal synapses. *J Neurosci*. (2013) 33:3706–24. doi: 10.1523/JNEUROSCI.4067-12.2013
107. Ireland J. *The Udana & The Itivuttaka: Inspired Utterances of the Buddha & The Buddha's Sayings*. Kandy: BPS Pariyatti Editions (2020).
108. Ramachandran S, Rodgriguez S, Potcoava M, Alford S. Single calcium channel nanodomains drive presynaptic calcium entry at lamprey reticulospinal presynaptic terminals. *J Neurosci*. (2022) 42:2385–403. doi: 10.1523/JNEUROSCI.2207-21.2022
109. Art JJ, Wu YC, Fettiplace R. The calcium-activated potassium channels of turtle hair cells. *J Gen Physiol*. (1995) 105:49–72. doi: 10.1085/jgp.105.1.49
110. Govindaraju AC, Quraishi IH, Lysakowski A, Eatock RA, Raphael RM. A Biophysical model of nonquantal transmission at the vestibular hair cell-calyx synapse: K(LV) currents modulate fast electrical and slow K(+) potentials in the synaptic cleft. *bioRxiv*. (2021):2021.11.18.469197. doi: 10.1101/2021.11.18.469197
111. Eatock RA. Specializations for fast signaling in the amniote vestibular inner ear. *Integr Comp Biol*. (2018) 58:341–50. doi: 10.1093/icb/icy069
112. McCue MP, Guinan JJ, Jr. Sound-evoked activity in primary afferent neurons of a mammalian vestibular system. *Am J Otol*. (1997) 18:355–60.
113. McCue MP, Guinan JJ, Jr. Spontaneous activity and frequency selectivity of acoustically responsive vestibular afferents in the cat. *J Neurophysiol*. (1995) 74:1563–72. doi: 10.1152/jn.1995.74.4.1563
114. McCue MP, Guinan JJ, Jr. Influence of efferent stimulation on acoustically responsive vestibular afferents in the cat. *J Neurosci*. (1994) 14:6071–83. doi: 10.1523/JNEUROSCI.14-10-06071.1994
115. Curthoys IS, Vulovic V. Vestibular primary afferent responses to sound and vibration in the guinea pig. *Exp Brain Res*. (2011) 210:347–52. doi: 10.1007/s00221-010-2499-5
116. Curthoys IS, Vulovic V, Sokolic L, Pogson J, Burgess AM. Irregular primary otolith afferents from the guinea pig utricular and saccular maculae respond to both bone conducted vibration and to air conducted sound. *Brain Res Bull*. (2012) 89:16–21. doi: 10.1016/j.brainresbull.2012.07.007
117. Curthoys IS, Vulovic V, Burgess AM, Sokolic L, Goonetilleke SC. The response of guinea pig primary utricular and saccular irregular neurons to

bone-conducted vibration (BCV) and air-conducted sound (ACS). *Hear Res*. (2016) 331:131–43. doi: 10.1016/j.heares.2015.10.019
118. Highstein SM, Mann MA, Holstein GR, Rabbitt RD. The quantal component of synaptic transmission from sensory hair cells to the vestibular calyx. *J Neurophysiol*. (2015) 113:3827–35. doi: 10.1152/jn.00055.2015
119. Sadeghi SG, Pyott SJ, Yu Z, Glowatzki E. Glutamatergic signaling at the vestibular hair cell calyx synapse. *J Neurosci*. (2014) 34:14536–50. doi: 10.1523/JNEUROSCI.0369-13.2014
120. Lysakowski A, Minor LB, Fernandez C, Goldberg JM. Physiological identification of morphologically distinct afferent classes innervating the cristae ampullares of the squirrel monkey. *J Neurophysiol*. (1995) 73:1270–81.
121. Kirkegaard M, Jorgensen JM. The inner ear macular sensory epithelia of the Daubenton's bat. *J Comp Neurol*. (2001) 438:433–44.
122. Jorgensen JM. Number and distribution of hair cells in the utricular macula of some avian species. *J Morphol*. (1989) 201:187–204. doi: 10.1002/jmor.1052010208
123. Jorgensen JM, Christensen JT. The inner ear of the common rhea (Rhea americana L.). *Brain Behav Evol*. (1989) 34:273–80. doi: 10.1159/000116512

Conflict of Interest: The authors declare that the research was conducted in the absence of any commercial or financial relationships that could be construed as a potential conflict of interest.

Publisher's Note: All claims expressed in this article are solely those of the authors and do not necessarily represent those of their affiliated organizations, or those of the publisher, the editors and the reviewers. Any product that may be evaluated in this article, or claim that may be made by its manufacturer, is not guaranteed or endorsed by the publisher.

Copyright © 2022 Contini, Holstein and Art. This is an open-access article distributed under the terms of the Creative Commons Attribution License (CC BY). The use, distribution or reproduction in other forums is permitted, provided the original author(s) and the copyright owner(s) are credited and that the original publication in this journal is cited, in accordance with accepted academic practice. No use, distribution or reproduction is permitted which does not comply with these terms.

frontiers | Frontiers in Neurology

ORIGINAL RESEARCH
published: 12 July 2022
doi: 10.3389/fneur.2022.897293

Low Gain Values of the Vestibulo-Ocular Reflex Can Optimize Retinal Image Slip

Stefan Glasauer[1,2*†] *and Hans Straka*[3†]

[1] Computational Neuroscience, Institute of Medical Technology, Brandenburg University of Technology Cottbus-Senftenberg, Cottbus, Germany, [2] Brandenburg Faculty for Health Sciences, Brandenburg University of Technology Cottbus-Senftenberg, Cottbus, Germany, [3] Faculty of Biology, Ludwig-Maximilians-University Munich, Planegg, Germany

The angular vestibulo-ocular reflex (aVOR) stabilizes retinal images by counter-rotating the eyes during head rotations. Perfect compensatory movements would thus rotate the eyes exactly opposite to the head, that is, eyes vs. head would exhibit a unity gain. However, in many species, but also in elderly humans or patients with a history of vestibular damage, the aVOR is far from compensatory with gains that are in part considerably lower than unity. The reason for this apparent suboptimality is unknown. Here, we propose that low VOR gain values reflect an optimal adaptation to sensory and motor signal variability. According to this hypothesis, gaze stabilization mechanisms that aim at minimizing the overall retinal image slip must consider the effects of (1) sensory and motor noise and (2) dynamic constraints of peripheral and central nervous processing. We demonstrate that a computational model for optimizing retinal image slip in the presence of such constraints of signal processing in fact predicts gain values smaller than unity. We further show specifically for tadpoles of the clawed toad, *Xenopus laevis* with particularly low gain values that previously reported VOR gains quantitatively correspond to the observed variability of eye movements and thus constitute an optimal adaptation mechanism. We thus hypothesize that lower VOR gain values in elderly human subjects or recovered patients with a history of vestibular damage may be the sign of an optimization given higher noise levels rather than a direct consequence of the damage, such as an inability of executing fast compensatory eye movements.

Keywords: semicircular canal, eye movement, extraocular motoneuron, optokinetic reflex, *Xenopus laevis*, sensorimotor noise

OPEN ACCESS

Edited by:
David Samuel Zee, Johns Hopkins University, United States

Reviewed by:
Faisal Karmali, Harvard Medical School, United States
Dan M. Merfeld, The Ohio State University, United States

****Correspondence:***
Stefan Glasauer
stefan.glasauer@b-tu.de

†ORCID:
Stefan Glasauer
orcid.org/0000-0002-4313-6210
Hans Straka
orcid.org/0000-0003-2874-0441

Specialty section:
This article was submitted to Neuro-Otology, a section of the journal Frontiers in Neurology

Received: *15 March 2022*
Accepted: *21 June 2022*
Published: *12 July 2022*

Citation:
Glasauer S and Straka H (2022) Low Gain Values of the Vestibulo-Ocular Reflex Can Optimize Retinal Image Slip. Front. Neurol. 13:897293. doi: 10.3389/fneur.2022.897293

INTRODUCTION

The angular vestibulo-ocular reflex (aVOR) is driven by semicircular canal afferent signals and becomes effective by counter-rotating the eyes during head movements, thereby stabilizing retinal images. A perfect compensatory stabilization would thus require that the eye movements have the same velocity as the head movement, only in the opposite direction, that is, eye vs. head motion should exhibit a VOR gain of −1 (gain: ratio of eye angular velocity to head angular velocity) (**Figure 1A**). Indeed, a VOR gain of (in absolute value) unity or very close to it can usually be found in healthy young humans. However, healthy elderly subjects (1) or patients with a clinical history of vestibular damage or dysfunction (2) can exhibit lower gain values, even though an age-related decline of the VOR gain in humans is relatively moderate or may even be absent (3, 4). In many non-human

vertebrate species, the VOR is far from compensatory with gains clearly lower than unity. For example, in rabbits, rotation at a frequency of 0.76 Hz is accompanied by eye movement gains of 0.57 (5), and in wildtype mice, during sinusoidal head rotation at a frequency of 0.8 Hz the VOR gain in darkness ranges from ∼0.4 (6) to ∼0.8 (7) largely depending on the eye motion recording technique. However, the reason for this is not that sufficiently fast eye movements cannot be generated: the mouse VOR gain in light at 0.8 Hz is ∼0.8 (6) to >0.9 (7), demonstrating that adequate gaze stabilization is not limited by the properties of the motor system. To the best of our knowledge, the reason for the apparent suboptimality of the VOR gain is so far unclear.

To explain this conundrum, we hypothesize that gain values smaller than unity can in fact be the optimal solution for gaze stabilization for two reasons. First, neural processing subserving the VOR includes the high-pass dynamics of the semicircular canals (partly compensated by the velocity storage mechanism) and elements such as the neural integrator that both can introduce phase shifts, which in turn increase retinal image slip at some frequencies due to the delay between head and eye movements (for an example, see **Figures 1B–D**). Consequently, if retinal image slip, due to the phase lag, must be avoided, a small gain may be desirable. However, in rabbits, the phase shift of the VOR at rotations with a frequency of 0.76 Hz was only 2.5°, by far too small to correspond to a gain of 0.57 (5). Therefore, a second aspect must be considered: signal-dependent sensory and motor noise (8) induces retinal image slip, and increases for faster and larger movements, which could outweigh the benefit of an appropriate compensatory gain value (example **Figures 1D–F**). Again, a smaller VOR gain would be more beneficial, because it would reduce the motor noise and consequently also the retinal image slip. This suggests that small VOR gain values are not necessarily the consequence of a general incapacity of a particular species to exert sufficiently large or fast eye movements but rather a strategy to minimize retinal image slip.

Here we tested this hypothesis by investigating the aVOR in *Xenopus laevis* tadpoles, which show a particularly small VOR gain at mid-larval stages despite being able to make fast and large

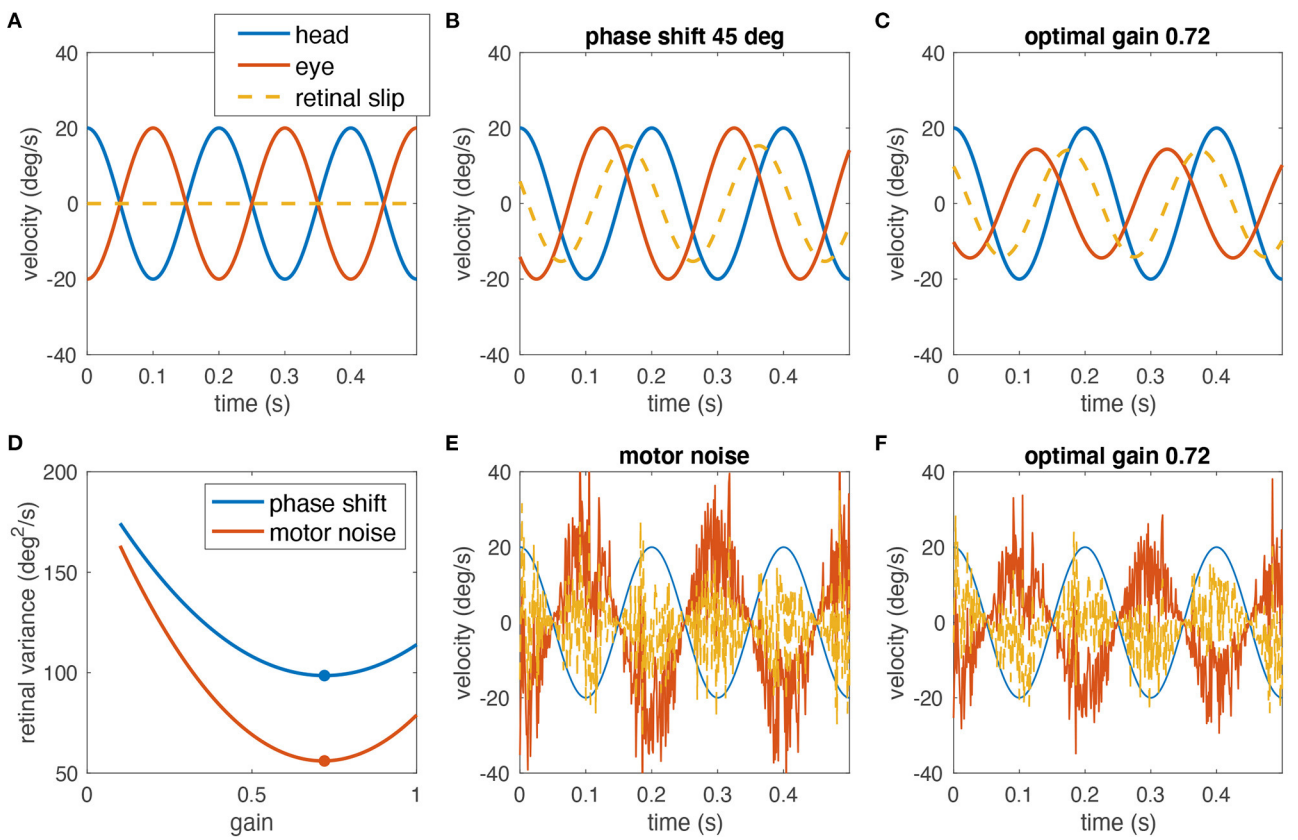

FIGURE 1 | Simulated example of why decreasing the gain of the VOR can help minimizing the retinal image slip. **(A)** A perfect compensatory VOR (gain = 1, no phase shift, no noise) results in zero retinal image slip (eye velocity in red, head velocity in blue, retinal image slip in dashed yellow). **(B)** In the presence of a 45° phase shift between eye and head rotation, a strong retinal image slip is present despite a gain of 1. **(C)** Reducing the VOR gain to 0.72 minimizes the overall retinal image slip. **(D)** Variance of the retinal slip plotted with respect to the VOR gain for phase shifts as in **(B,C)** (blue), and noise as in **(E,F)** (red). The plots have been obtained from numerical simulations. The optimal gain in both cases is ∼0.72 (red and blue dots). **(E)** Signal-dependent motor noise, proportional to eye velocity introduces a strong retinal image slip even if the gain = 1. **(F)** Reduction of the VOR gain also reduces the motor noise and thus the overall retinal image slip; retinal image slip plotted with respect to the VOR gain for this example is shown in **(D)** (red curve).

eye movements (9–11). While the phase of the aVOR oscillations can be computed from experimentally measured eye movements, neither sensory nor motor noise is directly accessible from eye movement data. If our hypothesis is correct, the variability of eye movements cannot be taken as proxy for sensorimotor noise, because the observed variability would be a consequence of optimization instead of directly reflecting internal noise from sensors or muscles. Therefore, a different approach was necessary to test the hypothesis. Accordingly, we modeled the dynamics of individual VOR responses to infer the internal noise level that corresponds to experimentally observed gain values assuming an optimal state. Using this model and applying sensory and motor noise corresponding to the gain, we were able to predict the variability of the eye position. Finally, these model predictions were then compared with the experimentally observed variability of the actual VOR-related eye movements in *Xenopus* tadpoles. If our hypothesis is true, predicted and observed variability should be quantitatively similar.

METHODS

Animal Experiments and Data Analysis

For this work we used eye movement data captured from six *Xenopus laevis* tadpoles, which had been published previously (11). The experimental protocol, stimulation and recording paradigms have been reported in full detail in the respective publication (11). All experiments were conducted *in vitro* on semi-intact preparations of *Xenopus laevis* tadpoles at developmental stages 53–54 (12) and complied with the "Principles of animal care," publication No. 86-23, revised 1985 of the National Institute of Health. All experiments were carried out in accordance with the ARRIVE guidelines and regulations. Permission for these experiments was granted by the ethics committee for animal experimentation of the legally responsible governmental institution (Regierung von Oberbayern) under the license code 55.2-1-54-2532.3-59-12. In addition, all experiments were performed in accordance with the relevant guidelines and regulations of the Ludwig-Maximilians-University Munich. Larvae of either sex were obtained from the in-house animal breeding facility at the Biocenter-Martinsried of the Ludwig-Maximilians-University Munich.

In brief, eye movements of *Xenopus* tadpoles were captured non-invasively during passive sinusoidal head rotations in darkness around an earth-vertical axis at 4 different stimulus frequencies (0.1, 0.2, 0.5, 1 Hz) with a peak velocity of ±30°/s as described previously (11). Two of the animals were not tested at 0.1 Hz. The recording duration varied between 35 s and 163 s depending on animal and stimulus frequency (mean number of stimulus cycles for each frequency: 0.1 Hz: 13.0; 0.2 Hz: 15.7; 0.5 Hz: 30.0; 1 Hz: 56.1). Eye movements were captured from above with a video camera (Grasshopper color; Point Gray Research) at a frame rate of 50 Hz (using FlyCap2) and analyzed offline using a custom-written video-processing algorithm (Matlab, The Mathworks) to compute eye position [for details, see (13)]. The raw eye position data was up-sampled to 1,000 Hz, slow drift was removed by piecewise cubic interpolation (Matlab function *makima*) and outliers (e.g., occasional fast phases) were discarded. The resulting eye position trace was averaged over all stimulus cycles and fitted to the averaged stimulus trace to determine gain and phase of the eye movements for each stimulus frequency.

In addition, the average variability of the eye position was computed from the averaged traces for comparison with model predictions (see also below). For m stimulus cycle repetitions with n time points in each cycle, first the standard deviation σ_i of the eye position at time point i over all m repetitions was computed, then the average $\overline{\sigma}$ over all n time points was used as variability measure:

$$\sigma_i = \frac{1}{m-1}\sqrt{\sum_{j=1}^{m}\left(p_{j,i}-\overline{p}_i\right)^2};\ \overline{\sigma} = \frac{1}{n}\sum_{i=1}^{n}\sigma_i$$

with $p_{j,i}$ being the eye position value at time point i and cycle j, and $\overline{p}_i$ the eye position at time point i averaged over all cycle repetitions. Thus, a possible dependency of variability across the cycle will not be visible in the variability measure $\overline{\sigma}$.

Mathematical Modeling

The model was constructed following classical aVOR models [see (14) for review] with semicircular canal signals as input (modeled as high-pass filter with a time constant of 5 s), the eye plant as final motor output [dominant time constant of 0.33 s and two non-dominant time constants, which can be interpreted as muscle activation, see (11)], and a brainstem processing algorithm by a leaky velocity-to-position integrator and a direct pathway that can be conceived as approximate inverse model of the eye plant. The integrator time constant and the two non-dominant eye plant time constants were fitted as free parameters by minimizing the phase difference between data and model. The overall model gain factor, an additional parameter, which has no influence on the phase of the response, was subsequently fitted to the average gain curve. The model fitting was performed for each animal separately.

The full VOR model, which describes the processing from angular head velocity ω to eye position p can be written in Laplace notation as

$$p(s) = -g \cdot s \cdot F_{SC}(s) \cdot F_{BS}(s) \cdot F_{EYE}(s) \cdot \omega(s) \quad (1)$$

with the free gain factor g, semicircular canal highpass $F_{SC}(s)$, brainstem processing $F_{BS}(s)$, and eye plant $F_{EYE}(s)$. The respective model components are:

$$F_{SC}(s) = \frac{\tau_{SC}s}{\tau_{SC}s+1} \quad (2)$$

$$F_{BS}(s) = \tau_E + \frac{\tau_I - \tau_E}{\tau_I s+1} \quad (3)$$

$$F_{EYE}(s) = \frac{1}{\tau_E s+1}\cdot\frac{1}{\tau_{M1}s+1}\cdot\frac{1}{\tau_{M2}s+1} \quad (4)$$

with the semicircular canal time constant τ_{SC} fixed to 5 s, leaky integrator time constant τ_I (free parameter), dominant eye plant time constant τ_E fixed to 0.33 s (11), and muscle activation time constants τ_{M1} and τ_{M2}.

Using the fitted model, the tadpole aVOR in response to sinusoidal head rotation at a single frequency (0.5 Hz) was simulated while being contaminated with sensory and motor noise. Both noise sources were modeled as signal-dependent noise (8), that is, the noise amplitude increased proportionally with increasing signal strength. For the sensor noise, the relevant signal was head velocity, for the motor noise it was the motor command signal, that is, the output of the extraocular motoneurons (output of brainstem processing, Equation 3). In the time domain, the noisy motor command $\boldsymbol{m}(\boldsymbol{t_i})$ at time step $\boldsymbol{t_i}$ can thus be written as

$$\boldsymbol{m}(\boldsymbol{t_i}) = \boldsymbol{b}(\boldsymbol{t_i}) + \varepsilon_{\boldsymbol{m}}(\boldsymbol{t_i}) \quad (5)$$

with $\boldsymbol{b}(\boldsymbol{t_i})$ being the output of the brainstem processing (Equation 3, sum of direct pathway and integrator) and $\varepsilon_{\boldsymbol{m}}(\boldsymbol{t_i})$ a normally distributed random number with zero mean and standard deviation $\boldsymbol{k_m} \cdot \boldsymbol{b}(\boldsymbol{t_i})$. The proportionality constant, or noise factor $\boldsymbol{k_m}$ thus describes the linear relationship between the standard deviation of motor noise and the motor command. Subsequently $\boldsymbol{m}(\boldsymbol{t_i})$ serves as input to Equation 4 to yield the eye position. Similarly, sensor noise was modeled as $\boldsymbol{\omega_n}(\boldsymbol{t_i}) = \boldsymbol{\omega}(\boldsymbol{t_i}) + \boldsymbol{\varepsilon_s}(\boldsymbol{t_i})$ with $\boldsymbol{\varepsilon_s}(\boldsymbol{t_i})$ as normally distributed random number with zero mean and standard deviation $\boldsymbol{k_s} \cdot \omega(\boldsymbol{t_i})$ and $\omega(\boldsymbol{t_i})$ as instantaneous head velocity at time step $\boldsymbol{t_i}$. The noisy head velocity $\omega_{\boldsymbol{n}}(\boldsymbol{t_i})$ serves as input to Equations 1 or 2.

From the simulated response, the variance of the retinal image slip was computed. The optimal gain factor that minimizes the variance of retinal image slip was determined by varying the gain factor. Sensory and motor noise were assumed to have equal noise factors, i.e., $\boldsymbol{k} = \boldsymbol{k_m} = \boldsymbol{k_s}$. The noise factor $\boldsymbol{k}$ was varied to find noise levels for which the optimal gain factor corresponds to the one that was found in the actual experiments.

As possible alternatives, we also simulated the model (1) with signal-independent (constant) additive sensor noise, (2) with only signal-dependent sensor noise, and (3) with only signal dependent motor noise. The fourth possibility, constant motor noise only, did not yield optimal gain values comparable to the ones found in tadpoles, because constant motor noise cannot be suppressed by small VOR gains.

The model was implemented in Matlab (The Mathworks) as Laplace transfer function using the Signal Processing Toolbox. For each frequency and amplitude, the amplitude and phase of the model response was derived by using the Matlab function *freqresp*. We first fitted the phase of the model response to the experimental data by using the Matlab function *fmincon* with lower and upper limits and the three time constants τ_{M1}, τ_{M2}, and τ_I as free parameters. Subsequently, the free overall gain factor $\boldsymbol{g}$ was fitted to the experimentally determined VOR gain values. For the model simulations, including sensor and motor noise, the model's differential equations were solved iteratively by using the Euler 1-step integration (time step 1 ms). Noise was simulated as normally distributed random variable with a mean of 0 at each time step (see Equation 5), with equal noise factors and uncorrelated sensor and motor noise for the main modeling approach (see Discussion).

For fitting the noise level (determined by the noise factor) that corresponds to an optimal gain factor minimizing retinal image slip, which is equal to the model gain factor, 1,000 s of aVOR eye movement recordings at a frequency of 0.5 Hz and $\pm 10^\circ$ head motion amplitude was simulated with different sensor and motor noise factors. The 0.5 Hz stimulus condition was chosen because it is located well within the frequency bandwidth of the VOR. Determining the noise for the 1 Hz, $\pm 5^\circ$ positional amplitude yielded quantitatively similar results (not shown). It should be noted that for finding the noise level, the dynamic model of each animal is used, rather than a specific response.

For comparison of the eye movement variability, the noise level and the optimal gain factor were used to simulate an aVOR at four experimental conditions. The duration of each simulation was chosen to approximately match the duration of the experimental data sets at each frequency (0.1 Hz: 150 s, 0.2 Hz: 80 s, 0.5 Hz: 50 s, 1 Hz: 50 s). The simulated head and eye position data were then fed through the same data analysis procedure as the experimental data to generate comparable average results.

Simulated data were compared to experimental data by using the coefficient of determination R^2 calculated as $R^2 = 1 - SS_{res}/SS_{tot}$ with $SS_{res} = \sum_i (y_i - f_i)^2$ being the residual sum of squares (data points y_i, model points f_i) and $SS_{tot} = \sum_i (y_i - \bar{y})^2$ the total sum of squares ($\bar{y}$ is the mean of the data points). The coefficient of determination can become negative, if the model used is inadequate, that is, worse than just taking the mean of the data, and thus produces a residual sum of squares larger than the total sum of squares.

Sequence of Analysis

The following lists the complete sequence of steps performed to test whether the experimentally observed variability of aVOR eye position traces is compatible with our hypothesis, which proposes that low aVOR gain values optimize the retinal image slip. The different steps are shown in **Figure 2** and explained below.

1) For each stimulus frequency, raw head and eye motion data (**Figure 2A**) are averaged over stimulus cycles to compute experimental gain and phase values (blue circles in **Figures 2B1,2**) for a given animal.
2) The computational model (see section Mathematical Modeling) is fit to the frequency response of each animal to extract individual model parameters (fitted model response, yellow circles and red lines in **Figures 2B1,2**). One of the model parameters is the aVOR gain factor for this animal.
3) The computational model is used to simulate responses at 0.5 Hz, $\pm 10^\circ$ amplitude with different noise factors, to calculate retinal image slip, and to find the noise level that requires an optimal gain factor corresponding to the experimentally observed VOR gain value (**Figure 2C**).
4) The predicted variability of eye position for the model simulation at the emerging noise level (**Figure 2D1**) is compared with the corresponding variability of the experimental data (**Figure 2D2**).

Note that the variability of the experimental data is an independent variable that has not been used in the entire process

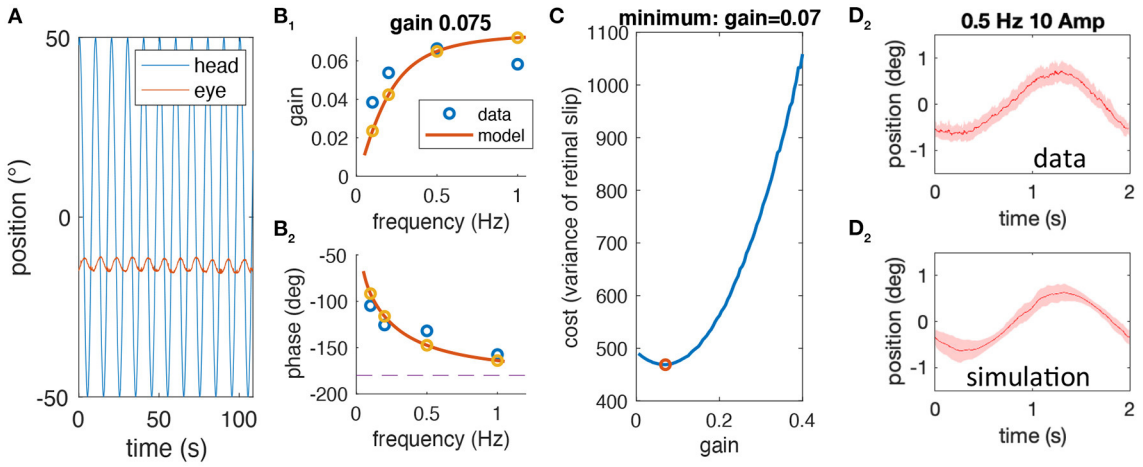

FIGURE 2 | Sequential steps of the methodological approach. **(A)** Example of raw head (blue) and eye (red) motion data obtained from one animal at a stimulus frequency of 0.1 Hz. **(B)** gain **(B_1)** and phase values **(B_2)** derived from raw data (blue) for a single animal along with the model simulation of the best fitting model; the gain value for this animal is 0.075. **(C)** Simulated cost function (retinal image slip variance) plotted with respect to the gain factor using the model derived in **(B)** for different noise factors; here, the simulation is shown for the optimal gain factor that matches the animal's actual gain factor. **(D)** Averaged eye position response during rotation at 0.5 Hz for the data **(D_1)** and the simulation **(D_2)**; note that the average eye position trace of data and simulation (mean, red line) is similar due to the prior model fitting, but that the variability, which is also similar (shaded red) is a prediction based on the noise level and gain factor.

until the comparison in step 4. Thus, if our hypothesis is correct, i.e., that low aVOR gain values optimize retinal image slip, then the variability, predicted by the model, and the experimental variability should be quantitatively similar.

RESULTS

Frequency Response

On average, experimentally observed gain values for all frequencies were rather low (<0.15) although with considerable differences between animals (**Figure 3A**). Based on the phase relation, responses were compensatory (−180°) on average only for rotations at 1 Hz but also differed strongly between animals (**Figure 3B**). As indicated above, a perfect aVOR response at a stimulus frequency of 1 Hz would require a phase shift of −180° but also a gain of 1. Experimentally, at frequencies of 0.5 and 1 Hz, we indeed found an optimal phase shift for some animals, but at the same time a gain far below unity. Thus, the low gain value is unlikely to derive from a compensation of an inappropriate phase shift, but must have other reasons, such as motor or sensory noise.

Modeling of Stimulus Frequency-Dependent Responses

The computational model was fitted to the responses obtained at different frequencies to extract an individual model for each animal. As expected from the individually different response dynamics (**Figure 3**), the model parameters also reflected these differences and variations between animals. The overall coefficient of determination (R^2, or variance explained by the model) between experimental and fitted phase values was 0.82, confirming a good model fit. The mean parameter values were for the integrator time constant 1.50 ± 1.73 s, the two muscle activation time constants 22 ± 17 and 21 ± 18 ms, and the model gain factor 0.14 ± 0.09.

Determination of the Noise Level

Using the individual model derived above, aVOR responses to a stimulus frequency of 0.5 Hz and ±10° stimulus amplitude including sensory and motor noise were numerically simulated. For a given noise factor, a cost function for different gain values was computed by determining the variance of retinal image slip over one stimulus cycle. The optimal gain for the given noise factor was determined as the minimum of the cost function (yellow dots in **Figure 4A**). This computation was repeated for different noise factors to find the optimal gain that corresponds to the experimentally encountered aVOR gain at that particular frequency (white dashed lines in **Figure 4A**; red dot in **Figure 4B**). The same was performed for the alternative noise models.

Comparison of Measured and Predicted Eye Movement Variability

Using the models obtained from individual animals and the noise factor determined above, all stimulus conditions were simulated (see Methods) and the simulated data (see **Figure 4C**) were analyzed using the same processing methods as applied to the real data (see **Figure 4D**). For the resulting average, simulated and real aVOR-related eye movements for each animal and frequency (see **Figure 5** for an example), the eye movement variability was determined as average standard deviation of the eye position over one stimulus cycle (**Figure 5**, shaded regions). Importantly, the variability of the data has not been employed so far in the analysis or modeling process and thus represents an independent variable. The simulated variability derived from a prediction of the model under the assumption that the aVOR gain factor that has been

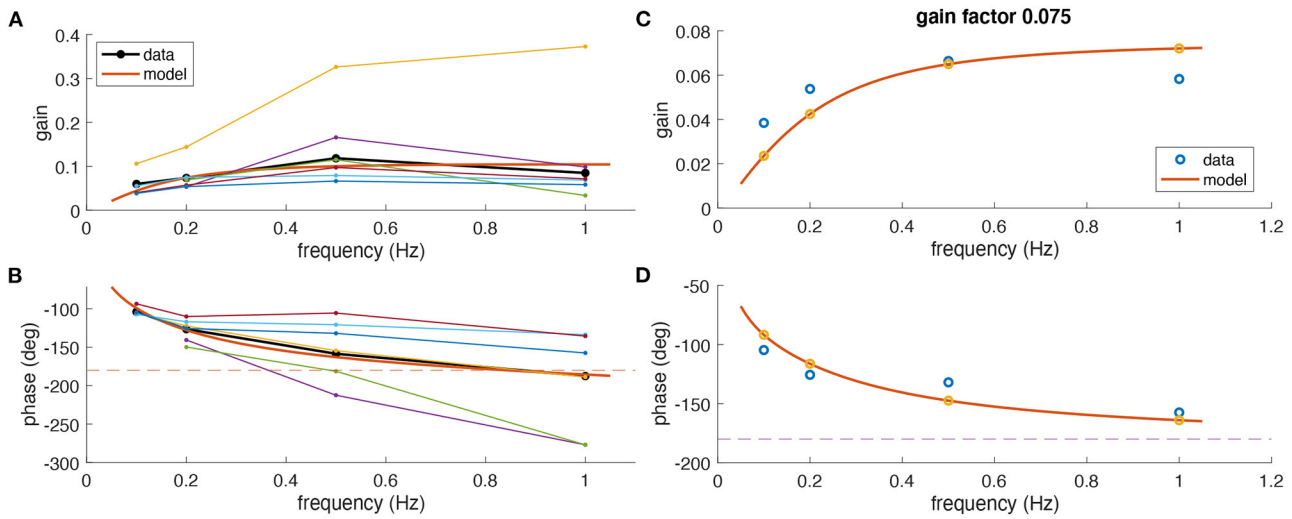

FIGURE 3 | Comparison of experimental and modeling data. **(A,B)** Experimental gain **(A)** and phase values **(B)** for eye movements of *Xenopus* tadpoles ($n = 6$) (colored small dots) along with average gain and phase values (large black dots); the red curve depicts simulated gain and phase values obtained from the computational model (red line) of the tadpole aVOR that have been fitted to the average results (black); note that an eye movement with a phase shift of −180° [dashed line in **(B)**] and a gain of 1 would perfectly compensate for the head rotation at all frequencies. **(C,D)** Example experimental data (blue circles) obtained from one animal (same as in **Figure 2**) and modeling results (red curve, yellow circles), with gain and phase values plotted in **(C,D)**, respectively.

determined from the data is optimized for the sensorimotor noise of an individual animal.

Despite considerable inter-individual differences in aVOR gain factors (**Figure 6A**), the calculated variability, predicted by the model, corresponds to the experimentally determined variability (see **Figure 6B**, coefficient of determination $R^2 = 0.46$, $n = 6$). A Bayes factor test corresponding to a paired t-test (15), comparing simulated (0.63 ± 0.49, mean ± SD) and experimental (0.58 ± 0.39) variability results in BF = 2.46, which is slightly in favor of the hypothesis that simulated and experimental variability are statistically not different. Thus, the similarity between predicted and experimentally occurring variability supports our hypothesis that small gain values, such as those found in *Xenopus* tadpoles, are possibly due to an optimization that minimizes retinal image slip. The alternative models show lower coefficients of determination (signal-dependent motor noise only: $R^2 = 0.104$) or negative values (constant sensor noise only: $R^2 = -4.71$; signal-dependent sensor noise only: $R^2 = -8.25$), suggesting that these models are unable to adequately explain the data. However, also for those models, the resulting simulated eye movement variability was still in the same range as found experimentally.

However, when plotting the experimental aVOR gain factors with respect to the variability found in the actual data, smaller gain values are found to be related to smaller eye position variability (**Figure 6C**). This finding seems at a first glance to contradict our hypothesis, because intuitively one would expect that in the optimized condition a larger aVOR gain can only be possible if the eye movement variability becomes smaller. This intuition, however, is erroneous for the rather low VOR gain values of tadpoles. This can be easily demonstrated by simulating a sinusoidal aVOR with a standard set of model parameters and varying noise levels. Accordingly, model simulations predict that, for the small aVOR gain regime (gain values <0.5), eye position variability will increase with increasing gain (**Figure 7A**). For higher gain values (>0.5), the variability decreases again (**Figure 7A**). The reason for this particular outcome can be best understood when considering the extremes: if there is no noise, eye position variability will be zero, and the best possible aVOR gain (disregarding phase shifts) will be unity. This corresponds to the lower right corner of **Figure 7A**. If there is an extremely high noise level, the best option is to set the aVOR gain to zero such that the noise cannot control the eye movements. In this case, eye position variability will also be zero (with signal-dependent motor noise), because the eyes do not move. This situation corresponds to the lower left corner of **Figure 7A**. Between these two extremes, eye position variability will necessarily be larger than zero and, at some point, reach a maximum (close to a gain of 0.5). Retinal slip will be smallest for zero noise and unity gain, and highest for zero eye movement. Consequently, eye position variability and standard deviation of retinal image slip also show a non-linear relationship (**Figure 7B**), while optimal aVOR gain values, as expected, decrease with increasing sensorimotor noise (**Figure 7C**).

DISCUSSION

Our model simulations demonstrated that for minimizing the retinal image slip for successful gaze stabilization, both, the internal dynamics of the sensorimotor processing and the sensorimotor noise represent important parameters. The optimal aVOR gain factor that minimizes retinal image slip should be lower than unity for dynamics involving delays or phase shifts and for systems involving sensorimotor noise. To illustrate these

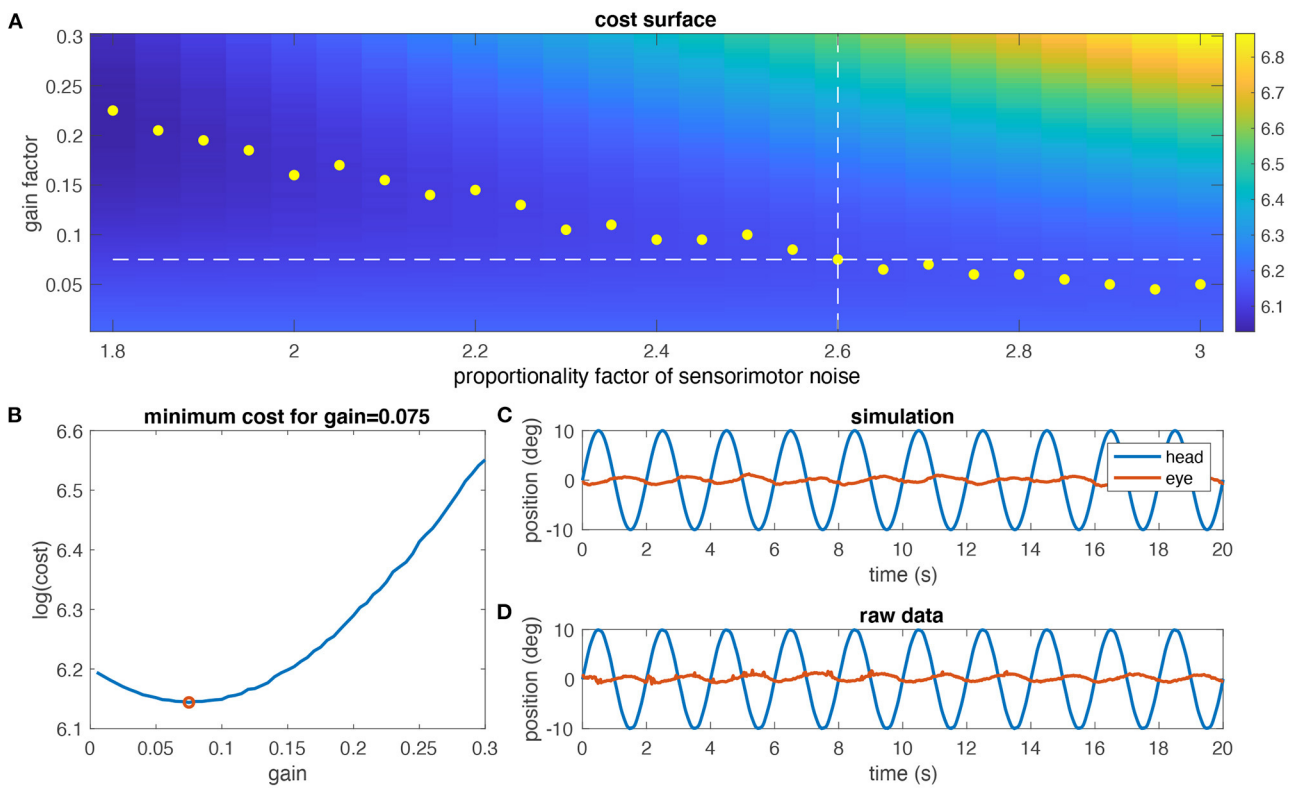

FIGURE 4 | Determination of the noise level. **(A)** Simulated cost surface [as log (cost)] for one animal (same as in **Figures 3C,D**) and for eye movements at a stimulus frequency of 0.5 Hz and ±10° head motion amplitude plotted as function of the noise factor of sensorimotor noise and model gain factor; the cost of the aVOR has been quantified by calculating the variance of the retinal image slip; yellow dots indicate the minimum cost for each noise factor; the dashed horizontal line is the experimentally determined gain value, and the vertical dashed line the noise factor at which the optimal gain value is closest to the experimental gain value (2.6 in this case). **(B)** Section through the cost surface for a noise factor of 2.6; the optimal gain is 0.075, as shown in **(A)**. **(C)** Simulated eye movements (red) for the optimal gain value determined in **(A,B)**. **(D)** Raw eye movement recordings (red) for this animal for comparison.

theoretical considerations, a simple, linear dynamic model of the VOR with non-ideal parameters (small integrator time constant, uncompensated muscle activation) and signal-dependent noise at both the sensor and the motor level was simulated. The variance of retinal image slip across repeated trials was used as cost function to be minimized. To experimentally test our considerations, we analyzed measurements of the aVOR of *Xenopus* tadpoles, which showed particularly low aVOR gains. For these data, our hypothesis suggests that the low gains are associated with high internal sensorimotor noise. However, the level of internal sensorimotor noise cannot be simply inferred from eye movement measurements, because the experimentally measured variability is a consequence of the optimization, but does not directly reflect the internal noise from sensors or muscles. Therefore, we have chosen an approach to predict the variability of individual eye movements by using the aVOR model with parameters based on measured responses at different frequencies and by assuming that the individual aVOR gain minimizes retinal image slip according to internal dynamics and sensorimotor noise. The variability of the model simulations showed an excellent quantitative match with respect to the measured data, thus supporting our hypothesis.

Optimality in Vestibular Processing

The present study is only one in a row of recent attempts to support the idea that vestibular signal processing underlying gaze stabilization or perception is optimized to account for the influence of internal noise (2, 16, 17). Vestibular processing during spatial orientation has long been described as optimal estimation [e.g., (18)], and more recent models also propose such an optimality strategy for the central processing of vestibular signals that assist in gaze stabilization [e.g., (19)]. Optimization has also been suggested as means to explain apparent deficits: perceptual vestibular thresholds of human subjects who fully recovered from unilateral vestibular deficits show a characteristic bilateral increase of the motion thresholds, which has been explained as being due to optimal adaptation to increased noise levels (2). More recently, it has been demonstrated that age-related changes in the dynamics of the human aVOR, that is, of the time constant, can be explained by an optimal estimation process that aims at adapting to the sensory signal-to-noise characteristics, which degrades with age (16). However, while all these studies consider optimal estimation in the presence of sensory noise, none of them considers motor noise together with the importance of retinal image slip as determining cost function.

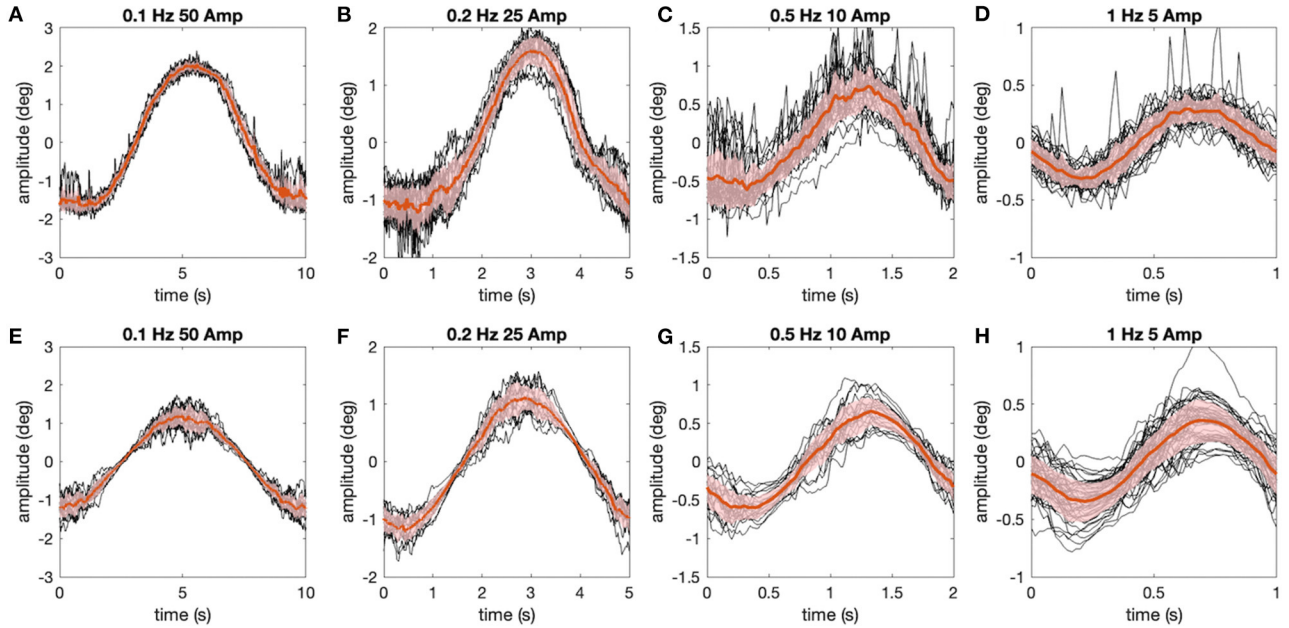

FIGURE 5 | Comparison of experimentally measured and simulated eye movements. **(A–H)** Eye movements (raw traces in black, red lines show average) shown for all stimulus motion cycles at different stimulus frequencies depicted for the representative animal in **Figure 4 (A–D)**, along with corresponding simulations **(E–H)** of the data using the aVOR model (with appropriately adapted parameters) and optimal gain values to minimize the retinal image slip caused by signal-dependent sensor and motor noise (see also **Figure 4**); shaded areas indicate one standard deviation of the mean response.

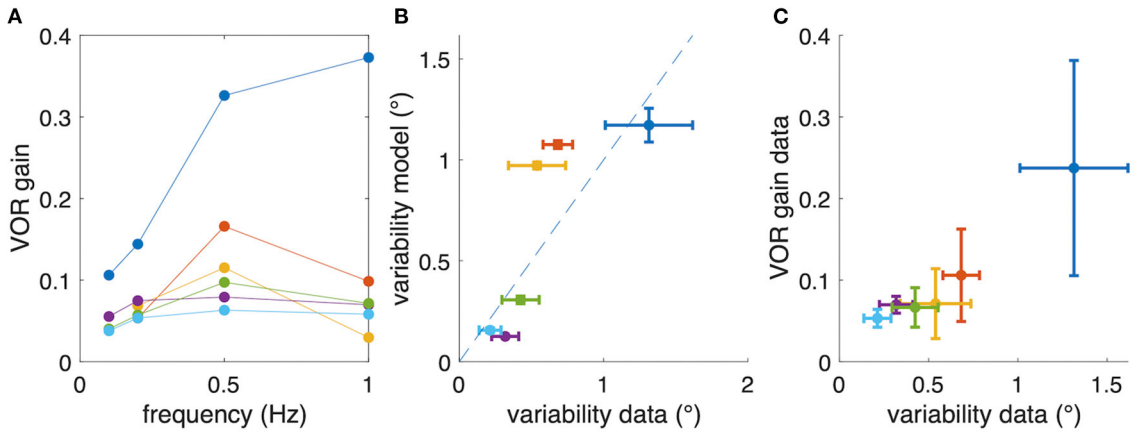

FIGURE 6 | Relation between aVOR gain and variability of eye movements. **(A)** For comparison, aVOR gain values (see **Figure 2**) are shown for each animal separately in different colors. **(B)** Variability of eye movements for each animal plotted with respect to the predicted variability, i.e., the variability of the model simulations. **(C)** Variability of eye movements for each animal plotted with respect to the aVOR gain. Each data point in **(B,C)** represents the mean across four stimulus frequencies; error bars denote the standard deviation; note that for the animals depicted in yellow and orange only data for three frequencies were available.

The Role of Dynamics Vs. Noise

While taking into account the internal dynamics of sensorimotor processing for our model, the deteriorating consequences of these dynamics (delays or phase shift) are not the main reason for the low gain values. A perfect compensatory aVOR, elicited at 1 Hz would require a unity gain and a phase shift of −180°. Experimentally, at 1 Hz an optimal phase shift on average (and very close to −180° for some individuals), but an average gain of 0.11, which is far below unity (**Figure 2**) was encountered. Thus, apart from semicircular canal size-related limitations in the sensitivity of the duct system in *Xenopus* tadpoles [(9, 10); see below], the generally low gain values in these animals cannot be simply explained by an inappropriate phase shift, but must have other reasons, such as motor or sensory noise as indicated above. Motor noise impacts motor commands at the level of motor unit recruitment (20) and would thus affect VOR responses

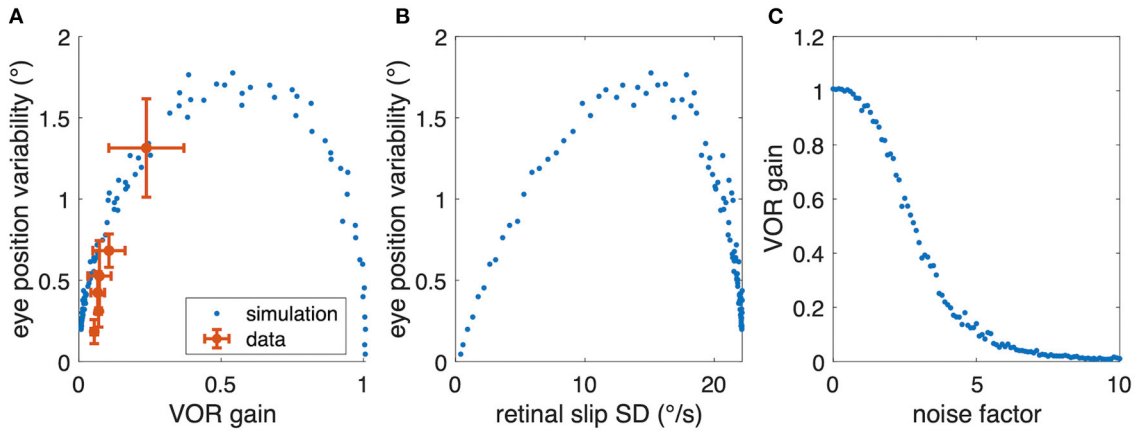

FIGURE 7 | Relation between aVOR gain and variability of eye movements. **(A)** Replot of data from **Figure 6C** (red) together with model simulations of the standard aVOR model with varying sensorimotor noise and optimized aVOR gain (all other model parameters kept constant); the model predicts that for low aVOR gain values, the eye position variability will increase with increasing gain values (<0.5), but decrease again for higher values (>0.5). **(B)** Variability of eye movements for each animal plotted with respect to the retinal image slip [same simulations as in **(B)**]. **(C)** Optimal aVOR gain values [model simulations as in **(A,B)**] decreases with the sensorimotor noise factor.

independent of the respective sensory origin (otolith organs or semicircular canals). However, as shown previously, VOR gain values of responses activated by semicircular canal plus otolith organ stimulation are considerably higher than those of responses produced by semicircular canal stimulation alone: in *Xenopus* tadpoles at stage 54, the horizontal VOR at 1 Hz has been reported to express a gain of 0.26, while for the torsional VOR (semicircular canal plus otolith organs) the gain was ∼0.6 (9, 10). Similar conclusions hold for combinations of vestibular and visual motion signals: in mice, the aVOR gain in light is twice as large as in darkness (6). Therefore, motor noise, even though it probably plays a considerable role, is likely insufficient to explain the low gain values of a horizontal, purely semicircular canal-driven aVOR. This thus requires reconsideration of the effect of sensory noise from the semicircular canals on aVOR responses and specifically on ocular motor responses related to retinal image slip.

Alternative Explanations for Low VOR Gains

An alternative reason for the low VOR gain observed in *Xenopus* tadpoles could be that the extraocular motor system in these animals might simply be unable to generate faster eye movements. However, this is not the case given the occasional expression of saccadic eye movements with velocities that are considerably higher than required for a perfect VOR (21). Yet another possibility to explain low gain values in *Xenopus* tadpoles is that semicircular canal-evoked responses saturate much earlier than expected and thus cannot transmit head velocities >30°/s. However, data presented previously show that this explanation is also unlikely [e.g., (9)], and the approximately sinusoidal shape of aVOR responses provides no evidence for a potential saturation of the VOR at the applied stimulus intensities (21), supported by direct measurements of extraocular motoneuronal spike discharge at increasing stimulus amplitudes (22). While unusually low in darkness, the aVOR of *Xenopus* tadpoles in light is supplemented by efficient, visuo-motor reflexes that naturally assist the maintenance of gaze stability (21). Even though the overall gain of the aVOR in light is only mildly enhanced, the phase of the aVOR in light matches much better an expected compensatory response (21). In fact, visuo-motor responses such as the optokinetic reflex are particularly prominent at low-frequencies, although the natural frequency of swimming in tadpoles is even higher than the imposed head motion frequency applied in the current study (23). While the swimming frequency gradually decreases with developmental age, the tadpole head oscillates approximately sinusoidally at about 5 Hz with an amplitude of 20° at stage 53–54 (23). The rather stereotyped motion dynamics and profile is exploited by the gaze stabilizing circuitry in *Xenopus* tadpoles by recruiting spinal locomotor efference copies to directly drive compensatory eye movements during swimming (10, 24). Therefore, an alternative explanation for low VOR gain values might be that gaze stabilization in *Xenopus* tadpoles becomes relevant only during high-frequency active swimming but might be more dispensable during passive motion at lower frequencies. However, the contribution of locomotor efference copies to gaze stabilization during active swimming likely provides a means to avoid excessive sensory noise introduced by vestibular sensory signals, which is fully compatible with the outcome of the modeling approach in the current study. Thus, to answer the question whether low gain values are indeed due to excessive sensory noise, it will be necessary to directly measure the variability of afferent vestibular signals during head rotation.

Limitations of the Current Study

The video capture of eye movements with a camera at 50 Hz likely introduces measurement noise that potentially contaminates the recordings and thus might critically influence the variability

of the eye position data determined in the final step of the analysis. However, camera-induced measurement noise is, in contrast to our assumptions for internal noise, independent of the signal (at least at the low stimulus frequencies used here) and thus can be considered as forming an additive noise to eye position signals. In contrast, sensorimotor noise is signal-dependent and acts on head velocity and subsequent neural activity. In addition, even if the measured variability would be affected by the measurement noise, it would overestimate rather than underestimate the variability. This might in fact explain why, for 4 out of 6 animals, the experimental variability was higher than predicted by the model (**Figure 6B**). It should be noted that instead of comparing the variability of the eye velocity or retinal image slip we have chosen to compare eye position variability, because this avoids the need to calculate the temporal derivative of eye position data, which would increase the effect of high-frequency measurement noise.

A further limitation of the current approach is that the relation of sensor to motor noise in the processing of aVOR signals is at present unknown. In the seminal work by Harris and Wolpert (8) on saccadic eye movements, and also in later work on combined goal-directed eye-head movements (25), the motor noise was responsible for the variability in final gaze position. For the present work, there is strong evidence from vertical VOR performance [(9), see above] that motor noise alone cannot be responsible for low gain values. Similarly, when gaze stabilization is driven by locomotor efference copies during active swimming (10, 24, 26), the gain is ∼0.6, demonstrating that higher VOR gain values are indeed possible, and that motor noise, which would affect all directional types of gaze stabilization components equally, cannot be the main reason for the observed low VOR gains. For human VOR responses it was recently reported that stimulus-dependent sensory noise is a likely explanation for the velocity-dependent variability of the VOR (16), matching the assumptions of the current study. However, for simplicity, in the present modeling approach equal amounts (in terms of noise factors) of sensor and motor noise were assumed, even though this assumption requires further exploration. Our finding that only sensor or only motor noise is unable to explain the data should be taken with caution until more data are available. It would be greatly beneficial to further investigate the dependency of variability on the eye position within the stimulus cycle, which can be clearly seen in the simulations (**Figures 5E,F**) and to a lesser extent also in the data (e.g., **Figure 5B**). One possibility for further experimentation would be to analyse the noise spectrum of eye movement responses, which, according to the model, differs for sensor noise (filtered by central processing and the eye plant) and motor noise (filtered only by the eye plant). Nonetheless, due to the presence and efficacy of the direct VOR pathway (27), these differences might only be subtle, and a direct measurement would be certainly more useful [see (28) for an exemplary study of vestibular afferents]. Therefore, future experiments would need to assess the level of sensor noise in vestibular nerve afferent responses vs. the level of motor noise, for example, when eye movements are driven by electrical stimulation at different levels of the processing (afferent semicircular canal nerve, vestibular nuclei, extraocular motor nuclei).

Importance for Human VOR

The hypothesis of the current study may apply not only to other vertebrate species with low VOR gain values, but might represent a general principle applicable to all mechanistic types of gaze stabilization. For example, VOR in light, i.e., with vision, usually improves the gain considerably, which under the present hypothesis is easily explainable if vestibular sensory noise plays a significant role: the additional optokinetic visual input might decrease the overall sensory noise, indicating that the corresponding optimal gain can be increased. As emphasized above, healthy elderly subjects (1) or subjects with a history of vestibular damage (2) may show considerably lower VOR gain values [but see (3, 4) for preserved gains in elderly]. Again, this effect, observed in both groups of humans, could be explained by increased sensory noise; in addition, in elderly, increased motor noise might also play a role. Even for smooth pursuit eye movements the same considerations may apply: if retinal image slip is the most important cost, then lower pursuit gains, for example in elderly, may be related to higher sensorimotor noise. Hence, small VOR gain values in elderly and patients may be an optimal adaptation to the changed sensorimotor properties rather than derive from a sensory deficiency: without such adaptation, gaze stabilization would be worse. This would add to the growing evidence that observable changes in motor or sensory abilities in recovering patients or elderly subjects are better understood as a consequence of sensorimotor optimization strategies to partly compensate for the damage, rather than being a direct effect of the damage. However, a recent study (29) on VOR responses in control subjects and patients with unilateral vestibular damage found no relationship between VOR gain and VOR variability (measured as root-mean-square error of eye velocity relative to the mean response for the early part of head-impulse tests). This finding apparently contradicts our hypothesis for the human VOR. One possibility is that for the human VOR the present theory is not applicable, because in humans high gain might be more important in order to keep the fovea approximately on target instead of minimizing retinal image slip. It should be noted that keeping minimal foveal distance also predicts that with high signal-dependent sensorimotor noise levels, the optimal VOR gain should be lower than unity. Another possibility, supported by preliminary model simulations (not shown) and compatible with the present hypothesis, is that additional variability, introduced by the trial-to-trial variability of head velocity in head-impulse tests, has obscured the expected gain-variability relationship. Yet another recent study in humans (30) shows that changes in dynamics, and possibly also of the gain of the aVOR in patients with unilateral damage are a consequence of optimal adaptation to elevated sensory noise levels relative to the available signal. Nonetheless, more experimental studies, specifically in humans, are necessary to resolve the question whether low gain values for gaze stabilization may be an optimal adaptation to increased sensorimotor noise.

DATA AVAILABILITY STATEMENT

The raw data supporting the conclusions of this article will be made available by the authors, without undue reservation.

ETHICS STATEMENT

The animal study was reviewed and approved by the Ethics Committee for animal experimentation of the Regierung von Oberbayern.

AUTHOR CONTRIBUTIONS

SG and HS conceived of the work, critically revised the work, and approved the final version. SG drafted the work, analyzed the data, and designed the model. All authors contributed to the article and approved the submitted version.

FUNDING

This work was supported by Deutsche Forschungsgemeinschaft (STR 478/3-1 and GL 342/2-1) and the Bernstein Center for Computational Neuroscience Munich (BT-1).

REFERENCES

1. Brzezny R, Glasauer S, Bayer O, Siebold S, Büttner U. Head impulses in three orthogonal planes of space: influence of age. *Ann NY Acad Sci.* (2003) 1004:473–7. doi: 10.1111/j.1749-6632.2003.tb00262.x
2. Cousins S, Kaski D, Cutfield N, Seemungal B, Golding JF, Gresty M, et al. Vestibular perception following acute unilateral vestibular lesions. *PLoS ONE.* (2013) 8:e61862. doi: 10.1371/journal.pone.0061862
3. Peterka R, Black F, Schoenhoff M. Age-related changes in human vestibuloocular reflexes: sinusoidal rotation and caloric tests. *J Vestib Res.* (1990) 1:49–59. doi: 10.3233/VES-1990-1106
4. McGarvie LA, MacDougall HG, Halmagyi GM, Burgess AM, Weber KP Curthoys IS. The video head impulse test (vHIT) of semicircular canal function – age-dependent normative values of VOR gain in healthy subjects. *Front Neurol.* (2015) 6:154. doi: 10.3389/fneur.2015.00154
5. Baarsma EA, Collewijn H. Vestibulo-ocular and optokinetic reactions to rotation and their interaction in the rabbit. *J Physiol.* (1974) 238:603–25. doi: 10.1113/jphysiol.1974.sp010546
6. van Alphen AM, Stahl JS, De Zeeuw CI. The dynamic characteristics of the mouse horizontal vestibulo-ocular and optokinetic response. *Brain Res.* (2001) 890:296–305. doi: 10.1016/S0006-8993(00)03180-2
7. Stahl JS. Using eye movements to assess brain function in mice. *Vision Res.* (2004) 44:3401–10. doi: 10.1016/j.visres.2004.09.011
8. Harris CM, Wolpert DM. Signal-dependent noise determines motor planning. *Nature.* (1998) 394:780–4. doi: 10.1038/29528
9. Lambert FM, Beck JC, Baker R, Straka H. Semicircular canal size determines the developmental onset of angular vestibuloocular reflexes in larval *Xenopus*. *J Neurosci.* (2008) 28:8086–95. doi: 10.1523/JNEUROSCI.1288-08.2008
10. Lambert FM, Bacqué-Cazenave J, Le Seach A, Arama J, Courtand G, Tagliabue M, et al. Stabilization of gaze during early *Xenopus* development by swimming-related utricular signals. *Curr Biol.* (2020) 30:1–8. doi: 10.1016/j.cub.2019.12.047
11. Dietrich H, Glasauer S, Straka H. Functional organization of vestibulo-ocular responses in abducens motoneurons. *J Neurosci.* (2017) 37:4032–45. doi: 10.1523/JNEUROSCI.2626-16.2017
12. Nieuwkoop PD, Faber J. *Normal Table of Xenopus laevis (Daudin): A Systematical and Chronological Survey of the Development From the Fertilized Egg Till the End of Metamorphosis*. New York, NY: Garland (1994).
13. Ramlochansingh C, Branoner F, Chagnaud BP, Straka H. Efficacy of tricaine methanesulfonate (MS-222) as an anesthetic agent for blocking sensory-motor responses in *Xenopus laevis* tadpoles. *PLoS ONE.* (2014) 9:e101606. doi: 10.1371/journal.pone.0101606
14. Glasauer S. Current models of the ocular motor system. *Dev Ophthalmol.* (2007) 40: 158–74. doi: 10.1159/000100485
15. Rouder JN, Speckman PL, Sun D, Morey RD, Iverson G. Bayesian t tests for accepting and rejecting the null hypothesis. *Psychon Bull Rev.* (2009) 16:225–37. doi: 10.3758/PBR.16.2.225
16. Karmali F, Whitman GT, Lewis RF. Bayesian optimal adaptation explains age-related human sensorimotor changes. *J Neurophysiol.* (2018) 119:509–20. doi: 10.1152/jn.00710.2017
17. Nouri S, Karmali F. Variability in the vestibulo-ocular reflex and vestibular perception. *Neuroscience.* (2018) 393:350–65. doi: 10.1016/j.neuroscience.2018.08.025
18. Glasauer S, Merfeld DM. Modeling three dimensional vestibular responses during complex motion stimulation. In: Fetter M. Haslwanter T, Misslich H, Tweed D, editors. *Three-Dimensional Kinematic Principles of Eye, Head, and Limb Movements in Health and Disease*. Amsterdam: Harwood Academic Publishers (1997). p. 387–98.
19. Laurens J, Angelaki DA. The functional significance of velocity storage and its dependence on gravity. *Exp Brain Res.* (2011) 210:407–22. doi: 10.1007/s00221-011-2568-4
20. Jones KE, Hamilton AFC, Wolpert DM. Sources of signal-dependent noise during isometric force production. *J Neurophysiol.* (2002) 88:1533–44. doi: 10.1152/jn.2002.88.3.1533
21. Soupiadou P, Gordy C, Forsthofer M, Sanchez-Gonzalez R, Straka H. Acute consequences of a unilateral VIIIth nerve transection on vestibulo-ocular and optokinetic reflexes in *Xenopus laevis* tadpoles. *J Neurol.* (2020) 267(Suppl. 1):S62–75. doi: 10.1007/s00415-020-10205-x
22. Gensberger KD, Kaufmann AK, Dietrich H, Branoner F, Banchi R, Chagnaud BP, et al. Galvanic vestibular stimulation: cellular substrates and response patterns of neurons in the vestibulo-ocular network. *J Neurosci.* (2016) 36:9097–110. doi: 10.1523/JNEUROSCI.4239-15.2016
23. Hänzi S, Straka H. Developmental changes in head movement kinematics during swimming in *Xenopus laevis* tadpoles. *J Exp Biol.* (2017) 220:227–36. doi: 10.1242/jeb.146449
24. Lambert FM, Combes D, Simmers J, Straka H. Gaze stabilization by efference copy signaling without sensory feedback during vertebrate locomotion. *Curr Biol.* (2012) 22:1649–58. doi: 10.1016/j.cub.2012.07.019
25. Saglam M, Lehnen N, Glasauer S. Optimal control of natural eye-head movements minimizes the impact of noise. *J Neurosci.* (2011) 31:16185–93. doi: 10.1523/JNEUROSCI.3721-11.2011
26. Bacqué-Cazenave J, Courtand G, Beraneck M, Lambert FM, Combes D. Temporal relationship of ocular and tail segmental movements underlying locomotor-induced gaze stabilization during undulatory swimming in larval *Xenopus*. *Front Neural Circuits.* (2018) 12:95. doi: 10.3389/fncir.2018.00095
27. Straka H, Dieringer N. Basic organization principles of the VOR: lessons from frogs. *Prog Neurobiol.* (2004) 73:259–309. doi: 10.1016/j.pneurobio.2004.05.003
28. Sadeghi SG, Chacron MJ, Taylor MC, Cullen KE. Neural variability, detection thresholds, and information transmission in the vestibular system. *J Neurosci.* (2007) 27:771–81. doi: 10.1523/JNEUROSCI.4690-06.2007
29. King S, Dahlem K, Karmali F, Stankovic KM, Welling DB, Lewis RF. Imbalance and dizziness caused by unilateral vestibular schwannomas correlate with vestibulo-ocular reflex precision and bias. *J Neurophysiol.* (2022) 127:596–606. doi: 10.1152/jn.00725.2020

30. Madhani A, Lewis RF, Karmali F. How peripheral vestibular damage affects velocity storage: a causative explanation. *JARO*. (2022). doi: 10.1007/s10162-022-00853-3. [Epub ahead of print].

Conflict of Interest: The authors declare that the research was conducted in the absence of any commercial or financial relationships that could be construed as a potential conflict of interest.

Publisher's Note: All claims expressed in this article are solely those of the authors and do not necessarily represent those of their affiliated organizations, or those of the publisher, the editors and the reviewers. Any product that may be evaluated in this article, or claim that may be made by its manufacturer, is not guaranteed or endorsed by the publisher.

Copyright © 2022 Glasauer and Straka. This is an open-access article distributed under the terms of the Creative Commons Attribution License (CC BY). The use, distribution or reproduction in other forums is permitted, provided the original author(s) and the copyright owner(s) are credited and that the original publication in this journal is cited, in accordance with accepted academic practice. No use, distribution or reproduction is permitted which does not comply with these terms.

frontiers | Frontiers in Neurology

ORIGINAL RESEARCH
published: 15 July 2022
doi: 10.3389/fneur.2022.850986

Self-Reported Measures Have a Stronger Association With Dizziness-Related Handicap Compared With Physical Tests in Persons With Persistent Dizziness

Lene Kristiansen[1,2], Liv H. Magnussen[1], Kjersti T. Wilhelmsen[1], Silje Maeland[3,4], Stein Helge G. Nordahl[2,5], Anders Hovland[6,7], Richard Clendaniel[8], Eleanor Boyle[9] and Birgit Juul-Kristensen[9]*

[1] Department of Health and Function, Faculty of Health and Social Sciences, Western Norway University of Applied Sciences, Bergen, Norway, [2] Norwegian National Advisory Unit on Vestibular Disorders, Department of Otorhinolaryngol and Head and Neck Surgery, Haukeland University Hospital, Bergen, Norway, [3] Department of Global Public Health and Primary Care, Faculty of Medicine, University of Bergen, Bergen, Norway, [4] Research Unit for General Practice in Bergen, The Norwegian Research Center, Bergen, Norway, [5] Department of Clinical Medicine, University of Bergen, Bergen, Norway, [6] Department of Clinical Psychology, University of Bergen, Bergen, Norway, [7] Solli District Psychiatric Centre, Bergen, Norway, [8] Physical Therapy Division, Department of Orthopaedics and Department of Head and Neck Surgery and Communication Sciences, Duke University School of Medicine, Durham, NC, United States, [9] Department of Sports Science and Clinical Biomechanics, University of Southern Denmark, Odense, Denmark

OPEN ACCESS

Edited by:
Joel Alan Goebel, Washington University in St. Louis, United States

Reviewed by:
Erin Gillikin Piker, James Madison University, United States
Hubertus Axer, Jena University Hospital, Germany

***Correspondence:**
Lene Kristiansen
lene.kristiansen@hvl.no

Specialty section:
This article was submitted to Neuro-Otology, a section of the journal Frontiers in Neurology

Received: *08 January 2022*
Accepted: *03 June 2022*
Published: *15 July 2022*

Citation:
Kristiansen L, Magnussen LH, Wilhelmsen KT, Maeland S, Nordahl SHG, Hovland A, Clendaniel R, Boyle E and Juul-Kristensen B (2022) Self-Reported Measures Have a Stronger Association With Dizziness-Related Handicap Compared With Physical Tests in Persons With Persistent Dizziness. Front. Neurol. 13:850986. doi: 10.3389/fneur.2022.850986

Background: Associations between dizziness-related handicap and a variety of self-reported measures have been reported. However, research regarding associations between dizziness-related handicap and aspects of functioning that includes both physical tests and self-reported measures is scarce.

Objective: The purpose of the study was to describe the variations in signs and symptoms in people with persistent dizziness using physical tests and self-reported outcomes across three severity levels of the Dizziness Handicap Inventory (DHI) and investigate their associations with the DHI.

Method: Participants with persistent dizziness ($n = 107$) were included in this cross-sectional study. The participants underwent (1) physical tests (gait tests, grip strength, body flexibility, and movement-induced dizziness) and completed questionnaires regarding (2) psychological measures (Mobility Inventory of Agoraphobia, Body Sensation Questionnaire, Agoraphobic Cognitions Questionnaire, and Hospital Depression and Anxiety Questionnaire), and (3) fatigue, dizziness severity, and quality of life (Chalders Fatigue Scale, Vertigo Symptom Scale-Short Form, and EQ visual analog scale), in addition to the DHI. Data were presented by descriptive statistics for three DHI severity levels (mild, moderate, and severe). A multiple linear backward regression analysis was conducted for each group of measures in relation to the DHI total score, with additional analyses adjusting for age and sex. Based on these results, significant associations were tested in a final regression model.

Results: With increasing severity levels of DHI, the participants demonstrated worse performance on most of the physical tests (preferred and fast gait velocity,

dizziness intensity after head movements), presented with worse scores on the self-reported measures (avoidance behavior, fear of bodily sensation, fear of fear itself, psychological distress, fatigue, dizziness severity, quality of life). After adjusting for age and sex, significant associations were found between total DHI and avoidance behavior, psychological distress, dizziness severity, and quality of life, but not with any of the physical tests, explaining almost 56% of the variance of the DHI total score.

Conclusion: There was a trend toward worse scores on physical tests and self-reported measurements with increasing DHI severity level. The DHI seems to be a valuable tool in relation to several self-reported outcomes; however, several signs and symptoms may not be detected by the DHI, and thus, a combination of outcomes should be utilized when examining patients with persistent dizziness.

Keywords: persistent dizziness, Dizziness Handicap Inventory, cross-sectional study, psychological characteristics, physical characteristics, regression analysis

INTRODUCTION

Dizziness is a common complaint (1, 2) with 16% reporting dizziness or balance problem in a recent Norwegian survey (3). It is a common feature in acute vestibular diseases where an abrupt start of symptoms, such as dizziness, nauseousness, reduced balance, and visual problems occurs (4). The symptoms usually subside within a couple of weeks; however, ∼30% of patients develop persistent symptoms (5, 6). When dizziness persists, it is important to also assess symptoms beyond those defined as vestibular (7). These signs and symptoms include reduced gait velocity (8), postural misalignment (9, 10), increased body sway (11, 12), pain (13), and rigid body movements (14), in addition to anxiety and depression (15–19), avoidance behavior (20), and reduced quality of life (QoL) (21). Fatigue has also been reported in patients with vestibular diagnoses (22). These symptoms may influence everyday life, but to our knowledge, a combination of physical tests and self-reported measures on the perception of dizziness-related handicap has not been investigated extensively.

A commonly used outcome measure related to dizziness is the Dizziness Handicap Inventory (DHI) (23), which was developed to evaluate perceived dizziness-related handicap (24). There seems to be less relationship between diagnostic vestibular function tests and DHI (25, 26), suggesting that dizziness-related handicap may be more associated with the perception of signs and symptoms that have a direct impact on everyday life. Previous studies have found relationships between DHI and functional balance tests involving locomotion (27), slower walking velocity and reduced step and stride lengths (28), and an increasing number of self-reported dizziness triggers (e.g., loud sounds and stress) (29). Severe scores on the DHI have also been associated with poorer psychological outcomes such as anxiety, depression, avoidance behavior, fear of bodily sensations, illness perception, and cognitive responses (5, 30). However, there seems to be a lack of knowledge regarding the relationship between DHI and other outcomes, such as muscle strength, body flexibility, movement-induced dizziness, dizziness-severity, and health-related QoL.

Dizziness Handicap Inventory is measured on a continuous scale (0–100 points). Attempts have been made to establish severity levels of the DHI that links to functional abilities on several occasions (31), but less seems to have been published apart from one study categorizing the DHI into mild (0–30 points), moderate (31–60 points), and severe handicap (61–100 points) (32). Patients with a severe DHI level have shown larger functional impairment on balance confidence and number of falls, compared with patients presenting with mild DHI level scores (32), implying that patients in the severe DHI level may need more clinical attention.

Several studies have reported correlations between DHI and a variety of signs and symptoms. However, there seems to be less scientific evidence examining the relationship between DHI and aspects of function which includes both physical tests and self-reported outcomes. This is an important knowledge in the clinical assessment and treatment of these patients. Therefore, the objectives of this study were to describe both physical tests and self-reported outcomes in people with persistent dizziness in relation to DHI severity levels and to investigate the associations between these outcomes and increasing severity of the DHI total score.

METHOD

Setting

This cross-sectional study used baseline data from a randomized controlled trial (RCT) for treating participants with persistent dizziness (LODIP) (33), and the data are presented according to the STROBE guidelines (34). No sample size calculation was conducted as this study was a part of a larger study and explorative in nature (33). Participants were recruited from primary health care, primarily from general practitioners (GPs), directly, or *via* the general public. Some were also recruited from physiotherapists and ear, nose, and throat specialists (ENTs). Participants attended the Western Norway University of Applied Sciences (HVL) for testing and data were collected from 1 February 2016 to 1 May 2019. Details regarding recruitment and testing procedures have been described elsewhere (33). The

LODIP trial was registered in ClinicalTrials.gov (NCT02655575) and approved by the Regional Committee for Medical Research Ethics (2014-00921).

Participants

A total of 107 participants were included in the LODIP trial. Participants were included if they were within working age (18–70 years old) and presented with perceived dizziness that had started abruptly with symptoms lasting for at least 3 months. In addition, the dizziness symptoms had to be initiated or exacerbated by movement. Exclusion criteria were the following: patient-reported non-vestibular reasons for dizziness, diagnoses with fluctuating vestibular symptoms (e.g., Ménière's disease), plans for/had treatment for benign paroxysmal positional vertigo (BPPV) within 1 month, conditions where fast head movements were contraindicated (e.g., whiplash-associated injuries, osteoporosis of the neck), and severe/terminal pathology (e.g., cancer, psychiatric diagnosis). People were also excluded if they had attended group therapy for dizziness within the past year, if they were unable to attend the testing location, or if they could not understand Norwegian sufficiently.

Data Collection Procedure

Data collection included physical testing and self-reported questionnaires. The physical testing was conducted according to an established protocol, and three physiotherapists were trained to conduct the testing. A detailed description of the testing procedure has been published earlier (33).

Variables

Dizziness Handicap Inventory (DHI) was used to quantify perceived dizziness-related handicap (24). It consists of 25 items where each item is scored "0" (no), "2" (sometimes), or "4" (yes), summing up to a score between 0 and 100 points. Higher scores represent higher levels of perceived dizziness-related handicap. The DHI scores were categorized into mild (0–30), moderate (31–60), or severe (60–100) dizziness-related handicap (32). It has been translated and validated in several languages, including Norwegian (35–38). The Norwegian version of the DHI has shown a high reliability (38).

Physical Tests

Preferred (walking at their preferred pace) and **fast** (walking as fast as they could) **gait velocity** was tested by timing the participants as they walked through the middle 6 m of an 8-m pathway. A number of two walking trials were performed for each condition, and the average gait velocity for preferred and fast gait was calculated. Gait velocity assessment has been shown to have high reliability in a vestibular population (39).

The **grip strength** test was used as an indicator of overall muscle strength (40). The test has also shown to inform regarding muscle mass, physical function, and health status, as well as to predict future physical function and health across various clinical populations (40). Maximal grip strength of the dominant hand was used as an indication of general muscle health (40) and was measured using a dynamometer (Mie Medical Systems myometer). The average strength (in kg) from two trials of the dominant hand was calculated. The grip strength test testing has shown to have a high reliability and validity in healthy individuals as well as in various patient populations (41).

A total of four elements (lumbosacral flexion, head-nod flexion, shoulder retraction, and elbow-drop) from the movement domain of the **Global Physiotherapy Examination (GPE**) (10, 14) were examined to investigate body flexibility. Each element was scored on a predefined ordinal scale with 15 levels between "−2.3" (hypotonus) and "+2.3" (hypertonus), with "0" representing the normal standard. The absolute values of the positive and negative scores were added to create a sum score, and the median scores were presented. The GPE body flexibility domain has been reported to be reliable and valid in individuals with musculoskeletal pain (42).

Dizziness severity after head movements was tested by a **head movement-induced dizziness test (NRS_dizziness**). The test involved active head oscillations at 1 Hz and guided by a metronome, for 1 min. The perceived intensity of dizziness after head movements was scored on a Numeric Rating Scale (NRS) from "0" (no dizziness) to "10" (as bad as it can be). The NRS has shown acceptable psychometric properties in patients with chronic pain (43).

Psychological Measures

Avoidance behavior when being alone was assessed using the **Mobility Inventory of Agoraphobia, alone (MI-A).** The MI-A contains 27 items, each rated from 1 (never avoid) to 5 (always avoid), and higher scores indicate greater avoidance behavior (44). The **Body Sensation Questionnaire (BSQ)** was used to evaluate fear of bodily sensations associated with panic and anxiety (45). It contains 18 items, each scoring from 1 (not at all frightened) to 5 (extremely frightened), and higher scores imply greater fear of somatic sensations. The **Agoraphobic Cognitions Questionnaire (ACQ)** was used to measure fear (45). It contains 14 items, each scoring from 1 (thought never occurs) to 5 (thought always occurs), and higher scores indicate greater levels of fear of physical, social, and mental consequences related to the symptoms of anxiety. All of these (MI-A, BSQ, and ACQ) have shown acceptable reliability and internal consistency in a population with anxiety (45). In addition, psychological distress was evaluated using the **Hospital Anxiety and Depression Scale (HADS)** (46). The HADS contains 14 items, each rated from 0 (not present) to 3 (considerably present). The sum score (0–42) is reported, and higher scores indicate higher levels of psychological distress. The scale has shown good internal consistency and acceptable validity in people with dizziness (47).

Fatigue, Dizziness Severity, and QoL Measures

To evaluate perceived fatigue, the participants completed the **Chalder Fatigue Questionnaire (CFQ)** (48). The score of the 11 items, with each item scoring from 0 (better than usual) to 3 (much worse than usual), is summed, and higher scores indicate more fatigue. The **Vertigo Symptom Scale-Short Form (VSS-SF)** measures the perceived severity of dizziness symptoms during the past month (49). The questionnaire is a 15-item scale, and each item is scored between 0 (never) and 4 (very often). The sum score (0–60) is reported, and a

TABLE 1 | Demographic data among participants with persistent dizziness, presented for the total population and categorized into three levels of severity of the Dizziness Handicap Inventory (DHI).

			DHI category	
	Total population 107)	**Mild (0–30 points) (*n* = 19, 18%)**	**Moderate (31–60 points) (*n* = 60, 56%)**	**Severe (61–100 points) (*n* = 28, 26%)**
Mean age, years (95% CI)	49 (46; 51)	54 (48; 61)	47 (43; 50)	49 (45;, 54)
Females, % (95% CI)	76 (0.66; 0.83)	84 (0.60; 0.97)	73 (0.60; 0.84)	75 (0.55; 0.89)
Median dizziness duration, months (95% CI)	23[a] (17; 40)	36[b] (17; 100)	33[c] (14; 74)	18[d] (6; 21)
24+ months, % (95% CI)	50 (0.49; 0.51)	53 (0.28; 0.77)	53 (0.39; 0.66)	39 (0.20; 0.61)
Educational level				
High school or below, % (95% CI)	31[e] (0.22; 0.41)	21 (0.06; 0.46)	32[f] (0.21; 0.46)	35[g] (0.17; 0.56)
Work situation				
Working, % (95% CI)	41[h] (0.31; 0.51)	58 (0.33; 0.80)	42[f] (0.30; 0.56)	25 (0.11; 0.45)
Sick leave or incapacity, % (95% CI)	42 (0.33; 0.52)	21 (0.06; 0.46)	41[f] (0.28; 0.54)	61 (0.41; 0.78)
Other, % (95% CI)	17 (0.10; 0.26)	21 (0.06; 0.46)	17[f] (0.84; 0.29)	14 (0.04; 0.33)

DHI, Dizziness Handicap Inventory; CI, Confidence Interval.
[a]n = 95, [b]n = 17, [c]n = 55, [d]n = 23, [e]n = 104, [f]n = 59, [g]n = 26, [h]n = 106. The term "other" includes students, persons staying at home, retired, and other.

TABLE 2 | Physical test (Group 1) and self-reported psychological measures (Group 2), and fatigue, dizziness severity and quality of life (Group 3) among participants with persistent dizziness, presented for the total population, and categorized into three levels of severity of the Dizziness Handicap Inventory (DHI).

					DHI categories			
	Total population		**Mild (0–30 points)**		**Moderate (31–60 points)**		**Severe (61–100 points)**	
	Mean	**(95% CI)**	**Mean**	**(95% CI)**	**Mean**	**(95% CI)**	**Mean**	**(95% CI)**
DHI	49	(45.3; 52.4)	24	(20.7; 27.8)	47	(44.5; 48.9)	72	(68.6; 75.6)
Physical tests (Group 1)								
Preferred gait velocity (m/s)	1.18	(1.10; 1.18)	1.22	(1.12; 1.32)	1.20	(1.15; 1.24)	1.11	(1.01; 1.20)
Fast gait velocity (m/s)	1.79	(1.74; 1.84)	1.80	(1.69; 1.91)	1.85	(1.78; 1.91)	1.66	(1.55; 1.77)
Grip strength (kg)*	25.4	(24.2; 27.0)	24.9	(22.2; 27.3)	26.2	(24.0; 28.4)	24.3	(21.7; 29.3)
GPE movement	3.80	(3.47; 4.13)	3.40	(2.65; 4.15)	3.78	(3.33; 4.23)	4.13	(3.44; 4.93)
NRS_dizziness*	6.0	(5.0; 7.0)	5.5	(3.0; 7.0)	6.0	(5.0; 7.0)	7.0	(6.0; 8.0)
Psychological measures (Group 2)								
MI-A*	1.41	(1.30; 1.70)	1.11	(1.04; 1.26)	1.39	(1.26; 1.76)	2.30	(1.70; 3.00)
BSQ*	1.70	(1.50; 1.82)	1.35	(1.12; 1.71)	1.59	(1.47; 1.82)	2.06	(1.76; 2.24)
ACQ*	1.30	(1.26; 1.42)	1.16	(1.11; 1.26)	1.37	(1.26; 1.42)	1.66	(1.32; 2.06)
HADS*	11.0	(9.0; 12.0)	5.0	(1.0; 7.0)	10.5	(9.0; 13.0)	15.5	(13.0; 22.0)
Fatigue, dizziness severity, QoL (Group3)								
CFQ*	18.0	(16.0; 20.0)	13.0	(11.0; 17.0)	18.5	(16.0; 21.0)	24.0	(18.0; 27.0)
VSS-SF	20.58	(18.66; 22.49)	12.53	(7.14–18.43)	20.22	(18.47; 22.76)	27.04	(23.39; 31.25)
EQ-VAS (%)	56.73	(53.52; 60.79)	73.22	(67.38–85.91)	59.05	(54.36; 62.76)	42.82	(36.69; 48.11)

**Indicates median score. DHI, Dizziness Handicap Inventory; CI, confidence interval; m/s, meters per second; kgs, kilograms; GPE, Global Physiotherapy Examination; NRS_dizziness, head movement-induced dizziness; MI-A, Mobility Inventory of Agoraphobia-Alone; BSQ, Body Sensation Questionnaire; ACQ, Agoraphobic Cognitions Questionnaire; HADS, Hospital Anxiety and Depression Scale; QoL, quality of life; CFQ, Chalders Fatigue Questionnaire; VSS-SF, Vertigo Symptom Scale-Short Form.*

higher score indicates greater symptom severity. The Norwegian version of VSS-SF has shown good reliability and construct validity (50). To evaluate the quality of life (QoL), the participants completed the **EQ-VAS** section of the **EQ5D-5L** (a generic quality of life measure) (51, 52). This section contains a visual analog scale scoring from 0 to 100, where higher scores indicate better health-related QoL. The **EQ-VAS** has shown good reliability in patients with rheumatoid arthritis (53).

Statistical Methods

Continuous data were checked for normality using Shapiro–Wilk tests and QQ plots. Demographic data (age, sex, duration of dizziness, educational level, and work situation) were collected and presented for the total population, as well as for the three dizziness-related handicap levels (described above). Depending on the nature of the measure, the data were presented using means, medians, or proportions and their respective 95% CI around the point estimate. Due to the number of measures

TABLE 3 | Associations between total DHI score and measures in the physical (Models 1 & 4), psychological (Models 2 & 5), and "other" domains (Models 3 & 6) in participants with persistent dizziness.

	Models				Models with covarites (Age, sex)			
	β	95% CI	*p*	Adjusted R^2	β	95% CI	*P*	Adjusted R^2
Physical tests		**Model 1**		**0.15**		**Model 4**		**0.13**
Preferred gait velocity (m/s)								
Fast gait velocity (m/s)	−12.69	−25.09; −0.29	0.045		−16.55	−29.95; −3.15	0.016	
Grip strength (kg)								
GPE movement								
NRS_dizziness	2.14	0.88; 3.40	0.001		2.04	0.79; 3.29	0.002	
Psychological questionnaires		**Model 2**		**0.44**		**Model 5**		**0.43**
MI-A	8.21	3.83; 12.59	<0.001		8.47	4.07:12.87	<0.001	
HADS	1.05	0.60; 1.50	<0.001		1.04	0.58; 1.50	<0.001	
BSQ								
ACQ								
Other questionnaires		**Model 3**		**0.44**		**Model 6**		**0.41**
CFQ								
VSS-SF	0.66	0.37; 0.95	<0.001		0.65	0.34; 0.96	<0.001	
EQ-VAS	−0.40	−0.55; −0.25	<0.001		−0.42	−0.57; −0.26	<0.001	

Shaded outcomes removed from models due to p-values above 0.100. β, beta coefficient; CI, confidence interval; p, p-value; GPE, Global Physiotherapy Examination; NRS_dizziness, head movement-induced dizziness; MI-A, Mobility Inventory of Agoraphobia-Alone; HADS, Hospital Anxiety and Depression Scale; BSQ, Body Sensation Questionnaire; ACQ, Agoraphobic Cognitions Questionnaire; CFQ, Chalders Fatigue Questionnaire; VSS-SF, Vertigo Symptom Scale-Short Form; EQ-VAS, self-rated quality of life.

TABLE 4 | Association between the significant outcomes from models 4–6 and the total Dizziness Handicap Inventory (DHI) score, in participants with persistent dizziness.

	Model 7				Model 8 (with covariates age, sex)			
	β	95% CI	*p*	Adjusted R^2	β	95% CI	*p*	Adjusted R^2
				0.58				**0.56**
Fast gait velocity (m/s)	−7.59	−16.92; 1.74	0.110		−6 to 69	−17.21; 3.83	0.209	
NRS_dizziness	0.35	−0.63; 1.33	0.483		0.33	−0.67; 1.32	0.518	
MI-A	6.34	2.21; 10.46	0.003		6.71	2.45; 10.98	0.002	
HADS	0.58	0.13; 1.03	0.012		0.60	0.14; 1.06	0.011	
VSS-SF	0.50	0.23; 0.77	<0.001		0.51	0.22; 0.79	<0.001	
EQ-VAS	−0.21	−0.36; −0.06	0.008		−0.20	−0.36; −0.04	0.015	

Shaded outcomes; p-values above 0.100. β, beta coefficient; CI, confidence interval; p, p-value; NRS_dz, head movement-induced dizziness; MI-A, Mobility Inventory of Agoraphobia-Alone; HADS, Hospital Anxiety and Depression Scale; VSS-SF, Vertigo Symptom Scale-Short Form.

investigated, they were split into three groups for all the analyses. Group 1 included measures collected during testing, termed "Physical tests," Group 2 was termed psychological measures and included measures related to anxiety, avoidance behavior, and psychological distress, whereas Group 3 comprised comprise other relevant self-reported measures (fatigue, dizziness severity, and QoL) which were also believed to have an impact on DHI scores. The measures were presented according to three groups of outcomes in relation to the severity level of the DHI. Possible differences between the DHI severity levels in each of the measures were investigated by comparing means/ medians in relation to CI in the different measures.

All the assumptions for linear regressions were met. Backward multiple linear regression analyses were used to test for associations between DHI total score and the measures within each group. Tests for assumptions were conducted to investigate for multicollinearity and normality of residuals. The regression analyses for each group were calculated as one model, including all the measures in each group, which resulted in three separate backward regression models. Regression analyses were afterward adjusted for age and sex. A positive beta coefficient implied a positive association with the DHI, whereas a negative beta coefficient indicated a negative association. The significant measures in each of the unadjusted models were presented in scatterplots in relation to DHI total score (**Figure 1**). Finally, a regression model including only the measures with *p*-values below 0.10 from each of the three models was conducted, with similar adjustments as conducted for the separate blocks.

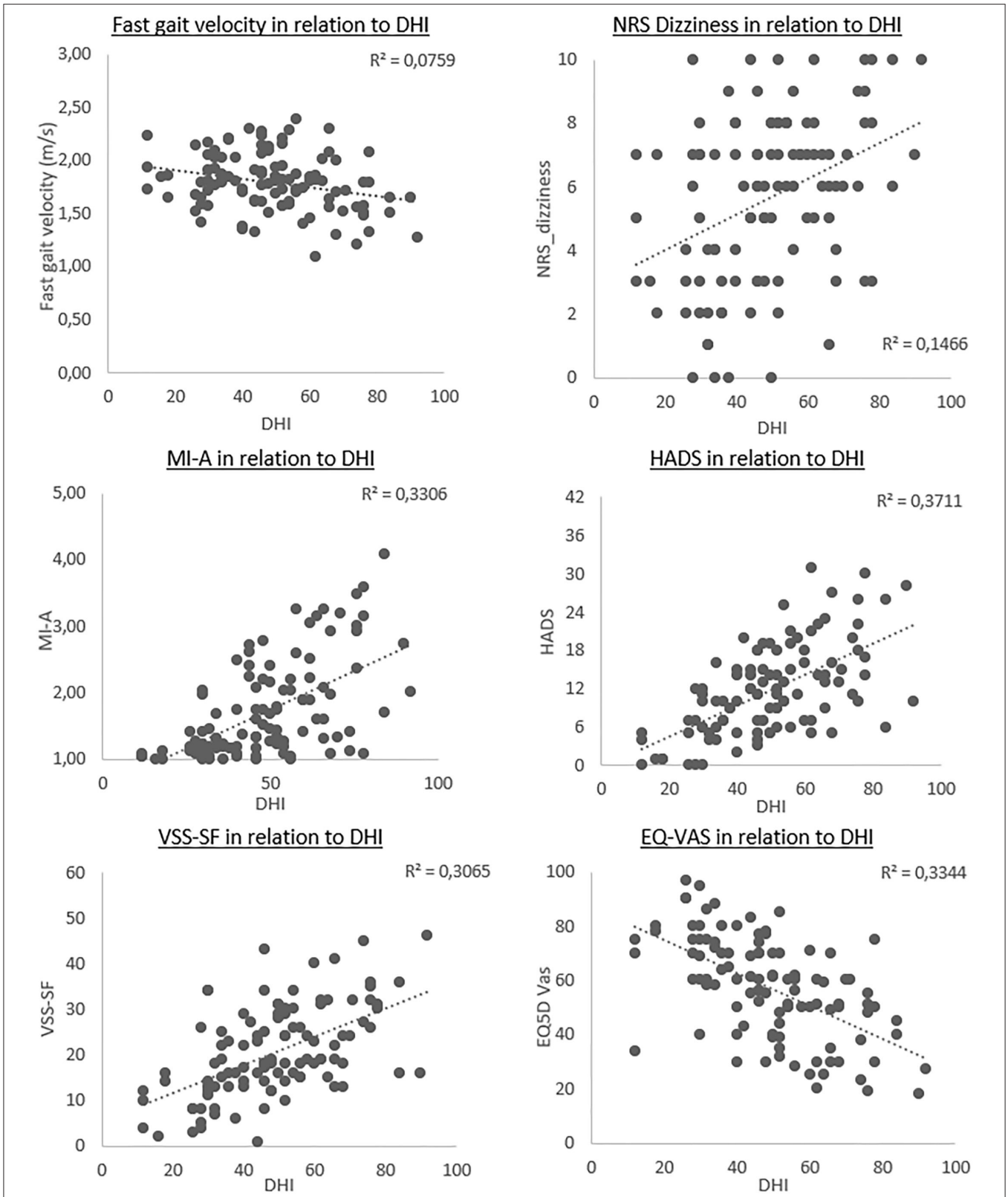

FIGURE 1 | Scatterplots of the outcomes significantly associated with the total Dizziness Handicap Inventory (DHI) score, in particicpants with persistent dizziness. Each plot presents the strength of the linear relationship, with DHI scores along *x*-axis and the different outcome measures on the *y*-axis. The dotted line represents the unadjusted regression coefficient for each outcome.

The statistical program IBM SPSS Statistics 26 was used for analysis, and p-values <0.05 were considered significant.

RESULTS

A total of 107 participants were included, with a mean age of 49 years (20–70 years), most of the participants were women (76%), and 50% of the participants reported a dizziness duration of at least 2 years (**Table 1**). The mean DHI score was 49 points (**Table 2**). Based on the DHI scores, 18% of the participants were classified as having mild dizziness-related handicap, 56% had moderate dizziness-related handicap, and 26% had severe dizziness-related handicap. Participants in the mild category tended to be older (mean age = 54 years) with a higher percentage of women (84%). A similar proportion of participants in the mild and moderate categories experienced dizziness for more than 24 months (53%), but almost two times as many in the moderate category (41%) were currently on sick leave compared with those in the mild category (21%), slightly over a third of the participants in the severe category presented with dizziness for more than 24 months; and 61% of these reported being on sick leave.

Participants presented with poorer scores in all groups of measures with increasing severity levels of DHI (**Table 2**). In Group 1, there was a tendency of higher preferred and fast gait velocities for those in the mild and moderate DHI categories compared with the severe category, and the participants in the mild DHI severity level demonstrated a trend toward lower NRS_dizziness scores compared with the severe group. The Group 2 measures all presented with low scores in the mild DHI severity level, which increased with DHI severity levels. The measures in Group 3 showed a similar trend of worsening symptoms with increasing severity levels of the DHI (increasing scores in CFQ and VSS-SF, decreasing scores on the EQ-VAS).

A total of three separate backward stepping multivariable models, with additional analyses including age and sex, were fitted to determine which measures within each group were associated with DHI (**Table 3**). After adjusting for age and sex, we found a significantly negative association between fast gait velocity and the DHI, and a significantly positive association between head movement-induced dizziness and the DHI (Model 4). For the measures in Group 2, the adjusted model showed significantly positive associations between both the MI-A and HADS scores and the DHI (Model 5). In Group 3, there was a significantly positive association between the VSS-SF scores and the DHI, and a significantly negative association between the EQ-VAS and the DHI after including age and sex in the model (Model 6). Model 4 could explain 13% of the variance in the DHI scores, whereas Models 5 and 6 explained 43 and 41% of the variance.

The independent variables associated with changes in DHI scores are presented as scatterplots (**Figure 1**). The plots showed a small negative association between DHI and fast gait, whereas NRS_dizziness presented with a larger variety of scores, with a small positive association. The MI-A, HADS, and VSS-SF all had a clear positive association, whereas the EQ5D-Vas illustrated a negative association with the DHI.

The independent variables in the final model (Model 7) could explain 58% of the variance (**Table 4**). After adjusting for age and sex, the MI-A, HADS, VSS-SF, and EQ-VAS (Model 8) remained significantly associated, and together, they explained 56% of the variance in the DHI scores.

DISCUSSION

There was a clear trend toward worse scores for the different outcomes in each of the DHI levels. In Group 1, gait velocity and head movement-induced dizziness (NRS_dizziness) became poorer with increasing severity level of the DHI. This also applied to avoidance behavior (MI-A), fear of bodily sensations (BSQ), fear itself (ACQ), and psychological distress (HADS) in Group 2, and fatigue (CFQ), dizziness severity (VSS-SF), and health-related QoL (EQ-VAS) in Group 3. In the adjusted multiple regression analyses, significant associations were found between increasing DHI severity and two measures within each of the three groups; fast gait velocity and NRS_dizziness in Group 1, MI-A and HADS in Group 2, and VSS-SF and EQ-VAS in Group 3. In the final adjusted combined model, only the MI-A, HADS, VSS-SF, and EQ-VAS remained significantly associated with increasing DHI severity, explaining 56% of the variance in the DHI score.

The participants scoring in the severe DHI category walked slower than the individuals in both the mild and moderate categories, at both preferred and fast velocities. The current results are in conflict with a previous study that demonstrated no significant difference in gait velocity between severity levels of DHI (32). The participants in this study were generally younger than those in the study by Whitney et al. (32) which could be one explanation for the different findings. However, different analysis methods and description of pace hamper direct comparisons. In this study, the adjusted regression analyses found that fast, but not preferred, gait velocity was significantly associated with DHI. This is in contrast to a previous study (28) and possibly due to the differences in versions of the DHI and statistical methods used. Since both studies suggest gait to influence DHI scores, results are considered not to be conflicting. The adjusted model also found significant associations between DHI and NRS_dizziness, but the lack of previous studies using this measure hampers comparison. Overall, less than half of the physical tests were significantly associated with the DHI, and the model explained only 13% of the DHI variance. These results indicate that the selected physical tests were unable to capture the current population's perception of dizziness-related handicap as measured by the DHI.

There was a trend for worse scores with increasing severity level of the DHI in the psychological measures. However, since ACQ and BSQ scores were within normal range (equal to a community sample) (54) across all DHI severity levels, the symptoms of panic and anxiety were of limited importance in this study population. Also, the MI-A (avoidance) and HADS

(psychological distress) scores increased with each DHI level, in line with the previous studies on populations with dizziness (30, 55, 56). Although only participants in the severe DHI level presented with abnormal scores for MI-A and HADS, [MI-A 2.30 points (cutoff value; 1.65 points (54), HADS 15.5 (cutoff value; 12 points (57)], the regression model including the psychological outcomes (Group 2) explained a relatively large part of the DHI variance (43%), with half of the selected measures being significantly associated with the DHI. This indicates that psychological outcomes may play an important role when dizziness-related handicap increase. This is in line with previous studies that have documented avoidance behavior in these patients (5, 30, 55), and that avoidance correlates with DHI scores (30). The same applies to HADS and association with DHI scores (56, 58) and was not surprising given the reported link between vestibular diseases and psychological complaints (18).

The outcomes in Group 3 (fatigue, dizziness severity, and QoL) also presented with worse scores with increasing DHI severity levels. It was surprising that the participants in the severe DHI level had CFQ scores similar to patients with chronic fatigue syndrome (mean; 24 points) (59), and that all three current levels of the DHI presented with severe dizziness according to VSS-SF (from 12.53 to 27.0, mean 20.58; cutoff 12 points) (60). The adjusted regression model showed significant associations between DHI and VSS-SF, in addition to EQ-VAS, in line with previous studies (29, 30, 38), whereas CFQ was not associated with DHI scores. This was somewhat surprising and may be explained by the fact that none of the items in DHI directly address questions related to fatigue.

The final adjusted model including significant measures from the previous models indicated that the self-reported outcomes covering avoidance (MI-A), anxiety, and depression (HADS) in addition to dizziness severity (VSS-SF) and QoL (EQ-VAS) and had a strong relationship with the DHI, whereas the physical tests did not. The model explained 56% of the variance in the DHI scores which was considered to be rather high, and in line with another study (30) who found that a model of different psychological outcomes could explain 62.7% of the variance in the DHI scores. Another study evaluating the relationship between demographic characteristics, mental health and dizziness-related characteristics also found significant associations between DHI and several outcomes which explained 63% of the variance (29). As far as we are aware of, this study is the only study to use multivariate regression analyses including both physical tests and self-reported outcomes in a stepwise backward model that at each step gradually eliminates variables from the regression model to find a reduced model that best explains the data. This represents a rather novel approach. As none of the physical tests were significant in the final model, it could indicate that the DHI is unable to capture problems associated with everyday physical activities using gait as an example. Diverging results are reported by others concerning such associations (27, 28, 32, 61). Studies using different static balance and functional tests have found moderate to strong correlations with the DHI, like for instance, single-leg stance and Dynamic Gait Index (27, 32, 61), whereas other outcomes such as Romberg test and single-leg stand test had weak or no correlation (27, 32). Whether other physical measures would have rendered the significant associations to remain in this study is, however, unclear. From our point of view, the DHI seems to be useful in collecting self-reported information concerning psychological problems, dizziness severity, and QoL. However, as people with dizziness often present with a variety of complaints, it is necessary to use a combination of tests and measures in the assessment of individual patients with persistent dizziness.

The study has several limitations. As data were collected in relation to an ongoing RCT, power calculations were not performed for this study. The study has a cross-sectional design, and data from this study do not allow for inferring conclusions regarding direction and causality. Even though there are risks of confounders that may influence the association in cross-sectional studies, this was not likely, since this study tested for assumptions for regression analyses, and no sign of multicollinearity was found.

A weakness of this study could conceivably be that diagnoses are not included as a confounder in the association analysis. However, we recruited persons with prolonged dizziness (average 24 months) without paying attention to diagnoses as they have shown to be of less importance for function when dizziness persists (13). We rather aimed to explore what functional challenges the participants had and if these problems influenced scores on the DHI. Another possible limitation is the use of three severity levels of the DHI (32), which is neither based on evidence nor consensus. However, we opted to use the categorization due to the clinical impression that scoring in the severe DHI level could be an indication for directing special attention toward these patients. Jacobson and Newman (24) also included subscales (physical, functional, and emotional) of the DHI. However, the validity of these subscales has been questioned (62) and the use of the total DHI score has been recommended (31, 35, 36, 38, 63), and thus, only the relationship between the total DHI and selected outcomes was examined in this study.

Strengths of the study include the inclusion of a relatively large population with persistent dizziness. Data were collected systematically following a published protocol (33) and trained testers were used. It is further a strength that the current age and sex distribution equal previous studies on populations with vestibular populations (13, 29, 30), and patients attending an oto-neurology clinic due to dizziness (30, 32), thereby increasing generalizability.

CONCLUSION

The use of a regression analysis including groups of physical tests and self-reported measures, to reveal the most important factors to explain the variance in DHI scores, represents a new approach in this field. The findings indicate that DHI seems to cover self-reported aspects such as avoidance, behavior, psychological distress, dizziness severity, and QoL. However, the relationship between DHI and physical tests was not established. From this study, it seems that DHI should be complemented with physical tests to establish

a more complete picture of the patients' complaints. However, further studies are needed to establish which physical test will be the most appropriate to use together with DHI.

DATA AVAILABILITY STATEMENT

The raw data supporting the conclusions of this article will be made available by the authors, without undue reservation.

ETHICS STATEMENT

The studies involving human participants were reviewed and approved by the Regional Committee for Medical Research Ethics. The patients/participants provided their written informed consent to participate in this study.

AUTHOR CONTRIBUTIONS

The primary investigator for the study was LK. She developed the study in collaboration with LM, SM, KW, SHN, RC, and BJ-K. LK was responsible for the screening and testing of participants, with assistance from LM. LK completed the statistical analysis in collaboration with EB. LK drafted the manuscript with contributions from all authors with critical revision. All authors have read and approved the final manuscript.

FUNDING

This study was funded by the Norwegian Fund for Postgraduate Training in Physiotherapy. The funding body had no active part in planning and conducting the study.

REFERENCES

1. Neuhauser HK, Lempert T. Vertigo: epidemiologic aspects. Seminar Neurol. (2009) 29:473–81. doi: 10.1055/s-0029-1241043
2. Bisdorff A, Bosser G, Gueguen R, Perrin P. The epidemiology of vertigo, dizziness, and unsteadiness and its links to co-morbidities. *Front Neurol.* (2013) 4:29. doi: 10.3389/fneur.2013.00029
3. Norway S. *Levekårsundersøkelse Statistisk sentralbyrå 2019.* (2019). Available from: https://www.ssb.no/statbank/table/04432/tableViewLayout1/ (accessed March 24, 2022).
4. Baloh RW. Clinical practice. Vestibular neuritis. *N Engl J Med.* (2003) 348:1027–32. doi: 10.1056/NEJMcp021154
5. Heinrichs N, Edler C, Eskens S, Mielczarek MM, Moschner C. Predicting continued dizziness after an acute peripheral vestibular disorder. *Psychosom Med.* (2007) 69:700–7. doi: 10.1097/PSY.0b013e318151a4dd
6. Godemann F, Siefert K, Hantschke-Bruggemann M, Neu P, Seidl R, Strohle A. What accounts for vertigo one year after neuritis vestibularis - anxiety or a dysfunctional vestibular organ? *J Psychiatr Res.* (2005) 39:529–34. doi: 10.1016/j.jpsychires.2004.12.006
7. Bisdorff A, Von Brevern M, Lempert T, Newman-Toker DE. Classification of vestibular symptoms: towards an international classification of vestibular disorders. *J Vestib Res.* (2009) 19:1–13. doi: 10.3233/VES-2009-0343
8. Schniepp R, Wuehr M, Huth S, Pradhan C, Brandt T, Jahn K. Gait characteristics of patients with phobic postural vertigo: effects of fear of falling, attention, and visual input. *J Neurol.* (2014) 261:738–46. doi: 10.1007/s00415-014-7259-1
9. Coelho Junior AN, Gazzola JM, Gabilan YP, Mazzetti KR, Perracini MR, Gananca FF. Head and shoulder alignment among patients with unilateral vestibular hypofunction. *Rev Bras Fisioter.* (2010) 14:330–6. doi: 10.1590/S1413-35552010005000022
10. Wilhelmsen K, Kvale A. Examination and treatment of patients with unilateral vestibular damage, with focus on the musculoskeletal system: a case series. *Phys Ther.* (2014) 94:1024–33. doi: 10.2522/ptj.20130070
11. Allum JH, Adkin AL, Carpenter MG, Held-Ziolkowska M, Honegger F, Pierchala K. Trunk sway measures of postural stability during clinical balance tests: effects of a unilateral vestibular deficit. *GaitPosture.* (2001) 14:227–37. doi: 10.1016/S0966-6362(01)00132-1
12. Horlings CG, Kung UM, Bloem BR, Honegger F, Van AN, Van Engelen BG, et al. Identifying deficits in balance control following vestibular or proprioceptive loss using posturographic analysis of stance tasks. *ClinNeurophysiol.* (2008) 119:2338–46. doi: 10.1016/j.clinph.2008.07.221
13. Wilhelmsen K, Ljunggren AE, Goplen F, Eide GE, Nordahl SH. Long-term symptoms in dizzy patients examined in a university clinic. *BMCEar Nose Throat Disord.* (2009) 9:2. doi: 10.1186/1472-6815-9-2
14. Kvale A, Wilhelmsen K, Fiske HA. Physical findings in patients with dizziness undergoing a group exercise programme. *Physiother Res Int.* (2008) 13:162–75. doi: 10.1002/pri.402
15. Eckhardt-Henn A, Breuer P, Thomalske C, Hoffmann S, Hopf H. Anxiety disorders and other psychiatric subgroups in patients complaining of dizziness. *J Anxiety Disord.* (2003) 17:369–88. doi: 10.1016/S0887-6185(02)00226-8
16. Edelman S, Mahoney AE, Cremer PD. Cognitive behavior therapy for chronic subjective dizziness: a randomized, controlled trial. *Am J Otolaryngol.* (2012) 33:395–401. doi: 10.1016/j.amjoto.2011.10.009
17. Holmberg J, Karlberg M, Harlacher U, Magnusson M. Experience of handicap and anxiety in phobic postural vertigo. *Acta Otolaryngol.* (2005) 125:270–5. doi: 10.1080/00016480410023001
18. Lahmann C, Henningsen P, Brandt T, Strupp M, Jahn K, Dieterich M, et al. Psychiatric comorbidity and psychosocial impairment among patients with vertigo and dizziness. *J Neurol Neurosurg Psychiatry* 86:302–8. doi: 10.1136/jnnp-2014-307601
19. Yardley L, Burgneay J, Nazareth I, Luxon L. Neuro-otological and psychiatric abnormalities in a community sample of people with dizziness: a blind, controlled investigation. *J Neurol Neurosurg Psychiatry.* (1998) 65:679–84. doi: 10.1136/jnnp.65.5.679
20. Neuhauser HK, Radtke A, von Brevern M, Lezius F, Feldmann M, Lempert T. Burden of dizziness and vertigo in the community. *Arch Intern Med.* (2008) 168:2118–24. doi: 10.1001/archinte.168.19.2118
21. Weidt S, Bruehl AB, Straumann D, Hegemann SC, Krautstrunk G, Rufer M. Health-related quality of life and emotional distress in patients with dizziness: a cross-sectional approach to disentangle their relationship. *BMC Health Serv Res.* (2014) 14:317. doi: 10.1186/1472-6963-14-317
22. Iglebekk W, Tjell C, Borenstein P. Pain and other symptoms in patients with chronic benign paroxysmal positional vertigo (BPPV). *Scand J Pain.* (2013) 4:233–40. doi: 10.1016/j.sjpain.2013.06.004
23. Fong E, Li C, Aslakson R, Agrawal Y. Systematic review of patient-reported outcome measures in clinical vestibular research. *Arch phys Med Rehabil.* (2015) 96:357–65. doi: 10.1016/j.apmr.2014.09.017
24. Jacobson GP, Newman CW. The development of the dizziness handicap inventory. *Arch Otolaryngol Head Neck Surg.* (1990) 116:424–7. doi: 10.1001/archotol.1990.01870040046011
25. Yip CW, Strupp M. The dizziness handicap inventory does not correlate with vestibular function tests: a prospective study. *J Neurol.* (2018) 265:1210–8. doi: 10.1007/s00415-018-8834-7
26. Patel M, Arshad Q, Roberts RE, Ahmad H, Bronstein AM. Chronic symptoms after vestibular neuritis and the high velocity vestibulo-ocular reflex. *Otol Neurotol.* (2016) 37:179. doi: 10.1097/MAO.0000000000000949

27. Vereeck L, Truijen S, Wuyts FL, Van De Heyning PH. The dizziness handicap inventory and its relationship with functional balance performance. *Otol Neurotol.* (2007) 28:87–93. doi: 10.1097/01.mao.0000247821.98398.0d
28. Zanotto D, Mamuyac EM, Chambers AR, Nemer JS, Stafford JA, Agrawal SK, et al. Dizziness handicap inventory score is highly correlated with markers of gait disturbance. *Otol Neurotol.* (2017) 38:1490–9. doi: 10.1097/MAO.0000000000001586
29. Formeister EJ, Krauter R, Kirk L, Zhu TR, Rizk HG, Sharon JD. Understanding the Dizziness Handicap Inventory (DHI): a cross sectional analysis of symptom factors that contribute to DHI variance. *Otol Neurotol.* (2020) 41:86–93. doi: 10.1097/MAO.0000000000002438
30. Herdman D, Norton S, Pavlou M, Murdin L, Moss-Morris R. Vestibular deficits and psychological factors correlating to dizziness handicap and symptom severity. *J Psychosom Res.* (2020) 132:109969. doi: 10.1016/j.jpsychores.2020.109969
31. Piker EG, Jacobson GP, Newman CW. Assessing dizziness-related quality of life. In: Jacobson GP, Shepard NT, Barin K, Janky K, McCaslin DL, editors. *Balance Function Assessment and Management*. 3rd ed. San Diego, CA: Plural publishing (2019). p. 143–66.
32. Whitney SL, Wrisley DM, Brown KE, Furman JM. Is perception of handicap related to functional performance in persons with vestibular dysfunction. *Otol Neurotol.* (2004) 25:139–43. doi: 10.1097/00129492-200403000-00010
33. Kristiansen L, Magnussen L, Wilhelmsen K, Mæland S, Nordahl S, Clendaniel R, et al. Efficacy of intergrating vestibular rehabilitation and cognitive behaviour therapy in persons with persistent dizziness in primary care-a study protocol for a randomised controlled trial. *Trials.* (2019) 20:575. doi: 10.1186/s13063-019-3660-5
34. Von Elm E, Altman DG, Egger M, Pocock SJ, Gøtzsche PC, Vandenbroucke JP. The Strengthening the Reporting of Observational Studies in Epidemiology (STROBE) statement: guidelines for reporting observational studies. *Ann Intern Med.* (2007) 147:573–7. doi: 10.7326/0003-4819-147-8-200710160-00010
35. Perez N, Garmendia I, Garcia-Granero M, Martin E, Garcia-Tapia R. Factor analysis and correlation between dizziness handicap inventory and dizziness characteristics and impact on quality of life scales. *Acta Otolaryngol Suppl.* (2001) 545:145–54. doi: 10.1080/0001648017503 88333
36. Vereeck L, Truijen S, Wuyts FL, Van De Heyning PH. Internal consistency and factor analysis of the Dutch version of the Dizziness Handicap Inventory. *Acta Otolaryngol.* (2007) 127:788–95. doi: 10.1080/00016480601 075464
37. Kurre A, van Gool CJ, Bastiaenen CH, Gloor-Juzi T, Straumann D, de Bruin ED. Translation, cross-cultural adaptation and reliability of the german version of the dizziness handicap inventory. *Otol Neurotol.* (2009) 30:359–67. doi: 10.1097/MAO.0b013e3181977e09
38. Tamber AL, Wilhelmsen KT, Strand LI. Measurement properties of the Dizziness Handicap Inventory by cross-sectional and longitudinal designs. *Health Qual Life Outcomes.* (2009) 7:101. doi: 10.1186/1477-7525-7-101
39. Hall CD, Herdman SJ. Reliability of clinical measures used to assess patients with peripheral vestibular disorders. *JNeurolPhysTher.* (2006) 30:74–81. doi: 10.1097/01.NPT.0000282571.55673.ed
40. Bohannon RW. Muscle strength: clinical and prognostic value of hand-grip dynamometry. *Curr Opin Clin Nutr Metab Care.* (2015) 18:465–70. doi: 10.1097/MCO.0000000000000202
41. Bobos P, Nazari G, Lu Z, MacDermid JC. Measurement properties of the hand grip strength assessment: a systematic review with meta-analysis. *Arch Phys Med Rehabil.* (2020) 101:553–65. doi: 10.1016/j.apmr.2019.10.183
42. Kvåle A, Ljunggren AE, Johnsen TB. Examination of movement in patients with long-lasting musculoskeletal pain: reliability and validity. *Physiother Res Int.* (2003) 8:36–52. doi: 10.1002/pri.270
43. Hawker GA, Mian S, Kendzerska T, French M. Measures of adult pain: Visual analog scale for pain (vas pain), numeric rating scale for pain (nrs pain), mcgill pain questionnaire (mpq), short-form mcgill pain questionnaire (sf-mpq), chronic pain grade scale (cpgs), short form-36 bodily pain scale (sf-36 bps), and measure of intermittent and constant osteoarthritis pain (icoap). *Arthritis Care Res/.* (2011) 63.S11:S240–S252. doi: 10.1002/acr.20543
44. Chambless DL, Caputo GC, Jasin SE, Gracely EJ, Williams C. The mobility inventory for agoraphobia. *Behav Res Ther.* (1985) 23:35–44. doi: 10.1016/0005-7967(85)90140-8
45. Chambless DL, Caputo GC, Bright P, Galalgher R. Assessment og fear of fear in agoraphobics: the body sensations questionnaire and the agoraphobic cognitions questionnaire. *J Consult Clin Psychol.* (1984) 52:10–1097. doi: 10.1037/0022-006X.52.6.1090
46. Zigmond A, Snaith R. The hospital anxiety and depression scale. *Acta Psychiatr Scand.* (1983) 67:361–70. doi: 10.1111/j.1600-0447.1983.tb09716.x
47. Piker EG, Kaylie DM, Garrison D, Tucci DL. Hospital anxiety and depression Scale: factor structure, internal consistency and convergent validity in Patients with dizziness. *Audiol Neurotol.* (2015) 20:394–9. doi: 10.1159/0004 38740
48. Chalder T, Berelowitz G, Pawlikowska T, Watts L, Wessely S, Wright D, et al. Development of a fatigue scale. *J Psychosom Res.* (1993) 37:147–53. doi: 10.1016/0022-3999(93)90081-P
49. Yardley L, Masson E, Verschuur C, Haacke N, Luxon L. Symptoms, anxiety and handicap in dizzy patients: development of the vertigo symptom scale. *J Psychosom Res.* (1992) 36:731–41. doi: 10.1016/0022-3999(92) 90131-K
50. Wilhelmsen K, Strand LI, Nordahl SH Eide GE, Ljunggren AE. Psychometric properties of the vertigo symptom scale - short form. *BMC Ear Nose Throat Disord.* (2008) 8:2. doi: 10.1186/1472-6815-8-2
51. Brooks R, Group E. EuroQol: the current state of play. *Health Policy.* (1996) 37:53–72. doi: 10.1016/0168-8510(96)00822-6
52. Van Reenen M, Janssen B. *EQ-5D-5L User Guide: Basic Information on How to Use the EQ-5D-5L Instrument*. (2015). Available online at: http://Euroqolorg: Euroqol (accessed August 20, 2020).
53. Hurst N, Kind P, Ruta D, Hunter M, Stubbings A. Measuring health-related quality of life in rheumatoid arthritis: validity, responsiveness and reliability of EuroQol (EQ-5D). *Br J Rheumatol.* (1997) 36:551–9. doi: 10.1093/rheumatology/36.5.551
54. Hovland A, Johansen H, Sjøbø T, Vøllestad J, Nordhus IH, Pallesen S, et al. A feasibility study on combining internet-based cognitive behaviour therapy with physical exercise as treatment for panic disorder—treatment protocol and preliminary results. *Cogn Behav Ther.* (2015) 44:275–87. doi: 10.1080/16506073.2015. 1022596
55. Jacob RG, Whitney SL, Detweiler-Shostak G, Furman JM. Vestibular rehabilitation for patients with agoraphobia and vestibular dysfunction: a pilot study. *J Anxiety Disord.* (2001) 15:131–46. doi: 10.1016/S0887-6185(00)00047-5
56. Cheng YY, Kuo CH, Hsieh WL, Lee SD, Lee WJ, Chen LK, et al. Anxiety, depression and quality of life (QoL) in patients with chronic dizziness. *Arch Gerontol Geriatr.* (2012) 54:131–5. doi: 10.1016/j.archger.2011.04.007
57. Hosaka T, Awazu H, Aoki T, Okuyama T, Yamawaki S. Screening for adjustment disorders and major depression in otolaryngology patients using the Hospital Anxiety and Depression Scale. *Int J Psychiatry Clin Pract.* (1999) 3:43–8. doi: 10.3109/13651509909024758
58. Roh KJ, Kim MK, Kim JH, Son EJ. Role of emotional distress in prolongation of dizziness: a cross-sectional study. *J Audiol Otol.* (2018) 22:6. doi: 10.7874/jao.2017.00290
59. Cella M, Chalder T. Measuring fatigue in clinical and community settings. *J Psychosom Res.* (2010) 69:17–22. doi: 10.1016/j.jpsychores.2009. 10.007
60. Yardley L, Donovan-Hall M, Smith HE, Walsh BM, Mullee M, Bronstein AM. Effectiveness of primary care-based vestibular rehabilitation for chronic dizziness. *Ann Intern Med.* (2004) 141:598–605. doi: 10.7326/0003-4819-141-8-200410190-00007
61. Gill-Body KM, Beninato M, Krebs DE. Relationship among balance impairments, functional performance, and disability in people with peripheral vestibular hypofunction. *Phys Ther.* (2000) 80:748–58. doi: 10.1093/ptj/80.8.748
62. Asmundson GJ, Stein MB, Ireland D, A. factor analytic study of the dizziness handicap inventory: does it assess phobic avoidance in vestibular referrals? *J Vestib Res.* (1999) 9:63–8. doi: 10.3233/VES-1999-9108

63. Koppelaar-van Eijsden HM, Schermer TR, Bruintjes TD. Measurement properties of the dizziness handicap inventory: a systematic review. *Otol Neurotol.* (2022) 43:e282–97. doi: 10.1097/MAO.0000000000003448

Conflict of Interest: The authors declare that the research was conducted in the absence of any commercial or financial relationships that could be construed as a potential conflict of interest.

Publisher's Note: All claims expressed in this article are solely those of the authors and do not necessarily represent those of their affiliated organizations, or those of the publisher, the editors and the reviewers. Any product that may be evaluated in this article, or claim that may be made by its manufacturer, is not guaranteed or endorsed by the publisher.

Copyright © 2022 Kristiansen, Magnussen, Wilhelmsen, Maeland, Nordahl, Hovland, Clendaniel, Boyle and Juul-Kristensen. This is an open-access article distributed under the terms of the Creative Commons Attribution License (CC BY). The use, distribution or reproduction in other forums is permitted, provided the original author(s) and the copyright owner(s) are credited and that the original publication in this journal is cited, in accordance with accepted academic practice. No use, distribution or reproduction is permitted which does not comply with these terms.

frontiers | Frontiers in Neurology

ORIGINAL RESEARCH
published: 18 July 2022
doi: 10.3389/fneur.2022.938740

Transcriptional Down-Regulation of Major Histocompatibility Complex as a Possible Pathogenesis for Meniere's Disease

*Kwang-Dong Choi[1], Eun Hye Oh[2], Hyun Sung Kim[2], Hyang-Sook Kim[2], Ji-Yun Park[3], Seo Young Choi[1] and Jae-Hwan Choi[2]**

[1] Department of Neurology, Pusan National University Hospital, Pusan National University School of Medicine and Biomedical Research Institute, Busan, South Korea, [2] Department of Neurology, Pusan National University School of Medicine, Research Institute for Convergence of Biomedical Science and Technology, Pusan National University Yangsan Hospital, Yangsan, South Korea, [3] Department of Neurology, Ulsan University Hospital, University of Ulsan College of Medicine, Ulsan, South Korea

OPEN ACCESS

Edited by:
Michael Strupp,
Ludwig Maximilian University of Munich, Germany

Reviewed by:
Daogong Zhang,
Shandong Provincial ENT Hospital, China
Teresa Requena,
University of Edinburgh, United Kingdom

***Correspondence:**
Jae-Hwan Choi
rachelbolan@hanmail.net

Specialty section:
This article was submitted to Neuro-Otology, a section of the journal Frontiers in Neurology

Received: 08 May 2022
Accepted: 20 June 2022
Published: 18 July 2022

Citation:
Choi K-D, Oh EH, Kim HS, Kim H-S, Park J-Y, Choi SY and Choi J-H (2022) Transcriptional Down-Regulation of Major Histocompatibility Complex as a Possible Pathogenesis for Meniere's Disease. Front. Neurol. 13:938740. doi: 10.3389/fneur.2022.938740

Objectives: This study aimed to determine the underlying pathogenesis of Meniere's disease (MD) using transcriptome analysis.

Methods: Total RNA was extracted from the peripheral blood mononuclear cells of 39 patients with MD and 39 controls. Through microarray analysis for nine patients and controls, the differentially expressed genes (DEGs) of those two groups were screened based on cut-off criteria (|fold changes| > 2.0 and adjusted p-value < 0.05). The functional enrichment analysis of DEGs was performed using Gene Ontology (GO).

Results: There were 996 DEGs identified in the MD group: 415 were upregulated and 581 were downregulated. A functional enrichment analysis indicated that the downregulated DEGs were significantly enriched in terms related to immune system processes. Among them, 17 genes were enriched in terms for the major histocompatibility complex (MHC) protein complex, and the relative messenger RNA (mRNA) levels of three markedly downregulated DEGs [fold changes < -5: human leukocyte antigen (HLA)-DMA, HLA-DRB1, and HLA-DPB1] were significantly decreased in another 30 patients with MD compared with normal controls by quantitative reverse transcription-polymerase chain reaction (qRT-PCR). However, there were no correlations between the expression levels of these three genes and clinical data, such as age, onset age, time course, or hearing threshold.

Conclusions: Our transcriptome analysis showed that the downregulated DEGs in MD were mainly associated with the immune system pathways including the MHC protein complex in MD. Remarkably, a breakdown in immunological tolerance mediated by MHC class II may contribute to the MD development, which has implications for targeted treatment.

Keywords: Meniere's disease, transcriptome analysis, immune system, MHC protein, differentially expressed gene

INTRODUCTION

Meniere's disease (MD) is a chronic disease of the inner ear characterized by episodic vertigo, fluctuating sensorineural hearing loss (SNHL) at low-to-medium frequencies, tinnitus, and aural fullness (1). Although endolymphatic hydrops (EH) is considered the histopathological hallmark of MD, the exact pathophysiology of MD is not yet fully understood. MD may be a multifactorial disorder associated with various etiologies, such as anatomical abnormalities, infections, and allergens. Autoimmunity has also been suggested as a potential cause of MD based on the increased prevalence of autoimmune diseases, the increased levels of autoantibodies, and the association with human leukocyte antigen (HLA) types in patients with MD (2–11). Since familial MD has been identified in 8−10% of cases, genetic factors might contribute to the MD development (2, 3, 12, 13). Next-generation sequencing and association studies using genomic DNA have revealed that numerous genes related to inner ear development, the immune-associated process, and systemic hemostatic derangement are associated with a susceptibility to MD (14–17). Polygenic multiallelic hypothesis has recently been proposed to explain the variable phenotype of MD (18). However, the genetic contribution to MD is still unclear due to the lack of a main validated gene across different populations.

Contrary to genome studies, transcriptome analysis using mRNA can establish the global pattern of gene expression and determine the biological functions of differentially expressed genes (DEGs) between two or more conditions (19). Therefore, transcriptome analysis has been widely used to identify the molecular pathogenesis and therapeutic targets in various malignancies and autoimmune diseases (20–22). However, only two previous studies have applied transcriptome analysis to MD (23, 24). One study using RNA sequencing found several DEGs associated with innate immune cells and autoimmune diseases in sporadic MD, suggesting that immune factors are involved in MD pathogenesis *via* regulation of immune system activities (23). Another study applied gene expression profiling for the differential diagnosis of MD and vestibular migraine, which revealed that the two disorders have different pro-inflammatory signatures (24).

This study aimed to provide novel insights into the pathogenesis and targeted treatment of MD using transcriptome analysis.

MATERIALS AND METHODS

We recruited 39 patients with definite MD according to the diagnostic criteria established by the Classification Committee of the Barany Society (1). The patients included 21 men and 18 women with an age ranging from 46 to 81 years (mean ± SD = 64.7 ± 8.1 years). The experiment has been conducted through the two-step process. Initially, the DEGs were screened using microarray analysis between nine patients with MD and normal controls. Then, the expression levels of selected DEGs were validated using quantitative reverse transcription-polymerase chain reaction (qRT-PCR) from other 30 patients with MD.

RNA Extraction and Microarray Analysis

As described previously (23), total RNA was extracted from peripheral blood mononuclear cells (PBMCs) of nine patients with MD and nine controls without any vertigo or hearing loss using the TRIzol Reagent. The purity and quantity of RNA were measured using a spectrophotometer (NanoDrop ND-1000, Thermo Fisher Scientific, Wilmington, DE, USA), and the quality of RNA was further measured using a bioanalyzer (Agilent 2100, Agilent Technologies).

Isolated total RNA was amplified, labeled, and hybridized using the Affymetrix Human Clariom S Assay according to the manufacturer's protocol. In brief, the purified RNA sample was transcribed to double-strand cDNA using the GeneChip Whole Transcript (WT) amplification kit. That cDNA was then fragmented and biotin-labeled with terminal deoxynucleotidyl transferase (TdT) using the GeneChip WT terminal labeling kit. Approximately 5.5 μg of the labeled cDNA was hybridized onto the Affymetrix GeneChip Array at 45°C for 16 h. After washing, the arrays were stained on the GeneChip Fluidics Station 450 and scanned using the GeneChip Scanner 3000. Raw data were analyzed using the Affymetrix GeneChip Command Console software.

Identification of DEGs and Functional Enrichment Analysis

To verify reproducibility between samples, Pearson's correlation test and multidimensional scaling (MDS) were performed. Raw data were summarized and normalized using the Robust Multi-array Average module implemented in Affymetrix Power Tools. The DEGs between MD and normal control samples were screened based on fold-change filtering combined with Student's *t*-tests. The false discovery rate (FDR) was controlled by the adjusted *p*-value using the Benjamini-Hochberg algorithm. Genes were considered to be differentially expressed when they conformed to the criteria of $|\text{fold changes}| > 2$ and adjusted $p\text{-value} < 0.05$.

To explain functional annotation for DEGs, the Gene Ontology (GO) enrichment analysis was performed using g:Profiler (https://biit.cs.ut.ee/gprofiler/). GO is a bioinformatics analysis that provides current scientific knowledge about the functions of genes and gene products and covers three biological terms: biological process (BP), cellular component (CC), and molecular function (MF). An adjusted *p*-value (FDR) <0.05 was used as the criterion for statistical significance.

Quantitative Reverse Transcription-Polymerase Chain Reaction (qRT-PCR)

The validation of selected DEGs was performed using qRT-PCR. Total RNA was extracted from PBMCs of other 30 patients with MD and healthy normal controls using the TRIzol Reagent (Life Technologies). Approximately 1 μg of total mRNA was reverse-transcribed into cDNA using M-MLV (Promega) according to the manufacturer's instructions. Gene expression was examined using qRT-PCR with the SYBR green PCR master mix and Rotor-Gene Q (both QIAGEN). The PCR conditions were as

TABLE 1 | Demographic and clinical characteristics of patients with the Meniere's disease (MD).

	Total ($n = 39$)	Microarray group ($n = 9$)	qRT-PCR group ($n = 30$)	*p*-value
Age, years, mean (SD)	65.0 (7.9)	67.1 (7.2)	64.7 (8.1)	0.379
Gender, female, *n* (%)	18 (46.2)	4 (44.4)	14 (46.7)	1.000
Age at onset, years, mean (SD)	57.5 (8.1)	59.0 (6.3)	57.3 (8.2)	0.436
Time course, years, mean (SD)	7.5 (4.3)	8.1 (5.4)	7.4 (4.1)	0.711
Family history, *n* (%)	3 (7.7)	1 (11.1)	2 (6.7)	0.556
Hearing loss at diagnosis, dB, mean (SD)	49.0 (18.1)	49.0 (21.9)	48.6 (17.7)	0.857
Delayed Meniere's disease, *n* (%)	5 (12.8)	1 (11.1)	4 (13.3)	1.000
Headache, *n* (%)	11 (28.2)	4 (44.4)	7 (23.3)	0.238
Migraine, *n* (%)	1 (2.6)	0 (0)	1 (3.3)	1.000
Autoimmune disease, *n* (%)	4 (10.3)	1 (11.1)	3 (10.0)	1.000
Hearing stage, *n* (%)				
1	5 (12.8)	2 (22.2)	3 (10.0)	0.572
2	9 (23.1)	1 (11.1)	8 (26.7)	0.654
3	20 (51.3)	4 (44.4)	16 (53.3)	0.716
4	5 (12.8)	2 (22.2)	3 (10.0)	0.572
Steroid treatment	9 (23.1)	3 (33.3)	6 (20.0)	0.406

follows: initial denaturation at 95°C for 5 min, followed by 40 cycles of denaturation at 95°C for 15 s, amplification at 60°C for 30 s, and extension at 72°C for 30 s. Glyceraldehyde 3-phosphate dehydrogenase (GAPDH) was used as the reference for PCR normalization, and all PCRs were performed in triplicate. The relative expression levels of genes were calculated using the $2^{-\Delta\Delta Ct}$ method.

Statistical Analysis

Statistical analyses were conducted using SPSS software (version 22, SPSS, Chicago, IL, USA) for the clinical data and relative gene expression levels. Between microarray analysis ($n = 9$) and qRT-PCR ($n = 30$) groups, continuous (age, age at onset, time course, and hearing threshold) and categorical (gender, family history, delayed MD, headache, migraine, autoimmune disease, hearing stage, and steroid treatment) variables were compared using the Mann–Whitney test or Fisher's exact test. The relative gene expression levels obtained from qRT-PCR between MD and normal control samples were compared using Student's *t*-test, and the correlation between the clinical data and relative gene expression levels were analyzed using Pearson's correlation coefficient. The significance criterion was set at $p < 0.05$.

RESULTS

Demographic and Clinical Characteristics

Detailed demographic and clinical characteristics of the patients are described in **Table 1**. The mean age at onset and time course was 57.5 ± 8.1 and 7.5 ± 4.3 years, respectively. It was found that three patients (7.7%) had a family history of episodic vertigo or SNHL. In total, 11 patients (28.2%) experienced a headache during attacks, but only one patient had migraine-type headache. In addition, four patients (10.3%) had a history of autoimmune diseases, such as rheumatoid arthritis ($n = 2$), inflammatory bowel disease ($n = 1$), and autoimmune hypothyroidism ($n = 1$). Nine patients (23.1%) had taken oral prednisolone or intratympanic dexamethasone injection to relieve vertigo attacks, all of whom showed a good response. There were no significant differences in demographic and clinical characteristics between the microarray analysis group ($n = 9$) and the qRT-PCR group ($n = 30$).

DEG Identification by Microarray Analysis

The reproducibility tests using Pearson's correlation test and MDS showed that there were positive correlations among the samples in the MD and control groups, and there was a great difference in gene expression patterns between the two groups (**Figures 1A,B**). These results indicate that the homogeneity of samples in the MD group and the heterogeneity of samples between the two groups.

The DEGs between the MD and control groups are depicted on the volcano plot in **Figure 1C**. Hierarchical cluster analysis of the upregulated and downregulated DEGs revealed distinctive expression patterns between them (**Figure 1D**). Based on the cut-off criteria (|fold changes| > 2 and adjusted *p*-value < 0.05), a total of 996 DEGs were detected between the MD and control samples, comprising 415 upregulated DEGs and 581 downregulated DEGs in the MD group (**Supplementary Table 1**). However, the number of DEGs with |fold changes| > 3 was considerably larger in the down-regulated DEGs than in the up-regulated DEGs (169 vs. 36). Furthermore, there were 41 genes with a distinct expression level (|fold changes| > 5) among the downregulated DEGs but only four among the upregulated DEGs.

Functional Enrichment Analysis of DEGs

The GO enrichment analysis was performed on all DEGs to identify their underlying functions. The upregulated DEGs were mostly enriched in BP terms for cellular

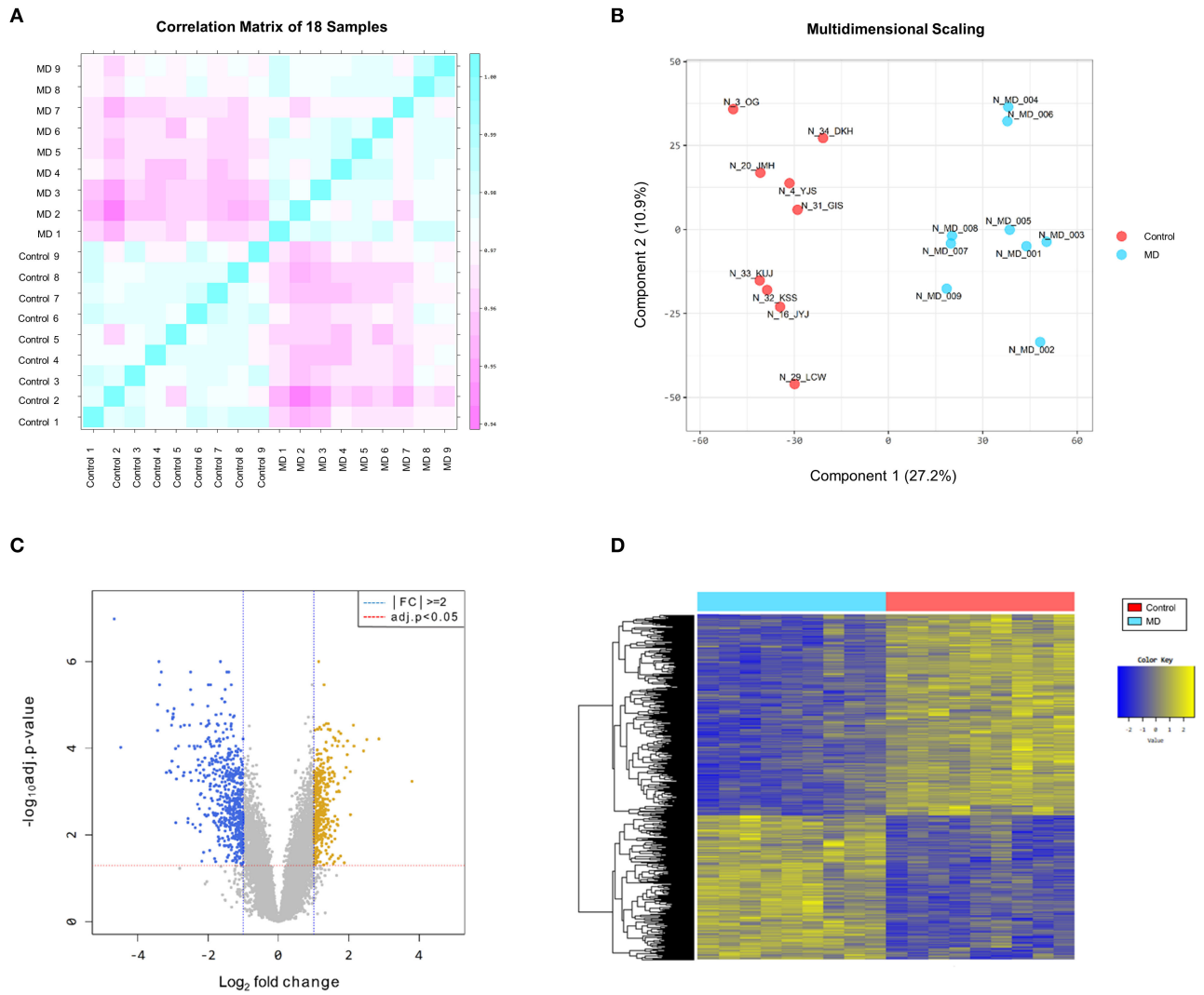

FIGURE 1 | (A) Pearson's correlation analysis of samples. The color reflects the intensity of the correlation. The closer the correlation coefficient is to 1, the more it represents the blue color. There are strong correlations among the samples in the Meniere's disease (MD) and control groups. **(B)** Multidimensional scaling of samples. There is a great difference in gene expression patterns between the MD (blue color) and control (red color) groups. **(C)** The volcano plot of differentially expressed genes (DEGs). Based on the cut-off criteria (|fold changes| > 2.0 and adjusted *p*-value < 0.05), 996 DEGs are identified between the MD and control samples, comprising 415 upregulated (yellow dots) and 581 downregulated (blue dots) in the MD group. **(D)** The results of a hierarchical clustering analysis of upregulated and downregulated DEGs between the MD and control groups. Each group includes nine individuals and each column represents one individual's sample. The yellow and blue colors indicate high and low relative expression levels, respectively.

localization and cellular metabolic processes, in CC terms for intracellular anatomical structure, and in MF terms for binding (**Supplementary Figure 1**). In contrast, most of the downregulated enrichments were related to BP terms for immune system processes, such as leukocyte activation, lymphocyte activation, and cellular response to cytokine stimulus (**Figure 2A**). For CC and MF, the downregulated DEGs were also enriched in terms related to the immune system processes, such as the major histocompatibility complex (MHC) class II protein complex, beta-catenin-TCF complex, MHC protein complex binding, and MHC class I protein binding (**Figures 2B,C**).

Validation of Downregulated DEGs by qRT-PCR

The GO enrichment analysis indicated that most upregulated DEGs were enriched in non-specific terms, whereas the downregulated DEGs were mostly enriched in terms for immune system processes. Among them, specific terms associated with the MHC protein complex were deemed to be of particular interest (**Table 2**) since different HLA gene alleles have been reported among patients with MD (6–11). In total, 17 genes were enriched in terms for MHC protein complex (**Table 3**), and the three markedly downregulated DEGs (fold changes < −5: HLA-DMA, HLA-DRB1, and HLA-DPB1) were analyzed to verify their

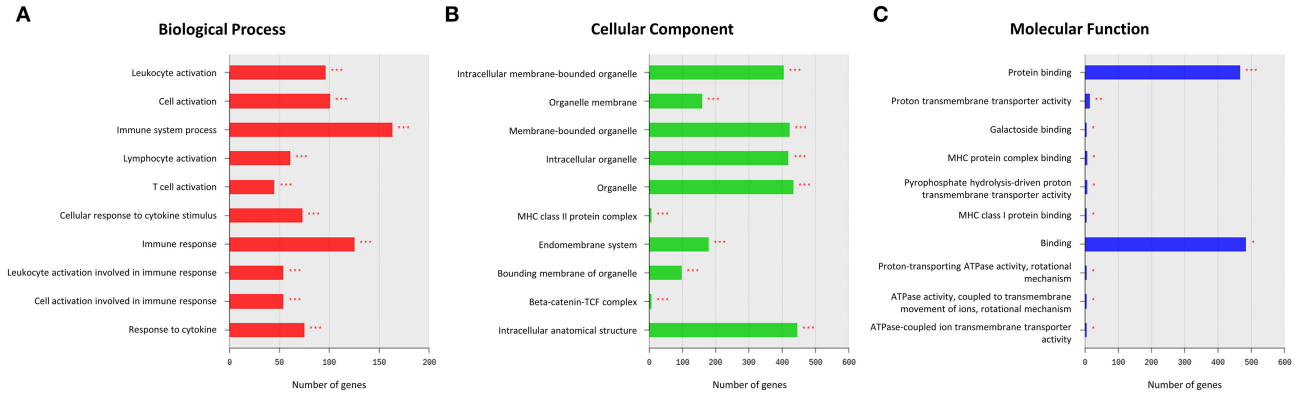

FIGURE 2 | Results of a Gene Ontology (GO) enrichment analysis of downregulated differentially expressed genes (DEGs) in the MD group. The top enriched GO terms for the biological process (BP) **(A)**, cellular component (CC) **(B)**, and molecular function (MF) **(C)** are shown. The *x*-axis represents the number of genes enriched in each GO term. The *y*-axis represents GO terms with adjusted *p*-values of <0.05 (*), <0.01 (**), and <0.001 (***).

TABLE 2 | Gene Ontology (GO) terms associated with the major histocompatibility complex (MHC) protein complex in downregulated differentially expressed genes (DEGs).

GO term	Specific term	*p*-value	Down-regulated DEGs
BP	GO:0002396-MHC protein complex assembly	3.4186e-05	*HLA-DMA, HLA-DRB1, HLA-DMB, TAPBPL, TAPBP*
	GO:0002501-peptide antigen assembly with MHC protein complex	0.00042583	*HLA-DMA, HLA-DRB1, HLA-DMB, TAPBPL*
	GO:0002399-MHC class II protein complex assembly	0.00277812	*HLA-DMA, HLA-DRB1, HLA-DMB*
	GO:0002503-peptide antigen assembly with MHC class II protein complex	0.00277812	*HLA-DMA, HLA-DRB1, HLA-DMB*
	GO:0019886-antigen processing and presentation of exogenous peptide antigen *via* MHC class II	0.00838024	*HLA-DMA, HLA-DRB1, HLA-DPB1, HLA-DMB, HLA-DOA, HLA-DPA1, FCER1G, CTSD, HLA-DQB1, DCTN3*
	GO:0002495-antigen processing and presentation of peptide antigen *via* MHC class II	0.01050122	*HLA-DMA, HLA-DRB1, HLA-DPB1, HLA-DMB, HLA-DOA, HLA-DPA1, FCER1G, CTSD, HLA-DQB1, DCTN3*
	GO:0002504-antigen processing and presentation of peptide or polysaccharide antigen *via* MHC class II	0.0127228	*HLA-DMA, HLA-DRB1, HLA-DPB1, HLA-DMB, HLA-DOA, HLA-DPA1, FCER1G, CTSD, HLA-DQB1, DCTN3*
	GO-2001190-positive regulation of T cell activation *via* T cell receptor contact with antigen bound to MHC molecule on antigen presenting cell	0.03779741	*LGALS9, HLA-DMB*
	GO-0002397-MHC class I protein complex assembly	0.03779741	*TAPBP, TAPBL*
CC	GO:0042613-MHC class II protein complex	1.0895e-05	*HLA-DMA, HLA-DRB1, HLA-DPB1, HLA-DMB, HLA-DOA, HLA-DPA1, HLA-DQB1*
	GO:0042611-MHC protein complex	0.00012583	*HLA-DMA, HLA-DRB1, HLA-DPB1, HLA-DMB, HLA-DOA, HLA-DPA1, HLA-DQB1*
MF	GO:0023023-MHC protein complex binding	0.01041392	*HLA-DMA, HLA-DRB1, HLA-DOA, LILRB2, HLA-DMB, TAPBPL*
	GO:0042288-MHC class I protein binding	0.02513155	*TAPBP, LILRB2, TUBB, PILRA, PILRB*

BP, biological process; CC, cellular component; DEG, differentially expressed gene; GO, gene ontology; MF, molecular function; MHC, major histocompatibility complex.

expression levels using qRT-PCR. The primer sequences used in the PCR analysis are listed in **Supplementary Table 2**. As shown in **Figure 3**, the relative mRNA expression levels of HLA-DMA, HLA-DRB1, and HLA-DPB1 were significantly decreased in 30 patients with MD compared with normal controls, which was consistent with the microarray data. However, there were no correlations between the expression levels of the three genes and clinical data, such as age, onset age, time course, or hearing threshold (**Table 4**).

DISCUSSION

Our transcriptome analysis revealed about 1,000 genes that were expressed differentially between the MD and control samples, comprising 415 upregulated and 581 downregulated genes in the MD group. However, the number of genes with markedly different expression levels was considerably larger in the downregulated than in the upregulated DEGs, the former being mostly enriched in terms of immune system processes,

such as MHC class II according to the bioinformatics analysis. Furthermore, qRT-PCR indicated that the expression levels of the three genes associated with MHC class II (HLA-DMA, HLA-DRB1, and HLA-DPB1) were significantly decreased in the validation cohort. These findings highlight a role of MHC class II in the immune system for MD pathogenesis.

In humans, the MHC class II protein complex is encoded by the HLA gene complex, such as HLA-DP, -DQ, -DR, -DM, and -DO (25). The MHC class II molecules are usually found on antigen-presenting cells, such as dendritic cells, macrophages, and B cells, and they play an important role in the immune system by presenting foreign antigens to $CD4^+$ T cells. This process is not only significant for the immune responses protecting against invading pathogens but also for self-tolerance maintenance (26). Indeed, specific allele polymorphisms of HLA genes have been found to be associated with susceptibility or resistance to various autoimmune diseases, such as rheumatoid arthritis, autoimmune hepatitis, and type 1 diabetes mellitus (27–29). Autoimmunity seems to be involved in the pathogenesis of some inner ear diseases, such as rapidly progressive bilateral SNHL and autoimmune inner ear disease. Similarly, it was speculated that MD might be associated with autoimmunity or immune-mediated process based on the increased prevalence of autoimmune diseases, the increased levels of autoantibodies, and the positive response to steroid therapy in MD (2–5). Among the included patients in the present study, some also had concurrent autoimmune diseases and showed a good response to steroid therapy.

Previous studies have investigated the association between HLA and MD and found that several HLA alleles, such as DRB1*1602, DRB1*0405, and DRB1*1101 were significantly increased or decreased in patients with MD (6–11). However, the results varied with the racial background, and the association was usually observed in specific groups of MD, such as DRB1*0405 in the anti-type II collagen antibody positive group and DRB1*1101 in bilateral MD (10, 11). Nevertheless, the association between HLA alleles and MD indicates that immunological alterations are involved with the MD pathogenesis. In the present study, many genes encoding MHC class II protein complex were downregulated in the MD group, which suggests that MHC class II offers resistance

TABLE 3 | Downregulated DEGs associated with the MHC protein complex.

Gene	Transcript ID	Fold change	Adjusted *p*-value
HLA-DMA	NM_006120	−7.819839	1.22843e-05
HLA-DRB1	NM_001243965	−6.434097	0.000362027
HLA-DPB1	NM_002121	−5.561917	0.000559052
LGALS9	NM_002308	−4.679215	0.00825859
TAPBPL	NM_018009	−3.642073	0.00018587
CTSD	NM_001909	−3.184350	0.00150167
FCER1G	NM_004106	−3.173098	0.00031412
HLA-DQB1	NM_001243961	−2.684463	0.01759631
LILRB2	NM_001080978	−2.619737	0.00048716
HLA-DMB	ENST00000414017	−2.599851	0.00010508
HLA-DPA1	NM_001242525	−2.528845	0.02204052
TAPBP	NM_003190	−2.486889	0.00909216
PILRA	NM_013439	−2.150609	0.00871555
DCTN3	NM_001281425	−2.119261	0.00042982
HLA-DOA	NM_002119	−2.106123	0.00434074
PILRB	NM_178238	−2.059781	0.00976276
TUBB	NM_001293214	−2.030527	0.00942943

DEG, differentially expressed gene; MHC, major histocompatibility complex.

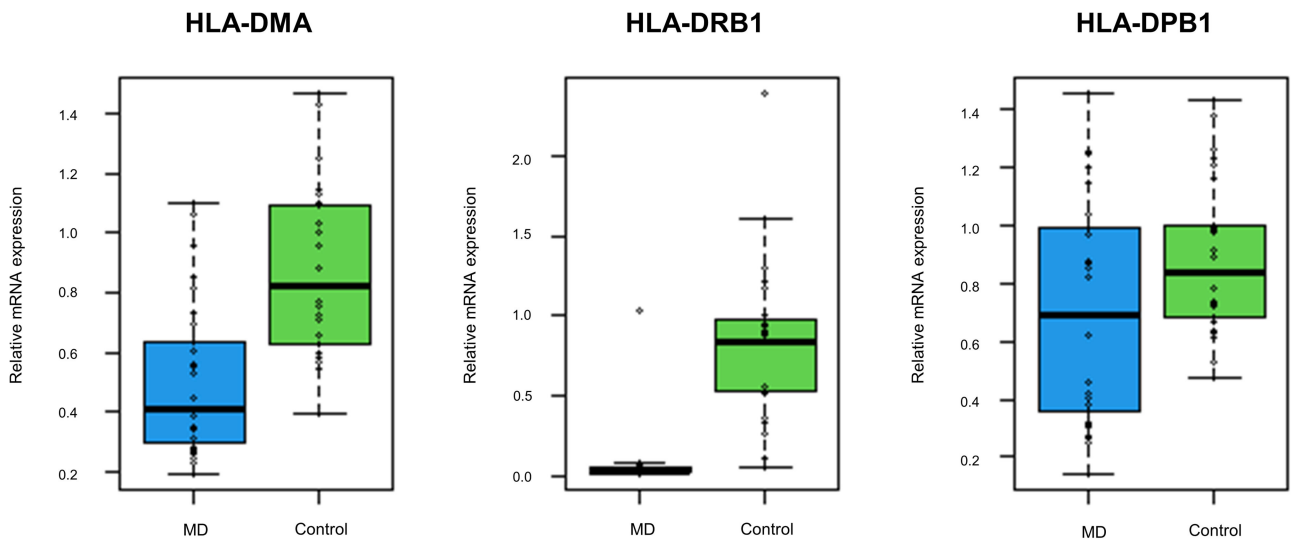

FIGURE 3 | The expression levels of the top three downregulated differentially expressed genes (DEGs) associated with the MHC protein complex using quantitative reverse transcription-polymerase chain reaction (qRT-PCR). Compared with normal controls, the mRNA expression levels of human leukocyte antigen (HLA)-DMA, HLA-DRB1, and HLA-DPB1 are significantly decreased in 30 validation cohort with the MD ($p < 0.001$, $p < 0.001$, and $p = 0.026$, respectively).

TABLE 4 | The correlation analysis between gene expression levels and clinical characteristics.

	HLA-DMA	*HLA-DRB1*	*HLA-DPB1*
Age	$r = -0.007$, $p = 0.972$	$r = 0.025$, $p = 1.000$	$r = 0.145$, $p = 0.454$
Onset age	$r = -0.147$, $p = 0.446$	$r = -0.012$, $p = 0.951$	$r = 0.020$, $p = 0.920$
Time course	$r = 0.313$, $p = 0.099$	$r = 0.247$, $p = 0.196$	$r = 0.211$. $p = 0.272$
PTA threshold	$r = 0.202$, $p = 0.293$	$r = 0.242$, $p = 0.205$	$r = 0.156$, $p = 0.419$

PTA, pure tone audiometry.

to MD development. It is still unclear whether this finding is directly related to MD pathogenesis or merely reflects an epiphenomenon caused by recurrent MD attacks. However, there was no obvious relationship between the expression levels of three major HLA genes and clinical data, such as age, onset age, time course, or hearing threshold, suggesting that the decreased expression levels of HLA genes were not caused by recurrent MD attacks. Perhaps, the downregulation of MHC class II protein complex would result in a breakdown in immunological tolerance to the underlying pathogens or self-antigens of MD. Several possible mechanisms could contribute to the downregulation of MHC class II protein complex, such as haplotype-specific variation, epigenetic mechanism, or environmental factors (26). Further studies are needed to investigate the role of the MHC class II protein complex in MD development.

The present study was subject to some potential limitations. First, we obtained gene expression profiling from the total RNA of peripheral PBMCs. This approach may not determine whether immunological alterations in peripheral blood levels greatly influence the initiation of specific immune responses in the inner ear. Thus, transcriptome analysis using endolymph in the inner ear could be a better method for identifying the underlying pathogenesis of MD. Second, we have verified expression levels of only three down-regulated DEGs by qRT-PCR. It is possible that there are discrepancies in the expression levels between microarray analysis and qRT-PCR. Thus, the expression levels of more DEGs should be validated using qRT-PCR for a large number of patients. However, the results of qRT-PCR for three DEGs were consistent with those of microarray analysis, and the reproducibility tests showed the homogeneity of samples in each (MD and control) group and the heterogeneity of samples between the two groups, suggesting that the intra-group data repeatability might be acceptable.

In conclusion, our transcriptome analysis identified the downregulated DEGs associated with the immune system pathway in MD. The findings of our bioinformatics analysis indicate that these DEGs are likely to contribute to MD development through a breakdown in immunological tolerance mediated by the MHC class II protein complex. The findings of the present study have meaningful implications for further biological investigations and targeted treatment for MD.

DATA AVAILABILITY STATEMENT

The datasets presented in this study can be found in online repositories. The name of the repository and accession number can be found below: National Center for Biotechnology Information (NCBI) Gene Expression Omnibus (GEO), https://www.ncbi.nlm.nih.gov/geo/query/acc.cgi?acc=GSE202657.

ETHICS STATEMENT

All experiments followed the tenets of the Declaration of Helsinki, and informed consents were obtained after the nature and possible consequences of this study had been explained to the participants. This study was approved by the institutional review boards of Pusan National University Yangsan Hospital (04-2020-029).

AUTHOR CONTRIBUTIONS

K-DC conducted the experiments and interpretation of the data, and wrote the manuscript. EO, HK, J-YP, and SC contributed to the interpretation and analysis of data. H-SK performed the experiment. J-HC conducted the design and conceptualization of the study, interpretation of the data, and revised the manuscript. All authors contributed to the article and approved the submitted version.

FUNDING

This research was supported by the Basic Science Research Program through the National Research Foundation of Korea funded by the Ministry of Education (NRF-2020R1I1A3071617).

SUPPLEMENTARY MATERIAL

The Supplementary Material for this article can be found online at: https://www.frontiersin.org/articles/10.3389/fneur.2022.938740/full#supplementary-material

REFERENCES

1. Lopez-Escamez JA, Carey J, Chung WH, Goebel JA, Magnusson M, Mandalà M, et al. Diagnostic criteria for Meniere's disease. *J Vestib Res.* (2015) 25:1–7. doi: 10.3233/VES-150549
2. Frejo L, Martín-Sanz E, Teggi R, Trinidad G, Soto-Varela A, Santos-Perez S, et al. Extended phenotype and clinical subgroups in unilateral Meniere disease: a cross-sectional study with cluster analysis. *Clin Otolaryngol.* (2017) 42:1172–80. doi: 10.1111/coa.12844

3. Frejo L, Soto-Varela A, Santos S, Aran I, Batuecas-Caletrio A, Perez-Guillen V, et al. Clinical subgroups in bilateral Meniere disease. *Front Neurol.* (2016) 7:182. doi: 10.3389/fneur.2016.00182
4. Kim SH, Kim JY, Lee HJ Gi M, Kim BG, Choi JY. Autoimmunity as a candidate for the etiopathogenesis of Meniere's disease: detection of autoimmune reactions and diagnostic biomarker candidate. *PLoS ONE.* (2014) 9:e111039. doi: 10.1371/journal.pone.0111039
5. Gazquez I, Soto-Varela A, Aran I, Santos S, Batuecas A, Trinidad G, et al. High prevalence of systemic autoimmune diseases in patients with Menere's disease. *PLoS ONE.* (2011) 6:e26759. doi: 10.1371/journal.pone.0026759
6. Xenellis J, Morrison AW, McClowskey D, Festenstein H, HLA. antigens in the pathogenesis of Meniere's disease. *J Laryngol Otol.* (1986) 100:21–4. doi: 10.1017/S0022215100098698
7. Bumm P, Muller EC, Grimm-Muller U, Schlimok G. T-lymphocyte subpopulation and HLA-DR antigens in hearing loss of vestibular neuropathy, Meniere's disease and Bell's palsy. *Laryngorhinootologie.* (1991) 70:260–6. doi: 10.1055/s-2007-998033
8. Koyama S, Mitsuishi Y, Bibee K, Watanabe I, Terasaki PI, HLA. associations with Meniere's disease. *Acta Otolaryngol.* (1993) 113:575–8. doi: 10.3109/00016489309135866
9. Melchiorri L, Martini A, Rizzo R, Berto A, Adinolfi E, Baricord OR. Human leukocyte antigen-A, -B, -C and -DR alleles and soluble human leukocyte antigen class I serum level in Meniere's disease. *Acta Otolaryngol Suppl.* (2002) 548:26–9. doi: 10.1080/00016480260094938
10. Koo JW, Oh SH, Chang SO, Park MH, Lim MJ, Yoo TJ, et al. Association of HLA-DR and type II collagen autoimmunity with Meniere's disease. *Tissue Antigens.* (2003) 61:99–103. doi: 10.1034/j.1399-0039.2003.610112.x
11. Lopez-Escamez JA, Vilchez JR, Soto-Varela A, Santos-Perez S, Perez-Garrigues H, Aran I, et al. HLA-DRB1*1101 allele may be associated with bilateral Meniere's disease in southern European population. *Otol Neurotol.* (2007) 28:891–5. doi: 10.1097/MAO.0b013e3180dca1cc
12. Requena T, Espinosa-Sanchez JM, Cabrera S, Trinidad G, Soto-Varela A, Santos-Perez S, et al. Familial clustering and genetic heterogeneity in Meniere's disease. *Clin Genet.* (2014) 85:245–52. doi: 10.1111/cge.12150
13. Lee JM, Kim MJ, Jung J, Kim HJ, Seo YJ, Kim SH. Genetic aspects and clinical characteristics of familial Meniere's disease in a South Korean population. *Laryngoscope.* (2015) 125:2175–80. doi: 10.1002/lary.25207
14. Requena T, Cabrera S, Martin-Sierra C, Price SD, Lysakowski A, Lopez-Escamez JA. Identification of two novel mutations in FAM136A and DTNA genes in autosomal-dominant familial Meniere's disease. *Hum Mol Genet.* (2015) 24:1119–26. doi: 10.1093/hmg/ddu524
15. Martín-Sierra C, Requena T, Frejo L, Price SD, Gallego-Martinez A, Batuecas-Caletrio A, et al. A novel missense variant in PRKCB segregates low-frequency hearing loss in an autosomal dominant family with Meniere's disease. *Hum Mol Genet.* (2016) 25:3407–15. doi: 10.1093/hmg/ddw183
16. Martín-Sierra C, Gallego-Martinez A, Requena T, Frejo L, Batuecas-Caletrío A, Lopez-Escamez JA. Variable expressivity and genetic heterogeneity involving DPT and SEMA3D genes in autosomal dominant familial Meniere's disease. *Eur J Hum Genet.* (2017) 25:200–7. doi: 10.1038/ejhg.2016.154
17. Oh EH, Shin JH, Kim HS, Cho JW, Choi SY, Choi KD, et al. Rare variants of putative candidate genes associated with sporadic Meniere's disease in east Asian population. *Front Neurol.* (2020) 10:1424. doi: 10.3389/fneur.2019.01424
18. Gallego-Martinez A, Lopez-Escamez JA. Genetic architecture of Meniere's disease. *Hear Res.* (2020) 397:107872. doi: 10.1016/j.heares.2019.107872
19. Oh EH, Rhee JK, Shin JH, Cho JW, Kim DS, Park JY, et al. Neutrophil-mediated immune response as a possible mechanism of acute unilateral vestibulopathy. *J Vestib Res.* (2020) 30:363–74. doi: 10.3233/VES-200044
20. Xia L, Yue Y, Li M, Zhang YN, Zhao L, Lu W, et al. CNN3 acts as a potential oncogene in cervical cancer by affecting RPLP1 mRNA expression. *Sci Rep.* (2020) 10:2427. doi: 10.1038/s41598-020-58947-y
21. Palmer NP, Silvester JA, Lee JJ, Beam AL, Fried I, Valtchinov VI, et al. Concordance between gene expression in peripheral whole blood and colonic tissue in children with inflammatory bowel disease. *PLoS ONE.* (2019) 14:e0222952. doi: 10.1371/journal.pone.0222952
22. Swindell WR, Sarkar MK, Liang Y, Xing X, Gudjonsson JE. Cross-disease transcriptomics: unique IL-17A signaling in psoriasis lesions and an autoimmune PBMC signature. *J Invest Dermatol.* (2016) 136:1820–30. doi: 10.1016/j.jid.2016.04.035
23. Sun Y, Zhang D, Sun G, Lv Y, Li Y, Li X, et al. RNA-sequencing study of peripheral blood mononuclear cells in sporadic Ménière's disease patients: possible contribution of immunologic dysfunction to the development of this disorder. *Clin Exp Immunol.* (2018) 192:33–45. doi: 10.1111/cei.13083
24. Flook M, Frejo L, Gallego-Martinez A, Martin-Sanz E, Rossi-Izquierdo M, Amor-Dorado JC, et al. Differential proinflammatory signature in vestibular migraine and Meniere disease. *Front Immunol.* (2019) 10:1229. doi: 10.3389/fimmu.2019.01229
25. Watts C. The exogenous pathway for antigen presentation on major histocompatibility complex class II and CD1 molecules. *Nat Immunol.* (2004) 5:685–92. doi: 10.1038/ni1088
26. Handunnetthi L, Ramagopalan SV, Ebers GC, Knight JC. Regulation of MHC class II gene expression, genetic variation and disease. *Genes Immun.* (2010) 11:99–112. doi: 10.1038/gene.2009.83
27. Gonzalez-Gay MA, Garcia-Porrua C, Hajeer AH. Influence of human leucocyte antigen DRA1 on the susceptibility and severity of rheumatoid arthritis. *Semin Arthritis Rheum.* (2002) 31:355–60. doi: 10.1053/sarh.2002.32552
28. Vázquez-García MN, Aláez C, Olivo A, Debaz H, Pérez-Luque E, Burguete A, et al. MHC class II sequences of susceptibility and protection in Mexicans with autoimmune hepatitis. *J Hepatol.* (1998) 28:985–90. doi: 10.1016/S0168-8278(98)80347-4
29. Nerup J, Platz P, Andersen OO, Christy M, Lyngsoe J, Poulsen JE, et al. HL-A antigens and diabetes mellitus. *Lancet.* (1974) 2:864–6. doi: 10.1016/S0140-6736(74)91201-X

Conflict of Interest: The authors declare that the research was conducted in the absence of any commercial or financial relationships that could be construed as a potential conflict of interest.

Publisher's Note: All claims expressed in this article are solely those of the authors and do not necessarily represent those of their affiliated organizations, or those of the publisher, the editors and the reviewers. Any product that may be evaluated in this article, or claim that may be made by its manufacturer, is not guaranteed or endorsed by the publisher.

Copyright © 2022 Choi, Oh, Kim, Kim, Park, Choi and Choi. This is an open-access article distributed under the terms of the Creative Commons Attribution License (CC BY). The use, distribution or reproduction in other forums is permitted, provided the original author(s) and the copyright owner(s) are credited and that the original publication in this journal is cited, in accordance with accepted academic practice. No use, distribution or reproduction is permitted which does not comply with these terms.

frontiers | Frontiers in Neurology

TYPE Original Research
PUBLISHED 25 July 2022
DOI 10.3389/fneur.2022.937703

Check for updates

OPEN ACCESS

EDITED BY
Sun-Young Oh,
Jeonbuk National University,
South Korea

REVIEWED BY
Young Sang Cho,
Sungkyunkwan University, South Korea
Wuqing Wang,
Fudan University, China

*CORRESPONDENCE
Ja-Won Koo
jwkoo99@snu.ac.kr

SPECIALTY SECTION
This article was submitted to
Neuro-Otology,
a section of the journal
Frontiers in Neurology

RECEIVED 06 May 2022
ACCEPTED 28 June 2022
PUBLISHED 25 July 2022

CITATION
Han SC, Kim YS, Kim Y, Lee S-Y, Song J-J, Choi BY, Kim J-S, Bae YJ and Koo J-W (2022) Correlation of clinical parameters with endolymphatic hydrops on MRI in Meniere's disease. *Front. Neurol.* 13:937703.
doi: 10.3389/fneur.2022.937703

COPYRIGHT
© 2022 Han, Kim, Kim, Lee, Song, Choi, Kim, Bae and Koo. This is an open-access article distributed under the terms of the Creative Commons Attribution License (CC BY). The use, distribution or reproduction in other forums is permitted, provided the original author(s) and the copyright owner(s) are credited and that the original publication in this journal is cited, in accordance with accepted academic practice. No use, distribution or reproduction is permitted which does not comply with these terms.

Correlation of clinical parameters with endolymphatic hydrops on MRI in Meniere's disease

Seung Cheol Han[1], Young Seok Kim[1], Yehree Kim[1], Sang-Yeon Lee[2], Jae-Jin Song[1], Byung Yoon Choi[1], Ji-Soo Kim[3], Yun Jung Bae[4] and Ja-Won Koo[1,5]*

[1]Department of Otorhinolaryngology, Seoul National University College of Medicine, Seoul National University Bundang Hospital, Seongnam, South Korea, [2]Department of Otorhinolaryngology, Seoul National University College of Medicine, Seoul National University Hospital, Seoul, South Korea, [3]Department of Neurology, Seoul National University College of Medicine, Seoul National University Bundang Hospital, Seongnam, South Korea, [4]Department of Radiology, Seoul National University College of Medicine, Seoul National University Bundang Hospital, Seongnam, South Korea, [5]Sensory Organ Research Institute, Seoul National University Medical Research Center, Seoul, South Korea

A clinical diagnosis of Ménière's disease (MD) is made based on medical history and audiometry findings. The 1995 American Academy of Otolaryngology-Head and Neck Surgery (AAO-HNS) guidelines requires histopathological confirmation of endolymphatic hydrops (EH) for a diagnosis of "certain" MD. Symptoms such as dizziness and ear fullness are important diagnostic features; however, the descriptions provided by patients are frequently vague and non-specific. A recently developed magnetic resonance imaging (MRI) protocol to document EH is, therefore, useful for the evaluation of inner ear status in patients with MD. In this study, patients with MD were assessed using MRI and the HYDROPS (HYbriD of Reversed image Of Positive endolymph signal and native image of positive perilymph Signal) protocol to investigate the effectiveness of MRI for visualization of the endolymphatic space in the diagnosis of MD by correlating clinical laboratory parameters with the grade of EH. Of the 123 patients with MD recruited in this study, 80 had definite MD, 11 had probable MD, and 32 had possible MD based on the 1995 AAO-HNS guidelines. The EH grade based on HYDROPS MRI was determined independently by two otorhinolaryngologists and compared with several clinical parameters, including the diagnostic scale of MD (1995 AAO-HNS guidelines), pure tone average (PTA), low tone average (LTA), canal paresis (CP) on the caloric test, and disease duration. Cochlear hydrops and vestibular hydrops were detected in 58 and 80% of 80 definite MD ears, in 33 and 58% of 12 probable MD ears, and in 5 and 27% of 37 possible MD ears, respectively. The proportion of higher hydrops grades increased significantly with grade according to the MD diagnostic scale ($p < 0.0001$). Both PTA and LTA were significantly higher in patients with hydrops grade 2 than hydrops grade 0 in both the cochlea and the vestibule. CP was significantly higher in

patients with grade 2 than grade 0 vestibular hydrops. Disease duration was not associated with hydrops grade. Radiological evaluation of MD using the HYDROPS protocol is useful for evaluation of the extent and severity of EH in the diagnosis of MD based on its pathophysiological mechanism.

KEYWORDS

Meniere disease, endolymphatic hydrops, labyrinth diseases, magnetic resonance imaging, clinical features

Introduction

Ménière's disease (MD) is a multifactorial disorder characterized by recurrent vertigo, fluctuating hearing change, ear fullness, and tinnitus. According to the 1995 Hearing and Equilibrium guidelines of the American Academy of Otorhinolaryngology-Head and Neck Surgery Committee (AAO-HNS), histopathological confirmation of endolymphatic hydrops (EH) is required for a diagnosis of "certain" MD. However, diagnosis of "certain" MD is practically impossible in living patients (1).

Some patients with cochleovestibular symptoms but who do not satisfy the criteria of the MD diagnostic guidelines may have EH, which is universally recognized as a component of MD pathogenesis (2–5). In contrast, not all patients with clinically diagnosed MD have endolymphatic hydrops (6–9). Furthermore, EH may be asymptomatic; when suspected, it must be distinguished from other otological disorders, such as inner ear trauma (1), viral infection, autoimmune processes (10), and cellular channelopathies (11).

A number of techniques have been developed to visualize EH using magnetic resonance imaging (MRI). In 2007, MRI visualization of the inner ear was facilitated by the intravenous (IV) injection of gadolinium-based contrast material (Gd) (12), rather than intratympanic (IT) injection (13). In MRI of the inner ear, despite the 4-h delay after injection, IV-Gd is faster and much less invasive than IT-Gd (14, 15). However, unlike MRI using IT-Gd, IV-Gd does not permit 3D inversion recovery sequences with a "real" reconstruction protocol (3D-real IR protocol) (16); the lower concentration of Gd in such sequences enables separate visualization of endolymph, perilymph, and bone in a single image. The recently developed "HYDROPS" (HYbriD of the reversed image of positive endolymph signal and native image of positive perilymph signal) imaging protocol addresses this limitation by enabling recognition of the endolymphatic space (17).

Further advances have yielded HYDROPS2, HYDROPS-Mi2, and HYDROPS2-Mi2, which use MR cisternography for better contrast in the production of positive perilymph images (PPIs) and positive endolymph images (PEIs) (18). Combined with the ratio of the endolymphatic space to the entire lymphatic space (%EL), the vestibular hydrops ratio (%VH), or the relative vestibular hydrops ratio (%RVH), these perilymph and endolymph images have been used in attempts to identify inner ear MRI findings associated with the clinical parameters of MD (19, 20). However, most studies have been performed only on small population of patients with definite MD who already have severe symptoms. In addition, it can be inferred that these patients have higher rates of severe EH. Therefore, the correlation between the clinical characteristics of MD and EH from MRI findings should be examined depending on the diagnostic scale of MD (possible, probable, and definite) and even unaffected subjects, determining the wider correlations between the severity of EH and clinical characteristics of patients with MD.

In this study, patients with clinically diagnosed MD defined according to the diagnostic scale of the 1995 AAO-HNS guidelines were examined by HYDROPS MRI. The correlations of EH grades based on HYDROPS MRI (21) with clinical and laboratory parameters were examined.

Materials and methods

Study setting and patients

HYDROPS MRI was performed in 166 patients with recurrent vertigo and hearing problems between 1 January 2020 and 31 August 2021. Detailed history taking, neurotological evaluation, and audiovestibular laboratory tests were performed. Forty-three patients were excluded due to tumors in the cerebellopontine angle, internal auditory canal, or inner ear; superior canal dehiscence syndrome; or recurrent dizziness that did not meet the diagnostic criteria of MD (1995 AAO-HNS guidelines). Finally, 123 patients (49 men, 74 women, mean age of 58.9 years) were included in this study. Based on the 1995 AAO-HNS guidelines, 32 patients had possible MD, 11 had probable MD, and 80 had definite MD. The left side was involved in 68 patients, while the right side was involved in 49 patients. Of the remaining six patients with bilateral MD, five had possible MD and one had probable MD. Among the 117 patients with unilateral MD, the contralateral side was clinically unaffected. Therefore, based on the MD classification, there were

TABLE 1 Demographic characteristics of 123 patients diagnosed with Ménière's disease.

Sex (male:female)	49:74
Age (years)	58.96 ± 13.63
Affected side (right:left:bilateral)	49:68:6
Unaffected:affected ears	117:129
Disease classification (definite:probable:possible)	80:11:32

117 unaffected ears and 129 affected (37 possible, 12 probable, and 80 definites) ears (Table 1). This study was approved by the review board of the Clinical Research Institute at Seoul National Bundang Hospital and was conducted in accordance with the Declaration of Helsinki (IRB-B-2111-720-106).

Inner ear MRI

MRI was performed using a 3.0 Tesla machine (Ingenia CX; Philips, Amsterdam, The Netherlands). MR scanning was performed 4 h after IV injection of Gadobutrol (Gadovist; Bayer, Leverkusen, Germany) (0.1 mmol/kg body weight).

Heavily T2-weighted MR cisternography (MRC) was performed for the anatomical reference of the total lymph fluid. Heavily T2-weighted-3D-FLAIR (hT2W-3D-FLAIR) scan with a repetition time (TR) of 16,000 ms was performed, with an inversion time of 2,900 ms at 4 h after IV injection of Gadobutrol in accordance with a previous report (22) and to distinguish PPI from other images. The hT2W-3D-FLAIR scan was performed with the same TR and inversion time of 2,000 ms at 4 h after IV injection of Gadobutrol to distinguish PEI. The perilymph signal is increased in images with an inversion time of 2,900 ms and suppressed in images with an inversion time of 2,000 ms. The endolymph signal is increased in images with an inversion time of 2,000 ms. The HYDROPS image was obtained by subtracting PEI from PPI at the scanner console. Negative signal values were allowed for the subtraction.

Detailed parameters for PPI and PEI were as follows: FLAIR–volume isotropic turbo spin-echo acquisition sequence; repetition time, 16,000 ms; echo time, 544 ms; echo train length, 173; matrix size, 332 × 328 mm; slice thickness, 1.6 mm; field of view, 200 × 200 mm; sensitivity encoding acceleration factor, two; number of excitations, two; scan time, 3 min 45 s.

Image analysis

Two otorhinolaryngologists blinded to the patient's clinical information, including disease site and history, independently rated the hydrops grade of the cochlea and vestibule using the grading system proposed by Nakashima et al. (21).

Briefly, in the cochlea, displacement of Reissner's membrane was defined as EH. Patients in whom the area of the cochlear duct exceeded the area of the scala vestibuli were diagnosed with significant hydrops. If the grade of EH differed between the basal and upper turns, a higher grade of EH was reported. In the vestibule, EH was defined as a ratio of the area of the endolymphatic space to that of the vestibular fluid space exceeding 1/3. Patients in whom the endolymphatic space was >50% of the fluid area in the vestibule were diagnosed with significant hydrops. Grade 0 was defined as no EH, grade 1 as mild EH, and grade 2 as significant EH (21) (Figure 1).

Interrater reliability analysis was performed between the two otorhinolaryngologists before reaching a consensus on the hydrops grading results. Cohen's kappa value was 0.870, indicating good agreement between the two otorhinolaryngologists. Grade rating was different in 6 ears (cochlea) and 25 ears (vestibule) by 1 grade. The final grade was determined after repeating the rating of these images by a third radiologist.

Clinical parameters

The diagnostic scale of the 1995 AAO-HNS guidelines was used for the analysis of clinical parameters in the diagnosis of MD. Pure tone audiometry and bithermal caloric tests were performed; if the tests were not performed on the day of HYDROPS MRI or their results were unavailable, the results of tests performed closest to the date of HYDROPS MRI were used for the analysis. The disease duration (in months) was calculated from the onset of the first episode of vertigo to the date of HYDROPS MRI confirmation.

All 123 patients underwent a hearing test using pure tone audiometry. Threshold results were obtained at frequencies of 0.25, 0.5, 1, 2, 3, 4, and 8 kHz in a soundproof audio booth. The pure tone average (PTA) was calculated based on the average of audiometry thresholds at 0.5, 1, 2, and 3 kHz according to the 2008 American Medical Association method for the estimation of hearing disability. The low tone average (LTA) was also calculated based on the average of the audiometry thresholds at 0.25, 0.5, and 1 kHz.

Bithermal caloric test results were available for 107 patients. The test was performed using a water caloric stimulator (NCI480; ICS Medical, Schaumburg, IL, USA) with the patient in the supine position and the head elevated at 30°. Caloric irrigation was delivered in the order of right cool (30°C), left cool (30°C), right warm (44°C), and left warm (44°C) for 30 s each, at a flow rate of 300 ml/min. The maximum slow-phase velocity of nystagmus was calculated after irrigation at each temperature; CP was determined using Jongkees' formula (23).

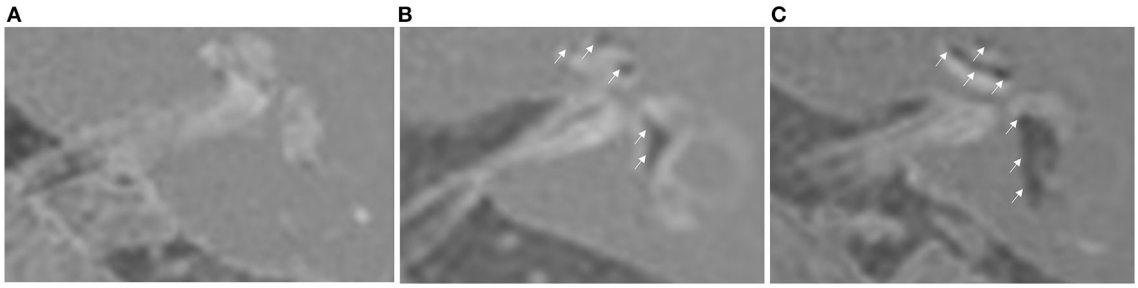

FIGURE 1
Hydrops grading based on HYDROPS MRI of the left ear. **(A)** Grade 0 cochlear hydrops with grade 0 vestibular hydrops. **(B)** Grade 1 cochlear hydrops with grade 1 vestibular hydrops. **(C)** Grade 2 cochlear hydrops with grade 2 vestibular hydrops.

Statistical analysis

The associations of hydrops grade with PTA, LTA, CP, and disease duration were analyzed by one-way ANOVA with Scheffé's *post-hoc* multiple comparison tests and by Welch's ANOVA with the Games-Howell's *post-hoc* multiple comparison test. The association between hydrops grade and MD classification was analyzed using the Fisher's exact test with *post-hoc* analysis consisting of pairwise Fisher's exact tests. The data were analyzed using R Studio version 1.4.1717 (R Studio Team, 2021) and R version 3.5.2 (R Core Team, 2018). In all analyses, $p < 0.05$ was taken to indicate statistical significance.

Results

Comparison of hydrops grade based on the diagnostic scale of MD

Of the total of 246 ears, 42 (17.1%) and 14 (5.7%) ears showed grade 1 and grade 2 cochlear hydrops, respectively, and 55 (22.4%) and 41 (16.7%) ears showed grade 1 and grade 2 vestibular hydrops, respectively. There were no hydropic changes (grade 0) in 190 ears (77.2%) for the cochlea and in 150 ears (60.9%) for the vestibule. Seven ears (2.8%) had only cochlear hydrops, and 47 (19.1%) ears had only vestibular hydrops. Both cochlear and vestibular hydrops were observed in 49 ears (19.9%).

The associations between the diagnostic scale of MD (unaffected, possible, probable, and definite) and the hydrops grade in the cochlea and vestibule were examined in 246 ears of 123 patients (Supplementary Table 1; Figure 2). Among the cases of definite MD, 46 of 80 ears (57.5%) showed grade 1 or 2 cochlear hydrops, and 64 ears (80%) showed grade 1 or 2 vestibular hydrops. Among the cases of probable MD, 4 of 12 ears (33%) showed grade 1 cochlear hydrops, and seven ears (58.3%) showed grade 1 or 2 vestibular hydrops. Among the cases of possible MD, two of 37 ears (5.4%) showed grade 1 or 2 cochlear hydrops, and 10 ears (27%) showed grade 1 or 2 vestibular hydrops. Among the 117 unaffected ears, 4 (3.4%) showed grade 1 cochlear hydrops and 15 (12.8%) showed grade 1 or 2 vestibular hydrops. Statistical analyses using Fisher's exact test showed that hydrops grade proportions were significantly different according to the diagnostic scale of MD both in the cochlea ($p < 0.0001$) and in the vestibule ($p < 0.0001$) (Supplementary Tables 2, 3). The proportions of hydrops grades 1 and 2 increased, while the proportion of hydrops grade 0 decreased as the diagnostic scale of MD increased in the order unaffected, possible, probable, and definite (Figure 2). The results of *post-hoc* analysis suggested that, for cochlear hydrops grade, the definite and probable MD groups differed significantly from the unaffected and possible MD groups (Supplementary Table 2). For the vestibular hydrops grade, the unaffected group differed significantly from all affected groups, and the possible group differed significantly from the definite group (Supplementary Table 3).

Comparison of hearing thresholds according to hydrops grade detected by MRI

Audiometry data for all 246 ears were analyzed (Supplementary Tables 4, 5; Figure 3) by one-way ANOVA followed by Scheffé's *post-hoc* multiple comparison tests; they were also analyzed using Welch's ANOVA followed by Games-Howell's *post-hoc* multiple comparison test. PTA and LTA increased significantly in patients with higher vestibular hydrops grades (Figures 3B,D). Both PTA and LTA were significantly lower in patients with grade 0 than grades 1 and 2 cochlear hydrops (i.e., the values were lower in ears without cochlear EH than in ears with cochlear EH) (Figures 3A,C).

Comparison of hearing thresholds according to the hydrops grade on MRI in ears with definite MD

Data from 80 ears with definite MD were analyzed (Supplementary Tables 6, 7; Figure 4) by one-way ANOVA with the Scheffé's *post-hoc* multiple comparison test. Analysis of both PTA and LTA values indicated that hearing thresholds were significantly higher in patients with hydrops grade 2 than hydrops grade 0 in both the cochlea and the vestibule.

Comparison of CP according to hydrops grade in MD ears

The association between CP and hydrops grade was analyzed after excluding six patients with bilateral MD and 10 patients who refused the caloric test. Accordingly, caloric test results were available for 107 ears. The association between CP and hydrops grade (0–2) in MD ears was analyzed by one-way ANOVA followed by the Scheffé's *post-hoc* multiple comparison test. The results are shown in Supplementary Table 8 and Figure 5. CP was significantly smaller in ears with grade 0 cochlear hydrops than in those with grade 1 cochlear hydrops (Supplementary Table 8; Figure 5A) and was significantly greater in ears with grade 2 vestibular hydrops than in those with grade 0 vestibular hydrops (Supplementary Table 8; Figure 5B).

Disease duration and hydrops grade

The association between disease duration and hydrops grade was analyzed in the ears of all 123 patients with MD (Supplementary Table 9; Supplementary Figures 1A,B). The results of one-way ANOVA followed by the Scheffé's *post-hoc* multiple comparison test showed no significant association between disease duration and hydrops grade.

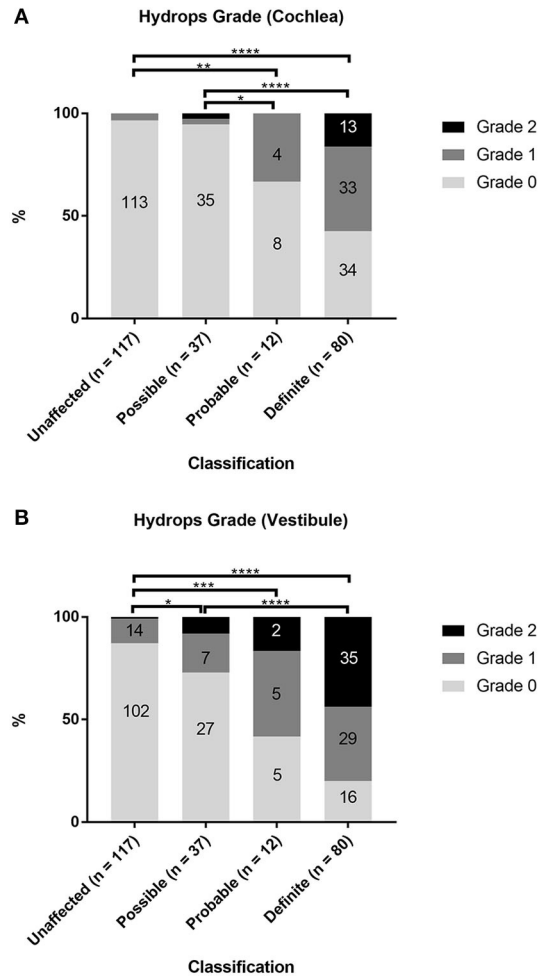

FIGURE 2
Comparison of hydrops grade according to the diagnosis of Ménière's disease (MD). The proportions of hydrops grades 0, 1, and 2 in unaffected ears and in ears with possible, probable, or definite MD were evaluated separately in the cochlea **(A)** and vestibule **(B)**. Fisher's exact test with pairwise Fisher's exact tests as *post-hoc* analysis. $*p < 0.05$; $**p < 0.01$; $***p < 0.001$; $****p < 0.0001$.

Discussion

In this study, the hydrops grade of the cochlea and the vestibule was examined in 246 ears of 123 patients. Cochlear hydrops and vestibular hydrops were detected in 58 and 80% of 80 definite MD ears, respectively, in 33 and 58% of 12 probable MD ears, and in 5 and 27% of 37 possible MD ears, respectively. The proportion of a higher hydrops grade increased significantly with increasing grade of MD classification (unaffected, possible, probable, and definite). The higher proportion of positive hydrops in definite MD suggested that EH is the pathophysiological mechanism of MD.

However, 3% of the cochleae and 13% of the vestibules of 117 unaffected ears also showed hydrops in this study. This is not surprising because varied rates of EH in unaffected ears have been reported in the literature. In a study conducted on a population of 29 patients with definite unilateral MD, 48 and 55% showed EH in the cochlea and the vestibule, respectively, in unaffected ears (24). In contrast, Wu et al. reported that 16.7% of 54 patients with unilateral definite MD revealed EH in the cochlea and/or vestibule (25). The possibility of subclinical involvement of the contralateral ear in patients with MD was not only documented in imaging studies using HYDROPS MRI but also demonstrated in an electrophysiological study. In a study to test the vestibular-evoked myogenic potential

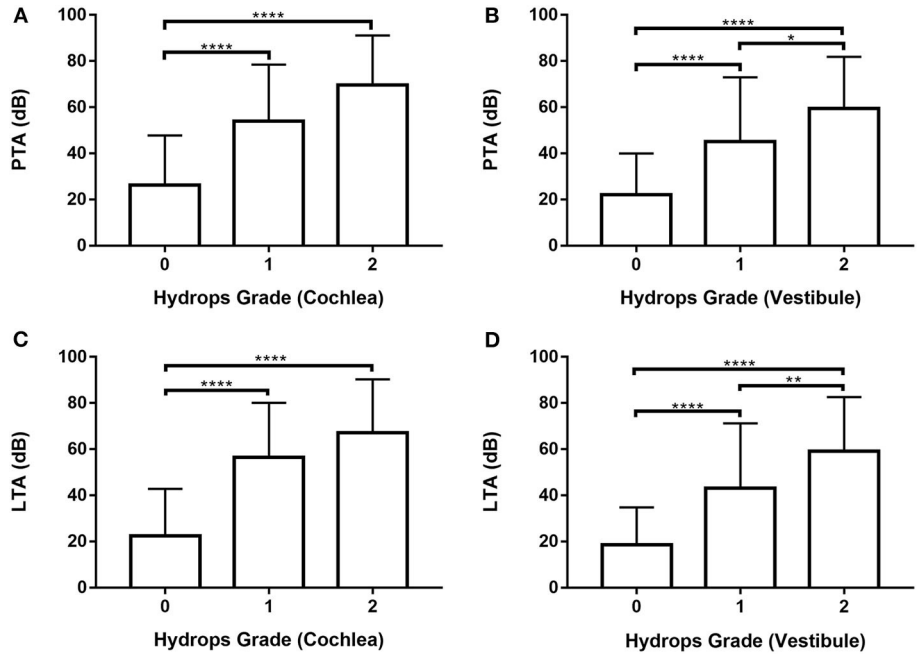

FIGURE 3
Analysis of pure tone average (PTA) and low tone average (LTA) according to cochlear and vestibular hydrops grades (0–2) in 246 ears of 123 patients. **(A)** and **(C)** One-way ANOVA with Scheffé's *post-hoc* multiple comparison test. **(B)** and **(D)** Welch's ANOVA with Games-Howell's *post-hoc* multiple comparison test. $*p < 0.05$; $**p < 0.01$; $****p < 0.0001$.

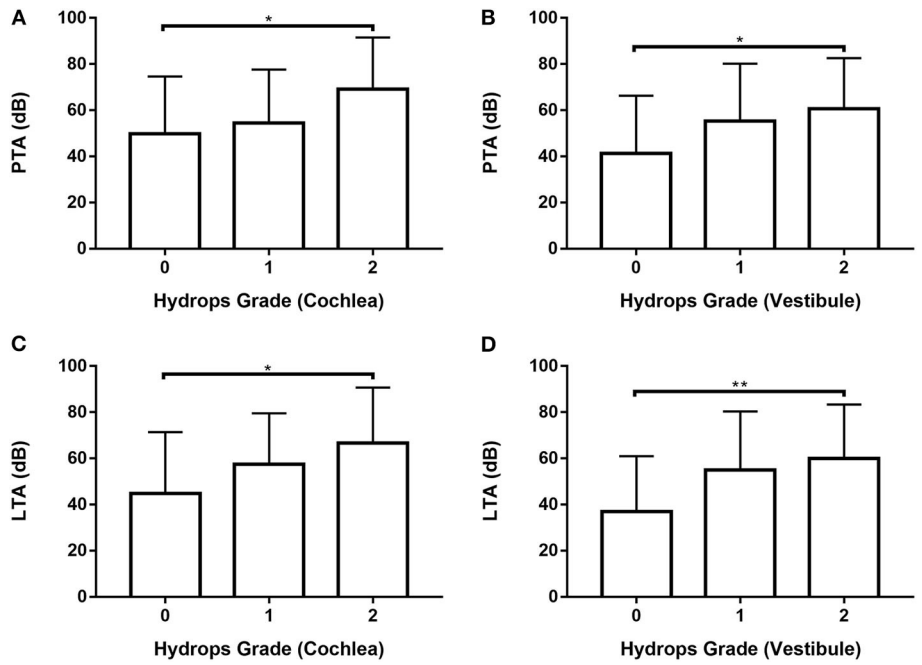

FIGURE 4
Analysis of PTA (**A**,**B**) and LTA (**C**,**D**) according to hydrops grade in the cochlea (**A**,**C**) and vestibule (**B**, **D**) in 80 ears with definite MD by one-way ANOVA with Scheffé's *post-hoc* multiple comparison test. $*p < 0.05$; $**p < 0.01$.

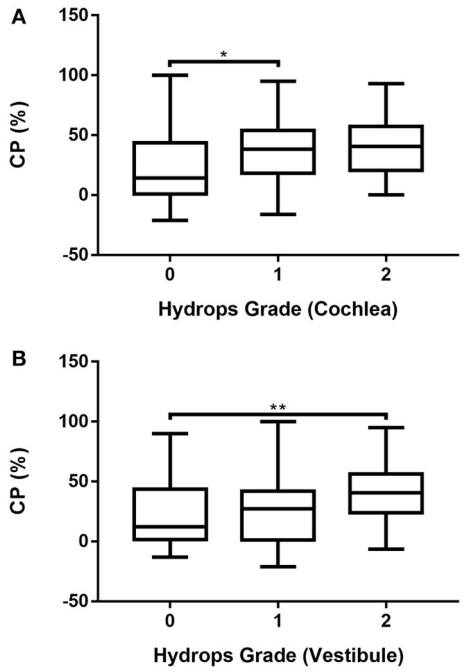

FIGURE 5
Associations of cochlear **(A)** and vestibular **(B)** hydrops grades 0, 1, and 2 with CP in 107 patients with unilateral MD determined by one-way ANOVA with Scheffé's *post-hoc* multiple comparison test. $*p < 0.05$; $**p < 0.01$.

(VEMP) in unilateral patients with MD, unaffected MD ears also showed a similar pattern to affected MD ears, such as elevated thresholds and frequency tuning around 1 kHz, unlike normal controls (26). These observations constitute evidence of subclinical involvement in the contralateral ear in unilateral MD. However, the incidence of EH in unaffected ears in our study was relatively low. This can be explained by the likely inclusion of patients with possible and probable MD in our study. As unaffected ears in MD may also have the potential to develop MD, it would be interesting to determine whether radiological EH without clinical symptoms (silent EH) precedes and eventually progresses to clinical EH.

Patients with clinically suspected MD, such as those with probable and possible MD, showed much lower incidences of EH. In probable MD, 33% showed cochlear hydrops and 58% showed vestibular hydrops. In possible MD, 5 and 27% of cases showed cochlear and vestibular hydrops, respectively. By adopting the 1995 AAO-HNS-defined definite, probable, and possible MD diagnostic scale (1) instead of the criteria of the 2015 Barany Society guidelines (27), we could learn the proportion of the patients having EH depending on the different diagnostic scales of MD since MD shows a wide spectrum of clinical presentations. True attacks of MD can have different visual analog scale (VAS) ranges and various hearing changes. There are also adjuvant spells of dizziness with different severities between true attacks of MD. In the 1995 AAO-HNS diagnostic scale (1), definite MD and certain MD are distinguished, which is now possible by the development of MRI protocol to visualize the endolymphatic space. It was interesting that 57 and 80% of definite MD ears showed hydrops in the cochlea or the vestibule, respectively, and those ears can be diagnosed as "certain" MD.

Using the 1995 AAO-HNS diagnostic scale (1), we can diagnose patients with the first attack of MD with low-frequency hearing loss, as probable MD, and patients with mild or moderate sensorineural hearing loss with flat audiometry results, as definite, probable, or possible MD depending on the pattern of the vertigo attacks. In this way, we could learn the proportion and the severity of hydrops in patients with the first attack of MD and patients with possible MD. In the 2015 Barany Society guidelines (27), these patients are not considered as MD even though they have recurrent inner ear symptoms and EH on MRI. Therefore, the 1995 AAO-HNS diagnostic scale (1) was more appropriate in our study to understand the underlying pathophysiology of this disease with a wide spectrum of clinical presentations. However, there may be some controversy regarding this point, so our choice of the 1995 AAO-HNS diagnostic scale (1) instead of the criteria of the 2015 Barany Society guidelines (27) as the main guidelines may represent a limitation of this study. The size of the study population consisting of 123 (246 ears) in our study was much larger than the sample sizes in previous studies of the associations between clinical parameters of MD and EH visualized by MRI (19, 20, 28–33).

In addition to a history of episodic vertigo with documented sensorineural hearing loss, inner ear MRI may substitute for histopathological evaluation by demonstrating EH to meet the "certain" classification of MD as defined by the AAO-HNS diagnostic scale. In our study, the endolymphatic space (as visualized on MRI using the HYDROPS protocol) was significantly expanded in patients with MD; EH grade on HYDROPS MRI exhibited associations with disease classification and clinical laboratory parameters. These results demonstrated the clinical importance of EH visualization in patients with MD using the HYDROPS MRI protocol.

Previous histopathological studies in postmortem samples of the temporal bones showed that, in the early stage of MD, hydrops predominantly involves the cochlear duct and saccule, while the utricle, ampulla, and overall endolymphatic system are affected in later stages (34–36). This sequence may reflect the mechanical compliance of the labyrinth membrane, which is higher in the saccule than the utricle (36, 37). In addition, the thick amorphous material in the ampulla and semicircular canal endows the labyrinth membrane with greater mechanical resistance (36). A relationship has been identified between the histological degree of cochlear involvement and the extent of hearing loss, which is more consistent than the relationship

between caloric test responses and histologically confirmed dilation of the vestibular structure (9, 38). Accordingly, the degree of hydrops is greater and involves a wider area in patients with severe MD, consistent with the analysis of the proportions of hydrops with respect to the MD classification.

Several recent studies analyzed MRI findings of EH and clinical data (19, 20, 28–31). Two Korean studies calculated the mean hydrops ratios in study populations of 29 and 16 patients with unilateral definite MD (19, 20). The mean hydrops ratios were 0.372 and 0.667 for the cochlea and the vestibule in one study (19) and 0.725 for the vestibule in the other study (20). Both studies analyzed correlations between the severity of EH and laboratory parameters, including audiometry, caloric test, cervical VEMP, and electrocochleography (ECoG), and showed that audiometry and caloric test results were correlated with the hydrops ratio, while VEMP and ECoG were not (19, 20). Other studies have also examined the correlation of EH with cervical VEMP in patients with unilateral definite MD (28, 29). In these studies, EH on MRI was present in 10 of 14 ears (29) and 12 of 20 ears (28), and hydrops grade (28) was correlated with the amplitude of cervical VEMP. In another study, in a population of 78 patients with unilateral definite MD, there were 57 cases of cochlear EH and 60 of vestibular EH, and these were related to the results of audiometry and caloric tests (30). In a study in which MRI was performed before the endolymphatic duct blockage procedure for unilateral definite MD, all affected ears had cochlear and vestibular EH (31).

MRI assessment of EH severity is usually based on the hydrops ratio or grade. Assessment based on the hydrops ratio uses the vestibular endolymphatic ratio, the cochlear endolymphatic ratio (32), and the cochlear hydrops ratio, along with the vestibular hydrops ratio (19, 20, 31) and the ratio of the area of the endolymphatic space to that of the entire lymphatic space (19). These ratios are obtained by drawing the region of interest for a specific slice of the MRI data and then calculating the number of pixels. Although an automated method for measurement of the hydrops ratio from the MRI findings was recently reported and showed considerable agreement with the existing calculation method, this automated measurement is not easy to set up for general clinical practice (39). Instead, the classification described by Nakashima et al. (21) can be easily adapted to determine the EH grade in daily clinical practice (29, 31–33). The grading systems proposed by Barath et al. (15), Kahn et al. (40), and Bernaerts et al. (41) have also been adopted for the analysis of EH in MD (28, 30); in some instances, these systems cannot be combined with MRI using the HYDROPS protocol. Therefore, the simplified grading system proposed by Nakashima et al. (21) was used in this study. Further advantages of this method include its ease of use for clinicians, as well as the absence of a requirement for another program or additional work for calculations. However, this grading system is subjective because it does not objectively determine the hydrops ratio.

Analysis of 80 ears with definite MD showed that both PTA and LTA were significantly higher in patients with hydrops grade 2 than grade 0 in both the cochlea and the vestibule. CP was significantly higher in patients with grade 2 vestibular hydrops than in those with grade 0 vestibular hydrops. Disease duration was not significantly associated with hydrops grade. These results were comparable with those of many previous studies. Audiometry results are closely associated with EH severity, assessed by grade or ratio (19, 29–32). The PTA results were significantly associated with the presence (19, 29) and severity (31, 32) of EH on MRI, as were the LTA results (19, 30, 32). In this study, we also examined the associations of vestibular hydrops grades 0, 1, and 2 with the PTA and LTA results in ears unaffected by MD, as well as their associations with possible, probable, and definite MD. Our results showed that in patients with MD, regardless of the classification, the presence of hydrops was significantly associated with the PTA and LTA results in both the cochlea and the vestibule. PTA and LTA findings seem to predict EH more accurately in definite MD.

There have been varied results regarding the correlation between radiological EH and the results of the caloric test, with some studies failing to show a relationship between radiological EH and CP (30, 32), while others have reported significant correlations (19, 20). The CP results were significantly correlated with the degree of EH in this study. We postulated that the correlation between cochlear hydrops and CP may be due to the confounding effect of cochlear hydrops and vestibular hydrops. The Cramer's V between cochlear hydrops grade and vestibular hydrops grade was 0.435 in 107 ears included in the analysis of CP. Therefore, the correlation between cochlear hydrops and CP may be affected by the correlation between vestibular hydrops and CP.

The disease duration and the severity of EH were not correlated with each other in this study. As the disease duration is defined as the period from the first occurrence of MD symptoms to the time of MRI, the severity of cochleovestibular dysfunction seems to be more closely related to the severity of EH than disease duration.

Conclusion

In our study, the EH grade, as visualized on HYDROPS MRI, was significantly associated with the diagnostic scale of MD according to the 1995 AAO-HNS guideline (1) and was also associated with the PTA, LTA, and CP results. However, the EH grade was not associated with disease duration. These results were obtained in the analysis of unaffected, possible, probable, and definite MD ears. Radiological assessment of EH using HYDROPS MRI is valuable for evaluating the extent and severity of MD,

as well as the pathophysiological relationship of MD with EH.

Data availability statement

The original contributions presented in the study are included in the article/Supplementary Material, further inquiries can be directed to the corresponding author/s.

Ethics statement

The studies involving human participants were reviewed and approved by Clinical Research Institute at Seoul National Bundang Hospital. The patients/participants provided their written informed consent to participate in this study. Written informed consent was obtained from the individual(s) for the publication of any potentially identifiable images or data included in this article.

Author contributions

SH and J-WK designed this study and wrote the manuscript. SH, YoK, YeK, and J-WK collected and analyzed data. All authors contributed to the article and approved the submitted version.

Funding

This study was supported by the Seoul National University Bundang Hospital Grant number (2021-019386).

Conflicts of interest

The authors declare that the research was conducted in the absence of any commercial or financial relationships that could be construed as a potential conflict of interest.

Publisher's note

All claims expressed in this article are solely those of the authors and do not necessarily represent those of their affiliated organizations, or those of the publisher, the editors and the reviewers. Any product that may be evaluated in this article, or claim that may be made by its manufacturer, is not guaranteed or endorsed by the publisher.

Supplementary material

The Supplementary Material for this article can be found online at: https://www.frontiersin.org/articles/10.3389/fneur.2022.937703/full#supplementary-material

References

1. Committee on Hearing and Equilibrium guidelines for the diagnosis and evaluation of therapy in Meniere's disease. American Academy of Otolaryngology-Head and Neck Foundation, Inc. *Otolaryngol Head Neck Surg.* (1995) 113:181–5. doi: 10.1016/S0194-5998(95)70102-8

2. Chen X, Zhang XD, Gu X, Fang ZM, Zhang R. Endolymphatic space imaging in idiopathic sudden sensorineural hearing loss with vertigo. *Laryngoscope.* (2012) 122:2265–8. doi: 10.1002/lary.23452

3. Kasai S, Teranishi M, Katayama N, Sugiura M, Nakata S, Sone M, et al. Endolymphatic space imaging in patients with delayed endolymphatic hydrops. *Acta Otolaryngol.* (2009) 129:1169–74. doi: 10.3109/00016480802691143

4. Kato M, Sugiura M, Shimono M, Yoshida T, Otake H, Kato K, et al. Endolymphatic hydrops revealed by magnetic resonance imaging in patients with atypical Meniere's disease. *Acta Otolaryngol.* (2013) 133:123–9. doi: 10.3109/00016489.2012.726374

5. Miyagawa M, Fukuoka H, Tsukada K, Oguchi T, Takumi Y, Sugiura M, et al. Endolymphatic hydrops and therapeutic effects are visualized in 'atypical' Meniere's disease. *Acta Otolaryngol.* (2009) 129:1326–9. doi: 10.3109/00016480802593513

6. Berggren S. Histological investigation of three cases with Menie're's syndrome. *Arch Otolaryngol.* (1949) 37:30–6. doi: 10.3109/00016484909120212

7. Arnvig J. Histological findings in a case of Menie're's disease, with remarks on the pathologic-anatomical basis of this lesion. *Acta Oto-Laryngologica.* (1947) 35:453–66. doi: 10.3109/00016484709123760

8. Belal A Jr, Ylikoski J. Pathologic significance of Meniere's symptom complex. A histopathologic and electron microscopic study. *Am J Otolaryngol.* (1980) 1:275–84. doi: 10.1016/S0196-0709(80)80030-5

9. Fraysse BG, Alonso A, House WF. Meniere's disease and endolymphatic hydrops: clinical-histopathological correlations. *Ann Otol Rhinol Laryngol Suppl.* (1980) 89:2–22. doi: 10.1177/00034894800896S201

10. Greco A, Gallo A, Fusconi M, Marinelli C, Macri GF, Vincentiis Mde. Meniere's disease might be an autoimmune condition? *Autoimmun Rev.* (2012) 11:731–8. doi: 10.1016/j.autrev.2012.01.004

11. P. Gates. Hypothesis: could Meniere's disease be a channelopathy? *Intern Med J.* (2005) 35:488–9. doi: 10.1111/j.1445-5994.2005.00891.x

12. Nakashima T, Naganawa S, Sugiura M, Teranishi M, Sone M, Hayashi H, et al. Visualization of endolymphatic hydrops in patients with Meniere's disease. *Laryngoscope.* (2007) 117:415–20. doi: 10.1097/MLG.0b013e31802c300c

13. Naganawa S, Yamazaki M, Kawai H, Bokura K, Sone M, Nakashima T. Visualization of endolymphatic hydrops in Meniere's disease with single-dose intravenous gadolinium-based contrast media using heavily T(2)-weighted 3D-FLAIR. *Magn Reson Med Sci.* (2010) 9:237–42. doi: 10.2463/mrms.9.237

14. Fang ZM, Chen X, Gu X, Liu Y, Zhang R, Cao DR, et al. A new magnetic resonance imaging scoring system for perilymphatic space appearance after intratympanic gadolinium injection, and its clinical application. *J Laryngol Otol.* (2012) 126:454–9. doi: 10.1017/S0022215112000060

15. Barath K, Schuknecht B, Naldi AM, Schrepfer T, Bockisch CJ, Hegemann SC. Detection and grading of endolymphatic hydrops in Meniere disease using MR imaging. *AJNR Am J Neuroradiol.* (2014) 35:1387–92. doi: 10.3174/ajnr.A3856

16. Naganawa S, Satake H, Kawamura M, Fukatsu H, Sone M, Nakashima T. Separate visualization of endolymphatic space, perilymphatic space and bone by a single pulse sequence; 3D-inversion recovery imaging utilizing real reconstruction after intratympanic Gd-DTPA administration at 3 Tesla. *Eur Radiol.* (2008) 18:920–4. doi: 10.1007/s00330-008-0854-8

17. Naganawa S, Yamazaki M, Kawai H, Bokura K, Sone M, Nakashima T. Imaging of Meniere's disease after intravenous administration of single-dose gadodiamide: utility of subtraction images with different inversion time. *Magn Reson Med Sci.* (2012) 11:213–9. doi: 10.2463/mrms.11.213

18. Naganawa S, Suzuki K, Nakamichi R, Bokura K, Yoshida T, Sone M, et al. Semi-quantification of endolymphatic size on MR imaging after intravenous injection of single-dose gadodiamide: comparison between two types of processing strategies. *Magn Reson Med Sci.* (2013) 12:261–9. doi: 10.2463/mrms.2013-0019

19. Cho YS, Ahn JM, Choi JE, Park HW, Kim YK, Kim HJ, et al. Usefulness of intravenous gadolinium inner ear MR imaging in diagnosis of Meniere's disease. *Sci Rep.* (2018) 8:17562. doi: 10.1038/s41598-018-35709-5

20. Choi JE, Kim YK, Cho YS, Lee K, Park HW, Yoon SH, et al. Morphological correlation between caloric tests and vestibular hydrops in Meniere's disease using intravenous Gd enhanced inner ear MRI. *PLoS ONE.* (2017) 12:e0188301. doi: 10.1371/journal.pone.0188301

21. Nakashima T, Naganawa S, Pyykkö I, Gibson WP, Sone M, Nakata S. Grading of endolymphatic hydrops using magnetic resonance imaging. *Acta Otolaryngol Suppl.* (2009) 129:5–8. doi: 10.1080/00016480902729827

22. Naganawa S, Kawai H, Taoka T, Sone M. Improved HYDROPS: imaging of endolymphatic hydrops after intravenous administration of gadolinium. *Magn Reson Med Sci.* (2017) 16:357–61. doi: 10.2463/mrms.tn.2016-0126

23. Furman JM, Jacob RG. Jongkees' formula re-evaluated: order effects in the response to alternate binaural bithermal caloric stimulation using closed-loop irrigation. *Acta Otolaryngol.* (1993) 113:3–10. doi: 10.3109/00016489309135759

24. Morimoto K, Yoshida T, Sugiura S, Kato M, Kato K, Teranishi M, et al. Endolymphatic hydrops in patients with unilateral and bilateral Meniere's disease. *Acta Otolaryngol.* (2016) 137:23–8. doi: 10.1080/00016489.2016.1217042

25. Wu Q, Dai C, Zhao M, Sha Y. The correlation between symptoms of definite Meniere's disease and endolymphatic hydrops visualized by magnetic resonance imaging. *Laryngoscope.* (2016) 126:974–9. doi: 10.1002/lary.25576

26. Lin MY, Timmer FC, Oriel BS, Zhou G, Guinan JJ, Kujawa SG, et al. Vestibular evoked myogenic potentials (VEMP) can detect asymptomatic saccular hydrops. *Laryngoscope.* (2006) 116:987–92. doi: 10.1097/01.mlg.0000216815.75512.03

27. Lopez-Escamez JA, Carey J, Chung WH, Goebel JA, Magnusson M, Mandala M, et al. Equilibrium Committee of the American Academy of, S Neck, and S Korean Balance, Diagnostic criteria for Meniere's disease. *J Vestib Res.* (2015) 25:1–7. doi: 10.3233/VES-150549

28. Shiraishi K, Ohira N, Kobayashi T, Sato M, Osaki Y, Doi K. Comparison of furosemide-loading cervical vestibular-evoked myogenic potentials with magnetic resonance imaging for the evaluation of endolymphatic hydrops. *Acta Otolaryngol.* (2020) 140:723–7. doi: 10.1080/00016489.2020.1769863

29. Murofushi T, Tsubota M, Kanai Y, Endo H, Ushio M. Association of cervical vestibular-evoked myogenic potential tuning property test results with MRI findings of endolymphatic hydrops in Meniere's disease. *Eur Arch Otorhinolaryngol.* (2021) 278:3267–73. doi: 10.1007/s00405-020-06410-z

30. Sluydts M, Bernaerts A, Casselman JW, Foer BDe, Blaivie C, Zarowski A, et al. The relationship between cochleovestibular function tests and endolymphatic hydrops grading on MRI in patients with Meniere's disease. *Eur Arch Otorhinolaryngol.* (2021) 278:4783–93. doi: 10.1007/s00405-021-06610-1

31. He J, Peng A, Hu J, Zhang Z, Chen Y, Wang Q, et al. Dynamics in endolymphatic hydrops & symptoms in Meniere's disease after endolymphatic duct blockage, preliminary results. *Front Neurol.* (2020) 11:622760. doi: 10.3389/fneur.2020.622760

32. Zhang W, Hui L, Zhang B, Ren L, Zhu J, Wang F, et al. The correlation between endolymphatic hydrops and clinical features of Meniere disease. *Laryngoscope.* (2021) 131:E144–50. doi: 10.1002/lary.28576

33. Xie J, Zhang W, Zhu J, Hui L, Li S, Ren L, et al. Differential diagnosis of endolymphatic hydrops between "Probable" and "Definite" Meniere's Disease *via* magnetic resonance imaging. *Otolaryngol Head Neck Surg.* (2021) 165:696–700. doi: 10.1177/0194599821990680

34. Ishiyama G, Lopez IA, Sepahdari AR, Ishiyama A. Meniere's disease: histopathology, cytochemistry, and imaging. *Ann N Y Acad Sci.* (2015) 1343:49–57. doi: 10.1111/nyas.12699

35. Schunknecht HF, Montandon P. Pathology of the ear in pneumococcal meningitis. *Arch Klin Exp Ohren Nasen Kehlkopfheilkd.* (1970) 195:207–25. doi: 10.1007/BF00302950

36. Nam SI. Endolymphatic Hydrops: Pathophysiology and Etiology. *Korean J Otorhinolaryngol Head Neck Surg.* (2011) 54:509–518. doi: 10.3342/kjorl-hns.2011.54.8.509

37. Wit HP, Warmerdam TJ, Albers FW. Measurement of the mechanical compliance of the endolymphatic compartments in the guinea pig. *Hear Res.* (2000) 145:82–90. doi: 10.1016/S0378-5955(00)00078-2

38. Salvinelli F, Greco F, Trivelli M, Linthicum FH Jr. Meniere's disease Histopathological changes: a post mortem study on temporal bones. *Eur Rev Med Pharmacol Sci.* (1999) 3:189–93.

39. Cho YS, Cho K, Park CJ, Chung MJ, Kim JH, Kim K, et al. Automated measurement of hydrops ratio from MRI in patients with Meniere's disease using CNN-based segmentation. *Sci Rep.* (2020) 10:7003. doi: 10.1038/s41598-020-63887-8

40. Kahn L, Hautefort C, Guichard JP, Toupet M, Jourdaine C, Vitaux H, et al. Relationship between video head impulse test, ocular and cervical vestibular evoked myogenic potentials, and compartmental magnetic resonance imaging classification in Meniere's disease. *Laryngoscope.* (2020) 130:E444–52. doi: 10.1002/lary.28362

41. Bernaerts A, Vanspauwen R, Blaivie C, van Dinther J, Zarowski A, Wuyts FL, et al. The value of four stage vestibular hydrops grading and asymmetric perilymphatic enhancement in the diagnosis of Meniere's disease on MRI. *Neuroradiology.* (2019) 61:421–9. doi: 10.1007/s00234-019-02155-7

frontiers | Frontiers in Neurology

TYPE Original Research
PUBLISHED 25 July 2022
DOI 10.3389/fneur.2022.955158

Check for updates

OPEN ACCESS

EDITED BY
Toshihisa Murofushi,
Teikyo University Mizonokuchi Hospital, Japan

REVIEWED BY
Tadashi Kitahara,
Nara Medical University, Japan
Chisato Fujimoto,
The University of Tokyo, Japan
Takeshi Tsutsumi,
Tokyo Medical and Dental University, Japan

*CORRESPONDENCE
Sun-Young Oh
ohsun@jbnu.ac.kr
Jong-Min Lee
ljm@hanyang.ac.kr

†These authors have contributed equally to this work and share first authorship

SPECIALTY SECTION
This article was submitted to Neuro-Otology, a section of the journal Frontiers in Neurology

RECEIVED 28 May 2022
ACCEPTED 27 June 2022
PUBLISHED 25 July 2022

CITATION
Oh S-Y, Kang J-J, Kim S, Lee J-M, Kim J-S and Dieterich M (2022) A preliminary trial of botulinum toxin type A in patients with vestibular migraine: A longitudinal fMRI study. *Front. Neurol.* 13:955158. doi: 10.3389/fneur.2022.955158

COPYRIGHT
© 2022 Oh, Kang, Kim, Lee, Kim and Dieterich. This is an open-access article distributed under the terms of the Creative Commons Attribution License (CC BY). The use, distribution or reproduction in other forums is permitted, provided the original author(s) and the copyright owner(s) are credited and that the original publication in this journal is cited, in accordance with accepted academic practice. No use, distribution or reproduction is permitted which does not comply with these terms.

A preliminary trial of botulinum toxin type A in patients with vestibular migraine: A longitudinal fMRI study

Sun-Young Oh[1,2*†], Jin-Ju Kang[1,2†], Sohui Kim[3†], Jong-Min Lee[4*], Ji-Soo Kim[5,6] and Marianne Dieterich[7,8,9]

[1]Department of Neurology, Jeonbuk National University Hospital and School of Medicine, Jeonju-si, South Korea, [2]Research Institute of Clinical Medicine of Jeonbuk National University-Biomedical Research Institute of Jeonbuk National University Hospital, Jeonju-si, South Korea, [3]Department of Electronic Engineering, Hanyang University, Seoul, South Korea, [4]Department of Biomedical Engineering, Hanyang University, Seoul, South Korea, [5]Department of Neurology, Seoul National University College of Medicine, Seoul, South Korea, [6]Department of Neurology, Dizziness Center, Clinical Neuroscience Center, Seoul National University Bundang Hospital, Seongnam-si, South Korea, [7]Department of Neurology, University Hospital, Ludwig-Maximilians-Universität, Munich, Germany, [8]German Center for Vertigo and Balance Disorders, University Hospital, Ludwig-Maximilians-Universität, Munich, Germany, [9]Munich Cluster for Systems Neurology (SyNergy), Munich, Germany

Objective: This study aims to investigate the efficacy of botulinum toxin type A (BTX-A) in the prophylactic management of vestibular migraine (VM) and to determine whether this treatment modulates intrinsic functional brain network.

Methods: Vestibular migraine patients ($n = 20$, mean age 45.4 years) who were resistant to conventional prophylactic therapies had BTX-A injection and rs-fMRI before and 2 months after the injection. We also measured the changes in the frequency of vertigo and migraine attacks, symptomatic functional disability scores, and neuropsychiatric inventories.

Results: After BTX-A injection, the mean monthly frequencies of migraine and vertigo episodes decreased significantly compared with the baseline ($p < 0.01$, paired t-test). The Headache Impact Test-6 score and the Migraine Disability Assessment, and the vertigo parameters, measured by the Dizziness Handicap Inventory and the Vertigo Symptom Scale, showed an improvement, as did the anxiety and depression scores 2 months after BTX-A treatment. The low-frequency fluctuation analysis of the rs-fMRI data found significant changes in the functional connectivity of the right superior temporal gyrus. Adoption of this cluster as the seed region increased the functional connectivity with the left post-central gyrus, right supramarginal gyrus, and right middle temporal gyrus after BTX-A treatment.

Conclusion: This prospective study suggests that BTX-A treatment is effective at ameliorating migraine and vertigo symptoms in VM patients who were resistant to conventional therapies. Along with symptomatic improvements, changes in the functional connectivity within the multisensory vestibular and pain networks suggest a dysmodulation of multimodal sensory integration and abnormal cortical processing of the vestibular and pain signals in VM patients.

KEYWORDS

vestibular migraine, botulinum toxin (BOTOX®), prophylactic therapy, migraine-associated vertigo, migraine, vertigo, dizziness, headache

TABLE 1 Diagnostic criteria for vestibular migraine (1).

A. At least five episodes with vestibular symptoms of moderate or severe intensity [a] lasting 5 min to 72 h
B. Current or previous history of migraine with or without aura according to the ICHD-3
C. One or more migraine features with at least 50% vestibular episodes:
a) headache with at least two of the following characteristics:
- unilateral location
- pulsating quality
- moderate or severe intensity
- aggravation by routine physical activity
b) photophobia and phonophobia
c) visual aura
D. Not better explained by another vestibular or ICHD diagnosis

[a]Vestibular symptoms are moderate when they interfere with but do not prevent daily activities and severe when they prevent such activities.

Introduction

The Bárány Society and the International Headache Society jointly proposed diagnostic consensus criteria for vestibular migraine (VM) included in the International Classification of Headache Disorders (ICHD-3) (Table 1) (1). VM is the most common cause of episodic vertigo in both adults and children, with a lifetime prevalence of 1% and a 1-year prevalence of 0.9% in the general population with a female preponderance (2). The underlying pathophysiology of VM is still unclear; however, possible mechanisms involve hyperactivity within the trigeminovascular system (TVS) and nociceptive brain stem centers, as well as an abnormal sensory modulation or integration in both pain and vestibular processing areas (3). Due to the absence of large, systematic, controlled clinical studies that specifically address VM, most therapeutic recommendations for VM are extrapolated from clinical trials on migraine with and without aura.

Botulinum toxin type A (BTX-A) has been used to treat different types of headache by blocking peripheral signals to the central nervous system, which inhibits central sensitization. The clinical efficacy of BTX-A in treating chronic migraine was previously demonstrated in the PREEMPT (Phase III Research Evaluating Migraine Prophylaxis Therapy) randomized clinical trial (4). BTX-A has also been used for other types of headaches, such as episodic migraine (<15 headache days per month) (5), chronic daily headache (>15 headache days per month) (6), and chronic tension-type headache, in a systematic series of exploratory controlled trials (7). In patients with frequent migraine headaches or vertigo attacks (15 days per month for more than 3 months), a trial of BTX-A might be reasonable; however, to date, there are no data on the management of chronic migraine headache or vertigo attacks in patients with VM.

Resting-state functional connectivity analysis in magnetic resonance imaging (rs-FC MRI) can visualize and measure the brain's intrinsic functional architecture, which aids in understanding the underlying mechanisms of various neurological disorders (8). The amplitude of low-frequency fluctuation (ALFF) changes in rs-FC MRI data is thought to be associated with local neuronal activity, and an ALFF analysis is effective for detecting fluctuations in spontaneous low-frequency oscillations.

The aim of this study was to evaluate the efficacy of BTX-A injection for the prophylactic treatment of VM. We hypothesized that a symptomatic improvement after BTX-A treatment would be reflected in changes in brain connectivity in areas that process and store vestibular and pain information. Therefore, rs-FC MRI data acquired pre- and post-BTX-A treatment were analyzed by comparing ALFF and seed-based rs-FC to detect changes in spontaneous brain activity in patients with VM.

Subjects and methods

Study design and participants

Patients at a dizziness clinic of Jeonbuk National University Hospital, Korea, who were diagnosed with VM using the criteria of the Headache Classification Committee of the International Headache Society (ICHD-3, appendix) and the Committee for the International Classification of Vestibular Disorders of the Bárány Society (9) were considered for inclusion in this study between May 2020 and January 2021 (Table 1). Twenty right-handed VM patients were included who suffered from moderate-to-severe vertigo attacks with migraine headache, with moderate impairment in daily life, despite treatment with several preventive drugs for at least 5 months. The use of migraine prophylactics was permitted if no changes in medications or dosages were made within the 2 months of study participation. Two or more categories of prophylactic medication were used prior to BTX-A injections in 75% (15/20) of patients. A calcium channel blocker (Nimodipine®) and topiramate were the two drugs most commonly prescribed in our patients; other preventive drugs used were cinnarizine, propranolol, valproate, and venlafaxine (antidepressant).

Patients were excluded if they had histories of medication overuse for headache or any medical condition or exposure to any agent that might have contraindicated the use of the BTX-A formulation, or if they had an infection or skin problem at any of the injection sites. Patients were also excluded if they had contraindications to MRI or had neurologic, psychiatric, audiovestibular, or systemic disorders or a history of complicated migraine attacks such as migrainous infarction or basilar migraine. Every patient underwent neurotological evaluations: video-oculography, video head impulse test, and

cervical and ocular vestibular-evoked myogenic potentials. The structural and resting-state functional MRI scans were performed during interictal periods before (baseline) and 2 months after BTX-A injection therapy. Patients were treated with BTX-A (BOTOX®, Allergan, Inc., Irvine, CA, USA) injections based on the PREEMPT injection paradigm of fixed-site and fix-dose injections; a total of 155U was injected (5U each into 31 designated sites corresponding to seven muscles of the head and neck areas) (10).

This study was approved by the Ethics Committee of Jeonbuk National University Hospital (IRB File No. 2020-10-033-001), and all participants voluntarily signed written informed consent forms before entering the study.

Efficacy measures

The primary efficacy measure was changes in the mean monthly frequency of vertigo and migraine headache episodes between the periods before and 2 months after the BTX-A injection. Headache or vertigo frequency was defined as calendar days on which a patient reported moderate to severe symptom episodes. The baseline for the efficacy measures was defined as the mean monthly frequency of vertigo or migraine episodes during the period of 2 months before the BTX-A injection.

We administered the following self-reported questionnaires before and after the treatment to gather data for our pre-specified secondary measure variables, which reflected mean monthly changes in the impact of headaches and vertigo on patient disability and psychiatric comorbidities: headache severity with visual analog scale (VAS), Headache Impact Test-6 (HIT-6), Migraine Disability Assessment (MIDAS) (11), Migraine-specific Quality of Life (MSQ), Vertigo Symptom Scale (VSS) (12), Dizziness Handicap Inventory (DHI) (13), Beck Depression Inventory (BDI), and Beck's Anxiety Inventory (BAI) (14).

Imaging data acquisition and analysis

Structural and functional MRI

Structural and functional images were acquired on a 3T MRI system (Magnetom Verio, Siemens Healthcare, Erlangen, Germany) with a 12-channel head coil. In a single session, 195 volumes (60 contiguous, axial, 2.5-mm-thick slices; 1-mm gap) were acquired with a gradient echo, echo-planar imaging (EPI) T2*-sensitive sequence (repetition time: 2,000 ms; echo time: 30 ms; flip angle: 90°; matrix: 64 × 64; field of view: 192 × 192 mm). Anatomical images included a T1-weighted magnetization-prepared rapid gradient echo sequence with a 256-mm field of view and 1.0 × 1.0 × 1.0 mm^3 isotropic spatial resolution (TE, 4.37 ms; TR, 2,100 ms; 160 slices). Resting-state fMRI data were preprocessed using SPM12 software (http://www.fil.ion.ucl.ac.uk/spm; Wellcome Trust Center for Neuroimaging, London, UK) implemented in Matlab® 2020A (MathWorks®, Natick, MA). We performed slice timing correction using the standard SPM procedure, and for subsequent processing, we used the DPARSFA toolbox (data processing assistant for resting-state fMRI, version 5.1; https://www.nitrc.org/projects/dparsf) (15) together with the SPM software. A detailed methodology was described in the previous reports (16).

Amplitude of low-frequency fluctuations analysis

The ALFF analysis was performed using the DPARSF software. After the preprocessing described above, the fMRI data were temporally band-pass filtered ($0.009 < f < 0.1$ Hz) to reduce low-frequency drift and high-frequency respiratory and cardiac noise. The time series of each voxel was transformed into the frequency domain, and the power spectrum was obtained. Because the power of a given frequency is proportional to the square of the amplitude of that frequency component, the square root was calculated at each frequency of the power spectrum, and the average square root was then obtained across 0.009–0.1 Hz at each voxel. This average square root was taken as the ALFF, which was assumed to reflect the absolute intensity of spontaneous brain activity (17).

Defining regions of interest (ROIs) and the seed-based functional connectivity analysis

To investigate functional alterations in the VM patients, we performed a seed-based FC analysis. Significant pre- and post-treatment ALFF changes were demonstrated in the right superior temporal gyrus (STG) region; therefore, that right STG cluster was used as the seed for the FC analysis. The MNI coordinates of the center of the 5-mm spherical ROI were determined using the peak t-score detected at the right STG. For the FC analysis, the mean time series was extracted from the seed region and correlated with the time series of each voxel in the whole brain for each subject. The correlation coefficients were transformed into z values using Fisher's r-to-z transformation to improve normality. An entire brain z-score map was created for each subject.

Statistical analyses

For each primary and secondary variable, the comparison between pre- and post-BTX-A treatment values was measured by an analysis of covariance in the change from baseline and the main effects of treatment. For all measures considered in this study, the data showed a normal distribution (Kolmogorov-Smirnov test, $p>0.05$). Paired t-tests were used to compare

the baseline (pre-BTX-A treatment) values with the results obtained 2 months after the BTX-A treatment. The significance level was set to $p<0.05$, and the Statistical Package for Social Sciences software (SPSS, Inc., Chicago, IL, USA) was used for all data analyses.

To examine differences in the ALFF and FC between the baseline and follow-up scans, a paired t-test of the ALFF maps and z-score maps, respectively, was performed with age as a covariate. Statistical images were assessed for cluster-wise significance using a cluster-defining threshold of $p < 0.05$ with family-wise error (FWE) and false discovery rate (FDR) correction for multiple testing unless otherwise stated.

Results

Demographic and clinical characteristics

The demographic and clinical characteristics of the patient population are listed in Table 2. Twenty patients were enrolled; they were all women and right-handers with a mean age of 45 years (range from 20 to 69 years). The mean disease duration was 7.6 ± 4.8 years (range, 0.5–20 years), and the mean monthly frequency of migraine episodes at baseline was 17.2 ± 0.5, with a mean headache severity of 5.9 ± 1.3 (VAS). Patients had a mean frequency of 14.0 ± 5.0 episodes of vertigo per month. The vestibular symptoms lasted at least 1 h and had a mean duration of 11.3 h. Every patient experienced vestibular symptoms corresponding to a score of 4 or higher; the mean vertigo intensity was 6.0, and 7 patients had severe symptoms that interfered with their daily lives. Most subjects (16/20, 80%) had recurrent, spontaneous vertigo; they described a sensation of movement when no motion was taking place or an altered sensation without any provoking movements. In our patients' group, four patients complained of additional ear symptoms such as tinnitus ($n = 3$) and aural fullness ($n = 1$), which were not correlated temporally with symptoms of vertigo or headache. We believe that an overlapping syndrome of VM and Meniere disease in our case series was not included. Most participants revealed normal vestibular function tests, except one subject who revealed caloric weakness (39%) and decreased amplitude of cervical vestibular-evoked myogenic potentials on the right side, but other findings, including the head-impulse test and oculography, were unremarkable. Another patient showed subtle spontaneous nystagmus on interictal VOG recordings (about 3°/s) without caloric paresis or abnormal vHIT, which was resolved a month after the BTX injection.

Efficacy measures after BTX-A treatment

There was an overall reduction in the mean monthly frequency of headache and vertigo episodes 2 months after

TABLE 2 Demographic and clinical characteristics of patients with vestibular migraine ($n = 20$).

	Patients ($n = 20$)
Demographics	
Sex (female)	20 (100%)
Age (mean ± SD, range, years)	45.4 ± 12.8, 20–69
Right handedness	20 (100%)
Migraine characteristics	
Disease duration (mean ± SD, range, years)	7.6 ± 4.8, 0.5–20
Frequency (mean ± SD, range, days/month)	17.2 ± 9.5, 3–30
Severity of headache (VAS, 0–10) (mean ± SD, range)	6.8 ± 1.3, 4–8
Episode duration (mean ± SD, range, h)	17.3 ± 19.0, 1–72
MwoA / MwA / Visual aura	13 (65%) / 7 (35%) / 7 (35%)
Headache side: right / Left / Bilateral	1 (5%) / 6 (30%) / 13 (65%)
Pulsating quality	7 (35%)
Photophobia / Phonophobia	2 (10%) / 4 (20%)
Vestibular symptoms	
Frequency (mean ± SD, range, days/month)	14.0 ± 5.0, 2–21
Duration (mean ± SD, range, h)	11.35 ± 16.9, 1–72
Intensity of vertigo (VAS-D, 0–10) (mean ± SD, range)[a]	6.0 ± 2.8, 4–10
Recurrent spontaneous / positional / visually induced vertigo	16 (80%) / 9 (45%) / 3 (15%)
Nausea or vomiting	14 (70%)
History of motion sickness	12 (60%)
Frequency of acute headache/vertigo treatment use (days/month)	15.0 ± 10.7
Prophylactic medications	20 (100%)
Use of two or more drugs	15 (75%)
Vestibular function tests	
Spontaneous nystagmus (VOG)	1 (5%)
vHIT (hVOR mean gain, R/L)	0.97 ± 0.05 / 0.98 ± 0.06
Abnormal vHIT hVOR gain / Presence of corrective saccades	0 / 0
VEMP (cVEMP, oVEMP)	
cVEMP p13 amplitude AR ≥ 40%	1 (5%)
cVEMP p13 amplitude AR (%)	20.19 ± 12.40
cVEMP p13 mean latency (ms, R/L)	13.17 ± 0.4/12.91 ± 0.5
oVEMP n10 amplitude AR ≥ 40%	0
oVEMP n10 amplitude AR (%)	18.42 ± 11.70
oVEMP n10 mean latency (ms, R/L)	10.11 ± 0.7/10.39 ± 0.5
Mean caloric response (°/s, R/L)	28.6 ± 15.4/26.4 ± 12.3
Caloric response AR	15.61 ± 21.9
Caloric response AR ≥ 35%	1/7 (14.3%)

AR, asymmetry ratio; vHIT, video head-impulse test; VOG, video oculography; VOR, video ocular reflex; VAS, Visual Analog Scale; VAS-D, Visual Analog Scale-Dizziness; R, right; L, left.

[a]To evaluate the intensity of vestibular symptoms, we used a scale similar to the numeric rating scale, with 0 set as none, 1–3 as mild (uninterrupted), 4–6 as moderate (disturbed but able to maintain daily activities), and more than 7 as severe (daily activities cannot be continued).

BTX-A treatment compared with baseline (Table 3). During the prospective baseline phase, VM patients had a mean monthly frequency of 17 migraine headaches and 14 vertigo episodes, which were significantly reduced to mean monthly frequencies of 9.5 (−8.3 days, $p = 0.001$, paired t-test) and 8.5 (−5.5 days, $p < 0.001$), respectively, 2 months after BTX-A injection. Some patients, however, did not show the effect of BTX-A treatment as <30% reduction ($n = 3$), no change ($n = 2$), or increase ($n = 2$) in the headache days per month.

Both the headache and vertigo profiles of our VM patients showed marked improvement after the BTX-A treatment (Table 3, Figure 1). The HIT−6 (−9.5, 95% CI, −13.1 to −5.9, $p < 0.001$, paired t–test), the MIDAS (−25.2, 95% CI, −38.0 to −14.2, $p = 0.001$), and the MSQ scores (+36.2, 95% CI, 20.6–53.2, $p<0.001$) were significantly improved after the BTX–A treatment. In the vertigo profiles, the VSS (−12.6, 95% CI, −18.1 to −8.0, $p < 0.001$, paired t–test) and the DHI (−20.1, 95% CI, −27.1 to −13.1, $p < 0.001$) were also improved after the injection. The mean scores of the BDI (−6.9, 95% CI, −10.3 to −3.5, $p < 0.001$) and BAI (−9.1, 95% CI, −14.0 to −4.5, $p = 0.001$) were improved 2 months after the BTX-A injection.

Resting-state ALFF values after BTX-A treatment

Compared with the baseline, the ALFF values were significantly higher in the right STG after BTX-A treatment ($p < 0.001$, FDR and FWE corrected, Table 4 and Figure 2A).

Seed-based functional connectivity

To further explore the role of the right STG in VM management using BTX-A injection, we applied an FC analysis using the peak of the overlapped cluster at the right STG (57, −36, 3, 5 mm) as the seed. After BTX-A treatment, the following FC values were increased between the right STG and (i) right supramarginal gyrus (SMG); (ii) left postcentral gyrus (PCG); (iii) right middle temporal gyrus (MTG) (Figure 2B, Table 5). Subanalyses revealed a significant negative correlation between the FC of the right STG–SMG and the migraine disability MIDAS ($r = -0.562$, $p = 0.019$, Pearson's correlation analysis) (Figure 3), and no other relevant subanalysis showed significant correlations.

Discussion

In this study, 155U BTX-A injections significantly reduced both vertigo attacks and migraine headache compared with

TABLE 3 Efficacy of botulinum toxin type A injection.

Parameters	Baseline	After treatment	p-value[a]
Headache profile			
Frequency (days/month)	17.8 ± 9.9	9.5 ± 10.1	0.001
Severity (VAS, 1–10)	6.8 ± 1.3	5.0 ± 2.6	<0.001
HIT-6 (6 questions, 78 points)	65.0 ± 7.4	55.2 ± 8.8	<0.001
Severe headache (HIT-6 ≥ 60 points)	17 (85%)	7 (35%)	0.002[b]
MIDAS (5 questions, days/3 month)	53.3 ± 29.4	28.3 ± 30.3	0.001
grade 1 (MIDAS score 0–5)	0 (0%)	8 (40%)	0.002[b]
grade 2 (MIDAS score 6–10)	0 (0%)	2 (10%)	
grade 3 (MIDAS score 11–20)	3 (15%)	0 (0%)	
grade 4 (MIDAS score ≥21)	17 (85%)	10 (50%)	
MSQ (14 questions, 100 points)	68.8 ± 47.1	105.0 ± 40.3	<0.001
MSQ_RR (7 questions)	23.9 ± 15.0	36.1 ± 13.7	0.001
MSQ_RP (4 questions)	24.3 ± 15.8	34.5 ± 14.4	0.003
MSQ_EF (3 questions)	20.7 ± 18.1	34.3 ± 16.8	0.001
Vestibular symptom profiles			
Frequency (days/month)	14.0 ± 5.0	8.5 ± 5.4	<0.001
Intensity (VAS-D, 0–10)	6.0 ± 2.8	3.7 ± 2.7	0.001
VSS (15 questions, 60 points)	30.1 ± 10.5	18.2 ± 11.3	<0.001
DHI (25 questions, 100 points)	52.4 ± 27.8	31.6 ± 22.9	<0.001
Physical (7 questions, 28 points)	11.6 ± 6.6	7.9 ± 5.2	0.001
Functional (9 questions, 36 points)	20.1 ± 11.9	13.8 ± 10.5	0.015
Emotional (9 questions, 36 points)	19.2 ± 10.0	10.1 ± 9.0	<0.001
Depression and anxiety profile			
BDI (21 questions, 63 points)	23.9 ± 15.6	16.0 ± 11.0	<0.001
BAI (21 questions, 63 points)	26.6 ± 14.7	16.7 ± 13.0	0.001

VAS, visual analog scale; HIT-6, Headache Impact Test-6; MIDAS, Migraine Disability Assessment; MSQ, Migraine Specific Quality of Life; RR, Role-function Restrictive; RP, Role-function Preventive; EF, Emotional Function; VAS-D, Visual Analog Scale-Dizziness; VSS, Vertigo Symptom Scale-short form; DHI, Dizziness Handicap Inventory; BDI, Beck Depression Inventory; BAI, Beck Anxiety Inventory.
[a]Paired t-test; [b]Pearson's chi-square test.

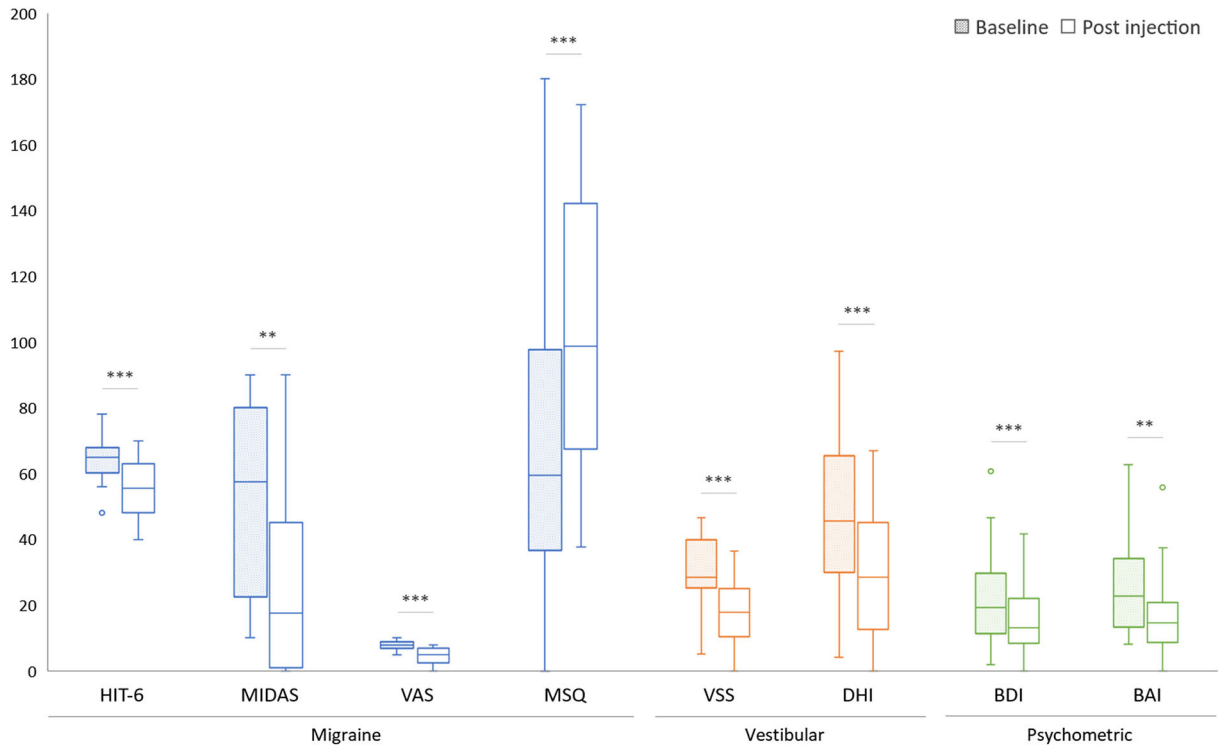

FIGURE 1
Comparison of symptomatic functional disability scores before (baseline) and after BTX-A treatment. $^{*}p < 0.05$, $^{**}p < 0.01$, $^{***}p < 0.001$.

TABLE 4 Brain regions with significant amplitude of low frequency fluctuation (ALFF) differences between pre- and post-BTX-A injection in vestibular migraine patients.

Cluster	Brain region	Cluster size	x	y	z	*t* value
Cluster 1	Right superior temporal gyrus	67	57	−36	3	5.94
			54	−21	3	5.61
			63	−24	−3	5.39

ALFF for contrast post-treatment > pre-treatment (FDR and FWE p < 0.05 corrected).

baseline in our 20 patients with VM. The patients also reported significant improvements in their functionality and the tolerability of migraine headache and vestibular symptoms after BTX-A treatment.

Although various mechanisms have been put forward to explain VM symptoms, interactions between nociceptive and vestibular pathways are broadly considered to represent the underlying pathophysiology of VM. The reciprocal connections between the vestibular nuclei and other brainstem structures, such as the raphe nuclei, the parabrachial nucleus, and the locus coeruleus, could modulate the sensitivity of the trigeminovascular system (TVS) and pain pathways (18), which could explain vestibular symptoms in VM. Altered neural activity within the TVS is considered to be the primary mechanism for migraine headache (19). Thus, TVS neuropeptides such as substance P and calcitonin gene-related peptide (CGRP), which cause vasodilation and neurogenic inflammation, might lead to throbbing pain and central sensitization (20). The TVS also innervates the inner ear, and some neurotransmitters, such as CGRP and serotonin, are expressed in the vestibular and cochlear systems and might also be involved in VM pathophysiology (21). Animal studies have shown increased CGRP expression in a rotational model of motion sickness (22), and CGRP null mice have a reduced vestibulo-ocular reflex (23), which gives more evidence that CGRP is expressed throughout various vestibular nuclei (24). These findings highlight the potential role of elevated CGRP signaling as an underlying mechanism in the association between migraine and vertigo (25). Parallel activation of the vestibular and nociceptive pathways, such as the periaqueductal gray and hypothalamic areas, has been proposed, and reciprocal connections between these systems could modulate neural activity within the TVS and vestibular system (26, 27). Furthermore, the response of both headache and vertigo symptoms to migraine prophylactic medications suggests that migraine headache

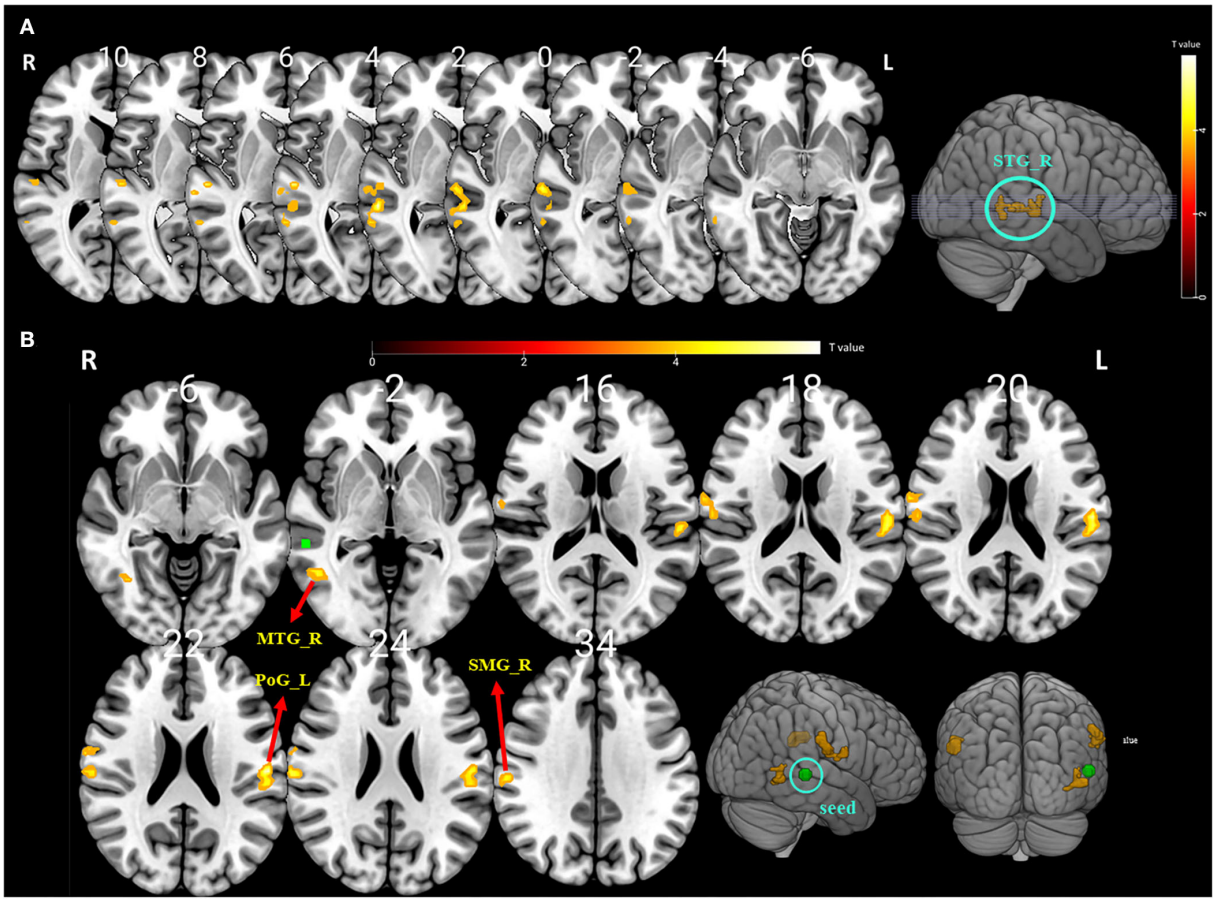

FIGURE 2
(A) The significantly altered amplitude of the low-frequency fluctuation (ALFF) map of the right superior temporal gyrus (STG) in vestibular migraine patients after BTX-A treatment (FDR and FWE $p < 0.05$ corrected). The color bar denotes the t-value. **(B)** Functional connectivity (FC) analysis using the peak of the overlapped cluster at the right STG (5-mm green sphere; 57, −36, 3) as the seed. Positive (hot color) t-value indicates increased FC (i) between the right STG and right supramarginal gyrus (SMG); (ii) between the right STG and left postcentral gyrus (PSG); and (iii) between the right STG and right middle temporal gyrus (MTG) (FDR and FWE $p < 0.05$ corrected).

and vertigo could share a common pathophysiology in the VM population (26).

Although the exact mechanism of action of BTX-A in VM is still a matter of speculation, animal studies suggest that BTX-A can block the release of nociceptive mediators such as substance P, glutamate, and CGRP, which reduces nociceptive input into the central nervous system from the periphery (28). Correspondingly, it has been shown that CGRP levels in chronic migraine patients strongly correlate with their response to BTX-A therapy (29), and CGRP levels after BTX-A treatment were significantly lower than before BTX-A treatment (median, 51.89 vs. 74.09 pg/ml, $p<0.001$) in patients with chronic migraine (30). Therefore, the activation of the TVS and vestibular system and the release of pain-producing molecules, especially CGRP, could be a potential therapeutic intervention during chronic migraine and VM attacks. Injections of BTX-A at the designated pericranial sites inhibit the release of CGRP, which would otherwise facilitate nociceptive transmission, contribute to the development of peripheral and central sensitization and possibly also contribute to pain processing and vestibular system modulation (20). Therefore, the primary mechanism of action for BTX-A in VM might be reversing peripheral and central sensitization by inhibiting the release of CGRP and (to a lesser degree) other pain-producing molecules from TVS neurons (31). In addition, it was suggested that BTX-A-mediated blockage of excitatory synapses might indirectly enhance inhibitory neurotransmission through an as yet unknown mechanism. Recently, it was reported that such a mechanism might be connected with the opioid and GABA-ergic systems in the central nervous system (32). Therefore, we speculate that the primary mechanism of BTX-A in patients with VM might involve the inhibition of TVS neuropeptide release such

as CGRP and the enhancement of endogenous opioidergic and GABA-ergic transmissions, which can modulate neural activity within both the TVS and the vestibular system. Supportively, BTX-A has been shown to be less effective in chronic tension-type headache, a condition in which CGRP levels have been shown to be normal (33).

TABLE 5 Results from the seed-based functional connectivity analysis showing altered right superior temporal gyrus (STG) functional connectivity (FC) pre- and post-treatment across patients.

Cluster	Brain region	Cluster size	x	y	z	*t* value
Cluster 1	Right supramarginal gyrus (SMG)	62	63	−24	30	5.9
			57	−21	36	4.96
			66	−6	21	4.87
Cluster 2	Left postcentral gyrus (PCG)	51	−57	−18	21	6.08
Cluster 3	Right middle temporal gyrus (MTG)	33	51	−57	−3	5.38
			36	−60	−6	4.72
			48	−57	6	4.67

FC with right STG for contrast post-treatment > pretreatment (FDR and FWE $p < 0.05$ corrected).

Cortical areas involved in processing vestibular information include the insular and retroinsular cortex, the parietal operculum, the STG, the temporo-parietal junction and posterior parietal cortex, the postcentral gyrus, the cingulum, the hippocampus, and the frontal cortices (34). These regions are multisensory areas in which the inputs of several sensory modalities, i.e., auditory, somatosensory, and visual, converge with vestibular information. Similarly, pain is a complex, multifactorial subjective experience, and a large distributed brain network is involved in nociceptive processing (35). Nociceptive-specific cortical and subcortical brain regions that are commonly activated by pain stimulation include the anterior cingulate cortex, insula cortex, frontal and pre-frontal cortices, primary and secondary somatosensory cortices, thalamus, basal ganglia, cerebellum, amygdala, hippocampus, and regions within the parietal and temporal cortices (36). The somatosensory and nociceptive cortical projections strongly overlap with the vestibular cortical projections, giving rise to vestibular-somatosensory and vestibular-nociceptive interactions, whose occurrence has been demonstrated by caloric and galvanic vestibular stimulation in humans (37). Therefore, it has been suggested that vestibular input could influence the processing of other tactile and nociception inputs.

In this study, alterations in spontaneous brain activity in VM patients were evaluated before and after BTX-A treatment using

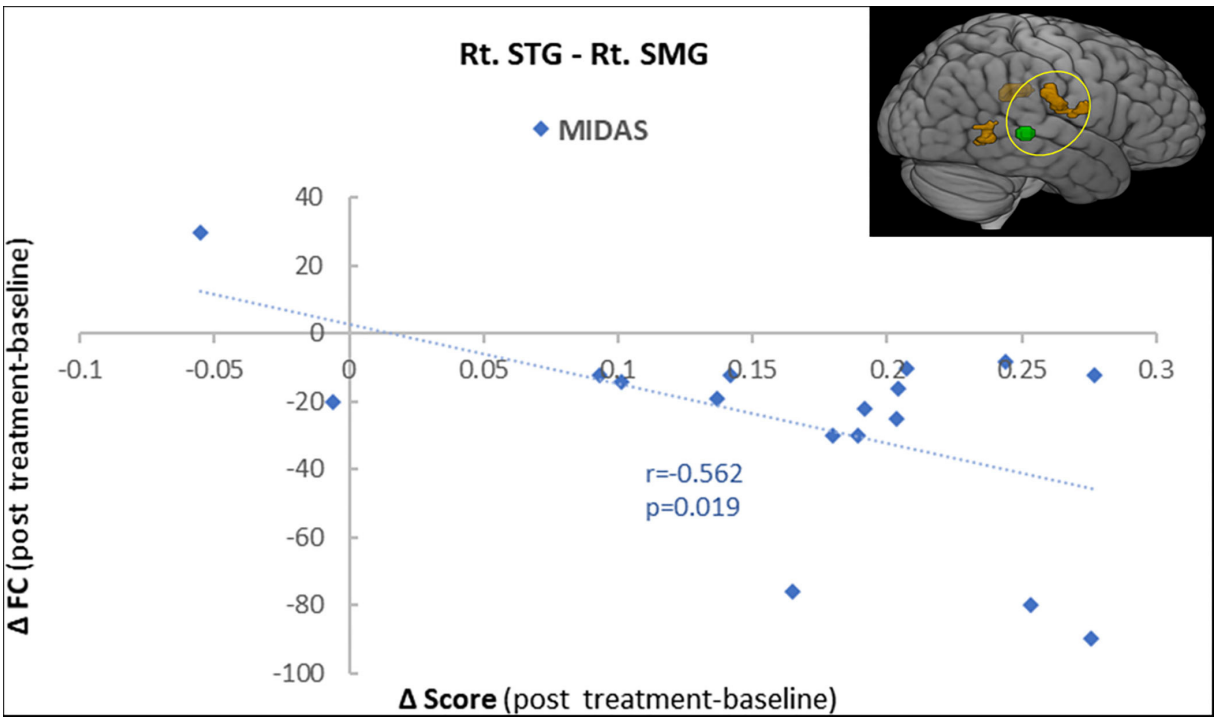

FIGURE 3
A correlation analysis showed a significant negative correlation between the functional connectivity of the right superior temporal gyrus (STG) with the supramarginal gyrus (SMG) and the MIDAS score ($r = -0.56$, $p = 0.001$).

two different sequential data-driven analyses, namely, ALFF and a seed-based functional connectivity (FC) analysis. Increased spontaneous activity was indicated by significantly higher ALFF values in the right temporal lobe (STG) after BTX-A treatment compared with the baseline. FC between the right STG and left PSG, right SMG, and right MTG was also increased after treatment. The enhanced regional functional activity after BTX-A treatment, mainly in the right temporal lobe, which contains the vestibular cortical core regions and participating pain processing regions, suggests that BTX-A injection can modulate the functional connectivity of the vestibular and pain cortices. The STG is an important area within the vestibular network and is closely connected to other multisensory brain regions. The posterior STG is consistently described as a core region for central vestibular processing, along with the posterior insula and parietal operculum, and as a secondary processing region for coordination of the eyes and head and spatial orientation. Structural and functional abnormalities of the STG have previously been demonstrated in both migraine patients (38) and patients with vestibular disorders (39). In chronic migraine, hypometabolism was reported in the bilateral temporal regions compared with healthy controls (38). On the contrary, hypermetabolism in the temporal lobe regions, including the temporal pole and STG, has been found in response to painful stimuli (40). In VM patients, an increased metabolism in the temporal areas was reported during a migraine attack (41). During the attack-free interval of VM patients, voxel-based morphometry in MRI showed a decrease in GM volume bilaterally in the inferior and middle temporal gyri, the cingulate cortex, and the posterior insula, as well as in the STG, supramarginal gyrus, dorsolateral prefrontal cortex, and inferior occipital gyrus (39). In this study, alterations in the ALFF values were observed only at the right side STG after treatment, which reflects the right-hemispheric dominance of the vestibular cortical network in right-handers in our VM patients (42).

The FC between the right STG and the right SMG increased after BTX-A treatment, and interestingly, the correlation analysis showed a negative correlation with the headache-related disability in the MIDAS score. The SMG and angular gyrus within the inferior parietal lobule (IPL) have been shown to be activated by vestibular stimulation (43). The IPL is also part of somatosensory processing, functions in the pain response and the sensing of temperature and pressure. In patients with migraine with or without aura, structural abnormalities of the SMG have been demonstrated (44). VM patients also have decreased GM volume in the SMG, the prefrontal cortex, and the posterior insula–operculum regions compared with healthy controls. Increased FC between the right STG and SMG and the negative correlation with the MIDAS score indicate that migrainous headaches improved after BTX-A treatment over time in parallel with the increased FC between the STG and SMG. We also found increased FC between the right STG and the PCG and MTG. These brain regions belong to the multisensory vestibular network, and the areas are activated by exposure to magnetic vestibular stimulation (45). The MTG in particular is considered to be functionally relevant to vestibular compensatory mechanisms and is strongly interconnected with other multisensory cortical areas that form a multisensory-integrative network (39). The increase in FC between the STG and regions of the MTG and PCG thus allows for two interpretations: first, it contributes to vestibular compensation during the recovery phases after BTX-A treatment, and second, the inclusion of somatosensory processing might reflect the integration between the vestibular and nociceptive systems.

This study has several limitations. First, the number of VM patients is relatively small in this longitudinal approach. Second, we choose a controlled before-after study which is a non-randomized design in that outcomes are measured before and after BTX-A treatment, both in a group that receives the treatment and in another comparison group. Typically this design could have a high risk of bias because of other differences between the groups that are being compared (confounders), and the placebo effect cannot be excluded. Third, it is difficult to assert that the change in the resting-state brain connectivity is a VM-specific finding because the comparative analysis was not conducted with a group of patients with migraine other than VM. Fourth, even though we did not change the use of preventive medications, we cannot exclude the possibility that the use of preventive therapies might have influenced the resting state of the brain and led to functional changes. Lastly, the follow-up of the patients for 2 months after the treatment might be too short; longer longitudinal studies are needed to evaluate the long-term effects of BTX-A in patients with VM.

In conclusion, our novel findings that BTX-A is effective in improving vertigo and migraine attacks in patients with VM and improved functional brain activity and connectivity in the vestibular and somatosensory (pain) processing regions after BTX-A treatment are intriguing and promising to expand our understanding of the pathophysiology of VM. With respect to the therapeutic mechanisms, botulinum toxin might enhance intrinsic vestibular, nociceptive, and cross-modal interactions within the multisensory vestibular cortical network in patients with VM. The findings suggest a disease-related dysfunction of multisensory (nociceptive, somatosensory, vestibular) cortical networks in VM patients.

Data availability statement

The original contributions presented in the study are included in the article/supplementary material, further inquiries can be directed to the corresponding authors.

Ethics statement

This study was approved by the Ethics Committee of Jeonbuk National University Hospital (IRB File No. 2020-10-033-001). The patients/participants provided their written informed consent to participate in this study.

Author contributions

S-YO was involved in the study concept and design and drafting a significant portion of the manuscript. J-JK was involved in the acquisition and analysis of data and drafting a significant portion of the manuscript and figures. SK and J-ML were involved in the acquisition and analysis of data. J-SK and MD were involved in the analysis of data and drafting a significant portion of the manuscript.

Funding

This study was supported by the Neurological Disorder Research Program of the National Research Foundation of Korea (NRF) grant funded by the Korean government (Ministry of Science and ICT) (Nos. 2022R1A2B5B01001933 and 2020M3E5D9080788) and by the Fund of the Biomedical Research Institute, Jeonbuk National University Hospital.

Conflict of interest

The authors declare that the research was conducted in the absence of any commercial or financial relationships that could be construed as a potential conflict of interest.

Publisher's note

All claims expressed in this article are solely those of the authors and do not necessarily represent those of their affiliated organizations, or those of the publisher, the editors and the reviewers. Any product that may be evaluated in this article, or claim that may be made by its manufacturer, is not guaranteed or endorsed by the publisher.

References

1. Lempert T, Olesen J, Furman J, Waterson J, Seemungal B, Carey J, et al. Vestibular migraine: diagnostic criteria. *J Vestib Res.* (2012) 22:167–72. doi: 10.3233/VES-2012-0453

2. Dieterich M, Obermann M, Celebisoy N. Vestibular migraine: the most frequent entity of episodic vertigo. *J Neurol.* (2016) 263:82–9. doi: 10.1007/s00415-015-7905-2

3. Huang T-C, Wang S-J, Kheradmand A. Vestibular migraine: an update on current understanding and future directions. *Cephalalgia.* (2020) 40:107–21. doi: 10.1177/0333102419869317

4. Lipton RB, Rosen NL, Ailani J, DeGryse RE, Gillard PJ, Varon SF. OnabotulinumtoxinA improves quality of life and reduces impact of chronic migraine over one year of treatment: pooled results from the PREEMPT randomized clinical trial program. *Cephalalgia.* (2016) 36:899–908. doi: 10.1177/0333102416652092

5. Blumenfeld AM, Schim JD, Chippendale TJ. Botulinum toxin type A and divalproex sodium for prophylactic treatment of episodic or chronic migraine. *Headache.* (2008) 48:210–20. doi: 10.1111/j.1526-4610.2007.00949.x

6. Lipton R, Varon S, Grosberg B, McAllister F, Aurora S, Dodick D, et al. OnabotulinumtoxinA improves quality of life and reduces impact of chronic migraine. *Neurology.* (2011) 77:1465–72. doi: 10.1212/WNL.0b013e318232ab65

7. Silberstein SD, Göbel H, Jensen R, Elkind AH, DeGryse R, Walcott JMCM, et al. Botulinum toxin type A in the prophylactic treatment of chronic tension-type headache: a multicentre, double-blind, randomized, placebo-controlled, parallel-group study. *Cephalalgia.* (2006) 26:790–800. doi: 10.1111/j.1468-2982.2006.01114.x

8. Cohen AL, Fair DA, Dosenbach NU, Miezin FM, Dierker D, Van Essen DC, et al. Defining functional areas in individual human brains using resting functional connectivity MRI. *Neuroimage.* (2008) 41:45–57. doi: 10.1016/j.neuroimage.2008.01.066

9. Arnold M. Headache classification committee of the international headache society (IHS) the international classification of headache disorders. *Cephalalgia.* (2018) 38:1–211. doi: 10.1177/0333102417738202

10. Blumenfeld A, Silberstein SD, Dodick DW, Aurora SK, Turkel CC, Binder WJ. Method of injection of onabotulinumtoxinA for chronic migraine: a safe, well-tolerated, and effective treatment paradigm based on the PREEMPT clinical program. *Headache.* (2010) 50:1406–18. doi: 10.1111/j.1526-4610.2010.01766.x

11. Stewart WF, Lipton RB, Dowson AJ, Sawyer J. Development and testing of the Migraine Disability Assessment (MIDAS) Questionnaire to assess headache-related disability. *Neurology.* (2001) 56:S20–8. doi: 10.1212/WNL.56.suppl_1.S20

12. Yardley L, Masson E, Verschuur C, Haacke N, Luxon L. Symptoms, anxiety and handicap in dizzy patients: development of the vertigo symptom scale. *J Psychosom Res.* (1992) 36:731–41. doi: 10.1016/0022-3999(92)90131-K

13. Jacobson GP, Newman CW. The development of the dizziness handicap inventory. *Arch Otolaryng Head Neck Surg.* (1990) 116:424–7. doi: 10.1001/archotol.1990.01870040046011

14. Fydrich T, Dowdall D, Chambless DL. Reliability and validity of the Beck anxiety inventory. *J Anxiety Disord.* (1992) 6:55–61. doi: 10.1016/0887-6185(92)90026-4

15. Yan C-G, Wang X-D, Zuo X-N, Zang Y-F, DPABI. data processing & analysis for (resting-state) brain imaging. *Neuroinformatics.* (2016) 14:339–51. doi: 10.1007/s12021-016-9299-4

16. Friston KJ, Williams S, Howard R, Frackowiak RS, Turner R. Movement-related effects in fMRI time-series. *Magnetic Resonance Med.* (1996) 35:346–55. doi: 10.1002/mrm.1910350312

17. Yu-Feng Z, Yong H, Chao-Zhe Z, Qing-Jiu C, Man-Qiu S, Meng L, et al. Altered baseline brain activity in children with ADHD revealed by resting-state functional MRI. *Brain Dev.* (2007) 29:83–91. doi: 10.1016/j.braindev.2006.07.002

18. Halberstadt A, Balaban C. Anterograde tracing of projections from the dorsal raphe nucleus to the vestibular nuclei. *Neuroscience.* (2006) 143:641–54. doi: 10.1016/j.neuroscience.2006.08.013

19. Pietrobon D, Moskowitz MA. Pathophysiology of migraine. *Annu Rev Physiol.* (2013) 75:365–91. doi: 10.1146/annurev-physiol-030212-183717

20. Furman JM, Marcus DA, Balaban CD. Migrainous vertigo: development of a pathogenetic model and structured diagnostic interview. *Curr Opin Neurol.* (2003) 16:5–13. doi: 10.1097/00019052-200302000-00002

21. Durham PL. Calcitonin gene-related peptide (CGRP) and migraine. *Headache.* (2006) 46:S3–8. doi: 10.1111/j.1526-4610.2006.00483.x

22. Xiaocheng W, Zhaohui S, Junhui X, Lei Z, Lining F, Zuoming Z. Expression of calcitonin gene-related peptide in efferent vestibular system and vestibular nucleus in rats with motion sickness. *PLoS ONE*. (2012) 7:e47308. doi: 10.1371/journal.pone.0047308

23. Luebke AE, Holt JC, Jordan PM, Wong YS, Caldwell JS, Cullen KE. Loss of α-calcitonin gene-related peptide (αCGRP) reduces the efficacy of the vestibulo-ocular reflex (VOR). *J Neurosci.* (2014) 34:10453–8. doi: 10.1523/JNEUROSCI.3336-13.2014

24. Kong W, Scholtz A, Hussl B, Kammen-Jolly K, Schrott-Fischer A. Localization of efferent neurotransmitters in the inner ear of the homozygous Bronx waltzer mutant mouse. *Hear Res.* (2002) 167:136–55. doi: 10.1016/S0378-5955(02)00382-9

25. Holland PR, Saengjaroentham C, Vila-Pueyo M. The role of the brainstem in migraine: potential brainstem effects of CGRP and CGRP receptor activation in animal models. *Cephalalgia.* (2019) 39:390–402. doi: 10.1177/0333102418756863

26. Furman JM, Marcus DA, Balaban CD. Vestibular migraine: clinical aspects and pathophysiology. *Lancet Neurol.* (2013) 12:706–15. doi: 10.1016/S1474-4422(13)70107-8

27. Koo J-W, Balaban C. Serotonin-induced plasma extravasation in the murine inner ear: possible mechanism of migraine-associated inner ear dysfunction. *Cephalalgia.* (2006) 26:1310–9. doi: 10.1111/j.1468-2982.2006.01208.x

28. Aoki K. Review of a proposed mechanism for the antinociceptive action of botulinum toxin type A. *Neurotoxicology.* (2005) 26:785–93. doi: 10.1016/j.neuro.2005.01.017

29. Cernuda-Morollón E, Martínez-Camblor P, Ramón C, Larrosa D, Serrano-Pertierra E, Pascual J, et al. and VIP levels as predictors of efficacy of Onabotulinumtoxin type A in chronic migraine. *Headache.* (2014) 54:987–95. doi: 10.1111/head.12372

30. Cernuda-Morollón E, Ramón C, Martínez-Camblor P, Serrano-Pertierra E, Larrosa D, Pascual J. OnabotulinumtoxinA decreases interictal CGRP plasma levels in patients with chronic migraine. *Pain.* (2015) 156:820–4. doi: 10.1097/j.pain.0000000000000119

31. Iyengar S, Johnson KW, Ossipov MH, Aurora SK, CGRP. and the trigeminal system in migraine. *Headache.* (2019) 59:659–81. doi: 10.1111/head.13529

32. Drinovac V, Bach-Rojecky L, Lacković Z. Association of antinociceptive action of botulinum toxin type A with GABA-A receptor. *J Neural Transm.* (2014) 121:665–9. doi: 10.1007/s00702-013-1150-6

33. Ashina M, Bendtsen L, Jensen R, Schifter S. Jansen–Olesen I, Olesen J. Plasma levels of calcitonin gene-related peptide in chronic tension-type headache. *Neurology.* (2000) 55:1335–40. doi: 10.1212/WNL.55.9.1335

34. Klingner CM, Volk GF, Flatz C, Brodoehl S, Dieterich M, Witte OW, et al. Components of vestibular cortical function. *Behav Brain Res.* (2013) 236:194–9. doi: 10.1016/j.bbr.2012.08.049

35. Peyron R, Laurent B, Garcia-Larrea L. Functional imaging of brain responses to pain. A review and meta-analysis 2000. *Neurophysiol Clin.* (2000) 30:263–88. doi: 10.1016/S0987-7053(00)00227-6

36. zu Eulenburg P, Baumgärtner U, Treede R-D, Dieterich M. Interoceptive and multimodal functions of the operculo-insular cortex: tactile, nociceptive and vestibular representations. *Neuroimage.* (2013) 83:75–86. doi: 10.1016/j.neuroimage.2013.06.057

37. Ferrè ER, Day BL, Bottini G, Haggard P. How the vestibular system interacts with somatosensory perception: a sham-controlled study with galvanic vestibular stimulation. *Neurosci Lett.* (2013) 550:35–40. doi: 10.1016/j.neulet.2013.06.046

38. Torres-Ferrus M, Pareto D, Gallardo VJ, Cuberas-Borrós G, Alpuente A, Caronna E, et al. Cortical metabolic and structural differences in patients with chronic migraine. An exploratory 18FDG-PET and MRI study. *J Headache Pain.* (2021) 22:1–11. doi: 10.1186/s10194-021-01289-5

39. Obermann M, Wurthmann S, Steinberg BS, Theysohn N, Diener H-C, Naegel S. Central vestibular system modulation in vestibular migraine. *Cephalalgia.* (2014) 34:1053–61. doi: 10.1177/0333102414527650

40. Maleki N, Becerra L, Brawn J, McEwen B, Burstein R, Borsook D. Common hippocampal structural and functional changes in migraine. *Brain Struct Funct.* (2013) 218:903–12. doi: 10.1007/s00429-012-0437-y

41. Shin JH, Kim YK, Kim H-J, Kim J-S. Altered brain metabolism in vestibular migraine: comparison of interictal and ictal findings. *Cephalalgia.* (2014) 34:58–67. doi: 10.1177/0333102413498940

42. Dieterich M, Kirsch V, Brandt T. Right-sided dominance of the bilateral vestibular system in the upper brainstem and thalamus. *J Neurol.* (2017) 264:55–62. doi: 10.1007/s00415-017-8453-8

43. Lopez C, Blanke O. The thalamocortical vestibular system in animals and humans. *Brain Res Rev.* (2011) 67:119–46. doi: 10.1016/j.brainresrev.2010.12.002

44. Rocca MA, Messina R, Colombo B, Falini A, Comi G, Filippi M. Structural brain MRI abnormalities in pediatric patients with migraine. *J Neurol.* (2014) 261:350–7. doi: 10.1007/s00415-013-7201-y

45. Bottini G, Karnath H-O, Vallar G, Sterzi R, Frith C, Frackowiak R, et al. Cerebral representations for egocentric space: functional–anatomical evidence from caloric vestibular stimulation and neck vibration. *Brain.* (2001) 124:1182–96. doi: 10.1093/brain/124.6.1182

frontiers | Frontiers in Neurology

TYPE Original Research
PUBLISHED 12 August 2022
DOI 10.3389/fneur.2022.955088

Check for updates

OPEN ACCESS

EDITED BY
Denise Utsch Gonçalves,
Federal University of Minas
Gerais, Brazil

REVIEWED BY
Theodore Raphan,
Brooklyn College (CUNY),
United States
Stefan Kammermeier,
Ludwig Maximilian University of
Munich, Germany

*CORRESPONDENCE
Sun-Young Oh
ohsun@jbnu.ac.kr

†These authors have contributed
equally to this work

SPECIALTY SECTION
This article was submitted to
Neuro-Otology,
a section of the journal
Frontiers in Neurology

RECEIVED 28 May 2022
ACCEPTED 18 July 2022
PUBLISHED 12 August 2022

CITATION
Nguyen TT, Kang J-J and Oh S-Y
(2022) Thresholds for vestibular and
cutaneous perception and oculomotor
response induced by galvanic
vestibular stimulation.
Front. Neurol. 13:955088.
doi: 10.3389/fneur.2022.955088

COPYRIGHT
© 2022 Nguyen, Kang and Oh. This is
an open-access article distributed
under the terms of the Creative
Commons Attribution License (CC BY).
The use, distribution or reproduction
in other forums is permitted, provided
the original author(s) and the copyright
owner(s) are credited and that the
original publication in this journal is
cited, in accordance with accepted
academic practice. No use, distribution
or reproduction is permitted which
does not comply with these terms.

Thresholds for vestibular and cutaneous perception and oculomotor response induced by galvanic vestibular stimulation

Thanh Tin Nguyen[1,2,3†], Jin-Ju Kang[2,4†] and Sun-Young Oh[1,2,4*]

[1]Jeonbuk National University College of Medicine, Jeonju, South Korea, [2]Department of Neurology, Jeonbuk National University Hospital and School of Medicine, Jeonju, South Korea, [3]Department of Pharmacology, Hue University of Medicine and Pharmacy, Hue University, Hue, Vietnam, [4]Research Institute of Clinical Medicine of Jeonbuk National University-Biomedical Research Institute of Jeonbuk National University Hospital, Jeonju, South Korea

Objectives: In this study, the specific threshold intensities and response characteristics of galvanic vestibular stimulation (GVS) on vestibular (conscious) and cutaneous (detrimental) perception as well as oculomotor nystagmus (reflex) were determined.

Methods: The threshold intensities for vestibular and cutaneous perception and oculomotor response induced by GVS were determined in 25 right-handed healthy subjects (32.6 ± 7.2 years of age; 56% female). The subjects were seated upright, and eye movements were recorded while a direct GVS current was applied with paradigms of cathode on the right and anode on the left (CRAL) and also cathode on the left and anode on the right (CLAR).

Results: Subjects experienced dizziness, sense of spinning, or fall tendency, which was more frequently directed to the cathode (76%) than the anode (24%, $p < 0.001$, chi-square one-variable test) at mean current greater than 0.98 ± 0.29 mA (mean vestibular threshold). The current also triggered a more frequent mild tingling sensation at the cathode (56%) than the anode (30%) or on both sides (14%; $p = 0.001$, chi-square one-variable test) when above the mean cutaneous threshold of 0.9 ± 0.29 mA. Above the mean oculomotor threshold of 1.61 ± 0.35 mA, combined horizontal and torsional nystagmus was more frequent toward the cathode (86%) than toward the anode ($p < 0.001$, chi-square one-variable test). The mean oculomotor threshold was significantly higher than both the vestibular ($p < 0.001$, Mann–Whitney *U*-test) and cutaneous ($p < 0.001$, Mann–Whitney *U*-test) thresholds, which were comparable ($p = 0.317$, Mann–Whitney *U*-test). There was no significant disparity in these specific thresholds between the two GVS paradigms. The vestibular threshold was significantly higher in males than in females [1 (0.5–1.25) mA vs. 0.75 (0.625–1.125) mA, $Z = -2.241$, $p = 0.025$, Mann–Whitney *U*-test]. However, the thresholds of cutaneous perception and oculomotor response did not differ by sex.

Conclusion: The findings indicate that thresholds for vestibular and somatosensory perception are lower than the oculomotor threshold. Therefore, a strategy to reduce GVS current intensity to the level of vestibular or somatosensory perception threshold could elicit beneficial vestibular effects while avoiding undesirable effects such as oculomotor consequences.

KEYWORDS

galvanic vestibular stimulation (GVS), vestibular perception threshold, cutaneous threshold, nystagmus, vertigo

Introduction

Vestibular afferents are sensitive to motion acceleration when the head translates and rotates in space, creating rapid and accurate reflexive responses to unpredictable and high acceleration. This function is critical in maintaining balance and visual stability (1, 2). The afferents provide continuous data for exploring and comprehending a vast range of physical motions encountered in daily life, acting as an inertial sensor and significantly contributing to spatial navigation (1). Notably, the vestibular system is multimodal and integrative (1, 3, 4), involving the fusion of otolith- and canal-derived signals at the level of vestibular nuclei and multisensory integration and convergence (such as vestibular-visual, vestibular-somatosensory, and vestibular-visual-somatosensory interactions) at the vestibular nuclei, thalamus, and cerebral cortices (1, 3, 4). The coherence integration of three systems (i.e., vestibular, visual, and somatosensory) imparts the ability to determine an internal representation of space and spatial perception and navigation in three-dimensional coordinates, using both egocentric and exocentric strategies (5, 6). The interaction between body and environmental space *via* navigation continuously occurs based on data from the navigable space (optic flow and visual cues) and the perception of self-motion (vestibular and somatosensory) (5, 6).

Over the past century, transcutaneous delivery of electric currents to the vestibular afferents, commonly referred to as galvanic vestibular stimulation (GVS), has been used to study and understand the function of the vestibular system (7). GVS is a technique that can stimulate the spike trigger zone of primary vestibular afferents associated with both semicircular canals (SCCs) and otolith organs (8, 9), allowing perception of vestibular sensations with excellent temporal control (10, 11). Firing rates of peripheral vestibular afferents are increased by galvanic currents at the cathode and decreased at the anode (9, 12, 13). The adaptive capacity of two types of vestibular afferent fibers to each GVS waveform is strikingly different that irregular fibers are sensitive to small-amplitude, highly dynamic currents (alternating current, AC), but fail to sustain tonic firing rates with constant currents (direct current, DC), whereas regular fibers are the opposite (14). GVS has also been used in functional neuroimaging studies to investigate the vestibular system (15) and in a variety of behavioral experiments on the effects of vestibular stimulation on locomotion and cognitive processes (16). In the framework of clinical therapeutic studies, favorable advantages of GVS have been shown in the improvement of postural stability (17–19), gait performance (20), functional mobility (21, 22), sensory perception (23–25), and cognition (26, 27).

Due to an increasing interest in GVS applications in clinical neuropsychiatry and rehabilitation, it is important to determine the stimulus parameters of waveforms (DC, sinusoidal or noisy), intensity, frequency, polarity, duration, and timing of stimulation, as well as electrode size and positioning (14). When altering these parameters, different amounts of electric current can be elicited, and diverse physiologic and adverse effects induced (14). In addition to the assessment of efficacy, electrical safety is crucial for the clinical application of GVS and must be considered in the intervention. Frequently reported detrimental effects of GVS include itching, tingling, and burning at the stimulation site. In addition, high GVS amplitude leads to significantly decreased performance in short-term spatial memory or egocentric mental rotation, supported by a significant decrease in cell proliferation in the hippocampus (28), induced postural instability (29), and decreased dynamic visual acuity (30). To achieve the optimal effect and simultaneously reduce detrimental effects, it is necessary to determine the GVS threshold defined by the lowest level of stimulus required to evoke vestibular responses. GVS currents also activate other sensory inputs including those of the cutaneous, visual, and auditory systems as well as the vestibular system, which encompasses somatosensory, oculomotor, and vestibular responses during an intervention (14). Therefore, investigating the thresholds for specific points of each sensory perspective, cutaneous and vestibular perception as well as oculomotor response, is necessary. Because precise sensory feedback from the visual, vestibular, and cutaneous systems is critical for maintaining balance and motor control, determining the appropriate individualized GVS threshold will maximize the therapeutic effects of GVS intervention while

minimizing the associated unpleasant sensations. In particular, due to increased clinical application of GVS, the threshold should be determined prior to the experimental session (31–33). Previous research has determined GVS threshold based on mostly vestibular perception, occasionally cutaneous feeling, and rarely oculomotor activity. To the best of our knowledge, no study has previously assessed these specific GVS thresholds concurrently. Thus, the most appropriate method to determine GVS threshold remains unclear. In this study, specific threshold intensities and response characteristics of GVS on vestibular and cutaneous perception as well as oculomotor response were determined.

Materials and methods

Participants

This study included 25 healthy subjects (32.6 ± 7.2 years; range 23–53 years; 11 males, 14 females, Table 1) recruited at Jeonbuk National University Hospital from July to September 2021. According to the Edinburgh Handedness Inventory (34), all participants were right-handed. Participants did not have any history of neurologic or neuro-otologic diseases and were not taking any medication. The subjects underwent neurotological evaluations including video oculography and head-impulse test and vestibular-evoked myogenic potential tests to screen for any vestibular impairment. They showed no abnormalities on examinations. The subjects provided written informed consent to participate in the study following an explanation of the study protocol. All experiments were reviewed and approved by the Institutional Review Board at Jeonbuk National University Hospital (No. 2021-07-013-007).

Experimental design and GVS procedure

Data from each participant were collected in two randomly ordered sessions of DC-GVS paradigms of cathode on the right and anode on the left (CRAL) or cathode on the left and anode on the right (CLAR; Tables 1, 2). The experimental design using "CLAR and CRAL" in right-handed participants is required in the context of handedness-dependent vestibular lateralization, in which the vestibular input and signaling pathways from the dominant side are more predominant than those from the non-dominant side (35, 36). This allowed the detection of any difference in the GVS threshold between CLAR and CRAL models. At the beginning of the sessions, participants received verbal and written instructions regarding the tasks. A CE-certified battery-driven constant current stimulator (neuroConn DC-Stimulator Plus; neuroConn, Ilmenau, Germany) was used to deliver the DC to subjects sitting upright in a chair *via* a pair of 35 cm^2 (5 × 7 cm) (37–39) rectangular conductive rubber electrodes (neuroConn) coated with electrode gel and placed binaurally over both mastoids. The maximum current density in this study was estimated to be 57.14 $\mu A/cm^2$ (corresponding to a charge density of 1.71 $Coloumb/cm^2$) at the skin surface, similar to previous studies (37, 38), and well below the safety limit for tissue damage (40–42). The electrodes were positioned on the mastoid, supplemented with a conductive gel prior to testing to reduce skin impedance, and secured in place by a rubber head strap. Participants were seated in a comfortable chair in front of a target bar of the three-dimensional video oculography instrument (3D-VOG, SMI, the Netherlands, sampling rate of 60 Hz) and wore goggles that tracked their ocular movements under the supervision of a senior neurotologist (S.Y. Oh). Threshold testing started with a low current (0.5 mA), gradually increasing by 0.25 mA for a 3-s period over a 5-min inter-step interval. In the inter-step interval, the subjects were asked to describe whether they experienced any tingling/pain (cutaneous perception threshold) or dizziness/unsteadiness (vestibular perception threshold) during GVS application. The senior neurotologist also monitored for the appearance of nystagmus when recording with the VOG (oculomotor threshold). These iterations were continued with a steady increase in current until the participant concurrently expressed tingling/pain, dizziness/unsteadiness, and nystagmus. To confirm the specific thresholds, the stimulus intensity was gradually decreased by 0.25 mA from 2 mA to the level at which the tingling/pain (cutaneous threshold), dizziness/unsteadiness (vestibular threshold), and ocular responses (oculomotor threshold) disappeared (Figure 1). The procedure was repeated two times to confirm the cutaneous, vestibular, and oculomotor thresholds (43–45). When thresholds differed between sessions, the mean value was used for analysis.

Thresholds for vestibular and cutaneous perception and oculomotor response

A verbal warning preceded each stimulus, and subjects were instructed to say "yes" when perceiving tingling, pain, or any other sensation at the electrodes. Subjects were asked to describe the sensory feelings and indicate the location of occurrence. Subjects were also instructed to focus on vestibular perception and asked to report any sense of dizziness with spinning or non-spinning and disequilibrium or any sense of motion. Each report was followed by feedback confirming the perceptions such as motion direction, and the current intensity was increased in the next step. Eye position and movement were binocularly recorded using the 3D-VOG during the entire experiment. Digitized data were analyzed using the MATLAB software (MathWorks, Natick, MA, USA). All data pertaining

TABLE 1 Thresholds for somatosensory and vestibular perception and oculomotor response and their characteristics in response to GVS with the cathode on the right and the anode on the left (CRAL).

Pts./sex/age	Handedness	Cutaneous perception		Vestibular perception		Oculomotor response			
		Threshold (mA)	Sensing site	Threshold (mA)	Description	Threshold (mA)	Degree (°/s)	Duration (s)	Direction
1/F/48	Rt.	0.5	Cathode (Rt.)	0.5	Rt. tilting and CW rotation, vertigo	1	2.1	5	RBN
2/F/36	Rt.	1	Cathode (Rt.)	1	Rt. tilting and CW rotation, vertigo	0.5	2.1	4.9	LBN
3/M/34	Rt.	0.5	Both	1	Rt. tilting and CW rotation,	1	2.5	5.4	RBN
4/M/33	Rt.	1	Cathode (Rt.)	1.5	Rt. tilting and CW rotation, vertigo	1.5	2	4.1	RBN
5/F/32	Rt.	0.5	Cathode (Rt.)	0.5	Rt. tilting and CW rotation, vertigo	2	1.8	4.3	RBN
6/M/34	Rt.	1	Cathode (Rt.)	2	CCW rotation	1.5	1.7	3.4	LBN
7/F/29	Rt.	1.5	Cathode (Rt.)	0.5	Rt. tilting and CW rotation	2	1.6	3.9	RBN
8/M/29	Rt.	1	Cathode (Rt.)	1	Lt. tilting and CCW rotation, vertigo	2	2.4	4.4	CW
9/M31	Rt.	0.5	Cathode (Rt.)	1	CW rotation	1	1.7	5.1	RBN
10/F/30	Rt.	1.5	Cathode (Rt.)	1	Lt. tilting and CCW rotation, vertigo	0.5	1.9	5	RBN
11/F/23	Rt.	1	Anode (Lt.)	0.5	Rt. tilting and CW rotation, vertigo	1.75	1.9	4.4	RBN
12/F/26	Rt.	1.5	Cathode (Rt.)	0.5	Rt. tilting and CW rotation, vertigo	1	2.5	5	CCW
13/F/25	Rt.	0.5	Both	0.5	CCW rotation	0.5	2.4	5.2	RBN
14/F/38	Rt.	0.5	Anode (Lt.)	0.5	Lt. tilting and CCW rotation, vertigo	1.5	1.8	4.5	CCW
15/F/44	Rt.	0.5	Both	0.5	Rt. tilting and CW rotation, vertigo	2	2.5	4.9	RBN
16/M/53	Rt.	1.25	Anode (Lt.)	1.5	Lt. tilting feeling	2	1.8	6	RBN
17/M/35	Rt.	0.5	Anode (Lt.)	1	CW rotation and vertigo	2	2.1	3.8	RBN
18/F/31	Rt.	0.5	Anode (Lt.)	0.75	Rt. tilting and CW rotation	1	2.3	8.7	RBN
19/F/26	Rt.	0.5	Cathode (Rt.)	0.75	Rt. tilting and CW rotation	2	1.7	5	LBN
20/F/28	Rt.	2	Cathode (Rt.)	2	Rt. tilting and CW rotation	2	1.6	4.2	RBN
21/M/25	Rt.	1.5	Cathode (Rt.)	1.75	CCW rotation	2	1.9	6.3	RBN
22/M/36	Rt.	1.25	Anode (Lt.)	1.25	Rt. tilting and CW rotation	2	2.2	5.8	RBN
23/M/33	Rt.	2	Cathode (Rt.)	2	Rt. tilting and vertigo	2	1.8	3.7	RBN
24/F/29	Rt.	1.25	Anode (Lt.)	1.25	Rt. tilting and CW rotation	1.75	1.7	4.3	RBN
25/M/27	Rt.	0.5	Anode (Lt.)	1	Rt. tilting and CW rotation	1.5	2.7	8	RBN, UBN

GVS, galvanic vestibular stimulation; Pts, participants; M, male; F, female; Rt., right; Lt., left; CW, clockwise; CCW, counter-clockwise; RBN, right-beating nystagmus; LBN, left-beating nystagmus.

10.3389/fneur.2022.955088

TABLE 2 Thresholds for somatosensory and vestibular perception and oculomotor response and their characteristics in response to GVS with the cathode on the left and the anode on the right (CLAR).

Pts./sex/age	Handedness	Cutaneous perception		Vestibular perception		Oculomotor response			
		Threshold (mA)	Sensing site	Threshold (mA)	Description	Threshold (mA)	Degree (°/s)	Duration (s)	Direction
1/F/48	Rt.	0.5	Cathode (Lt.)	0.5	Lt. tilting and CCW rotation	1.5	2.2	5.1	LBN
2/F/36	Rt.	0.5	Cathode (Lt.)	0.75	Lt. tilting and CCW rotation	1	2.7	5.7	LBN
3/M/34	Rt.	0.5	Cathode (Lt.)	0.5	Lt. tilting and CCW rotation, vertigo	1.5	1.5	4.9	LBN
4/M/33	Rt.	1	Anode (Rt.)	0.75	Lt. tilting and CCW rotation, vertigo	1.75	1.9	4.6	LBN
5/F/32	Rt.	1.25	Cathode (Lt.)	1.25	Lt. tilting and CCW rotation	2	1.8	3.8	LBN
6/M/34	Rt.	1.5	Both	1.25	Rt. tilting and CW rotation	1.5	2.1	4.5	RBN
7/F/29	Rt.	0.5	Cathode (Lt.)	0.5	Lt. tilting and CCW rotation	1.5	2.3	5	LBN
8/M/29	Rt.	0.75	Cathode (Lt.)	0.75	Lt. tilting and CCW rotation	1.75	2.4	4	LBN
9/M31	Rt.	1	Anode (Rt.)	1.25	Lt. tilting and CCW rotation	2	1.4	6	LBN
10/F/30	Rt.	1	Anode (Rt.)	1	Rt. tilting and CW rotation	1.5	1.8	4.4	LBN
11/F/23	Rt.	0.5	Cathode (Lt.)	1	Lt. tilting and CCW rotation	1.5	2.2	5	LBN
12/F/26	Rt.	1.25	Cathode (Lt.)	1.5	Rt. tilting and CW rotation, vertigo	2	2.6	4.8	LBN
13/F/25	Rt.	1	Cathode (Lt.)	1	Lt. tilting and CCW rotation	1.5	2	5.9	LBN
14/F/38	Rt.	0.75	Cathode (Lt.)	0.75	Lt. tilting and CCW rotation	2	2.7	6	LBN
15/F/44	Rt.	1	Both	1	Lt. tilting and CCW rotation, vertigo	2	2	4.5	LBN, DBN, CCW
16/M/53	Rt.	0.75	Cathode (Lt.)	0.75	CCW rotation	1.5	1.1	4.7	LBN
17/M/35	Rt.	0.5	Anode (Rt.)	1	Lt. tilting and vertigo	2	1.8	3	LBN, DBN
18/F/31	Rt.	0.5	Cathode (Lt.)	0.75	Lt. tilting and CCW rotation	1.5	2.3	6	LBN
19/F/26	Rt.	1	Anode (Rt.)	1.25	Rt. tilting and CW rotation	1.5	1.8	5	LBN
20/F/28	Rt.	0.5	Both	0.5	Lt. tilting and CCW rotation, vertigo	2	1.7	4	LBN
21/M/25	Rt.	1	Cathode (Lt.)	1	Lt. tilting and CCW rotation	1.5	1.2	6.1	LBN
22/M/36	Rt.	1.75	Cathode (Lt.)	1.75	Lt. tilting and CCW rotation	2	2	6.2	LBN
23/M/33	Rt.	0.5	Both	0.75	Lt. tilting and CCW rotation	2	2.6	5.3	LBN
24/F/29	Rt.	1	Anode (Rt.)	1.25	Lt. tilting and CCW rotation	1.5	2.1	7.7	RBN
25/M/27	Rt.	0.75	Anode (Rt.)	0.5	Rt. tilting and CW rotation	2	1.8	4.5	LBN

10.3389/fneur.2022.955088

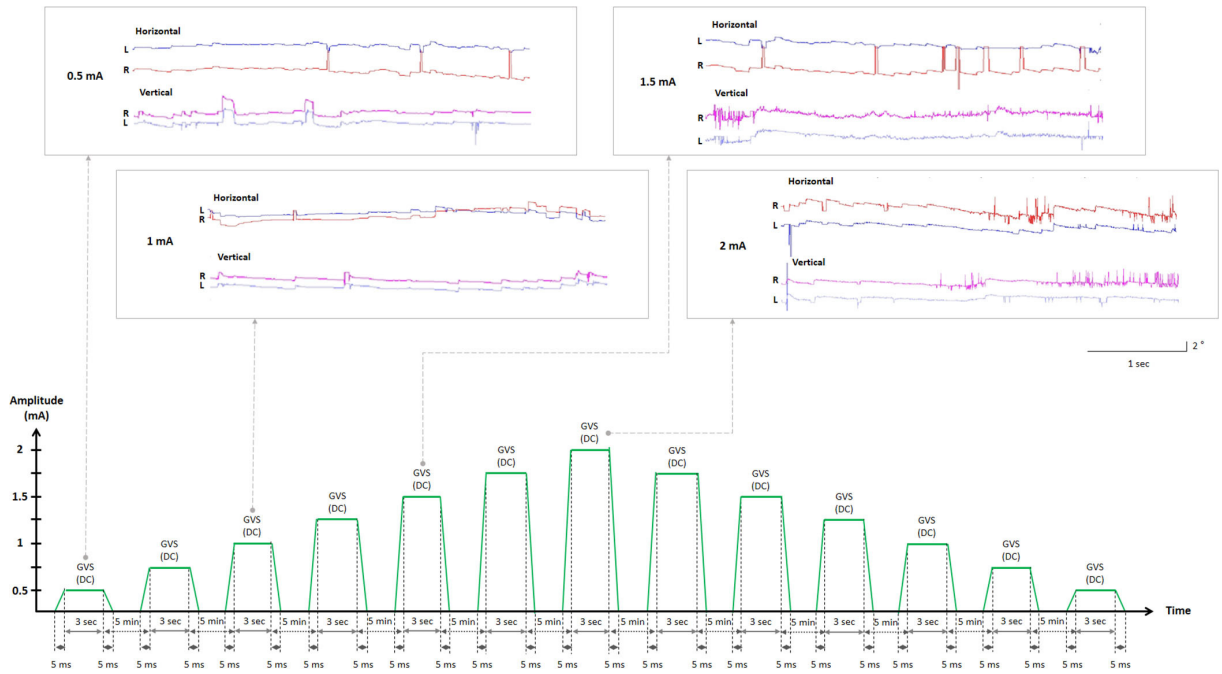

FIGURE 1
Experimental design flowchart. Representations of ocular movements during GVS application (in the boxes). The two-step approach to determining GVS thresholds. GVS, galvanic vestibular stimulation; DC, direct current; L, left eye (blue); R, right eye (red).

to the results reported in this article (text and figures) will be shared.

Statistical analysis

All data were analyzed using SPSS Statistics version 23.0 (IBM Corp., Armonk, NY, USA). For each parameter, the normality of the distribution was assessed using the Shapiro-Wilk test. The variables were presented as mean ± standard deviation. The non-parametric variables were indicated as median (95% confidence interval), and the significant difference was determined using the Kruskal-Wallis test (between group comparison) and the Mann-Whitney *U*-test (pairwise comparisons). The chi-square one-variable test was used to compare the difference between variables in multiple categories. The Spearman's correlation coefficient was used to assess the correlations between age and the vestibular, cutaneous, and oculomotor thresholds. Statistical significance was set at a 0.05 level.

Results

Although GVS is mildly unpleasant, no participant reported particular discomfort or withdrew from the study. All participants perceived cutaneous and vestibular sensations and showed oculomotor responses confirmed by VOG recordings (Figure 1).

Thresholds for cutaneous and vestibular perceptions and oculomotor response

Subjects experienced mild cutaneous tingling or stinging sensations above the mean stimulation intensity of 0.9 ± 0.29 mA (cutaneous threshold, 0.85 ± 0.35 mA on CLAR, and 0.97 ± 0.50 mA on CRAL; Figure 2). These somatosensory perceptions were more frequent on the cathode (56%) than the anode (30%) or both sides (14%; $p = 0.001$, chi-square one-variable test; Figure 3A). Subjects also experienced various vestibular sensations evoked by GVS, as described in the subject's self-report. Some participants experienced dizziness and vertigo, likely the manifestation of whole-body angular rotation or a sense of rotation of the environment as if the objects around them were spinning. Other participants described the feeling of change in gravity. These sensations persisted for several seconds even after cessation of the stimulation above the mean stimulation intensity of 0.98 ± 0.29 mA (vestibular threshold, 0.93 ± 0.33 mA on CLAR, and 1.03 ± 0.52 mA on CRAL; Figure 2). Rotating and falling sensations were more frequently experienced toward the cathode (76%) than the anode (24%, $p < 0.001$, chi-square one-variable test;

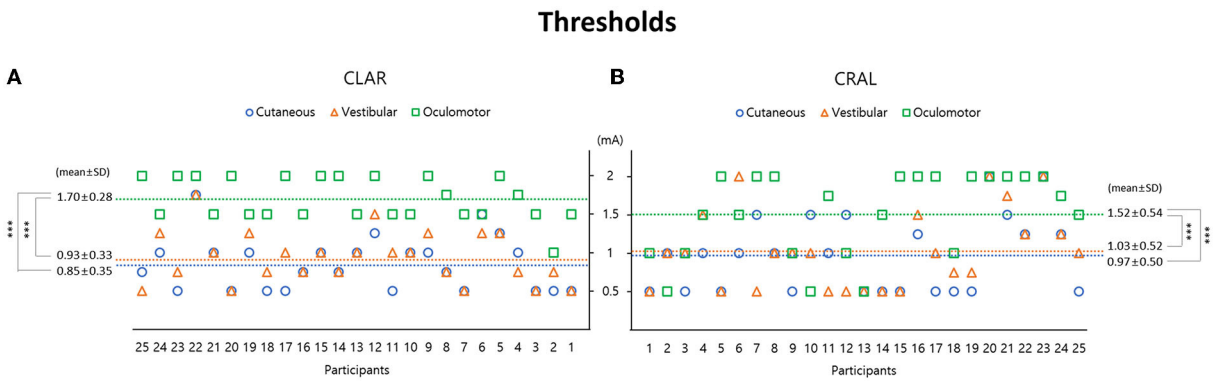

FIGURE 2
Galvanic vestibular stimulation (GVS) thresholds are presented separately: cutaneous and vestibular perceptions and oculomotor response using two stimulating paradigms of the cathode on the left and anode on the right (CLAR) **(A)** and the cathode on the right and anode on the left (CRAL) **(B)**. In the CLAR paradigm, the oculomotor threshold (1.7 ± 0.28 mA) was significantly higher than the vestibular perception threshold (0.93 ± 0.33 mA, $p < 0.001$, Bonferroni test) and cutaneous perception threshold (0.85 ± 0.35 mA, $p < 0.001$, Bonferroni test) **(A)**. In the CRAL paradigm, the oculomotor threshold (1.52 ± 0.54 mA) was also significantly higher than the vestibular perception threshold (1.03 ± 0.52 mA, $p <$ 0.001, Bonferroni test) and cutaneous perception threshold (0.97 ± 0.5 mA, $p < 0.001$, Bonferroni test) **(B)**. GVS threshold values are presented as mean ± standard deviation (mA).

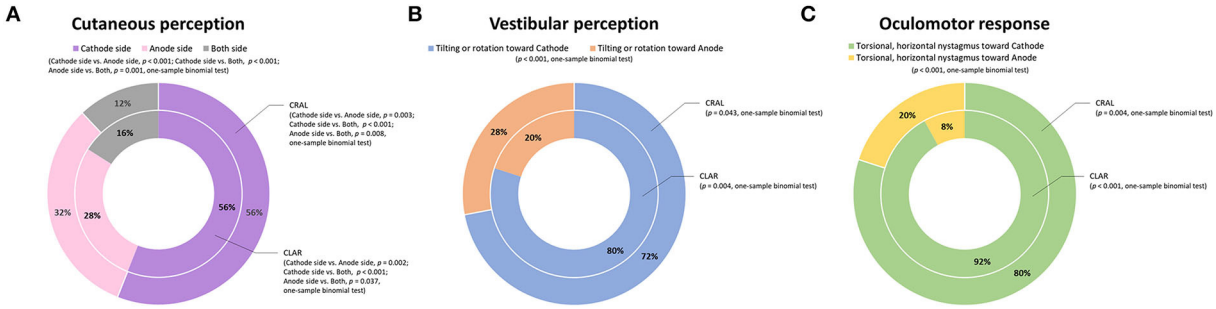

FIGURE 3
Characteristics of galvanic vestibular stimulation (GVS)-induced cutaneous and vestibular perception and oculomotor responses depending on the stimulating paradigms; the cathode on the left and the anode on the right (CLAR, inside annulus) and the cathode on the right and the anode on the left (CRAL, outside annulus). Cutaneous perceptions were more frequent on the cathode side (56%) than the anode (30%) or both sides (14%; $p = 0.001$, chi-square one-variable test) **(A)**. Rotating and falling sensations were more frequently experienced toward the cathode (76%) than the anode (24%, $p < 0.001$, chi-square one-variable test) direction **(B)**. Nystagmoid ocular movements were observed more frequently with horizontal and torsional nystagmus toward the cathode (86%) than toward the anode (14%, $p < 0.001$, chi-square one-variable test) **(C)**. Values are presented as percentages.

Figure 3B). The vestibular threshold in males was significantly higher than in females [1 (0.5–1.25) mA vs. 0.75 (0.625–1.125) mA, $Z = -2.241$, $p = 0.025$, Mann–Whitney U-test]. However, significant differences were not observed in cutaneous perception and oculomotor response between the sexes. Correlations were not found between age and vestibular, cutaneous, and oculomotor thresholds.

Short-latency eye movements were also observed above the mean stimulation intensity of 1.61 ± 0.35 mA (oculomotor threshold, 1.70 ± 0.28 mA on CLAR, and 1.52 ± 0.54 mA on CRAL; Figure 2). Nystagmoid ocular movements were observed more frequently with horizontal and torsional nystagmus toward the cathode (86%) than toward the anode (14%, $p < 0.001$, chi-square one-variable test; Figure 3C). The mean amplitude and the mean duration of nystagmus were, respectively, 2.03 ± 0.33°/s and 5.01 ± 1.23 s for CRAL and 2 ± 0.43°/s and 5.07 ± 0.98 s for CLAR (Table 3). Notably, the oculomotor threshold [1.75 (1.5–1.75) mA] was significantly higher than the vestibular perception threshold [1 (0.75–1.125) mA, $Z = -4.866$, $p < 0.001$, Mann–Whitney U-test] and the cutaneous perception threshold [0.875 (0.75–1.125) mA, $Z = -5.184$, $p < 0.001$, Mann–Whitney U-test; $\chi^2 = 34.488$, $p < 0.001$, Kruskal-Wallis test, Figure 2]. A comparison of the properties of cutaneous and vestibular perception and oculomotor responses between the CRAL and CLAR paradigms revealed no significant differences between them (Table 3).

TABLE 3 Comparison of the properties of cutaneous and vestibular perception and oculomotor response depending on the CRAL and CLAR GVS paradigms.

	Participants ($n = 25$)		*P*-value
	CRAL	CLAR	
Cutaneous perception			
Threshold, median (IQR) (mA)	1 (0.5–1.38)	0.75 (0.5–1)	0.542
Intensity, median (IQR) (1–10)	1 (1–2)	1 (1–1.5)	0.176
Nature			1.000
Neutral sensation, *n* (%)	23 (92)	24 (96)	
Painful sensation, *n* (%)	2 (8)	1 (4)	
Site			0.901
Cathode side, *n* (%)	14 (56)	14 (56)	
Anode side, *n* (%)	8 (32)	7 (28)	
Both, *n* (%)	3 (12)	4 (16)	
Vestibular perception			
Threshold, median (IQR) (mA)	1 (0.5–1.38)	1 (0.75–1.25)	0.441
Intensity, median (IQR) (1–10)	1 (1–2)	1 (1–2)	0.371
Nature			0.742
Tilting and rotation toward the cathode, *n* (%)	18 (72)	20 (80)	
Tilting and rotation toward the anode, *n* (%)	7 (28)	5 (20)	
Oculomotor response			
Threshold, median (IQR) (mA)	1.75 (1–2)	1.5 (1.5–2)	0.075
Degree, median (IQR) (°/s, Rt. eye)	1.9 (1.75–2.35)	2 (1.8–2.3)	0.794
Duration, median (IQR) (s)	4.9 (4.25–5.3)	5 (4.5–5.95)	0.567
Direction			0.417
Horizontal or torsional nystagmus toward the cathode, *n* (%)	20 (80)	23 (92)	
Horizontal or torsional nystagmus toward the anode, *n* (%)	5 (20)	2 (8)	

CRAL, the cathode on the right and the anode on the left; CLAR, the cathode on the left and the anode on the right; IQR, interquartile range.

Discussion

Vestibular and cutaneous perception and oculomotor response thresholds were measured in 25 healthy young subjects during DC GVS with both CRAL and CLAR paradigms, using a two-step approach with gradual increase and decrease in intensities. Vestibular and somatosensory perception thresholds were lower than the oculomotor threshold, indicating the use of the vestibular or somatosensory perception threshold to determine the GVS thresholds in the majority of human trials due to its sensitivity with minimal oculomotor responses. Theoretically, the vestibular threshold might reflect the vestibular function more directly and precisely than other motor response thresholds such as the vestibulo-ocular reflex (VOR) and the vestibulo-spinal reflex (VSR), which may be involved in central adaptation (1, 2, 14, 46, 47). Furthermore, the vestibular threshold could provide a comprehensive assay of peripheral vestibular function including the SSCs or otoliths (48, 49).

A previous study with a similar model reported a vestibular perception threshold of DC of 1.0 ± 0.2 mA, which is very similar to the results of our study (45). Recently, the vestibular threshold was shown to significantly increase after the age of 40 years (49), which has been considered a central gain enhancement for compensating the reduced peripheral vestibular input due to age-related degeneration of vestibular hair cells and afferents (50–52). In particular, prior studies have demonstrated that the aging-related degeneration of vestibular irregular afferent fibers, which are six times more sensitive to GVS than regular fibers, was faster and more potent than those in regular fibers (51, 53). Significant changes, however, have not been observed in the GVS threshold dependent on temporal effects, polarity effects, or body positions (10). Additionally, this study confirmed that there were no significant differences in the specific thresholds between the CRAL and CLAR configurations. Notably, a substantial difference associated with sex was found in vestibular perception but did not occur in cutaneous and oculomotor response thresholds, consistent with a recent trial (54). These sex-related threshold differences were most likely because they have a substantially different size of vestibular apparatus and numbers of vestibular afferent fibers (55, 56). In particular, the total number of myelinated axons in vestibular nuclei is significantly lower in females than in males (55). Regarding the otolith organs, the surface areas of the utricular and saccular maculae, the width of the utricular macula, and the length of the saccular macula are significantly greater in males than in females (56). In addition, diameters of the three SCCs are larger in males than in females, and the difference was statistically significant for the superior SCC (56). These anatomical distinctions might cause vestibular-related behavioral differences. For example, the GVS-induced ocular vestibular-evoked myogenic potential (oVEMP) amplitude was reported higher in males than in females (57). Males were shown to normally perform better in vestibular function-related tasks, in particular, visuospatial cognition such as 3D figures, spatial orientation, and maze navigation (58, 59).

Cutaneous sensations underneath and around the stimulus electrodes, such as burning, tingling, itching, and pain, mostly depend on the stimulus amplitude (14, 33) and have commonly been described as minor adverse effects of GVS intervention. The use of large surface electrodes on the mastoid, covering with electrode gel or topical anesthesia, or controlling the current amplitude helps to minimize the risk of skin irritations, burns, and patient discomfort (14, 60). The cutaneous threshold, also known as the nociceptive threshold, was determined to help manage these disruptions and enhance treatment compliance

(17, 26, 61, 62). The cutaneous threshold was determined to be 0.9 mA in this study, with tingling sensation occurring mostly at the cathode side (Figure 3A). The findings were in agreement with a previous study conducted on healthy volunteers utilizing the staircase approach to assess the cutaneous threshold in which a mean value of 0.8 mA was reported (63). Although several previous studies have revealed that a threshold of ∼1 mA produced no significant difference in somatosensory sensations between the anode and cathode sides (64–68), the sensory ratings were consistently higher at the cathode than at the anode for pain, tingling, piercing, electrifying, tugging, and pinching senses in other recent studies (Figure 3A) (68, 69). The tingling and itching sensations under the electrodes were usually short lasting and disappeared after a few seconds, similar to our findings. However, in some studies, the sensations were reportedly prolonged (64, 65, 70).

Regarding the characteristics of the vestibular responses to bipolar GVS, rotation and tilt were more frequently experienced toward the cathode (76%) than toward the anode (Figure 3B). Our present findings were in agreement with results from previous studies showing that DC-form GVS induces a tilt of subjective vertical toward the anode and simultaneously induces some illusion of self-tilt or spin toward the cathodal side (8, 71, 72). This dissociation between subjective vertical and body orientation elicited by GVS is mainly determined by central multisensory integration processes involved in the estimation of sensory cue reliability (72). Interestingly, the direction of tilt illusion was associated with posture only when the duration of the GVS was longer than 5 s, and it was toward the anode in freestanding posture, and toward the cathode in an immobilized posture (71). GVS-induced perception of motion is as context-dependent as oculomotor and postural responses, which are specified by the anatomic orientation of the SCC (SCC-driven signals) and the macular surfaces in the otolith organs (otolith-driven signals) (8). Cathodal GVS increases the firing rate of all responsive afferents, and anodal GVS decreases the firing rate of all responsive afferents; consequently, their effects at a canal are represented by a sum of geometric rotational stimuli (9, 40, 73). After calculating both the position of the canals in the plane of the head during upright standing and the incomplete orthogonal of SCCs, the summing vector representing the synergistic effects of SCC afferent activation evoked by GVS from both sides will be a signal roll with a yaw component, both directed toward the cathode, and a perceived visual tilt toward the anode (8, 11, 73). Furthermore, bilateral bipolar GVS produces a utricular firing pattern consistent with a natural stimulus of linear acceleration toward the cathodal side or visual tilt toward the anodal side (8, 11). However, in some psychophysical studies, the otolith contributions to GVS-induced postural responses were negligible compared with the canal input (74, 75).

As GVS can elicit ocular movement in the absence of head movement, it is frequently used to characterize potential pathologies in peripheral and central vestibular signal transmission (14). GVS activates both afferent fibers, including regular and irregular afferents, from all three SCCs to generate a horizontal-torsional nystagmus as a summative effect (14, 76). Regarding the time-related eye movements evoked by the application of a constant current application (DC-GVS) in this study, horizontal nystagmus frequently appeared at the onset of stimuli and immediately subsided, which was consistent with rapid activation but prompt adaptation characterized by thick, irregular fibers. However, non-adapting ocular torsion prevailed for the duration of the stimulus, which was the result of regular SCC fiber activation (14). Due to the oculomotor response threshold as the only method for estimating the GVS threshold in animal trials, it was often used as a control GVS (16, 77). In humans, however, due to discomforts such as oscillopsia and blurred vision caused by ocular movements, measurement of oculomotor threshold is less widely used to trigger vestibular stimulation with GVS. In previous studies with vestibular dysfunction patients, the GVS-induced eye movements were used to evaluate the reduction or absence of oculomotor contribution from the vestibular end organs (60, 78–80). Patients with bilateral vestibular nerve dissection or other pathological disorders affecting both vestibular nerves did not reveal GVS-induced oculomotor responses; therefore, these GVS-induced eye movements are considered a strong predictor of the residual function of the injured vestibular nerve (81–83). In this study, the oculomotor threshold was significantly higher than the vestibular and cutaneous perception thresholds (1.61 mA vs. 0.98 mA and 0.9 mA, Figure 2). Some previous studies have investigated GVS-induced nystagmus in normal subjects (80, 84), in which the oculomotor response appeared with intensities above 1.5 mA, similar to this study (80). Because the entire populations of both SCCs and otolith afferents are susceptible to GVS (76), GVS-induced oculomotor responses are likely to be exceedingly diversified, including the roll, yaw, and pitch components (76). In this study, the most prevalent components were horizontal and torsional nystagmus, primarily beating toward the cathode, compatible with vectored activation of afferent fibers from all three SCCs on one side (51, 76). Other studies have reported obvious GVS-induced oculomotor response of mainly conjugate ocular torsion with the upper pole of both eyes rotating toward the side of the anode, slight skew deviation with hypertropia of the eye ipsilateral to the cathode and hypotropia with the eye of the anode, and small conjugate horizontal eye movements toward the anode (80). Amplitudes of GVS-induced eye movements apparently depend on the stimulating current level or the group of vestibular afferents engaged with regular or irregular firing rates (76, 80, 85). Furthermore, GVS-induced nystagmus was suppressed by visual fixation in light (60,

79, 85), and horizontal nystagmus was mainly observed at the onset and offset of the current step, with ocular torsion prevailing for the entire duration of the stimulus up to several minutes (79).

The DC-GVS is useful for rescuing vestibular function in unilateral vestibular disorders by rebalancing the vestibular deafferentation effect proved in previous studies (77, 86). Therefore, in this study, we investigated only the GVS thresholds using DC. Based on the components of tonic or phasic vestibular fibers that are likely to be recruited for the GVS response, we surmise threshold differences between DC and AC stimulation. Thus, further research is needed to determine the GVS thresholds for the AC (sinusoidal, noisy). Regarding the statistically non-significant results in our study such as age-related GVS threshold, it could be due to a type 2 error related to the small sample size.

In conclusion, GVS is a safe stimulation method when certain standard procedures are followed. Due to the variables influencing GVS-induced cortical excitability, the same quantity of current is likely to have non-uniform effects in each subject with different conditions. Individual factors are a source of heterogeneity in clinical research, which is a significant obstacle for routine use in clinical settings. Therefore, the patient-specific customized threshold should be determined rather than population thresholds. The results of this study show more sensitive vestibular and somatosensory perception thresholds than the oculomotor threshold, which allows the selection of the appropriate current that induces the vestibular effect while simultaneously preventing disturbing ocular movements during the intervention.

Data availability statement

The original contributions presented in the study are included in the article/supplementary material, further inquiries can be directed to the corresponding author.

Ethics statement

All experiments were reviewed and approved by the Institutional Review Board at Jeonbuk National University Hospital (No. 2021-07-013-007). The patients/participants provided their written informed consent to participate in this study.

Author contributions

TTN collected data, conducted the experiment, and wrote the manuscript. J-JK collected data and drew the figures. S-YO designed and supervised the study and wrote the manuscript. All authors contributed to the article and approved the submitted version.

Funding

This study was supported by a National Research Foundation of Korea (NRF) grant funded by the Korean Government (Ministry of Science and ICT; No. 2022R1A2B5B01001933) and by the Fund of the Biomedical Research Institute, Jeonbuk National University Hospital.

Conflict of interest

The authors declare that the research was conducted in the absence of any commercial or financial relationships that could be construed as a potential conflict of interest.

Publisher's note

All claims expressed in this article are solely those of the authors and do not necessarily represent those of their affiliated organizations, or those of the publisher, the editors and the reviewers. Any product that may be evaluated in this article, or claim that may be made by its manufacturer, is not guaranteed or endorsed by the publisher.

References

1. Angelaki DE, Cullen KE. Vestibular system: the many facets of a multimodal sense. *Annu Rev Neurosci.* (2008) 31:125–50. doi: 10.1146/annurev.neuro.31.060407.125555

2. Vidal P-P, Cullen K, Curthoys I, Du Lac S, Holstein G, Idoux E, et al. *The Vestibular System. The Rat Nervous System*. Amsterdam: Elsevier (2015). p. 805–64. doi: 10.1016/B978-0-12-374245-2.00028-0

3. Ferrè ER, Walther LE, Haggard P. Multisensory interactions between vestibular, visual and somatosensory signals. *PLoS ONE.* (2015) 10:e0124573. doi: 10.1371/journal.pone.0124573

4. Zaleski-King AC, Lai W, Sweeney AD. *Anatomy and Physiology of the Vestibular System. Diagnosis and Treatment of Vestibular Disorders*. Berlin: Springer (2019). p. 3–16. doi: 10.1007/978-3-319-97858-1_1

5. Brandt T. *Vestibular Cortex: Its Locations, Functions, and Disorders*. New York, NY: Vertigo (2003). p. 219–31. doi: 10.1007/978-1-4757-3801-8_13

6. Pissaloux E, Velázquez R. On spatial cognition and mobility strategies. *Mobility oVisually Impaired People.* (2018) 2018:137–66. doi: 10.1007/978-3-319-54446-5_5

7. Brunoni AR, Nitsche MA, Bolognini N, Bikson M, Wagner T, Merabat L, et al. Clinical research with transcranial direct current stimulation (tDCS): challenges and future directions. *Brain Stimul.* (2012) 5:175–95. doi: 10.1016/j.brs.2011.03.002

8. Fitzpatrick RC, Day BL. Probing the human vestibular system with galvanic stimulation. *J Appl Physiol.* (2004) 96:2301–16. doi: 10.1152/japplphysiol.00008.2004

9. Goldberg J, Smith CE, Fernandez C. Relation between discharge regularity and responses to externally applied galvanic currents in vestibular nerve afferents of the squirrel monkey. *J Neurophysiol.* (1984) 51:1236–56. doi: 10.1152/jn.1984.51.6.1236

10. Ertl M, Klimek M, Boegle R, Stephan T, Dieterich M. Vestibular perception thresholds tested by galvanic vestibular stimulation. *J Neurol.* (2018) 265:54–6. doi: 10.1007/s00415-018-8808-9

11. Bent LR, McFadyen BJ, Merkley VF, Kennedy PM, Inglis JT. Magnitude effects of galvanic vestibular stimulation on the trajectory of human gait. *Neurosci Lett.* (2000) 279:157–60. doi: 10.1016/S0304-3940(99)00989-1

12. Minor LB, Goldberg JM. Vestibular-nerve inputs to the vestibulo-ocular reflex: a functional-ablation study in the squirrel monkey. *J Neurosci.* (1991) 11:1636–48. doi: 10.1523/JNEUROSCI.11-06-01636.1991

13. Courjon J, Precht W, Sirkin D. Vestibular nerve and nuclei unit responses and eye movement responses to repetitive galvanic stimulation of the labyrinth in the rat. *Exp Brain Res.* (1987) 66:41–8. doi: 10.1007/BF00236200

14. Dlugaiczyk J, Gensberger KD, Straka H. Galvanic vestibular stimulation: from basic concepts to clinical applications. *J Neurophysiol.* (2019) 121:2237–55. doi: 10.1152/jn.00035.2019

15. Bense S, Stephan T, Yousry TA, Brandt T, Dieterich M. Multisensory cortical signal increases and decreases during vestibular galvanic stimulation (fMRI). *J Neurophysiol.* (2001) 85:886–99. doi: 10.1152/jn.2001.85.2.886

16. Nguyen TT, Nam G-S, Kang J-J, Han GC, Kim JS, Dieterich M, et al. Galvanic vestibular stimulation improves spatial cognition after unilateral labyrinthectomy in mice. *Front Neurol.* (2021) 2021:1261. doi: 10.3389/fneur.2021.716795

17. Iwasaki S, Yamamoto Y, Togo F, Kinoshita M, Yoshifuji Y, Fujimoto C, et al. Noisy vestibular stimulation improves body balance in bilateral vestibulopathy. *Neurology.* (2014) 82:969–75. doi: 10.1212/WNL.0000000000000215

18. Goel R, Kofman I, Jeevarajan J, De Dios Y, Cohen HS, Bloomberg JJ, et al. Using low levels of stochastic vestibular stimulation to improve balance function. *PLoS ONE.* (2015) 10:e0136335. doi: 10.1371/journal.pone.0136335

19. Stefani SP, Serrador JM, Breen PP, Camp AJ. Impact of galvanic vestibular stimulation-induced stochastic resonance on the output of the vestibular system: a systematic review. *Brain Stimul.* (2020) 13:533–5. doi: 10.1016/j.brs.2020.01.006

20. Iwasaki S, Fujimoto C, Egami N, Kinoshita M, Togo F, Yamamoto Y, et al. Noisy vestibular stimulation increases gait speed in normals and in bilateral vestibulopathy. *Brain Stimul.* (2018) 11:709–15. doi: 10.1016/j.brs.2018.03.005

21. Mulavara AP, Kofman IS, De Dios YE, Miller C, Peters BT, Goel R, et al. Using low levels of stochastic vestibular stimulation to improve locomotor stability. *Front Syst Neurosci.* (2015) 9:117. doi: 10.3389/fnsys.2015.00117

22. Putman EJ, Galvan-Garza RC, Clark TK. The effect of noisy galvanic vestibular stimulation on learning of functional mobility and manual control nulling sensorimotor tasks. *Front Hum Neurosci.* (2021) 15:756674. doi: 10.3389/fnhum.2021.756674

23. Voros JL, Sherman SO, Rise R, Kryuchkov A, Stine P, Anderson AP, et al. Galvanic vestibular stimulation produces cross-modal improvements in visual thresholds. *Front Neurosci.* (2021) 15:311. doi: 10.3389/fnins.2021.640984

24. Keywan A, Wuehr M, Pradhan C, Jahn K. Noisy galvanic stimulation improves roll-tilt vestibular perception in healthy subjects. *Front Neurol.* (2018) 9:83. doi: 10.3389/fneur.2018.00083

25. Kerkhoff G, Hildebrandt H, Reinhart S, Kardinal M, Dimova V, Utz KS, et al. long-lasting improvement of tactile extinction after galvanic vestibular stimulation: two Sham-stimulation controlled case studies. *Neuropsychologia.* (2011) 49:186–95. doi: 10.1016/j.neuropsychologia.2010.11.014

26. Hilliard D, Passow S, Thurm F, Schuck NW, Garthe A, Kempermann G, et al. Noisy galvanic vestibular stimulation modulates spatial memory in young healthy adults. *Sci Rep.* (2019) 9:1–11. doi: 10.1038/s41598-019-45757-0

27. Wilkinson D, Zubko O, DeGutis J, Milberg W, Potter J. Improvement of a figure copying deficit during subsensory galvanic vestibular stimulation. *J Neuropsychol.* (2010) 4:107–18. doi: 10.1348/174866409X468205

28. Dilda V, MacDougall HG, Curthoys IS, Moore ST. Effects of Galvanic vestibular stimulation on cognitive function. *Exp Brain Res.* (2012) 216:275–85. doi: 10.1007/s00221-011-2929-z

29. MacDougall HG, Moore ST, Curthoys IS, Black FO. Modeling postural instability with Galvanic vestibular stimulation. *Exp Brain Res.* (2006) 172:208–20. doi: 10.1007/s00221-005-0329-y

30. Moore ST, MacDougall HG, Peters BT, Bloomberg JJ, Curthoys IS, Cohen HS. Modeling locomotor dysfunction following spaceflight with galvanic vestibular stimulation. *Exp Brain Res.* (2006) 174:647–59. doi: 10.1007/s00221-006-0528-1

31. Kennedy PM, Cressman EK, Carlsen AN, Chua R. Assessing vestibular contributions during changes in gait trajectory. *Neuroreport.* (2005) 16:1097–100. doi: 10.1097/00001756-200507130-00013

32. Bent LR, Bolton PS, Macefield VG. Modulation of muscle sympathetic bursts by sinusoidal galvanic vestibular stimulation in human subjects. *Exp Brain Res.* (2006) 174:701–11. doi: 10.1007/s00221-006-0515-6

33. Utz KS, Korluss K, Schmidt L, Rosenthal A, Oppenländer K, Keller I, et al. Minor adverse effects of galvanic vestibular stimulation in persons with stroke and healthy individuals. *Brain Injury.* (2011) 25:1058–69. doi: 10.3109/02699052.2011.607789

34. Oldfield RC. The assessment and analysis of handedness: the Edinburgh inventory. *Neuropsychologia.* (1971) 9:97–113. doi: 10.1016/0028-3932(71)90067-4

35. Dieterich M, Kirsch V, Brandt T. Right-sided dominance of the bilateral vestibular system in the upper brainstem and thalamus. *J Neurol.* (2017) 264:55–62. doi: 10.1007/s00415-017-8453-8

36. Kirsch V, Boegle R, Keeser D, Kierig E, Ertl-Wagner B, Brandt T, et al. Handedness-dependent functional organizational patterns within the bilateral vestibular cortical network revealed by fMRI connectivity based parcellation. *Neuroimage.* (2018) 178:224–37. doi: 10.1016/j.neuroimage.2018.05.018

37. Sandrini M, Fertonani A, Cohen LG, Miniussi C. Double dissociation of working memory load effects induced by bilateral parietal modulation. *Neuropsychologia.* (2012) 50:396–402. doi: 10.1016/j.neuropsychologia.2011.12.011

38. Poreisz C, Boros K, Antal A, Paulus W. Safety aspects of transcranial direct current stimulation concerning healthy subjects and patients. *Brain Res Bull.* (2007) 72:208–14. doi: 10.1016/j.brainresbull.2007.01.004

39. Nooristani M, Maheu M, Houde M-S, Bacon B-A, Champoux F. Questioning the lasting effect of galvanic vestibular stimulation on postural control. *PLoS ONE.* (2019) 14:e0224619. doi: 10.1371/journal.pone.0224619

40. Utz KS, Dimova V, Oppenländer K, Kerkhoff G. Electrified minds: transcranial direct current stimulation (tDCS) and galvanic vestibular stimulation (GVS) as methods of non-invasive brain stimulation in neuropsychology—a review of current data and future implications. *Neuropsychologia.* (2010) 48:2789–810. doi: 10.1016/j.neuropsychologia.2010.06.002

41. Nitsche MA, Liebetanz D, Lang N, Antal A, Tergau F, Paulus W. Safety criteria for transcranial direct current stimulation (tDCS) in humans. *Clin Neurophysiol.* (2003) 114:2220–3. doi: 10.1016/S1388-2457(03)00235-9

42. Yuen TG, Agnew WF, Bullara LA, Jacques S, McCreery DB. Histological evaluation of neural damage from electrical stimulation: considerations for the selection of parameters for clinical application. *Neurosurgery.* (1981) 9:292–9. doi: 10.1227/00006123-198109000-00013

43. Helmchen C, Machner B, Rother M, Spliethoff P, Göttlich M, Sprenger A. Effects of galvanic vestibular stimulation on resting state brain activity in patients with bilateral vestibulopathy. *Hum Brain Mapp.* (2020) 41:2527–47. doi: 10.1002/hbm.24963

44. Helmchen C, Rother M, Spliethoff P, Sprenger A. Increased brain responsivity to galvanic vestibular stimulation in bilateral vestibular failure. *NeuroImage.* (2019) 24:101942. doi: 10.1016/j.nicl.2019.101942

45. Preuss N, Kalla R, Müri R, Mast FW. Framing susceptibility in a risky choice game is altered by galvanic vestibular stimulation. *Sci Rep.* (2017) 7:1–7. doi: 10.1038/s41598-017-02909-4

46. Hartmann M, Furrer S, Herzog MH, Merfeld DM, Mast FW. Self-motion perception training: thresholds improve in the light but not in the dark. *Exp Brain Res.* (2013) 226:231–40. doi: 10.1007/s00221-013-3428-1

47. Cullen K. Chapter 2—Physiology of central pathways. In: Furman JM, editors, *Handbook of Clinical Neurology*. Amsterdam: T. Lempert, Elsevier B.V, (2016). p. 17–40. doi: 10.1016/B978-0-444-63437-5.00002-9

48. Priesol AJ, Valko Y, Merfeld DM, Lewis RF. Motion perception in patients with idiopathic bilateral vestibular hypofunction. *Otolaryngology.* (2014) 150:1040–2. doi: 10.1177/0194599814526557

49. Bermúdez Rey MC, Clark TK, Wang W, Leeder T, Bian Y, Merfeld DM. Vestibular perceptual thresholds increase above the age of 40. *Front Neurol.* (2016) 7:162. doi: 10.3389/fneur.2016.00162

50. Peters RM, Blouin J-S, Dalton BH, Inglis JT. Older adults demonstrate superior vestibular perception for virtual rotations. *Exp Gerontol.* (2016) 82:50–7. doi: 10.1016/j.exger.2016.05.014

51. Jahn K, Naeßl A, Schneider E, Strupp M, Brandt T, Dieterich M. Inverse *U*-shaped curve for age dependency of torsional eye movement responses to galvanic vestibular stimulation. *Brain.* (2003) 126:1579–89. doi: 10.1093/brain/awg163

52. Dalton BH, Blouin J-S, Allen MD, Rice CL, Inglis JT. The altered vestibular-evoked myogenic and whole-body postural responses in old men during standing. *Exp Gerontol.* (2014) 60:120–8. doi: 10.1016/j.exger.2014.09.020

53. Goldberg JM. Afferent diversity and the organization of central vestibular pathways. *Exp Brain Res.* (2000) 130:277–97. doi: 10.1007/s002210050033

54. Geng B, Yoshida K, Jensen W. Impacts of selected stimulation patterns on the perception threshold in electrocutaneous stimulation. *J Neuroeng Rehabil.* (2011) 8:1–10. doi: 10.1186/1743-0003-8-9

55. Moriyama H, Itoh M, Shimada K, Otsuka N. Morphometric analysis of fibers of the human vestibular nerve: sex differences. *Eur Archiv Oto-rhino-laryngol.* (2007) 264:471–5. doi: 10.1007/s00405-006-0197-5

56. Sato H, Sando I, Takahashi H. Computer-aided three-dimensional measurement of the human vestibular apparatus. *Otolaryngology.* (1992) 107:405–9. doi: 10.1177/019459989210700311

57. Sung P-H, Cheng P-W, Young Y-H. Effect of gender on ocular vestibular-evoked myogenic potentials *via* various stimulation modes. *Clin Neurophysiol.* (2011) 122:183–7. doi: 10.1016/j.clinph.2010.06.004

58. Rilea SL. A lateralization of function approach to sex differences in spatial ability: a reexamination. *Brain Cogn.* (2008) 67:168–82. doi: 10.1016/j.bandc.2008.01.001

59. Mueller SC, Jackson CP, Skelton RW. Sex differences in a virtual water maze: an eye tracking and pupillometry study. *Behav Brain Res.* (2008) 193:209–15. doi: 10.1016/j.bbr.2008.05.017

60. MacDougall HG, Brizuela AE, Curthoys IS. Linearity, symmetry and additivity of the human eye-movement response to maintained unilateral and bilateral surface galvanic (DC) vestibular stimulation. *Exp Brain Res.* (2003) 148:166–75. doi: 10.1007/s00221-002-1289-0

61. Yamamoto Y, Struzik ZR, Soma R, Ohashi K, Kwak S. Noisy vestibular stimulation improves autonomic and motor responsiveness in central neurodegenerative disorders. *Ann Neurol.* (2005) 58:175–81. doi: 10.1002/ana.20574

62. Wuehr M, Nusser E, Krafczyk S, Starube A, Brandt T, Jahn K, et al. Noise-enhanced vestibular input improves dynamic walking stability in healthy subjects. *Brain Stimul.* (2016) 9:109–16. doi: 10.1016/j.brs.2015.08.017

63. Wilkinson D, Nicholls S, Pattenden C, Kilduff P, Milberg W. Galvanic vestibular stimulation speeds visual memory recall. *Exp Brain Res.* (2008) 189:243–8. doi: 10.1007/s00221-008-1463-0

64. Ambrus GG, Paulus W, Antal A. Cutaneous perception thresholds of electrical stimulation methods: comparison of tDCS and tRNS. *Clin Neurophysiol.* (2010) 121:1908–14. doi: 10.1016/j.clinph.2010.04.020

65. Dundas J, Thickbroom G, Mastaglia F. Perception of comfort during transcranial DC stimulation: effect of NaCl solution concentration applied to sponge electrodes. *Clin Neurophysiol.* (2007) 118:1166–70. doi: 10.1016/j.clinph.2007.01.010

66. Ferrè ER, Day BL, Bottini G, Haggard P. How the vestibular system interacts with somatosensory perception: a sham-controlled study with galvanic vestibular stimulation. *Neurosci Lett.* (2013) 550:35–40. doi: 10.1016/j.neulet.2013.06.046

67. Lenggenhager B, Lopez C, Blanke O. Influence of galvanic vestibular stimulation on egocentric and object-based mental transformations. *Exp Brain Res.* (2008) 184:211–21. doi: 10.1007/s00221-007-1095-9

68. McFadden JL, Borckardt JJ, George MS, Beam W. Reducing procedural pain and discomfort associated with transcranial direct current stimulation. *Brain Stimul.* (2011) 4:38–42. doi: 10.1016/j.brs.2010.05.002

69. Borckardt JJ, Linder K, Ricci R, Li X, Anderson B, Arana A, et al. Focal electrically administered therapy (FEAT): device parameter effects on stimulus perception in humans. *J ECT.* (2009) 25:91. doi: 10.1097/YCT.0b013e318183c6a4

70. Gandiga PC, Hummel FC, Cohen LG. Transcranial DC stimulation (tDCS): a tool for double-blind sham-controlled clinical studies in brain stimulation. *Clin Neurophysiol.* (2006) 117:845–50. doi: 10.1016/j.clinph.2005.12.003

71. Wardman DL, Taylor JL, Fitzpatrick RC. Effects of galvanic vestibular stimulation on human posture and perception while standing. *J Physiol.* (2003) 551:1033–42. doi: 10.1113/jphysiol.2003.045971

72. Mars F, Vercher J-L, Popov K. Dissociation between subjective vertical and subjective body orientation elicited by galvanic vestibular stimulation. *Brain Res Bull.* (2005) 65:77–86. doi: 10.1016/j.brainresbull.2004.11.012

73. Day B, Severac Cauquil A, Bartolomei L, Pastor M, Lyon I. Human body-segment tilts induced by galvanic stimulation: a vestibularly driven balance protection mechanism. *J Physiol.* (1997) 500:661–72. doi: 10.1113/jphysiol.1997.sp022051

74. Mian OS, Dakin CJ, Blouin JS, Fitzpatrick RC, Day BL. Lack of otolith involvement in balance responses evoked by mastoid electrical stimulation. *J Physiol.* (2010) 588:4441–51. doi: 10.1113/jphysiol.2010.195222

75. Cathers I, Day BL, Fitzpatrick RC. Otolith and canal reflexes in human standing. *J Physiol.* (2005) 563:229–34. doi: 10.1113/jphysiol.2004.079525

76. Zink R, Bucher S, Weiss A, Brandt T, Dieterich M. Effects of galvanic vestibular stimulation on otolithic and semicircular canal eye movements and perceived vertical. *Electroencephalogr Clin Neurophysiol.* (1998) 107:200–5. doi: 10.1016/S0013-4694(98)00056-X

77. Nam G-S, Nguyen TT, Kang J-J, Han GC, Oh S-Y. Effects of galvanic vestibular stimulation on vestibular compensation in unilaterally labyrinthectomized mice. *Front Neurol.* (2021) 12:736849. doi: 10.3389/fneur.2021.736849

78. MacDougall H, Brizuela A, Burgess A, Curthoys I, Halmagyi G. Patient and normal three-dimensional eye-movement responses to maintained (DC) surface galvanic vestibular stimulation. *Otol Neurotol.* (2005) 26:500–11. doi: 10.1097/01.mao.0000169766.08421.ef

79. MacDougall HG, Brizuela AE, Burgess AM, Curthoys IS. Between-subject variability and within-subject reliability of the human eye-movement response to bilateral galvanic (DC) vestibular stimulation. *Exp Brain Res.* (2002) 144:69–78. doi: 10.1007/s00221-002-1038-4

80. Cauquil AS, Faldon M, Popov K, Day BL, Bronstein AM. Short-latency eye movements evoked by near-threshold galvanic vestibular stimulation. *Exp Brain Res.* (2003) 148:414–8. doi: 10.1007/s00221-002-1326-z

81. Curthoys IS. A critical review of the neurophysiological evidence underlying clinical vestibular testing using sound, vibration and galvanic stimuli. *Clin Neurophysiol.* (2010) 121:132–44. doi: 10.1016/j.clinph.2009.09.027

82. Dieterich M, Zink R, Weiss A, Brandt T. Galvanic stimulation in bilateral vestibular failure: 3-D ocular motor effects. *Neuroreport.* (1999) 10:3283–7. doi: 10.1097/00001756-199911080-00007

83. Aw ST, Todd MJ, Lehnen N, Aw GE, Weber KP, Eggert T, et al. Electrical vestibular stimulation after vestibular deafferentation and in vestibular schwannoma. *PLoS ONE.* (2013) 8:e82078. doi: 10.1371/journal.pone.0082078

84. Kim HJ, Choi JY, Son EJ, Lee WS. Response to galvanic vestibular stimulation in patients with unilateral vestibular loss. *Laryngoscope.* (2006) 116:62–6. doi: 10.1097/01.mlg.0000184525.14825.f4

85. Curthoys IS, MacDougall HG. What galvanic vestibular stimulation actually activates. *Front Neurol.* (2012) 3:117. doi: 10.3389/fneur.2012.00117

86. Nguyen TT, Nam G-S, Kang J-J, Han GC, Kim JS, Dieterich M, et al. The differential effects of acute right-vs. left-sided vestibular deafferentation on spatial cognition in unilateral labyrinthectomized mice. *Front Neurol.* (2021) 12:789487. doi: 10.3389/fneur.2021.789487

frontiers | Frontiers in Neurology

TYPE Review
PUBLISHED 02 September 2022
DOI 10.3389/fneur.2022.986302

Check for updates

OPEN ACCESS

EDITED BY
Sun-Young Oh,
Jeonbuk National University,
South Korea

REVIEWED BY
Andreas Zwergal,
Ludwig Maximilian University of
Munich, Germany
Gay R. Holstein,
Icahn School of Medicine at Mount
Sinai, United States
Vito Enrico Pettorossi,
University of Perugia, Italy

*CORRESPONDENCE
Paul F. Smith
paul.smith@otago.ac.nz

SPECIALTY SECTION
This article was submitted to
Neuro-Otology,
a section of the journal
Frontiers in Neurology

RECEIVED 04 July 2022
ACCEPTED 08 August 2022
PUBLISHED 02 September 2022

CITATION
Smith PF (2022) Recent developments
in the understanding of the
interactions between the vestibular
system, memory, the hippocampus,
and the striatum.
Front. Neurol. 13:986302.
doi: 10.3389/fneur.2022.986302

COPYRIGHT
© 2022 Smith. This is an open-access
article distributed under the terms of
the Creative Commons Attribution
License (CC BY). The use, distribution
or reproduction in other forums is
permitted, provided the original
author(s) and the copyright owner(s)
are credited and that the original
publication in this journal is cited, in
accordance with accepted academic
practice. No use, distribution or
reproduction is permitted which does
not comply with these terms.

Recent developments in the understanding of the interactions between the vestibular system, memory, the hippocampus, and the striatum

Paul F. Smith[1,2]*

[1]Department of Pharmacology and Toxicology, School of Biomedical Sciences and Brain Health Research Centre, University of Otago, Dunedin, New Zealand, [2]Eisdell Moore Centre for Hearing and Balance Research, University of Auckland, Auckland, New Zealand

Over the last two decades, evidence has accumulated to demonstrate that the vestibular system has extensive connections with areas of the brain related to spatial memory, such as the hippocampus, and also that it has significant interactions with areas associated with voluntary motor control, such as the striatum in the basal ganglia. In fact, these functions are far from separate and it is believed that interactions between the striatum and hippocampus are important for memory processing. The data relating to vestibular-hippocampal-striatal interactions have considerable implications for the understanding and treatment of Alzheimer's Disease and Parkinson's Disease, in addition to other neurological disorders. However, evidence is accumulating rapidly, and it is difficult to keep up with the latest developments in these and related areas. The aim of this review is to summarize and critically evaluate the relevant evidence that has been published over the last 2 years (i.e., since 2021), in order to identify emerging themes in this research area.

KEYWORDS

vestibular system, memory, hippocampus, Alzheimer's disease, striatum, Parkinson's disease

Introduction

The last two decades have seen significant advances in our understanding of the contributions of the vestibular system to functions beyond the vestibulo-ocular and vestibulo-spinal reflexes, such as higher cognitive functions [see (1) for a recent review]. This evidence has obvious implications for the etiology and treatment of dementia, such as Alzheimer's Disease (AD) [see (2) for a review]. To a lesser extent, evidence has been gradually accumulating to suggest that the vestibular system has a significant impact on voluntary motor control, though connections with the striatum, a part of the basal ganglia that is also important for memory [see (3) for a review]. This evidence has important implications for our understanding and treatment of Parkinson's Disease (PD) as well as other disorders of the basal ganglia. In the last 2 years,

many studies in these two areas have been published, consolidating existing hypotheses and advancing new ones. The aim of this review is to summarize and critically evaluate what I consider to be the most important of these studies, with a view to delineating some of the next steps in these research areas. Since this Special Topic concerns "Insights in Neuro-Otology: 2021", papers published prior to 2021 will not be included, unless they are directly relevant to the topic under discussion, and no attempt will be made to be exhaustive.

The vestibular system and cognitive function

Spatial memory in humans

Although studies of the relationship between the vestibular system and cognition date back to the 1960's and 1970's, by the 2000's, systematic, well-controlled behavioral studies were reported which demonstrated the importance of the vestibular system for spatial memory, in particular [see (1) for a recent review]. These studies were initially mostly animal studies, but since then many studies have been published that support the hypothesis that vestibular loss can cause varying degrees of cognitive impairment in patients with vestibular disorders (1). At the same time, animal studies have revealed that vestibular loss is associated with the dysfunction of various spatially-responsive neurons in the brain, such thalamic head direction cells, hippocampal place cells and entorhinal grid cells (1). Even in just the last 2 years, many studies have been published which support and extend the view that the vestibular system makes important contributions to memory, especially spatial memory.

Xie et al. (4) studied cognitive function in 126 neuro-otology clinic outpatients, using interviews and cognitive questionnaire scores. Sixty percent of the patients reported experiencing cognitive problems. Using linear regression, they found that the patients, compared to non-vertiginous controls, scored significantly worse on the total Neuropsychological Vertigo Inventory (NVI, which measures cognitive, emotional, visual, and motor symptoms), and the NVI cognitive composite and 3 individual NVI cognition subscales (i.e., Attention, Space Perception, and Time Perception), but not the Everyday Memory Questionnaire (EMQ; tests general memory ability). The cognitive questionnaire scores were also positively correlated with the overall Depression, Anxiety and Stress Scale (DASS) scores, suggesting a relationship with emotional symptoms. The patients exhibited a heterogeneous range of vestibular disorders (e.g., vestibular migraine, Meniere's Disease, Benign Paroxsymal Positional Vertigo) and their hearing status was not clear. This is an important issue in terms of separating the contributions of vestibular vs. auditory deficits to cognitive dysfunction [see (5) for a discussion].

Schöberl et al. (6) studied 14 patients with either complete or incomplete bilateral vestibulopathy (BVP) and compared their performance with age-matched healthy controls in a navigation task requiring the retracing of familiar spatial routes and the combination of novel routes in order to locate objects in real space. [^{18}F]-Fluorodeoxyglucose PET was used to describe their brain activation during the task and the subjects also wore a gaze-controlled, head fixed camera in order to quantify visual search behavior. Although the performance of the patients was not significantly different from the controls when retracing familiar routes, they performed significantly worse when having to combine novel routes, which was correlated with the degree of the BVP. At the same time, the right hippocampus and entorhinal cortex exhibited lower activity and the bilateral parahippocampal areas more activity in the patients during the navigation process. The results of this study suggest that vestibular loss may specifically affect the neural representation of *novel* spatial information.

Gammeri et al. (7) studied the navigation strategies of patients with vestibular loss using a virtual reality reverse T-maze to distinguish "allocentric" (a spatial strategy based on external landmarks) and "egocentric" (response, e.g., left vs. right turn) strategies. They compared 23 patients with unilateral vestibular loss (UVL) to 23 with bilateral vestibular loss (BVL) and 23 healthy controls matched for age, sex and education. The authors reported that for both the UVL and BVL groups, the odds of using a specific egocentric or allocentric strategy in the T maze were reduced. They observed that only a right UVL appeared to reduce the odds of adopting an allocentric spatial strategy. For those patients who used a specific strategy to navigate, the chances of using an allocentric strategy were reduced for the BVL patients, whereas the chances of using an egocentric strategy were reduced for the UVL patients. The authors acknowledged that hearing loss was a possible confounding factor in the study.

Bosmans et al. (8) studied cognitive function in 34 patients with bilateral vestibulopathy (BVP) compared to 34 controls, matched for age, sex and hearing status. BVP patients performed worse on the Repeatable Battery for the Assessment of Neuropsychological Status (RBANS-H) relative to the controls on all subscales, but with a medium statistical effect size (i.e., Cohen's *d*) for attention and a large effect size for visuospatial processing (i.e., processing visual stimuli in order to understand spatial relationships) (Figure 1). The authors found a positive correlation between Performance-Oriented Mobility Assessment (POMA) scores and RBANS-H scores, suggesting that the cognitive deficits were related to the degree of balance and gait dysfunction. An important aspect of this study was that the subjects were matched for hearing status, and therefore hearing loss cannot easily explain the cognitive deficits in the BVP patients (5).

Bigelow et al. (9) and Lacroix et al. (10) have recently published studies indicating that the vestibular system is

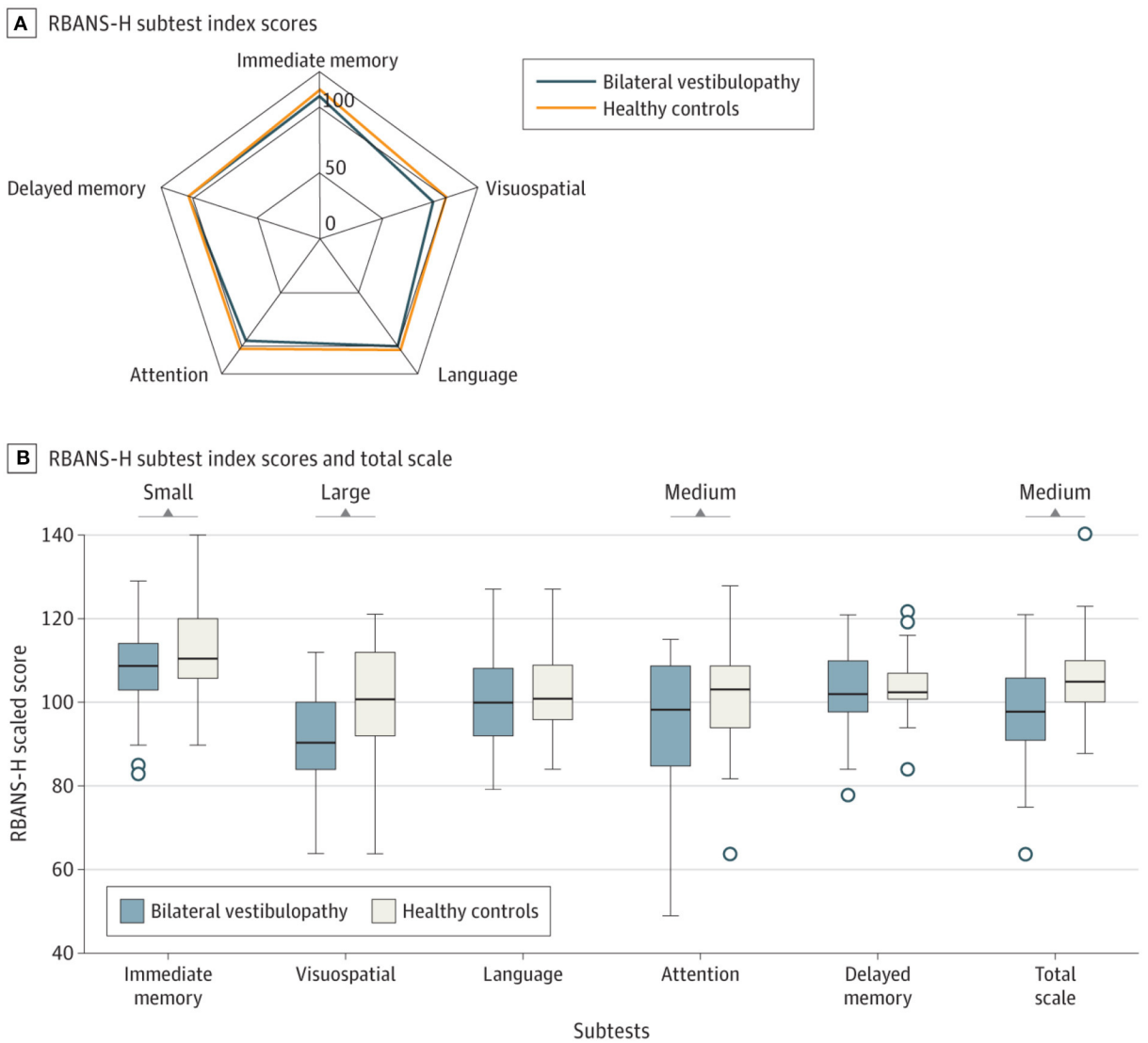

FIGURE 1
Effects of bilateral vestibulopathy on the Repeatable Battery for the Assessment of Neuropsychological Status (RBANS-H) scores in different cognitive domains. Comparison of RBANS-H scores between individuals with bilateral vestibulopathy and their matched healthy controls. **(A)** The relationship between the scores for immediate memory, delayed memory, attention, language and visuospatial function for bilateral vestibulopathy patients and healthy controls. **(B)** Whiskers indicate range; boxes, interquartile range (IQR); circles indicate outliers; bold line, median *d*. Small (Cohen's $d = 0.2$), medium (Cohen's $d = 0.5$), and large (Cohen's $= 0.8$) indicate clinically meaningful Cohen's *d* effect sizes. While there were medium and large differences for attention and visuospatial memory, there were only small effects for immediate memory, language and delayed memory. Reproduced from Bosmans et al. (8).

important for a child's cognitive development. Stimulated by such studies, Van Hecke et al. (11) have published a new protocol to further investigate the involvement of the vestibular system in children's cognitive development. This will be an important area of investigation for developmental problems in children.

Lacroix et al. (12) have suggested that Kahneman's Capacity Model of Attention might be usefully applied to the understanding of cognitive deficits associated with vestibular loss, and especially the variability in these amongst patients. The concept is that there is a limited quantity of cognitive resources that can be allocated to cognitive tasks during recovery from vestibular loss. They suggest that those patients who exhibit cognitive impairment may do so partly as a cost of compensating for their vestibular loss, whereas those people who not compensate very effectively, still have their full cognitive capacity (see Figure 2). This may be why the cognitive effects

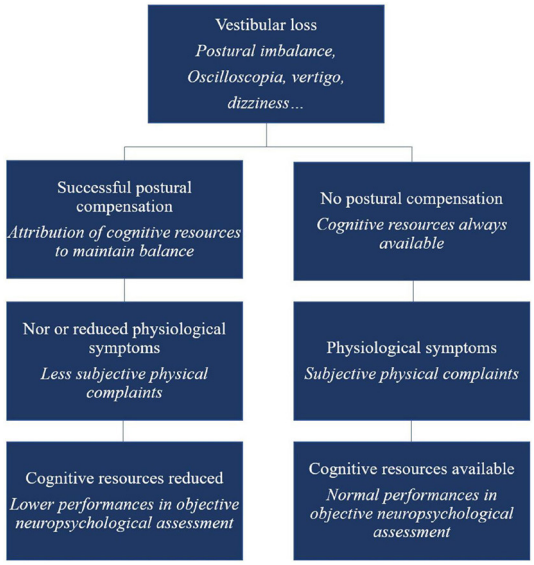

FIGURE 2
Schematic overview of the cognitive-vestibular compensation hypothesis—adaptation of the Kahneman's Capacity Model of Attention to vestibular damaged patients. Reproduced from Lacroix et al. (12).

of vestibular dysfunction vary so much from one clinical study to another.

Spatial orientation in humans

Borel et al. (13) studied the effects of unilateral vestibular neurotomy on the perception of the subjective straight ahead (SSA). They found that during the early phase of the recovery, the patients exhibited the typical translatory and rotatory bias toward the operated side; however, by 2 months post-op., they exhibited a translatory rightward bias of the SSA, without a rotation bias, irrespective of the side of the neurotomy. The authors interpreted these findings as indicative of a long-term change in body representation which is reminiscent of spatial neglect following hemispheric lesions. Both the left and right neurotomy groups suffered hearing loss of approximately equal magnitude.

Brain volume and Alzheimer's disease

There have been a number of studies published recently which extend what is known about the effects of vestibular dysfunction on brain volume, following the study by Brandt et al. (14) which demonstrated a bilateral atrophy of the hippocampus in patients with BVL. Dordevic et al. (15) studied 15 patients with chronic (at least 6 months), mild unilateral or bilateral vestibulopathy and compared them with healthy controls. None of the patients suffered from severe hearing loss as might occur in Meniere's Disease. They observed that the patients performed significantly worse on the clinical balance test, the triangle completion test for path integration (a test of spatial navigation) and the rotational memory test, but not on the Berlin intelligence structure test or the d2-R test for attention and concentration. However, in contrast to some previous studies [e.g., (14)], they found no significant differences in volumetric gray matter, including in the medial temporal lobe. Cohen et al. (16) studied patients with AD and cognitive impairment and found that they exhibited vestibular dysfunction according to Dix-Hallpike maneuvers and cervical vestibular-evoked myogenic potentials (cVEMPs), a measure of saccular function. However, they also found that patients with impaired cVEMPs exhibited significantly reduced left hippocampal volumes compared to those with normal cVEMPs. A number of previous studies have reported a link between abnormal otolithic function and AD [see (2) for a review]. Interestingly, there has been a recent report of punctate hippocampal lesions being associated with an acute vestibular syndrome (17). At the current time, there is no obvious explanation for the discrepancies relating to vestibular dysfunction and hippocampal atrophy, between the different studies.

Previous studies have reported that vestibular dysfunction increases the risk of AD by several-fold [see (2) for a review]. A number of studies have investigated the possibility of using aspects of vestibular function as potential biomarkers for AD. Wang et al. (18) compared visuo-spatial, executive and attentional function, and EEG and P300 responses, in 21 patients with age-related vestibular loss, 19 patients with cognitive impairment and 21 age- and sex-matched healthy controls. The three groups were also matched for hearing threshold and central auditory processing in order to exclude differences in hearing as a confounding factor. They found that the vestibular-impaired group exhibited deficits in these cognitive functions, a reduced P300 response and decreased gamma connectivity between the right Brodmann area 19 (B19, the right cuneus) and Brodmann area 7 (BA7) in the left superior parietal gyrus, in both the vestibular-impaired and cognitively-impaired group, relatve to the controls. The authors suggested that the changes in P300 and functional connectivity in the patients with age-related vestibular loss may serve as useful biomarkers for vestibular-related cognitive dysfunction. Ide et al. (19) have reported significantly poorer index of postural stability (IPS) scores in AD patients compared to those with mild cognitive impairment, in the closed eyes/hard surface condition. Biju et al. (20) have also reported that AD patients exhibit increased medio-lateral sway in both eyes open and eyes closed conditions.

Despite the evidence linking vestibular dysfunction and AD, there is no reason, based on currently published data, to think that there is a specific connection to this form of dementia, rather than dementia in general. For example, vestibular

abnormalities have been detected in frontotemporal dementia, which also presents with an impairment of visuospatial function (21). It is possible that if vestibular loss does contribute to cognitive dysfunction, it is involved in many forms of dementia.

Putman et al. (22) have recently published the results of a study in which they showed that noisy galvanic vestibular stimulation (nGVS), which has been shown to enhance motor control in PD [e.g., (23)], enhanced task learning in a functional mobility task (navigating an obstacle course on a compliant surface with degraded visual cues) compared to sham controls. Interestingly, the benefits of the nGVS were maintained even following the cessation of the stimulus. However, the enhancement was not observed in a manual control task (using a joy-stick to null self-roll tilt in response to a pseudo-random disturbance in the dark).

Animal studies

Over the last 2 years, Nguyen et al. have published a series of studies which investigated the effects of GVS on spatial cognition in mice. In the first study, they compared animals with UVL that received GVS with UVL animals that did not, as well as a control group (24). Cognitive function was assessed at 3, 7, and 14 days using the Y maze and Morris Water Maze (MWM) tests. Importantly, the UVL was created using a surgical method so that it was more specific to the vestibular system than a chemical lesion. The GVS, which was a bipolar, sinusoidal current at 1 Hz, was subthreshold for inducing nystagmus and the cathodal electrode was positioned on the right (lesioned) side. GVS was delivered for 5 days post-UVL with 30 min sessions each day. Mice with UVL exhibited significant impairments in cognitive function, which were reduced by GVS treatment. This was the case for both the Y maze test and the MWM test (see Figures 3, 4). In a follow-up study, they compared left- and right-sided UVL and found that the spatial cognitive deficits differed depending on the side of the lesion (25). Spatial cognition was more impaired in the left-sided UVL group compared to the right-sided, suggesting a laterality effect, although GVS accelerated recovery in both groups when the cathode was on the side of the lesion (25).

In Nguyen et al. (26), they applied the same experimental paradigm to mice that had received an incomplete surgical BVL. Again, the effects of GVS were compared on performance in the Y maze and MWM at 3, 7, and 14 days post-op. Similar to previous studies [e.g., (27, 28)], they found that BVL impaired spatial memory in both the Y maze and MWM. However, GVS accelerated the recovery from the spatial memory deficits (Figure 5).

Taken together, the studies published since 2021 reinforce the previous evidence that normal vestibular function is necessary for intact cognition, especially spatial cognitive processes. More evidence for this has been published in both humans and animals; however, the human studies present a more complex and varied picture, with some studies showing less severe effects or more circumscribed effects [e.g., novel spatial information but not familiar spatial information (5)]. Inevitably, because the studies in patients involve an heterogeneous array of vestibular disorders, with different degrees of vestibular dysfunction, sometimes confounded by concurrent hearing loss, and different time courses, the effects of vestibular loss on cognition are bound to be more variable, and may be explained partly by Lacroix et al.'s (12) reference to Kahneman's Capacity Model of Attention. The evidence that vestibular loss increases the risk of AD is also gradually accumulating (2).

The vestibular system and the hippocampus

Since the early 2000's, many animal studies have been published which show that the thalamus and hippocampus undergo abnormal plasticity following the loss of vestibular function (1). This has been followed by studies in patients with vestibular disorders which, in the majority of cases, have demonstrated structural changes in the hippocampus, such as bilateral atrophy [e.g., (14)]. A number of specialized spatially tuned neurons in the medial temporal lobe and thalamus are known to be important for spatial memory [see (29) for a review]. However, despite the fact that spatial memory deficits associated with vestibular loss are often attributed to the dysfunction of place cells in the hippocampus, there are still only two specific studies that have demonstrated abnormal place cell activity in the hippocampus (30, 31) and one study that has demonstrated abnormal grid cell activity in the entorhinal cortex (32). Although there have been no further studies of these neuronal types directly related to the effects of vestibular loss over the last 2 years, there have been some studies published which are relevant to understanding the effects of vestibular dysfunction on these areas of the brain.

Van Rompaey et al. (33) studied the effects of hearing and vestibular loss caused by the oral intake of allynitrile in mice, and found, similar to previous studies, deficits in spatial memory, using the Barnes Maze. They also used doublecortin immunohistochemistry to investigate the number of immature neurons in the hippocampus, as an indication of neurogenesis. Surprisingly, they found a significant decrease in doublecortin-+ve cells in the left, but not right hippocampus, compared to the control group. This result suggests that the combination of hearing and vestibular loss may impact on neurogenesis in the left hippocampus. Whether the immature neurons in these studies would have become place cells is, of course, unknown; however, a decrease in neurogenesis could have an impact on place cell numbers. Previous studies have reported an increase in

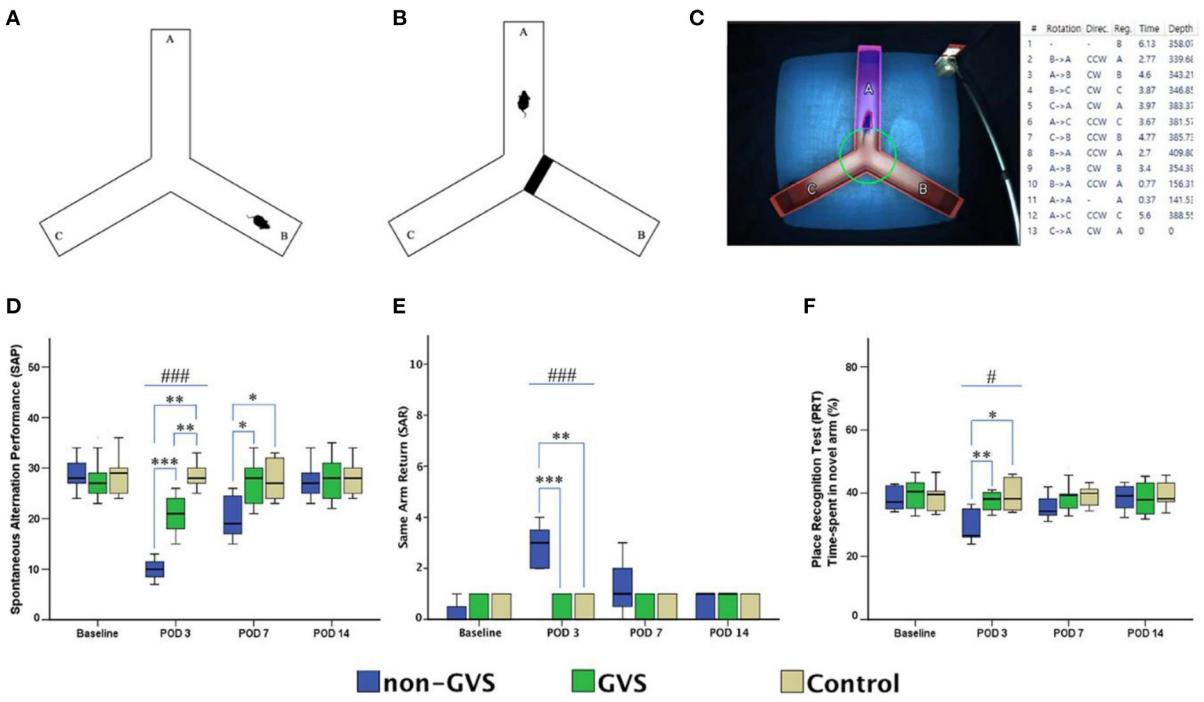

FIGURE 3
Evaluation of locomotor activities and spatial navigation through the Y maze test. The mice move freely within three arms **(A)**. Mice were trained with a block in the B arm for 3 min, then the block was removed, and the mouse activity for exploring the B arm was assessed, i.e., the place recognition test **(B)**. Mice activities in the three groups of non-GVS, GVS, and control groups were tracked and computed by analysis software in 6 min at four time points: baseline, and post-operative days (PODs) 3, 7, and 14 **(C)**. There was a significant difference between the groups in the spontaneous alternation performance at PODs 3 ($\chi^2 = 17.11$, $p < 0.001$, Kruskal–Wallis test). This decline in the non-GVS group continued until POD 7 as compared to the GVS group ($Z = -2.12$, $p < 0.05$) and control group ($Z = -1.95$, $p < 0.05$) **(D)**. There was also a significant difference between the groups in the same arm return at POD 3 ($\chi^2 = 15.23$, $p < 0.001$, Kruskal–Wallis test) **(E)**. The place recognition test indicates spatial reference memory and it shows a significant difference between the groups at POD 3 ($\chi^2 = 7.63$, $p < 0.05$, Kruskal–Wallis test) **(F)**. Values of significant difference were calculated by using the Kruskal–Wallis test for between groups and the Mann–Whitney *U*-tests for pairwise comparisons. *Significantly different between two groups; #Significantly different between three groups; $^{*,\#}p < 0.05$; $^{**,\#\#}p < 0.01$; $^{***,\#\#\#}p < 0.001$. Reproduced from Nguyen et al. (25).

cell proliferation following BVL (34), although GVS was found to reduce neurogenesis in the left hippocampus (35).

Historically, most hippocampal place cell studies have been conducted in freely moving rats and mice and there has been some question as to whether place cells behave similarly in primates. In the first study of spatial coding in freely moving macaques, Mao et al. (36) found hippocampal neurons that were more complex than those described in rodents and which were tuned to many different spatial variables, including horizontal position, head height, linear speed, azimuth head direction, head tilt, head-facing location in 3 dimensions, egocentric boundary (i.e., relative to the arena boundary) and angular head velocity. They observed that the firing of hippocampal neurons was mainly modulated by position (26%), speed (22%), and head direction (41%), with 26% exhibiting conjunctive firing. Interestingly, neuronal activity was strongly modulated by eye movement. This is very significant given the differences in eye movements between primates and rodents, i.e., eye movements in rodents are mainly reflexive, as opposed to voluntary saccadic and smooth pursuit movements. "Place cells", as defined in rodents, were relatively rare but similar to other studies in monkeys. Only 1% of neurons showed grid-like modulation as in rodents. There was an intermittent, low frequency (∼4 Hz) theta activity specific to movement onset, speed-dependent and to which many neurons were phase-locked. Theta phase precession was rare. This study strongly suggests that to understand the neural basis of spatial memory deficits associated with vestibular loss in the hippocampus, the differences in hippocampal processing of spatial information between rodents and primates is crucial to keep in mind. Keshavarzi et al. (37) have recently reported angular head velocity responses, highly dependent on vestibular input, in the retrospenial cortex of the mouse. Their gain was enhanced by the addition of visual information; one might speculate on how much more complex these cells could be in the primate retrospenial cortex.

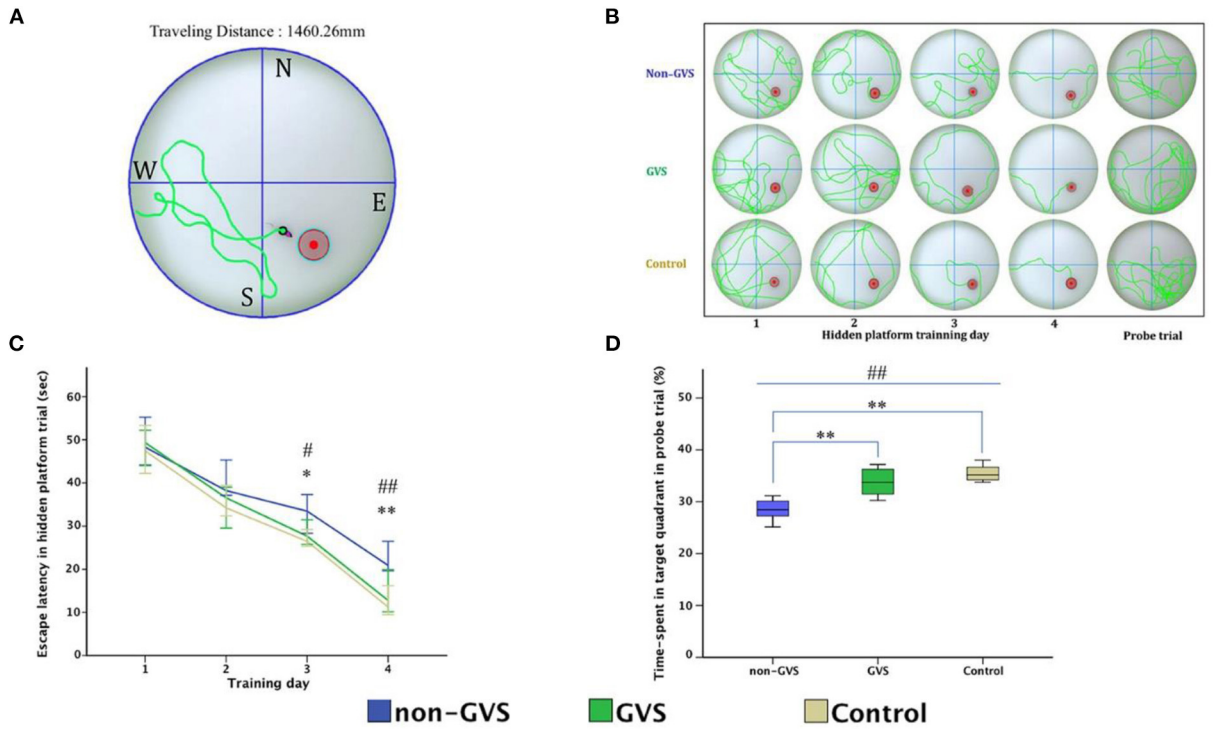

FIGURE 4
Evaluation of motor coordination and spatial navigation of mice through the Morris water maze (MWM). The analysis package divided the searching area into four quadrants, one of which contains the escape platform (red circle) **(A)**. The process of finding the escape platform from the starting point was tracked in the mice (pink) for 1 min **(A)**. Mice were trained with the visible platform at post-operative day (POD) 8 (not depicted) and hidden platform for 4 consecutive days (POD 10–13) and no platform in the probe trial at POD 14 **(B)**. Longer values of escape latency to find the hidden platform indicate an inadequate acquisition of spatial memory and navigation, which showed differences between groups at the last two training days ($\chi^2 = 6.54$, $p < 0.05$ and $\chi^2 = 10.52$, $p < 0.01$, Kruskal–Wallis test). Non-GVS mice had a longer escape latency (33.5 s on the third day and 20.9 s on the fourth day of hidden platform trials) than those of the GVS group (27.67 s, $Z = -2.07$, $p < 0.05$ on the third day and 17.39 s, $Z = -2.73$, $p < 0.01$ on the fourth day) and the control group (26.47 s, $Z = -2.19$, $p < 0.05$ on the third day and 11.25 s, $Z = -2.61$, $p < 0.01$ on the fourth day) (Mann–Whitney *U*-test) **(C)**. During the probe trial at POD 14, there was a significant decrease in the percentage of time spent in the target quadrant in the non-GVS mice [28.5% (26.2–30.6%)] compared to the control group [35.2% (34.0–37.3%), $Z = -2.61$, $p < 0.01$, Mann–Whitney *U*-test] **(D)**. GVS intervention substantially enhanced recovery of this deficit [33.7% (30.9–36.5%), $Z = -2.73$, $p < 0.01$, Mann–Whitney *U*-test], and they were no different from the control group **(D)**. *Significantly different between two groups; #Significantly different between three groups; $^{*,\#}p < 0.05$; $^{**,\#\#}p < 0.01$. Values of significant difference were calculated by using the Kruskal–Wallis test for between groups and the Mann–Whitney *U*-tests for pairwise comparisons. Reproduced from Nguyen et al. (25).

There has been recent progress in understanding the nature of the projections from the vestibular system to the hippocampus in the last 2 years. Hitier et al. (38) selectively electrically stimulated the different parts of the vestibular labyrinth in the rat—the horizontal, anterior, posterior semicircular canals and the utricle and saccule—and recorded triphasic local field potential responses throughout the bilateral hippocampi using a 16 electrode microarray (Figure 6). They found responses of varying amplitudes and latencies throughout the dorsal and ventral hippocampus following stimulation of the different vestibular sensors, but with generally larger amplitudes on the side contralateral to the stimulation and in response to saccular and utricular stimulation (Figures 6, 7). The greater response to otolithic stimulation is consistent with the view that information about gravitational vertical is especially important for the hippocampus [see (39) for a review]. The responses were polysynaptic and long latency in all cases, and it remains to be seen how much and what kinds of vestibular input are transmitted to the hippocampus *via* various pathways from the vestibular nucleus vs. the cerebellum.

Taken together, the studies of vestibular-hippocampal interaction published over the last 2 years, although there have been only a few, have increased our understanding of the way the hippocampus may process vestibular information. Up to now, there has been a wealth of evidence demonstrating that the hippocampus becomes abnormal following vestibular loss, but less information about *how* the hippocampus uses vestibular sensory input. The study by Van Rompaey et al. (33) suggests that vestibular input may actually be necessary for the normal level of neurogenesis in the hippocampus. The study by Hitier et al. (38) shows that vestibular input to the hippocampus is much more widespread than previously thought and also may be

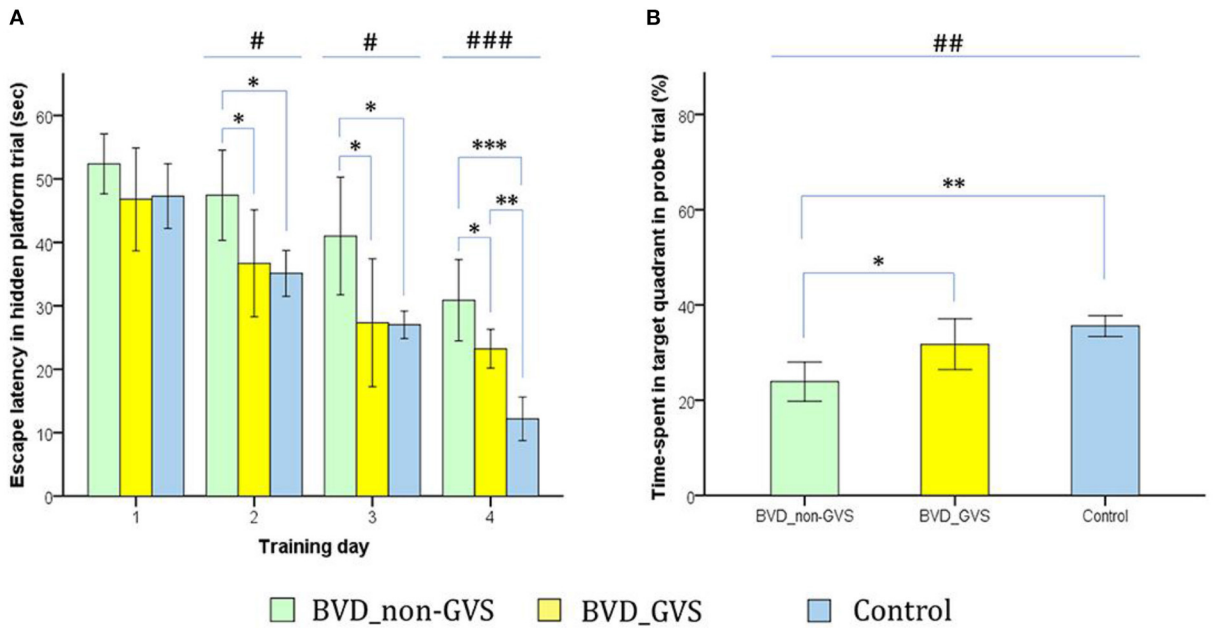

FIGURE 5
Evaluation of long-term spatial reference memory using the Morris water maze (MWM). The escape latencies to find the hidden platform gradually decreased through the training sessions, indicating ongoing learning. Longer values of escape latency to find the hidden platform indicate an inadequate acquisition of spatial memory and navigation. Differences between the groups were observed on training days (TDs) 2 ($p = 0.012$, ANOVA), 3 ($p = 0.013$, ANOVA), and 4 ($p < 0.001$, ANOVA). The BVD non-GVS group had longer escape latency than the control group on TDs 2 ($p = 0.022$, Bonferroni test), 3 ($p = 0.032$, Bonferroni test), and 4 ($p < 0.001$, Bonferroni test). The BVD GVS group had shorter escape latency than the BVD non-GVS group on TDs 2 ($p = 0.037$, Bonferroni test), 3 ($p = 0.028$, Bonferroni test), and 4 ($p = 0.024$, Bonferroni test) **(A)**. Residual impairments in long-term spatial memory were also indicated by a lower percentage of time spent in the target quadrant (probe trial) on POD 14 in the BVD non-GVS compared with both the control ($p = 0.001$, Bonferroni test) and BVD GVS groups ($p = 0.012$, Bonferroni test) ($p = 0.001$, ANOVA) **(B)**. The values are indicated as the mean ± SD. Statistical significance was calculated using one-way ANOVA with *post-hoc* tests. *Significant differences between two groups; #Significant differences among three groups: $^{*,\#}p < 0.05$; $^{**,\#\#}p < 0.01$; $^{***,\#\#\#}p < 0.001$. Reproduced from Nguyen et al. (25).

lateralized, even in rats. Perhaps the most important study is that by Mao et al. (36), which demonstrates for the first time that the nature of spatially-responsive hippocampal neurons in primates may be much more complex than predicted from studies in rats and mice and that therefore the effects of vestibular loss may be similarly complex.

The vestibular system and the striatum

Studies of connections between the vestibular system and the basal ganglia date back to the 1960's, with speculation about how vestibular information might contribute to the control of non-reflexive movement [see (3) for a review]. However, the results of early electrophysiological studies have been inconsistent and difficult to reconcile; therefore vestibulo-strital pathways have remained a mystery [see (3) for a review]. Connections between the vestibular system and the striatum have often been investigated because of their possible relevance to PD. However, the dorsal striatum (i.e., the putamen and the caudate nucleus) is also known to be important in learning and memory and interacts with the hippocampus to compare cognitive information [see (40) for a review].

Since 2021 there have been a number of major studies relating to vestibulo-striatal interactions and PD. One of the possible pathways for the transmission of vestibular information to the striatum is *via* the pedunculopontine tegmental nucleus (Figure 8), which, along with the striatum, has been demonstrated to undergo plasticity following BVL [(41–43); see (44) for a review]. Özkan et al. (45) have recently reported the results of a study in which they injected fluoro-gold tracer into the pedunculopontine tegmental nucleus of rats and observed labeling in the vestibular nucleus both ipsilateral and contralateral to the injection. Similar results were obtained in humans using diffuser tensor imaging and data from the Human Connectome Project.

Bohnen et al. (46) studied vesicular acetylcholine transporter expression using positron emission tomography imaging in PD patients, as an indicator of the integrity of cholinergic pathways. They found evidence of cholinergic deficits in many different brain regions but one of them was the cholinergic

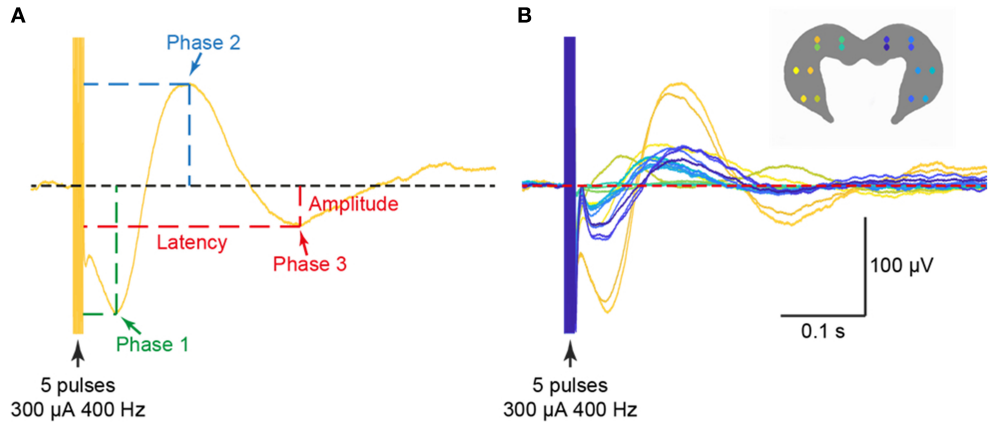

FIGURE 6
Examples of triphasic waveforms **(A)** from all 16 electrodes **(B)** evoked in the ipsilateral and contralateral hippocampus from electrical stimulation of the saccule. The stimulus used was 300 µA at 400 Hz. Reproduced with permission from Hitier et al. (38).

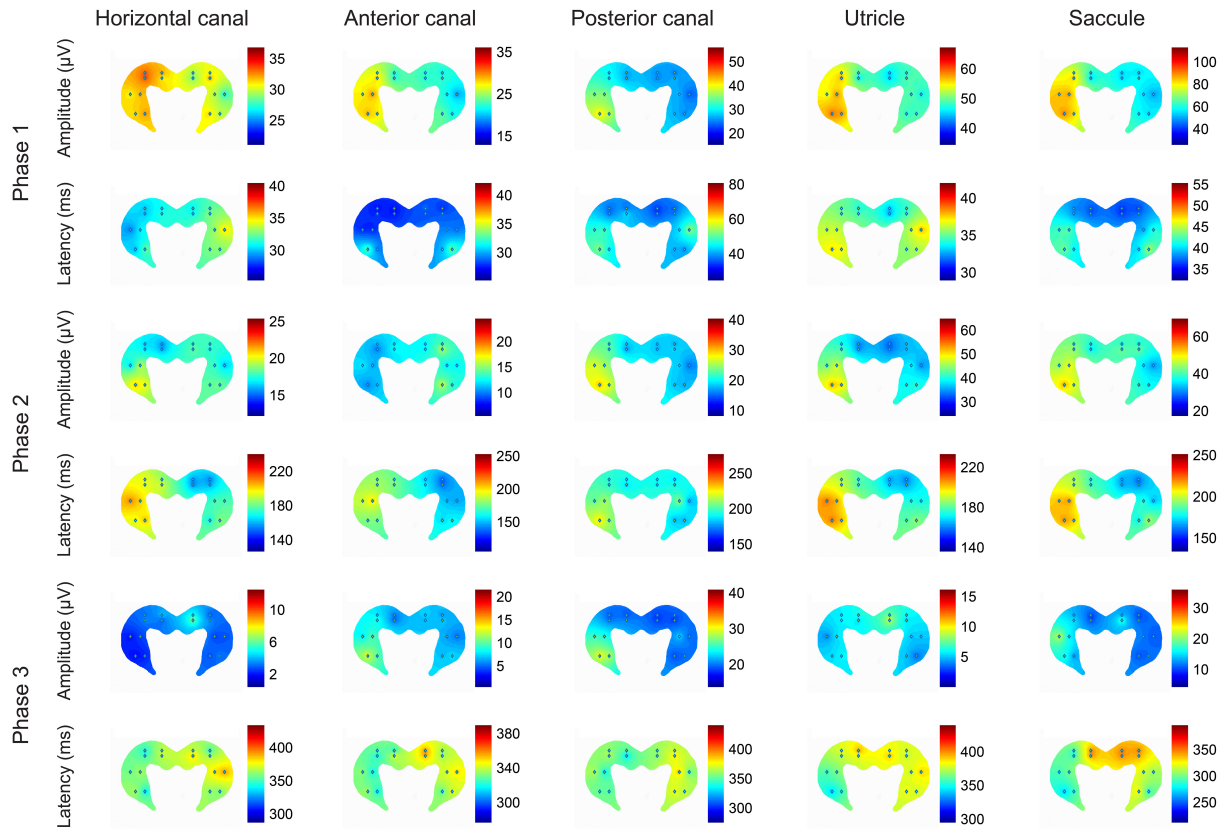

FIGURE 7
Heat plots of the patterns of amplitudes and latencies of the 3 phases of the local field potentials (LFPs) evoked in the hippocampus by electrical stimulation of the horizontal canal (HC), anterior canal (AC) or posterior canal (PC) ampullae, or the utricle or saccule, where the hot colors represent the highest amplitudes and the longest latencies. The heat maps represent the data from all of the rats used in the experiments. The left side on the figures represents the right hippocampus and is contralateral to the stimulation. This is a heatmap scaled by itself, i.e., every single heatmap has maximum and minimum colors. The advantage of this heatmap is that it helps to understand how stimulation of the different sensors activates different areas of the hippocampus. The stimulus used was 300 µA at 400 Hz in all cases. Reproduced with permission from Hitier et al. (38).

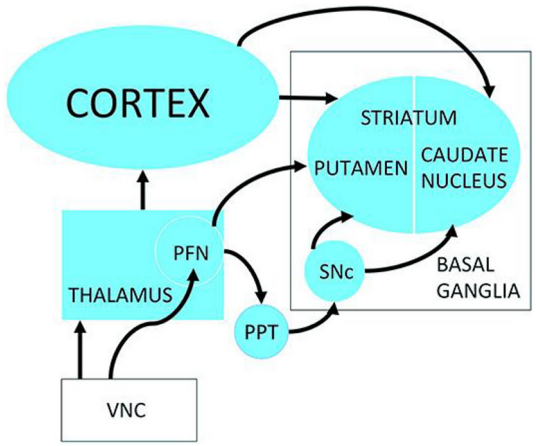

FIGURE 8
Possible neuronal pathways connecting the vestibular nucleus complex to the striatum. PFN, Parafascicular nucleus; PPT, pedunculopontine tegmental nucleus; SNc, Substantia nigra pars compacta; VNC, vestibular nucleus complex. Reproduced from Smith (3).

pathway arising from the medial vestibular nucleus. In a further study, the authors demonstrated that such cholinergic deficits were specifically associated with postural instability and gait difficulties (47).

Antons et al. (48) undertook a large longitudinal dual tracer study in rats following BVL, using positron emission tomography with computer tomography to measure functional and structural plasticity throughout the brain at 1, 3, 5, 7, and 9 weeks post-lesion. They found significant decreases in glucose metabolism in both the left and right striatum, coupled with increases in synaptic density. The BVL was induced by the intratympanic injection of bupivacaine and p-arsanilic acid; therefore, effects on the auditory system could not be excluded. However, these results suggest that the striatum undergoes substantial plasticity following BVL, consistent with the results of previous studies [e.g., (41)].

Hawkins et al. have undertaken a series of systematic studies of vestibulo-ocular reflex and otolith function in a sample of 40 patients with PD and 40 healthy controls. Using the video head impulse test, they found, somewhat surprisingly, no significant differences in the gain of horizontal or vertical vestibulo-ocular reflex function (49). This is in contrast to some previous studies [see (3) for a review]. They obtained similar results using the suppression head impulse paradigm, although they did observe saccadic dysfunction in PD patients (50). In studying otolith function, they found that the PD patients exhibited significantly more absent cervical-evoked myogenic potentials to both clicks and taps, indicating saccular dysfunction, consistent with previous studies [(51); see (3) for a review]. In a further study (52), they used a virtual reality task and demonstrated that PD patients displayed poorer balance which correlated with the severity of the disease, age, vestibulo-ocular reflex function and proprioceptive ability. These studies are particularly significant because of the size of the sample of PD patients and also the use of the same number of controls.

As with AD, although PD has been the focus of attention for the effects of vestibular loss on the basal ganglia, there is no reason to think that this is specific to PD, and it is conceivable that vestibular loss is associated with other basal ganglia disorders. For example, neuronal loss in the vestibular nuclei has been reported in Huntington's Disease [e.g., (53)].

In recent years GVS has been investigated extensively as a potential treatmenf for PD [see (54) for a review]. In what is the most recent study, Lee et al. (23) investigated 18 patients with PD and 20 healthy controls using a simple reaction time task while receiving subthreshold GVS. Because there has been considerable controversy surrounding the type of GVS that might have optimal effects, they decided to compare 9 different types of GVS, including random noise GVS, which has been used most often, and 7 different kinds of multisine stimuli, in both on- and off-medication conditions. Since random noise GVS is supposed to work by the stochastic resonance principle, the purpose of comparing sine wave stimuli of different frequencies (4–200 Hz) to random noise GVS was to test whether stochastic resonance was necessary to improve PD symptoms and also to determine whether the sine wave GVS could be optimized to individuals. They found that the multisine-γ GVS (30–50 Hz) was associated with the shorter response time in both the PD off-medication and control groups compared to the random noise group. The response time for the PD off-medication groups also decreased during the multisine-β (13–30 Hz) GVS. The authors concluded that the optimal GVS frequency to ameliorate PD symptoms may vary considerably between patients and that random noise GVS is not necessarily the best GVS stimulus.

Taken together, the few studies of vestibulo-striatal interaction and vestibular modulation of PD have advanced our understanding of this area. Although the details are still to be elucidated, it is becoming clear that the pedunculopontine tegmental nucleus, which is known to project to the striatum, is also connected to the vestibular nucleus; furthermore, it is evident that PD is associated with major changes in cholinergic pathways involving the vestibular system. The study by Antons et al. (48) reinforces previous evidence that vestibular loss is associated with major functional changes in the striatum. Evidence continues to be reported that GVS can modulate the symptoms of PD (23). Finally, a series of recent studies by Hawkins et al. (49–52) has suggested that vestibular symptomatology in PD may be most prominent for the otoliths and not for the semi-circular canals and vestibulo-ocular reflexes.

Conclusions

Many studies have been published during the last 2 years which have had an impact on our understanding of the contribution of vestibular function to cognition, the hippocampus and the striatum. A number of these studies have reinforced and extended our understanding of the cognitive effects of vestibular dysfunction (4–8, 10). New evidence has been reported on the possible association between vestibular dysfunction and AD (16), as well as vestibular deficits as possible biomarkers for the disease (18–20). Although Dordevic et al. (15) reported no significant change in hippocampal volume associated with vestibular loss, Cohen et al. (16) found that in AD patients, cervical-evoked myogenic potential deficits were associated with a reduction in the volume of the left hippocampus. Further evidence has been published in support of the use of GVS to enhance recovery from vestibular loss in rats (24–26). Consistent with previous studies, Hitier et al. (38) have demonstrated that vestibular input is extensively represented in the rat hippocampus and that all of the vestibular sensors—the horizontal, anterior and posterior semi-circular canals and the utricle and saccule—transmit information there in a stratified fashion, with preferential input from the otoliths and to the contralateral side.

In terms of the striatum, recent studies indicate that major changes occur in the cholinergic pathways involving the vestibular nucleus in PD (46, 47), and that BVL is associated with plasticity in the bilateral striatum. Hawkins et al. (49–52) have also published a series of systematic, well controlled studies of PD patients showing that vestibulo-ocular reflex function is not significantly affected but that cervical-evoked myogenic potential function is degraded.

Taken together, these studies support the idea that vestibular information is important for normal hippocampal and striatal function, may be relevant to AD and PD, as well as other disorders, and that a greater understanding of the processing of vestibular input in these two structures, and how they interact, may benefit our understanding of neurological disorders.

Author contributions

The author confirms being the sole contributor of this work and has approved it for publication.

Funding

This research was supported by a Grant from the Health Research Council (HRC) of New Zealand 20/399.

Conflict of interest

The author declares that the research was conducted in the absence of any commercial or financial relationships that could be construed as a potential conflict of interest.

Publisher's note

All claims expressed in this article are solely those of the authors and do not necessarily represent those of their affiliated organizations, or those of the publisher, the editors and the reviewers. Any product that may be evaluated in this article, or claim that may be made by its manufacturer, is not guaranteed or endorsed by the publisher.

References

1. Smith PF. The vestibular system and cognition. *Curr Opin Neurol.* (2017) 30:84–9. doi: 10.1097/WCO.0000000000000403

2. Agrawal Y, Smith PF, Rosenberg PB. Vestibular impairment, cognitive decline and Alzheimer's disease: Balancing the evidence. Aging Mental Health. (2020) 24:705–8. doi: 10.1080/13607863.2019.1566813

3. Smith PF. Vestibular functions and Parkinson's Disease. *Front Neurol.* (2018) 9:1085. doi: 10.3389/fneur.2018.01085

4. Xie D, Welgampola MS, Miller LA, Young AS, D'Souza M, Breen N, et al. Subjective cognitive dysfunction in patients with dizziness and vertigo. *Audiol Neurootol.* (2022) 27:122–32. doi: 10.1159/000518188

5. Smith PF. Hearing loss versus vestibular loss as contributors to cognitive dysfunction. *J Neurol.* (2022) 269:87–99. doi: 10.1007/s00415-020-10343-2

6. Schöberl F, Pradhan C, Grosch M, Brendel M, Jostes F, Obermaier K, et al. Bilateral vestibulopathy causes selective deficits in recombining novel routes in real space. *Sci Rep.* (2021) 11:2695. doi: 10.1038/s41598-021-82427-6

7. Gammeri R, Léonard J, Toupet M, Hautefort C, van Nechel C, Besnard S, et al. Navigation strategies in patients with vestibular loss tested in a virtual reality T-maze. *J Neurol.* (2022) 269:4333–348. doi: 10.1007/s00415-022-11069-z

8. Bosmans J, Gommeren H, Mertens G, Cras P, Engelborghs S, Van Ombergen A, et al. Associations of bilateral vestibulopathy with cognition in older adults matched with healthy controls for hearing status. *JAMA Otolaryngol Head Neck Surg.* (2022) 148:731–39. doi: 10.1001/jamaoto.2022.1303

9. Bigelow RT, Semenov YR, Hoffman HJ, Agrawal Y. Association between vertigo, cognitive and psychiatric conditions in US children: 2012 National Health Interview Survey. *Int J Pediatr Otorhinolaryngol.* (2020) 130:109802. doi: 10.1016/j.ijporl.2019.109802

10. Lacroix E, Edwards MG, De Volder A, Noël MP, Rombaux P, Deggouj N. Neuropsychological profiles of children with vestibular loss. *J Vest Res.* (2020) 30:25–33. doi: 10.3233/VES-200689

11. Van Hecke R, Deconinck FJA, Wiersema JR, Clauws C, Danneels M, Dhooge I, et al. Balanced Growth project: a protocol of a single-centre observational study on the involvement of the vestibular system in a child's motor and cognitive development. *BMJ Open.* (2021) 11:e049165. doi: 10.1136/bmjopen-2021-049165

12. Lacroix E, Deggouj N, Edwards MG, Van Cutsem J, Van Puyvelde M, Pattyn N. The cognitive-vestibular compensation hypothesis: How cognitive impairments might be the cost of coping with compensation. *Front Hum Neurosci.* (2021) 15:732974. doi: 10.3389/fnhum.2021.732974

13. Borel L, Honoré J, Bachelard-Serra M, Lavieille JP, Saj A. Representation of body orientation in vestibular-defective patients before and after unilateral vestibular loss. *Front Syst Neurosci.* (2021) 15:733684. doi: 10.3389/fnsys.2021.733684

14. Brandt T, Schautzer F, Hamilton DA, Brüning R, Markowitsch HJ, Kalla R, et al. Vestibular loss causes hippocampal atrophy and impaired spatial memory in humans. *Brain.* (2005) 128:2732–41. doi: 10.1093/brain/awh617

15. Dordevic M, Sulzer S, Barche D, Dieterich M, Arens C, Müller NG. Chronic, Mild vestibulopathy leads to deficits in spatial tasks that rely on vestibular input while leaving other cognitive functions and brain volumes intact. *Life.* (2021) 11:1369. doi: 10.3390/life11121369

16. Cohen HS, Lincoln CM, Pavlik VN, Sangi-Haghpeykar H. Changes in measures of vestibular and balance function and hippocampus volume in Alzheimer's Disease and mild cognitive impairment. *Otol Neurotol.* (2022) 43:e663–70. doi: 10.1097/MAO.0000000000003540

17. Kim KT, Lee SU, Jung I, Kim JB Yu S, Kim JS. Punctuate hippocampal lesions presenting with acute vestibular syndrome. *J Neurol.* (2022) 269:2210–3. doi: 10.1007/s00415-021-10853-7

18. Wang Y, Huang X, Feng Y, Luo Q, He Y, Guo Q, et al. Resting-state electroencephalography and P300 evidence: age-related vestibular loss as a risk factor contributes to cognitive decline. *J Alzheimers Dis.* (2022) 86:1107–21. doi: 10.3233/JAD-215467

19. Ide R, Ota M, Hada Y, Watanabe S, Takahashi T, Tamura M, et al. Dynamic balance deficit and the neural network in Alzheimer's disease and mild cognitive impairment. *Gait Posture.* (2022) 93:252–8. doi: 10.1016/j.gaitpost.2022.01.018

20. Biju K, Oh E, Rosenberg P, Xue QL, Dash P, Burhanullah MH, et al. Vestibular function predicts balance and fall risk in patients with Alzheimer's Disease. *J Alzheimers Dis.* (2022) 86:1159–68. doi: 10.3233/JAD-215366

21. Nakamagoe K, Kadono K, Koganezawa T, Takiguchi M, Terada M, Yamamoto F, et al. Vestibular impairment in frontotemporal dementia syndrome. *Dement Geriatr Cogn Dis Extra.* (2016) 6:194–204. doi: 10.1159/000445870

22. Putman EJ, Galvan-Garza RC, Clark TK. The effect of noisy galvanic vestibular stimulation on learning of functional mobility and manual control nulling sensorimotor tasks. *Front Hum Neurosci.* (2021) 15:756674. doi: 10.3389/fnhum.2021.756674

23. Lee S, Smith PF, Lee WH, McKeown MJ. Frequency specific effects of galvanic vestibular stimulation on response time performance in Parkinson's disease. *Front Neurol (Mov Disord).* (2021) 12:758122. doi: 10.3389/fneur.2021.758122

24. Nguyen TT, Nam GS, Kang JJ, Han GC, Kim JS, Dieterich M, et al. Galvanic vestibular stimulation improves spatial cognition after unilateral labyrinthectomy in mice. *Front Neurol.* (2021) 12:716795. doi: 10.3389/fneur.2021.716795

25. Nguyen TT, Nam GS, Kang JJ, Han GC, Kim JS, Dieterich M, et al. The differential effects of acute right- vs. left-sided vestibular deafferentation on spatial cognition in unilateral labyrinthectomized mice. *Front Neurol.* (2021) 12:789487. doi: 10.3389/fneur.2021.789487

26. Nguyen TT, Nam GS, Han GC, Le C, Oh SY. The effect of galvanic vestibular stimulation on visuospatial cognition in an incomplete bilateral vestibular deafferentation mouse model. *Front Neurol.* (2022) 13:857736. doi: 10.3389/fneur.2022.857736

27. Zheng Y, Goddard M, Darlington CL, Smith PF. Long-term deficits on a foraging task after bilateral vestibular deafferentation in rats. *Hippocampus.* (2009) 19:480–48. doi: 10.1002/hipo.20533

28. Baek J-H, Zheng Y, Darlington CL, Smith PF. Evidence that spatial memory deficits in rats following bilateral vestibular loss are probably permanent. *Neurobiol Learn Mem.* (2010) 94:402–13. doi: 10.1016/j.nlm.2010.08.007

29. Moser I, Kropff E, Moser MB. Place cells, grid cells, and the brain's spatial representation system. *Ann Rev Neurosci.* (2008) 31:69–89. doi: 10.1146/annurev.neuro.31.061307.090723

30. Stackman RW, Clark AS, Taube JS. Hippocampal spatial representations require vestibular input. *Hippocampus.* (2002) 12:291–303. doi: 10.1002/hipo.1112

31. Russell N, Horii A, Smith PF, Darlington CL, Bilkey D. The long-term effects of permanent vestibular lesions on hippocampal spatial firing. *J. Neurosci.* (2003) 23:6490–8. doi: 10.1523/JNEUROSCI.23-16-06490.2003

32. Jacob PY, Poucet B, Liberge M, Save E, Sargolini F. Vestibular control of entorhinal cortex activity in spatial navigation. *Front Integr Neurosci.* (2014) 8:38. doi: 10.3389/fnint.2014.00038

33. Van Rompaey V, Liesenborghs A, Goyvaerts K, Herd DD, Verdoodt D, Lammers M, et al. Decreased doublecortin (DCX) immunoreactivity in hippocampus after profound sensorineural hearing loss and vestibular dysfunction in adult mice. *B-ENT.* (2021) 17:223–33. doi: 10.5152/B-ENT.2021.21452

34. Zheng Y, Balabhadrapatruni S, Chung P, Gliddon CM, Zhang M, Napper R, et al. The effects of bilateral vestibular loss on hippocampal volume, neuronal number and cell proliferation in rats. *Front Neuro-Otol.* (2012) 3:1–8. doi: 10.3389/fneur.2012.00020

35. Zheng Y, Geddes L, Sato G, Stiles L, Darlington CL, Smith PF. Galvanic vestibular stimulation impairs cell proliferation and neurogenesis in the rat hippocampus but not spatial memory. *Hippocampus.* (2014) 24:541–52. doi: 10.1002/hipo.22247

36. Mao D, Avila E, Caziot B, Laurens J, Dickman JD, Angelaki DE. Spatial modulation of hippocampal activity in freely moving macaques. *Neuron.* (2021) 109:3521–34.e6. doi: 10.1016/j.neuron.2021.09.032

37. Keshavarzi S, Bracey EF, Faville RA, Campagner D, Tyson AL, Lenzi SC, et al. Multisensory coding of angular head velocity in the retrosplenial cortex. *Neuron.* (2022) 110:532–43.e9. doi: 10.1016/j.neuron.2021.10.031

38. Hitier M, Zhang Y, Sato G, Besnard S, Zheng Y, Smith PF. Stratification of hippocampal electrophysiological activation evoked by selective electrical stimulation of different linear and angular acceleration sensors in the rat peripheral vestibular system. *Hear Res.* (2021) 403:108173. doi: 10.1016/j.heares.2021.108173

39. Smith PF. The growing evidence for the importance of the otoliths for spatial memory. *Front Neural Circ.* (2019) 3:1–14. doi: 10.3389/fncir.2019.00066

40. Mancini A, de Iure A, Picconi B. Basic mechanisms of plasticity and learning. *Handb Clin Neurol.* (2022) 184:21–34. doi: 10.1016/B978-0-12-819410-2.00002-3

41. Aitken P, Benoit A, Zheng Y, Philoxene B, Le Gall A, Denise P, et al. Hippocampal and striatal M_1-muscarinic acetylcholine receptors are down-regulated following bilateral vestibular loss in rats. *Hippocampus.* (2016) 26:1509–14. doi: 10.1002/hipo.22651

42. Aitken P, Zheng Y, Smith PF. Effects of bilateral vestibular deafferentation in rat on hippocampal theta response to somatosensory stimulation, acetylcholine release and cholinergic neurons in the pedunculopontine tegmental nucleus. *Brain Struct Funct.* (2017) 222:3319–32. doi: 10.1007/s00429-017-1407-1

43. Benoit A, Besnard S, Guillamin M, Philoxene B, Sola B, Le Gall A, et al. Differential regulation of NMDA receptor-expressing neurons in the rat hippocampus and striatum following bilateral vestibular loss demonstrated using flow cytometry. *Neurosci Letts.* (2018) 683:43–7. doi: 10.1016/j.neulet.2018.06.035

44. Aitken P, Zheng Y, Smith PF. The modulation of hippocampal theta rhythm by the vestibular system. *J Neurophysiol.* (2018) 119:548–62. doi: 10.1152/jn.00548.2017

45. Özkan M, Köse B, Algin O, Oguz S, Erden ME, Çavdar S. Non-motor connections of the pedunculopontine nucleus of the rat and human brain. *Neurosci Lett.* (2022) 767:136308. doi: 10.1016/j.neulet.2021.136308

46. Bohnen NI, Kanel P, Koeppe RA, Sanchez-Catasus CA, Frey KA, Scott P, et al. Regional cerebral cholinergic nerve terminal integrity and cardinal motor features in Parkinson's disease. *Brain Commun.* (2021) 3:fcab109. doi: 10.1093/braincomms/fcab109

47. Bohnen NI, Kanel P, Roytman S, Scott PJH, Koeppe RA, Albin RL, et al. Cholinergic brain network deficits associated with vestibular sensory conflict deficits in Parkinson's disease: correlation with postural and gait deficits. *J Neural Transm.* (2022) 129:1001–9. doi: 10.1007/s00702-022-02523-3

48. Antons M, Lindner M, Grosch M, Oos R, Palumbo G, Brendel M, et al. Longitudinal [^{18}]UCB-H/[^{18}F]FDG imaging depicts complex patterns of structural and functional neuroplasticity following bilateral vestibular loss in the rat. *Sci Rep.* (2022) 12:6049. doi: 10.1038/s41598-022-09936-w

49. Hawkins KE, Chiarovano E, Paul SS, Burgess AM, MacDougall HG, Curthoys IS. Vestibular semicircular canal function as detected by video Head Impulse Test (vHIT) is essentially unchanged in people with Parkinson's disease compared to healthy controls. *J Vestib Res.* (2022) 32:261–9. doi: 10.3233/VES-201626

50. Hawkins KE, Rey-Martinez J, Chiarovano E, Paul SS, Valldeperes A, MacDougall HG, et al. Suppression head impulse test paradigm (SHIMP) characteristics in people with Parkinson's disease compared to healthy controls. *Exp Brain Res.* (2021) 239:1853–62. doi: 10.1007/s00221-021-06107-7

51. Hawkins KE, Chiarovano E, Paul SS, MacDougall HG, Curthoys IS. Static and dynamic otolith reflex function in people with Parkinson's disease. *Eur Arch Otorhinolaryngol.* (2021) 278:2057–65. doi: 10.1007/s00405-020-06446-1

52. Hawkins KE, Paul SS, Chiarovano E, Curthoys IS. Using virtual reality to assess vestibulo-visual interaction in people with Parkinson's disease compared to healthy controls. *Exp Brain Res.* (2021) 239:3553–64. doi: 10.1007/s00221-021-06219-0

53. Rüb U, Hentschel M, Stratmann K, Brunt E, Heinsen H, Seidel K, et al. Huntington's disease (HD): degeneration of select nuclei, widespread occurrenceof neuronal nuclear and axonal inclusions in the brainstem. *Brain Pathol.* (2014) 24:247–60. doi: 10.1111/bpa.12115

54. Lee S, Liu A, McKeown MJ. Current perspectives on galvanic vestibular stimulation in the treatment of Parkinson's disease. *Expert Rev Neurother.* (2021) 21:405–18. doi: 10.1080/14737175.2021.1894928

frontiers | Frontiers in Neurology

TYPE Original Research
PUBLISHED 02 September 2022
DOI 10.3389/fneur.2022.917413

Check for updates

OPEN ACCESS

EDITED BY
Toshihisa Murofushi,
Teikyo University Mizonokuchi Hospital, Japan

REVIEWED BY
Takao Imai,
Osaka University Hospital, Japan
Leigh Andrew McGarvie,
Royal Prince Alfred Hospital, Australia
Erich Schneider,
Brandenburg University of Technology Cottbus-Senftenberg, Germany

*CORRESPONDENCE
Maksim Pleshkov
maksim.o.pleshkov@gmail.com

SPECIALTY SECTION
This article was submitted to Neuro-Otology, a section of the journal Frontiers in Neurology

RECEIVED 11 April 2022
ACCEPTED 05 August 2022
PUBLISHED 02 September 2022

CITATION
Pleshkov M, Zaitsev V, Starkov D, Demkin V, Kingma H and van de Berg R (2022) Comparison of EOG and VOG obtained eye movements during horizontal head impulse testing. *Front. Neurol.* 13:917413. doi: 10.3389/fneur.2022.917413

COPYRIGHT
© 2022 Pleshkov, Zaitsev, Starkov, Demkin, Kingma and van de Berg. This is an open-access article distributed under the terms of the Creative Commons Attribution License (CC BY). The use, distribution or reproduction in other forums is permitted, provided the original author(s) and the copyright owner(s) are credited and that the original publication in this journal is cited, in accordance with accepted academic practice. No use, distribution or reproduction is permitted which does not comply with these terms.

Comparison of EOG and VOG obtained eye movements during horizontal head impulse testing

Maksim Pleshkov[1]*, Vasilii Zaitsev[2], Dmitrii Starkov[1], Vladimir Demkin[2], Herman Kingma[1] and Raymond van de Berg[1]

[1]Department of Otorhinolaryngology and Head and Neck Surgery, Division of Balance Disorders, Maastricht University Medical Center, School for Mental Health and Neuroscience, Maastricht, Netherlands, [2]Faculty of Physics, National Research Tomsk State University, Tomsk, Russia

Introduction: Video head impulse testing is frequently used to evaluate the vestibular function. During this test, eye movement responses are recorded with video-oculography (VOG). However, the use of VOG can sometimes be challenging, especially due to pupil detection problems (e.g., blinking, droopy eyelids, etc.). Therefore, this study investigated whether electro-oculography (EOG), a technique that does not depend on pupil tracking but on the orientation of the corneoretinal potential, might be an alternative to VOG for quantifying eye movement responses during head impulse testing.

Subjects and methods: Head impulse testing was performed in 19 healthy subjects without a prior history of vestibular symptoms. Horizontal eye movements were recorded simultaneously with EOG (using an EOG system) and VOG (using a VHIT system: ICS Impulse). The eye movement responses to each side of both techniques were compared using a concordance correlation coefficient (r_C), *t*-testing, and Bayes Factor (BF) paired *t*-testing.

Results: EOG and VOG obtained eye movement traces that correlated well with each other during head impulse testing (average $r_C = 0.89$). Average VOR gains obtained with EOG and VOG were not significantly different from each other for all subjects during left head impulses. However, VOG gains differed between both techniques regarding right head impulses. VOG showed significant VOR gain asymmetry (5% to the right), whereas EOG showed no significant asymmetry (1% to the right).

Conclusion: This study demonstrated the use of EOG to record eye movements during head impulse testing for the first time. EOG and VOG obtained eye movement traces that correlated well with each other during horizontal head impulse testing. In addition, EOG showed smaller VOR gain asymmetry in healthy individuals, in contrast to VOG. These findings indicate that EOG might potentially be applicable as an alternative to VOG for collecting eye movement responses during head impulse testing.

Trial registration number: 10192021-38 dated 19.10.21.

KEYWORDS

electro-oculography, video-oculography, head impulse test, eye velocity, asymmetry

Introduction

The vestibular organ is a part of the inner ear, located in the temporal bone on both sides of the head (1). Each organ consists of three semicircular canals sensitive to head angular accelerations and two otolith organs sensitive to head linear accelerations and gravity (2).

One of the semicircular canals functions is to stabilize images on the retina during head movements. This is established by the vestibulo-ocular reflex (VOR), which moves the eyes, velocity controlled, in the opposite direction of the head movement (3). For example, when the head rotates to the right, the eyes rotate to the left, keeping the image of a tracked object almost stationary on the retina. However, various diseases and injuries of the inner ear can lead to an impairment of the vestibular function (4), leading to a reduced VOR (5).

A frequently used test to assess vestibular function is the head impulse test (HIT) (6). During HIT, the examiner performs abrupt, unpredictable, fast, and small amplitude rotational movements of the patient's head (also called head impulses), while the patient tries to fixate on an earth-fixed target placed in front of the patient. During the head impulse, the eye movements are observed and analyzed. If the VOR is intact, eye and head velocities will be in opposite direction but of the same magnitude, resulting in a smooth eye movement without interruptions. However, if the VOR is impaired, the patient's eyes will not move or move too slowly, and the visual fixation of the target will be lost. In order to regain target fixation, corrective saccades will be made either during (covert saccade) or after (overt saccades) the head impulse to bring the eyes back on target. The HIT can evaluate the VOR in all three dimensions and investigate the function of all six semicircular canals (6).

Various eye-tracking methods have been developed to quantify the VOR (7, 8). Electro-oculography (EOG) and video-oculography (VOG) are the most commonly used techniques in clinical practice. EOG is a low-cost technique, already used for decades, based on the fact that the eye can be considered as a dipole since the electrical activity in the retina leads to a corneoretinal potential. During the eye movements, the orientation of this dipole changes, which can be detected by electrodes placed around the eyes (9–11). VOG is a more recently developed technique based on pupil detection, using an infrared video camera that is (in most devices) mounted on relatively expensive goggles (12–14).

In order to quantify the VOR during HIT, the video head impulse test (VHIT) was developed using low-weight goggles with a built-in motion sensor and a high-speed infrared camera. These commercially available devices can track eye and head movements during HIT (12–15). The recorded eye and head velocities are then analyzed to quantify the VOR using the most crucial outcome parameter "gain": the relation between eye and head velocities during HIT (15). The VHIT also identifies corrective covert and overt saccades that compensate for the defective VOR. Currently, most VHIT devices use one infrared camera (VOG) mounted on the goggles, which tracks eye movements of one eye. Unfortunately, during the fast head impulses with peak velocities between 200 and 300 deg/s, the mass inertia of the goggles can induce substantial artifacts due to slippage of the goggles over the head, despite the minimal weight and very tight strapping (16, 17). The accuracy of the VHIT relies also on an accurate pupil position detection, which can be hampered by eye blinking, drooping eyelids, and eyelids covering the pupil (e.g., narrow eyelids or big pupils) and other issues. The sample frequencies of the VHIT systems are currently limited to 250 Hz, and the camera position (right or left eye) has been suggested to induce a non-physiological asymmetry in VOR gain (18). Although VHIT is a clinically highly relevant and frequently used vestibular function test, it is no "plug and play." It requires substantial expertise and training to manually perform the correct head impulses and to recognize and deal with problems of eye-tracking and goggle slippage artifacts. Commercially available VHIT devices are still relatively expensive due to their special goggle design, hardware, and software.

The advantage of EOG over VOG is that it works in almost any subject, even with eyes partially or completely closed. Eye blinks are one of the main sources of artifact with EOG, like in VOG. EOG is also a less expensive but very robust technique, using electrodes (either disposable or reusable) and a simple multichannel differential amplifier able to detect horizontal and vertical eye movements at high sampling rates, especially also for fast eye movements like saccades (19).

However, EOG is not a "plug and play" technique. It requires special expertise and training to mount the electrodes correctly in order to minimize the signal-to-noise ratio and drift. Furthermore, the light intensity in the examination room needs to be kept constant, because the corneoretinal potential directly depends on the intensity of the incident light on the retina. These aspects require a regular calibration of the corneoretinal potential as a measure of the eye rotation. To obtain an optimal signal-to-noise ratio, a bright minimum of 200 lux illumination for the HIT experiments is used and recommended. Physical contact with the electrodes or movement of the skin has to be prevented when using EOG for HIT, as they induce severe artifacts (similar to goggle movements with VOG).

This study aims to check the feasibility of using EOG as an eye movement detection technique during horizontal HIT, by comparing eye movement responses detected with EOG to those simultaneously obtained with VOG. Secondly, it investigates whether the gain asymmetry for leftward and rightward head impulses as has been reported when using VOG in healthy individuals can be confirmed when detecting the eye movements with EOG.

Methods and materials

Study design

HIT was performed in 19 healthy subjects, while eye movements were recorded simultaneously with EOG (using an EOG system) and VOG (using a VHIT system). Horizontal eye movements were compared between EOG and VOG using concordance correlation and Bayes factor analysis as well as *t*-testing.

Study population

Nineteen healthy subjects without a prior history of vestibular symptoms were included in this study. A group of subjects included 14 men aged 23.0 ± 3.8 years (mean ± standard deviation) and 9 women aged 24.7 ± 4.1 years (mean ± standard deviation).

EOG setup and preparation

The EOG system consisted of a custom-made 8-channel differential amplifier with a 20 Bits ADC, ± 50 *mV* measurement range, and 0.1 μV resolution (MPAQ, IDEE, Maastricht University, the Netherlands). The amplifier was connected to the PC *via* a USB interface. Custom-made software (IDEEQ, IDEE, Maastricht University, the Netherlands) was used for signal acquisition and preprocessing. The recorded signal was hardware filtered using a 50-Hz low-pass filter. The signal amplification factor (gain) was set at 3,200.

To detect the corneoretinal potential, three disposable Ag/AgCl electrodes (Ambu Blue sensor N-50-K/25, prewired, 30 by 22 mm size, 1.5 mm connector, Ballerup, Denmark) were used. The skin located to the right and left of the right eye, and the skin on each subject's forehead, were cleaned with petroleum ether to optimize the electrical contact and allow proper electrode fixation. Two electrodes were put on the left and right sides of the right eye (monocular, naso-temporal derivation of the eye position). The reference electrode was placed on the subject's forehead (Figure 1A). The EOG sampling rate was set at 250 Hz.

The EOG system was calibrated manually. Three markers were placed along with a horizontal line on a well-illuminated white painted wall (cold white light of fluorescent lamps, 200 lux ± 4%, measured by an RGK LM-20 lux meter) with a fixation distance of 2 m. Light conditions were carefully kept constant to avoid changes in corneoretinal potential. After placing the electrodes, subjects were sitting for 15 min in front of the illuminated wall, to allow the corneoretinal potential to be stabilized. The calibration markers were placed on the wall at a mutual distance of 7.5°. The healthy subject was then asked to look at the markers one by one while the head was kept stable by the examiner. The degree-voltage relation for EOG can be assumed to be linear, especially for the small amplitude of eye movements (10–15°) (20). Therefore, calibration was performed by fitting the linear regression on three data points. The electro-corneal potentials ranged between 0.49 and 1.20 UV per degree of eye rotation for all 19 subjects.

VHIT setup and preparation

ICS Impulse goggles (GN Otometrics, Taastrup, Denmark) were used for VHIT. This device incorporates a high-speed infrared camera recording the right eye and a set of gyroscopes to detect head movements. To avoid contact, the goggles were put on the subject's face above the already-fixed EOG electrodes (Figure 1B). It was tightly strapped on the subject's head to prevent slippage. The sampling rate was set at default 246 Hz in OtoSuite software (GN Otometrics, Taastrup, Denmark).

For calibration, an automatic built-in horizontal two-point laser calibration was used with a fixation distance of 2 m. The same well-illuminated wall was used for EOG calibration (see above). A detailed description can be found in the ICS Impulse Reference Manual: https://partners.natus.com/asset/resource/file/otometrics/asset/2019-07/7-50-2060-EN_05.PDF.

HIT testing

Horizontal eye movements during horizontal HIT were recorded by EOG and VOG simultaneously. Subjects were seated on a chair. Subjects then were asked to fixate a stable dark blue target at a distance of 2 m, placed at a height of 1.17 m from the floor on the well-illuminated wall (see above). The head of the subject was flexed for 20° to ensure that the impulses were made approximately in the plane of the horizontal canals and to ensure a good pupil capture by the VOG camera, also at lateral gaze (± 7.5° from the center). One trained examiner (VZ) performed all impulses: small amplitude (10–15°) fast (>120°/s) head impulses in the horizontal plane. These outward unpredictable head impulses always started from the center and were randomly applied to the left and right until the ICS Impulse detected 20 valid impulses to each side.

Data processing

The data were processed in Matlab 2014b software. First, a 30-Hz software low-pass filter was used to reduce the noise of all traces (21). After that, the VOG velocity trace was additionally filtered with a 20-Hz low-pass filter since it contained a relatively low-frequency (20–30 Hz) noise. For EOG, eye velocities were

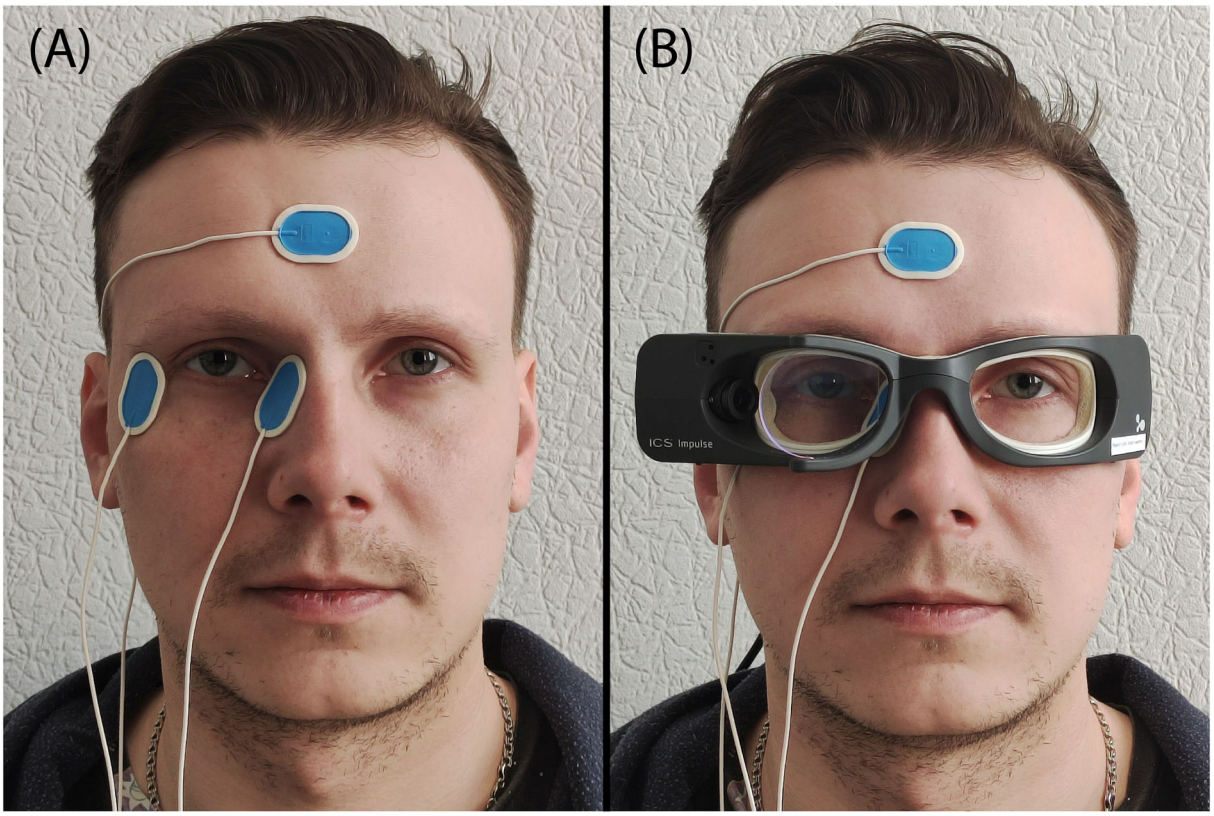

FIGURE 1
Illustration of the placement of the electrodes and VOG goggles. **(A)** Location of the EOG electrodes, **(B)** ICS Impulse goggles together with the EOG electrodes.

calculated by the first-order 5-point central difference of the recorded eye position. Both signals were resampled to 245 Hz, using spline interpolation to eliminate sampling time instabilities and allow further point-to-point comparison.

The VOG and EOG eye velocity traces were first synchronized in time by finding the cross-correlation maximum (best-match) between the whole eye velocity traces, whereas VOG eye and head velocity traces were already synchronized by means of the built-in VOG system procedures. The position of every head impulse was identified by determining the timing of head peak velocities. For the analysis, 800 ms of each head impulse test was selected: 200 ms before the head peak velocity and 600 ms after the head peak velocity. Impulses were only included in the data cleaning process, if they were accepted by the VHIT system. Therefore, no artifacts were additionally removed from the EOG velocity traces. For each subject, data cleaning implied that head impulses were included in the analysis if the head peak velocity ranged between 120 and 250 deg/s.

The signal-to-noise ratio (SNR) was calculated for unfiltered, correlated, and length-adjusted EOG and VOG eye velocity traces as $SNR = 10^{*}log10(\frac{P_{signal}}{P_{noise}})$ [in dB], where P_{signal} and P_{noise} are the signal and noise power, respectively. The signal and noise power were calculated as a square of the amplitudes in a frequency domain after performing the Fourier transform. The signal was considered to be present in a range (0, 30] Hz (21), the noise consequently took the rest of the bandwidth [30, 122.5] Hz.

The VOR gains were calculated for every EOG and VOG obtained trace, as the ratio of the areas under the eye velocity and head velocity curves [area under the curve from 40 ms before to 80 ms after peak head velocity as introduced in Synapsis system (22)] and were then averaged per subject.

Asymmetry was calculated again for every included impulse as $asymmetry = \frac{Gain_{Left} - Gain_{Right}}{Gain_{Left} + Gain_{Right}}$, where $Gain_{Left}$ and $Gain_{Right}$ comprised gains calculated as described above, during left and right impulses, respectively. This implies that negative asymmetry values indicated an asymmetry to the right, and vice versa. The value of 0 indicated the absence of asymmetry.

It should be noted that for both VOG and EOG the motion sensors in the VOG goggles were used to detect head movements. Hence, in this study, it was not possible to investigate difference in latencies using EOG or VOG (see limitations of this study).

Data analysis

For every subject, concordance correlation analysis was performed for each impulse and for each side, to estimate the correlation between eye velocity traces recorded by EOG and VOG. On top of that, the concordance correlation analysis was applied for the head velocity traces and VOG and EOG obtained eye velocity traces. The obtained concordance correlation coefficients (r_c) were first z-transformed (by Fischer), then averaged per subject, averaged per group, and finally the average r_c was obtained for the whole tested group after the inverse Fisher z-transform. r_c values close to 1 implied perfect concordance, whereas a value of zero indicated the absence of concordance. Bayesian factor (BF) paired t-testing was used to compare the average VOR gains obtained by EOG and VOG to each side; t-testing was applied to separately compare VOR gain asymmetries of EOG and VOG obtained eye velocity traces with the value of 0 (indicating absence of asymmetry). BF values >1 indicated evidence of an alternative hypothesis (significant difference), values <1 implicated evidence for the null hypothesis (no significant difference), and a value of 1 indicated no evidence for any hypothesis. T-test p-values lower than 0.05 were considered statistically significant.

Results

Comparison of eye velocities obtained with EOG and VOG

Peak head velocity during head impulses ranged from 120.7 to 249.2 deg/s (mean ± standard deviation 174.4 ± 20.4 deg/s). The SNR for VOG and EOG was equal to 6.1 dB and 3.2 dB, respectively.

After data cleaning, every subject had at least 19 valid head impulses to each side; therefore, 19 head impulses were used for the analysis. The latency between the peak head velocity and the peak eye velocity detected by VOG in this study was on average 6.6 ms to the right and 8.7 ms to the left. Figure 2 presents an example of the obtained eye velocity traces in a single subject during 19 head impulses to the left and the right, recorded by EOG (gray traces) and VOG (yellow traces).

The average r_c coefficient of all subjects was equal to 0.89, indicating a positive correlation between EOG and VOG eye velocity traces. The average r_c when comparing VOG eye velocity and head velocity traces was 0.96, whereas average r_c for EOG was 0.89.

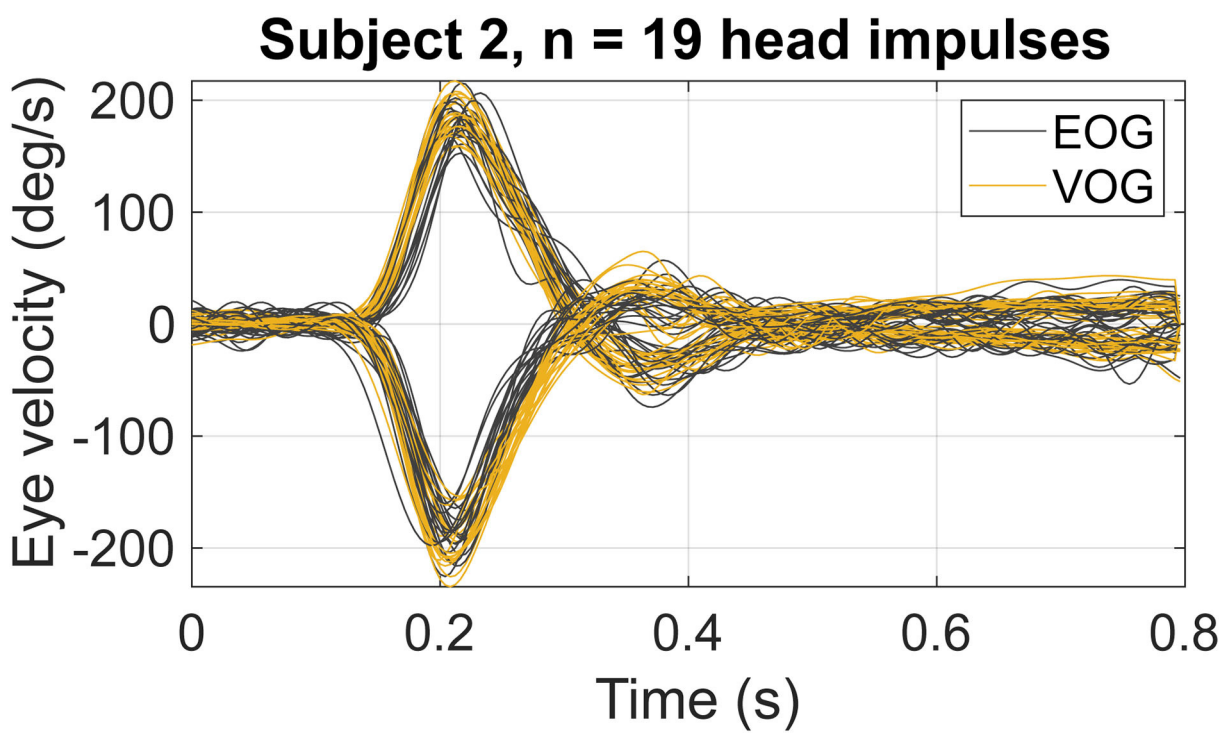

FIGURE 2
An example of eye velocity traces in a single subject (subject 2), during 19 head impulses to the left (positive velocities) and to the right (negative velocities), recorded by EOG (gray traces) and VOG (yellow traces).

TABLE 1 Mean VOR gains for left and right impulses and their standard deviations for each oculography system ($n = 19$).

EOG		VOG	
Left	**Right**	**Left**	**Right**
0.93 ± 0.11	0.95 ± 0.17	0.94 ± 0.10	1.04 ± 0.12

Comparison of VOR gain between EOG and VOG

The mean VOR gains for left and right head impulses and their standard deviations for both EOG and VOG are illustrated in Table 1. Using a BF-paired *t*-test, the difference between the average VOR gain for EOG and VOG was not significantly different from zero for all subjects for left head impulses (mean difference = −0.01, df = 18, t = −0.41, $p = 0.169$, BF = 0.26). VOG gains differed between both techniques regarding head impulses to the right (mean difference = −0.08, df = 18, t = −2.32, $p = 0.03$, BF = 2.03).

Comparison of VOR gain asymmetry between EOG and VOG

Figure 3 shows the VOR gain asymmetries obtained with EOG and VOG during horizontal HIT for the whole group. The mean VOR gain asymmetry obtained with EOG was 1% to the right, which was not significantly different from 0% asymmetry (*t*-test: mean = −0.01, df = 18, t = −0.49, $p = 0.62$). On the opposite, the mean VOR gain asymmetry obtained with VOG was 5% to the right, which was significantly different from 0% (*t*-test: mean = −0.05, df = 18, t = −7.41, $p < 0.001$). Furthermore, EOG and VOG gain asymmetries were not significantly different from each other (paired *t*-test: mean difference = 0.04, df = 18, t = 1.75, $p = 0.10$). EOG-obtained VOR gain asymmetries were more dispersed than those obtained with VOG (Figure 3).

Discussion

This study compared eye movement traces of the right eye, which were simultaneously collected using EOG and VOG during horizontal head impulse testing, in a group of 19 healthy subjects. The EOG and VOG obtained eye movement traces correlated well with each other. Nevertheless, the VOG eye velocity correlated better with the head velocity traces than the EOG as compared to concordance correlation coefficients. The obtained SNR in VOG eye velocity traces was 3 dB higher before filtering compared with EOG SNR. The VOG obtained latencies between peak head and peak eye velocities agree with the values reported in the literature for the latency of the VOR (23). The VOR gains were not statistically different between EOG and VOG methods during impulses to the left but significantly differed during impulses to the right. Furthermore, a 1% not significant and a 5% significant VOR gain asymmetries to the right were present in the eye movement traces obtained with EOG and VOG, respectively. These findings indicate that EOG might potentially be applicable as an alternative to VOG for collecting eye movement responses during head impulse testing.

EOG and VOG eye movement responses correlated well, although both techniques do not exactly provide the same type of traces, which is inherent to their different physical backgrounds (24). After all, EOG recordings can be distorted by electrode polarization processes, motion artifacts, power-line interferences, muscle contraction, intrinsic device noise, and other processes (25). These factors probably resulted in greater values of noise (less precision), as can be seen from SNR values assuming the same signal magnitude. Nevertheless, the applied filtering should have equalized the SNR for EOG and VOG, although the levels of low-frequency (<30 Hz) noises remain unknown. VOG recordings, on the other hand, can mainly be distorted by pupil detection problems (e.g., due to small eyelids, blinking, etc.) (26). So far, VOG seems to better detect eye movements in terms of the recorded velocity traces, assuming the (nearly) perfect concordence between head and eye velocities in the case of intact VOR.

Furthermore, the observed correlation between eye movement responses measured with both oculography methods does not imply that the same VOR gains should be obtained with both techniques. Therefore, both the correlation and VOR gain should be considered when investigating the feasibility of EOG as a method for head impulse testing. It can be concluded that EOG reliably detects high-velocity eye movements during horizontal head impulse testing, since (a) this study showed a well correlation between eye velocity traces recorded by both techniques; (b) the VOR gains were very similar between both techniques despite a significant difference for head impulses to the right (not to the left). After all, the significant VOR gain difference of 0.08 is most likely not clinically significant. Although using EOG is more time-consuming than VOG, EOG has several advantages: (1) Pupil detection is not necessary. This suggests that small eyelids, droopy eyelids, lens implants, and testing with lateral gaze (head impulses in the vertical plane with only a little space for the pupil before it disappears behind the eyelids) (27, 28) might not lead to artifacts in the traces. Even mini-blinks might not lead to substantial artifacts, as long as the horizontal EOG trace is not significantly interrupted by the blink; (2) Both eyes can easily be measured by applying electrodes around both eyes (29). Most current VOG systems for head impulse testing only use one camera to record one eye; (3) EOG does not require goggles to measure the eye movements. Therefore, the shape (size) of the head is less important to perform this examination (e.g., small children) (30). Many currently available VOG systems for head impulse

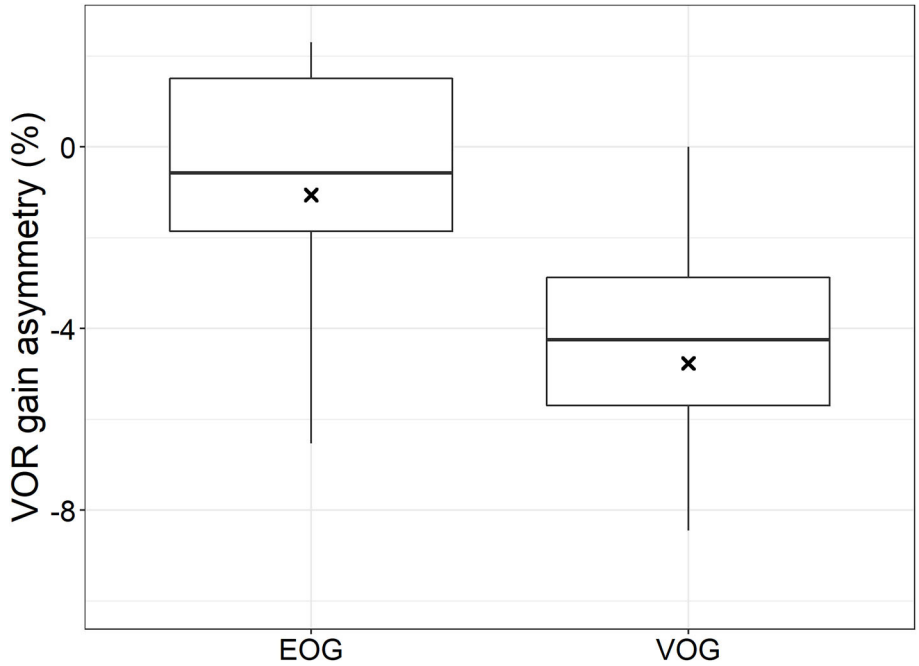

FIGURE 3
Boxplot: left-right asymmetry in VOR gain calculated for EOG and VOG obtained traces. Black crosses indicate mean values, black bars indicate medians, boxes represent first and third quartiles, and dots represent outliers.

testing still use a camera mounted on goggles. Taking all these factors into account, this might imply that EOG could be used as an alternative to, or complementary to, VOG for head impulse testing in the future. Nevertheless, if EOG would be used for head impulse testing, still a solution should be found to measure head movements. After all, in VHIT most often gyroscopes are incorporated in the head-mounted goggles, while EOG does not use head-mounted goggles.

Regarding VOR gain asymmetry, it was found that EOG-obtained eye movement responses showed small but not statistically significant asymmetry of 1% to the right, while those obtained by VOG did demonstrate a significant asymmetry of 5% to the right (which is the side of the camera and the recorded eye). These differences in asymmetry are congruent with the significant differences in VOR gain between EOG and VOG, regarding head impulses to the right. The 5% asymmetry obtained with VOG, with higher VOR gains obtained during head impulses to the side of the camera, corresponds with the literature (18). Several hypotheses were previously proposed to account for a physiological basis of this VOG detected asymmetry, for example: (1) Adduction requires an additional neuron compared to abduction. Therefore, during a head impulse to the right, the adducting (right) eye has a longer latency and needs a higher velocity to catch up with the head movement (18, 31); (2) The axis of head rotation and distance to the fixation target might influence VOR gain in favor of the side of the camera (18, 32). The asymmetries observed in this study together with those reported in the literature (31) suggest that it is not likely the artifact of one of the oculography systems itself. Also, the left-right asymmetry present at relatively low head velocities (∼180 deg/s) might be too small (31) to be detected by EOG for instance due to the lower resolution (8) compared with VOG. On top of that, a previously described asymmetry in corneoretinal potential (a lower potential when the eye is turning from right to left) might counterbalance the inherent asymmetry of the oculomotor system (19, 33) leading therefore to lower asymmetry values in the EOG recorded traces using monocular recording.

This study demonstrated that EOG can reliably detect eye movements during head impulses. However, in order to explore whether EOG is feasible for head impulse testing per se, more research is needed. In particular, EOG should be tested during head impulse testing in patients with vestibular pathology, in order to assess whether EOG can accurately detect compensatory saccades which occur in the case of vestibular hypofunction (22). In addition, the EOG technique could be optimized, e.g.,: vertical electrodes could be used to explore the feasibility of vertical head impulse testing with EOG and to detect vertical eye velocities that present in eye blinks. The use of binocular eye recordings with EOG might compensate for a possible VOR gain asymmetry (resulting in less dispersion of VOR gain asymmetries in the EOG recordings, see Figure 3)

since the electrodes are not placed symmetrically around the eyes with respect to the optical axis (21).

Limitations

Main limitation of this study involved data selection: only impulses were used, which were accepted by the vHIT device (i.e., VOG eye movement responses). This implies that a selection bias was present with respect to VOG recordings. After all, if e.g., an eye movement response during head impulse testing was rejected by the vHIT device due to pupil detection failure, this would not necessarily have been a problem for EOG, since it does not depend on pupil detection. Therefore, this study did not facilitate a comparison between EOG and VOG regarding the influence of artifacts on VOR outcomes. Therefore, dedicated new algorithms have to be developed to identify correct impulses appropriate for quantification of vestibular function, before EOG will be used for HIT.

For both eye movement detection techniques, the motion sensors in the VOG goggles were used to detect the head movements. Hence, in this study, goggle slippage might have affected the latency between eye and head movements for both EOG and VOG recordings in the same way. The latency between the peak head velocity and the peak eye velocity detected by VOG in this study was on average 6.6 ms to right and 8.7 ms to the left and falls within the normal range of the VOR latency. The absolute latency of the EOG measurements defined as the time span between the onset of the eye movement and the change in the corneoretinal potential is virtually non-existent, as these phenomena are mechanically coupled. The detection of the corneoretinal potential change depends therefore on the signal processing in the data-acquisition system. The delay in this system is specified as 80 μs. The delay of the eye movement detection in the VOG system is not specified, but as this is based on image processing and a frame rate of 246 Hz, it is longer than 4 ms, which is order of magnitude longer than the delay in the EOG system. The detection of the real onset of the eye movement in both systems is determined by algorithms that depend on the signal-to-noise ratio.

Compared to motion sensors in the goggles, a head-fixed motion sensor mounted on a bite bar (34) might probably provide more accurate information about the head movements, as this ensures close contact with the skull. It is well known that eye movement detection with VOG can be disturbed by the movement of the goggles relative to the eyes (26). Similarly, movement of the electrodes with EOG can disturb the eye movement detection, but most likely in a very different way and should be avoided at all expenses. So recognition of specific artifacts when using EOG for HIT is of similar importance as when using VOG for HIT. Nevertheless, the VOG and EOG recorded eye movement traces showed a close correlation, which suggests that in this study no major or very similar electrode or goggle movement artifacts were present in the eye movements recorded by both techniques. Moreover, using a separate head movement sensor (e.g. on a bite bar) will allow to include all impulses independent of the rejection algorithms of any oculography system. It will be implemented in the follow-up studies aimed to analyze the vertical (LARP and RALP) HITs.

Future perspectives

This study investigated the feasibility of EOG to accurately detect eye movements during the horizontal HIT, which was confirmed based on the close correlation between EOG and VOG recorded eye velocities. This could pave the way for the development of an EOG-based HIT system, incorporating a motion sensor (e.g., mounted on a bite board), and determining its accuracy for clinical use. Furthermore, this study could be extended to vertical HITs, in which especially the use of VOG can be challenging due to pupil detection difficulties [i.e., the pupil can be covered by the eyelids, (35)], whereas EOG might be easier to apply with sufficient accuracy (36).

Using a head-fixed motion sensor together with a reliable synchronization pulse between the two oculography systems (e.g., a special eye movement pattern added in the beginning and/or at the end of the recording) might give an insight in slippage sensitivities of both eye movement recording techniques. This could also facilitate evaluating the delays between head and eye traces, and therefore, estimate possible gain calculation errors due to goggle slippage (26).

EOG and VOG methods can be compared in terms of the signal-to-noise ratio and accuracy or resolution using both raw and unfiltered traces. The resolution for EOG is believed to be close to 0.5°, whereas for VOG, it is quantified at about 0.01° (8). However, these average numbers can substantially vary from patient to patient and very strongly depend on the typical features of pupil detection vs. corneoretinal potential detection.

Conclusion

To our knowledge, this is the first description of using the EOG technique to record eye movements during head impulse testing. EOG and VOG obtained eye movement traces correlate well with each other during horizontal head impulse testing. In addition, EOG did not show significant VOR gain asymmetry in healthy individuals, in contrast to VOG. These findings indicate that EOG might potentially be applicable as an alternative to VOG for collecting eye movement responses during head impulse testing.

Data availability statement

The raw data supporting the conclusions of this article will be made available by the authors, without undue reservation.

Ethics statement

The studies involving human participants were reviewed and approved by local Ethical Committee of Tomsk State University. The patients/participants provided their written informed consent to participate in this study.

Author contributions

MP and VZ collected the data. MP, VZ, and DS conducted the analysis and wrote the manuscript. VD, HK, and RB supervised the study and edited the manuscript. All authors contributed to the article and approved the submitted version.

Conflict of interest

The authors declare that the research was conducted in the absence of any commercial or financial relationships that could be construed as a potential conflict of interest.

Publisher's note

All claims expressed in this article are solely those of the authors and do not necessarily represent those of their affiliated organizations, or those of the publisher, the editors and the reviewers. Any product that may be evaluated in this article, or claim that may be made by its manufacturer, is not guaranteed or endorsed by the publisher.

References

1. Baloh RW, Honrubia V, Kerber KA. Baloh and Honrubia's clinical neurophysiology of the vestibular system. In: *Handbook of Clinical Audiology*. 4th ed. Oxford University Press (2011). doi: 10.1093/med/9780195387834.001.0001

2. Khan S, Chang R. Anatomy of the vestibular system: a review. *NeuroRehabilitation*. (2013) 32:437–43. doi: 10.3233/NRE-130866

3. Fetter M. Vestibulo-ocular reflex. In: Straube A, Buttner U, editors. *Neuro-Ophthalmology*. Basel: KARGER (2007). p. 35–51.

4. Ciuman RR. Inner ear symptoms and disease: pathophysiological understanding and therapeutic options. *Med Sci Monit*. (2013) 19:1195–210. doi: 10.12659/MSM.889815

5. Wallace B, Lifshitz J. Traumatic brain injury and vestibulo-ocular function: current challenges and future prospects. *Eye Brain*. (2016) 8:153–64. doi: 10.2147/EB.S82670

6. Halmagyi GM, Curthoys IS. A clinical sign of canal paresis. *Arch Neurol*. (1988) 45:737–9. doi: 10.1001/archneur.1988.00520310043015

7. Wuyts FL, Furman J, Vanspauwen R, Van de Heyning P. Vestibular function testing. *Curr Opin Neurol*. (2007) 20:19–24. doi: 10.1097/WCO.0b013e3280140808

8. Eggert T. Eye movement recordings: methods. *Dev Ophthalmol*. (2007) 40:15–34. doi: 10.1159/000100347

9. Siddiqui U, Shaikh AN. An overview of "Electrooculography." *Int J Adv Res Comput Commun Eng*. (2013) 2:4328–30.

10. Creel DJ. The electrooculogram. In: *Handbook of Clinical Neurology*. Elsevier B.V (2019). p. 495–9.

11. Merino M, Rivera O, Gómez I, Molina A, Dorronzoro E. A method of EOG signal processing to detect the direction of eye movements. In: *In: 2010 First International Conference on Sensor Device Technologies and Applications*. (2010). p. 100–5. doi: 10.1109/SENSORDEVICES.2010.25

12. Welgampola MS, Taylor RL, Halmagyi GM. Video head impulse testing. *Adv Otorhinolaryngol*. (2019) 82:56–66. doi: 10.1159/000490272

13. Alhabib SF, Saliba I. Video head impulse test: a review of the literature. *Eur Arch Oto-Rhino-Laryngology*. (2017) 274:1215–22. doi: 10.1007/s00405-016-4157-4

14. Halmagyi GM, Chen L, MacDougall HG, Weber KP, McGarvie LA, Curthoys IS. The video head impulse test. *Front Neurol*. (2017) 8:1. doi: 10.3389/fneur.2017.00258

15. MacDougall HG, Weber KP, McGarvie LA, Halmagyi GM, Curthoys IS. The video head impulse test: diagnostic accuracy in peripheral vestibulopathy. *Neurology*. (2009) 73:1134–41. doi: 10.1212/WNL.0b013e3181bacf85

16. Suh MW, Park JH, Kang S. Il, Lim JH, Park MK, Kwon SK. Effect of goggle slippage on the video head impulse test outcome and its mechanisms. *Otol Neurotol*. (2017) 38:102–9. doi: 10.1097/MAO.0000000000001233

17. Heuberger M, Grill E, Saglam M, Ramaioli C, Müller M, Strobl R, et al. Usability of the video head impulse test: lessons from the population-based prospective KORA study. *Front Neurol*. (2018) 9:659. doi: 10.3389/fneur.2018.00659

18. Strupp M, Kichler A, McGarvie L, Kremmyda O. The video head impulse test: a right–left imbalance. *J Neurol*. (2018) 265:40–3. doi: 10.1007/s00415-018-8986-5

19. Wierts R, Janssen MJA, Kingma H. Measuring saccade peak velocity using a low-frequency sampling rate of 50 Hz. *IEEE Trans Biomed Eng*. (2008) 55:2840–2. doi: 10.1109/TBME.2008.925290

20. Jia Y, Tyler CW. Measurement of saccadic eye movements by electrooculography for simultaneous EEG recording. *Behav Res Methods*. (2019) 51:2139–51. doi: 10.3758/s13428-019-01280-8

21. López A, Ferrero FJ, Valledor M, Campo JC, Postolache O. A study on electrode placement in EOG systems for medical applications. In: *2016 IEEE International Symposium on Medical Measurements and Applications*. IEEE (2016). p. 1–15. doi: 10.1109/MeMeA.2016.7533703

22. van Dooren TS, Starkov D, Lucieer FMP, Vermorken B, Janssen AML, Guinand N, et al. Comparison of three video head impulse test systems for the diagnosis of bilateral vestibulopathy. *J Neurol*. (2020) 267:256–64. doi: 10.1007/s00415-020-10060-w

23. Collewijn H, Smeets JBJ. Early components of the human vestibulo-ocular response to head rotation: latency and gain. *J Neurophysiol*. (2000) 84:376–89. doi: 10.1152/jn.2000.84.1.376

24. Blakley BW, Chan L. Methods considerations for nystagmography. *J Otolaryngol Head N*. (2015) 44:1–5. doi: 10.1186/s40463-015-0078-2

25. López A, Ferrero F, Villar JR, Postolache O. High-performance analog front-end (AFE) for EOG systems. *Electron*. (2020) 9:1–15. doi: 10.3390/electronics9060970

26. Mantokoudis G, Saber Tehrani AS, Kattah JC, Eibenberger K, Guede CI, Zee DS, et al. Quantifying the vestibulo-ocular reflex with video-oculography: nature and frequency of artifacts. *Audiol Neurotol*. (2015) 20:39–50. doi: 10.1159/000362780

27. Larrazabal AJ, García Cena CE, Martínez CE. Video-oculography eye tracking towards clinical applications: a review. *Comput Biol Med*. (2019) 108:57–66. doi: 10.1016/j.compbiomed.2019.03.025

28. Ganança MM, Caovilla HH, Ganança FF. Electronystagmography vs. videonystagmography. *Braz J Otorhinolaryngol.* (2010) 76:399–403. doi: 10.1590/S1808-86942010000300021

29. Kumar A, Krol G. Binocular infrared oculography. *Laryngoscope.* (1992) 102:367–78. doi: 10.1288/00005537-199204000-00002

30. Finocchio D V, Preston KL, Fuchs AF. Obtaining a quantitative measure of eye movements in human infants: a method of calibrating the electrooculogram. *Vision Res.* (1990) 30:1119–28. doi: 10.1016/0042-6989(90)90169-L

31. Weber KP, Aw ST, Todd MJ, McGarvie LA, Pratap S, Curthoys IS, Halmagyi GM. Inter-ocular differences of the horizontal vestibulo-ocular reflex during impulsive testing. *Prog Brain Res.* (2008) 171:195–8. doi: 10.1016/S0079-6123(08)00626-2

32. Crane BT, Viirre ES, Demer JL. The human horizontal vestibulo-ocular reflex during combined linear and angular acceleration. *Exp Brain Res.* (1997) 114:304–20. doi: 10.1007/PL00005639

33. Liu H, Liao F, de la Villa P. Ocular asymmetry in electrooculographic responses. *Symmetry.* (2021) 13:1809. doi: 10.3390/sym13101809

34. Ramaioli C, Cuturi LF, Ramat S. Lehnen N. Vestibulo-ocular responses and dynamic visual acuity during horizontal rotation and translation. *Front Neurol.* (2019) 10:1–11. doi: 10.3389/fneur.2019.00321

35. MacDougall HG, McGarvie LA, Halmagyi GM, Curthoys IS, Weber KP. The Video Head Impulse Test (vHIT) detects vertical semicircular canal dysfunction. *PLoS ONE.* (2013) 8:e61488. doi: 10.1371/journal.pone.0061488

36. Janssen MJA. *Vestibular Exploration : On Advanced Diagnostics and Therapy*. Maastricht University (2011). p. 143.

frontiers | Frontiers in Neurology

TYPE Original Research
PUBLISHED 20 October 2022
DOI 10.3389/fneur.2022.1033955

Check for updates

OPEN ACCESS

EDITED BY
Michael Strupp,
Ludwig Maximilian University of Munich, Germany

REVIEWED BY
Jorge Rey-Martinez,
Donostia University Hospital, Spain
Eduardo Martin-Sanz,
Hospital de Getafe, Spain
Maurizio Versino,
Humanitas Mater Domini, Italy

*CORRESPONDENCE
Hyun Ah Kim
kha0206@dsmc.or.kr

†These authors have contributed equally to this work and share first authorship

SPECIALTY SECTION
This article was submitted to Neuro-Otology, a section of the journal Frontiers in Neurology

RECEIVED 01 September 2022
ACCEPTED 06 October 2022
PUBLISHED 20 October 2022

CITATION
Park J-Y, Lee H and Kim HA (2022) The frequency and relationship with vestibular function test results of positional preference in acute vestibular neuritis.
Front. Neurol. 13:1033955.
doi: 10.3389/fneur.2022.1033955

COPYRIGHT
© 2022 Park, Lee and Kim. This is an open-access article distributed under the terms of the Creative Commons Attribution License (CC BY). The use, distribution or reproduction in other forums is permitted, provided the original author(s) and the copyright owner(s) are credited and that the original publication in this journal is cited, in accordance with accepted academic practice. No use, distribution or reproduction is permitted which does not comply with these terms.

The frequency and relationship with vestibular function test results of positional preference in acute vestibular neuritis

Ji-Yun Park[1†], Hyung Lee[2,3†] and Hyun Ah Kim[2,3*]

[1]Department of Neurology, Ulsan University Hospital, University of Ulsan College of Medicine, Ulsan, South Korea, [2]Department of Neurology, Keimyung University School of Medicine, Daegu, South Korea, [3]Brain Research Institute, Keimyung University School of Medicine, Daegu, South Korea

Objective: To assess the prevalence and relationship with vestibular function test results of positional preference in acute vestibular neuritis (VN).

Methods: We prospectively recruited 33 patients with VN during the acute phase. We assessed the severity of vertigo with a visual analog scale (VAS) and the degree of spontaneous nystagmus (SN) during sitting, the head rolling to the affected, and the healthy side. Patients performed other vestibular function tests, including ocular and cervical vestibular evoked myogenic potential (VEMP), on the same day or the next day of VNG testing.

Results: Twelve patients (12/33, 36%) with VN complained of more severe vertigo during lying on the affected side compared to the healthy side under visual fixation. Compared to patients without positional preference (without positional preference group), patients with positional preference (with positional preference group) showed a significantly higher VAS and maximal slow phase velocity (SPV) of SN at all positions except lying on the lesion side. However, there was no difference in the SPV gap between the two groups. 30% (10/33) of patients with VN complained of more severe vertigo while lying on the affected side compared to the healthy side without visual fixation. Maximal SPV of SN was not different between the two groups. There was no other significant difference in both canalith and otolith function test results between the two groups regardless of the visual fixation.

Conclusions: One-third of patients with acute VN had more severe vertigo while lying on the affected side than in the supine position. The positional preference was not directly related to the SN intensity or VEMP results. The positional preference might reflect the otolith damage in the setting of activation of the sustained otolith system, not the transient otolithic system.

KEYWORDS

vestibular neuritis, positional preference, otolith function, spontaneous nystagmus, visual analog scale

Introduction

Vestibular neuritis (VN) is a common neuro-otologic syndrome characterized by acute prolonged vertigo (lasting several days), nausea, and vomiting without other accompanying neurologic or audiological symptoms or signs (1, 2). During the acute attack, patients usually lie with their eyes closed on a side with a healthy ear down (2). However, the frequency and mechanism of the positional preference in acute VN are unknown.

When a patient with acute VN sits up, especially with the head bending 30 degrees, the horizontal semicircular canal lies on the horizontal plane (3), and the effect of gravity on the semicircular canal and otolith organ on both sides would be the same. On the other hand, the difference of gravity between both vestibular organs would be the maximum on the lesion side up. The mechanism of this positional preference implies an interaction between inputs from the otoliths and the semicircular canals (4, 5). It has been suggested that the medial portion of the utricle may respond best to the pull of gravity (6). A previous study found that some of the patients with VN showed the inhibition of spontaneous nystagmus (SN) when they lay toward the healthy side and an increase of SN when they lay toward the lesion side (5). Authors suggested that an alteration in the influence of gravitation on the otolith organs can change SN in both a positive and a negative direction (5). Therefore, we assumed that the positional preference might be related to the utricular function tests such as subjective visual vertical (SVV) and ocular vestibular evoked myogenic potential (oVEMP) tests. We sought to investigate the frequency of positional preference and its relationship with semicircular and otolithic vestibular function tests in acute VN.

Methods

We prospectively recruited patients with VN during the acute phase at Keimyung University Dongsan Hospital and Ulsan University Hospital from April 2019 to April 2020. All patients met the clinical diagnostic criteria for VN (1, 2, 7), including (1) sudden onset of prolonged vertigo (more than 1 day) within 1 week, (2) unidirectional spontaneous horizontal–torsional nystagmus, (3) the head-thrust test showed an ipsilateral deficit of the horizontal semicircular canal (gain < 0.8) or caloric asymmetry ($>25\%$). Exclusion criteria were (1) the presence of auditory or other neurologic findings, (2) a previous history of neuro-otologic diseases, (3) abnormal audiogram or middle ear function, (4) acute lesion on diffusion-weighted brain MRI, (5) Severe cognitive impairment (Mini-mental state examination < 15). Diffusion-weighted MRI was performed on all patients to exclude a central lesion mimicking peripheral vestibulopathy.

Videonystagmography (VNG) was used to record SN, head-shaking nystagmus (HSN), head-impulse test (HIT), and caloric responses. The maximal slow phase velocity (SPV) of SN was calculated during sitting, supine, lying on the affected side, and healthy side. We assessed the severity of vertigo with a visual analog scale (VAS) during each position (Figure 1). We defined the presence of positional preference if there is any difference in VAS between lying on the lesion and healthy sides. We checked maximal SPV and VAS with and without visual fixation. We also calculated the gap between maximal SPV and VAS between lying on the healthy and the lesion sides with the revised Jongkees difference equation (8).

SPV gap = (SPV_L– SPV_H)/SPV_L*100, where SPV_L is maximal SPV lying on the lesion side, and SPV_H is maximal SPV lying on the healthy side.

VAS gap = (VAS_L – VAS_H)/VAS_L*100, where VAS_L is VAS lying on the lesion side, and VAS_H is VAS lying on the healthy side.

Patients also performed oVEMP, cervical vestibular evoked myogenic potential (cVEMP), and SVV on the same day or the next day of VNG. We used a Nicolet Viking Select unit (Nicolet-Biomedical, Madison, WI, USA) to measure the surface electromyography (EMG) activity for cVEMP and oVEMP. A cVEMP was performed with the patient in a supine position, raising the head approximately 30° and rotating contralaterally to activate the sternocleidomastoid (SCM) muscles. The active electrode was placed over the belly of the contracted SCM after subtracting activity from a reference electrode located on the medial clavicle. A ground electrode was attached to the forehead. A short alternating tone burst (110 dB nHL; 500 Hz; ramp = 2 ms; plateau = 3 ms) was given at 2.1 Hz monoaurally using a headphone. To compare the amplitude of p13-n23 on the affected side (Aa) with that on the unaffected side (Au), the asymmetry ratio of each patient was calculated as (Aa – Au) / (Aa + Au) × 100 (9). We monitored the patients to ensure adequate levels of activation, enable fine adjustment of head position to match the EMG levels for each side, and allow measurement of background contraction levels and calculation of normalized amplitudes (9). Tests were considered abnormal if interaural differences in amplitude of p13 or n23 were outside the average value + 2 SDs (i.e., asymmetry of amplitude of cVEMPs $>$ 28%) or no wave formation. Normative data were obtained from 36 age-matched healthy controls (14 men, mean age = 58.17 ± 10.59, t-test, $p = 0.146$) without a history of auditory or vestibular disorders.

To record oVEMP, the subject was supine on a bed, with the head supported on a pillow. An active electrode was placed 1 cm below the center of the lower eyelid, and the reference electrode was attached to the cheek 2 cm below the active electrode (10). The ground electrode was located on the forehead. During testing, the subject looked up approximately 25° above straight

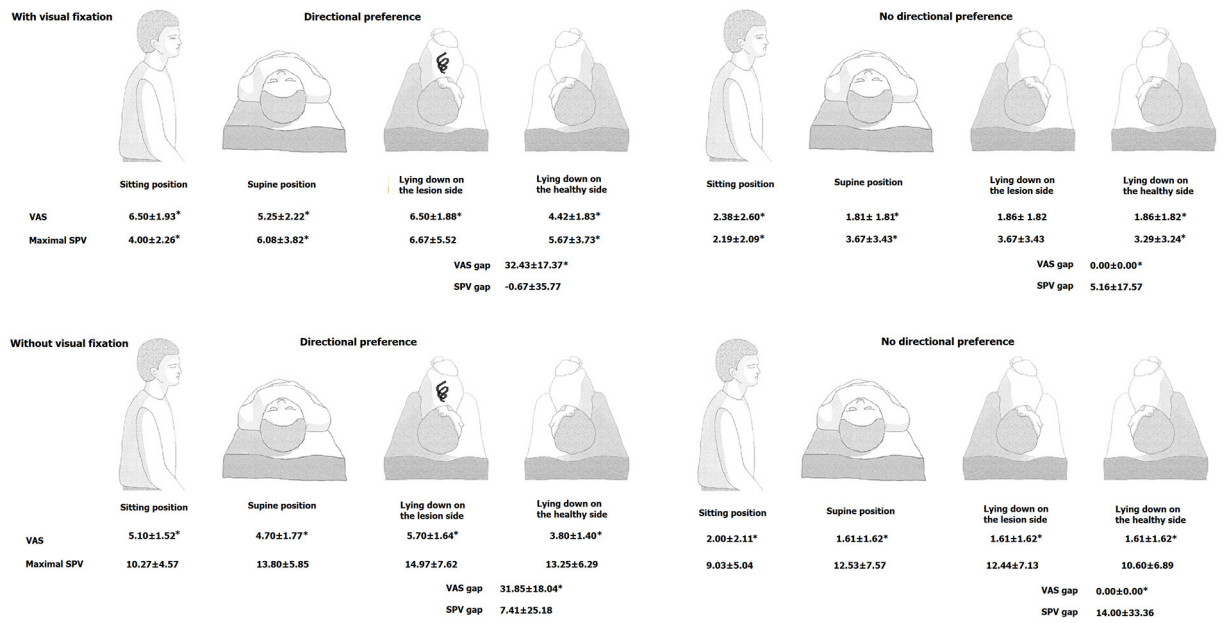

FIGURE 1
Comparison of the intensity of spontaneous nystagmus (maximal SPV) and vertigo severity (VAS) at each position between patients with vs. without positional preference. **(Upper)**: under the visual fixation, **(Lower)**: without visual fixation. SP, slow phase velocity; SN, spontaneous nystagmus; VAS, visual analog scale. *$p < 0.05$: with vs. without positional preference.

ahead and maintained a small fixation point ∼60 cm from the eyes. oVEMPs were elicited by tapping the hairline using an electric reflex hammer (VIASYS Healthcare, CA, USA). Bilateral responses were simultaneously obtained whenever tapping stimuli were applied. Ocular VEMPs in response up to 60 stimuli were averaged for each test. The average latency of the initial negative peak (n10) and the n10 – p10 amplitude were analyzed. The interaural difference ratio of the amplitude of the ocular VEMPs was calculated as the interaural difference ratio (%) (Aa – Au) / (Aa + Au) × 100, where Aa and Au are the n10 – p10 amplitude on the affected and unaffected sides, respectively (10). Tests were considered abnormal if interaural differences in amplitude or latencies of n10 were outside the average value ± 2 SDs (i.e., asymmetry of amplitude of oVEMPs > 29%, amplitude of n10-p10 < 1.5 μV or latency of n10 > 21.5 ms) or no wave formation. Normative data were obtained from 28 age-matched healthy controls (19 men, mean age = 50.89 ± 11.54, *t*-test, $p = 0.346$) without a history of auditory or vestibular disorders.

The SVV tilt in the patients was defined as abnormal when the degree of SVV tilt exceeded the mean ± 2SD obtained from 80 normal controls (normal range: −2.0∼2.0° for binocular viewing; the negative value indicates a counterclockwise tilt) (7). The detailed methods for recording SVV have been described previously (11).

Numerical parameters between patients with or without positional preference were calculated with a Mann-Whitney U test. A Fisher's exact test was performed for percentage comparison of nominal data, and Spearman's correlation was used for correlation analysis between parameters. Two-way ANOVA was used to determine both the independent effect of fixation and positional preference as well as to test whether there was a significant interaction between these variables.

All experiments complied with the tenets of the Declaration of Helsinki, and the study protocol was reviewed and approved by the Institutional Review Board of the School of Medicine at Keimyung University.

Results

Thirty-three patients with acute VN were enrolled. The mean age was 53.9 ± 13.2 years. Approximately 76% of the patients were male, and 49% had VN on the right side. The time from onset to VNG was 53.0 ± 38.1 h.

Vertigo severity and maximal SPV of SN at different positions with and without fixation

Under the visual fixation, the mean VAS during sitting position was 3.9 ± 3.1 and during supine position was 3.1 ± 2.6. Mean maximal SPV during sitting position was 2.8 ± 2.3 deg/sec and during supine position was 4.6 ± 3.8 deg/sec. The mean VAS during lying on the affected side was 3.6 ± 2.9, while

TABLE 1 Correlation analysis between the intensity of spontaneous nystagmus (maximal SPV) and vertigo severity (VAS) at each position.

	Maximal SPV with fixation (deg/sec)					Maximal SPV without fixation (deg/sec)				
VAS	**Sitting**	**Supine**	**Lying on the lesion side**	**Lying on the healthy side**	**SPV gap**	**Sitting**	**Supine**	**Lying on the lesion side**	**Lying on the healthy side**	**SPV gap**
Sitting	0.554**	0.487**	0.483**	0.592**	−0.149	0.320	0.283	0.354*	0.342	−0.030
Supine	0.568**	0.532**	0.503**	0.578**	−0.037	0.283	0.242	0.337	0.310	0.065
Lying on the lesion side	0.590**	0.552**	0.518**	0.602**	−0.039	0.278	0.249	0.330	0.342	0.002
Lying on the healthy side	0.508**	0.469**	0.478**	0.542**	−0.032	0.240	0.209	0.292	0.235	0.092
VAS gap	0.456**	0.377*	0.333	0.414*	−0.021	0.158	0.131	0.143	0.279	−0.136

Spearman's correlation coefficient.
*$p < 0.05$, **$p < 0.01$.
SPV, slow phase velocity; VAS, visual analog scale.

TABLE 2 Sex, lesion side, otolithic function test results between patients with and without positional preference.

	With visual fixation			Without visual fixation		
	No positional preference	**With positional preference**	***p*-value**	**No positional preference**	**With positional preference**	***p*-value**
Sex (Female)	3/21 (14.3%)	5/12 (41.7%)	0.106	3/23 (13%)	5/10(50%)	0.036*
Lesion side (Lt)	13/21 (61.9%)	4/12 (33.3%)	0.157	14/23 (60.9%)	3/10 (30%)	0.141
Abnormal SVV	13/18 (72.2%)	9/11 (81.8%)	0.677	15/20 (75%)	7/9 (77.8%)	1.000
Abnormal oVEMP	11/21 (52.4%)	8/12 (66.7%)	0.486	12/23 (52.2%)	7/10 (70%)	0.455
Abnormal cVEMP	10/21 (47.6%)	3/12 (27.3%)	0.450	10/23 (43.5%)	3/9 (33.3%)	0.704

Fisher's exact test, *$p < 0.05$.
SVV, subjective visual vertical; oVEMP, ocular vestibular evoked myogenic potential; cVEMP, cervical vestibular evoked myogenic potential.

lying on the healthy side was 2.8 ± 2.2. The mean maximal SPV during lying on the affected side was 4.8 ± 4.5 deg/sec, while lying on the healthy side was 4.2 ± 3.6 deg/sec. The mean VAS gap and SPV gap were 11.79 ± 18.83 and 3.10 ± 25.31, respectively.

When goggles were covered on the eyes (without visual fixation), the mean VAS during sitting position was 2.9 ± 2.4 and during supine position was 2.6 ± 2.2. Mean maximal SPV was 9.4 ± 4.9 deg/sec during sitting and 13.0 ± 7.1 deg/sec during supine position. The mean VAS during lying on the affected side was 2.9 ± 2.5, while lying on the healthy side was 2.3 ± 1.8. The mean maximal SPV during lying on the affected side was 13.3 ± 7.4 deg/sec, while lying on the healthy side was 11.6 ± 6.7 deg/sec. The mean VAS gap and SPV gap were 9.65 ± 17.67 and 12.00 ± 30.87, respectively.

Thirty-six percent (12/33) of the patients with VN complained of more severe vertigo during lying on the affected side compared to the healthy side (i.e., with directional preference group) under the visual fixation. The other patients reported no difference in vertigo severity while lying on the healthy side compared to the affected side (i.e., without positional preference group). Maximal SPVs during supine, sitting, and lying on the lesion side were significantly higher in the with positional preference group than those without positional preference group under the fixation. However, the mean SPV gaps between the two groups were no different (−0.67 ± 35.77 vs. 5.16 ± 17.57, respectively) (Figure 1 and Supplementary Table 1).

When goggles were covered on the eyes (without visual fixation), 30% (10/33) of patients with VN complained of more severe vertigo during lying on the affected side compared to the healthy side. There was no difference in maximal SPVs at any positions between the two groups without visual fixation. Maximal SPV and VAS at each position under two main factors (positional preference and visual fixation) with a two-way ANOVA showed no interaction between positional preference and visual fixation (Supplemental Table 1). There were significant positive correlations of VAS with maximal SPV at all positions under the visual fixation, but the VAS gap did not correlate with the SPV gap. There was no significant correlation of VAS with maximal SPV at all positions except lying on the lesion side (Table 1).

TABLE 3 Vestibular function test results between patients with and without positional preference.

	With visual fixation					Without visual fixation				
	No positional preference ($n = 21$)		With positional preference ($n = 12$)			No positional preference ($n = 23$)		With positional preference ($n = 10$)		
	Mean	SD	Mean	SD	*p*-value	Mean	SD	Mean	SD	*p*-value
Age	55.95	13.12	50.42	13.24	0.410	54.87	13.83	51.80	12.16	0.681
Time interval from onset to test (hrs)	59.95	44.40	40.83	19.52	0.261	60.30	42.62	36.20	16.30	0.136
CP (%)	59.27	18.75	63.76	19.79	0.475	60.72	18.61	61.04	20.86	0.917
hHIT	0.37	0.15	0.33	0.12	0.370	0.35	0.15	0.35	0.12	0.903
pHIT	0.82	0.20	0.85	0.17	0.969	0.84	0.20	0.82	0.17	0.428
aHIT	0.60	0.15	0.65	0.10	0.258	0.60	0.15	0.66	0.09	0.230
SVV (°)	3.59	2.55	3.25	1.75	0.928	3.77	2.55	2.78	1.26	0.509
oVEMP (%)	50.21	37.71	49.16	38.09	1.000	50.86	38.25	47.50	36.78	0.935
n10 latency (ms)	6.93	6.52	9.33	6.78	0.270	7.17	6.91	9.28	6.00	0.312
n10-p10 amplitude (μV)	6.38	5.20	24.42	38.56	0.120	11.75	27.12	16.20	20.33	0.142
cVEMP (%)	44.50	39.02	26.56	28.68	0.184	41.71	38.31	29.41	30.91	0.358
HSN (deg/sec)	16.89	7.30	17.17	4.86	0.938	17.17	7.01	16.60	5.17	0.652

Mann-Whitney U-test.
SD, standard deviation; CP, canal paresis; hHIT, horizonal canal gain of head-impulse test; pHIT, posterior canal gain of head-impulse test; aHIT, anterior canal gain of head-impulse test; SVV, subjective visual vertical; oVEMP, ocular vestibular evoked myogenic potential; cVEMP, cervical vestibular evoked myogenic potential; HSN, head-shaking nystagmus.

Vestibular function test results in patients with and without positional preference

There was no difference in age, lesion side, and time interval from symptom onset to the test between the two groups, regardless of the visual fixation. Female sex was significantly more frequent in patients with positional preference when the visual fixation was removed (13% vs. 50%, $p = 0.036$) (Table 2). The presence of positional preference was not different in patients with and without the abnormality of SVV, oVEMP, or cVEMP (Table 2). There was also no significant difference in canalith and otolith vestibular function test results between patients with and without positional preference (Table 3). The VAS and SPV gaps did not correlate with age, time interval from symptom onset to the test, or vestibular function test results, regardless of the visual fixation (Table 4).

Discussion

About 30% of patients with acute VN had positional preference, and all had more severe vertigo during lying on the affected side compared to the healthy side. Because SN intensity during lying on the lesion side was more prominent than lying on the healthy side (gravity-dependence) in the present study, we could assume that asymmetry of the vestibulo-ocular reflex may be reinforced during lying on the affected side and affect the SN intensity. However, the difference in vertigo severity between lying on the lesion and the healthy side did not relate to the gap in SN intensity. Moreover, SVV and VEMP test results were not associated with the gravity-dependence of SN intensity and positional preference.

Positional preference in VN has been thought to be due to the effect of gravity on the horizontal component of SN mediated by otolith-ocular reflex (5, 12). Because SN intensity in VN increased or inhibited according to head position, an alteration in the influence of gravitation on the otolith organs could change SN, which might be related to positional preference in patients with VN (13). As in the previous study (5, 13), patients with VN showed gravity-dependence of SN intensity in the present study. The mean maximal SPV was highest during lying on the affected side and lowest during the supine position. In the previous study, HSN in patients with unilateral VN is also modulated by the static attitude of the head and is more intense with the affected ear down (14). It has been suggested that an asymmetric suppression of vestibular nystagmus by the unilaterally impaired otolith organs could result in positional preference (5). Because the anterior semicircular canal is important in distinguishing between utricular activation by linear acceleration during lateral head tilt and by lateral head translation (15, 16), misinterpreted signals about head translation and head tilt in acute superior VN were suggested as a possible mechanism of positional preference. Another possible explanation for positional preference is linear vertigo. In patients with BPPV, the discrepancy between the internal representation of gravito-inertial acceleration provided by the otolith and the internal estimation of actual gravity direction increases an erroneous inertial acceleration (17–19). Similarly, we could assume that vestibular imbalance in VN

TABLE 4 Correlation analysis of the gap of vertigo severity (VAS gap) and the gap of the intensity of spontaneous nystagmus (SPV gap) while lying on the lesion and healthy sides with vestibular function test results.

	With fixation				Without fixation			
	SPV gap		VAS gap		SPV gap		VAS gap	
	r	p	*r*	p	*r*	p	*r*	p
Age	−0.140	0.436	−0.139	0.441	0.089	0.623	−0.102	0.570
Time interval from onset to test (hrs)	−0.088	0.627	−0.171	0.341	0.127	0.480	−0.290	0.102
CP (%)	0.115	0.531	0.064	0.728	0.190	0.297	−0.030	0.872
hHIT	0.072	0.694	−0.170	0.352	−0.328	0.067	0.004	0.983
pHIT	−0.257	0.155	−0.033	0.858	0.024	0.895	−0.120	0.513
aHIT	0.003	0.987	0.158	0.389	0.023	0.899	0.230	0.206
SVV (°)	0.101	0.602	0.046	0.812	0.185	0.337	−0.129	0.504
oVEMP (%)	0.067	0.717	−0.010	0.957	−0.071	0.701	0.007	0.972
n10 latency (ms)	0.022	0.903	0.178	0.331	0.087	0.634	0.158	0.388
n10-p10 amplitude (μV)	0.010	0.958	0.309	0.085	−0.094	0.609	0.259	0.152
cVEMP (%)	0.023	0.901	−0.243	0.188	0.163	0.380	−0.133	0.475
HSN (deg/sec)	0.243	0.180	−0.023	0.901	0.000	0.999	−0.093	0.614

Spearman's correlation coefficient.
SPV, slow phase velocity; VAS, visual analog scale; CP, canal paresis; hHIT, horizonal canal gain of head-impulse test; pHIT, posterior canal gain of head-impulse test; aHIT, anterior canal gain of head-impulse test; SVV, subjective visual vertical; oVEMP, ocular vestibular evoked myogenic potential; cVEMP, cervical vestibular evoked myogenic potential; HSN, head-shaking nystagmus.

could cause linear vertigo from transient central canal-otolithic perception change. If linear vertigo is additional to the original dizziness from the vestibular imbalance, it could cause positional preference in patients with VN.

Even though we could see gravity-dependent SN in patients with VN, the change of SN intensity during position change did not correlate with positional preference. Moreover, positional preference was not related to other semicircular or otolith function test results, including anterior canal gain of HIT, SVV, or VEMP in the present study. VEMP tests are clinical tests of transient otolith function evoked by brief sound and vibration stimuli and reflect the unilateral otolithic loss (20). In contrast, the sustained otolithic system concerned with signaling low-frequency gravitoinertial force stimuli could be tested with ocular counterrolling to roll-tilt or tests using linear translation. Although the SVV primarily reflects the asymmetry of utricular inputs between the sides of the vestibular system (21), the SVV most likely does not only reflect otolith function, but also depends directly and indirectly (*via* internal references) on the canal and proprioceptive function, and is affected by eye torsion upon the head roll (22). It seems that otolithic function test results in the present study could not simply reflect the stimulation of sustained otolithic system from lying on the lesion or healthy side.

Proprioception participates in the appreciation of body orientation and configuration, which is essential in vestibular rehabilitation in the acute stage (23). Asymmetric neck muscle proprioceptive signals from passive sustained head turning caused asymmetric functioning of the VOR in a previous study (24). Proprioception may also contribute to the generation of SVV change during head tilt (25, 26). There has been no previous study on the effect of lying to the healthy or lesion side on VOR. However, we could assume that the proprioceptive signal from lying also could affect the positional preference in acute VN.

Our study has some limitations. First, because the number of patients was relatively small, the possible contribution of the positional preference to the severity of vertigo and SN should be investigated again with larger sample size. Second, even though patients with VN usually prefer to lie in bed on the side with their healthy ears down and their eyes closed, they sometimes do not notice any difference in the severity of vertigo between lying on either side (2). We assessed the degree of vertigo during performing VNG, which could be different with positional preference in bed. Finally, some patients performed SVV, cVEMP, and oVEMP on the next day of VNG. We could not exclude the possibility of changing otolith functions within 1 day.

Data availability statement

The raw data supporting the conclusions of this article will be made available by the authors, without undue reservation.

Ethics statement

The studies involving human participants were reviewed and approved by Institutional Review Board of the School of Medicine at Keimyung University. The patients/participants

provided their written informed consent to participate in this study.

Author contributions

HK conducted the design and conceptualization of the study, interpretation of the data, and drafting and revising the manuscript. HL and J-YP interpreted the data and revised the manuscript. All authors contributed to the article and approved the submitted version.

Funding

This work was supported by the research promoting grant from the Keimyung University Dongsan Medical Center in 2018.

Conflict of interest

HL serves on the editorial boards of the Research in Vestibular Science, Frontiers in Neuro-otology, and Current Medical Imaging Review.

The remaining authors declare that the research was conducted in the absence of any commercial or financial relationships that could be construed as a potential conflict of interest.

Publisher's note

All claims expressed in this article are solely those of the authors and do not necessarily represent those of their affiliated organizations, or those of the publisher, the editors and the reviewers. Any product that may be evaluated in this article, or claim that may be made by its manufacturer, is not guaranteed or endorsed by the publisher.

Supplementary material

The Supplementary Material for this article can be found online at: https://www.frontiersin.org/articles/10.3389/fneur.2022.1033955/full#supplementary-material

References

1. Strupp M, Brandt T. Vestibular neuritis. *Adv Otorhinolaryngol.* (1999) 55:111–36. doi: 10.1159/000059060

2. Baloh RW. Clinical practice. Vestibular neuritis. *N Engl J Med.* (2003) 348:1027–32. doi: 10.1056/NEJMcp021154

3. Curthoys IS, Oman CM. Dimensions of the horizontal semicircular duct, ampulla and utricle in the human. *Acta Otolaryngol.* (1987) 103:254–61. doi: 10.3109/00016488709107280

4. Leigh RJ. *The Neurology of Eye Movements*. New York, NY: Oxford University Press (2006).

5. Fluur E. Interaction between the utricles and the horizontal semicircular canals. IV tilting of human patients with acute unilateral vestibular neuritis. *Acta Otolaryngol.* (1973) 76:349–52. doi: 10.3109/00016487309121520

6. Lempert T, Gianna C, Brookes G, Bronstein A, Gresty M. Horizontal otolith-ocular responses in humans after unilateral vestibular deafferentation. *Exp Brain Res.* (1998) 118:533–40. doi: 10.1007/s002210050309

7. Kim HA, Hong JH, Lee H, Yi HA, Lee SR, Lee SY, et al. Otolith dysfunction in vestibular neuritis: recovery pattern and a predictor of symptom recovery. *Neurology.* (2008) 70:449–53. doi: 10.1212/01.wnl.0000297554.21221.a0

8. Wexler DB. Nonlinearity of the Jongkees difference equation for vestibular hypofunction. *Otolaryngol Head Neck Surg.* (1994) 111:485–7. doi: 10.1177/019459989411100416

9. Welgampola MS, Colebatch JG. Characteristics and clinical applications of vestibular-evoked myogenic potentials. *Neurology.* (2005) 64:1682–8. doi: 10.1212/01.WNL.0000161876.20552.AA

10. Iwasaki S, Smulders YE, Burgess AM, McGarvie LA, Macdougall HG, Halmagyi GM, et al. Ocular vestibular evoked myogenic potentials to bone conducted vibration of the midline forehead at Fz in healthy subjects. *Clin Neurophysiol.* (2008) 119:2135–47. doi: 10.1016/j.clinph.2008.05.028

11. Yi HA, Kim HA, Lee H, Baloh RW. Body lateropulsion as an isolated or predominant symptom of a pontine infarction. *J Neurol Neurosurg Psychiatry.* (2007) 78:372–4. doi: 10.1136/jnnp.2006.106237

12. Kim JS. When the room is spinning: experience of vestibular neuritis by a neurotologist. *Front Neurol.* (2020) 11:157. doi: 10.3389/fneur.2020.00157

13. Wang H, Li Z, Zhang S, He J, Yu D. Horizontal nystagmus is gravity-dependent in patients with vestibular neuritis. *Am J Otolaryngol.* (2021) 42:102967. doi: 10.1016/j.amjoto.2021.102967

14. Palla A, Marti S, Straumann D. Head-shaking nystagmus depends on gravity. *J Assoc Res Otolaryngol.* (2005) 6:1–8. doi: 10.1007/s10162-004-4052-3

15. Green AM, Angelaki DE. An integrative neural network for detecting inertial motion and head orientation. *J Neurophysiol.* (2004) 92:905–25. doi: 10.1152/jn.01234.2003

16. Zupan LH, Merfeld DM, Darlot C. Using sensory weighting to model the influence of canal, otolith and visual cues on spatial orientation and eye movements. *Biol Cybern.* (2002) 86:209–30. doi: 10.1007/s00422-001-0290-1

17. Choi JY, Park YM, Lee SH, Choi J, Hyun SW, Song JM, et al. Linear vertigo in benign paroxysmal positional vertigo: prevalence and mechanism. *Cerebellum.* (2021) 20:160–8. doi: 10.1007/s12311-020-01196-6

18. Choi JY, Glasauer S, Kim JH, Zee DS, Kim JS. Characteristics and mechanism of apogeotropic central positional nystagmus. *Brain.* (2018) 141:762–75. doi: 10.1093/brain/awx381

19. Laurens J, Angelaki DE. The functional significance of velocity storage and its dependence on gravity. *Exp Brain Res.* (2011) 210:407–22. doi: 10.1007/s00221-011-2568-4

20. Curthoys IS. The anatomical and physiological basis of clinical tests of otolith function. A tribute to yoshio uchino. *Front Neurol.* (2020) 11:566895. doi: 10.3389/fneur.2020.566895

21. Müller JA, Bockisch CJ, Tarnutzer AA. Spatial orientation in patients with chronic unilateral vestibular hypofunction is ipsilesionally distorted. *Clin Neurophysiol.* (2016) 127:3243–51. doi: 10.1016/j.clinph.2016.07.010

22. Pavlou M, Wijnberg N, Faldon ME, Bronstein AM. Effect of semicircular canal stimulation on the perception of the visual vertical. *J Neurophysiol.* (2003) 90:622–30. doi: 10.1152/jn.00960.2002

23. Pavri BB, Ruskin JN, Brooks R. The yield of head-up tilt testing is not significantly increased by repeating the baseline test. *Clin Cardiol.* (1996) 19:494–6. doi: 10.1002/clc.4960190610

24. Padoan S, Karlberg M, Fransson PA, Magnusson M. Passive sustained turning of the head induces asymmetric gain of the vestibulo-ocular reflex in healthy subjects. *Acta Otolaryngol.* (1998) 118:778–82. doi: 10.1080/00016489850182431

25. Yelnik AP, Lebreton FO, Bonan IV, Colle FM, Meurin FA, Guichard JP, et al. Perception of verticality after recent cerebral hemispheric stroke. *Stroke.* (2002) 33:2247–53. doi: 10.1161/01.STR.0000027212.26686.48

26. Bronstein AM. The interaction of otolith and proprioceptive information in the perception of verticality. The effects of labyrinthine and CNS disease. *Ann N Y Acad Sci.* (1999) 871:324–33. doi: 10.1111/j.1749-6632.1999.tb09195.x

Frontiers in Neurology

Explores neurological illness to improve patient care

The third most-cited clinical neurology journal explores the diagnosis, causes, treatment, and public health aspects of neurological illnesses. Its ultimate aim is to inform improvements in patient care.

Discover the latest Research Topics

See more →

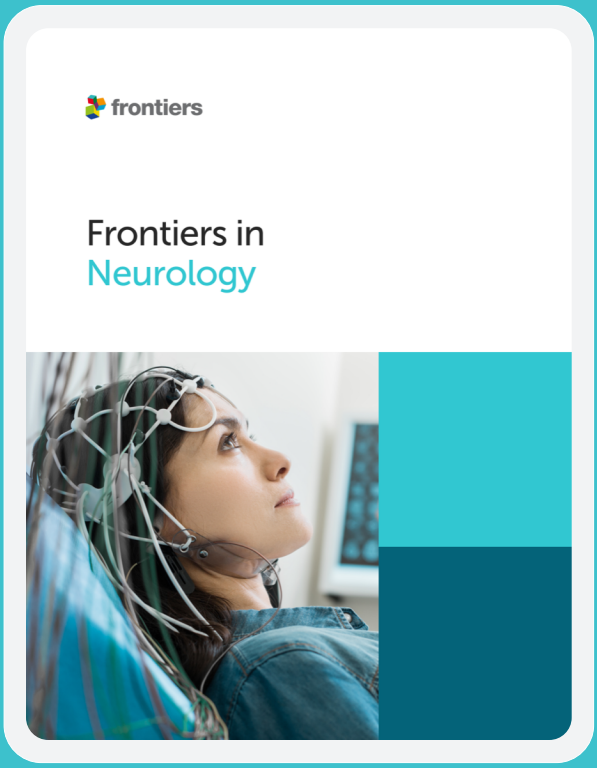

Frontiers

Avenue du Tribunal-Fédéral 34
1005 Lausanne, Switzerland
frontiersin.org

Contact us

+41 (0)21 510 17 00
frontiersin.org/about/contact